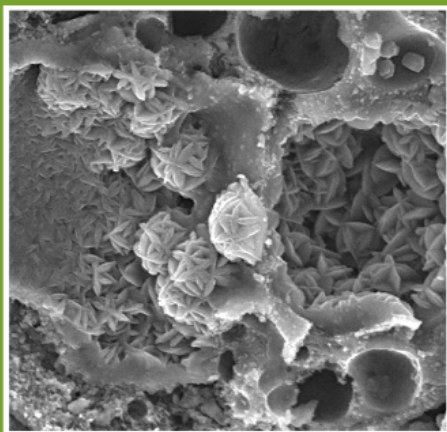


WOODHEAD PUBLISHING IN MATERIALS



Geopolymers

Structure, processing,
properties and
industrial applications

Edited by John L. Provis and
Jannie S. J. van Deventer



WP

Geopolymers

Related titles:

Developments in the formulation and reinforcement of concrete

(ISBN 978-1-84569-263-6)

Developments in the formulation and reinforcement of concrete are of great topical interest to the construction industry worldwide, with applications in high-rise, offshore, nuclear and bridge structures, and in pre-cast concrete. This authoritative book addresses the current lack of information on the latest developments in the formulation and reinforcement of concrete in one source. The book discusses the latest types of concrete and reinforcement and includes chapters on hot weather concreting, cold weather concreting and the use of recycled materials in concrete. It presents current research from leading innovators in the field.

Geosynthetics in civil engineering

(ISBN 978-1-85573-607-8)

Geosynthetics are essential to civil engineering and have a multitude of applications. The first part of the book looks at design principles for geosynthetics, their material properties and durability, and at the range of national and international standards governing their use. Part II reviews the range of applications of synthetics as well as quality assurance issues. There are chapters on geosynthetic applications as filters, separators and barrier materials, in improving building foundations and landfill sites, and as limited design life materials.

Advanced civil infrastructure materials

(ISBN 978-1 85573-943-7)

In recent decades, developments in response to the call for more durable infrastructures have led to many exciting advancements in materials science and mechanics. This book provides an up-to-date review of several emerging infrastructure materials – especially in advanced composites – that may have a significant impact on repair and/or new construction. Each chapter concludes with selective examples of real world applications using advanced materials. This book will be an invaluable resource for undergraduate and graduate students of civil engineering, materials, architecture and building engineering.

Details of these and other Woodhead Publishing materials books can be obtained by:

- visiting our web site at www.woodheadpublishing.com
- contacting Customer Services (e-mail: sales@woodheadpublishing.com; fax: +44 (0) 1223 893694; tel.: +44 (0) 1223 891358 ext. 130; address: Woodhead Publishing Limited, Abington Hall, Granta Park, Great Abington, Cambridge CB21 6AH, UK)

If you would like to receive information on forthcoming titles, please send your address details to: Francis Dodds (address, tel. and fax as above; e-mail: francis.dodds@woodheadpublishing.com). Please confirm which subject areas you are interested in.

Geopolymers

Structure, processing, properties
and industrial applications

Edited by
John L. Provis and
Jannie S. J. van Deventer



CRC Press
Boca Raton Boston New York Washington, DC

WOODHEAD PUBLISHING LIMITED
Oxford Cambridge New Delhi

Published by Woodhead Publishing Limited, Abington Hall, Granta Park, Great Abington, Cambridge CB21 6AH, UK
www.woodheadpublishing.com

Woodhead Publishing India Private Limited, G-2, Vardaan House, 7/28 Ansari Road, Daryaganj, New Delhi – 110002, India

Published in North America by CRC Press LLC, 6000 Broken Sound Parkway, NW, Suite 300, Boca Raton, FL 33487, USA

First published 2009, Woodhead Publishing Limited and CRC Press LLC
© 2009, Woodhead Publishing Limited
The authors have asserted their moral rights.

This book contains information obtained from authentic and highly regarded sources. Reprinted material is quoted with permission, and sources are indicated. Reasonable efforts have been made to publish reliable data and information, but the authors and the publishers cannot assume responsibility for the validity of all materials. Neither the authors nor the publishers, nor anyone else associated with this publication, shall be liable for any loss, damage or liability directly or indirectly caused or alleged to be caused by this book.

Neither this book nor any part may be reproduced or transmitted in any form or by any means, electronic or mechanical, including photocopying, microfilming and recording, or by any information storage or retrieval system, without permission in writing from Woodhead Publishing Limited.

The consent of Woodhead Publishing Limited does not extend to copying for general distribution, for promotion, for creating new works, or for resale. Specific permission must be obtained in writing from Woodhead Publishing Limited for such copying.

Trademark notice: Product or corporate names may be trademarks or registered trademarks, and are used only for identification and explanation, without intent to infringe.

British Library Cataloguing in Publication Data

A catalogue record for this book is available from the British Library.

Library of Congress Cataloging in Publication Data

A catalog record for this book is available from the Library of Congress.

Woodhead Publishing ISBN 978-1-84569-449-4 (book)

Woodhead Publishing ISBN 978-1-84569-638-2 (e-book)

CRC Press ISBN 978-1-4398-0970-9

CRC Press order number: N10092

The publishers' policy is to use permanent paper from mills that operate a sustainable forestry policy, and which has been manufactured from pulp which is processed using acid-free and elemental chlorine-free practices. Furthermore, the publishers ensure that the text paper and cover board used have met acceptable environmental accreditation standards.

Typeset by Replika Press Pvt Ltd

Printed by TJ International Limited, Padstow, Cornwall, UK

Contents

<i>Contributor contact details</i>	<i>xi</i>
1 Introduction to geopolymers	1
J L PROVIS and J S J VAN DEVENTER, University of Melbourne, Australia	
1.1 History of geopolymer technology	1
1.2 Geopolymer terminology	3
1.3 Geopolymer science	4
1.4 Geopolymer applications	6
1.5 Conclusions	6
1.6 References	7
Part I Geopolymer synthesis and characterisation	
2 Fly ash glass chemistry and inorganic polymer cements	15
L M KEYTE, University of Melbourne, Australia	
2.1 Introduction	15
2.2 Origin and history of coal fly ash	16
2.3 Coal fly ash particle morphology	19
2.4 Aluminosilicate glass chemistry	22
2.5 Examining coal fly ash glass chemistry	24
2.6 Coal fly ash glass behaviour in IPC formation	29
2.7 Conclusions	33
2.8 References	33
3 Geopolymer precursor design	37
P DUXSON, University of Melbourne, Australia	
3.1 Introduction	37
3.2 Metallurgical slags	38
3.3 Fly ash	39
3.4 Availability of aluminium	42

vi	Contents	
3.5	An optimal two-part geopolymer?	43
3.6	Designing one-part geopolymer cements	44
3.7	Geopolymers and the future cement industry	45
3.8	Conclusions	45
3.9	References	46
4	Activating solution chemistry for geopolymers J L PROVIS, University of Melbourne, Australia	50
4.1	Introduction	50
4.2	Alkali hydroxide solutions	51
4.3	Alkali silicate solutions	56
4.4	Other activators	64
4.5	Conclusions	66
4.6	References	66
5	Nanostructure/microstructure of metakaolin geopolymers J L PROVIS, S L YONG and P DUXSON, University of Melbourne, Australia	72
5.1	Introduction	72
5.2	Metakaolin	73
5.3	Formation of metakaolin geopolymers	75
5.4	Nanostructure of metakaolin geopolymers	76
5.5	Microstructure of metakaolin geopolymers	81
5.6	Calcium in metakaolin geopolymers	84
5.7	Conclusions	85
5.8	References	85
6	Nanostructure/microstructure of fly ash geopolymers A FERNÁNDEZ-JIMÉNEZ and A PALOMO, Eduardo Torroja Institute, Spain	89
6.1	Introduction: general characteristics of cementitious gels	89
6.2	Polymerisation: a conceptual model	92
6.3	Characterisation of N-A-S-H gel	96
6.4	Microstructure of the fly ash geopolymer	111
6.5	Conclusions	114
6.6	References	114
7	Geopolymer synthesis kinetics J L PROVIS and C A REES, University of Melbourne, Australia	118
7.1	Introduction	118
7.2	In situ infrared spectroscopy	119
7.3	Calorimetry	125

7.4	Rheology	126
7.5	Diffraction techniques	127
7.6	Nuclear magnetic resonance (NMR)	129
7.7	Microscopy	130
7.8	Modelling	130
7.9	Conclusions	133
7.10	References	133

Part II Manufacture and properties of geopolymers

8	Accelerated ageing of geopolymers R R LLOYD, University of Melbourne, Australia	139
8.1	Introduction	139
8.2	Crystallisation during synthesis of geopolymer gels	140
8.3	Crystallisation during ageing of geopolymer gels	141
8.4	Accelerated ageing tests of geopolymers	142
8.5	Ageing of geopolymers synthesised from metakaolin	145
8.6	Ageing of geopolymers synthesised from fly ash	153
8.7	Conclusions	163
8.8	References	164
9	Chemical durability of geopolymers A FERNÁNDEZ-JIMÉNEZ and A PALOMO, Eduardo Torroja Institute, Spain	167
9.1	Introduction: general aspects	167
9.2	Sulphate attack and sea water attack resistance	168
9.3	Acid attack	172
9.4	Resistance to corrosion of steel reinforcement	176
9.5	Alkali silica reaction	180
9.6	High temperature and fire resistance	183
9.7	Resistance to extreme environment: frost attack	189
9.8	Conclusions	190
9.9	References	190
10	Life-cycle analysis of geopolymers M WEIL, Institute for Technology Assessment and Systems Analysis, Germany, K DOMBROWSKI, Technische Universität Bergakademie Freiberg Germany and A BUCHWALD, Bauhaus University Weimar, Germany	194
10.1	Introduction	194
10.2	Life cycle assessment	195
10.3	Influence of the geopolymer composition on environmental impacts	198

10.4	Influence of the geopolymer production process on environmental impacts	200
10.5	LCA comparison of geopolymers to other product systems	202
10.6	Geopolymers and the utilisation of secondary resources	208
10.7	Conclusions	209
10.8	Acknowledgement	209
10.9	References	210
11	Engineering properties of geopolymer concrete B V RANGAN, Curtin University of Technology, Australia	211
11.1	Introduction	211
11.2	Geopolymer concrete	212
11.3	Mixture design, production, and curing	213
11.4	Short-term properties of geopolymer concrete	216
11.5	Long-term properties of geopolymer concrete	219
11.6	Conclusions	225
11.7	References	225
12	Producing fire- and heat-resistant geopolymers G KOVALCHUK and P V KRIVENKO, Kyiv National University for Civil Engineering and Architecture, Ukraine	227
12.1	Introduction	227
12.2	Phase composition of alkaline aluminosilicate cements after curing at normal and elevated temperature	229
12.3	Interrelation between mix proportion, phase composition after hydration and dehydration, and properties	250
12.4	Experience of application	257
12.5	Conclusions	261
12.6	References	263
13	Utilization of mining wastes to produce geopolymer binders F PACHECO-TORGAL and S JALALI, University of Minho, Portugal and J P CASTRO-GOMES, University of Beira Interior, Portugal	267
13.1	Introduction	267
13.2	Influence of calcination operations in the reactivity of mine wastes	268
13.3	Strength gain and mix design parameters	271
13.4	Physical and mechanical properties	276
13.5	Durability and environmental performance	286
13.6	Future research trends	289
13.7	References	291

14	Utilisation of non-thermally activated clays in the production of geopolymers K J D MACKENZIE, Victoria University of Wellington, New Zealand	294
14.1	Introduction	294
14.2	Dehydroxylation of 1:1 layer-lattice aluminosilicate minerals	296
14.3	Dehydroxylation of 2:1 layer-lattice aluminosilicate minerals	299
14.4	Reactions of thermally dehydroxylated clays with alkali	300
14.5	Methods for reproducing the effects of thermal dehydroxylation in clays	302
14.6	Other methods for forming aluminosilicate geopolymers	308
14.7	Conclusions	311
14.8	References	312
15	Thermal properties of geopolymers A VAN RIESSEN and W RICKARD, Curtin University of Technology, Australia and J SANJAYAN, Monash University, Australia	315
15.1	Introduction	315
15.2	Thermal expansion	316
15.3	Thermoanalysis	324
15.4	Thermophysical properties	326
15.5	Fire resistance	327
15.6	Mechanical strength evolution	330
15.7	Phase changes at elevated temperatures	333
15.8	Microstructural changes	335
15.9	High temperature applications of geopolymers	338
15.10	References	339
16	Utilisation of low-calcium slags to improve the strength and durability of geopolymers K KOMNITSAS and D ZAHARAKI, Technical University of Crete, Greece	343
16.1	Introduction	343
16.2	Materials and methodology	345
16.3	Factors affecting compressive strength	347
16.4	Durability studies	356
16.5	Mineralogical studies	360
16.6	Prospects for industrial applications	369
16.7	Conclusions	369
16.8	Sources of further information and advice	371
16.9	References	371

Part III Applications of geopolymers

17	Commercialization of geopolymers for construction – opportunities and obstacles P DUXSON and J S J VAN DEVENTER, University of Melbourne, Australia	379
17.1	Introduction	379
17.2	Alkaline activation: is this a new idea?	380
17.3	Why has AAM technology not been commercialized before now?	381
17.4	How the standards and regulations framework is addressed	385
17.5	Analysis of the cement market	390
17.6	How climate change and carbon trading create opportunities	393
17.7	Opportunities for AAM	398
17.8	Conclusions	399
17.9	References	400
18	Geopolymers for nuclear waste immobilisation E R VANCE and D S PERERA, Institute of Materials Engineering, Australia	401
18.1	Nuclear wastes around the world	401
18.2	Cementitious LLW/ILW waste forms	405
18.3	Future trends	415
18.4	Conclusions	415
18.5	Sources of further information and advice	416
18.6	Acknowledgements	416
18.7	References	416
19	Immobilisation of toxic wastes in geopolymers J L PROVIS, University of Melbourne, Australia	421
19.1	Introduction	421
19.2	Main group elements	424
19.3	Transition metals	430
19.4	Other wastes	435
19.5	Conclusions	436
19.6	References	436
	<i>Index</i>	441

Contributor contact details

(* = main contact)

Chapter 1

John L. Provis* and Jannie S. J.
van Deventer
Department of Chemical and
Biomolecular Engineering
University of Melbourne
Victoria 3010
Australia

E-mail: jprovis@unimelb.edu.au

Chapter 2

Louise M. Keyte
Department of Chemical and
Biomolecular Engineering
University of Melbourne
Victoria 3010
Australia

E-mail: lkeyte@unimelb.edu.au

Chapter 3

Peter Duxson
Department of Chemical and
Biomolecular Engineering
The University of Melbourne
Victoria 3010
Australia

E-mail: duxsonp@unimelb.edu.au

Chapter 4

John L. Provis
Department of Chemical and
Biomolecular Engineering
University of Melbourne
Victoria 3010
Australia

E-mail: jprovis@unimelb.edu.au

Chapter 5

John L. Provis*, Syet Li Yong and
Peter Duxson
Department of Chemical and
Biomolecular Engineering
University of Melbourne
Victoria 3010
Australia

E-mail: jprovis@unimelb.edu.au
slyong@pgrad.unimelb.edu.au

Chapters 6 and 9

A. Palomo* and A. Fernández-
Jiménez

Department of Synthesis
Eduardo Torroja Institute
C/ Serrano galvache
Nº4, Madrid 28033
Spain

E-mail: anafj@ietcc.csic.es
palomo@ietcc.csic.es

Chapter 7

John L. Provis* and Catherine A.
Rees

Department of Chemical and
Biomolecular Engineering
University of Melbourne
Victoria 3010
Australia

E-mail: jprovis@unimelb.edu.au

Chapter 8

Redmond R. Lloyd
Department of Chemical and
Biomolecular Engineering
University of Melbourne
Victoria 3010
Australia

E-mail: rlloyd@unimelb.edu.au

Chapter 10

M. Weil*

Forschungszentrum Karlsruhe
Institute for Technology
Assessment and Systems
Analysis
Department of Technology-Induced
Material Flow (ITAS-ZTS)
Hermann-von-Helmholtz-Platz 1
Germany

E-mail: marcel.weil@kit.edu

K. Dombrowski

Technische Universität
Bergakademie Freiberg
Institute of Ceramic, Glass, and
Construction Materials
Germany

A. Buchwald

Bauhaus University Weimar
Chair of Building Chemistry
Germany

Chapter 11

B. Vijaya Rangan

Emeritus Professor of Civil
Engineering
Curtin University of Technology
Perth
Australia

E-mail: V.Rangan@curtin.edu.au

Chapter 12

G. Kovalchuk* and P. V. Krivenko
V. D. Glukhovskiy State Scientific
Research Institute for Binders
and Materials

Kyiv National University for Civil
Engineering and Architecture
Povitroflotskiy prosp., 31
PO Box 161
03037 Kyiv
Ukraine

E-mail: george.kiev@mail.ru
pavlo.kryvenko@gmail.com

Chapter 13

F. Pacheco-Torgal*
C-TAC Research Unit
Sustainable Construction Group
University of Minho
Campus de Azurem
4800-058 Guimarães
Portugal

E-mail: f.pachecotorgal@gmail.com

J. Castro Gomes
Department of Civil Engineering
and Architecture
University of Beira Interior
Rua Marques D'Avila e Bolama
6201-001 Covilhã
Portugal

E-mail: castro.gomes@ubi.pt

Said Jalali
Department of Civil Engineering
University of Minho
Campus de Azurem
4800-058 Guimarães
Portugal

E-mail: said@uminho.pt

Chapter 14

Kenneth J. D. MacKenzie
MacDiarmid Institute for Advanced
Materials and Nanotechnology
Victoria University of Wellington
P.O. Box 600 Wellington
New Zealand

E-mail: kenneth.mackenzie@vuw.
ac.nz

Chapter 15

Arie van Riessen* and William
Rickard
Centre for Materials Research
Curtin University of Technology
GPO Box U1987
Perth
Western Australia 6845
Australia

E-mail: A.VanRiessen@curtin.edu.au

Jay Sanjayan
Department of Civil Engineering
Monash University
Clayton
Victoria 3800
Australia

Chapter 16

Kostas Komnitsas* and Dimitra Zaharaki
Department of Mineral Resources Engineering
Technical University of Crete
73100 Hania
Greece

E-mail: komni@mred.tuc.gr

Chapter 17

Peter Duxson* and Jannie S.J. van Deventer
Department of Chemical and Biomolecular Engineering
The University of Melbourne
Victoria 3010
Australia

E-mail duxsonp@unimelb.edu.au

Chapter 18

E. R. Vance* and D. S. Perera
Institute of Materials Engineering,
Australian Nuclear Science and Technology Organisation
Menai, NSW 2234
Australia

E-mail: erv@ansto.gov.au

Chapter 19

John L. Provis
Department of Chemical and Biomolecular Engineering
University of Melbourne
Victoria 3010
Australia

E-mail: jprovis@unimelb.edu.au

J L PROVIS and J S J VAN DEVENTER,
University of Melbourne, Australia

Abstract: This introductory chapter provides a brief overview of some important aspects of geopolymer technology, in particular its historical development and the terminology by which geopolymers are described. An introduction to geopolymer technology from a scientific viewpoint is also given. The scope of this review is confined to predominantly low-calcium materials, i.e. ‘traditional’ alkali-aluminosilicate geopolymers, to the exclusion of alkali-activated slags and other related materials.

Key words: geopolymer, inorganic polymer, aluminosilicate, alkali activation.

1.1 History of geopolymer technology

The term ‘geopolymer’ was coined in the 1970s by the French scientist and engineer Prof. Joseph Davidovits, and applied to a class of solid materials synthesised by the reaction of an aluminosilicate powder with an alkaline solution (Davidovits 1982a, 1991, 2008). These materials were originally developed as a fire-resistant alternative to organic thermosetting polymers following a series of fires in Europe, and products based on this initial work have since found application as coatings for fire protection for cruise ships (Talling 2002), as a resin in high-temperature carbon-fibre composites (Lyon *et al.* 1997), in thermal protection of wooden structures (Giancaspro *et al.* 2006), as a heat-resistant adhesive (Bell *et al.* 2005, Krivenko and Kovalchuk 2007), as a monolithic refractory (Comrie and Kriven 2003, Kriven *et al.* 2004), and in various other niche applications. However, as can be seen from a brief perusal of the Table of Contents of this book, the primary application for geopolymer binders has since shifted to uses in construction. This is primarily due to the observation, first published by Wastiels *et al.* (1993), that it is possible to generate reliable, high-performance geopolymers by alkaline activation of fly ash, a by-product of coal combustion.

The synthesis of construction materials by alkaline activation of solid, non-Portland cement precursors (usually high-calcium metallurgical slags) was first demonstrated by Purdon (1940). Detailed lists of key historical references and milestones in the development of alkali-activated binders have been presented in various review papers (Malone *et al.* 1985, Krivenko 1994, Roy 1999, Krivenko 2002); the majority of these relate to the alkaline

activation of blast furnace slags, and so are beyond the scope of the current discussion. A very extensive review focussed predominantly on alkali activation of metallurgical slags has recently been published (Shi *et al.* 2006), and the reader is referred to that excellent book for information in that area. The key distinction to be made here is that the alkaline activation of slags produces a fundamentally calcium silicate hydrate-based gel (Richardson *et al.* 1994, Wang and Scrivener 1995, Shi *et al.* 2006), with silicon present mainly in one-dimensional chains and some substitution of Al for Si and Mg for Ca, whereas the geopolymer gel is a three-dimensional alkali aluminosilicate framework structure (Duxson *et al.* 2007b). The role of calcium in geopolymers is a matter still under investigation; some of the subtleties of calcium chemistry in geopolymers will be discussed throughout this book.

Much of the early published research into aluminosilicate geopolymers was published in the patent literature (for example: Davidovits 1982b, 1984), and so contains little scientific detail. Probably the most valuable documents summarising work throughout the 1980s are the proceedings of a conference (*Geopolymer '88*) held in France in 1988 (Davidovits and Orlinski 1988), and a review paper authored by Davidovits (1991). Shortly after this, Palomo and Glasser published the first detailed scientific study of metakaolin geopolymers (Palomo and Glasser 1992), followed shortly afterwards by an extremely valuable three-part series by Rahier *et al.* (1996a, 1996b, 1997). These papers laid the groundwork for both broader and deeper study of metakaolin geopolymers in the ensuing decade, in particular work by groups in Spain (Granizo and Blanco 1998, Palomo *et al.* 1999b, Alonso and Palomo 2001), New Zealand (Barbosa *et al.* 2000, Barbosa and MacKenzie 2003), Germany (Kaps and Buchwald 2002, Buchwald *et al.* 2003, Buchwald 2006), and Australia (Yip and van Deventer 2003, Duxson *et al.* 2005, Perera *et al.* 2005, Singh *et al.* 2005, Steveson and Sagoe-Crentsil 2005). The proceedings of Geopolymer conferences held in 1999 (Davidovits *et al.* 1999), 2002 (Lukey 2002) and 2005 (Davidovits 2005) also provide valuable information regarding both technical developments in the field and the worldwide growth in geopolymers research during this period. A book published recently by Davidovits (2008) also summarises a good deal of work that was only previously available in the patent literature.

Research into fly ash geopolymers has grown from the aforementioned conference paper by Wastiels *et al.* (1993) to now form the bulk of applications-oriented research in this field. Fly ash has long been used in Portland cement concretes to enhance flow and other properties (Diamond 1986, Bouzoubaâ *et al.* 1999, Manz 1999), to reduce the carbon footprint of concrete, as well as simply a means of disposing of some of the many millions of tonnes of fly ash produced worldwide each year. Additional early reports of geopolymerisation of ASTM Class F (low-calcium) fly ash were provided by a number of researchers (van Jaarsveld *et al.* 1997, 1998,

Palomo *et al.* 1999a, van Jaarsveld 2000, Krivenko and Kovalchuk 2002, Lee and van Deventer 2002, Swanepoel and Strydom 2002, Fernández-Jiménez and Palomo 2003, Rostami and Brendley 2003, Hardjito *et al.* 2004, Palomo *et al.* 2004), along with a proliferation of patents. Possibly due to the inherent difficulty associated with detailed scientific analysis of highly heterogeneous fly ash-based geopolymers, the level of understanding of fly ash geopolymers currently appears to lag behind their metakaolin-based counterparts. Metakaolin geopolymers are often used as a ‘model system’ by which the more commercially relevant fly ash-based materials may be better understood (van Deventer *et al.* 2007), and the exact degree to which this relationship holds has been the subject of some recent scrutiny (Lloyd 2008).

It is also necessary to note that various theories have been proposed attempting to link aspects of geopolymerisation technology to the construction of ancient structures, most particularly the Pyramids of Egypt (Davidovits and Davidovits 2001, Barsoum *et al.* 2006). While the veracity of such arguments is still under quite intense debate in some circles, it is clear that whether or not the Pyramids were ‘poured’ as synthetic stone blocks, the chemistry involved in such an undertaking would have been some distance away from the alkali-activated aluminosilicate systems which today are described as geopolymers (Barsoum *et al.* 2006). However, it is not the role of this Introduction to attempt to speculate regarding such issues.

1.2 Geopolymer terminology

In the context of this book, a ‘geopolymer’ is in general defined as a solid and stable aluminosilicate material formed by alkali hydroxide or alkali silicate activation of a precursor that is usually (but not always) supplied as a solid powder. The same term has also been used to describe organic polymers formed under geological conditions (e.g., coal); in spite of some highly speculative discussions to the contrary (Davidovits 2008), these materials are entirely unrelated to aluminosilicate geopolymers and will not be discussed in detail here.

The materials referred to here as ‘geopolymers’ have also been described in the academic literature as ‘mineral polymers’, ‘inorganic polymers’, ‘inorganic polymer glasses’, ‘alkali-bonded ceramics’, ‘alkali ash material’, ‘soil cements’, ‘hydroceramics’, and a variety of other names. The major impact of this proliferation of different names for essentially the same material is that researchers who are not intimately familiar with the field will either become rapidly confused about which terms refer to which specific materials, or they will remain unaware of important research that does not appear upon conducting a simple keyword search on an academic search engine. A prime example of this is the very valuable early work of Rahier and colleagues

(Rahier *et al.* 1996a, 1996b, 1997), who used the term ‘inorganic polymer glass’ rather than ‘geopolymer,’ and so these papers have received far fewer citations than their quality and importance deserve. The terms ‘geopolymer’ and ‘inorganic polymer’ are gaining increasing ubiquity in the academic research field, and will be used essentially interchangeably throughout this book. Geopolymers are a subset of the broader class of alkali-activated binders (Shi *et al.* 2006), which also includes materials formed by alkali-, silicate-, carbonate- or sulfate-activation of metallurgical slags and giving a product that is predominantly calcium silicate hydrate, as mentioned in Section 1.1. The defining characteristic of a geopolymer is that the binding phase comprises an alkali aluminosilicate gel, with aluminium and silicon linked in a three-dimensional tetrahedral gel framework that is relatively resistant to dissolution in water (MacKenzie 2003, Rees *et al.* 2007).

More than 25 years ago, Davidovits introduced the ‘sialate’ nomenclature to describe aluminosilicate structures (Davidovits 1982a). The linkage type Si-O-Al was named a sialate bond, and Si-O-Si a siloxo bond. This provided a means of describing the composition of geopolymers according to their Si/Al ratio, with a ratio of 1.0 being a poly(sialate), 2.0 being a poly(sialate-siloxo), and 3.0 a poly(sialate-disiloxo). Unfortunately, the term ‘sialate’ was already in use (since the 1950s) to describe any of the salts of sialic acid, a nine-carbon monosaccharide and an important component of several biochemical systems within the human body. Also, this system of nomenclature implies certain aspects of the geopolymer gel structure which do not correspond to reality; firstly, it describes only integer Si/Al ratios, and secondly, it provides a one-dimensional description of a three-dimensional network, which will almost invariably prove inadequate. This nomenclature system did for some time find relatively widespread use in academic research (Barbosa *et al.* 2000, Zoulgami *et al.* 2002, Zhang *et al.* 2005, Subaer and van Riessen 2007), often to describe systems with non-integer Si/Al ratios but generally without comment as to its applicability in such cases, but appears to be fading in popularity as researchers discover its limitations.

1.3 Geopolymer science

Given that a large part of the purpose of this book is to provide an overview of the state of the art in various aspects of geopolymer science, it would be superfluous to provide a detailed description in this Introduction. Nonetheless, some preliminary comments are in order.

Initially, it must be said that geopolymers are a complex class of materials. The principal means of synthesising geopolymers is to combine an alkaline solution with a reactive aluminosilicate powder, in particular metakaolin (calcined kaolinite clay) or fly ash (a by-product of coal combustion). This results in the formation of a disordered alkali aluminosilicate gel phase,

known as the geopolymeric gel binder phase. Embedded within this phase are unreacted solid precursor particles, and the pore network of the gel contains the water that was used in mixing the precursors (usually supplied via the alkaline ‘activating solution’). Unlike in a calcium silicate hydrate gel, the water does not form an integral part of the chemical structure of a geopolymer binder; from a practical perspective this presents both advantages and disadvantages. The fundamental framework of the gel is a highly connected three-dimensional network of aluminate and silicate tetrahedra, with the negative charge due to Al^{3+} in four-fold coordination localised on one or more of the bridging oxygens in each aluminate tetrahedron and balanced by the alkali metal cations provided by the activating solution. There have been a variety of attempts to draw schematic diagrams of the three-dimensional geopolymer structure; such efforts will almost certainly be fraught with difficulty due to the disorder inherent in the geopolymer and also the difficulty of accurately representing a three-dimensional framework in two dimensions. The picture presented recently by Rowles *et al.* (2007) is probably the most useful of those currently available.

It has also been shown that the geopolymeric gel binder displays structural similarities, on an atomic to nanometre length scale, to zeolitic materials. In some cases – particularly in the presence of high water content, elevated synthesis temperature and low Si/Al ratio – this extends so far as to be visible as the formation of nanocrystallites within the geopolymer gel (Provis *et al.* 2005). However, even where none of these factors is present and the geopolymer displays no structural ordering on a length scale exceeding 1 nm, there are still strong structural motifs on an atomic length scale which correlate well with those observed in zeolites (Bell *et al.* 2008).

From this basis, the structural analysis presented in various chapters of this book represents the results of detailed investigations by various research groups over a number of years. Very little about the structural analysis of geopolymers is straightforward, as they comprise a mixture of various X-ray amorphous phases (reaction product as well as unreacted precursor material), and are formed in a corrosive reaction environment which complicates in situ analysis (as discussed in detail in Chapter 4). Nonetheless, much information has been obtained through careful experimental design and data analysis. In most areas of science, it is the case that either ‘easy’ (i.e. routine) methods of analysis are applied to ‘challenging’ materials, or ‘challenging’ methods of analysis are applied to ‘easy’ (i.e., pure and well characterised) material classes. Geopolymers, in common with Portland cements, are a ‘challenging’ class of materials whose chemistry necessitates the use of ‘challenging’ techniques for characterisation; this means that the science involved in understanding ‘low-technology’ construction materials is in fact at the cutting edge of materials science in general.

1.4 Geopolymer applications

As was mentioned in Section 1.1, the primary area of application of geopolymer technology is currently in the development of reduced-CO₂ construction materials as an alternative to Portland-based (calcium silicate) cements. Various other properties of geopolymers provide technological advantages over traditional construction materials, but performance in itself will not be sufficient to drive a revolutionary change in construction materials technology (Duxson *et al.* 2007a). A new material cannot be forced onto an unwilling market; the market itself must demand a new material, and this is beginning to be the case for geopolymers in construction, as will be discussed in detail in Chapter 17 of this book.

Other applications for geopolymers include as a host matrix in waste encapsulation, as a low-cost ceramic (either used directly or as a precursor for calcination), and in fire protection of structures. Part III of this book is dedicated to the description of some of the prime applications for geopolymers at present.

1.5 Conclusions

Geopolymers are a class of materials, whose potential remains to be fully unlocked. It is only through a detailed understanding of geopolymer science that full use can be made of the properties of geopolymers in specific applications. However, such science would rapidly become irrelevant in the absence of commercial success; a material that is well characterised but not used in the real world is in effect useless. From a scientific perspective, debates regarding nomenclature and semantics are entirely counterproductive, so long as the existing nomenclature is adequate to the task at hand. What is more important is that the understanding of geopolymers is built to the point where binder properties can be tailored *a priori* by rational mix design, and the understanding of the binder structure is sufficient to explain why these properties can be expected to last for a sufficient period of time to render the material fit for purpose in an engineering sense.

There is a growing demand for new construction materials that have low greenhouse gas emissions associated with their manufacture. Therefore, geopolymeric concrete could potentially be used widely as a replacement for Portland cement concrete, but this will only happen when both an efficient supply chain for raw materials and a distribution network for the products are in place. Recent commercial initiatives in this regard are encouraging, but it will take some time to make geopolymeric concrete a scaleable commodity available on a global basis. In the meantime, it is imperative that the localised demonstration of geopolymer technology grows, especially for converting coal ash into concrete with a low carbon footprint. This book

provides essential background to those interested in pursuing this exciting technology.

1.6 References

- Alonso, S. and Palomo, A. (2001) Calorimetric study of alkaline activation of calcium hydroxide-metakaolin solid mixtures. *Cement and Concrete Research*, 31, 25–30. doi:10.1016/S0008-8846(00)00435-X.
- Barbosa, V. F. F. and Mackenzie, K. J. D. (2003) Synthesis and thermal behaviour of potassium sialate geopolymers. *Materials Letters*, 57, 1477–1482. doi:10.1016/S0167-577X(02)01009-1.
- Barbosa, V. F. F., Mackenzie, K. J. D. and Thaumaturgo, C. (2000) Synthesis and characterisation of materials based on inorganic polymers of alumina and silica: sodium polysialate polymers. *International Journal of Inorganic Materials*, 2, 309–317. doi:10.1016/S1466-6049(00)00041-6.
- Barsoum, M. W., Ganguly, A. and Hug, G. (2006) Microstructural evidence of reconstituted limestone blocks in the Great Pyramids of Egypt. *Journal of the American Ceramic Society*, 89, 3788–3796. doi:10.1111/j.1551-2916.2006.01308.x
- Bell, J. L., Gordon, M. and Kriven, W. M. (2005) Use of geopolymeric cements as a refractory adhesive for metal and ceramic joins. *Ceramic Engineering and Science Proceedings*, 26, 407–413.
- Bell, J. L., Sarin, P., Provis, J. L., Haggerty, R. P., Driemeyer, P. E., Chupas, P. J., van Deventer, J. S. J. and Kriven, W. M. (2008) Atomic structure of a cesium aluminosilicate geopolymer: A pair distribution function study, *Chemistry of Materials*, 20, 4768–4776. doi 10.1021/cm703369s.
- Bouzoubaâ, N., Zhang, M. H., Malhotra, V. M. and Golden, D. M. (1999) Blended fly ash cements – A review. *ACI Materials Journal*, 96, 641–650.
- Buchwald, A. (2006) What are geopolymers? Current state of research and technology, the opportunities they offer, and their significance for the precast industry. *Betonwerk + Fertigteil-Technik*, 72, 42–49.
- Buchwald, A., Kaps, C. and Hohmann, M. (2003) Alkali-activated binders and pozzolan cement binders – Complete binder reaction or two sides of the same story? *Proceedings of the 11th International Conference on the Chemistry of Cement*, Durban, South Africa, 1238–1246.
- Comrie, D. C. and Kriven, W. M. (2003) Composite cold ceramic geopolymer in a refractory application. *Ceramic Transactions*, 153, 211–225.
- Davidovits, J. (1982a) The need to create a new technical language for the transfer of basic scientific information. *Transfer and Exploitation of Scientific and Technical Information, EUR 7716*. Luxembourg, Commission of the European Communities.
- Davidovits, J. (1982b) Mineral polymers and methods of making them, U.S. Patent 4,349,386.
- Davidovits, J. (1984) Synthetic mineral polymer compound of the silicoaluminates family and preparation process, U.S. Patent 4,472,199.
- Davidovits, J. (1991) Geopolymers – Inorganic polymeric new materials. *Journal of Thermal Analysis*, 37, 1633–1656. doi:10.1007/BF01912193.
- Davidovits, J. (2005) *Geopolymer, Green Chemistry and Sustainable Development Solutions: Proceedings of World Congress Geopolymer 2005*. Saint-Quentin, France.

- Davidovits, J. (2008) *Geopolymer Chemistry and Applications*, Saint-Quentin, France, Institut Géopolymère.
- Davidovits, J. and Davidovits, F. (2001) *The Pyramids: An Enigma Solved*. 2nd Revised Ed., Saint-Quentin, France, Éditions J. Davidovits.
- Davidovits, J. and Orlinski, J. (1988) *Proceedings of Geopolymer '88 – First European Conference on Soft Mineralogy*. Compeigne, France.
- Davidovits, J., Davidovits, R. and James, C. (1999) *Proceedings of Géopolymère '99 – Second International Conference*. Saint-Quentin, France.
- Diamond, S. (1986) Particle morphologies in fly ash. *Cement and Concrete Research*, 16, 569–579. doi:10.1016/0008-8846(86)90095-5.
- Duxson, P., Lukey, G. C., Separovic, F. and Van Deventer, J. S. J. (2005) The effect of alkali cations on aluminum incorporation in geopolymeric gels. *Industrial and Engineering Chemistry Research*, 44, 832–839. doi:10.1021/ie0494216.
- Duxson, P., Provis, J. L., Lukey, G. C. and Van Deventer, J. S. J. (2007a) The role of inorganic polymer technology in the development of 'Green concrete'. *Cement and Concrete Research*, 37, 1590–1597. doi:10.1016/j.cemconres.2007.08.018.
- Duxson, P., Fernández-Jiménez, A., Provis, J. L., Lukey, G. C., Palomo, A. and Van Deventer, J. S. J. (2007b) Geopolymer technology: The current state of the art. *Journal of Materials Science*, 42, 2917–2933. doi:10.1007/s10853-006-0637-z.
- Fernández-Jiménez, A. and Palomo, A. (2003) Characterisation of fly ashes. Potential reactivity as alkaline cements. *Fuel*, 82, 2259–2265. doi:10.1016/S0016-2361(03)00194-7.
- Giancaspro, J., Balaguru, P. N. and Lyon, R. E. (2006) Use of inorganic polymer to improve the fire response of balsa sandwich structures. *Journal of Materials in Civil Engineering*, 18, 390–397. doi:10.1061/(ASCE)0899-1561(2006)18:3(390).
- Granizo, M. L. and Blanco, M. T. (1998) Alkaline activation of metakaolin - An isothermal conduction calorimetry study. *Journal of Thermal Analysis*, 52, 957–965. doi:10.1023/A:1010176321136.
- Hardjito, D., Wallah, S. E., Sumajouw, D. M. J. and Rangan, B. V. (2004) On the development of fly ash-based geopolymer concrete. *ACI Materials Journal*, 101, 467–472.
- Kaps, C. and Buchwald, A. (2002) Property controlling influences on the generation of geopolymeric binders based on clay. *Geopolymers 2002. Turn Potential into Profit*, Melbourne, Lukey, G. C. (Ed.), CD-ROM Proceedings.
- Kriven, W. M., Bell, J. L. and Gordon, M. (2004) Geopolymer refractories for the glass manufacturing industry. *Ceramic Engineering and Science Proceedings*, 25, 57–79.
- Krivenko, P. V. (1994) Alkaline cements. *Proceedings of the First International Conference on Alkaline Cements and Concretes*, Kiev, Ukraine, Krivenko, P. V. (Ed.), 11–129.
- Krivenko, P. V. (2002) Alkaline cements: From research to application. *Geopolymers 2002. Turn Potential into Profit*, Melbourne, Australia, Lukey, G. C. (Ed.), CD-ROM Proceedings.
- Krivenko, P. V. and Kovalchuk, G. Y. (2002) Heat-resistant fly ash based geocements. *Geopolymers 2002. Turn Potential into Profit*, Melbourne, Australia, Lukey, G. C. (Ed.), CD-ROM Proceedings.
- Krivenko, P. V. and Kovalchuk, G. Y. (2007) Directed synthesis of alkaline aluminosilicate minerals in a geocement matrix. *Journal of Materials Science*, 42, 2944–2952. doi:10.1007/s10853-006-0528-3.
- Lee, W. K. W. and Van Deventer, J. S. J. (2002) The effect of ionic contaminants on the early-age properties of alkali-activated fly ash-based cements. *Cement and Concrete Research*, 32, 577–584. doi:10.1016/S0008-8846(01)00724-4.

- Lloyd, R. R. (2008) PhD Thesis, Department of Chemical and Biomolecular Engineering, University of Melbourne, Australia.
- Lukey, G. C. (2002) *Proceedings of Geopolymers 2002 – Turn Potential into Profit*, Melbourne, Australia.
- Lyon, R. E., Balaguru, P. N., Foden, A., Sorathia, U., Davidovits, J. and Davidovics, M. (1997) Fire-resistant aluminosilicate composites. *Fire and Materials*, 21, 67–73. doi:10.1002/(SICI)1099-1018(199703)21:2<67::AID-FAM596>3.0.CO;2-N.
- Mackenzie, K. J. D. (2003) What are these things called geopolymers? A physico-chemical perspective. *Ceramic Transactions*, 153, 175–186.
- Malone, P. G., Randall, C. J. and Kirkpatrick, T. (1985) *Potential applications of alkali-activated aluminosilicate binders in military operations*. GL-85-15, Geotechnical Laboratory Department of the Army, Washington DC.
- Manz, O. E. (1999) Coal fly ash: a retrospective and future look. *Fuel*, 78, 133–136. doi:10.1016/S0016-2361(98)00148-3
- Palomo, A. and Glasser, F. P. (1992) Chemically-bonded cementitious materials based on metakaolin. *British Ceramic Transactions and Journal*, 91, 107–112.
- Palomo, A., Grutzeck, M. W. and Blanco, M. T. (1999a) Alkali-activated fly ashes – A cement for the future. *Cement and Concrete Research*, 29, 1323–1329. doi:10.1016/S0008-8846(98)00243-9.
- Palomo, A., Blanco-Varela, M. T., Granizo, M. L., Puertas, F., Vazquez, T. and Grutzeck, M. W. (1999b) Chemical stability of cementitious materials based on metakaolin. *Cement and Concrete Research*, 29, 997–1004. doi:10.1016/S0008-8846(99)00074-5.
- Palomo, A., Alonso, S., Fernández-Jiménez, A., Sobrados, I. and Sanz, J. (2004) Alkaline activation of fly ashes: NMR study of the reaction products. *Journal of the American Ceramic Society*, 87, 1141–1145. doi:10.1111/j.1551-2916.2004.01141.x
- Perera, D. S., Aly, Z., Vance, E. R. and Mizumo, M. (2005) Immobilization of Pb in a geopolymer matrix. *Journal of the American Ceramic Society*, 88, 2586–2588. doi:10.1111/j.1551-2916.2005.00438.x
- Provis, J. L., Lukey, G. C. and Van Deventer, J. S. J. (2005) Do geopolymers actually contain nanocrystalline zeolites? – A re-examination of existing results. *Chemistry of Materials*, 17, 3075–3085. doi:10.1021/cm050230i.
- Purdon, A. O. (1940) The action of alkalis on blast-furnace slag. *Journal of the Society of Chemical Industry – Transactions and Communications*, 59, 191–202.
- Rahier, H., Van Mele, B., Biesemans, M., Wastiels, J. and Wu, X. (1996a) Low-temperature synthesized aluminosilicate glasses. 1. Low-temperature reaction stoichiometry and structure of a model compound. *Journal of Materials Science*, 31, 71–79. doi:10.1007/BF00355128.
- Rahier, H., Van Mele, B. and Wastiels, J. (1996b) Low-temperature synthesized aluminosilicate glasses. 2. Rheological transformations during low-temperature cure and high-temperature properties of a model compound. *Journal of Materials Science*, 31, 80–85. doi:10.1007/BF00355129.
- Rahier, H., Simons, W., Van Mele, B. and Biesemans, M. (1997) Low-temperature synthesized aluminosilicate glasses. 3. Influence of the composition of the silicate solution on production, structure and properties. *Journal of Materials Science*, 32, 2237–2247. doi:10.1023/A:1018563914630.
- Rees, C. A., Provis, J. L., Lukey, G. C. and Van Deventer, J. S. J. (2007) Attenuated total reflectance Fourier transform infrared analysis of fly ash geopolymer gel ageing. *Langmuir*, 23, 8170–8179. doi:10.1021/la700713g.
- Richardson, I. G., Brough, A. R., Groves, G. W. and Dobson, C. M. (1994) The

- characterization of hardened alkali-activated blast-furnace slag pastes and the nature of the calcium silicate hydrate (C-S-H) paste. *Cement and Concrete Research*, 24, 813–829. doi:10.1016/0008-8846(94)90002-7.
- Rostami, H. and Brendley, W. (2003) Alkali ash material: A novel fly ash-based cement. *Environmental Science and Technology*, 37, 3454–3457. doi:10.1021/es026317b.
- Rowles, M. R., Hanna, J. V., Pike, K. J., Smith, M. E. and O'Connor, B. H. (2007) ^{29}Si , ^{27}Al , ^1H and ^{23}Na MAS NMR study of the bonding character in aluminosilicate inorganic polymers. *Applied Magnetic Resonance*, 32, 663–689. doi:10.1007/s00723-007-0043-y.
- Roy, D. (1999) Alkali-activated cements – Opportunities and challenges. *Cement and Concrete Research*, 29, 249–254. doi:10.1016/S0008-8846(98)00093-3.
- Shi, C., Krivenko, P. V. and Roy, D. M. (2006) *Alkali-Activated Cements and Concretes*, Abingdon, UK, Taylor and Francis.
- Singh, P. S., Bastow, T. and Trigg, M. (2005) Structural studies of geopolymers by ^{29}Si and ^{27}Al MAS-NMR. *Journal of Materials Science*, 40, 3951–3961. doi:10.1007/s10853-005-1915-x.
- Stevenson, M. and Sagoe-Crentsil, K. (2005) Relationships between composition, structure and strength of inorganic polymers. Part I – Metakaolin-derived inorganic polymers. *Journal of Materials Science*, 40, 2023–2036. doi:10.1007/s10853-005-1226-2.
- Subaer and Van Riessen, A. (2007) Thermo-mechanical and microstructural characterisation of sodium-poly(sialate-siloxo) (Na-PSS) geopolymers. *Journal of Materials Science*, 42, 3117–3123. doi:10.1007/s10853-006-0522-9.
- Swanepoel, J. C. and Strydom, C. A. (2002) Utilisation of fly ash in a geopolymeric material. *Applied Geochemistry*, 17, 1143–1148. doi:10.1016/S0883-2927(02)00005-7
- Talling, B. (2002) Geopolymers give fire safety to cruise ships. *Geopolymers 2002. Turn Potential into Profit*, Melbourne, Australia, Lukey, G. C. (Ed.), CD-ROM Proceedings.
- Van Deventer, J. S. J., Provis, J. L., Duxson, P. and Lukey, G. C. (2007) Reaction mechanisms in the geopolymeric conversion of inorganic waste to useful products. *Journal of Hazardous Materials*, A139, 506–513. doi:10.1016/j.jhazmat.2006.02.044.
- Van Jaarsveld, J. G. S. (2000) PhD Thesis, Department of Chemical Engineering, University of Melbourne, Australia.
- Van Jaarsveld, J. G. S., Van Deventer, J. S. J. and Lorenzen, L. (1997) The potential use of geopolymeric materials to immobilise toxic metals. 1. Theory and applications. *Minerals Engineering*, 10, 659–669. doi:10.1016/S0892-6875(97)00046-0.
- Van Jaarsveld, J. G. S., Van Deventer, J. S. J. and Lorenzen, L. (1998) Factors affecting the immobilization of metals in geopolymerized flyash. *Metallurgical and Materials Transactions B – Process Metallurgy and Materials Processing Science*, 29, 283–291. doi:10.1007/s11663-998-0032-z.
- Wang, S. D. and Scrivener, K. L. (1995) Hydration products of alkali-activated slag cement. *Cement and Concrete Research*, 25, 561–571. doi:10.1016/0008-8846(95)00045-E.
- Wastiels, J., Wu, X., Faignet, S. and Patfoort, G. (1993) Mineral polymer based on fly ash. *Proceedings of the 9th International Conference on Solid Waste Management*, Philadelphia, PA, 8pp.
- Yip, C. K. and Van Deventer, J. S. J. (2003) Microanalysis of calcium silicate hydrate gel formed within a geopolymeric binder. *Journal of Materials Science*, 38, 3851–3860. doi:10.1023/A:1025904905176.
- Zhang, Y., Sun, W. and Li, Z. (2005) Hydration process of interfacial transition in

- potassium polysialate (K-PSDS) geopolymer concrete. *Magazine of Concrete Research*, 57, 33–38. doi:10.1680/mac.57.1.33.57865.
- Zoulgami, M., Lucas-Girot, A., Michaud, V., Briard, P., Gaudé, J. and Oudadesse, H. (2002) Synthesis and physico-chemical characterization of a polysialate-hydroxyapatite composite for potential biomedical application. *European Physical Journal – Applied Physics*, 19, 173–179. doi:10.1051/epjap:2002063.

Fly ash glass chemistry and inorganic polymer cements

L M KEYTE, University of Melbourne, Australia

Abstract: In this chapter, the importance of developing a detailed understanding of coal fly ash as the basis for the analysis of inorganic polymer formation is outlined, and many of the factors controlling ash properties are discussed. The properties of fly ash are seen to depend very significantly on the composition of the coal burned, as well as the combustion conditions. The usual compositional ranges in which fly ashes fall display some very complex chemistry in the $\text{Al}_2\text{O}_3\text{-SiO}_2$ system, which must be considered in analysis of ash-derived inorganic polymers.

Key words: fly ash, glass chemistry, inorganic polymer cement, coal, combustion, aluminosilicate.

2.1 Introduction

One of the main driving forces for the development of inorganic polymer technology is the potential of a viable alternative to Portland cement. Inorganic polymer cements (IPCs) can be synthesised by alkali-activation of a variety of materials including thermally activated clays, coal fly ash and blast furnace slag to produce a hardened material with mechanical properties potentially suitable for Portland cement replacement (Duxson *et al.*, 2007). Inorganic polymer binders synthesised from the alkali-activation of metakaolin (thermally activated kaolinite) require large volumes of water to create workable pastes. Despite their water demand, hardened metakaolin based inorganic polymers can exhibit comparable or superior mechanical properties to Portland cement (Davidovits, 1991). IPCs based on coal fly ash are of particular interest as they can display superior paste workability with less than a quarter of the water required to produce a metakaolin inorganic polymer paste, which may result in improved mechanical properties (Lloyd and Keyte, 2007). In particular, coal fly ash with low calcium content (< 5 wt% CaO) is an abundant industrial by-product which is currently underutilised worldwide (Ingram and Crookes, 2005).

The mechanical properties of inorganic polymers synthesised from coal fly ash can vary substantially (van Jaarsveld *et al.*, 1997). To assess the potential of an IPC to be a replacement for Portland cement, its compressive strength is usually determined. This measurement gives a simple practical assessment of the extent of binder formation; an IPC binder can only be useful if a

new phase with appreciable strength forms. The dissolution mechanisms of coal fly ash during inorganic polymer synthesis, and the influence of these mechanisms on the final hardened material, are still unclear. This is also, in part, due to most research investigations generally being performed on a single coal fly ash sample, rather than a selection of different ashes.

A scientific understanding of coal fly ash glass chemistry is necessary to begin to understand the complex dissolution and reprecipitation processes occurring during IPC formation. This chapter will discuss the origin and history of low calcium coal fly ash, and how the coal from which the ash originates influences the nature and morphology of the phases present in the ash. The dissolution behaviour of coal fly ash during IPC formation will also be discussed in relation to the chemistry of the reactive phases present in the ash.

2.2 Origin and history of coal fly ash

One of the most primitive ways to generate heat is to ignite an organic material which will continue to generate heat in the presence of oxygen until all of the material has combusted. Coal, an organic sedimentary rock, is mined throughout the world and most of it used to generate electricity in power stations by utilising the heat generated when the coal is combusted.

The formation of coal, known as coalification, occurs when a great deal of plant material is buried quickly before significant decay has occurred. The layer of sediment covering the plant material must be substantial enough that oxygen and sunlight are excluded and further decay cannot occur. Over millions of years, the weight of the sediment compresses the plant matter, squeezing out water and converting the dehydrated plant debris into the material known as coal (Cook, 2003).

Coal deposits are usually formed in depressions in the Earth's crust called basins. The coal deposits are usually found in layers of sedimentary rocks and are referred to as either coal beds or coal seams. A deposit may consist of very thick seams of almost pure coal or may have thinner seams separated by layers of shale, siltstones and sandstones.

Coal is an organic sediment consisting of a complex mixture of substances; however, it is nearly always associated with incombustible inorganic material, some of which cannot be separated from the organic matter prior to combustion. This inorganic matter forms the majority of the waste stream from a coal-fired boiler in a power station, along with char and any other residues.

There are three common types of coal-fired boilers used in power stations: dry-bottom boilers, wet-bottom boilers and cyclone furnaces (Tishmack, 1996). The most common type is the dry-bottom furnace and when pulverised coal is combusted in this boiler, around 80% of all the ash produced leaves the furnace entrained in the flue gas and is generally collected using electrostatic

precipitation (Tishmack, 1996). This material, commonly referred to as coal fly ash, or fly ash, differs from other types of power station ash and by-products with respect to particle size, composition and utilisation potential. Coal fly ash is the fine particulate residue of each individual coal particle after combustion. As the coal particles are carried in a gas stream and are only briefly exposed to high temperatures, there is little possibility for interaction between the fragments. As a consequence, the mineral matter present in each particle is also briefly exposed to high temperatures, which may cause physical and chemical transformation of the minerals, and carried out in the same stream as individual particles (Diamond, 1986).

The particle size distribution and chemical composition of many coal fly ashes, as well as the generally spherical particle shape and low cost, make fly ash an ideal material for use as a supplementary cementitious material in concrete (Idorn, 1985). As coal seams can contain between 2 and 35% mineral matter, a constant supply of coal fly ash will be available as long as coal-fired power stations continue to operate.

The addition of coal fly ash to cement has been well examined. It is generally agreed that the fly ash can be reactive in this system and improve properties in freshly mixed concrete such as (Idorn, 1985; Butler and Mearing, 1985; Hemmings and Berry, 1987):

- Improved workability imparted by the spherical ash particles and the associated water reduction that minimises separation of water from the cement mixture.
- Improved compressive strength and other mechanical properties as a result of the reduced water demand.
- Reduced concrete cost as the value of coal fly ash is lower than that of cement.
- Reduced CO₂ emission as less cement is required.
- Improved durability, and in some cases improved strength, in hardened concrete due to the pozzolanic reaction with calcium hydroxide generated during cement hydration increasing the volume of calcium silicate hydrate binder, which helps fill the reduced water voids and thus creates a more durable and less permeable concrete.

The amount of coal fly ash that can be added to cement varies depending on its chemical composition. Coal fly ashes that contain high concentrations of calcium (>15% w/w CaO) can replace much more Portland cement than those with low concentrations (<5% w/w CaO). In some cases, up to 40% of the cement in concrete can be replaced with coal fly ash (Wei *et al.*, 1992). This is due to the coal fly ash being able to contribute significantly to the reactions occurring during cement hydration, as well as the benefit of reduced water demand.

Australia produces around 13 Mt of fly ash annually, but only around 4

Mt is utilised in a beneficial manner (Ingram and Crookes, 2005). The rest is simply disposed of in ponds or land-fill. The chemical composition of coal fly ash in Australia varies; however, all commercially available sources contain relatively low concentrations of calcium. As a result, less of the coal fly produced in Australia can be utilised in Portland cement concrete than is desirable. Coal fly ash with low calcium content is typically referred to as Class F fly ash, although the actual definition of a Class F fly ash is when the sum of the silica, alumina and iron oxide present is greater than 70% (ASTM C 618-05, 2005). Development of inorganic polymer cements that can utilise large amounts of Class F coal fly ash is of particular interest.

Coal fly ash is the residue of the mineral matter present in the coal, and the composition of the ash will be related to the type and concentration of these minerals. Inorganic materials, known as mineral matter, occur in coal deposits as the plant materials themselves contain inorganic and organo-metallic complexes. Minerals may also be washed into the coal forming environment during coalification or may be present in the environment from volcanic activity. Other minerals may precipitate out of ground water or may occur in the surface and pore water of the coal. The mineral matter may occur in thin bands with the coal deposit or may fill cracks and fissures and be intimately associated with the coal. It may also be finely dispersed within the actual coal matter (Gammidge, 2004).

The types of mineral matter in coal include clays, carbonates, sulphides and oxides, and the type and concentration can vary substantially throughout a basin. The most abundant minerals are phyllosilicates and include kaolinite, illite and montmorillonite; however, these clays can have considerable substitution of many other ions in their structure. Table 2.1 lists the minerals that have been observed in Australian coals (Ward, 1989).

There exists substantial literature on the minerals present in coal seams as the information is relevant to many fields of research and the occurrence and abundance of minerals in Australian coal seams has been examined by many researchers (Ward, 1978; Ward and Christie, 1993; Ward and Taylor, 1996; Creelman and Ward, 1996; Uysal *et al.*, 2000; Ward, 2002; Ruan and Ward, 2002; Wigley and Williamson, 2005). Coal seam samples from New South Wales and Queensland were examined by Ward to determine the type and concentration of mineral matter present (Ward, 1978). A total of 40 different samples from 28 seams were examined, with quartz, kaolinite and other layered silicates found to be the dominant species. Carbonate, sulphate and phosphate minerals were also found to be abundant in some samples.

During coal combustion, the temperatures to which the particles are exposed can exceed 1600°C, which is sufficiently high to melt most inorganic materials present in coal (Hemmings and Berry, 1987). As the type, concentrations and composition of the mineral matter on each coal particle can vary substantially, the size and chemical composition of each coal fly ash particle

Table 2.1 Major minerals identified by various authors in Australian bituminous coals (Ward, 1989)

<i>Silicates</i>	<i>Carbonates</i>
Kaolinite $\text{Al}_2\text{Si}_2\text{OH}_5(\text{OH})_4$	Calcite CaCO_3
Illite $\text{KAl}_2(\text{Al},\text{Si}_3)\text{O}_{10}(\text{OH})_2$	Siderite FeCO_3
Montmorillonite $\text{Na}(\text{Al},\text{Mg})\text{Si}_4\text{O}_{10}(\text{OH})_2$	Dolomite $\text{CaMg}(\text{CO}_3)_2$
Chlorite $(\text{Mg},\text{Fe},\text{Al})_6(\text{Al},\text{Si})_4\text{O}_{10}(\text{OH})_8$	Ankerite $(\text{Ca},\text{Fe},\text{Mg})\text{CO}_3$
Interstratified (mixed-layer) clay minerals	Dawsonite $\text{NaAlCO}_3(\text{OH})_2$
Quartz SiO_2	Strontianite SrCO_3
Chalcedony SiO_2	Aragonite CaCO_3
Feldspar KAlSi_3O_8	
<i>Sulphides</i>	<i>Sulphates</i>
Pyrite FeS_2	Gypsum $\text{CaSO}_4 \cdot 2\text{H}_2\text{O}$
Marcasite FeS_2	Barite BaSO_4
Sphalerite ZnS_2	Anhydrite CaSO_4
Galena PbS	Coquimbite $\text{Fe}_2(\text{SO}_4)_3 \cdot 9\text{H}_2\text{O}$
Millerite NiS	Szomolnokite $\text{FeSO}_4 \cdot \text{H}_2\text{O}$
Chalcocopyrite CuFeS_2	Natrojarosite $\text{NaFe}_3(\text{SO}_4)_2(\text{OH})_6$
	Thenardite Na_2SO_4
	Bassanite $\text{CaSO}_4 \cdot \frac{1}{2}\text{H}_2\text{O}$
	Celestite SrSO_4
<i>Phosphates</i>	<i>Other minerals</i>
Apatite $\text{Ca}_5\text{F}(\text{PO}_4)_3$	Anatase TiO_2
Goyazite $\text{SnAl}_3(\text{PO}_4)_2(\text{OH})_5 \cdot 5\text{H}_2\text{O}$	Rutile TiO_2
	Bohemite $\text{AlO}(\text{OH})$
	Haematite Fe_2O_3
	Goethite $\text{Fe}(\text{OH})_3$
	Zircon ZrSiO_4

can be completely different to any other particle (Diamond, 1986). Even if the types and concentrations of the minerals present in the feed coal were known, the resultant particles could exhibit wide variances in composition. Moreover, as the coal is blended to optimise calorific value, power stations which blend coals from different deposits can be producing a coal fly ash with a composition that may vary significantly from day to day.

2.3 Coal fly ash particle morphology

Coal fly ash is a complex material, and although the presence of non-crystalline and crystalline constituents was recognised in the 1950s and 1960s (Simons and Jeffery, 1960), it was only in the 1980s that serious attempts to understand the chemical nature of fly ash particles were made (Hemmings and Berry, 1987).

An excellent review of the abundance of research which occurred around this time is provided by Hemmings and Berry (1987). They present a summary of the key research that was performed on the characterisation of coal fly ash

particles; the reactive glass fraction of the coal fly ash being of most interest. It is generally agreed that most of the inorganic matter present in coal melts during combustion as the temperature inside the boiler is often in excess of 1600°C. Quartz, which is generally present in Australian coal seams, is an exception and remains largely unchanged. Quartz is thus generally always observed in Australian coal fly ashes.

The major mineral constituents in Australian coals are the silicates; kaolinite clays are generally predominant in the coals although illite and montmorillonite are also common. These aluminosilicates will melt during coal combustion and mainly form spherical droplets of molten liquid which cool rapidly as they are carried out of the boiler. The spherical nature of fly ash is a result of surface tension forces acting on the melt to minimise surface free energy. Some of the particles also become bloated by gases released by the combusting gas, or by the clay material itself (Hemmings and Berry, 1987). Some clays in particular cause many bloated spheres to form and these hollow spheres, referred to as cenospheres, are collected and used as lightweight additives to a variety of industries (Ngu *et al.*, 2007).

As the molten aluminosilicate droplets are carried out of the boiler, they cool rapidly and form amorphous to semi-crystalline phases. The amorphous phase is described as an aluminosilicate phase, and mullite may crystallize from this glass if the particle does not cool rapidly enough (Diamond, 1986; Hemmings and Berry, 1987; Henry *et al.*, 2004). Mullite crystals have been observed in Australian Class F coal fly ashes (van Jaarsveld *et al.*, 2003). It is widely accepted that an aluminosilicate melt forms during combustion from which mullite crystallisation occurs, rather than direct conversion to mullite from existing mineral phases (Henry *et al.*, 2004).

The shapes and sizes of the ash particles depend on many factors including their size, gaseous inclusions and/or proximity to other molten droplets (which may result in coalescences and collisions). Further contributing to heterogeneity in fly ash is the presence of other mineral matter in the coal. Minerals rich in iron, titanium, sulphur, phosphorus, boron, alkali metal and alkali earth cations are common and their distribution through the seam is variable. Each coal particle may contain different amounts of a variety of inorganic matter and so the resultant ash may be highly heterogeneous. Hemmings and Berry (1987) discuss how the consequences of these variations can be examined at three distinct levels of magnitude: (a) *macrostructure* – differences in composition, morphology, size, density, etc., between different particle classes (inter-particle speciation); (b) *microstructure* – differences within a given particle (intra-particle speciation); and (c) *nanosstructure* – variations in the glass at the molecular level (phase separation).

Inter-particle speciation is almost universal in Class F fly ashes, particularly for those containing more than 1–2 wt% iron. Particles rich in iron are often evident in such fly ashes, as are particles completely devoid of iron and a

range in between. Crystalline quartz is also often present as discrete particles in coal fly ashes.

Intra-particle speciation is also common in many fly ashes, particularly due to the crystallisation of mullite from aluminosilicate glasses. Many particles will contain mullite crystals embedded in an aluminosilicate glass and these may be observed by briefly exposing the fly ash particles to a 1% hydrofluoric acid solution (Diamond, 1986).

Intra-particle speciation also occurs in many iron-rich particles. Magnetic separation is an easy way to collect particles rich in magnetite. Diamond (1986) exposed a magnetically separated sample of fly ash to hydrofluoric acid dissolution and found most of the material was attacked to some degree. Many of the residual particles were found to be magnetite structures which probably contained an iron rich glass around the framework before dissolution occurred. Warren and Dudas (1989) also examined magnetically separated fly ash particles and found that most of them consisted of three distinct phases: a highly soluble exterior glassy veneer, a crystalline magnetite highly substituted in a variety of metals, and a less soluble aluminosilicate glass interstitial to the magnetite. Gomes *et al.* (1999) characterised the magnetite present in a Class F coal fly ash and found it to be highly substituted with magnesium, manganese, calcium and silicon.

Titanium is also generally present in Australian coal fly ash, as an impurity in kaolin and other clays. Titanium is known to be a good nucleating agent for crystallisation from glasses (Diamond, 1986; Shelby, 2005). Gomes and Francois (2000) also characterised the crystalline mullite present in a coal fly ash and found it to be substituted with titanium as well as iron.

Other impurities such as sulphur, phosphorus and boron are often present in low concentrations in coal fly ash but may have a significant impact on behaviour. For example, a coal fly ash produced in New Zealand has limited utility as a Portland cement replacement due to its low but significant (~0.1 wt%) boron content which is believed to retard the setting of Portland cement (South, 2005).

Alkali cations and alkali earth cations may also have an effect on the coal fly ash phases, particularly in terms of nanostructure. Phase separation is reported to occur in the glass phases present in coal fly ash (Hemmings and Berry, 1987). The major glassy phase present in most Australian Class F coal fly ash is an aluminosilicate; this glass forms from the molten clays present in the coal. As mentioned previously, mullite is known to crystallise from this glass during cooling. This occurs because of phase separation, the term used to describe liquid–liquid immiscibility in glass.

Other types of particles can also be present in coal fly ash including reactive calcium silicate phases, similar to those found in Portland cement. These particles are the result of pore filling cements present in the coal, as discussed previously, and can remain discrete during combustion (Uysal *et*

al., 2000). All of these complex phases can be present in coal fly ash the bulk composition of elements present is often a mere reflection of complexity within.

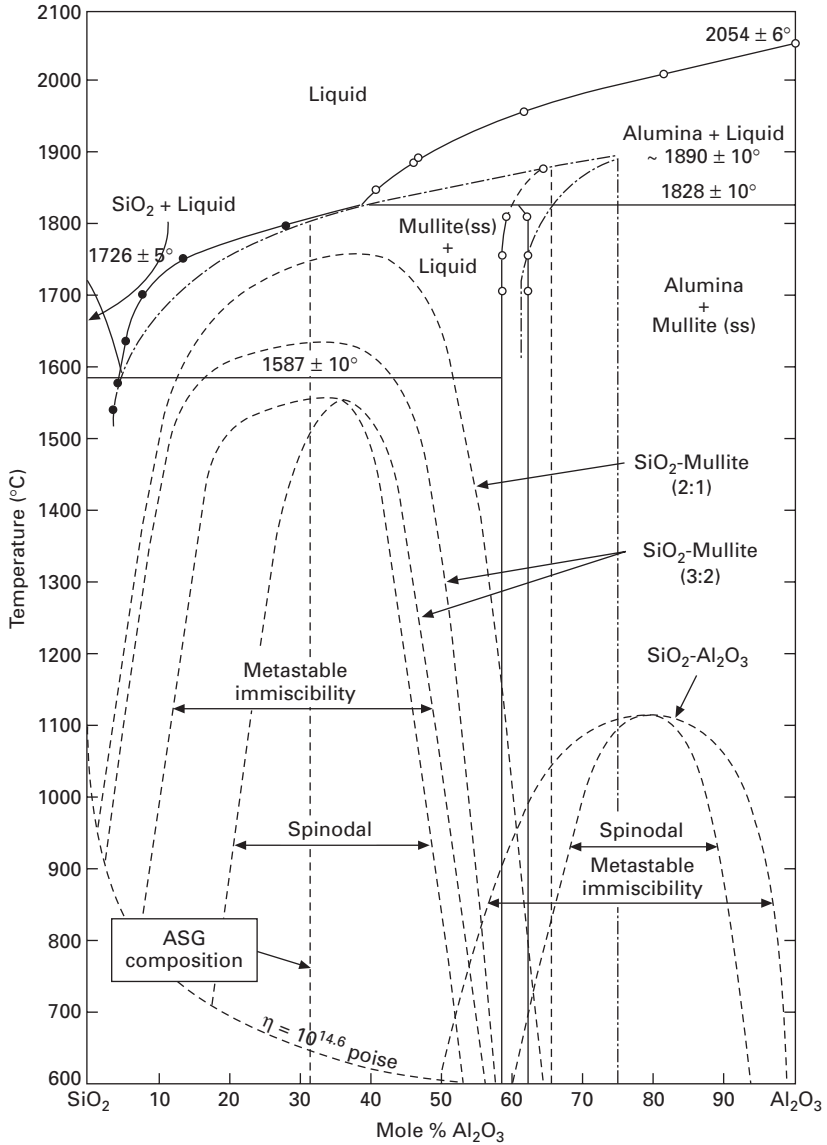
2.4 Aluminosilicate glass chemistry

The predominant reactive glassy phases present in low calcium coal fly ashes are those formed from the melting of clays present in the coal. These molten aluminosilicate droplets cool as they are carried out of the boiler and form amorphous and crystalline phases.

Phase separation occurs over most of the compositional range for aluminosilicate glasses, including the compositions likely to be present in coal fly ash. The molten particles will separate into two phases: a silica rich phase with composition close to SiO_2 and an alumina rich phase with composition close to $\text{Al}_6\text{Si}_2\text{O}_{13}$ (Aramaki and Roy, 1961). The most developed phase diagram for the Al_2O_3 - SiO_2 is shown in Fig. 2.1 (Risbud and Pask, 1977). The alumina rich phase has a composition close to mullite and unless rapid cooling rates are employed, some or all of this phase will crystallise (Johnson *et al.*, 2001; Li *et al.*, 2002).

As discussed by Shelby (2005), many glass-forming melts exhibit liquid-liquid immiscibility, though the degree to which separation occurs is dependent on several factors. For example, if a crucible containing a melt with two highly fluid, immiscible liquids is cooled carefully enough, the resulting material can be completely separated into two distinct glasses, and the separation is visible to the naked eye. If the same melt was quenched rapidly, however, the immiscibility may be more like an emulsion and the phase separation may only be observed using high magnification. Also, if the melt is highly viscous, the degree of separation will be also very small. Coal fly ash particles cool at different rates, depending on their size and residence time in the boiler; however, the quenching is rapid enough to suppress the crystallisation of the silica-rich phase. The aluminosilicate-rich phase generally exhibits some degree of crystallisation, as evidenced by the presence of mullite.

Alkali and alkali earth metal cations can have a significant impact on the behaviour of aluminosilicate melts. Aluminium can occur in tetrahedral coordination when an alkali cation is present, and these tetrahedra can substitute directly into the silica glass network. As alkali content increases within the melt, less and less phase separation will occur (Shelby, 2005). As most low calcium coal fly ashes contain far less charge balancing cations than aluminium, high concentrations of phase separated aluminosilicate glasses are likely to still be present. Also, as the distribution of cations is generally heterogeneous, many aluminosilicate particles may contain no charge balancing cations.



2.1 Calculated miscibility gaps superimposed in stable and metastable phase equilibrium diagrams for the $\text{SiO}_2\text{-Al}_2\text{O}_3$ system. The gaps shown with spinodal regions are considered the most probable thermodynamically. Adapted from Risbud and Pask (1977).

2.5 Examining coal fly ash glass chemistry

Thermal treatment without melting to induce phase transformations (devitrification) can be performed to examine the amorphous phases in coal fly ash using X-ray diffractometry (XRD). Multi-phase glass systems are often devitrified to induce the crystallisation of a particular phase for a variety of reasons (Johnson *et al.*, 2001; Shelby, 2005). Devitrification can be a useful tool for examining amorphous phases if the liquidus temperature of the glassy material being examined is higher than the temperature at which any of the amorphous phases present will begin to crystallise. If this is the case then devitrification will cause the amorphous phases to crystallise, and they will thus be discernable by XRD. In a simple glass system, these new crystalline phases can be a representation of the amorphous phases which exist in the material.

If this technique is carefully applied to coal fly ash, it is possible that the nature of the glass phases present may be determined by analysing the XRD pattern of the coal fly ash after thermal treatment, assisted by the measured oxide composition. To ensure that this provides an accurate representation, the chemistry of the coal from which the ash was generated should also be examined. The coal fly ash is formed from the mineral inclusions within the coal, meaning that the phases expected to form during combustion can be predicted to some extent by analysis of the coal chemistry.

The use of devitrification to examine the glassy phases of fly ash was first performed by Hemmings and Berry (1985). They demonstrated that fly ash samples classified by density displayed marked differences in their XRD diffraction patterns after thermal treatment at 900°C for 24–27 hours (Hemmings and Berry, 1987). This allowed a better understanding of the phases present in the fly ash under observation, as it was found that different crystals formed in samples with different densities. The devitrification temperature chosen for thermal treatment was 900°C, as differential thermal analysis (DTA) of the samples had shown exothermic events to begin to occur around this point. There is, however, little more research than this into the determination of the glassy phases in fly ash and they are generally still only considered with respect to the bulk amorphous content.

Although this technique provides useful information about the amorphous phases in fly ash, Hemmings and Berry's work did not yield a complete understanding of all of the phases present. As each fly ash sample may contain a multitude of different glass phases, it is possible that each of these phases will begin to crystallise at different temperatures. Also, as each of the fly ash particles themselves may be completely different to another, it is possible that some particles may melt at a temperature that others will not, and may give misleading results.

Thermal treatment of low calcium coal fly ash samples has been performed

at a range of temperatures for differing periods of time to observe phase transformations using XRD (Keyte, 2008). A synthetic aluminosilicate glass (ASG) with known properties (Glasson, 2006), synthesised from high purity SiO_2 and Al_2O_3 , was first examined for comparison with the coal fly ash samples. The devitrification characteristics of this material have been well studied as the material is fabricated and sold as a ceramic refractory fibre. As there is concern over the use of any fibrous material that may contain crystalline silica, it has been important to observe the devitrification of these materials (Ganz and Krönert, 1982).

As discussed previously, the binary Al_2O_3 - SiO_2 system exhibits phase separation over most of the compositional range from mullite to silica. The melts are homogeneous at temperatures above the liquidus ($\sim 1850^\circ\text{C}$) but spontaneously separate metastably into two amorphous phases upon cooling (Aramaki and Roy, 1961; MacDowell and Beall, 1969; Aksay and Pask, 1975; Risbud and Pask, 1977; Beall and Duke, 1983). The oxide composition of ASG examined by Keyte (2008) is in the composition range between mullite and silica (Table 2.2) with around 31.4 mole% Al_2O_3 , indicating that phase separation will occur in this material (Fig. 2.1). If the ASG is cooled rapidly enough, an X-ray amorphous heterogeneous material should result, consisting of two inter-connected phases; one with a composition close to that of mullite and the other close to that of silica (Beall and Duke, 1983). The alumina-rich glass requires a much higher cooling rate than the siliceous portion to remain amorphous, and is more likely to crystallise during cooling. The ASG is cooled rapidly to ensure that crystallisation does not occur and as a result, the material will be X-ray amorphous.

The two amorphous phases present, one close to mullite in composition and the other close to silica, will crystallise at different temperatures. The first observable change should be the crystallisation of mullite around 980°C , although the temperature may be as low as 900°C (Ganz and Krönert, 1982). The formation of mullite crystals will continue to increase as the temperature is increased, and the mullite content will reach a maximum at around 1300°C . The second observable change should be the crystallisation of cristobalite, and the temperature at which this occurs will be a function of the purity of the silica. It has been shown that the presence of impurities such as iron oxide and titanium dioxide may cause cristobalite formation to occur at lower temperatures (Ganz and Krönert, 1982; MacDowell and Beall, 1969). As ASG is synthesised from high purity raw materials, the temperature of

Table 2.2 Major oxide composition of ASG (wt%)

	SiO_2	Al_2O_3	Na_2O	K_2O	CaO	TiO_2	Other
ASG	55.7	43.3	0.2	0.0	0.0	0.0	0.8

crystallisation should be close to the ideal temperature of 1250°C to 1300°C (Ganz and Krönert, 1982).

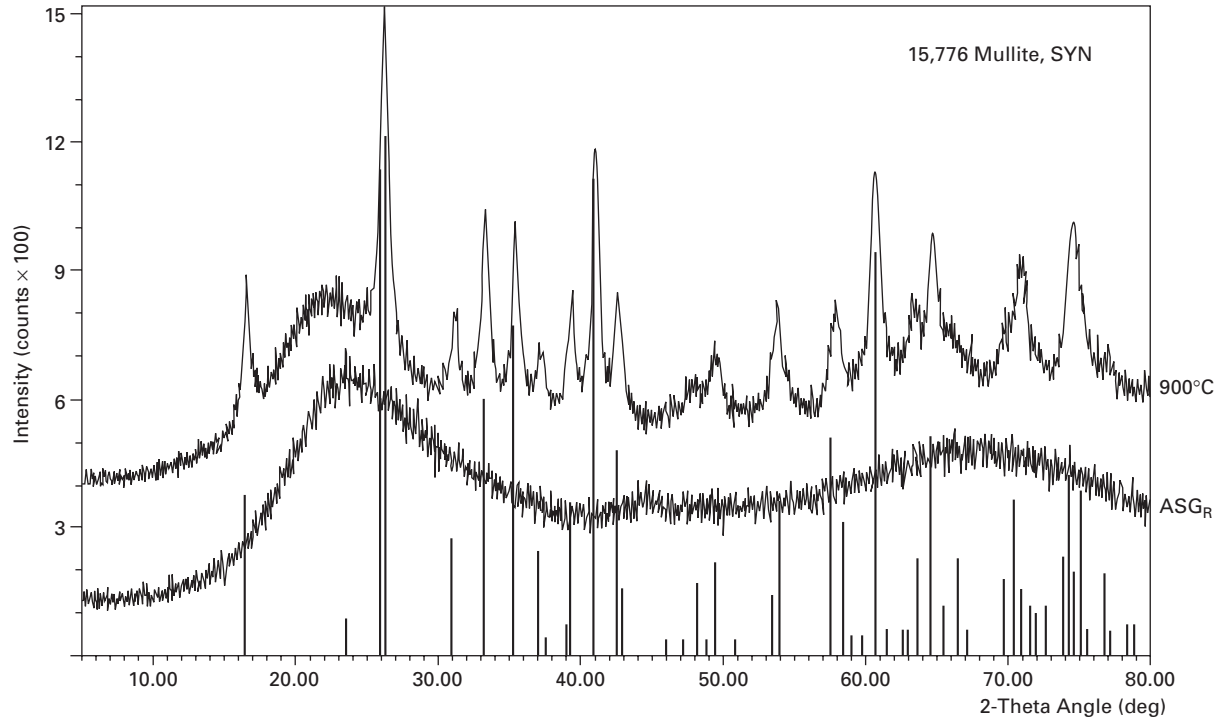
The XRD patterns of ASG reference sample (ASG_R) confirmed the X-ray amorphous nature of the material, showing only broad amorphous humps (Keyte, 2008). Thermal treatment of this material was initially performed by Keyte (2008) by subjecting the samples to a constant temperature for 24 hours. After this time, the samples were allowed to cool slowly over several hours with a cooling rate of less than 100°C per hour. Samples were heated at 600°C, 700°C and 800°C for 24 hours, and the XRD patterns showed no identifiable phase transformations. Mullite was identified in the XRD pattern of ASG after thermal treatment at 900°C for 24 hours, confirming the presence of an amorphous phase with a composition close to that of mullite in the unheated glass. A large amorphous hump is still apparent, however, indicative of the amorphous silica still present (Fig. 2.2).

Samples thermally treated at 1000°C, 1100°C and 1200°C for 24 hours reveal no other new phases in their XRD patterns. This is expected as amorphous silica should not crystallise to cristobalite until around 1300°C, due the high purity of the raw materials used to synthesise ASG. Although no new phases are observed, there is a noticeable difference in the intensity and resolution of the mullite peaks over this temperature range. The increased size and intensity of these peaks, accompanied by a decrease in the amorphous hump is due to the increasing concentration of mullite. Although mullite first crystallises around 900°C, it is only a small amount of the total. Ganz and Krönert (1982) observed mullite crystallisation in this system at around 980°C, forming about 20–25% mullite. The proportion of mullite was then found to increase significantly with increasing temperatures up to 1050°C. Thereafter, the amount of mullite increased more rapidly and linearly up to about 1200°C, with mullite content remaining constant between 1200°C and 1300°C. Keyte (2008) found the XRD patterns for ASG to be consistent with their observations.

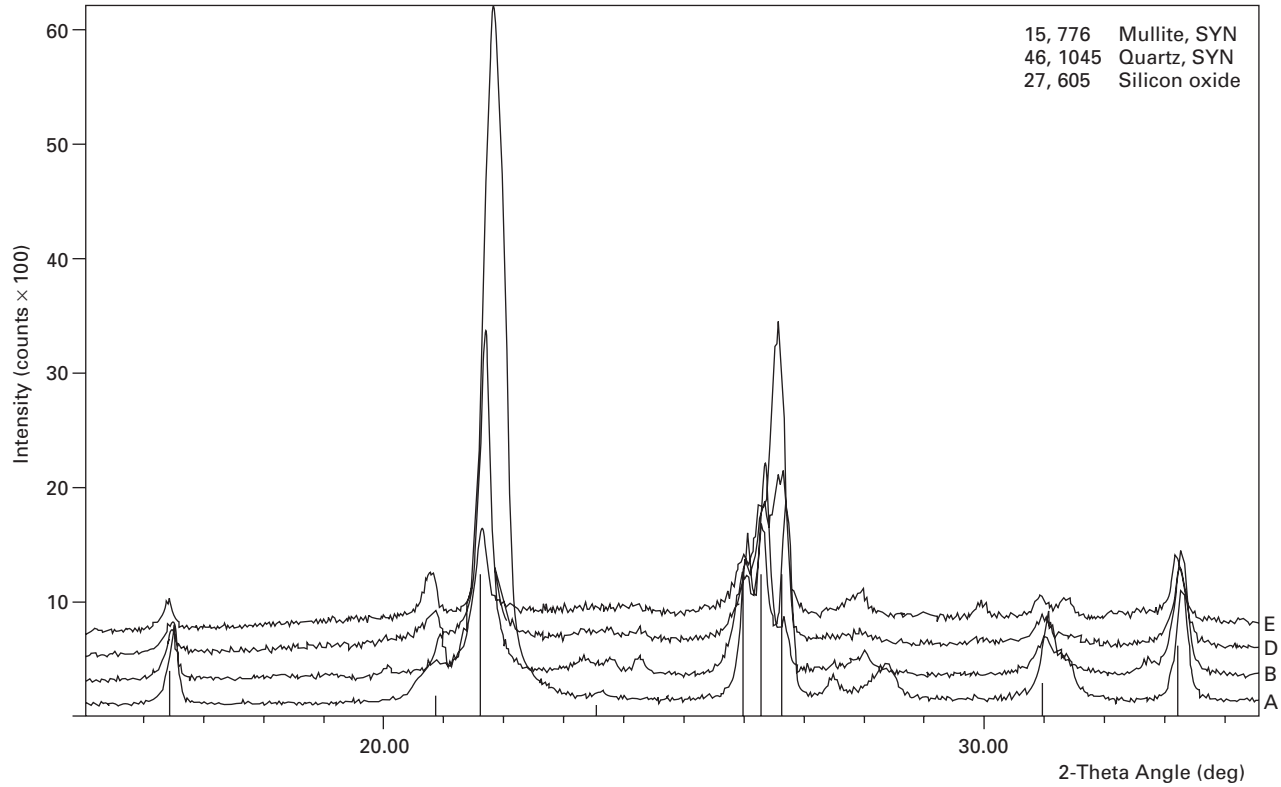
Thermal treatment at 1300°C was found to be sufficient to cause the crystallisation of cristobalite, as observed by XRD. As this work allowed the glass phases to be determined using devitrification, as crystallisation occurred below the liquidus, the technique was applied to coal fly ash samples.

Keyte (2008) further demonstrated that four different Australian low calcium coal fly ash samples contained amorphous Al₆Si₂O₁₃ phases (some phases already crystallised as mullite) and amorphous silica (SiO₂) rich phases, as predicted (Fig. 2.3). Other minor reactive phases were also found to be present in these coal fly ash samples including calcium silicate phases.

Low-calcium coal fly ash predominantly consists of phase separated aluminosilicate glasses. The differences between these types of coal ashes can be related to the degree of crystallisation of these glasses, mainly the degree of mullite formation, as well as the presence of other minor reactive phases.



2.2 XRD patterns of ASG before and after thermal treatment at 900°C.



2.3 XRD patterns of four different Australian coal fly ashes (A, B, D and E), after thermal treatment at 1200°C for A and 1000°C for B, D and E.

2.6 Coal fly ash glass behaviour in IPC formation

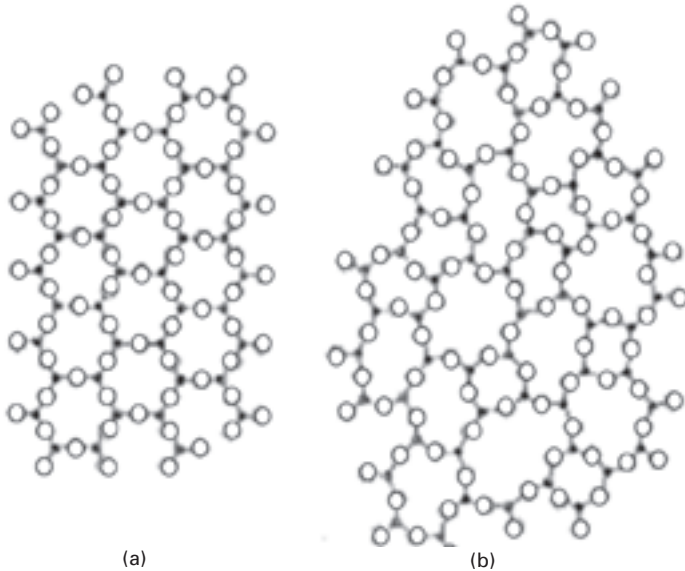
IPCs are synthesised by dissolving aluminosilicate-rich phases from raw materials, including coal fly ash. As discussed, the predominant phases in low-calcium coal fly ash are the phase separated aluminosilicate glasses, some of which generally crystallises to form mullite. Minor amounts of quartz, amorphous and crystalline iron-rich phases and calcium-rich phases may also be present.

The dissolution of minerals and glasses has been well studied for many systems including the behaviour of silicate and aluminosilicate glasses under highly alkaline conditions (Nordberg, 1964; Doremus, 1973; Shelby, 2005). The distinction between a crystalline material and an amorphous material is important when considering dissolution behaviour. It has previously been stated that coal fly ash contains some crystalline phases, such as quartz and mullite, and that these phases are considered unreactive (Criado *et al.*, 2005, Fernández-Jiménez *et al.*, 2006). This is because their rate of reaction in alkali-silicate solutions is considered to be extremely slow when compared to amorphous materials; the crystalline materials present in the raw materials are always observed by XRD in the IPC in similar quantities, even after lengthy curing (Lee and van Deventer, 2002).

The rate constant for hydrolysis of vitreous silica is more than 45 times higher than that of quartz (Iler, 1979), and this difference is not overcome with strongly alkaline solutions. If the structures of crystalline silica and amorphous silica are considered, it is not immediately obvious why one should be more reactive than another (Fig. 2.4).

In crystalline silica polymorphs, there are regular repeating units; each silicon being associated with four oxygen atoms in SiO_4 tetrahedra (with the exception of stishovite, which has SiO_6 octahedra). Each of the oxygen atoms is associated with two silicon atoms in a three-dimensional structure possessing long-range order. A silica melt cooled sufficiently fast to produce vitreous silica also contains almost identical SiO_4 tetrahedra. These tetrahedra have a high degree of internal order, and thus short-range order is preserved. The disorder in the amorphous structure arises from the variability in the Si-O-Si angle connecting adjacent tetrahedra. Additional disorder is introduced by rotation of adjacent tetrahedra around the point occupied by the oxygen atom linking the tetrahedra and also by rotation of the tetrahedra around the line connecting the linking oxygen with one of the silicon atoms (Hemmings and Berry, 1987; Shelby, 2005). As a result, long-range order is lost as the Si-O-Si angle and the rotations are now described by a distribution of values rather than the single values found in crystal lattices. This also makes the glasses X-ray amorphous.

Diffraction studies have shown there to be little difference in the shortest Si-O and O-O distances of amorphous and crystalline silica, illustrating the



2.4 Schematic representations in two dimensions of the structure of (a) crystalline silica, (b) vitreous silica. Hollow circles are Si atoms, filled circles are O atoms. After Hemmings and Berry (1987).

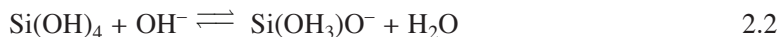
high degree of order within the short range represented by the basic tetrahedral SiO_4 building block. When observing the distances between the silica atoms in the centres of linked tetrahedra, however, a range of values is found in the amorphous structure as a result of the distribution in bond angles. The distributions become broader when observing the distances between silicon atoms and the second next closest oxygen and so forth (Shelby, 2005).

The Si-O-Si bond angles are thought to range from 120° to 180° with a maximum around 147° (Clark *et al.*, 2004), though most are thought to lie within $\pm 10\%$ of 144° (Shelby, 2005). Shelby further notes that the structure of vitreous silica thus has regions of highly stressed bonds and defects such as oxygen vacancies, represented by Si-Si bonds, and peroxy defects, represented by Si-O-O-Si bonds. These highly strained bonds weaken the resistance of the glass to water and a range of aggressive agents including alkaline solutions. This is different from the very ordered bonds present in crystalline materials which, although they will eventually react, they are considered to contribute little to IPC formation.

Aluminosilicate glasses also have strained bonds, oxygen vacancies and peroxy bonds. The glasses present in low-calcium fly ash are mainly those from the binary $\text{SiO}_2\text{-Al}_2\text{O}_3$ system. Owing to the ratio of aluminium to silicon, the glasses are the result of phase separation into a vitreous silica-rich phase and a vitreous alumina-rich phase. The vitreous silica-rich phase

rate controlled by the surface chemical reaction would be observed. However, this is not the case (Doremus, 1973). Also, it has also been found that larger molecular units apparently dissolve first and hydrolyse only slowly to the equilibrium monomolecular $\text{Si}(\text{OH})_4$ form found in the neutral solutions, further complicating matters (Doremus, 1973).

When the pH of the solution is increased, however, diffusion of water molecules into the structure no longer becomes a rate controlling step as the surface is dissolving too rapidly. At high pH, ionisation of silanol groups occurs rapidly:



The remaining silicon-oxygen bonds are hence weakened and more susceptible to attack by water molecules, and rapid dissolution occurs (Doremus, 1973; Xiao and Lasaga, 1996; Shelby, 2005). The rate of dissolution of silica glass at high pH is not very different from that of alkali-silicate glasses (Doremus, 1973). The high pH of the activating solution is causing such rapid destruction of the silicon-oxygen bonds that the non-bridging oxygens in alkali-silicate glasses provide little enhancement. The silica-rich phases present in coal fly ash would thus be expected to dissolve rapidly in alkaline solutions.

Addition of alumina to the glass is reported to lower the rate of dissolution in alkaline solutions, though the reasons are unclear (Nordberg, 1964; Doremus, 1973). Further examination of the literature found that all studies on the alkali dissolution of aluminosilicate glasses nearly always relate to silica glasses containing charge-balanced aluminium (Nordberg, 1964; Doremus, 1973; Shelby, 2005). Aluminium-rich silicate glass with composition close to that of mullite, as found in phase separated aluminosilicate glasses, has an entirely different structure to silicate glasses containing charge-balanced aluminium. A preliminary study by Keyte (2008) found there to be no evidence to suggest that the rate of dissolution of an aluminium-rich glass with composition $\text{Al}_6\text{Si}_2\text{O}_{13}$ was any different to that of a glass with composition close to SiO_2 .

As the glass phase with composition close to $\text{Al}_6\text{Si}_2\text{O}_{13}$ will crystallise to some degree in most coal fly ashes, the amount of aluminium which can dissolve can vary considerably between different ash sources. This will influence the silicon to aluminium ratio of the gel which forms, and ultimately the strength of the IPC binder. The compressive strength of IPCs has been shown to be a function of the Si/Al ratio (Rowles and O'Connor, 2003; Duxson *et al.*, 2005) and it is generally agreed that ratios of greater than around 2.5 result in poor mechanical properties. IPCs produced from coal fly ashes with low available aluminium may result in poor mechanical properties.

2.7 Conclusions

Low-calcium coal fly ash is a complex multi-phase material and its behaviour during IPC formation is influenced by a range of factors. The ratio of silicon to aluminium in the reactive glassy phases can vary between similar sources due to the crystallisation of mullite. A coal fly ash that cools slowly may crystallise large amounts of mullite, leaving little aluminium in the reactive glassy phases.

Modelling the dissolution of aluminosilicate glasses in IPC systems would provide further insight into the mechanisms occurring and allow for greater understanding of the new phases forming.

2.8 References

- Aksay, I. A. and Pask J. P. (1975). 'Stable and metastable equilibria in the system $\text{SiO}_2\text{-Al}_2\text{O}_3$.' *Journal of the American Ceramic Society*, **58**: 507–512.
- Aramaki, S. and Roy R. (1961). 'Revised phase diagram for the system $\text{Al}_2\text{O}_3\text{-SiO}_2$.' *Journal of the American Ceramic Society*, **45**: 229–242.
- ASTM (2005). Standard Specification for Coal Fly Ash and Raw Calcined Natural-Pozzolan for Use as a Mineral Admixture in Concrete, Designation C61805, ASTM International, PO Box 700, West Conshohocken, PA 19428–2959, USA.
- Beall, G. H. and Duke D. A. (1983). Glass-ceramic technology. *Glass: Science and Technology*, D. R. Uhlmann and N. J. Kreidl, Eds. New York, Academic Press. **1**: 419–422.
- Butler, W. B. and Mearing M. A. (1985). 'Fly ash beneficiation and utilization in theory and in practice.' Materials Research Society Symposia Proceedings. V 65. Fly Ash and Coal Conversion By-Products: Characterization, Utilization and Disposal II, Boston, Massachusetts, U.S.A., McCarthy, G. J., Glasser, F. P., Roy, D. M. Eds.: 11–18.
- Clark, T. M., Grandinetti, P. J., Florian P. and Stebbins J. F. (2004). 'Correlated structural distributions in silica glass.' *Physical Review B* **70**: 064202.
- Cook, B. (2003). 'Coal in a sustainable future.' *Introduction to Australia's minerals*, Adelaide, Osmond Earth Sciences, 24pp.
- Creelman, R. A. and Ward C. R. (1996). 'A scanning electron microscope method for automated, quantitative analysis of mineral matter in coal.' *International Journal of Coal Geology*, **30**: 249–269.
- Criado, M., Palomo A. and Fernández-Jiménez A. (2005). 'Alkali activation of fly ashes. Part 1: Effect of curing conditions on the carbonation of the reaction products.' *Fuel*, **84**: 2048–2054.
- Davidovits, J. (1991). 'Geopolymers: inorganic polymeric new materials.' *Journal of Thermal Analysis*, **37**: 1633–1656.
- Diamond, S. (1986). 'Particle morphologies in fly ash.' *Cement and Concrete Research*, **16**: 569–579.
- Doremus, R. H. (1973). *Glass Science*, John Wiley and Sons Inc., 345pp.
- Duxson, P., Mallicoat, S. W., Lukey, G. C., Kriven W. M. and van Deventer J. S. J. (2005). 'Understanding the relationship between geopolymer composition, microstructure and mechanical properties.' *Colloids and Surfaces A: Physicochemical and Engineering Aspects*, **269**: 47–58.

- Duxson, P., Fernández-Jiménez, A., Provis, J. L., Lukey, G. C., Palomo A. and van Deventer J. S. J. (2007). 'Geopolymer technology: the current state of the art.' *Journal of Materials Science*, **42**: 2917–2933.
- Fernández-Jiménez, A., de la Torre, A. G., Palomo, A., Lopez-Olmo, G., Alonso M. M. and Aranda M. A. G. (2006). 'Quantitative determination of phases in the alkali activation of fly ash. Part I. Potential ash reactivity.' *Fuel*, **85**: 625–634.
- Gammidge, L. (2004). Coal: an introduction. <http://www.newcastle.edu.au/discipline/geology/research/cfk/undp.htm>, Department of Geology, University of Newcastle, Australia, March 2005.
- Ganz, R. and Krönert W. (1982). 'Crystallisation behaviour of high temperature ceramic fibres of the $\text{Al}_2\text{O}_3\text{-SiO}_2$ system.' *Interceram*, **31**(2): 136.
- Glasson, L. (2006). Private communication, Unifrax Australia Pty Ltd.
- Gomes, S. and Francois M. (2000). 'Characterization of mullite in silicoaluminous fly ash by XRD, TEM, and ^{29}Si MAS NMR.' *Cement and Concrete Research*, **30**: 175–181.
- Gomes, S., Francois, M., Abdelmoula, M., Refait, P., Pellissier C. and Evrard O. (1999). 'Characterization of magnetite in silico-aluminous fly ash by SEM, TEM, XRD, magnetic susceptibility, and Mössbauer spectroscopy.' *Cement and Concrete Research*, **29**: 1705–1711.
- Hemmings, R. T. and Berry E. E. (1985). 'Speciation in size and density fractionated fly ash'. Materials Research Society Symposia Proceedings: V. 65. Fly Ash and Coal Conversion By-Products: Characterization, Utilization, and Disposal II, Boston, Massachusetts, U. S. A., McCarthy, G. J., Glasser, F. P., Roy, D. M. Eds.: 91–104.
- Hemmings, R. T. and Berry E. E. (1987). 'On the Glass in Coal Fly Ashes: Recent Advances.' Materials Research Society Symposia Proceedings. V 113. Fly Ash and Coal Conversion By-Products: Characterization, Utilization, and Disposal IV, Boston, Massachusetts, U. S. A., McCarthy, G. J., Glasser, F. P., Roy, D. M., Hemmings, R. T., Eds.: 3–38.
- Henry, J., Towler, M. R., Stanton, K. T., Querol X. and Moreno N. (2004). 'Characterisation of the glass fraction of a selection of European coal fly ashes.' *Journal of Chemical Technology and Biotechnology*, **79**: 540–546.
- Idorn, G. M. (1985). 'The research-technology interface in the fly ash-concrete regime.' Materials Research Society Symposia Proceedings: V. 65. Fly Ash and Coal Conversion By-Products: Characterization, Utilization and Disposal II, Boston, Massachusetts, U.S.A., McCarthy, G. J., Glasser, F. P., Roy, D. M., Eds.: 3–10.
- Iler, R. K. (1979). *The Chemistry of Silica*, John Wiley and Sons Inc., 835pp.
- Ingram, C. and B. Crookes (2005). *Inorganic Polymer Technology: Technical Overview and Market Study of Key Raw Materials*, Department of Chemical and Biomolecular Engineering, The University of Melbourne, Australia.: 157pp.
- Johnson, B. R., Kriven W. M. and Schneider J. (2001). 'Crystal structure development during devitrification of quenched mullite.' *Journal of the European Ceramic Society*, **21**: 2541–2562.
- Keyte, L. M. (2008). PhD thesis, The University of Melbourne, Australia.
- Krishnan, S., Weber, J. R. K., Ansell, S., Hixson A. D. and Nordine P. C. (2000). 'Structure of liquid $\text{Al}_6\text{Si}_2\text{O}_{13}$ (3:2 Mullite).' *Journal of the American Ceramic Society*, **83**: 2777–2780.
- Lee, W. K. W. and van Deventer J. S. J. (2002). 'Structural reorganisation of class F fly ash in alkaline silicate solutions.' *Colloids and Surfaces A: Physicochemical and Engineering Aspects*, **211**: 49–66.

- Li, M., Nagashio K. and Kuribayashi K. (2002). 'Containerless solidification of highly undercooled mullite melts: Crystal growth behavior and microstructure formation.' *Metallurgical and Materials Transactions A*, **33A**: 2677–2683.
- Linh, N. N. and Hoang V. V. (2007). 'Structural and amorphous properties of simulated liquid and amorphous aluminium silicates.' *Physica Scripta*, **76**: 165–172.
- Lloyd, R. R. and Keyte L. M. (2007). Unpublished research. Melbourne.
- MacDowell, J. F. and Beall G. H. (1969). 'Immiscibility and crystallization in Al_2O_3 - SiO_2 glasses.' *Journal of the American Ceramic Society*, **52**: 17–25.
- Morikawa, H., Miwa, S., Miyake, M., Marumo F. and Sata T. (1982). 'Structural analysis of SiO_2 - Al_2O_3 glasses.' *Journal of the American Ceramic Society*, **65**: 78–81.
- Ngu, L. N., Wu H. and Zhang D. K. (2007). 'Characterization of ash cenospheres in fly ash from Australian power stations.' *Energy Fuels* **21**(6): 3437–3445.
- Nordberg, M. E. (1964). *Chemical Durability*, Corning Glass Works Library: 13pp.
- Risbud, S. H. and Pask J. P. (1977). 'Calculated thermodynamic data and metastable immiscibility in the system SiO_2 - Al_2O_3 .' *Journal of the American Ceramic Society*, **60**: 418–424.
- Rowles, M. R. and O'Connor B. (2003). 'Chemical optimisation of the compressive strength of aluminosilicate geopolymers synthesised by sodium silicate activation of metakaolinite.' *Journal of Materials Chemistry*, **13**: 1161–1165.
- Ruan, C. and Ward C. R. (2002). 'Quantitative X-ray powder diffraction analysis of clay minerals in Australian coals using Rietveld methods.' *Applied Clay Science*, **21**: 227–240.
- Shelby, J. E. (2005). *Introduction to Glass Science and Technology*, The Royal Society of Chemistry, 241pp.
- Simons, H. S. and Jeffery J. W. (1960). 'An X-ray study of pulverised fuel ash.' *Journal of Applied Chemistry*, **10**: 328–336.
- South, W. (2005). Personal communication. Melbourne.
- Tishmack, J. K. (1996). 'Bulk chemical and mineral characteristics of coal combustion by-products (CCB).' Proceedings of the Coal Combustion By-Products Associated with Coal Mining – Interactive Forum, SIU at Carbondale, Chugh, Y.P, Sangunetti, B.M., Vories, K.C., Eds.: 13–19.
- Uysal, I. T., Golding S. D. and Glikson M. (2000). 'Petrographic and isotope constraints on the origin of authigenic carbonate minerals and the associated fluid evolution in Late Permian coal measures, Bowen Basin (Queensland), Australia.' *Sedimentary Geology*, **136**: 189–206.
- van Jaarsveld, J. G. S., van Deventer J. S. J. and Lorenzen L. (1997). 'The potential use of geopolymeric materials to immobilise toxic metals: Part I. Theory and applications.' *Minerals Engineering*, **10**: 659–669.
- van Jaarsveld, J. G. S., van Deventer J. S. J. and Lukey G. C. (2003). 'The characterisation of source materials in fly ash-based geopolymers.' *Materials Letters*, **57**: 1272–1280.
- Ward, C. R. (1978). 'Mineral matter in Australian bituminous coals.' *Proceedings of the Australasian Institute of Mining and Metallurgy*, **267**: 7–25.
- Ward, C. R. (1989). 'Minerals in bituminous coals of the Sydney basin (Australia) and the Illinois basin (USA).' *International Journal of Coal Geology*, **13**: 455–479.
- Ward, C. R. (2002). 'Analysis and significance of mineral matter in coal seams.' *International Journal of Coal Geology*, **50**: 135–168.
- Ward, C. R. and Christie P. J. (1993). 'Clays and other minerals in coal seams of the Moura-Baralaba area, Bowen Basin, Australia.' *International Journal of Coal Geology*, **25**: 287–309.

- Ward, C. R. and Taylor J. C. (1996). 'Quantitative mineralogical analysis of coals from the Callide Basin, Queensland, Australia using X-ray diffractometry and normative interpretation.' *International Journal of Coal Geology*, **30**: 211–229.
- Warren, C. J. and Dudas M. J. (1989). 'Leachability and partitioning of elements in ferromagnetic fly ash particles.' *The Science of the Total Environment*, **84**: 223–236.
- Wei, L., Naik T. R. and Golden D. M. (1992). Construction Materials Made with Coal Combustion By-Products, Center for By-Products Utilization, University of Wisconsin, Milwaukee. CBU 1992–24.
- Wigley, F. and Williamson J. (2005). *Coal mineral transformations – Effects on boiler ash behaviour*. London, Department of Materials, Imperial College of Science, Technology and Medicine: 43pp.
- Winkler, A. and Horbach J. (2004). 'Structure and diffusion dynamics in amorphous aluminium silicate: A molecular dynamics computer simulation.' *Journal of Chemical Physics*, **120**(1): 384–393.
- Xiao, Y. and Lasaga A. C. (1996). 'Ab initio quantum mechanical studies of the kinetics and mechanisms of quartz dissolution: OH⁻ catalysis.' *Geochimica et Cosmochimica Acta*, **60**: 2283–2295.

Abstract: This chapter outlines the possibility of designing raw materials for use in geopolymers. The opportunities presented by the development of one-part ‘just add water’ geopolymer formulations complement the potential of the traditional two-part (solid plus alkaline activator solution) mix design. The key roles played by network-modifying (alkali and alkaline earth) cations and alumina in rendering glassy precursors favourable for geopolymerization are discussed, and the potential value of ASTM Class C ashes in synthesis of high-performance geopolymers becomes evident. This provides a significant step towards the commercial application of geopolymer binders in the construction industry worldwide, and raises a number of important challenges for researchers in the field of geopolymer and cement technology.

Key words: geopolymer, precursors, fly ash, slag, glass chemistry, network modifiers.

3.1 Introduction

This chapter explores different raw materials used in geopolymer manufacture, and provides in some sense a significantly abbreviated form of the discussion presented by Duxson and Provis (2008); the reader is referred to that paper for a more detailed coverage of many of the issues raised here. The primary aim of the discussion is to understand what makes a ‘good’ raw material for generic two-part (solid source plus alkaline activator) geopolymer synthesis, and with that in mind to move towards the design of a successful one-part ‘just add water’ geopolymer formulation. Such a product would then potentially be capable of competing on an equal footing with Portland cement technology – whereas a two-part mix is less practical in many applications.

The three most common raw material classes used in geopolymerization are slags, calcined clays and coal fly ashes. Each of these has been widely studied as a supplementary cementitious material in Portland cement-based systems, and the reader is referred to the cement literature for a detailed discussion of their performance and properties in that context (ACI Committee 226 1987, Bouzoubaâ *et al.* 1999, Sabir *et al.* 2001, Richardson 2004). Calcined clays (predominantly metakaolin) have been relatively widely used in geopolymer synthesis, but their plate-like particle morphologies present tend to give an unfeasibly high water demand in geopolymer concrete applications. Other types of raw materials have also been used for two-part geopolymer synthesis,

including some synthetic powder precursors (Hos *et al.* 2002, Gordon *et al.* 2005); however, their use is not yet widespread.

3.2 Metallurgical slags

Blast furnace slag (abbreviated GGBFS, for ‘ground granulated blast furnace slag’) is broadly described as a mixture of poorly crystalline phases with compositions resembling gehlenite ($2\text{CaO}\cdot\text{Al}_2\text{O}_3\cdot\text{SiO}_2$) and akermanite ($2\text{CaO}\cdot\text{MgO}\cdot 2\text{SiO}_2$), as well as depolymerized calcium silicate glasses. The degree of depolymerization largely controls reactivity. As slag is generated at high temperature as a liquid in the blast furnace during iron production and subsequently quenched, its composition is essentially that of an over-charge-balanced calcium aluminosilicate framework – i.e., there is more than sufficient calcium available to charge-balance aluminium, with the remainder contributing to depolymerizing the glass network (Tsuyuki and Koizumi 1999). In the context of geopolymer synthesis from slag glasses, the key glass network forming cations are Al^{3+} and Si^{4+} ; the divalent Ca^{2+} and Mg^{2+} act as network modifiers along with any alkalis present.

Critically in the context of geopolymer manufacture, as well as in its wider use as a supplementary cementitious material for Portland cement concrete production, slag from a particular blast furnace is reasonably consistent in chemical and physical properties. However, despite this quality control within individual locations, slag compositions do vary between specific furnaces and ores. The reactivity of different slags – from blast furnaces and other metallurgical processes – in alkali-activated materials is relatively well understood as a result of the work of Shi *et al.* (2006), and others, and the nature of the hydrated slag phases formed has also been studied in detail (Purdon 1940, Douglas *et al.* 1992, Richardson *et al.* 1994, Wang and Scrivener 1995, Puertas *et al.* 2000, Song *et al.* 2000, Fernández-Jiménez *et al.* 2003, Wang and Scrivener 2003, Gruskovnjak *et al.* 2006, Xu *et al.* 2008). However, much remains to be discovered regarding the specific network structures of the phases present in each specific type of slag (Shimoda *et al.* 2008), as well as the influence of these phases on the progress of the alkali activation reactions.

It is also well known that the reactions of slag are dominated by small particles. Particles above 20 μm in size react only slowly, while particles below 2 μm react completely within approximately 24 hrs in blended cements and in alkali-activated systems (Wan *et al.* 2004, Wang *et al.* 2005). Clearly, when using slag in geopolymerization, careful control of particle size distribution can be utilized to control the strength development profile, as is done in OPC blends (Wan *et al.* 2004).

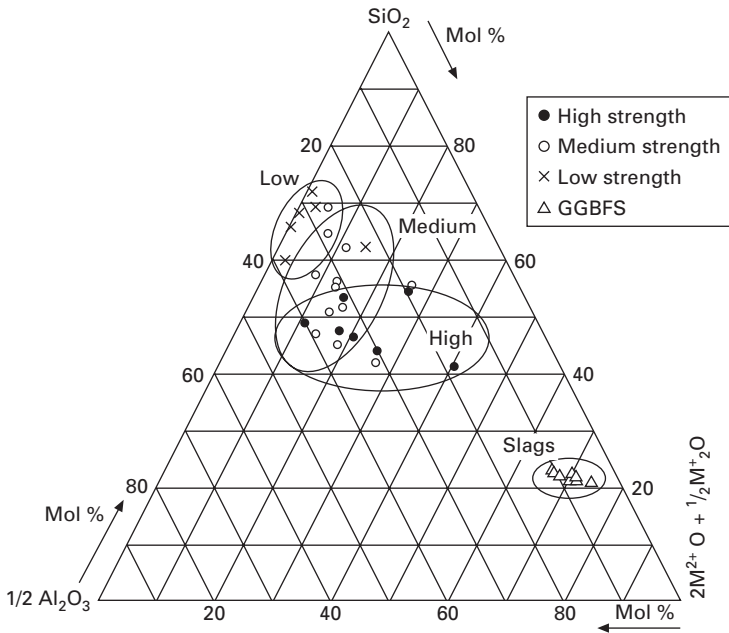
3.3 Fly ash

Fly ash consists of the remnants of clays, sand and organic matter present in coal, which leave via the chimney of the furnace during combustion. These compounds may melt in the furnace, but are then quenched rapidly in air to produce small, generally spherical glass particles. However, crystalline phases are also present, and heterogeneity is observed on both interparticle and intraparticle levels (Hemmings and Berry 1988, Hower *et al.* 1999, Nugteren 2007). Therefore, fly ash is a highly variable material that is dependent not only on the impurities present in the coal prior to combustion, but also on the particulars of the combustion and quenching process. The fly ashes that are most widely used in geopolymer synthesis are low in Ca, i.e. Class F according to ASTM C618. Published work on higher-Ca (Class C) ashes is scarcer, possibly due to the rapidity with which setting may occur in systems of ‘standard’ geopolymer design. As such, these two classes of fly ash will be dealt with separately here.

3.3.1 Class F ash

The reactivities of fly ashes, and the nature of the geopolymeric products produced from them, vary dramatically, and some of the reasons for this were discussed in detail in Chapter 2 of this book. However, there are additional trends that can be identified by comparison of the ash composition and geopolymer strength data, as shown in Fig. 3.1 (adapted from Duxson and Provis (2008)). This plot shows the overall oxide compositions of a number of ashes, as well as an indication of the strength achievable by activation of those ashes. Given that the data are obtained from a variety of literature sources from different research groups, meaning that samples were formulated and cured very differently, the exact strength data are not directly comparable. Regardless, categorization as ‘high’, ‘medium’ or ‘low’ strength does provide some useful insight. The multicomponent compositional data are converted to pseudo-ternary data by combining the alkaline earth ($M^{2+}O$) and alkali metal (M_2^+O) oxides and representing these components by the sum of the charges on all network-modifying cations – so an alkali metal cation counts as one charge unit, and an alkaline earth cation as two. Iron, titanium, residual carbon and other elements present are not included in this simplified analysis, and the compositions are normalized to account for this.

From Fig. 3.1, it is clear that ashes with low network modifier content tend to produce low-strength geopolymer products, with strength generally increasing as a function of network modifier content for Class F ashes. The only ash depicted that is not Class F is the rightmost of the black points shown; this is a Class C ash, and its alkali activation gives products of high strength (Keyte *et al.* 2005). Figure 3.1 also shows the compositions of some



3.1 Pseudo-ternary composition diagram for fly ashes, showing ashes which give alkali activation products in approximate strength ranges as indicated. Alkali and alkaline earth oxides are summed, and represented as the total number of charges on the respective cations. Composition and strength data are compiled from the literature (Duxson and Provis 2008). For comparison, compositions of a selection of blast furnace slags (data from Shi *et al.* 2006) are also shown.

representative blast furnace slags, which are very high in Ca and low in Al compared to fly ashes (Shi *et al.* 2006). There is a significant overlap in Fig. 3.1 between the ‘medium’ and ‘high’ categories, which indicates that, as expected, there are important additional factors influencing strength – in particular particle size, crystallinity, and other elements such as iron or carbon that are not accounted for in Fig. 3.1. However, it is observed that high-strength geopolymers are in general derived from ashes in the higher-alumina part of the compositional region shared by these two categories. Another (related) point of note is that the only ‘low-strength’ ash with a significant network modifier content (sourced from Mount Piper, Australia) is also close to the lowest in Al_2O_3 of all the ashes depicted.

3.3.2 Class C fly ash

The observation that network modifier content is an indicator of the potential utility of a given fly ash in geopolymerization will obviously bring attention

to the use of Class C (high-calcium) fly ashes. This class of ashes has not been subjected to the same level of analysis in the academic literature as Class F, with only a handful of publications to date (Roy *et al.* 1996, Perera *et al.* 2004, Xu *et al.* 2004, Keyte *et al.* 2005, Chindaprasirt *et al.* 2007). Roy *et al.* (1996) and Lukey *et al.* (2006) have shown that not only is it possible to utilize Class C fly ash in geopolymers, but in fact it can be largely preferable if the rheology of the mix can be adequately controlled. Class C fly ash could be viewed (within reason) as compositionally in between Class F fly ash and GGBFS. The fact that GGBFS–Class F ash mixes are often preferred in the production of geopolymers (Puertas *et al.* 2000, Goretta *et al.* 2004, Li and Liu 2007, and numerous instances in the patent literature) also provides an indication of the potential of Class C ashes. However, if there exists an optimal precursor composition for geopolymer formation, then it is clear that a better understanding of the role of glass chemistry in fly ash is required, not least because Class C fly ash is less abundant than Class F ash.

3.3.3 Fly ashes and glass chemistry

Unlike the more homogeneous glassy phases in GGBFS, fly ash contains many different phases, with both interparticle and intraparticle inhomogeneity observed (Hemmings and Berry 1988). Despite this complexity, much information is available in the literature detailing the nature and reactivity of the phases present in fly ashes (Gomes and François 2000, Henry *et al.* 2001, Ramesh and Koziński 2001, Brouwers and van Eijk 2002, Williams *et al.* 2005, Brindle and McCarthy 2006, Ward and French 2006, Nugteren 2007, Yazhenskikh *et al.* 2008).

It is clear that the exact details of the geopolymerization process depend on the individual ash source selected, and that no two ashes will follow exactly the same mechanism. Analysis must therefore be based on an understanding of how each phase observed in fly ashes reacts under geopolymerization conditions. Knowledge of which phases are present – and, critically, which are accessible during geopolymerization – will then enable the correct mechanistic analysis to be applied to each ash source. This is far from a trivial task, as it necessitates the development of a database of the chemistry, reactivity, leaching rates and dissolution mechanisms of all the different glasses observed in fly ashes, along with a detailed mineralogical and crystallographic analysis of every batch of ash to be processed. Some preliminary work has been completed involving linking the concepts and techniques developed by Hemmings and Berry (1988) with geopolymer chemistry and in modelling of ash dissolution. However, the laborious nature of this work necessitates a more technologically and intellectually accessible approach, the implementation of which remains the subject of

ongoing discussion and research, and is likely to remain so for many years to come (Duxson and Provis 2008).

3.4 Availability of aluminium

It is well known that the availability of aluminium controls to a large degree the properties of geopolymers (Weng *et al.* 2005, Fernández-Jiménez *et al.* 2006, Duxson *et al.* 2007). The amount of available aluminium, and possibly more importantly the rate of its release throughout reaction, affect geopolymer strength, setting characteristics, acid resistance, microstructure, and in particular control the strength development profile. Geopolymerization is known to be a strongly kinetically controlled process (Provis and van Deventer 2007), and so factors influencing both the rate of release of aluminium and its subsequent availability for geopolymer formation (which can be controlled in various ways (Rees *et al.* 2008)) must be understood. The availability of silicon is also important, but ultimately less critical as any deficiencies in the solid source can be accounted for by direct addition of soluble silicate to the activating solution. Therefore, by understanding the release rate of aluminium from a precursor, it becomes possible to predict and control the properties of the resultant geopolymer.

Only a small change in aluminium incorporation rates is observed when activating metakaolin with alkaline solutions containing different alkali metals, indicating that the aluminium in metakaolin is readily available (Duxson *et al.* 2005). In contrast, the release of aluminium from fly ash is in general slower, and is greatly affected by alkali concentration and type (van Jaarsveld and van Deventer 1999, Lee and van Deventer 2002, Fernández-Jiménez and Palomo 2003). This indicates that the availability of aluminium from the glassy phases in fly ash is limited by the nature of those phases.

Thermodynamic calculations (de Jong and Brown 1980, Hamilton *et al.* 2001) and sorption/speciation arguments (Blum and Lasaga 1991, Hamilton *et al.* 2001) show that most Al(IV)-O-Si bonds are more readily broken than Si-O-Si bonds, and bonds between network-forming and network-modifying species are weaker yet (Oelkers and Gislason 2001). Once network-modifying cations are introduced into aluminosilicate glasses above the level required for charge-balancing of tetrahedral aluminium – which is the case in slags, as was discussed earlier in this chapter – these associate predominantly with silicon sites, which become depolymerized (Lee and Stebbins 2006). These depolymerized glasses are the phases most likely to provide aluminium during geopolymerization – and this explains in part the higher reactivity of over-charge-balanced slag glasses compared to most fly ashes. Conversely, if there is insufficient network-modifying charge available in a phase, the solubility of aluminium from that phase is greatly reduced as it tends to take on 6-coordination (e.g., mullite-type glasses).

The presence of alkaline earth cations in a glass also gives an increased tendency towards framework disorder, including the formation of a small concentration of (weak, reactive) Al-O-Al bonds if the Al content is sufficiently high, as well as an NBO content higher than is strictly required by stoichiometry (Stebbins and Xu 1997, Lee and Stebbins 2006). It is thus easy to understand how slag, rich in Ca^{2+} and Mg^{2+} as modifiers, provides an excellent raw material for alkali activation.

3.5 An optimal two-part geopolymer?

Following the work of Hemmings and Berry (1988) as well as the discussion above, it is possible to identify a ‘good’ ash for geopolymerization by using XRD in conjunction with compositional analysis and other techniques (including devitrification and/or quantitative scanning electron microscopy) to determine the chemistry and compositions of the reactive phases. However, in practical terms, the supply of ‘good’ ashes is often both limited in volume and geographically isolated from major concrete markets. There is a high likelihood that of the selection of ‘local’ materials available at a given site, few if any will have highly favourable glass chemistry, and even if one does, it is likely to be in high demand (either by OPC concrete or rival geopolymer manufacturers). Therefore, it is critical that alternative, apparently less ‘good,’ ashes need to be used if a true geopolymer industry is to be created, and possibly also that poor ashes may be somehow upgraded to a higher quality at an acceptably low cost. GGBFS provides an obvious source of highly reactive glass, but is priced similarly to OPC in many markets and so drives up cost. Clearly, the key is to optimise reactive glass content while keeping price and performance within commercial parameters.

This real-world trade-off introduces the concept of a product ‘sweet spot’, where price, reactivity, water demand and strength characteristics are optimized. This will be different for every geographic location, taking into account the properties and costs of the available raw materials, as well as the demands of the local market and environment. For example, chloride resistance is critical in marine climates, sulphate resistance in areas with acid sulphate soils, and freeze-thaw resistance is critical in much of Europe and northern North America but relatively unimportant at lower latitudes. So, in terms of a real-world geopolymer industry, there is no such thing as a single globally ‘optimal’ geopolymer composition, but rather a collection of possible mix designs utilizing a broad variety of raw materials to achieve a balance of commercial and technical goals. As raw material availability, quality or price change (and all will certainly change over periods of years, and sometimes day-to-day as well), a producer must be able to react quickly to compensate in a timely and cost-competitive manner. The intellectual complexity of this process is clear from the discussion above, and is not

conducive to large-scale commercial implementation. For a true geopolymer industry to develop, a simple and effective method must be formulated.

3.6 Designing one-part geopolymer cements

OPC is formed by the very deliberate manufacture of a reactive, predominantly calcium silicate material, containing the correct constituents and phases to provide the nutrients required for reactions at a given rate in the presence of water. The dissolution behaviour of OPC is determined predominantly by chemical composition and particle fineness, and has been refined over close to 200 years of large-scale production. Calcium is present in sufficient quantities to depolymerise the silicon, giving extremely rapid initial dissolution when compared to a slag or a fly ash under the same conditions of near-neutral initial pH. As the pH increases later in the OPC hydration process, any slag and/or ash present will then begin to react. This is why the chemistry of these components is known to be beneficial primarily in development of later-term properties of blended cements; they simply do not react rapidly enough at pH ~10-11 to contribute significantly to the initial period of cement hydration. The spherical particles in fly ash are in fact beneficial in fresh cement rheology as well, but this is entirely independent from dissolution chemistry. In terms of the discussion in the preceding section, OPC presents itself as the 'sweet spot' composition for calcium silicate chemistry, and it is possible that a similar approach may be able to be used for manufacturing a one-part 'just add water' aluminosilicate-based geopolymer cement. OPC chemistry has been developed over a period of many decades using the predominantly empirical means of analysis that have historically been available; geopolymer technology does not have the same luxury in terms of a waiting market and lack of competing products, and so advanced scientific techniques must be applied to the development of a fuller understanding of the 'sweet spot' principle in this case.

The fineness of cement is also routinely used to control reactivity, by means of milling. However, this has the deleterious effect of increasing water demand due to the irregular shapes generated by the fracture of brittle particles subjected to intense mechanical forces during milling (Wan *et al.* 2004). Water demand depends strongly on the surface area of the solid precursor, meaning that fine, irregular particles require the addition of much more water to the mix for equivalent workability. Spherical fly ash particles will in general have a low water demand as spheres have the lowest surface area per unit volume. Low-energy, short-duration milling of fly ashes actually decreases water demand further, by breaking down irregular particle agglomerates and perospheres (hollow particles filled with smaller spheres), without affecting the majority of the other particles present (Bouzoubaâ *et al.* 1997, 1999). However, high-energy milling of the type required for significant particle-

size reduction causes fracture of the majority of particles present, leading to the observed increase in water demand.

Water reduction is desirable in terms of many of the properties of concretes, as well as from an environmental perspective. In particular, lower water/binder ratios give reductions in porosity and thus permeability, meaning that corrosion of steel reinforcing due to chloride or sulphate attack is greatly reduced. The design of a one-part geopolymer precursor should take this into account also, meaning that fine spherical particles are preferred over larger particles milled to a smaller size but irregular shapes.

3.7 Geopolymers and the future cement industry

Geopolymers do not necessarily need to be a product which competes on a global scale with the existing OPC industry infrastructure, but rather may be viewed as a technology which may be utilized by cement producers to offer a broader range of cementitious products to the market. Clearly a one-part process is the ideal mechanism for large-scale deployment of geopolymer cements, as most of the quality control processes can be dealt with centrally rather than requiring extensive control and understanding of chemistry on the part of the end user. However, this is not to say that this proposition is currently feasible or close to market readiness. In contrast, two-part geopolymer concrete production is ready for commercialization, given that sufficient expertise is available to ensure sufficient quality control and access to appropriate technology to either cope with or remove the need for regular mix-design adjustments. Such an operation commenced medium-scale production in Australia early in 2008 (Nowak 2008).

3.8 Conclusions

In designing and tailoring 'ideal' precursors for geopolymerization, it is critical to be able to control the dissolution rates of the glassy phases present. This can be achieved by optimization of the network modifier (alkali or alkaline earth cation) content during precursor synthesis. By use of standard glass synthesis methodology, it should be entirely possible to generate a precursor of the necessary composition to enable synthesis of geopolymers by 'just adding water.' By generating the precursor as spherical glass particles, it will be possible to retain the benefits of spherical particle shape observed in fly ash. The need for addition of alkali (i.e., a two-part mix formulation) may be greatly reduced or even eliminated if the correct glass, or combination of glasses, can be selectively synthesized to enable a commercially viable one-part mix ('just add water') geopolymer.

3.9 References

- ACI Committee 226 (1987) Ground granulated blast-furnace slag as a cementitious constituent in concrete. *ACI Materials Journal*, 84, 327–342.
- Blum, A. E. and Lasaga, A. C. (1991) The role of surface speciation in the dissolution of albite. *Geochimica et Cosmochimica Acta*, 55, 2193–2201. doi:10.1016/0016-7037(91)90096-N.
- Bouzoubaâ, N., Zhang, M. H., Bilodeau, A. and Malhotra, V. M. (1997) The effect of grinding on the physical properties of fly ashes and a portland cement clinker. *Cement and Concrete Research*, 27, 1861–1874. doi:10.1016/S0008-8846(97)00194-4.
- Bouzoubaâ, N., Zhang, M. H., Malhotra, V. M. and Golden, D. M. (1999) Blended fly ash cements – A review. *ACI Materials Journal*, 96, 641–650.
- Brindle, J. H. and McCarthy, M. J. (2006) Chemical constraints on fly ash glass compositions. *Energy and Fuels*, 20, 2580–2585. doi:10.1021/ef0603028.
- Brouwers, H. J. H. and van Eijk, R. J. (2002) Fly ash reactivity: Extension and application of a shrinking core model and thermodynamic approach. *Journal of Materials Science*, 37, 2129–2141. doi:10.1023/A:1015206305942.
- Chindaprasirt, P., Chareerat, T. and Sirivivatnanon, V. (2007) Workability and strength of coarse high calcium fly ash geopolymer. *Cement and Concrete Composites*, 29, 224–229. doi:10.1016/j.cemconcomp.2006.11.002.
- de Jong, B. H. W. S. and Brown, G. E. (1980) Polymerization of silicate and aluminate tetrahedra in glasses, melts, and aqueous solutions -I. Electronic structure of $H_6Si_2O_7$, $H_6AlSiO_7^{1-}$, and $H_6Al_2O_7^{2-}$. *Geochimica et Cosmochimica Acta*, 44, 491–511. doi:10.1016/0016-7037(80)90046-0.
- Douglas, E., Bilodeau, A. and Malhotra, V. M. (1992) Properties and durability of alkali-activated slag concrete. *ACI Materials Journal*, 89, 509–516.
- Duxson, P. and Provis, J. L. (2008) Designing precursors for geopolymer cements. *Journal of the American Ceramic Society*, 91, 3864–3869. doi:10.1111/j.1551-2916.2008.02787.x
- Duxson, P., Lukey, G. C., Separovic, F. and van Deventer, J. S. J. (2005) The effect of alkali cations on aluminum incorporation in geopolymeric gels. *Industrial and Engineering Chemistry Research*, 44, 832–839. doi:10.1021/ie0494216.
- Duxson, P., Fernández-Jiménez, A., Provis, J. L., Lukey, G. C., Palomo, A. and van Deventer, J. S. J. (2007) Geopolymer technology: The current state of the art. *Journal of Materials Science*, 42, 2917–2933. doi:10.1007/s10853-006-0637-z.
- Fernández-Jiménez, A. and Palomo, A. (2003) Characterisation of fly ashes. Potential reactivity as alkaline cements. *Fuel*, 82, 2259–2265. doi:10.1016/S0016-2361(03)00194-7.
- Fernández-Jiménez, A., Puertas, F., Sobrados, I. and Sanz, J. (2003) Structure of calcium silicate hydrates formed in alkaline-activated slag: Influence of the type of alkaline activator. *Journal of the American Ceramic Society*, 86, 1389–1394. doi:10.1111/j.1151-2916.2003.tb03481.x.
- Fernández-Jiménez, A., Palomo, A., Sobrados, I. and Sanz, J. (2006) The role played by the reactive alumina content in the alkaline activation of fly ashes. *Microporous and Mesoporous Materials*, 91, 111–119. doi:10.1016/j.micromeso.2005.11.015.
- Gomes, S. and François, M. (2000) Characterization of mullite in silicoaluminous fly ash by XRD, TEM, and ^{29}Si MAS NMR. *Cement and Concrete Research*, 30, 175–181. doi:10.1016/S0008-8846(99)00226-4.
- Gordon, M., Bell, J. L. and Kriven, W. M. (2005) Comparison of naturally and synthetically derived, potassium-based geopolymers. *Ceramic Transactions*, 165, 95–106.

- Goretta, K. C., Chen, N., Gutierrez-Mora, F., Routbort, J. L., Lukey, G. C. and van Deventer, J. S. J. (2004) Solid-particle erosion of a geopolymer containing fly ash and blast-furnace slag. *Wear*, 256, 714–719. doi:10.1016/S0043-1648(03)00463-0.
- Gruskovnjak, A., Lothenbach, B., Holzer, L., Figi, R. and Winnefeld, F. (2006) Hydration of alkali-activated slag: comparison with ordinary Portland cement. *Advances in Cement Research*, 18, 119–128. doi: 10.1680/adcr.2006.18.3.119.
- Hamilton, J. P., Brantley, S. L., Pantano, C. G., Criscenti, L. J. and Kubicki, J. D. (2001) Dissolution of nepheline, jadeite and albite glasses: Toward better models for aluminosilicate dissolution. *Geochimica et Cosmochimica Acta*, 65, 3683–3702. doi:10.1016/S0016-7037(01)00724-4.
- Hemmings, R. T. and Berry, E. E. (1988) On the glass in coal fly ashes: Recent advances. *Fly Ash and Coal Conversion By-Products: Characterization, Utilization, and Disposal IV*, Warrendale, PA, McCarthy, G. J. (Ed.), 3–38.
- Henry, J., Towler, M. R., Stanton, K. T., Querol, X. and Moreno, N. (2001) Characterisation of the glass fraction of a selection of European coal fly ashes. *Journal of Chemical Technology and Biotechnology*, 79, 540–546. doi:10.1002/jctb.1023.
- Hos, J. P., McCormick, P. G. and Byrne, L. T. (2002) Investigation of a synthetic aluminosilicate inorganic polymer. *Journal of Materials Science*, 37, 2311–2316. doi:10.1023/A:1015329619089.
- Hower, J. C., Rathbone, R. F., Robertson, J. D., Peterson, G. and Trimble, S. (1999) Petrology, mineralogy, and chemistry of magnetically separated sized fly ash. *Fuel*, 78, 197–203. doi:10.1016/S0016-2361(98)00132-X.
- Keyte, L. M., Lukey, G. C. and van Deventer, J. S. J. (2005) The effect of coal ash glass chemistry on the tailored design of waste-based geopolymeric products. *WasteEng 2005*, Albi, France, Nzihou, A. (Ed.), CD-ROM proceedings.
- Lee, S. K. and Stebbins, J. F. (2006) Disorder and the extent of polymerization in calcium silicate and aluminosilicate glasses: O-17 NMR results and quantum chemical molecular orbital calculations. *Geochimica et Cosmochimica Acta*, 70, 4275–4286. doi:10.1016/j.gca.2006.06.1550.
- Lee, W. K. W. and van Deventer, J. S. J. (2002) Structural reorganisation of class F fly ash in alkaline silicate solutions. *Colloids and Surfaces A – Physicochemical and Engineering Aspects*, 211, 49–66. doi:10.1016/S0927-7757(02)00237-6.
- Li, Z. and Liu, S. (2007) Influence of slag as additive on compressive strength of fly ash-based geopolymer. *Journal of Materials in Civil Engineering*, 19, 470–474. doi:10.1061/(ASCE)0899-1561(2007)19:6(470).
- Lukey, G. C., Mendis, P. A., van Deventer, J. S. J. and Sofi, M. (2006) Advances in inorganic polymer concrete technology. In Day, K. W. (Ed.) *Concrete Mix Design, Quality Control and Specification*, 3rd Edition. London, Routledge.
- Nowak, R. (2008) Geopolymer concrete opens to reduce CO₂ emissions. *New Scientist*, 197, 28–29. doi:10.1016/S0262-4079(08)60229-8.
- Nugteren, H. W. (2007) Coal fly ash: From waste to industrial product. *Particle and Particle Systems Characterisation*, 24, 49–55. doi:10.1002/ppsc.200601074.
- Oelkers, E. H. and Gislason, S. R. (2001) The mechanism, rates and consequences of basaltic glass dissolution: I. An experimental study of the dissolution rates of basaltic glass as a function of aqueous Al, Si and oxalic acid concentration at 25°C and pH = 3 and 11. *Geochimica et Cosmochimica Acta*, 65, 3671–3681. doi:10.1016/S0016-7037(01)00664-0.
- Perera, D. S., Nicholson, C. L., Blackford, M. G., Fletcher, R. A. and Trautman, R. A. (2004) Geopolymers made using New Zealand flyash. *Journal of the Ceramic Society of Japan*, 112, S108–S111.

- Provis, J. L. and van Deventer, J. S. J. (2007) Geopolymerisation kinetics. 2. Reaction kinetic modelling. *Chemical Engineering Science*, 62, 2318–2329. doi:10.1016/j.ces.2007.01.028.
- Puertas, F., Martínez-Ramírez, S., Alonso, S. and Vázquez, E. (2000) Alkali-activated fly ash/slag cement. Strength behaviour and hydration products. *Cement and Concrete Research*, 30, 1625–1632. doi:10.1016/S0008-8846(00)00298-2.
- Purdon, A. O. (1940) The action of alkalis on blast-furnace slag. *Journal of the Society of Chemical Industry – Transactions and Communications*, 59, 191–202.
- Ramesh, A. and Koziński, J. A. (2001) ^{29}Si , ^{27}Al and ^{23}Na solid-state nuclear magnetic resonance studies of combustion-generated ash. *Fuel*, 80, 1603–1610. doi:10.1016/S0016-2361(01)00041-2.
- Rees, C. A., Provis, J. L., Lukey, G. C. and van Deventer, J. S. J. (2008) Geopolymer gel formation with seeded nucleation. *Colloids and Surfaces A – Physicochemical and Engineering Aspects*, 318, 97–105. doi:10.1016/j.colsurfa.2007.12.019.
- Richardson, I. G. (2004) Tobermorite/jennite- and tobermorite/calcium hydroxide-based models for the structure of C-S-H: applicability to hardened pastes of tricalcium silicate, β -dicalcium silicate, Portland cement, and blends of Portland cement with blast-furnace slag, metakaolin, or silica fume. *Cement and Concrete Research*, 34, 1733–1777. doi:10.1016/j.cemconres.2004.05.034.
- Richardson, I. G., Brough, A. R., Groves, G. W. and Dobson, C. M. (1994) The characterization of hardened alkali-activated blast-furnace slag pastes and the nature of the calcium silicate hydrate (C-S-H) paste. *Cement and Concrete Research*, 24, 813–829. doi:10.1016/0008-8846(94)90002-7.
- Roy, A., Schilling, P. J. and Eaton, H. C. (1996) Alkali activated class C fly ash cement, U.S. Patent 5,565,028.
- Sabir, B. B., Wild, S. and Bai, J. (2001) Metakaolin and calcined clays as pozzolans for concrete: a review. *Cement and Concrete Composites*, 23, 441–454. doi:10.1016/S0958-9465(00)00092-5.
- Shi, C., Krivenko, P. V. and Roy, D. M. (2006) *Alkali-Activated Cements and Concretes*, Abingdon, UK, Taylor and Francis.
- Shimoda, K., Tobu, Y., Kanehashi, K., Nemoto, T. and Saito, K. (2008) Total understanding of the local structures of an amorphous slag: Perspective from multi-nuclear (^{29}Si , ^{27}Al , ^{17}O , ^{25}Mg , and ^{43}Ca) solid-state NMR. *Journal of Non-Crystalline Solids*, 354, 1036–1043. doi:10.1016/j.jnoncrysol.2007.08.010.
- Song, S., Sohn, D., Jennings, H. M. and Mason, T. O. (2000) Hydration of alkali-activated ground granulated blast furnace slag. *Journal of Materials Science*, 35, 249–257. doi:10.1023/A:1004742027117.
- Stebbins, J. F. and Xu, Z. (1997) NMR evidence for excess non-bridging oxygen in an aluminosilicate glass. *Nature*, 390, 60–62. doi:10.1038/36312.
- Tsuyuki, N. and Koizumi, K. (1999) Granularity and surface structure of ground granulated blast-furnace slags. *Journal of the American Ceramic Society*, 82, 2188–2192. doi:10.1111/j.1151-2916.1999.tb02061.x.
- van Jaarsveld, J. G. S. and van Deventer, J. S. J. (1999) Effect of the alkali metal activator on the properties of fly ash-based geopolymers. *Industrial and Engineering Chemistry Research*, 38, 3932–3941. doi:10.1021/ie980804b.
- Wan, H., Shui, Z. and Lin, Z. (2004) Analysis of geometric characteristics of GGBS particles and their influences on cement properties. *Cement and Concrete Research*, 34, 133–137. doi:10.1016/S0008-8846(03)00252-7.
- Wang, P. Z., Trettin, R. and Rudert, V. (2005) Effect of fineness and particle size distribution

- of granulated blast-furnace slag on the hydraulic reactivity in cement systems. *Advances in Cement Research*, 17, 161–166. doi: 10.1680/adcr.2005.
- Wang, S. D. and Scrivener, K. L. (1995) Hydration products of alkali-activated slag cement. *Cement and Concrete Research*, 25, 561–571. doi:10.1016/0008-8846(95)00045-E.
- Wang, S.-D. and Scrivener, K. L. (2003) ^{29}Si and ^{27}Al NMR study of alkali-activated slag. *Cement and Concrete Research*, 33, 769–774. doi:10.1016/S0008-8846(02)01044-X.
- Ward, C. R. and French, D. (2006) Determination of glass content and estimation of glass composition in fly ash using quantitative X-ray diffractometry. *Fuel*, 85, 2268–2277. doi:10.1016/j.fuel.2005.12.026.
- Weng, L., Sagoe-Crentsil, K., Brown, T. and Song, S. (2005) Effects of aluminates on the formation of geopolymers. *Materials Science and Engineering, B: Solid-State Materials for Advanced Technology*, 117, 163–168. doi:10.1016/j.mseb.2004.11.008.
- Williams, P. J., Biernacki, J. J., Rawn, C. J., Walker, L. and Bai, J. (2005) Microanalytical and computational analysis of Class F fly ash. *ACI Materials Journal*, 102, 330–337.
- Xu, H., Lukey, G. C. and van Deventer, J. S. J. (2004) The activation of Class C-, Class F-fly ash and blast furnace slag using geopolymerisation. *Proceedings of 8th CANMET/ACI International Conference on Fly Ash, Silica Fume, Slag and Natural Pozzolans in Concrete*, Las Vegas, NV, Malhotra, V. M. (Ed.), 797–819.
- Xu, H., Provis, J. L., van Deventer, J. S. J. and Krivenko, P. V. (2008) Characterization of aged slag concretes. *ACI Materials Journal*, 105, 131–139.
- Yazhenskikh, E., Hack, K. and Müller, M. (2008) Critical thermodynamic evaluation of oxide systems relevant to fuel ashes and slags. Part 3: Silica–alumina system. *Calphad*, 32, 195–205. doi:10.1016/j.calphad.2007.05.004.

Activating solution chemistry for geopolymers

J L PROVIS, University of Melbourne, Australia

Abstract: This chapter discusses the different solutions that are used as activators in geopolymer synthesis: alkali metal hydroxides and silicates. The phase behaviour, speciation and physical properties of different potential activating solutions are discussed. The use of alternative activators is also briefly mentioned.

Key words: sodium, potassium, silicate, hydroxide, speciation, viscosity, alkalinity.

4.1 Introduction

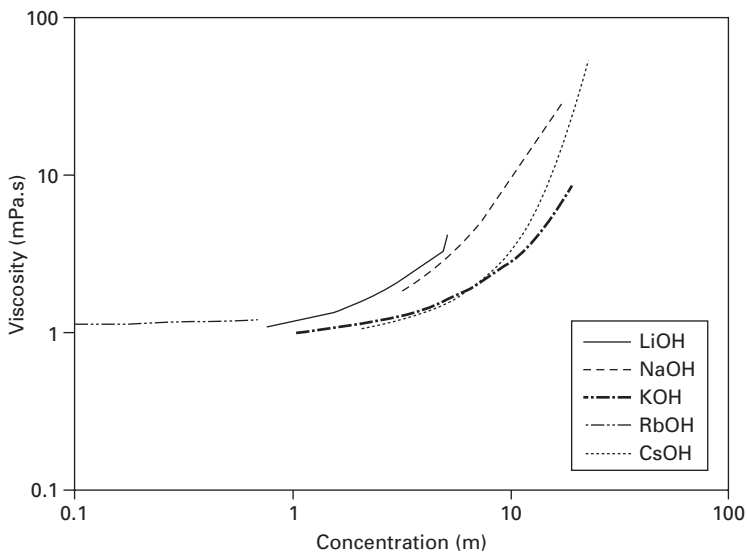
In addition to the reactive solid components as described in Chapter 3, a chemical activator is required to initiate the geopolymerisation reaction. In general, aluminosilicate binder materials activated by alkali hydroxides or silicates under high-pH conditions are classified as being geopolymers, and these will be the main focus of the discussion here. For an overview of reactions involving carbonate or sulphate activating solutions, the reader is referred to the book by Shi, Krivenko and Roy (2006). The chemistry of alkali silicate solutions is also critical to the understanding of zeolite synthesis (McCormick and Bell 1989, Swaddle *et al.* 1994, Cheng and Shantz 2006, Knight *et al.* 2006, 2007), so much of the knowledge that is available regarding these solutions has originally been developed in that context. Much of this information is also valuable in the analysis of geopolymer activating solution chemistry, but with the caveat that the concentrations involved in zeolite synthesis are often much lower than the very high levels required for geopolymer synthesis.

This chapter is essentially divided into three sections. The first section gives a brief discussion of the chemistry of alkali hydroxide solutions, as the simplest activating solution used in geopolymer synthesis. The second section provides an overview of key chemistry and engineering aspects of alkali silicate solutions, outlining the issues controlling their (often complex) behaviour during geopolymerisation, and some of the implications of this behaviour. Finally, the possibility of using different activating solutions will be addressed; specifically, the use of sodium aluminate as an activator, and also a brief discussion of ‘just-add-water’ geopolymer formulations as described in Chapter 3.

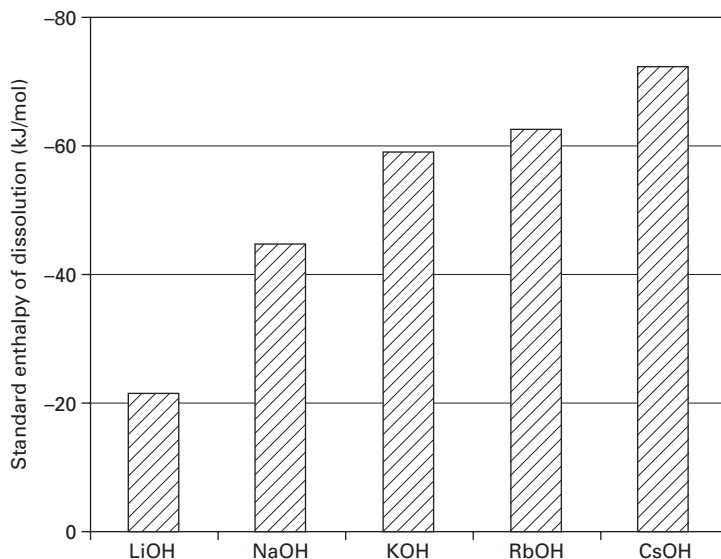
4.2 Alkali hydroxide solutions

The alkali hydroxides most commonly used as activators in geopolymer synthesis are sodium and/or potassium, with only a handful of publications to date addressing the use of small proportions mixed with one or both of sodium and potassium. In a processing context and aside from their obviously high corrosivity, the most important properties of concentrated hydroxide solutions that must be considered are viscosity and heat of dissolution. Figure 4.1 shows the variation of viscosity with concentration at 25°C for each of the alkali hydroxides; the data sets are in some cases incomplete because the data are not available in the academic literature. However, it is clear that a consistent trend is followed by all the solutions depicted, with a very gradual increase in viscosity up to about 1.0M, at which point the viscosity does not differ markedly from that of water. After this, there is a significant increase whose steepness depends on the identity of the alkali cation (noting that Fig. 4.1 is plotted on logarithmic axes). There does not appear to be a systematic trend in viscosity as a function of cation size, but there is a significant degree of uncertainty introduced by the scarcity of data for some of the systems shown.

Figure 4.2 depicts the standard enthalpy of dissolution to infinite dilution, $\Delta_{aq}H^{\circ}_{298.15K}$, of each of the alkali hydroxides as a function of cation size. The importance of the heat of dissolution is that, in preparing a concentrated hydroxide solution, a significant temperature increase will take place, which



4.1 Viscosities of alkali hydroxide solutions as a function of molality. Data from Laliberté (2007) for LiOH, NaOH and KOH, Fricke (1924) for RbOH, and Sipos *et al.* (2000) for CsOH.



4.2 Standard enthalpies of dissolution of MOH (M: alkali metal) to infinite dilution at 298.15K. Data from the reviews of Gurvich *et al.* (1996, 1997).

may be problematic. The actual heat released by dissolution into a highly concentrated solution will be somewhat less than the infinite-dissolution values plotted in Fig. 4.2, as the heat of dilution incurred by moving to infinite dilution will not be significant in preparing geopolymer activating solutions. However, the enthalpy of dissolution dominates the dilution effects, and so the data plotted in Fig. 4.2 provide a useful estimate of the heat that will be released. From inspection of the data tables in the reviews of Gurvich *et al.* (1996, 1997), it is estimated that dilution from $\sim 10\text{M}$ to infinite dilution contributes around 10% of the enthalpy of dissolution of NaOH, with dissolution of the crystalline solid providing the other 90%. The data of Simonson *et al.* (1989) show that the enthalpy of dissolution of NaOH(aq) is only weakly concentration-dependent at 25°C , but does depend somewhat more strongly on temperature. As a ballpark estimate rather than an exact figure is being sought here, the figure of 10% will be sufficiently accurate for the purposes of this calculation.

The data in Fig. 4.2 can then be used to calculate the approximate temperature increase expected when dissolving solid alkali hydroxides to the concentrations required for geopolymer synthesis. If it is assumed that dissolving 10 moles of NaOH into a litre of water releases 90% of the heat that would be released in moving to infinite dissolution, as discussed above, then this will be around 400 kJ. Taking the mean heat capacity of NaOH solution to be approximately equal to that of water, as indicated by

the results of Simonson *et al.* (1989), this quantity of heat will be sufficient to raise the temperature of the water by over 90°C. In most cases, some of the heat will be lost to the surroundings and some will be expended by vapourisation of some percentage of the solution. However, it is clear that such a temperature rise in a highly caustic solution will need to be very carefully considered and monitored if hydroxide solutions are to be routinely prepared from solid precursors in an industrial production setting. As shown in Fig. 4.2, the heat of dissolution increases with cation size, so solutions prepared containing high levels of KOH will suffer an even larger temperature rise than is observed in the NaOH case.

Next, issues specific to each of the five alkali metal hydroxides as concentrated aqueous solutions will be briefly discussed in the context of geopolymer synthesis.

4.2.1 Lithium hydroxide, LiOH

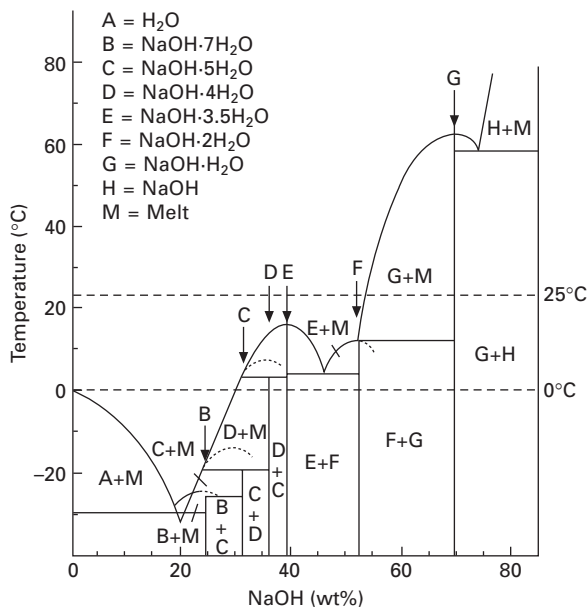
The solubility of LiOH at 298.15K is just under 5.4 *m* (Monnin and Dubois 2005), which is at the lower end of the useful alkalinity range for hydroxide activating solutions in geopolymer synthesis. The majority of references to the use of lithium in geopolymers come from the patent literature. These either involve its use as an accelerator for polymerisation, analogous to its known enhancement of colloid formation in silicate sols (Gaboriaud *et al.* 1999), or simply listing lithium as a possible alkali metal cation when making a broad claim relating to geopolymer materials of a range of compositions. It must therefore be considered to be of relatively minor importance in the investigation of geopolymers. The primary role of Li⁺ in cement and concrete technology is to minimise degradation due to the alkali-aggregate (alkali-silica) reaction in the presence of a reactive aggregate (Lumley 1997). Given that alkali-aggregate reactions have not been observed to be problematic in geopolymers (Li *et al.* 2006, García-Lodeiro *et al.* 2007), and that the reaction between alkali from pore solutions and reactive silicate/aluminosilicate aggregates is expected to generate more geopolymer gel binder rather than any deleterious products, the use of lithium in this context in geopolymers is not expected to become as prevalent as it is in Portland cement systems.

4.2.2 Sodium hydroxide, NaOH

The thermodynamic properties of NaOH solutions have been analysed and modelled in some detail over the past several decades (Pabalan and Pitzer 1987, Simonson *et al.* 1989, Petrenko and Pitzer 1997). NaOH is the most commonly used hydroxide activator in geopolymer synthesis, being both the cheapest and most widely available of the alkali hydroxides. The use of NaOH as an activator in geopolymer synthesis, from both fly ash and metakaolin

precursors, is very widespread due to its low cost, wide availability and low viscosity. However, the highly corrosive nature of concentrated NaOH or any other alkali hydroxide means that very specialised processing equipment would be required to produce large volumes of hydroxide-activated geopolymers, and for this reason (in addition to structural and performance issues discussed in detail throughout this book) silicate activation is often preferred. The solubility of NaOH at 25°C is 53.3% by mass (28.57 *m*), but falls below 30 wt% (10.73 *m*) at 0°C with the formation of a complex sequence of solid hydrates between 30 and 50 wt% NaOH and 0 and 25°C, as shown in the phase diagram presented as Fig. 4.2 (Pickering 1893, Kurt and Bittner 2006). This may be of significance if concentrated hydroxide activating solutions are to be used for geopolymer production in cooler climates.

The use of sodium hydroxide activators in geopolymers is well known to lead to the formation of observable zeolitic structures (Provis *et al.* 2005b), particularly after extended periods of curing under moist conditions or after even a brief period at elevated temperature. Investigations are still ongoing into whether this phenomenon will be linked to any change in material performance; some correlation between zeolite formation and decreased strength has been observed in certain systems. However, it is not yet clear whether this is specifically a causative effect (i.e., zeolite formation leading



4.3 Phase diagram for the system NaOH-H₂O. Adapted from Kurt and Bittner (2006).

to loss of performance), or whether a deeper underlying factor or combination of factors causes both zeolite formation and strength decrease.

Efflorescence (formation of white sodium carbonate or bicarbonate crystals) is also a known issue in geopolymers activated with too high a concentration of hydroxide solutions, where the excess alkali reacts with atmospheric CO₂. This is unsightly, but not always harmful to the structural integrity of the material.

4.2.3 Potassium hydroxide, KOH

The solubility of KOH at 25°C is approximately 21 *m*, and this does not decrease dramatically with decreasing temperature (Pickering 1893). The phase diagram is also much simpler than that of the NaOH-H₂O system, without the complex assemblage of hydrate phases. It is therefore unlikely that precipitation from potassium hydroxide activating solutions will be problematic under any realistic geopolymer processing conditions.

Zeolite formation is also well known to take place in KOH-activated geopolymers, similar to their NaOH-containing counterparts. However, crystallisation is less rapid in KOH/metakaolin geopolymers compared to the NaOH/metakaolin system (Duxson *et al.* 2007), and very significantly suppressed in KOH/fly ash systems compared to NaOH/fly ash (Fernández-Jiménez *et al.* 2006). Carbonation of KOH-activated geopolymers is also a potential issue (Fernández-Jiménez *et al.* 2006), although this has not been analysed in detail in the literature.

4.2.4 Rubidium hydroxide, RbOH

Rubidium hydroxide has not been studied in detail in geopolymerisation, due mainly to its cost and relative scarcity. In fact, the dearth of information regarding the behaviour and properties of RbOH is evidenced by the fact that the best currently available thermochemical data for this compound, as reviewed by Gurvich *et al.* (1997), was obtained from experimental data published in 1906 for a sample of unknown purity. The solubility of RbOH at 15°C is 17.6 *m*, or around 180g RbOH per 100 mL H₂O (Lenk and Prinz 2005).

4.2.5 Caesium hydroxide, CsOH

Caesium hydroxide has been used in geopolymerisation in some instances, but predominantly in silicate rather than hydroxide-activated systems. It is less rare than rubidium, but still sufficiently exotic to be considered unlikely to see large-scale commercial use in geopolymers except in niche ceramic-type applications where the higher thermal resistance and very low thermal

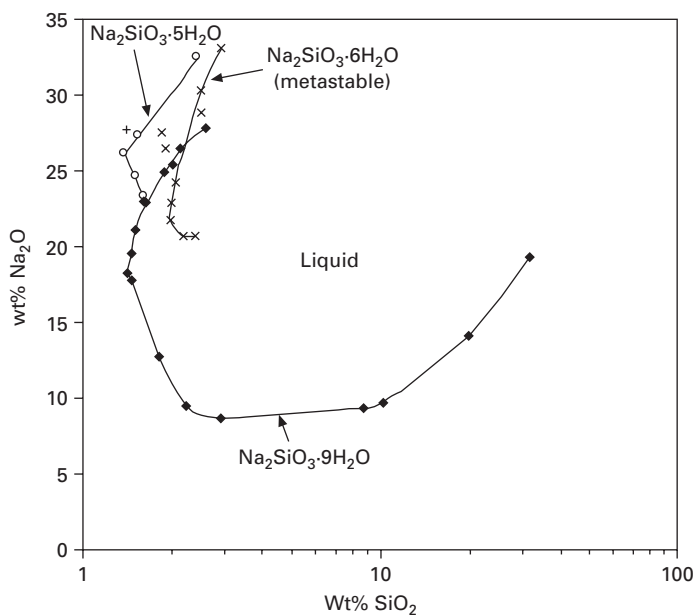
expansion of aluminosilicates containing larger alkali cations (Kriven *et al.* 2006) would be desirable. The solubility of CsOH in water at room temperature is around 27 m (~400g CsOH/100 mL H₂O) (Bick and Prinz 2005), so precipitation of CsOH or its hydrates is unlikely to be problematic in geopolymer synthesis.

The immobilisation of radioactive caesium in geopolymers has been relatively widely studied (Khalil and Merz 1994, Bao *et al.* 2005, Fernández-Jiménez *et al.* 2005, Perera *et al.* 2006, Blackford *et al.* 2007), but with one notable exception (Berger *et al.* 2007) this has generally been as a minor component in mixed-alkali systems. The other studies of pure caesium aluminosilicate geopolymers have been designed around X-ray scattering studies, where the fact that it provides very good X-ray contrast in a matrix of lighter elements such as Al and Si has been utilised to give detailed information (Provis 2006, Bell *et al.* 2008).

4.3 Alkali silicate solutions

4.3.1 Solubility and phase equilibria

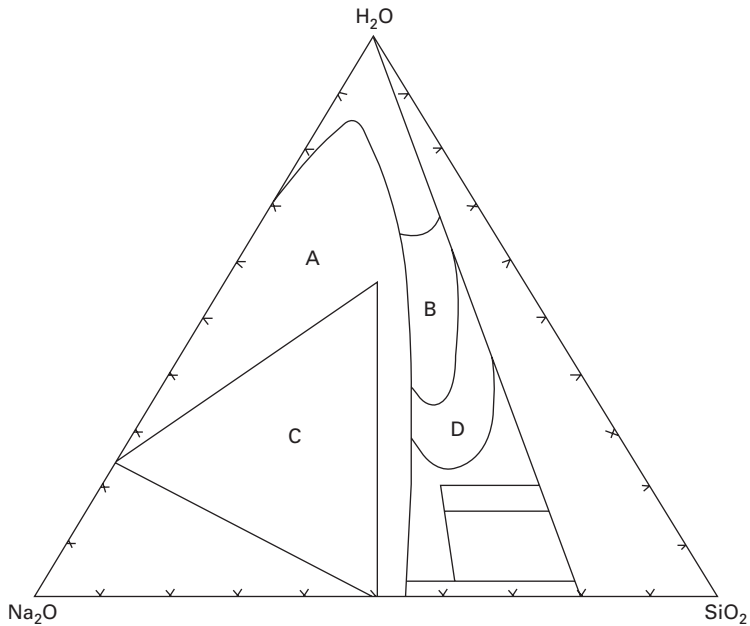
Figure 4.4 shows a portion of the Na₂O-SiO₂-H₂O composition space with crystallisation isotherms at 25°C, plotted from the data of Wills (1950). A full



4.4 Crystallisation isotherms for hydrated sodium metasilicate phases at 25°C and ambient pressure, plotted from the tabulated data of Wills (1950). The phase Na₃HSiO₄·5H₂O, which is reported at relatively high Na₂O and low SiO₂ concentrations, is not depicted.

phase diagram for this system is not easy to determine, due in large part to the formation of metastable aqueous silicate solutions which, if they will ever precipitate, will do so very very slowly (Brown 1990). Further evidence for this is provided by the observation that in the table of 'Typical commercial sodium silicates' given by Weldes and Lange (1969), all the compositions given for common commercially available sodium silicate solutions actually fall in the region in which precipitation of $\text{Na}_2\text{SiO}_3 \cdot 9\text{H}_2\text{O}$ would be expected. Note that the silica concentrations in Fig. 4.4 are plotted on a logarithmic scale, to enable more ready viewing of the data at low silica content. Brown (1990) plotted these data with the axes representing the tenth root of the respective concentrations, to enable the display of isotherm data spanning seven orders of magnitude in the concentration of each component, and that paper should be consulted if a more detailed and/or extensive plot is desired. However, for the purposes of the present discussion of geopolymer activating solutions, the higher-silica region of the diagram is sufficient.

Vail (1952) gives a diagram showing the full ternary Na_2O - SiO_2 - H_2O system at ambient temperature, divided into regions with a brief description of the properties and uses of the materials obtained in each compositional region; Fig. 4.5 is adapted from that source.



4.5 Compositional regions leading to different types of product in the Na_2O - SiO_2 - H_2O system, after Vail (1952). Regions of importance in geopolymer synthesis are discussed in the text.

The regions of Fig. 4.5 that are of primary importance in geopolymer synthesis are region A ('partially crystalline mixtures'; many low-silica activating solutions are metastable compositions in this region) or region B (most commercial silicate solutions fall in this region). Solutions prepared with composition in region C are highly prone to crystallisation, often as hydrated sodium metasilicates as shown in Fig. 4.4, and region D tends to give inconveniently high viscosities. The metastability of activator compositions in region 6 can be clearly shown by the fact that these solutions gradually crystallise if stored for extended periods, or rapidly if the ambient temperature drops. Descriptions of the importance and properties of mixtures in other compositional regions can be found in Vail (1952) or in Weldes and Lange (1969). Similar diagrams for potassium silicate solutions are not widely used; the precipitation of hydrated potassium silicate phases is much less prevalent than in the sodium case, and the stability range of the homogeneous aqueous solution is much wider.

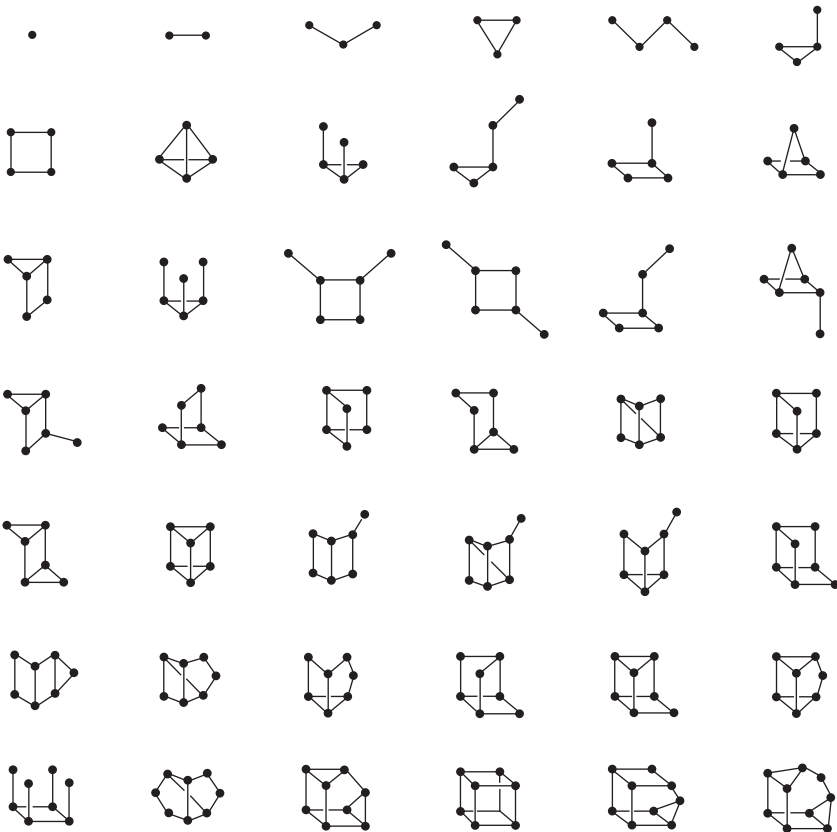
Lithium silicate solutions are discussed briefly by Vail (1952) and by Iler (1979). Lithium silicate preparation is hindered by the low solubility of hydrated lithium metasilicate phases, particularly at elevated temperature (Vail 1952), although commercially viable techniques for the production of these solutions have been developed. Where sodium and potassium silicates are usually prepared by direct dissolution into water of glasses of appropriate composition, lithium silicate is instead generated by dissolution of amorphous silica into aqueous LiOH (Iler 1979). Rubidium and caesium silicate solutions, similar to the potassium case, are not subject to such issues as the solubility of their respective metasilicate phases is very high. Rubidium silicates are discussed briefly by Vail (1952); Weldes and Lange (1969) comment that rubidium and caesium silicate solutions 'have been made but not studied extensively and at present have no commercial importance', a situation which appears not to have changed in the four decades since that review was written.

4.3.2 Speciation

The chemistry (aqueous and solid-state) of silica is probably more complex than that of any other element other than carbon, and as such is relatively poorly understood from a fundamental standpoint. In concentrated alkaline solutions, silica polymerises into an array of small species, the identities and structures of several of which are only now being resolved. ^{29}Si NMR in its various forms has proven to be an invaluable tool in identifying the species present in silicate solutions (Engelhardt *et al.* 1974, Harris and Knight 1983a, 1983b, Cho *et al.* 2006, Knight *et al.* 2007), and useful information has also recently been obtained by mass spectroscopy (Pelster *et al.* 2006). Infrared spectroscopy has also been used (Halasz *et al.* 2007), but the

interpretation of spectral features remains uncertain and at present does not always correlate well with the results of NMR experiments. The isolation and attempted quantification of silicate species by extraction as trimethylsilyl or silicomolybdate compounds was popular prior to the widespread availability of advanced spectroscopic techniques (Lentz 1964, Ray and Plaisted 1983, Dietzel and Usdowski 1995). However, the required chemical processing (in particular acidification) is likely to cause severe disruption to the structures of the species present, and these techniques have largely fallen out of favour for analysis of speciation in concentrated alkaline solutions.

Figure 4.6 shows some of the structures that are known to exist in alkaline silicate solutions, as identified by high-resolution two-dimensional NMR



4.6 Species identified by ^{29}Si NMR of alkaline silicate solutions. Lines represent Si-O-Si bonds and dots are Si atoms, all Si sites are tetrahedral, and hydroxyl groups are not shown. Where multiple stereoisomers of a species are possible, only one is depicted. Species shown are those identified by Knight *et al.* (2007) in ^{29}Si -enriched potassium silicate solutions.

study of isotopically enriched solutions (Knight *et al.* 2007). There are other species postulated by some researchers to take place in the formation of specific zeolite structure types (Kirschhock *et al.* 1999), but the existence of many of these is controversial (Knight and Kinrade 2002, Knight *et al.* 2006) and is beyond the scope of this review. The equilibria between a selected representative subset of these species are able to be represented by a free energy minimisation model using the Pitzer activity coefficient framework (Provis *et al.* 2005a). Tetrahedral sites within silicate species (and solid structures) are denoted Q^n , where n is the number of bonds to other tetrahedral sites; so a silicate monomer $\text{Si}(\text{OH})_4$ is denoted Q^0 , and a fully coordinated site is Q^4 . In aluminosilicate structures, the notation is also extended to describe the numbers of Si-O-Al bonds; for example, a $Q^3(2\text{Al})$ site hosts two Si-O-Al bonds, one Si-O-Si bond and one Si-O-H bond.

Aluminium substitution into these silicate oligomers where dissolved Al is present appears to be widespread; although detailed characterisation of Al populations in each of the species depicted above has not been carried out, the consensus appears to be that Al can replace Si in essentially all of the species depicted in Fig. 4.3 (Swaddle *et al.* 1994, Swaddle 2001), with a preference towards being located in more highly coordinated sites at high Al concentration, and towards lower coordination at lower Al concentration (Samadi-Maybodi *et al.* 2005). The process of resolving and assigning peaks in the ^{27}Al NMR spectra of aluminosilicate solutions is, however, far from simple (Samadi-Maybodi *et al.* 2001).

In the context of geopolymerisation, the most important aspect of the existence of a distribution of silicate species is the variability in lability between the different species present. This was noted initially by Engelhardt and Hoebbel (1984), who proposed that the cyclic trimer and the prismatic hexamer were notably slower to exchange silicate units than were chain structures or larger rings. However, the work of Knight *et al.* (1988) using enriched silicate solutions found that the cyclic trimer showed a particularly rapid intramolecular ring opening/closing reaction. The other exchange processes identified in this paper were all either intramolecular rearrangements or involved exchange of monomers. Bahlmann *et al.* (1997) found that on a timescale of approximately 0.1s, mixing was only observed between sites of connectivity n with those of connectivity $n - 1$ or $n + 1$; i.e., the connectivity of a given site did not change by more than one bond within this timeframe. The cubic octamer is also known to be particularly stable in tetraalkylammonium silicate solutions (Caratzoulas *et al.* 2005), but this is most likely due to effects specific to the geometry of the tetraalkylammonium cations, as this species does not account for such a significant fraction of the dissolved species formed in the presence of alkali cations. Vallazza *et al.* (1998) obtained rate constants for reactions involving exchange of silicate units between small species, and later work from the same research group

(North and Swaddle 2000, Anseau *et al.* 2005) showed that aluminate sites are significantly more labile than their silicate counterparts.

It has been proposed that the species which dominate silicate exchange kinetics are monomers carrying a low density of deprotonated hydroxyl sites (Kinrade and Swaddle 1988). Highly charged species will obviously repel each other, hindering exchange, and exchange processes involving larger oligomers will require the breakage and formation of a greater number of bonds than those involving monomers. Provis and Vlachos (2006) proposed a kinetic model for silica polymerisation where the main reaction was between either a neutral monomer and a charged site on an oligomer, or a deprotonated monomer and a neutral site on an oligomer. Reactions between two charged sites, or involving multiple-deprotonated sites, were not considered to be significant, consistent with the observation of Kinrade and Swaddle (1988) that silicate exchange processes become greatly slowed at very high pH. This model was able to qualitatively capture the effect of various parameters on clear-solution zeolite synthesis, and so may prove to be of some value in understanding analogous processes taking place during geopolymerisation.

Pelster *et al.* (2007) have recently shown, via a very elegant set of experiments, that exchange processes in isotopically labelled solutions containing a high proportion of cubic octamers can involve exchange of entire cube faces rather than monomers. However, this is a special case providing a counterexample to the general trend of exchange via smaller species. Bahlmann *et al.* (1997) also showed a marked trend in self-diffusion coefficients, which decrease with increasing oligomer size; this may also be significant in determining exchange rates in the highly viscous environment of a concentrated alkali silicate solution.

Operating in parallel with the effects of silicate oligomer formation in concentrated solutions are acid-base reactions. Monomeric silica, $\text{Si}(\text{OH})_4$, is also known as ‘orthosilicic acid,’ and behaves as a polyprotic weak acid under alkaline conditions. Approximate pK_a values of the silicate monomer (4 acidic protons) and dimer (6 acidic protons) were calculated by efčik and McCormick (1997) assuming a linear progression in pK_a with increasing extent of deprotonation for the higher charge states where direct measurements are very difficult, and the values obtained are given here in Table 4.1.

Geopolymer activating solutions generally fall in the range 1–10 *m* MOH (M: alkali metal), and 1–10 *m* SiO_2 . From Table 4.1, it can be seen that the majority of the silicate sites present in these solutions will be deprotonated either once or twice (i.e. $n = 1$ or 2 for the monomer, between 1 and 4 for the dimer), depending on the exact $\text{SiO}_2/\text{M}_2\text{O}$ ratio selected. Obviously, Q^3 sites can only undergo a single deprotonation; Rimer *et al.* (2005) calculated an effective pK_2 of 11.2 for Q^3 sites in larger silicate clusters, but this also includes electrostatic repulsion effects due to the localisation of charges on a cluster. An intrinsic pK_a of 8.4 for hydroxyl protons on Q^3 sites was

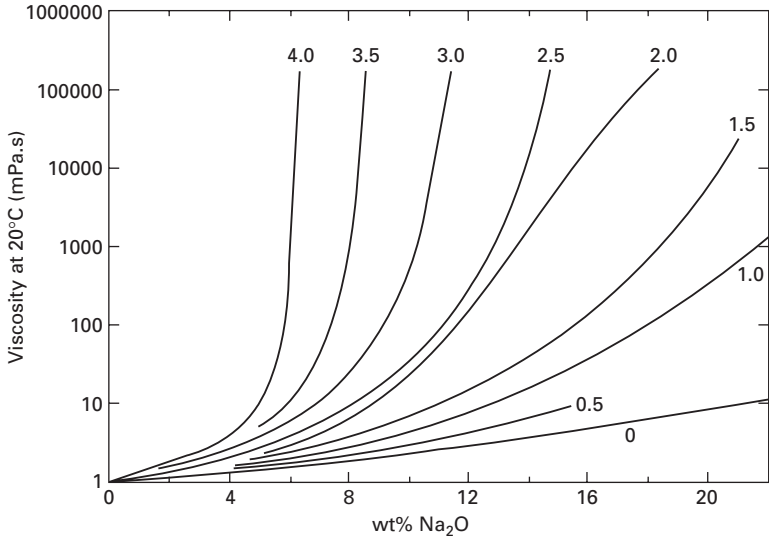
Table 4.1 Equilibrium constants for the successive deprotonations of the silicate monomer and dimer

Reaction	<i>n</i>					
	1	2	3	4	5	6
$\text{SiO}_{n-1}(\text{OH})_{5-n} \rightleftharpoons \text{SiO}_n(\text{OH})_{4-n} + \text{H}^+$	9.5	12.6	15.7	18.8	–	–
$\text{Si}_2\text{O}_n(\text{OH})_{7-n} \rightleftharpoons \text{Si}_2\text{O}_{n+1}(\text{OH})_{6-n} + \text{H}^+$	9.0	10.7	12.4	14.1	15.8	17.5

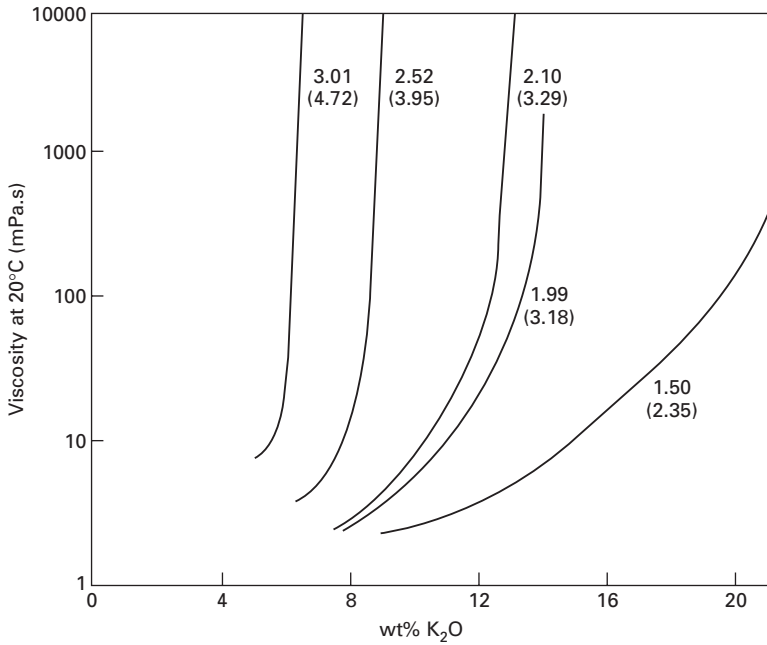
calculated via a model accounting directly for these effects, and appears to better represent their actual behaviour. Taking into account the distribution of species present and their respective pK_a values, most silicate activating solutions used in geopolymerisation are buffered at approximately pH 11–12 by the silicate deprotonation equilibria, and yet can provide a much higher level of ‘available alkalinity’ when compared to hydroxide solutions at the same pH due to the buffering effect providing a ready source of basic species. Obviously, the hydroxide activating solutions discussed in Section 4.2 will have a higher pH than this prior to mixing with the solid geopolymer source materials, but the dissolution of even a small amount of silica into such a solution will rapidly bring the pH into this region during the reaction process. As the reaction nears completion and the majority of the silica precipitates from the remaining aqueous phase (which is, by this point, the pore solution of a hardened geopolymer), the pH will increase again due to the removal of this buffering effect.

4.3.3 Engineering properties

Figures 4.7 and 4.8 present the viscosities of sodium and potassium silicate solutions as a function of composition, showing data obtained from Vail (1952). The data are plotted in terms of mass ratio $\text{SiO}_2/\text{M}_2\text{O}$ (M: alkali metal); this is very close to the molar ratio in sodium silicates, as the ratio of the molecular masses of SiO_2 and Na_2O is 0.97. However, this ratio in the potassium case is 0.64, so the molar ratio corresponding to each mass ratio is marked on Fig. 4.8 to enable comparison with Fig. 4.7. Note that in both figures, viscosities are plotted on a logarithmic scale, and viscosity increases dramatically at higher silica content. Potassium silicate solutions show a markedly lower viscosity than sodium silicates of comparable composition, even accounting for the conversion from mass to mole ratios. This is often of value in the laboratory study of geopolymers, where the higher cost of potassium silicate solutions is less important than in commercial production; when it is desirable to use the lowest possible activator/binder ratio, the more favourable rheology of a potassium-containing activator will make mixing and moulding samples more straightforward. Sodium silicates, particularly in the composition range favoured in geopolymer synthesis, are also very



4.7 Viscosities of sodium silicate solutions with mass ratio $\text{SiO}_2/\text{Na}_2\text{O}$ as marked. Mole ratios are 3% greater than the mass ratios shown. Data from Vail (1952).



4.8 Viscosities of potassium silicate solutions with mass ratio (mole ratio) $\text{SiO}_2/\text{K}_2\text{O}$ as marked. Data from Vail (1952).

much more ‘tacky’ than potassium silicates (Weldes and Lange 1969), which can also be problematic as the fresh sodium-containing geopolymer mixture tends to stick to mixing equipment rather than being easily flowable.

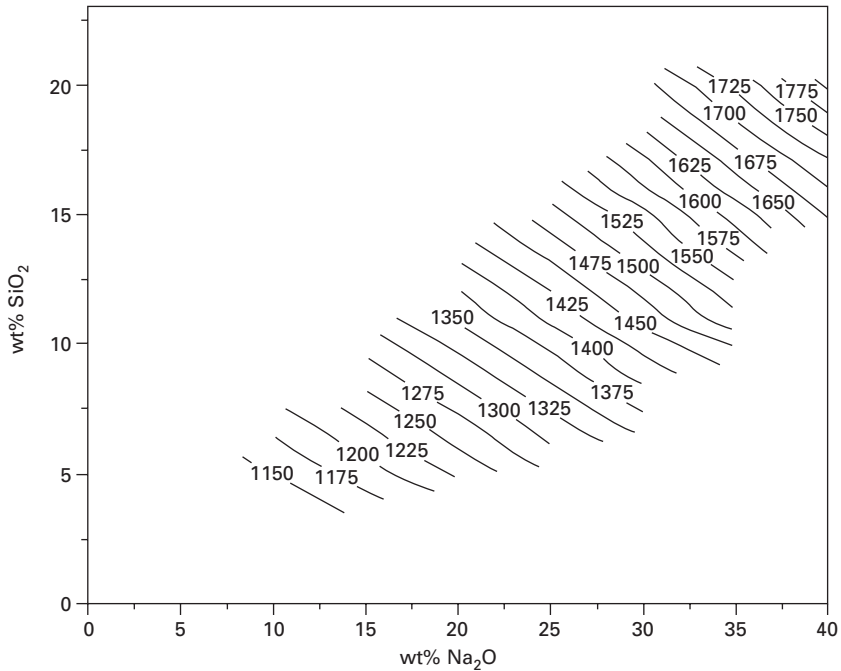
The viscosity behaviour of mixed-alkali silicate solutions is believed to be relatively complex; Vail (1952) noted that some high-silica mixed alkali solutions show a much higher viscosity than either of the pure-alkali solutions that were mixed to produce them. Ingram *et al.* (1981) did not reproduce such an effect at lower silica content and high concentration, although they did observe a subtle mixed-alkali effect in conductivity data at low potassium content. Grant and Masson (1972) showed that the viscosity of sodium silicate solutions over a relatively wide concentration range is independent of shear rate, even at high $\text{SiO}_2/\text{Na}_2\text{O}$ ratio; the oligomerisation of the dissolved silica does not give ‘polymer solution-like’ rheology, most likely because the oligomers tend to be condensed rather than forming extended chains as do organic polymers.

Yang *et al.* (2008b) showed that the viscosity of sodium silicate solutions decreases markedly with increasing temperature, dropping by a factor of approximately 8 upon heating from 20°C to 40°C and then further decreasing above this point. However, the solubility of some sodium metasilicate phases begins to decrease at elevated temperature (Vail 1952), meaning that heating is not a guaranteed way to ensure or accelerate the dissolution of solid precursors during preparation of a geopolymer activating solution. The enthalpy of solution of solid anhydrous sodium metasilicate into concentrated solutions varies strongly as a function of concentration (Vail 1952); the inability of the dissolved species to achieve full hydration at very high concentration means that the heat released per mole of Na_2SiO_3 dissolved into a 40 wt% aqueous solution is significantly lower than at 20 wt%.

Figure 4.9 shows the variation in sodium silicate solution density as a function of composition. Potassium silicates also follow a similar trend, although the data available in the literature are less extensive. The data depicted here are based on the plots given by Vail (1952); densities have been converted into SI units and the data re-plotted. Vail also comments that knowing the density and viscosity of a silicate solution is sufficient to calculate its composition without the need for a chemical analysis, as these properties can be reliably and repeatably measured even for metastable solutions.

4.4 Other activators

Many researchers over the past several decades have addressed the use of alkali carbonate solutions for activation of (generally high-calcium) slags (Shi *et al.* 2006), but their use in the activation of fly ash is much less widespread. Fernández-Jiménez *et al.* (2006) report that the use of mixed hydroxide-



4.9 Density of sodium silicate solutions as a function of composition. Data from Vail (1952).

carbonate activating solutions gives a poorly reacted, porous product, but it is not clear what is the specific contribution of the carbonate component of the activating solution. It appears that the generally lower reactivity of Class F fly ashes compared to slags means that a higher level of available alkalinity is required than can be supplied by a carbonate solution, and so a stronger base than M_2CO_3 (M: Na and/or K) is required.

There have also been a handful of studies on the use of sodium aluminate as an activator in geopolymer synthesis. In particular, Phair and van Deventer (2002) and Rees (2007) each produced viable geopolymers by activation of fly ash with aqueous sodium aluminate, while Brew and MacKenzie (2007) used aqueous sodium aluminate and silica fume to produce a high-purity aluminosilicate geopolymer. There has also been some work aimed at the use of solid sodium aluminate in ‘just add water’-type one-part mix geopolymers, using solid geothermal silica as a silicate source (Hajimohammadi *et al.* 2008, Rees 2007), although this is still at the early development stage and is probably most useful as a system for scientific investigation of reaction mechanisms rather than large-scale utilisation due to the difficulty of scaling-up the process.

Some recent work has also been conducted on alternative methods of achieving a just-add-water geopolymer mix; either by mixing a sufficiently

finely milled solid sodium silicate with fly ash (Yang *et al.* 2008a) or by calcining metakaolin together with an alkali hydroxide powder (Koloušek *et al.* 2007). Further investigations into each of these methods would definitely appear justified, considering the difficulties associated with the handling of concentrated caustic activating solutions as discussed in the earlier parts of this chapter.

4.5 Conclusions

Various different types of solutions have been used as activators in geopolymer synthesis, and the chemical and physical properties of each will play a role in determining the properties and value of geopolymers synthesised using them. Sodium and potassium silicate and hydroxide are the most commonly used activating solutions, with sodium-based solutions being less expensive, but potassium-based solutions displaying more favourable phase behaviour and rheology. Alternative activating solutions include carbonates, aluminates and even water, but none of these have seen widespread use in the synthesis of aluminosilicate geopolymers to date. Future work needs to focus particularly on interactions between silicate activating solutions and dissolved calcium; this is an area which remains poorly understood but which is critical to the early-age properties and later structure development of fly ash-based geopolymers.

4.6 References

- Anseau, M. R., Leung, J. P., Sahai, N. and Swaddle, T. W. (2005) Interaction of silicate ions with zinc(II) and aluminum(III) in alkaline aqueous solution. *Inorganic Chemistry*, 44, 8023–8032. doi:10.1021/ic050594c.
- Bahlmann, E. K. F., Harris, R. K., Metcalfe, K., Rockliffe, J. W. and Smith, E. G. (1997) Silicon-29 NMR self-diffusion and chemical-exchange studies of concentrated sodium silicate solutions. *Journal of the Chemical Society – Faraday Transactions*, 93, 93–98. doi:10.1039/a604878a.
- Bao, Y., Grutzeck, M. W. and Jantzen, C. M. (2005) Preparation and properties of hydroceramic waste forms made with simulated Hanford low-activity waste. *Journal of the American Ceramic Society*, 88, 3287–3302. doi:10.1111/j.1551-2916.2005.00775.x.
- Bell, J. L., Sarin, P., Provis, J. L., Haggerty, R. P., Driemeyer, P. E., Chupas, P. J., van Deventer, J. S. J., Kriven, W. M. (2008) Atomic structure of a cesium aluminosilicate geopolymer: A pair distribution function study, *Chemistry of Materials*, 20(14), 4768–4776. doi 10.1021/cm703369s.
- Berger, S., Frizon, F., Fournel, V. and Cau-Dit-Comes, C. (2007) Immobilization of cesium in geopolymeric matrix: A formulation study. *12th International Congress on the Chemistry of Cement*, Montreal, Canada, Beaudoin, J. J. (Ed.).
- Bick, M. and Prinz, H. (2005) Cesium and cesium compounds. *Ullmann's Encyclopedia of Industrial Chemistry*. Wiley-VCH Verlag. doi:10.1002/14356007.a06_153.

- Blackford, M. G., Hanna, J. V., Pike, K. J., Vance, E. R. and Perera, D. S. (2007) Transmission electron microscopy and nuclear magnetic resonance studies of geopolymers for radioactive waste immobilization. *Journal of the American Ceramic Society*, 90, 1193–1199. doi:10.1111/j.1551-2916.2007.01532.x.
- Brew, D. R. M. and Mackenzie, K. J. D. (2007) Geopolymer synthesis using silica fume and sodium aluminate. *Journal of Materials Science*, 42, 3990–3993. doi:10.1007/s10853-006-0376-1.
- Brown, P. W. (1990) The system $\text{Na}_2\text{O}-\text{CaO}-\text{SiO}_2-\text{H}_2\text{O}$. *Journal of the American Ceramic Society*, 73, 3457–3561. doi:10.1111/j.1151-2916.1990.tb06475.x.
- Caratzoulas, S., Vlachos, D. G. and Tsapatsis, M. (2005) Molecular dynamics studies on the role of tetramethylammonium cations in the stability of the silica octamers $\text{Si}_8\text{O}_{20}^{8-}$ in solution. *Journal of Physical Chemistry B*, 109, 10429–10434. doi:10.1021/jp0500891.
- Cheng, C.-H. and Shantz, D. F. (2006) ^{29}Si NMR studies of zeolite precursor solutions. *Journal of Physical Chemistry B*, 110, 313–318. doi:10.1021/jp055124i.
- Cho, H., Felmy, A. R., Craciun, R., Keenum, J. P., Shah, N. and Dixon, D. A. (2006) Solution state structure determination of silicate oligomers by ^{29}Si NMR spectroscopy and molecular modeling. *Journal of the American Chemical Society*, 128, 2324–2335. doi:10.1021/ja0559202.
- Dietzel, M. and Usdowski, E. (1995) Depolymerization of soluble silicate in dilute aqueous solutions. *Colloid and Polymer Science*, 273, 590–597. doi:10.1007/BF00658690.
- Duxson, P., Mallicoat, S. W., Lukey, G. C., Kriven, W. M. and Van Deventer, J. S. J. (2007) The effect of alkali and Si/Al ratio on the development of mechanical properties of metakaolin-based geopolymers. *Colloids and Surfaces A – Physicochemical and Engineering Aspects*, 292, 8–20. doi:10.1016/j.colsurfa.2006.05.044.
- Engelhardt, G. and Hoebbel, D. (1984) ^{29}Si NMR spectroscopy reveals dynamic SiO_4^{4-} group exchange between silicate anions in aqueous alkaline silicate solutions. *Journal of the Chemical Society – Chemical Communications*, 514–516. doi:10.1039/C39840000514.
- Engelhardt, G., Jancke, H., Hoebbel, D. and Wiek, W. (1974) Strukturuntersuchungen an Silikatanionen in wässriger Lösung mit Hilfe der ^{29}Si -NMR-Spektroskopie. *Zeitschrift für Chemie*, 14, 109–110.
- Fernández-Jiménez, A., Macphee, D. E., Lachowski, E. E. and Palomo, A. (2005) Immobilization of cesium in alkaline activated fly ash matrix. *Journal of Nuclear Materials*, 346, 185–193. doi:10.1016/j.jnucmat.2005.06.006.
- Fernández-Jiménez, A., Palomo, A. and Criado, M. (2006) Alkali activated fly ash binders. A comparative study between sodium and potassium activators. *Materiales de Construcción*, 56, 51–65.
- Fricke, R. (1924) Zähigkeit von Rubidiumhydroxydlösungen. *Zeitschrift für Anorganische und Allgemeine Chemie*, 139, 419–420. doi:10.1002/zaac.19241390126.
- Gaboriaud, F., Nonat, A., Chaumont, D., Craievich, A. and Hanquet, B. (1999) ^{29}Si NMR and small-angle X-ray scattering studies of the effect of alkaline ions (Li^+ , Na^+ , and K^+) in silico-alkaline sols. *Journal of Physical Chemistry B*, 103, 2091–2099. doi:10.1021/jp984074x.
- García-Lodeiro, I., Palomo, A. and Fernández-Jiménez, A. (2007) Alkali-aggregate reaction in activated fly ash systems. *Cement and Concrete Research*, 37, 175–183. doi:10.1016/j.cemconres.2006.11.002.
- Grant, R. and Masson, C. R. (1972) Viscosity of sodium silicate solutions. *Journal of Colloid and Interface Science*, 41, 606–607. doi:10.1016/0021-9797(72)90383-9.

- Gurvich, L. V., Bergman, G. A., Gorokhov, L. N., Iorish, V. S., Leonidov, V. Y. and Yungman, V. S. (1996) Thermodynamic properties of alkali metal hydroxides. Part 1. Lithium and sodium hydroxides. *Journal of Physical and Chemical Reference Data*, 25, 1211–1276.
- Gurvich, L. V., Bergman, G. A., Gorokhov, L. N., Iorish, V. S., Leonidov, V. Y. and Yungman, V. S. (1997) Thermodynamic properties of alkali metal hydroxides. Part 2. Potassium, rubidium, and cesium hydroxides. *Journal of Physical and Chemical Reference Data*, 26, 1031–1110.
- Hajimohammadi, A., Provis, J. L. and Van Deventer, J. S. J. (2008) One-part geopolymer mixes from geothermal silica and sodium aluminate. *Industrial & Engineering Chemistry Research*, 47, 9396–9405. doi: 10.1021/ie8006825.
- Halasz, I., Agarwal, M., Li, R. and Miller, N. (2007) Vibrational spectra and dissociation of aqueous Na_2SiO_3 solutions. *Catalysis Letters*, 117, 34–42. doi:10.1007/s10562-007-9141-6.
- Harris, R. K. and Knight, C. T. G. (1983a) Silicon-29 nuclear magnetic resonance studies of aqueous silicate solutions. Part 5. First-order patterns in potassium silicate solutions enriched with silicon-29. *Journal of the Chemical Society – Faraday Transactions II*, 79, 1525–1538. doi:10.1039/F29837901525.
- Harris, R. K. and Knight, C. T. G. (1983b) Silicon-29 nuclear magnetic resonance studies of aqueous silicate solutions. Part 6. Second-order patterns in potassium silicate solutions enriched with silicon-29. *Journal of the Chemical Society – Faraday Transactions II*, 79, 1539–1561. doi:10.1039/F29837901539.
- Iler, R. K. (1979) *The Chemistry of Silica: Solubility, Polymerization, Colloid and Surface Properties, and Biochemistry*, New York, Wiley.
- Ingram, M. D., King, K., Kranbuehl, D. and Adel-Hadadi, M. (1981) Mixed-alkali effect in aqueous silicate solutions. *Journal of Physical Chemistry*, 85, 289–294. doi:10.1021/j150603a015.
- Khalil, M. Y. and Merz, E. (1994) Immobilization of intermediate-level wastes in geopolymers. *Journal of Nuclear Materials*, 211, 141–148. doi:10.1016/0022-3115(94)90364-6.
- Kinrade, S. D. and Swaddle, T. W. (1988) Silicon-29 NMR studies of aqueous silicate solutions. 2. Transverse ^{29}Si relaxation and the kinetics and mechanism of silicate polymerization. *Inorganic Chemistry*, 27, 4259–4264. doi:10.1021/ic00296a035.
- Kirschhock, C. E. A., Ravishankar, R., Verspeurt, F., Grobet, P. J., Jacobs, P. A. and Martens, J. A. (1999) Identification of precursor species in the formation of MFI zeolite in the TPAOH-TEOS- H_2O system. *Journal of Physical Chemistry B*, 103, 4965–4971. doi:10.1021/jp990297r.
- Knight, C. T. G. and Kinrade, S. D. (2002) Comment on ‘Identification of precursor species in the formation of MFI zeolite in the TPAOH-TEOS- H_2O system’. *Journal of Physical Chemistry B*, 106, 3329–3332. doi:10.1021/jp012286f.
- Knight, C. T. G., Kirkpatrick, R. J. and Oldfield, E. (1988) Two-dimensional silicon-29 nuclear magnetic resonance spectroscopic study of chemical exchange pathways in potassium silicate solutions. *Journal of Magnetic Resonance*, 78, 31–40. doi:10.1016/0022-2364(88)90154-0.
- Knight, C. T. G., Wang, J. and Kinrade, S. D. (2006) Do zeolite precursor species really exist in aqueous synthesis media? *Physical Chemistry Chemical Physics*, 8, 3099–3103. doi:10.1039/b606419a.
- Knight, C. T. G., Balec, R. J. and Kinrade, S. D. (2007) The structure of silicate anions in aqueous alkaline solutions. *Angewandte Chemie – International Edition*, 46, 8148–8152. doi:10.1002/anie.200702986.

- Koloušek, D., Brus, J., Urbanova, M., Andertova, J., Hulinsky, V. and Vorel, J. (2007) Preparation, structure and hydrothermal stability of alternative (sodium silicate-free) geopolymers. *Journal of Materials Science*, 42, 9267–9275. doi:10.1007/s10853-007-1910-5.
- Kriven, W. M., Kelly, C. A. and Comrie, D. C. (2006) *Geopolymers for structural ceramic applications*. Air Force Office of Scientific Research Report FA9550–04-C-0063.
- Kurt, C. and Bittner, J. (2006) Sodium hydroxide. *Ullmann's Encyclopedia of Industrial Chemistry*. Wiley-VCH Verlag. doi:10.1002/14356007.a24_345.pub2.
- Laliberté, M. (2007) Model for calculating the viscosity of aqueous solutions. *Journal of Chemical and Engineering Data*, 52, 321–335. doi:10.1021/jc0604075.
- Lenk, W. and Prinz, H. (2005) Rubidium and rubidium compounds. *Ullmann's Encyclopedia of Industrial Chemistry*. Wiley-VCH Verlag. doi:10.1002/14356007.a23_473.
- Lentz, C. W. (1964) Silicate minerals as sources of trimethylsilyl silicates and silicate structure analysis of sodium silicate solutions. *Inorganic Chemistry*, 3, 574–579. doi:10.1021/ic50014a029.
- Li, K.-L., Huang, G.-H., Jiang, L.-H., Cai, Y.-B., Chen, J. and Ding, J.-T. (2006) Study on abilities of mineral admixtures and geopolymer to restrain ASR. *Key Engineering Materials*, 302–303, 248–254.
- Lumley, J. S. (1997) ASR suppression by lithium compounds. *Cement and Concrete Research*, 27, 235–244. doi:10.1016/S0008-8846(97)00003-3.
- Mccormick, A. V. and Bell, A. T. (1989) The solution chemistry of zeolite precursors. *Catalysis Reviews – Science and Engineering*, 31, 97–127.
- Monnin, C. and Dubois, M. (2005) Thermodynamics of the LiOH+H₂O system. *Journal of Chemical and Engineering Data*, 50, 1109–1113. doi:10.1021/jc0495482.
- North, M. R. and Swaddle, T. W. (2000) Kinetics of silicate exchange in alkaline aluminosilicate solutions. *Inorganic Chemistry*, 39, 2661–2665. doi:10.1021/ic0000707.
- Pabalan, R. T. and Pitzer, K. S. (1987) Thermodynamics of NaOH(aq) in hydrothermal solutions. *Geochimica et Cosmochimica Acta*, 51, 829–837. doi:10.1016/0016-7037(87)90096-2.
- Pelster, S. A., Schrader, W. and Schüth, F. (2006) Monitoring temporal evolution of silicate species during hydrolysis and condensation of silicates using mass spectrometry. *Journal of the American Chemical Society*, 128, 4310–4317. doi:10.1021/ja057423r.
- Pelster, S. A., Weimann, B., Schaak, B. B., Schrader, W. and Schüth, F. (2007) Dynamics of silicate species in solution studied by mass spectrometry with isotopically labeled compounds. *Angewandte Chemie – International Edition*, 46, 6674–6677. doi:10.1002/anie.200701927.
- Perera, D. S., Vance, E. R., Aly, Z., Davis, J. and Nicholson, C. L. (2006) Immobilization of Cs and Sr in geopolymers with Si/Al ~ 2. *Ceramic Transactions*, 176, 91–96.
- Petrenko, S. V. and Pitzer, K. S. (1997) Thermodynamics of aqueous NaOH over the complete composition range and to 523 K and 400 MPa. *Journal of Physical Chemistry B*, 101, 3589–3595. doi:10.1021/jp963707+.
- Phair, J. W. and Van Deventer, J. S. J. (2002) Characterization of fly-ash-based geopolymeric binders activated with sodium aluminate. *Industrial and Engineering Chemistry Research*, 41, 4242–4251. doi:10.1021/ie010937o.
- Pickering, S. U. (1893) The hydrates of sodium, potassium and lithium hydroxides. *Journal of the Chemical Society, Transactions*, 63, 890–909. doi: 10.1039/CT8936300890.
- Provis, J. L. (2006), Ph.D. Thesis, Department of Chemical and Biomolecular Engineering, University of Melbourne.

- Provis, J. L. and Vlachos, D. G. (2006) Silica nanoparticle formation in the TPAOH-TEOS-H₂O system: A population balance model. *Journal of Physical Chemistry B*, 110, 3098–3108. doi:10.1021/jp056658m.
- Provis, J. L., Duxson, P., Lukey, G. C., Separovic, F., Kriven, W. M. and Van Deventer, J. S. J. (2005a) Modeling speciation in highly concentrated alkaline silicate solutions. *Industrial and Engineering Chemistry Research*, 44, 8899–8908. doi:10.1021/ie050700i.
- Provis, J. L., Lukey, G. C. and Van Deventer, J. S. J. (2005b) Do geopolymers actually contain nanocrystalline zeolites? – A reexamination of existing results. *Chemistry of Materials*, 17, 3075–3085. doi:10.1021/cm050230i.
- Ray, N. H. and Plaisted, R. J. (1983) The constitution of aqueous silicate solutions. *Journal of the Chemical Society – Dalton Transactions*, 475–481. doi:10.1039/DT9830000475.
- Rees, C. A. (2007), PhD Thesis, Department of Chemical and Biomolecular Engineering, University of Melbourne.
- Rimer, J. D., Lobo, R. F. and Vlachos, D. G. (2005) Physical basis for the formation and stability of silica nanoparticles in basic solutions of monovalent cations. *Langmuir*, 21, 8960–8971. doi:10.1021/la0511384.
- Samadi-Maybodi, A., Azizi, S. N., Naderi-Manesh, H., Bijanzadeh, H., Mckeag, I. H. and Harris, R. K. (2001) Highly resolved ²⁷Al NMR spectra of aluminosilicate solutions. *Journal of the Chemical Society – Dalton Transactions*, 633–638. doi:10.1039/b008718l.
- Samadi-Maybodi, A., Goudarzi, N. and Bijanzadeh, H. (2005) Aluminum-27 NMR investigations of aqueous and methanolic aluminosilicate solutions. *Journal of Solution Chemistry*, 34, 283–295. doi:10.1007/s10953-005-3049-9.
- efčík, J. and McCormick, A. V. (1997) Thermochemistry of aqueous silicate solution precursors to ceramics. *AIChE Journal*, 43, 2773–2784.
- Shi, C., Krivenko, P. V. and Roy, D. M. (2006) *Alkali-Activated Cements and Concretes*, Abingdon, UK, Taylor and Francis.
- Simonson, J. M., Mesmer, R. E. and Rogers, P. S. Z. (1989) The enthalpy of dilution and apparent molar heat capacity of NaOH(aq) to 523 K and 40 MPa. *Journal of Chemical Thermodynamics*, 21, 561–584. doi:10.1016/0021-9614(89)90172-9
- Sipos, P. M., Hefter, G. and May, P. M. (2000) Viscosities and densities of highly concentrated aqueous MOH solutions (M⁺ = Na⁺, K⁺, Li⁺, Cs⁺, (CH₃)₄N⁺) at 25.0 °C. *Journal of Chemical and Engineering Data*, 45, 613–617. doi:10.1021/je000019h.
- Swaddle, T. W. (2001) Silicate complexes of aluminum(III) in aqueous systems. *Coordination Chemistry Reviews*, 219–221, 665–686. doi:10.1016/S0010-8545(01)00362-9.
- Swaddle, T. W., Salerno, J. and Tregloan, P. A. (1994) Aqueous aluminates, silicates, and aluminosilicates. *Chemical Society Reviews*, 23, 319–325. doi:10.1039/CS9942300319.
- Vail, J. G. (1952) *Soluble Silicates: Their Properties and Uses*, New York, Reinhold.
- Vallazza, E., Bain, A. D. and Swaddle, T. W. (1998) Dynamics of silicate exchange in highly alkaline potassium silicate solutions. *Canadian Journal of Chemistry – Revue Canadienne De Chimie*, 76, 183–193. doi:10.1139/cjc-76-2-183.
- Weldes, H. H. and Lange, K. R. (1969) Properties of soluble silicates. *Industrial and Engineering Chemistry*, 61, 29–44. doi:10.1021/ie50712a008.
- Wills, J. H. (1950) A review of the system Na₂O-SiO₂-H₂O. *Journal of Physical and Colloid Chemistry*, 54, 304–310. doi:10.1021/j150477a002.

- Yang, K.-H., Song, J.-K., Ashour, A. F. and Lee, E.-T. (2008a) Properties of cementless mortars activated by sodium silicate. *Construction and Building Materials*, 22, 1981–1989. doi:10.1016/j.conbuildmat.2007.07.003.
- Yang, X., Zhu, W. and Yang, Q. (2008b) The viscosity properties of sodium silicate solutions. *Journal of Solution Chemistry*, 37, 73–83. doi:10.1007/s10953-007-9214-6.

Nanostructure/microstructure of metakaolin geopolymers

J L PROVIS, S L YONG and P DUXSON,
University of Melbourne, Australia

Abstract: This chapter provides discussion of the formation, structure and properties of metakaolin geopolymers. While unlikely to see large-scale utilisation as a construction material due to issues related to high water demand and corresponding drying shrinkage, metakaolin geopolymers display properties that will be of use in some specific applications as well as providing a useful ‘model system’ through which geopolymer chemistry can be better understood.

Key words: geopolymer, metakolin, aluminosilicate, microstructure, nanostructure.

5.1 Introduction

Probably the chemically simplest system in which geopolymers are formed is the alkali hydroxide/silicate activation of metakaolin. In fact, it was to these materials that the term ‘geopolymer’ was initially applied (Davidovits 1982, 1991, 2008), with wider application of this name to materials based on fly ash and other aluminosilicate sources following soon afterwards. The reaction between alkalis and metakaolin at slightly elevated temperatures, to form one or more of a variety of zeolites depending on exact reaction conditions, was well known for a decade or more prior to the introduction of ‘geopolymerisation’ (Barrer and Mainwaring 1972a, 1972b). Metakaolin is also used as a pozzolanic additive to Portland cement concretes, or activated directly by mixing with lime (Sabir *et al.* 2001). The first detailed scientific study of the alkali activation of metakaolin was published in 1992 (Palomo and Glasser 1992), and research has intensified since that time as the value of this system as a model for some chemical aspects of more complex (particularly fly ash-based) geopolymerisation systems has become more evident. The primary focus of this chapter will be on the geopolymerisation of metakaolin and the structure of the products thus formed; the exact extent of the transferability (or otherwise) of this understanding to the study of fly ash geopolymers remains the subject of detailed investigation (van Deventer *et al.* 2007, Lloyd 2008).

The main drawback of metakaolin-based geopolymers for large-scale applications is that the very high surface area and plate-like particle shape

of the metakaolin mean that the water demand of a reacting metakaolin mix is very high. This in turn causes difficulties related to drying shrinkage and cracking, as the excess water (which is not chemically bound to the geopolymer structure) leaves the hardened geopolymer over a period of time. Additionally, the use of any excess of alkali solution can lead to efflorescence issues, which are more pronounced in metakaolin geopolymers than in fly ash-based systems due to the higher alkali content of these materials. Nonetheless, there are situations in which the properties of metakaolin geopolymers are desirable for specific applications, as will be discussed in later sections of this book, and so they do provide genuine 'real-world' value in addition to their use as a model system. Additionally, the reactions involving materials such as calcined paper sludges (containing kaolin), as well as some alternative precursors including clay-rich mining wastes, closely resemble the metakaolin geopolymerisation process.

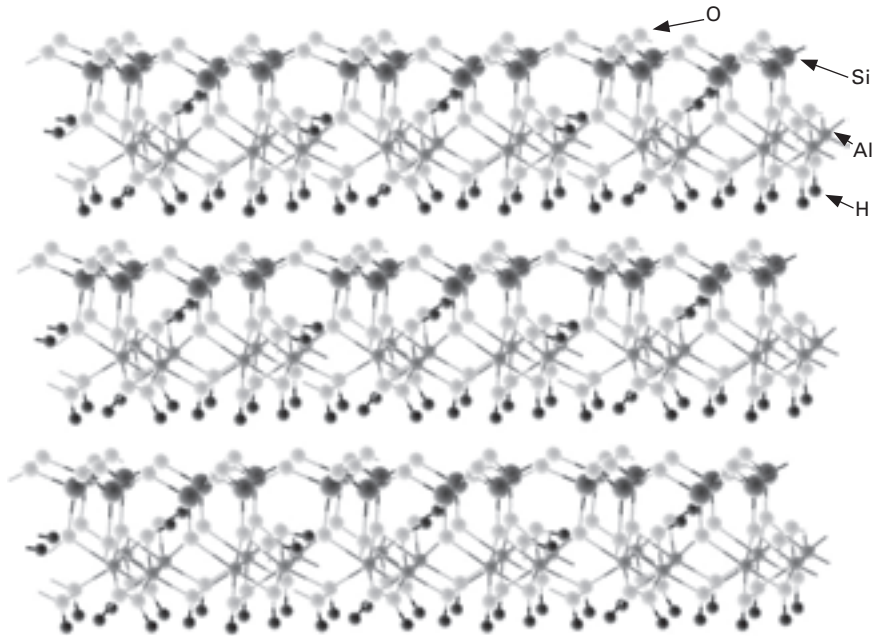
5.2 Metakaolin

Metakaolin is itself a relatively complex material, being generated by calcination of kaolinite clay at temperatures ranging from 500–800°C depending on the purity and crystallinity of the precursor clay (MacKenzie *et al.* 1985, Rocha and Klinowski 1990, Granizo and Blanco 1998, Badogiannis *et al.* 2005, Granizo *et al.* 2007).

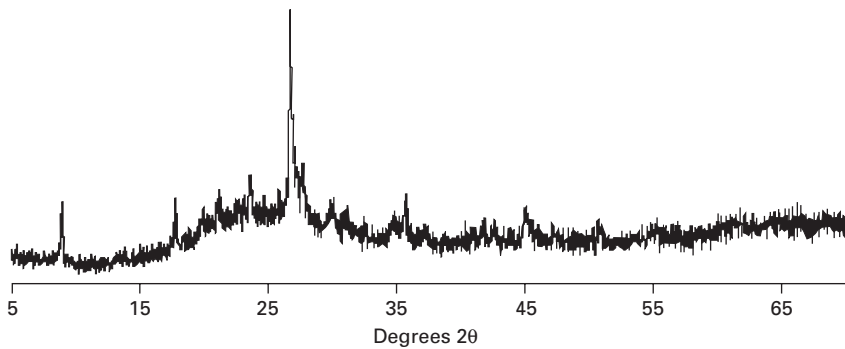
The structure of metakaolin appears disordered to X-ray analysis (Fig. 5.2), although the fact that it is derived by the removal of hydroxyl groups from the layered kaolinite structure (Fig. 5.1) means that at some degree of ordering must remain. This is observed by electron diffraction (Lee *et al.* 2003) and also by the fact that the dehydroxylation process is at least partially reversible (Rocha *et al.* 1990). In essence, metakaolin consists of alternating buckled silicate and aluminate layers, with the silicon in 4-coordination and the aluminium in a mixture of 4-, 5- and 6-coordination.

There has been some debate and speculation regarding the exact roles of each of the three different coordination states of Al with regard to the behaviour of metakaolin in geopolymerisation (Davidovits 2008), but it is generally accepted that the key to the reactivity of metakaolin (as compared to kaolinite) is the strain in the bonding network induced by thermal dehydroxylation. Other means of inducing such strains in clay minerals to render them active in geopolymerisation have been studied recently (MacKenzie *et al.* 2007) and are outlined in some detail in Chapter 14.

The metakaolin sources used in geopolymerisation vary markedly in particle size, purity and in the crystallinity of the kaolinite from which they were derived. Each of these factors is important in the use of metakaolin for geopolymer production, and will mean that it is very unlikely that there will exist a specific 'recipe' which is optimal for geopolymers derived from



5.1 Layered structure of kaolinite. Removal of hydroxyl groups by calcination results in a reduction in Al coordination number and buckling of the layers, with a corresponding loss of long-range order.



5.2 Cu K_{α} diffractogram of a commercial metakaolin (Metastar 402, Imerys, UK). All sharp peaks are attributed to a slight muscovite impurity; the broad peak at 15–35° 2θ is characteristic of the metakaolin structure.

a wide range of sources. The work presented in this chapter is based on one specific metakaolin source, Metastar 402, supplied by Imerys Minerals, UK, which has a molar ratio $\text{SiO}_2/\text{Al}_2\text{O}_3$ of 2.3, a BET surface area of $12.7 \text{ m}^2/\text{g}$, and a mean particle size d_{50} of $1.58 \mu\text{m}$ (Duxson 2006). Also, all activating solutions are formulated according to their $\text{Na}_2\text{O}/\text{SiO}_2$ molar ratio (between 0

and 2), with $H_2O/Na_2O = 11$, and blended with metakaolin stoichiometrically to give an overall Na/Al ratio of 1.

5.3 Formation of metakaolin geopolymers

The process of metakaolin geopolymerisation has been studied by a variety of experimental and modelling techniques over the past two decades. Direct *in situ* observation of geopolymerisation is challenging due to a combination of factors, as will be discussed in detail in Chapter 7 of this book. However, the process may be summarised briefly as follows:

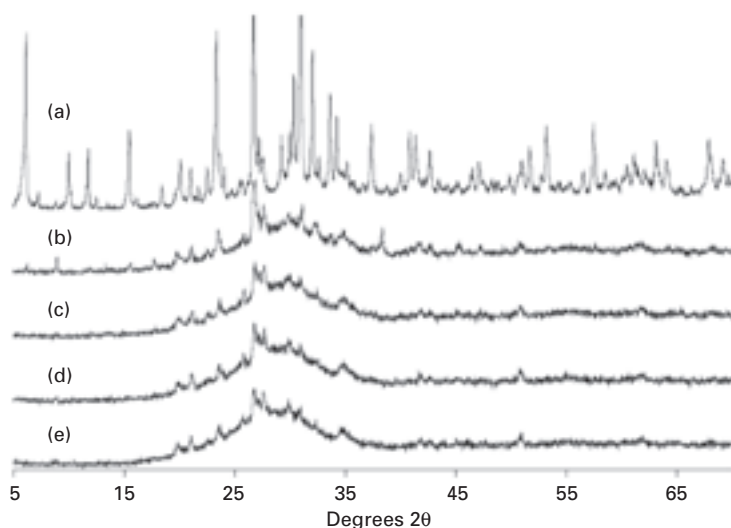
- (1) Alkaline attack on the metakaolin structure results in the release of silicate and aluminate species into solution, with 5- and 6-coordinated Al being converted to 4-coordination upon dissolution (Duxson *et al.* 2005c). It has been proposed that the initial release of Al may be more rapid than that of Si (Weng and Sagoe-Crentsil 2007) – and this may be rationalised by considering the additional lattice strain in the Al layers in the metakaolin compared to the Si layers. Modelling of NMR data produces results consistent with the presence of partially dealuminated remnant metakaolin particles within the hardened geopolymer structure (Provis *et al.* 2005a).
- (2) Interactions between the small dissolved species, and also involving any silicate initially supplied by the activating solution, lead to the formation of aluminosilicate oligomers.
- (3) Dissolution proceeds to the point where the concentration of dissolved aluminate is sufficiently high to destabilise the silicate solution, and precipitation of dissolved species to form a gel commences. This step will also be influenced by factors such as mechanical disruption (shearing or ultrasonication), and also the presence of additional particle surfaces (aggregates and/or other added oxides), which may provide nucleation sites. Note also that dissolution continues while gelation is occurring, meaning that the coating of gel on the particle surfaces will impact the dissolution process by hindering mass transport. This is a primary reason why simple leaching tests are unable to give a full understanding of the dissolution kinetics of metakaolin (Feng *et al.* 2004); reprecipitation of dissolved species complicates such experiments severely.
- (4) Geopolymer gel grows to the point where the reacting slurry solidifies. The time taken for this depends strongly on the mix design and curing temperature, as well as the presence of any contaminants. Setting can be almost instantaneous, or can take a number of days, depending on the mix design and the curing environment. Reaction processes do in fact continue for quite some time after the point of setting, as is evident from ongoing strength development and also the growth of X-ray observable zeolitic crystallites in some samples (Duxson *et al.* 2007b).

This reaction process has been modelled by a coupled set of reaction rate equations (Provis and van Deventer 2007), which will also be outlined in more detail in Chapter 7 of this book. In the case of metakaolin geopolymers, the achievable extent of reaction (i.e., conversion of metakaolin to geopolymer gel) is in many cases quite high, particularly if the samples are cured in sealed moulds at slightly elevated temperature for some period of time. The geopolymer gel will, if maintained warm and sealed, eventually begin to crystallise to form zeolites, most commonly giving relatively simple structure types such as the sodalite, faujasite, gismondine and Linde type A frameworks. This is most notable at lower Si/Al ratios (i.e. more alkaline systems) (Provis *et al.* 2005b), and Fig. 5.3 shows an example of this trend for the case of geopolymers synthesised by reaction of sodium hydroxide/silicate with metakaolin.

5.4 Nanostructure of metakaolin geopolymers

5.4.1 Nuclear magnetic resonance

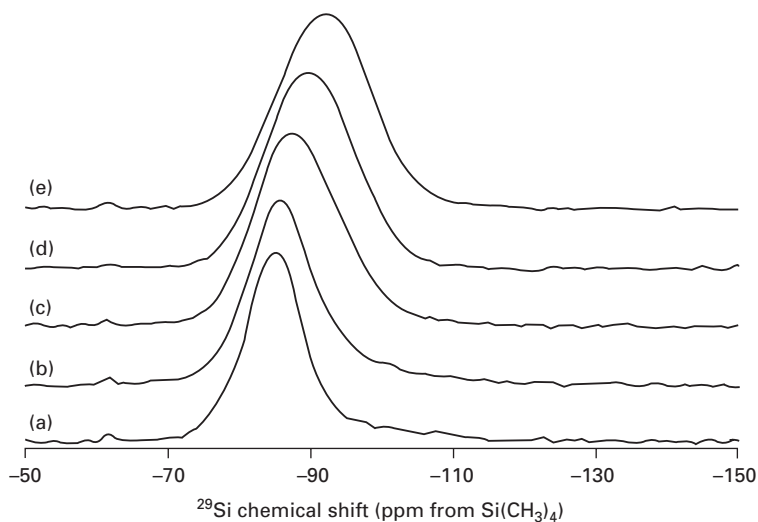
Solid-state magic angle spinning nuclear magnetic resonance spectroscopy (MAS NMR) has proven to be a technique of significant value in the



5.3 $\text{Cu K}\alpha$ X-ray diffractograms of geopolymers synthesised by mixing metakaolin with (a) sodium hydroxide solution, and (b–e) sodium silicate solutions with mole ratios $\text{SiO}_2/\text{Na}_2\text{O} = 0.5, 1.0, 1.5$ and 2.0 respectively. The small sharp peaks common to all samples are due to the muscovite impurity in the metakaolin; sample (a) shows the formation of appreciable crystallinity in the form of faujasite and minor contributions from other zeolites, and (b) also shows slight crystallinity. From Duxson (2006).

investigation of metakaolin geopolymers in particular. While the study of fly ash geopolymers by NMR spectroscopy is often problematic due to the presence of iron in many fly ashes, NMR was one of the first advanced analytical techniques applied to the study of metakaolin geopolymers (Davidovits 1988), and has continued to provide valuable information ever since (Rahier *et al.* 1996a, Barbosa *et al.* 2000, Duxson *et al.* 2005a,b, Singh *et al.* 2005, Duxson *et al.* 2006, Rowles *et al.* 2007).

Figure 5.4 presents ^{29}Si MAS NMR spectra of samples of compositions corresponding to those shown in Fig. 5.3. While the spectra do appear relatively featureless, detailed analysis of peak positions and widths provides insight into the extent of ordering and Si/Al substitution in the geopolymer frameworks (Duxson *et al.* 2005a). Substitution of Al into the silicate network results in a less negative chemical shift (Engelhardt and Michel 1987), and it is clear that, as expected, geopolymers synthesised with a higher Si/Al ratio show a greater extent of Al substitution and a lower distribution of connectivity types $Q^4(n\text{Al})$ (tetrahedral Si surrounded by 4 -OAl bonds and $(4-n)$ -OSi bonds). Deconvolution of these spectra into component peaks (one peak for each value of n) then enables comparison with the expected connectivity distribution computed from statistical thermodynamics (Provis *et al.* 2005a). These comparisons showed that the extent of framework disorder (Si/Al ordering violation) was higher in K-aluminosilicate geopolymers than in Na-aluminosilicate geopolymers. It should also be noted that such deconvolution



5.4 ^{29}Si MAS NMR spectra of geopolymers synthesised by mixing metakaolin with (a) sodium hydroxide solution, and (b–e) sodium silicate solutions with mole ratios $\text{SiO}_2/\text{Na}_2\text{O} = 0.5, 1.0, 1.5$ and 2.0 respectively. Data from Duxson (2006).

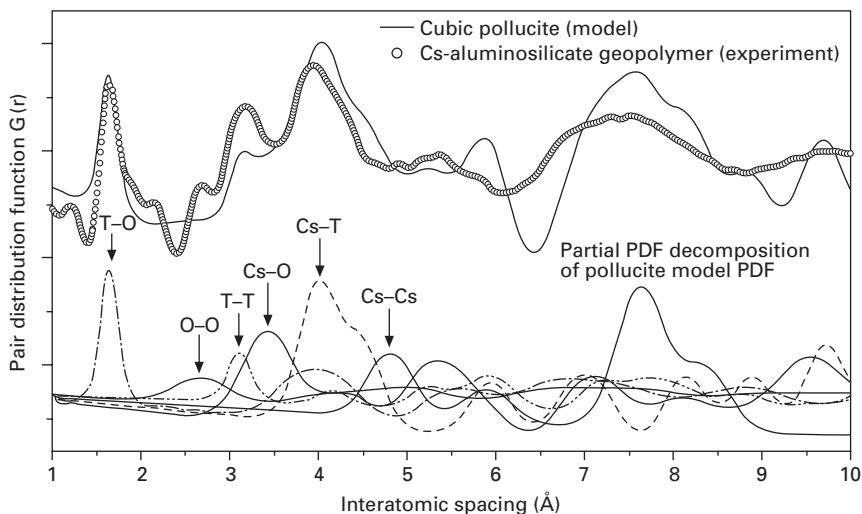
must be adequately constrained if the results are to be meaningful; the calculated Si/Al ratio must match the known Si/Al ratio of the samples, and sufficiently accurate sub-peak positions and widths must be used. Deconvolution also relies on the assumption that all sites within the geopolymer framework are Q^4 (i.e., fully connected to other framework species). This was shown by 2H MAS NMR to be accurate for the stoichiometrically formulated (Na/Al = 1.0) and well-cured samples (20h at 40°C then 2 weeks at room temperature) studied here (Duxson *et al.* 2005c), but provides a limitation on the use of similar methods for partially-cured or non-stoichiometric geopolymer mixes (although this is sometimes attempted regardless, see for example Zhang *et al.* 2008).

Various other nuclei are also useful in NMR studies of metakaolin geopolymers. ^{27}Al MAS NMR gives an indication of the extent of conversion of metakaolin to geopolymer gel, as any residual Al(VI) is clearly evident as distinct from the tetrahedral Al in the geopolymer gel. The quantity of residual Al(VI) as a percentage of all the Al present does not exactly represent the quantity of unreacted metakaolin, as the three different coordination states of Al in metakaolin are expected to react at different rates. However, it provides a useful measure by which a series of samples may be compared (Duxson *et al.* 2005c). Comparison of the ^{23}Na and ^{39}K MAS NMR spectra of mixed-alkali geopolymers at low Si/Al ratio and early age has also been used to show that K^+ is preferentially incorporated into the gel while Na^+ remains solvated for longer (Duxson *et al.* 2005c, 2006). Two-dimensional triple-quantum MAS NMR also provides the opportunity to distinguish various sites which would otherwise overlap each other in a simple MAS spectrum, using quadrupolar nuclei including ^{17}O (Duxson 2006, Duxson *et al.* 2007a) and ^{23}Na (Rowles *et al.* 2007).

5.4.2 X-ray pair distribution function analysis

The NMR spectra of geopolymers generally appear relatively featureless in most situations, although some short-range ordering does begin to appear in isolated cases. However, recent work using X-ray pair distribution function (PDF) analysis based on synchrotron X-ray scattering data (Provis 2006, Bell *et al.* 2008) has shown that, even in samples which appear ‘amorphous’ to standard X-ray diffractometry, there is a significant extent of short-range order. In particular, comparing the short-range atomic ordering in a caesium aluminosilicate geopolymer with a model pollucite structure (Fig. 5.5) shows that there are very marked similarities in the short-range structures of Cs-geopolymer and crystalline pollucite.

The main short-range difference between the two structures appears to be a slight shift in the position of the Cs^+ atom upon crystallisation; however, more significant differences begin to become apparent at longer length



5.5 Comparison of the pair distribution functions of cubic pollucite ($\text{CsAlSi}_2\text{O}_6$) and a caesium aluminosilicate geopolymer of corresponding composition. The partial PDF decomposition shows the atom-atom correlations between each pair of atoms, where T is a tetrahedral Si or Al site; these atoms cannot be distinguished within the resolution of the data due to their very similar X-ray scattering properties. Model and partial PDF data were computed using the program PDFFIT (Proffen and Billinge 1999); data from Bell *et al.* (2008).

scales as the extent of ordering in the geopolymer decreases. Structural correlations in the geopolymer diminish rapidly as a function of distance, with essentially no deviation from randomness observed on length scales beyond 10\AA , whereas any identifiably crystalline pollucite structure will show a much longer coherence length (Bell *et al.* 2008). X-ray PDF studies have also been conducted on sodium and potassium aluminosilicate geopolymers (Bell 2008); however, the relatively lower X-ray contrast in these systems means that data analysis is less straightforward.

5.4.3 Structural models

Over the past two decades, various authors have proposed a wide range of structural models for metakaolin geopolymers, and some of the more noteworthy contributions will be briefly discussed here. Davidovits (1991) used a structural depiction based on different zeolite framework types, selected according to the Si/Al ratio and alkali cation of the specific geopolymer, but did not provide any indications either of the role of water, or of how structural disorder influences the framework connectivity. Rahier and colleagues

(Rahier *et al.* 1996a, b, 1997) used a polymer science paradigm to describe the geopolymer structure as a ‘low-temperature inorganic polymer glass,’ and the group led by Grutzeck described metakaolin geopolymers cured at elevated temperature as ‘hydroceramics’ (Siemer 2002, Bao *et al.* 2005). Barbosa *et al.* (2000) provided advances on the Davidovits (1991) structural model by generating a structural diagram explicitly showing water and alkali cations associated with the aluminosilicate framework, but still showed a very ordered aluminosilicate backbone for the gel.

The link between geopolymers and zeolites has been suggested many times, and was elaborated in detail in a review paper by Provis *et al.* (2005b), with the presence of zeolitic units in the nanostructure of the disordered geopolymer gel discussed in detail by those authors. Rowles *et al.* (2007) have recently presented what is almost certainly the most advanced nanostructural depiction of metakaolin geopolymers based on their NMR data, depicting both positional and connectivity disorder as well as non-framework species. However, this depiction – along with all other local-scale two-dimensional attempts to depict a complex, disordered, multiscale, three-dimensional structure – cannot possibly provide any more than an indicative view of specific aspects of the geopolymer framework.

Because of the danger of oversimplifying what is undoubtedly a highly complex local structure, no similar depiction will be presented in this chapter; while it is undoubtedly possible to obtain some information of value from such diagrams, the pitfalls associated with their use are highly significant (Provis and van Deventer 2009). However, what can be confidently stated regarding the nanostructure of metakaolin geopolymers is as follows:

- The gel structure is that of a charge-balanced aluminosilicate, with local order strongly resembling that observed in zeolites and related aluminosilicate minerals. This may potentially be better understood by analogy with calcium silicate hydrate gels; these show nanostructural features resembling minerals such as tobermorite and/or jennite, but are not long-range ordered and so appear largely amorphous to X-ray diffraction analysis (Richardson 2008). Similarly, the geopolymer gel shares nanostructural features of zeolites, but lacks long-range crystalline order.
- The exact details of the local structure (i.e., which zeolite framework type the gel resembles on a local level) are determined to a significant extent by the Si/Al ratio and the nature of the alkali cation(s) present.
- Each tetrahedral aluminium site is charge-balanced by an alkali metal cation. The alkali metal cation will not associate directly with the (positively-charged) Al atom, but rather will associate with one or more – depending on steric issues – of the (negatively-charged) oxygen atoms surrounding the aluminium.

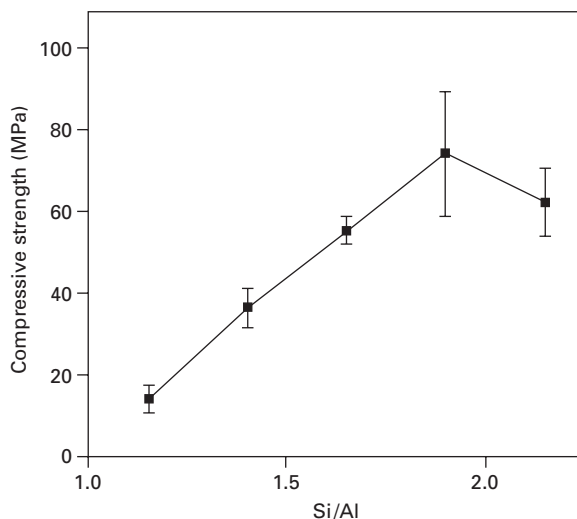
- The gel formed in a stoichiometric ($M^+/Al = 1$, M: alkali metal), well-cured metakaolin geopolymer is predominantly fully connected, with few non-bridging oxygens. If excess alkali is present, or if the geopolymer is incompletely cured, there will be non-bridging oxygen sites associated with some of the framework positions. Non-bridging oxygens attached to a silicon atom may either be protonated, or deprotonated and charge-balanced by an alkali cation; if any non-bridging oxygens are present on aluminium sites, they will remain protonated due to the very high pKa of the aluminol (Al-OH) group.
- The scarcity of bound hydroxyls means that the water present is generally localised in the pores, which range from nanopores up to macropores in varying proportions depending on the chemistry and thermal history of the sample. This is one of the main differences between an aluminosilicate geopolymer and the hydrated calcium silicates which form many of the binding phases in Portland cement concretes; geopolymers do not rely on water as an integrally bound component of the matrix.
- Within the framework, Al(IV)-O-Al(IV) bonding is disfavoured, although not exclusively – the preference is a thermodynamic (i.e., probabilistic) one rather than being due to steric or other stricter reasons. Al sites thus tend to be surrounded by four silicon neighbours in a fully-coordinated geopolymer framework.

5.5 Microstructure of metakaolin geopolymers

Detailed analysis of the microstructure of metakaolin geopolymers has been published by Duxson *et al.* (2005b, 2007b), and by others (Kriven *et al.* 2003, Schmücker and MacKenzie 2005, Zhang *et al.* 2007, Lloyd 2008). The discussion presented here will be brief rather than exhaustive, and is predominantly derived from the arguments presented in the Duxson *et al.* papers.

The prime importance of the microstructural details of geopolymers is twofold. Firstly, the mechanical strength of the binder is clearly related to its composition (Fig. 5.6), and this is able to be correlated to the details of the reaction process via analysis of the binder microstructure (Duxson *et al.* 2005b). Secondly, the pore network of the geopolymer binder will play a highly significant role in determining its durability; the main degradation mechanisms of geopolymers involve attack by aggressive agents, and if these agents cannot enter the material due to a tortuous or disconnected pore network, they cannot damage the chemical structure or cause corrosion of embedded reinforcing (Lloyd 2008).

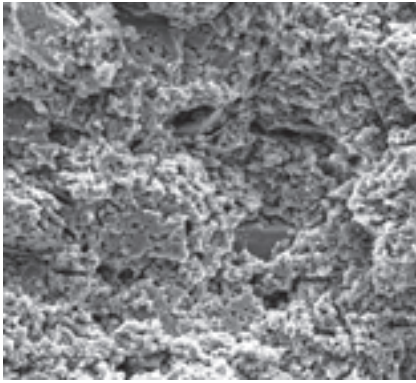
The data presented in Fig. 5.6 show a clear optimum in strength at high silica content, which correlates very well with the corresponding scanning electron microscope (SEM) images in Fig. 5.7. These images show a very



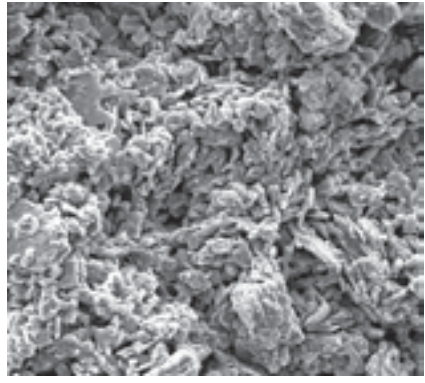
5.6 Compressive strengths of geopolymers synthesised by reaction of metakaolin with $\text{Na}_2\text{O}/\text{SiO}_2$ ratios corresponding to those presented in Figs 5.3 and 5.4. The data are plotted here in terms of overall Si/Al ratio, where Si/Al = 1.15 is metakaolin with NaOH solution, and Si/Al = 2.15 is metakaolin with a solution of composition $\text{Na}_2\text{O}/\text{SiO}_2 = 2.0$. Data from Duxson *et al.* (2005b).

rough, disconnected binder structure at low silica content giving way to a smooth, relatively homogeneous binder when more silica is added (Duxson *et al.* 2005b, Duxson 2006). It has also been argued that much of the roughness of the low-silica samples can be attributed to the low strength of these samples causing fracture during polishing (Lloyd 2008) – and certainly the degree of smoothness achieved on these samples is less than for the stronger, higher-silica samples – but this is unlikely to give such a dramatic difference in texture as is observed in Fig. 5.7.

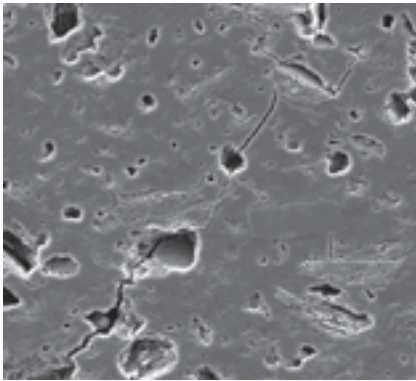
The analysis of porosimetry data for metakaolin geopolymers remains the subject of significant discussion (Duxson *et al.* 2005b, Lloyd 2008), due largely to the complications inherent in obtaining pore distribution data by either gas or mercury porosimetry from a pore network as tortuous and complex as that of a geopolymer. However, it is apparent that the skeletal density of the geopolymer matrix does not vary to anywhere near the extent that would be expected simply from observation of SEM images such as Fig. 5.7; the apparently highly homogeneous gel in the higher-silica geopolymers is in fact also highly porous, but on a length scale that is too small to observe in standard-resolution SEM imaging. There are also significant trends in pore structure in mixed-alkali geopolymer series, with the mean pore size decreasing almost monotonically as sodium is progressively replaced by potassium in the geopolymer mix (Kriven and Bell 2004).



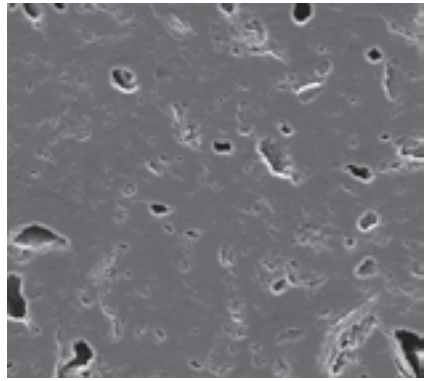
(a)



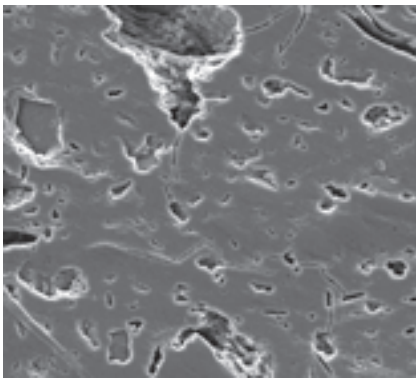
(b)



(c)



(d)



(e)

10 μm

5.7 Microstructures of geopolymers synthesised by mixing metakaolin with (a) sodium hydroxide solution, and (b–e) sodium silicate solutions with mole ratios $\text{SiO}_2/\text{Na}_2\text{O} = 0.5, 1.0, 1.5$ and 2.0 respectively. Images from Duxson (2006).

5.6 Calcium in metakaolin geopolymers

The calcium hydroxide-metakaolin system is in itself of interest as a means of analysing the pozzolanic reaction in Portland cement concretes, entirely separate from any discussion of geopolymer chemistry. However, the introduction of an additional alkali source, as is the case in calcium-containing metakaolin geopolymers, introduces additional complexity into the range of phases that can form in this reaction system. In particular, the possibility of phase separation and metastable coexistence of calcium (alumino)silicate hydrate, C-(A)-S-H, and sodium aluminosilicate hydrate, N-A-S-H, gels is an issue of very significant interest (Granizo *et al.* 2002, Yip and van Deventer 2003, Buchwald *et al.* 2007, García-Lodeiro *et al.* 2008, Yip *et al.* 2008, Yong 2009).

The addition of a sufficient quantity of calcium to geopolymers in the form of calcium hydroxide can lead to the formation of phase-separated C-(A)-S-H and geopolymer (N-A-S-H) gels. This is known to be more prevalent at relatively low alkalinity - low NaOH concentrations in hydroxide-activated systems (Alonso and Palomo 2001), or higher SiO₂/Na₂O ratios in silicate-activated systems (Yong 2009). It is likely that the common ion effect involving OH⁻ in highly alkaline solutions means that the dissolution of Ca(OH)₂ is hindered in such systems, and it is also possible that very highly alkaline conditions will lead to dissolution of any C-S-H type phases which are formed. Slag-metakaolin geopolymers show a significant extent of phase coexistence, as well as relatively high strength compared to many other metakaolin geopolymers (Yip and van Deventer 2003, Buchwald *et al.* 2007).

When adding calcium to geopolymers in the form of various calcium silicates (minerals, blast furnace slag and Portland cement), Yip *et al.* (2008) found that the replacement of 20% of the metakaolin in a geopolymer mix had varying effects depending on the specific nature of the calcium silicate source and also the alkalinity of the geopolymer-forming system. At low alkalinity, the compressive strength of geopolymer matrices prepared with predominantly amorphous calcium silicates (blast furnace slag) or containing crystalline phases specifically manufactured for reactivity (cement) was much higher than when the calcium was supplied as crystalline silicate minerals. The compressive strength of matrices containing natural calcium silicates improved with increasing alkalinity, however the opposite trend was observed in matrices synthesised with processed calcium silicate sources. The difference in compressive strength between matrices synthesised using different calcium silicate sources was significantly reduced at high alkalinity. At high alkalinity, calcium played a lesser role in determining the nature of the final binder, as it formed hydroxide precipitates rather than hydrated gels.

5.7 Conclusions

To develop a more detailed understanding of the process of metakaolin geopolymerisation, the structure and chemistry of metakaolin must first be better understood. Such understanding will then be able to be used to analyse the interactions between the disordered layered structure of metakaolin and the alkaline activating solutions, which will provide further insight into the mechanistic issues underpinning the differences in microstructure (and thus mechanical performance) between high-silica and low-silica metakaolin geopolymers. This information will then be valuable both in the analysis of metakaolin geopolymers themselves, and also in contributing to the discussion of to what extent metakaolin geopolymers are able to be useful as a model for understanding the chemistry of fly ash geopolymers.

5.8 References

- Alonso, S. and Palomo, A. (2001) Calorimetric study of alkaline activation of calcium hydroxide-metakaolin solid mixtures. *Cement and Concrete Research*, 31, 25–30. doi:10.1016/S0008-8846(00)00435-X.
- Badogiannis, E., Kakali, G. and Tsvilis, S. (2005) Metakaolin as supplementary cementitious material. Optimization of kaolin to metakaolin conversion. *Journal of Thermal Analysis and Calorimetry*, 81, 457–462. doi: 10.1007/s10973-005-0806-3.
- Bao, Y., Grutzeck, M. W. and Jantzen, C. M. (2005) Preparation and properties of hydroceramic waste forms made with simulated Hanford low-activity waste. *Journal of the American Ceramic Society*, 88, 3287–3302. doi:10.1111/j.1551-2916.2005.00775.x.
- Barbosa, V. F. F., MacKenzie, K. J. D. and Thaumaturgo, C. (2000) Synthesis and characterisation of materials based on inorganic polymers of alumina and silica: sodium polysialate polymers. *International Journal of Inorganic Materials*, 2, 309–317. doi:10.1016/S1466-6049(00)00041-6.
- Barrer, R. M. and Mainwaring, D. E. (1972a) Chemistry of soil minerals. Part XI. Hydrothermal transformations of metakaolinite in potassium hydroxide. *Journal of the Chemical Society – Dalton Transactions*, 1254–1265. doi: 10.1039/DT9720001254.
- Barrer, R. M. and Mainwaring, D. E. (1972b) Chemistry of soil minerals. Part XIII. Reactions of metakaolinite with single and mixed bases. *Journal of the Chemical Society – Dalton Transactions*, 2534–2546. doi: 10.1039/DT9720002534.
- Bell, J. L. (2008) PhD Thesis, Department of Materials Science and Engineering, University of Illinois at Urbana-Champaign.
- Bell, J. L., Sarin, P., Provis, J. L., Haggerty, R. P., Driemeyer, P. E., Chupas, P. J., van Deventer, J. S. J. and Kriven, W. M. (2008) Atomic structure of a cesium aluminosilicate geopolymer: A pair distribution function study. *Chemistry of Materials*, 20, 4768–4776. doi 10.1021/cm703369s.
- Buchwald, A., Hilbig, H. and Kaps, C. (2007) Alkali-activated metakaolin-slag blends – Performance and structure in dependence on their composition. *Journal of Materials Science*, 42, 3024–3032. doi: 10.1007/s10853-006-0525-6.
- Davidovits, J. (1982) Mineral polymers and methods of making them, US Patent 4,349,386.

- Davidovits, J. (1988) Structural characterization of geopolymeric materials with X-ray diffractometry and MAS-NMR spectrometry. *Proceedings of Geopolymer '88 – First European Conference on Soft Mineralurgy*, Compeigne, France, Davidovits, J. and Orlinski, J. (Eds.), 149–166.
- Davidovits, J. (1991) Geopolymers – Inorganic polymeric new materials. *Journal of Thermal Analysis*, 37, 1633–1656. doi:10.1007/BF01912193.
- Davidovits, J. (2008) *Geopolymer Chemistry and Applications*, Saint-Quentin, France, Institut Géopolymère.
- Duxson, P. (2006) PhD Thesis, Department of Chemical and Biomolecular Engineering, University of Melbourne.
- Duxson, P., Provis, J. L., Lukey, G. C., Separovic, F. and van Deventer, J. S. J. (2005a) ^{29}Si NMR study of structural ordering in aluminosilicate geopolymer gels. *Langmuir*, 21, 3028–3036. doi:10.1021/la047336x.
- Duxson, P., Provis, J. L., Lukey, G. C., Mallicoat, S. W., Kriven, W. M. and van Deventer, J. S. J. (2005b) Understanding the relationship between geopolymer composition, microstructure and mechanical properties. *Colloids and Surfaces A – Physicochemical and Engineering Aspects*, 269, 47–58. doi:10.1016/j.colsurfa.2005.06.060.
- Duxson, P., Lukey, G. C., Separovic, F. and van Deventer, J. S. J. (2005c) The effect of alkali cations on aluminum incorporation in geopolymeric gels. *Industrial and Engineering Chemistry Research*, 44, 832–839. doi:10.1021/ie0494216.
- Duxson, P., Provis, J. L., Lukey, G. C., van Deventer, J. S. J., Separovic, F. and Gan, Z. H. (2006) ^{39}K NMR of free potassium in geopolymers. *Industrial and Engineering Chemistry Research*, 45, 9208–9210. doi:10.1021/ie060838g.
- Duxson, P., Gehman, J. D., White, C. E., Provis, J. L., Separovic, F., Gan, Z. and van Deventer, J. S. J. (2007a) ^{17}O MQMAS NMR characterisation of geopolymers. *Chemeca 2007*, Melbourne, Australia, CD-ROM proceedings.
- Duxson, P., Mallicoat, S. W., Lukey, G. C., Kriven, W. M. and van Deventer, J. S. J. (2007b) The effect of alkali and Si/Al ratio on the development of mechanical properties of metakaolin-based geopolymers. *Colloids and Surfaces A – Physicochemical and Engineering Aspects*, 292, 8–20. doi:10.1016/j.colsurfa.2006.05.044.
- Engelhardt, G. and Michel, D. (1987) *High-Resolution Solid-State NMR of Silicates and Zeolites*, Chichester, John Wiley and Sons.
- Feng, D., Tan, H. and van Deventer, J. S. J. (2004) Ultrasound enhanced geopolymerisation. *Journal of Materials Science*, 39, 571–580. doi: 10.1023/B:JMSC.0000011513.87316.5c.
- García-Lodeiro, I., Fernández-Jiménez, A., Blanco, M. T. and Palomo, A. (2008) FTIR study of the sol–gel synthesis of cementitious gels: C-S-H and N-A-S-H. *Journal of Sol-Gel Science and Technology*, 45, 63–72. doi:10.1007/s10971-007-1643-6.
- Granizo, M. L. and Blanco, M. T. (1998) Alkaline activation of metakaolin – An isothermal conduction calorimetry study. *Journal of Thermal Analysis*, 52, 957–965. doi:10.1023/A:1010176321136.
- Granizo, M. L., Alonso, S., Blanco-Varela, M. T. and Palomo, A. (2002) Alkaline activation of metakaolin: Effect of calcium hydroxide in the products of reaction. *Journal of the American Ceramic Society*, 85, 225–231. doi: 10.1111/j.1151-2916.2002.tb00070.x.
- Granizo, M. L., Blanco Varela, M. T. and Martínez-Ramírez, S. (2007) Alkali activation of metakaolins: Parameters affecting mechanical, structural and microstructural properties. *Journal of Materials Science*, 42, 2934–2943. doi: 10.1007/s10853-006-0565-y.
- Kriven, W. M. and Bell, J. L. (2004) Effect of alkali choice on geopolymer properties. *Ceramic Engineering and Science Proceedings*, 25, 99–104.

- Kriven, W. M., Bell, J. L. and Gordon, M. (2003) Microstructure and microchemistry of fully-reacted geopolymers and geopolymer matrix composites. *Ceramic Transactions*, 153, 227–250.
- Lee, S., Kim, Y. J. and Moon, H. S. (2003) Energy-filtering transmission electron microscopy (EF-TEM) study of a modulated structure in metakaolinite, represented by a 14 Å modulation. *Journal of the American Ceramic Society*, 86, 174–176. doi: 10.1111/j.1151-2916.2003.tb03297.x.
- Lloyd, R. R. (2008) PhD Thesis, Department of Chemical and Biomolecular Engineering, University of Melbourne, Australia.
- MacKenzie, K. J. D., Brown, I. W. M., Meinhold, R. H. and Bowden, M. E. (1985) Outstanding problems in the kaolinite-mullite reaction sequence investigated by ^{29}Si and ^{27}Al solid-state nuclear magnetic resonance: I. Metakaolinite. *Journal of the American Ceramic Society*, 68, 293–297. doi: 10.1111/j.1151-2916.1985.tb15228.x.
- MacKenzie, K. J. D., Brew, D. R. M., Fletcher, R. A. and Vagana, R. (2007) Formation of aluminosilicate geopolymers from 1:1 layer-lattice minerals pre-treated by various methods: A comparative study. *Journal of Materials Science*, 42, 4667–4674. doi: 10.1007/s10853-006-0173-x.
- Palomo, A. and Glasser, F. P. (1992) Chemically-bonded cementitious materials based on metakaolin. *British Ceramic Transactions and Journal*, 91, 107–112.
- Proffen, T. and Billinge, S. J. L. (1999) PDFFIT, a program for full profile refinement of the atomic pair distribution function. *Journal of Applied Crystallography*, 32, 572–575. doi: 10.1107/S0021889899003532.
- Provis, J. L. (2006) PhD Thesis, Department of Chemical and Biomolecular Engineering, University of Melbourne.
- Provis, J. L. and van Deventer, J. S. J. (2007) Geopolymerisation kinetics. 2. Reaction kinetic modelling. *Chemical Engineering Science*, 62, 2318–2329. doi:10.1016/j.ces.2007.01.028.
- Provis, J. L. and van Deventer, J. S. J. (2009) Discussion of ‘Synthesis and microstructural characterization of fully-reacted potassium-poly(sialate-siloxo) geopolymeric cement matrix’, by Y. Zhang *et al.* *ACI Materials Journal*, 106, 95–96.
- Provis, J. L., Duxson, P., Lukey, G. C. and van Deventer, J. S. J. (2005a) Statistical thermodynamic model for Si/Al ordering in amorphous aluminosilicates. *Chemistry of Materials*, 17, 2976–2986. doi:10.1021/cm050219i.
- Provis, J. L., Lukey, G. C. and van Deventer, J. S. J. (2005b) Do geopolymers actually contain nanocrystalline zeolites? – A re-examination of existing results. *Chemistry of Materials*, 17, 3075–3085. doi:10.1021/cm050230i.
- Rahier, H., van Mele, B., Biesemans, M., Wastiels, J. and Wu, X. (1996a) Low-temperature synthesized aluminosilicate glasses. 1. Low-temperature reaction stoichiometry and structure of a model compound. *Journal of Materials Science*, 31, 71–79. doi:10.1007/BF00355128.
- Rahier, H., van Mele, B. and Wastiels, J. (1996b) Low-temperature synthesized aluminosilicate glasses. 2. Rheological transformations during low-temperature cure and high-temperature properties of a model compound. *Journal of Materials Science*, 31, 80–85. doi:10.1007/BF00355129.
- Rahier, H., Simons, W., van Mele, B. and Biesemans, M. (1997) Low-temperature synthesized aluminosilicate glasses. 3. Influence of the composition of the silicate solution on production, structure and properties. *Journal of Materials Science*, 32, 2237–2247. doi:10.1023/A:1018563914630.

- Richardson, I. G. (2008) The calcium silicate hydrates. *Cement and Concrete Research*, 38, 137–158. doi: 10.1016/j.cemconres.2007.11.005.
- Rocha, J. and Klinowski, J. (1990) Solid-state NMR studies of the structure and reactivity of metakaolinite. *Angewandte Chemie – International Edition, English*, 29, 553–554. doi: 10.1002/anie.199005531.
- Rocha, J., Adams, J. M. and Klinowski, J. (1990) The rehydration of metakaolinite to kaolinite: Evidence from solid-state NMR and cognate techniques. *Journal of Solid State Chemistry*, 89, 260–274. doi:10.1016/0022-4596(90)90267-2.
- Rowles, M. R., Hanna, J. V., Pike, K. J., Smith, M. E. and O'Connor, B. H. (2007) ^{29}Si , ^{27}Al , ^1H and ^{23}Na MAS NMR study of the bonding character in aluminosilicate inorganic polymers. *Applied Magnetic Resonance*, 32, 663–689. doi:10.1007/s00723-007-0043-y.
- Sabir, B. B., Wild, S. and Bai, J. (2001) Metakaolin and calcined clays as pozzolans for concrete: a review. *Cement and Concrete Composites*, 23, 441–454. doi:10.1016/S0958-9465(00)00092-5.
- Schmücker, M. and MacKenzie, K. J. D. (2005) Microstructure of sodium polysialate siloxo geopolymer. *Ceramics International*, 31, 433–437. doi:10.1016/j.ceramint.2004.06.006.
- Siemer, D. D. (2002) Hydroceramics, a 'new' cementitious waste form material for US defense-type reprocessing waste. *Materials Research Innovations*, 6, 96–104. doi:10.1007/s10019-002-0193-3.
- Singh, P. S., Bastow, T. and Trigg, M. (2005) Structural studies of geopolymers by ^{29}Si and ^{27}Al MAS-NMR. *Journal of Materials Science*, 40, 3951–3961. doi:10.1007/s10853-005-1915-x.
- van Deventer, J. S. J., Provis, J. L., Duxson, P. and Lukey, G. C. (2007) Reaction mechanisms in the geopolymeric conversion of inorganic waste to useful products. *Journal of Hazardous Materials*, A139, 506–513. doi:10.1016/j.jhazmat.2006.02.044.
- Weng, L. and Sagoe-Crentsil, K. (2007) Dissolution processes, hydrolysis and condensation reactions during geopolymer synthesis: Part I – Low Si/Al ratio systems. *Journal of Materials Science*, 42, 2997–3006. doi: 10.1007/s10853-006-0820-2.
- Yip, C. K. and van Deventer, J. S. J. (2003) Microanalysis of calcium silicate hydrate gel formed within a geopolymeric binder. *Journal of Materials Science*, 38, 3851–3860. doi:10.1023/A:1025904905176.
- Yip, C. K., Lukey, G. C., Provis, J. L. and van Deventer, J. S. J. (2008) Effect of calcium silicate sources on geopolymerisation. *Cement and Concrete Research*, 38, 554–564. doi: 10.1016/j.cemconres.2007.11.001.
- Yong, S. L. (2009) PhD Thesis, Department of Chemical and Biomolecular Engineering, University of Melbourne.
- Zhang, Y., Sun, W. and Li, Z. (2007) Preparation and microstructure of K-PSDS geopolymeric binder. *Colloids and Surfaces A – Physicochemical and Engineering Aspects*, 302, 473–482. doi:10.1016/j.colsurfa.2007.03.031.
- Zhang, Y., Sun, W. and Li, Z. (2008) Synthesis and microstructural characterization of fully-reacted potassium-poly(sialate-siloxo) geopolymeric cement matrix. *ACI Materials Journal*, 105, 156–164.

Nanostructure/microstructure of fly ash geopolymers

A FERNÁNDEZ-JIMÉNEZ and A. PALOMO,
Eduardo Torroja Institute, Spain

Abstract: Alkali aluminosilicate polymers, or ‘geopolymers’, a family of minerals with cementitious properties, constitute a promising future source of materials for the construction industry. These polymers combine certain properties of ordinary cements, traditional ceramic materials and zeolites. ^{29}Si , ^{27}Al and ^{23}Na MAS-NMR spectroscopy were used to characterise the reaction products resulting from the alkali activation of a type F fly ash. Specifically, analysis focused on the influence of the degree of polymerisation of the activating solution. The results obtained show that the nature of the alkali activator plays an important role in the kinetics, structure and composition of the gel initially formed. The alkaline aluminosilicate gel formed exhibits short-range order, with the silicon appearing in a wide variety of $\text{Q}^4(n\text{Al})$ ($n = 0, 1, 2, 3$ and 4) environments.

Key words: ^{29}Si , ^{27}Al , ^{23}Na , MAS-NMR, nano-microstructure model.

6.1 Introduction: general characteristics of cementitious gels

Most of the physical, chemical and mechanical properties of conventional cements and concretes can be attributed to C-S-H (hydrated calcium silicate) gel, the main reaction product of Portland cement hydration. The ‘CaO-SiO₂-H₂O’ system in which the gel is described was the subject of a substantial number of studies conducted in the twentieth century under ambient temperature and equilibrium conditions. Over 30 C-S-H crystalline phases have been identified (Taylor 1990).

Taylor (1986), who fathered the chemistry of cement, suggested in 1986 that the C-S-H gel forming as a result of the hydration of Ca_3SiO_5 contained two types of local structures, one similar to 1.4 nm tobermorite and the other jennite-like. In tobermorite, two silica chains flank a central Ca-O layer. The chains have a ‘dreierketten’ structure (Taylor 1992), in which two tetrahedra – called paired tetrahedra – share an oxygen atom, while the second member of the pair also shares one of its O atoms with a third (‘outer’) tetrahedron. The latter is known as the bridging tetrahedron because it shares a second oxygen with the first tetrahedron of the following pair in the chain. Finally, all the paired tetrahedra are linked to the inner Ca-O layer across their two remaining oxygens. Water molecules and additional calcium cations occupy

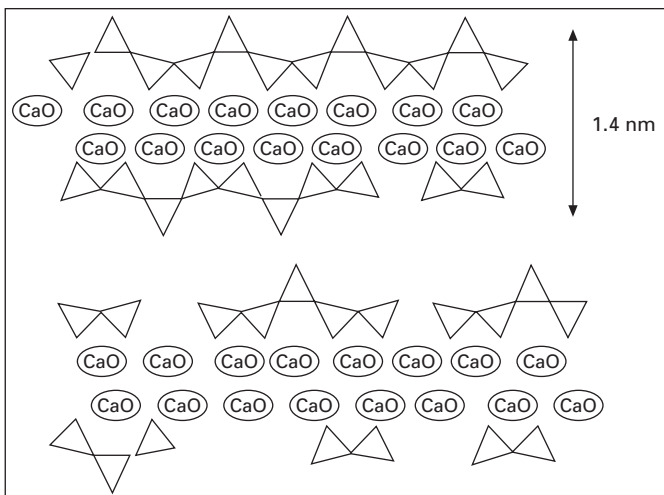
the interlayer. The Ca/Si ratio is generally around 0.83, but this value varies in less crystalline forms (see Fig. 6.1). Like tobermorite, jennite consists in a central layer of CaO in between two rows of (dreierketten-type) silicates with calcium atoms and water molecules in the interlayer. The chief difference between the two structures is that in jennite some of the silica tetrahedra in the simple dreierketten chain are replaced by OH groups, causing substantial undulation in the CaO layer.

Richardson *et al.* (1993), in turn, proposed a model for C-S-H similar to Taylor's, assuming that the aluminium could replace the silicon in the bridging tetrahedra, as ²⁹Si NMR studies revealed the presence of a signal at -82 ppm attributed to Q²(1Al) units. The charges would be balanced in this model by alkali cations or Ca²⁺ ions in the interlayer region.

Many factors affect both C-S-H gel composition and structure: temperature, relative humidity, pH, presence of alkalis and so on. Many studies have been published on the effects of all these parameters on C-S-H gels (Glasser and Hong 2003, Richardson 2000, Cong and Kirkpatrick 1995).

At the same time, a host of methods have been developed for synthesizing C-S-H gels, ranging from hydrothermal treatments of SiO₂, CaO and H₂O at high temperatures (the most common in the literature) to calcium silicate reactions (C₃S or β-C₂S) at ambient temperature in an aqueous suspension (Sharara *et al.* 1994, Chen *et al.* 2004). Sol-gel procedures can likewise be used to synthesize C-S-H.

The quest for a new construction material less environmentally detrimental and more durable than traditional Portland cement has generated increasing interest in the study of alkali activation as a procedure for obtaining alternative



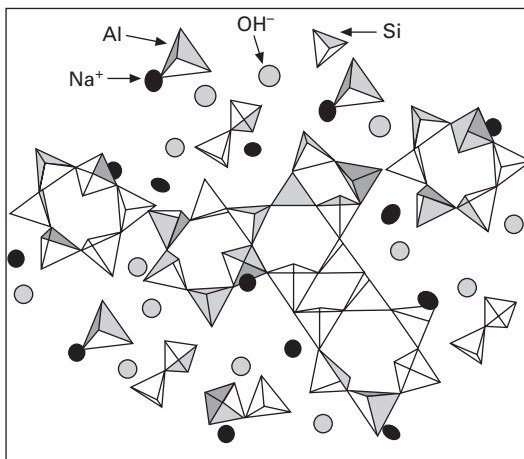
6.1 Structural model proposed for C-S-H gel (after Taylor 1990).

cementitious systems. Two major groups of materials are presently under study for the production of alkali-activated cements: calcium-, silicon- and aluminium-rich materials (primarily blast furnace slag) on the one hand, and silica- and alumina-rich materials (such as metakaolin or type F fly ash) on the other. The main reaction product generated by the first group is a hydrated calcium silicate or C-S-H gel similar to the gel formed in Portland cement hydration.

The chemistry and structure of the products generated in the second group of systems, however, vary substantially from Portland cement hydration products in those respects. In fact, the main reaction product of the alkali activation of both fly ash and metakaolin is an alkaline silicoaluminate (geopolymer) containing silicon and aluminium tetrahedra arranged to form a three-dimensional structure (Davidovits 1994, Barbosa *et al.* 2000, Palomo *et al.* 2004a, Fernandez-Jimenez *et al.* 2006a, Criado *et al.* 2007b, Duxson *et al.* 2007a). The cavities formed within the network can accommodate alkaline cations to compensate the charge imbalance resulting from the replacement of Si(IV) by an Al(III). Terminal hydroxyl groups are also found on the gel surface, although their presence has little bearing on the structure of the material (see Fig. 6.2).

As in the case of C-S-H gel, many factors affect the structure and chemical composition of alkaline aluminosilicate gel.

A wide range of possibilities for producing such gels can be found in the literature. In some methods the initial reagents are natural raw materials or industrial by-products (slag, metakaolin, fly ash, and others) (Shi *et al.* 2006, Palomo and Glasser 1992, Duxson *et al.* 2007b, Davidovits 2008, Palomo *et al.* 1999, Fernandez-Jimenez and Palomo 2003), while in others



6.2 Two-dimensional representation of the structural model proposed for N-A-S-H gel (Data from Criado 2007).

synthesis involves the use of laboratory reagents (Ikeda 1997, Barbosa *et al.*, 2000, Barbosa and MacKenzie 2003, Fernandez-Jimenez *et al.* 2006b). The characteristics of the product formed are directly affected by the characteristics of the prime materials, activator type and concentration, curing time and temperature and so on.

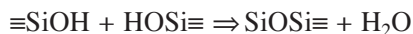
6.2 Polymerisation: a conceptual model

Although interest in the sol-gel process as a method for synthesising inorganic clay-based products and vitreous materials dates back to the early nineteenth century, the first major breakthroughs came in the mid-twentieth century, with the works of Carman (1940) and Iler (1955) introduced the theory of silicic acid polymerisation, according to which the process takes place in three now well-known steps:

- (i) monomer polymerisation and particle formation
- (ii) particle growth
- (iii) inter-particle bonding to form branched chains, networks and ultimately the gel.

Iler (1955), in his book *The Chemistry of Silica*, provided an exhaustive description of the chemistry of silica in aqueous systems, treating aspects of solubility, mechanisms of polymerisation, and so on. The basis for the mechanisms of polymerisation proposed by Iler is the tendency of silicic acid monomers ($\text{Si}(\text{OH})_4$) to polymerise via siloxane bridges (Si-O-Si) to form dimers, cyclical molecules and particles which, depending on the alkalinity of the medium, evolve in one way or another. For pH values of under 7, or between 7 and 10 in the presence of salts (which act as flocculating agents), the particles aggregate to form a three-dimensional structure; by contrast, at pH values of 7–10 but in the absence of salts, the particles grow in size and decline in number to form a sol.

Experimental studies have confirmed these early results and the general consensus is that polymerisation entails an increase in the molecular weight of silica, implying the condensation of silanol groups:



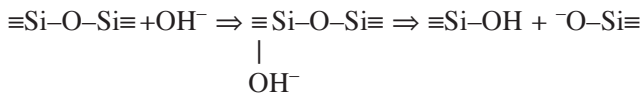
The term polymerisation is used in a loose sense, in which the condensation of $\text{Si}(\text{OH})$ units may generate larger units either by enlarging the size of the spherical particles or by increasing the number of particles comprising the aggregate. Spherical particle formation and growth take place under certain conditions, while particle aggregation and the concomitant formation of viscous sols or gels require a different set of conditions. These two types of polymerisation may occur simultaneously.

Taking these theories as a starting point, Glukhovsky (1967) proposed a

general model to describe the mechanisms that govern the alkali activation of aluminosiliceous materials. His model divides the process into three main stages.

First stage: ‘Destruction–Coagulation’

This first disaggregation process is based on severing the Me–O, Si–O–Si, Al–O–Al and Al–O–Si bonds in the starting material. Severance of covalent Si–O–Si and Al–O–Al bonds calls for reactivity conditions that can only be attained if the ionic force is varied by adding electron donor ions (such as alkaline metals) to the medium to raise the pH. The OH[−] ions initiate the rupture of the Si–O–Si bonds:



This takes place by the action of the OH[−] redistributing the electron density around the silicon atom and rendering the Si–O–Si bond more susceptible to rupture. The degree of silicon hydroxylation may rise to more than two or three units, forming intermediate complexes that decompose into silicic acid Si(OH)₄ as well as oligomeric, anionic species containing ≡Si–O[−] groups. The presence of alkaline metal cations neutralises the resulting negative charge. The appearance of ≡Si–O[−]–Na⁺ bonds hinders the reverse reaction from forming siloxane bonds. These alkaline silicates may also take part in ion exchange reactions with divalent ions to form ≡Si–O–Ca–OH type complexes.

Inasmuch as the hydroxyl groups affect the Al–O–Si bond in the same way, the aluminates in the alkaline solution form complexes, predominantly Al(OH)₄[−] (Radnai *et al.* 1998).

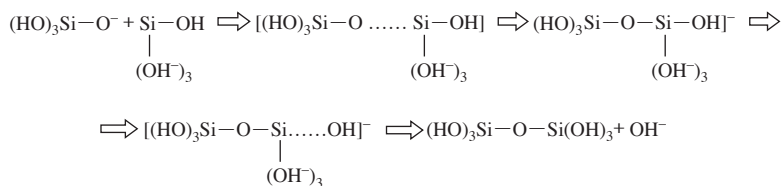
The –Si–O–Na⁺ complexes, which are stable in alkaline media, create conditions suitable for the transport of the reacting structural units and the development of the coagulated structure. Therefore, the cation catalyses these reactions, maintaining the ionic force needed to destroy the covalent bonds and thereby participating in the conversion of the bonds destroyed into a colloidal phase.

Second stage: ‘Coagulation–Condensation’

In this second stage accumulation enhances contact among the disaggregated products, forming a coagulated structure where polycondensation takes place.

The condensability of silicic acid rises with high pH values, at which it is slightly dissociated or in a molecular state. Therefore, at pH > 7, the

disaggregation of the Si-O-Si bond gives rise to a hydroxylated complex, $\text{Si}(\text{OH})_4$, which condenses to form a new Si-O-Si bond and generate the following dimer:



This reaction is catalysed by the OH^- ion. The clusters formed by the polymerisation of orthosilicic acid may grow in all directions, generating colloidal particles. Aluminate also participates in these polymerisation reactions, substituting isomorphously for silicate tetrahedra. While the alkaline metal catalyses destruction in the first stage, in the following two it is a structural component.

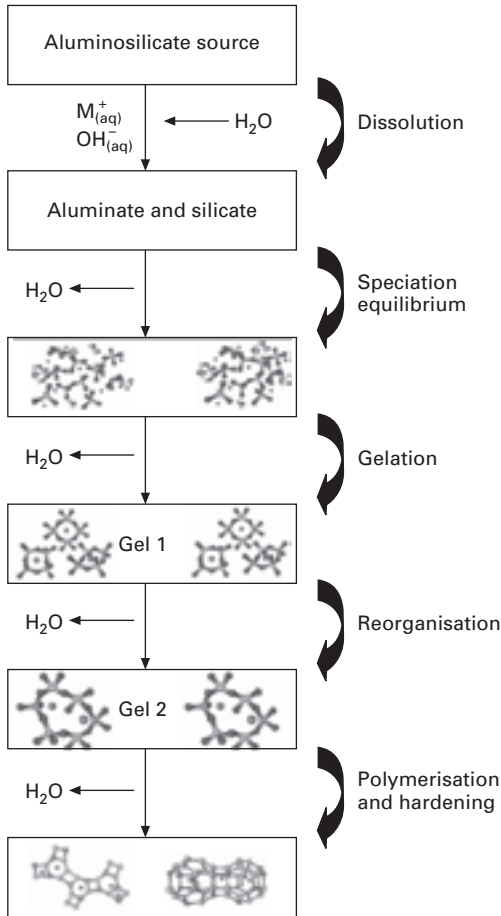
Third stage: 'Condensation-Crystallisation'

Like the appearance of microparticles resulting from the condensed structure, the presence of particles in the initial solid phase prompts the precipitation of products whose composition is determined by the mineralogical and chemical composition of the initial phase, the nature of the alkaline component and hardening conditions.

More recently, other authors have developed and expanded on Glukhovsky's theories and applied the existing knowledge of zeolite synthesis to explain the formation of alkaline inorganic polymers in greater detail.

In 2005, for instance, Fernández-Jiménez *et al.* (2005a) and Palomo *et al.* (2005a) provided a graphic description of the mechanism governing the alkali activation of aluminosilicates. (The authors subsequently changed the model slightly, in close collaboration with Duxson, Provis and van Deventer.) In that study the authors described some of the unknown details about the nanostructure of the reaction products generated during the alkali activation of this type of materials (Duxson *et al.* 2007a). Among other novelties, the model incorporates the two stages that govern zeolite synthesis: (i) a first or nucleation stage in which the aluminosilicates dissolve in the alkaline medium, favouring the formation of zeolite precursors (a stage that encompasses Glukhovsky's first two stages and is heavily dependent upon kinetic and thermodynamic parameters); and (ii) a second stage in which several nuclei reach a critical size and crystals begin to develop.

Figure 6.3 shows the various stages comprising the transformation of a source of aluminosilicates into an alkaline inorganic polymer (although the processes are shown linearly, these stages are actually simultaneous; the overall



6.3 Conceptual model for geopolymerisation from Duxson *et al.* (2007a).

process is heterogeneous). Initially, the contact between the solid particles and the alkaline solution causes the vitreous/amorphous component of these particles to dissolve (this is the mechanism that governs the dissolution of solid particles in the early stages), releasing aluminates and silicates, probably as monomers.

These monomers inter-react to form dimers, which in turn react with other monomers to form trimers, tetramers and so on. When the solution reaches saturation an aluminosilicate gel precipitates. Initially this is an aluminium-rich gel (denominated Gel I, an intermediate reaction product). Its formation may be explained by the higher Al^{3+} ion content in the alkaline medium in the early stages of the process (from the first few minutes to the first four or five hours), since reactive aluminium dissolves more rapidly

than silicon because Al-O bonds are weaker than Si-O bonds and therefore easier to sever (Fernandez-Jimenez *et al.* 2006a). As the reaction progresses, more Si-O groups in the initial solid source dissolve, increasing the silicon concentration in the medium and gradually raising the proportion of silicon in the zeolite precursor gel (Gel 2).

These structural reorganisation processes determine the final composition of the polymer as well as pore microstructure and distribution in the material, which are critical factors in the development of many physical properties of the resulting cement (Fernandez-Jimenez *et al.* 2006c, Sofi *et al.* 2007).

Today this gel is known to be a product containing large numbers of zeolite-like nanocrystals. In fact, many cementitious systems made from inorganic polymers are observed to contain small amounts of perfectly crystallised zeolites (chabazite-Na, analcime, Linde A and so on), which would appear to confirm this hypothesis. Zeolite formation, however, calls for a minimum amount of liquid and crystallisation takes some time (Barrer 1982).

6.3 Characterisation of N-A-S-H gel

The term 'N-A-S-H' as an acronym for the sodium aluminosilicate gel forming as the main reaction product in the alkali activated fly ash materials first appeared in the literature in 2005 (Fernandez-Jimenez and Palomo 2005b). It has since been widely accepted by cement professionals (scientific community and technical circles), by contrast to 'geopolymer', which continues to be thought of more as a commercial than a scientifically rigorous term. Several reasons may underlie the acceptance of the term 'N-A-S-H gel':

- Its terminological analogy to C-S-H gel (main OPC binding product).
- Its descriptive analogy to actual gel composition (sodium aluminosilicate hydrate 'N-A-S-H'), providing for product positioning in phase equilibrium diagrams.
- Its methodological analogy to C-S-H gel in terms of gel characterisation, in light of the physical similarity between these two cementitious gels (C-S-H and N-A-S-H).
- They are physically similar and both are cementitious.

As is the case for C-S-H gels, N-A-S-H gels are difficult to characterise with XRD due to their amorphous or nanocrystalline nature. The use of other characterisation techniques such as FTIR or electron microscopy (SEM, BSEM, TEM) can furnish valuable information about gel nanostructure and composition (Criado *et al.* 2007a, 2007c, Duxson *et al.* 2005, 2007a, Fernandez-Jimenez *et al.* 2005b, 2006d, Palomo *et al.* 2004a, 2005a, 2005b). The technique that has contributed most substantially to an understanding of N-A-S-H (as well as C-S-H) gel in the last ten years, however, is the nuclear magnetic resonance of solids.

Davidovits (1988, 1994 and 2008) was the first author, in the 1980s, to use the nuclear magnetic resonance of solids to explore the structure of N-A-S-H, K-A-S-H and similar gels (which he called geopolymers) generated by the alkali activation of metakaolin. A full understanding of the structure of these gels was not possible for several years, however, because of the poor spectral resolution available. Fortunately, today's equipment is more powerful and sophisticated, able to generate higher resolution spectra. The foregoing is applicable to the gels derived from metakaolin (Davidovits 1994, Duxson *et al.* 2007a, 2007b), and fly ash (Criado *et al.* 2007b, Fernandez-Jimenez *et al.* 2006a, Palomo *et al.* 2004a) as it is to synthetic N-A-S-H gels (Fernandez-Jimenez *et al.* 2006b, Ikeda 1997, Phair *et al.* 2003).

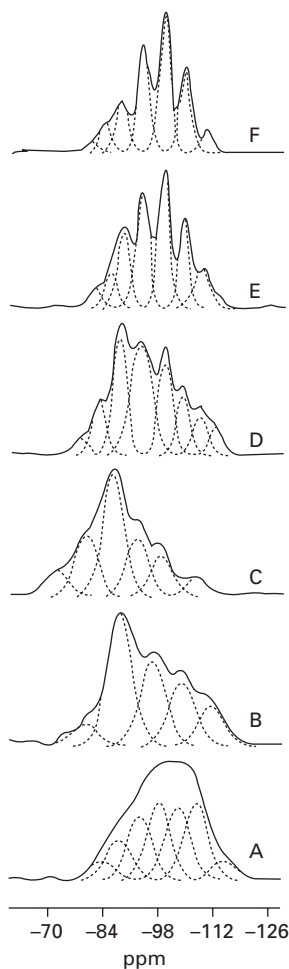
A detailed description of the role of the three components, Si, Al and Na, given below, is based primarily on MAS-NMR results.

6.3.1 The role of silicon in N-A-S-H gel structure

As mentioned above, all the studies published to date concur that the main reaction product of the alkali activation of aluminosilicates, and more specifically the alkali activation of fly ash, is an alkaline hydrated aluminosilicate gel with a three-dimensional structure consisting in $Q^4(mAl)$ ($m = 0, 1, 2, 3, 4$) units. Nonetheless, significant differences can be found in gel structure depending on the degree of ash reaction, curing temperature and especially the presence of soluble silica in the alkali activator.

In Fig. 6.4 (spectrum A) the ^{29}Si NMR spectra of a normal type fly ash is shown. The deconvolution of this spectrum shows the presence of 7 components. Peaks detected at -83 ppm, -91.8 ppm, -96.9 ppm and -103 ppm correspond to the starting vitreous material, while the peak at -87.4 ppm corresponds to crystalline mullite present in the fly ash. Finally, the peaks at -109.3 and -114 [signals $Q^4(0Al)$] have been ascribed to the presence of different crystalline silica phases (Fernandez-Jimenez and Palomo 2003).

The ^{29}Si MAS-NMR spectra of fly ash activated with 8M NaOH and cured at $85^\circ C$ for from two hours to seven days (spectra B to F) are also given in Fig. 6.4. The changes detected in spectra A to F reveal the chemical transformations taking place during alkali activation of the initial fly ash at different reaction times. The most relevant change is observed in the early stages. The most intense signal appearing between the second and the eighth hour at $85^\circ C$, at around $-86/-87$ ppm, is associated with the formation of an Al-rich alkaline silicoaluminate gel with a predominance of $Q^4(4Al)$ silicon units [Gel I]. The signals detected at lower values ($\approx -82/-80$ and $-79/-77$ and $-72/-70$ ppm), whose intensity decreases as the reaction progresses, are attributed to the presence of less condensed, i.e. monomer and dimer, species. Assignment of the signals observed at over -88 ppm, indicative of



6.4 (a) ^{29}Si MAS-NMR spectra of the starting fly ash (A) and the fly ash alkali activated with 8M NaOH solution and cured at 85°C for: B = 2 hours; C = 5 hours; D = 8 hours; E = 20 hours and F = 7 days (data from Fernandez-Jimenez *et al.* 2006a).

a lower degree of reaction, is difficult because they overlap with the signals for the unreacted ash.

Spectra E and F (24 hours and 7 days of thermal curing) are similar and reveal the existence of several components. Five of these are associated with the presence of silicon respectively surrounded by zero, one, two, three or four aluminium tetrahedra in the silico-aluminat gel, whose signals appear at around -110, -104, -98, -93, and -88 ppm, attributed to the formation of a new tectosilicate rich in Si (Gel 2). The signals detected at -74.5 and -81.0 ppm in some of these spectra are associated with the presence of less

condensed, residual species, probably monomer or dimer units with silanol groups.

At intermediate reaction times, the ^{29}Si NMR spectra (see spectrum D) consist of a superposition of the two aluminosilicates formed.

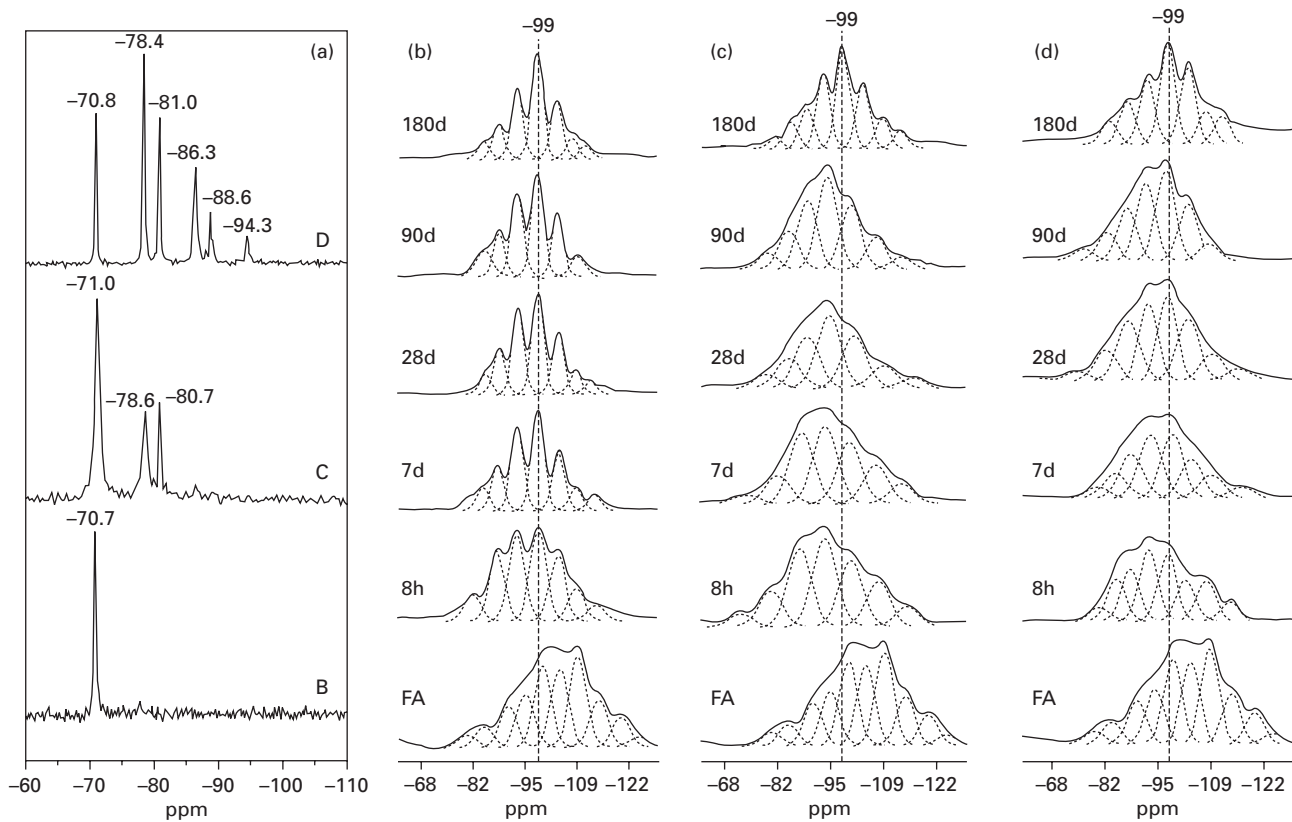
The Si/Al ratio of the gel formed can be found by applying Engelhardt's equation (Engelhardt + Michel 1987) (this equation assumes that everything is $\text{Q}^4(n\text{Al})$ units) to the eight-hour spectra, where only minor overlapping with the unreacted ash is observed. In the present case the 8- and 24-hour and 7-day values obtained were 1.42, 1.92 and 1.8, respectively (spectra D, E and F). At a curing time of 85°C , these data confirm that as the reaction time increases, the Al-rich *meta-stable/intermediate* phase (Gel 1) changes to a more stable Si-rich phase or Gel 2 (Ostwald's rule). The dissolution rates for the Al- and Si-rich phases of the N-A-S-H gel, a 'zeolite precursor', indicate that the latter is more stable.

Studies by a number of authors (Bakharev 2005, Criado *et al.* 2005, Fernandez-Jimenez *et al.* 2005b, Krivenko 1992, Palomo *et al.* 2004a) have shown that both the curing temperature and the nature of the alkali activator may affect process kinetics. More specifically the reaction rate increases with increasing curing temperature. Moreover, different reaction products can be obtained by varying the reaction time and curing temperature. Longer reaction times lead to higher proportions of Si in the end product, with the concomitant enhancement of mechanical properties (Fernandez-Jimenez *et al.* 2005b, Palomo *et al.* 2004a, Duxson *et al.* 2007a).

With regard to the nature of the alkali activator, the Si which forms part of the N-A-S-H gel need not come solely from the raw material used as the primary source of the binder: it may also be present in the alkali activator. In fact, the silica present in sodium silicate (one of the activators most commonly used in these systems) is highly soluble and consequently incorporated immediately into the N-A-S-H gel. Nonetheless, most importantly, the degree of silica polymerisation in the sodium silicate (*waterglass*) solution, which depends on the $\text{SiO}_2/\text{Na}_2\text{O}$ ratio, decisively conditions the (*intermediate*, *metastable*) structural stages involved in N-A-S-H formation.

Figure 6.5(a) shows the ^{29}Si NMR spectra of three sodium silicate solutions with an Na_2O content of $\sim 8\%$ and different $\text{SiO}_2/\text{Na}_2\text{O}$ ratios (0.17, 0.60 and 1.90, respectively, for solutions B, C and D). Figures 6.5(b), (c) and (d), in turn, give the ^{29}Si MAS-NMR spectra for the products forming over time during fly ash activation with the three sodium silicate solutions. (The experimental profiles were deconvoluted with WIN NMR 1D software, using the assignments reported in previous studies (Fernandez-Jimenez *et al.* 2005b, Palomo *et al.* 2004a, Duxson *et al.* 2007a). In the present analysis, a constant bandwidth was assumed for all components.)

The main conclusion which can be extracted from Fig. 6.5 (Criado *et al.* 2007b) is that the nature of the alkali activator plays an instrumental role



6.5 (a) ^{29}Si NMR spectra of the alkaline solutions used; ^{29}Si MAS NMR-MAS spectra of AAFA pastes activated with solution (b) B, (c) C or (d) D (Criado *et al.* 2007b)

in the kinetics, structure and composition of the gel initially formed. The addition of soluble silica affects the intermediate stages of the activation reaction but not the end result.

Figure 6.5 also shows that the effects of a higher degree of polymerisation of the predominant silica species in the activating solutions include: (1) the time required for monomers and dimers to induce gel-forming reactions is shorter; (2) the presence of a high percentage of dimers leads to the speedier formation of gels, which are, however, less thermodynamically stable; and (3) the presence of cyclic silicate trimers (solution D Fig. 6.5(a), signal at -81 , -86 , -88 , and -94) or large species in general gives rise to initially more stable gels that retard the subsequent reaction of the ash.

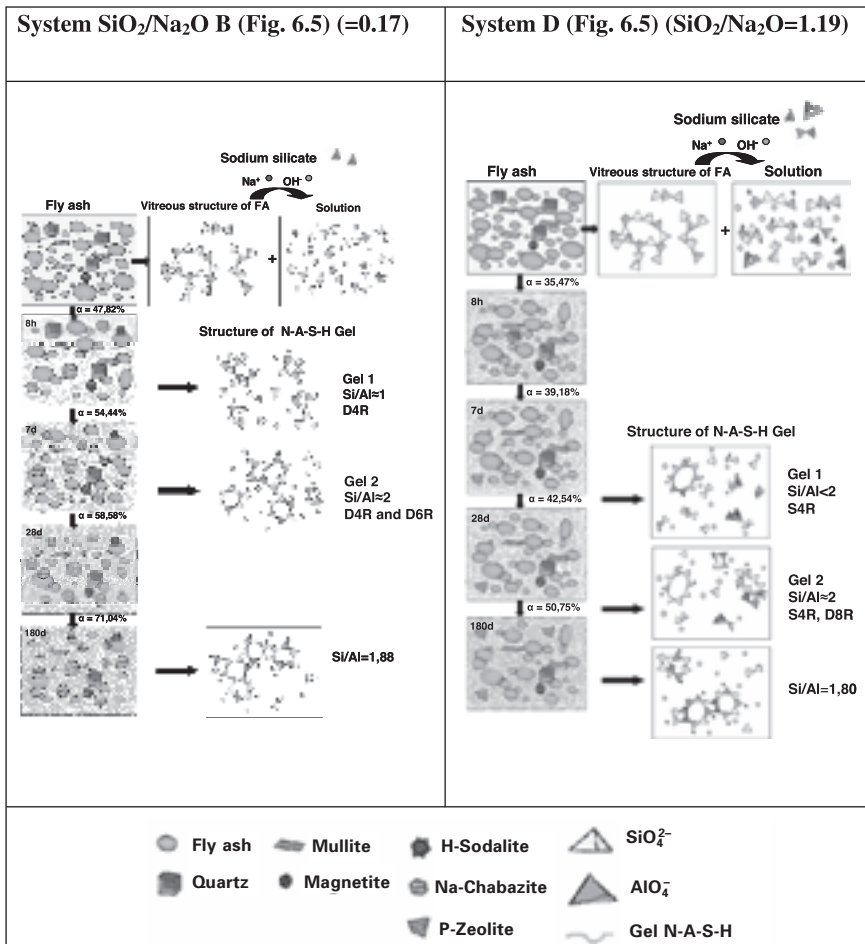
These findings show that the Si/Al ratio should not be increased indefinitely. There appears to be a threshold value of around 2, toward which the composition of these systems tends regardless of the initial conditions, possibly for reasons of thermodynamic stability.

In 2007, Criado *et al.*, (2007a, 2007b and 2007c) interpreting data obtained by a number of techniques (Rietveld XRD, FTIR and NMR) proposed different structural models to describe fly ash activation based on the amount of soluble silica used in the activation process. By way of example, Fig. 6.6 shows the nanostructural evolution of two of the systems studied by that author. This model illustrates the dissolution of the vitreous structure of the ash in the alkaline solution. The dissolved species interact, forming more polymerised structures, to ultimately precipitate as N-A-S-H gel when the system reaches saturation.

The presence of highly polymerised silica, such as in system D, affects N-A-S-H gel formation kinetics, retarding the degree of ash reaction and the zeolite crystallisation rate. Nonetheless, with time the system evolves toward a more thermodynamically stable product (see the 180-day spectra in Fig. 6.5).

6.3.2 The role of aluminium in N-A-S-H gel

Highly concentrated solutions of alkaline silicate are generally metastable and of moderate pH; consequently, the presence of soluble silicate is not in itself sufficient to produce a chemically hardened material. Compounds formed by silicates re-dissolve in water. Alkaline aluminosilicate solubility is extremely low, however, even when present in very small concentrations (on the order of mmol/l) (Glasser and Harvey 1984, Gasteiger *et al.* 1992). When silicate and aluminate solutions come into contact, the resulting aluminosilicate solution gels or precipitates to form zeolites or pre-zeolites (Ejaz *et al.* 1999, Patra and Ganguli 1994). In alkaline aluminosilicates, the condensation reactions are chemically initiated by the aluminium. Although no definitive studies on how to enhance or reduce aluminium availability



6.6 Nanostructural models of N-A-S-H gels with different doses of sodium silicate (Criado 2007).

during the synthesis of alkaline mineral polymers have been forthcoming, both the activator and the raw materials have been shown to be able to control the release of the element.

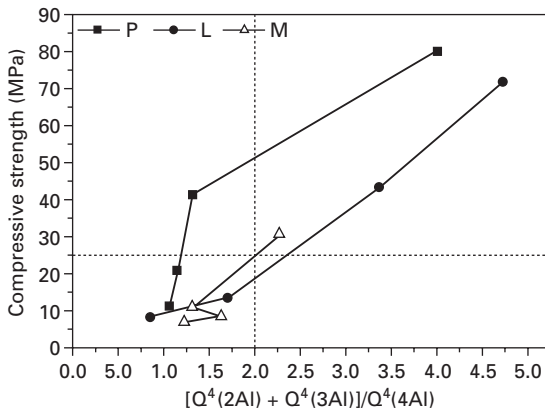
Determining the amount of aluminium available in the reactive system is crucial to properly formulating alkaline mineral polymers.

Fernández-Jiménez *et al.* (2005c, 2006a, 2006e), interpreting FTIR and NMR results for fly ash with similar reactive silica contents but different percentages of reactive alumina, demonstrated the importance of the role of reactive aluminium in gel formation kinetics and the mechanical performance of these materials. If an ash has a high initial reactive alumina content, large amounts of aluminium are released into the solution, and as a result, the ash is highly reactive. On the contrary, ash with a low percentage of reactive

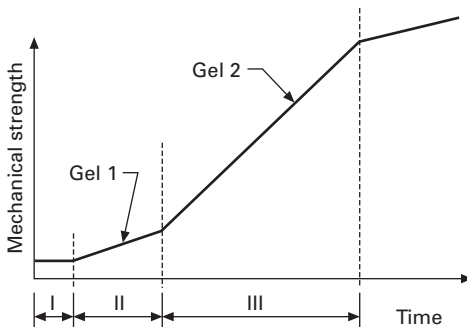
alumina, which is consumed in the early phases of the reaction, exhibits low reactivity.

Their findings indicate that the reactive alumina in fly ash must exceed a certain threshold ($\approx 20\%$) for the resulting material to exhibit good mechanical properties. Furthermore, excess aluminium concentration in the reactive medium shortens setting times and leads to more crystalline reaction products (De Silva *et al.*, 2007).

Fernández-Jiménez *et al.* (2006a) analysed the ^{29}Si MAS NMR spectra of the gel generated by the alkali activation of a number of types of fly ash, establishing relationships between mechanical strength and the proportions of $\text{Q}^4(3\text{Al}) + \text{Q}^4(2\text{Al})$ units (see Fig. 6.7). They concluded from the findings that



(a)



(b)

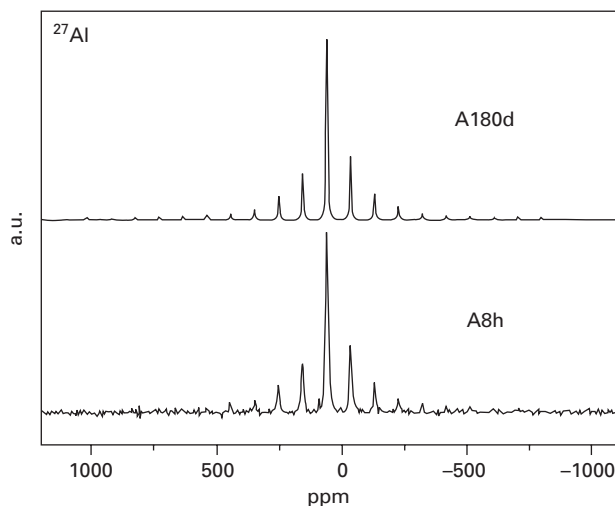
6.7 (a) Mechanical strength vs $\text{Q}^4(2\text{Al}) + \text{Q}^4(3\text{Al})/\text{Q}^4(4\text{Al})$ ratios deduced by NMR spectroscopy for three fly ashes with different alumina content ($P \approx 18.0\%$; $L \approx 22.5\%$; $M \approx 12.6\%$); (b) Schematic description of mechanical properties evolution with reaction time. The increase in mechanical performance is related to the Si/Al ratio in the gel (data from Fernández-Jiménez *et al.* 2006a).

the mechanical strength of mineral polymers increases during the formation of an aluminium-rich aluminosilicate gel (Gel 1) in the first stage of alkali activation of fly ash particles, but substantially more when the material is Si-enriched (Gel 2 formation).

In the 1980s Davidovits (1988, 1994) used nuclear magnetic resonance to study the structure of metakaolin-based inorganic polymers, reporting that Al(IV) prevails in these products, which also contain traces of Al(VI).

The spectra for fly ash alkali activated with an 8M NaOH solution are shown in Fig. 6.8 and Fig. 6.9. In ^{27}Al ($I = 5/2$) MAS-NMR spectra, central and satellite transitions are modulated by equally spaced side bands generated when the sample spins (Fig. 6.8). The spinning sidebands observed correspond to the central $(-1/2, 1/2)$ and satellite $[(-3/2, -5/2), (-1/2, -3/2), (1/2, 3/2)$ and $(3/2, 5/2)]$ transitions. The quadrupolar constants C_Q and η (C_Q , the quadrupolar coupling constant, provides information on the magnitude of polyhedral distortions, while η represents the asymmetry of the electric field gradient tensor at nuclear sites) can be estimated by simulating ^{27}Al MAS NMR spectra (first order quadrupolar effects). In the early stages of the reaction the materials are amorphous and exhibit no clearly defined environments. The mean values for the quadrupolar constants are $C_Q = 0.3$ MHz and $\eta = 0.5$. The similarity of the values for all the samples analysed is an indication that their structural characteristics are likewise similar.

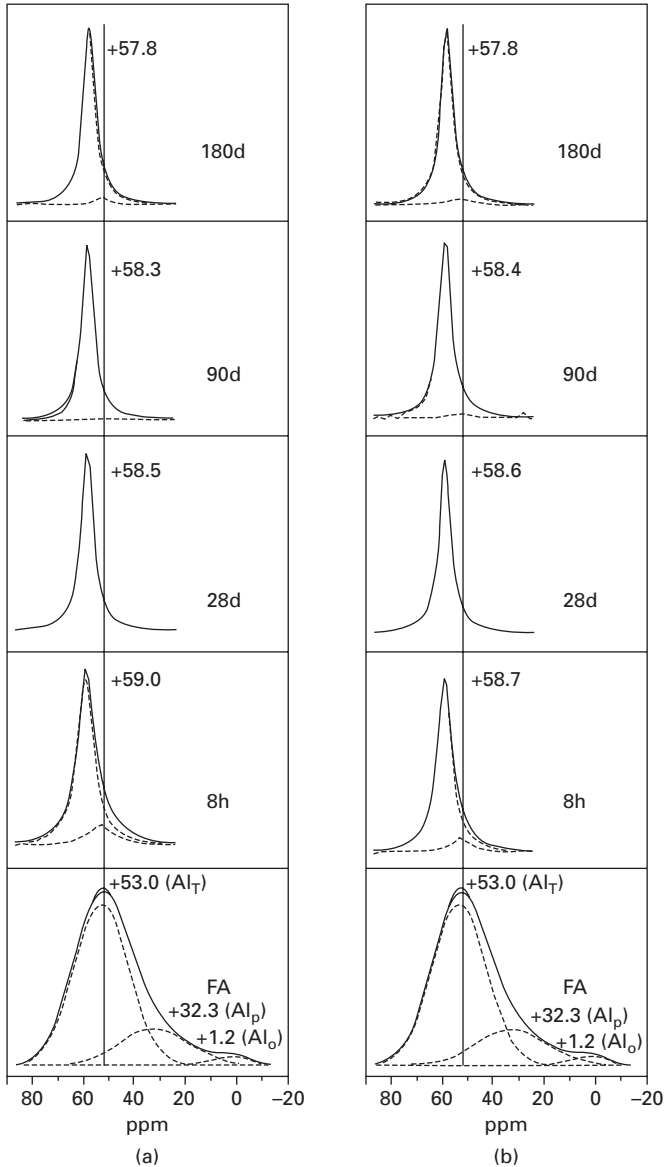
The experimental envelopes for several activated materials were analysed with the WINFIT software package to estimate quadrupolar interactions. In all



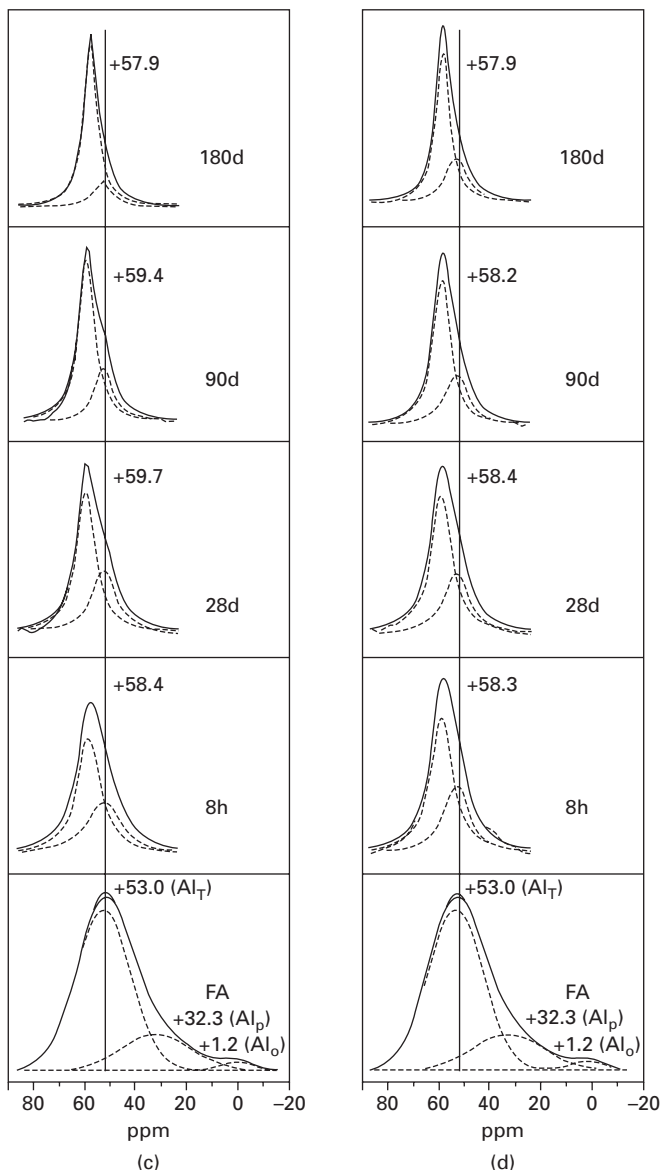
6.8 ^{27}Al MAS-NMR spectra of ash pastes activated with an 8M NaOH solution. Quadrupolar sideband patterns are visible in these spectra (data from Criado 2007).

samples, tetrahedral ^{27}Al MAS-NMR components, located at approximately +58 ppm, were scantily impacted by second order quadrupolar effects.

Note that the central components of the ^{27}Al MAS NMR spectrum for



6.9 Central component of the ^{27}Al MAS NMR spectra for fly ash pastes activated with (a) 8M NaOH solution; (b) Solution B in Fig. 6.5; (c) solution C in Fig. 6.5; (d) solution D in Fig. 6.5 (data from Criado 2007).



6.9 Cont'd

the initial ash include an intense tetrahedral aluminium peak at $\sim +60$ ppm (Fernandez-Jimenez *et al.* 2006a) (see Fig. 6.9). When the alkaline solution comes into contact with the ash, the tetrahedral aluminium signal narrows, as aluminium is quickly consumed during N-A-S-H gel formation. No octahedral aluminium is detected in these spectra, probably because the original mullite

phase with octahedral aluminium is partially attacked under such aggressive conditions (Criado *et al.* 2007c).

The experimental profiles are scarcely affected by the uptake of the soluble silica in the activating solution. In all cases Al is surrounded by four tetrahedral Si sites (Lowenstein rule). As the reaction time increases from 8 hours to 180 days, the spectra for all the activated materials exhibit similar changes. Zeolite formation, in particular, generates more clearly defined environments. In these phases, the spinning bands occupy a larger area of the spectrum, C_Q values rise (0.8 MHz) and η values remain unchanged ($\eta=0.5$) (Criado (2007)).

The line widths of the recorded spectra also vary, depending on the activating solutions used and thermal curing times. The line width of the Al_T component in the initial ash (at +53.0 ppm) declines with curing time, as the reaction is progressing and the percentage of unreacted ash is falling. In systems A and B, where reaction kinetics are faster, the amount of unreacted ash is smaller and the peak widths are narrower than in the other two systems (see Fig. 6.9).

At the highest reaction time, however, 180 days, the Al_T peak position is similar in all the materials. According to earlier studies (Palomo *et al.* 2004a, Criado *et al.* 2007a), behaviour in these systems follows the Ostwald ripening rule. Here also, the nature of the alkali activator affects the intermediate stages but not the end result of the reaction.

6.3.3 The role of sodium in the N-A-S-H gel structure

Although the role of alkali cations in the structure of the hydrated aluminosilicate gel appears to be related to balancing the negative charge generated during the uptake of AlO_4 tetrahedral units, little information is presently available in this regard.

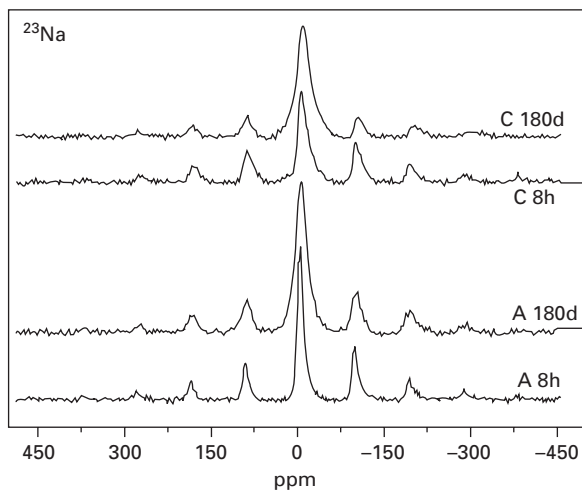
Duxson *et al.* (2005) showed that sodium can neutralise the negative charge in two ways. And in fact two peaks are visible on the ^{23}Na MAS NMR spectra for sodium aluminosilicates. One, at -4 ppm, is attributed to the sodium associated with aluminium inside the gel structure (compensation of the charge deficit). The other, at 0 ppm, appearing in the spectra for sodium aluminosilicates with a Si/Al ratio ≤ 1.40 , is associated with the sodium present in the solution that fills the pores, where it neutralizes the charge on $Al(OH)_4^-$ groups. These studies were conducted not on fly ash, but on metakaolin geopolymers (Rowles *et al.* 2007).

More recently Criado *et al.* (2007a) studied the position of Na in the structure of the N-A-S-H gel forming when fly ash is alkali activated. In dehydrated zeolites, sodium ions are known to coordinate intensely with oxygen ions, leading to highly negative chemical shifts. This dehydrated material is characterised by substantial polyhedral distortions, while quadrupolar

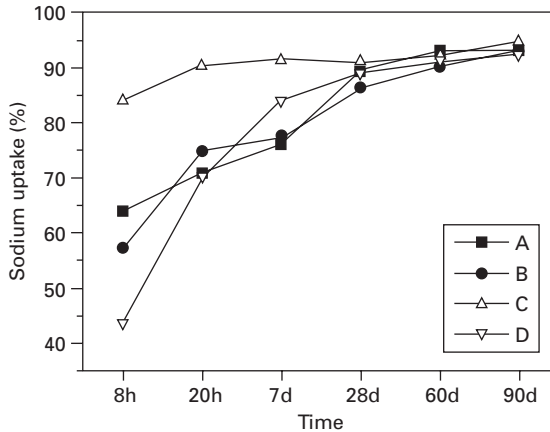
interactions induce large deviations in the chemical shifts of ^{23}Na , which normally appear at values lower than -20 ppm (Barbosa *et al.* 2000, Hannus *et al.* 1998, 1999). The chemical shift is toward more positive values as the water content rises. Fig. 6.10, show a broad, intense signal centred over -6.5 to -10 ppm. This signal is associated with the presence of partially hydrated sodium coordinated with the aluminium replacing the silicon in a charge balancing arrangement.

Note that in the ^{23}Na MAS NMR spectra, when sodium is totally or partially hydrated, the chemical environment around these ions is very similar, giving rise to scant variation in chemical shifts; low quadrupole interaction is likewise observed in such cases. These materials exhibit small quadrupolar interactions with the concomitant small deviations in quadrupolar shifts. In all cases, the mean values for the quadrupolar constants are $C_Q \approx 0.06\text{--}0.07$ MHz and $\eta \approx 0.4\text{--}0.5$, indicating, as in the case of aluminium, that the structural features are similar in all samples.

As in the ^{27}Al spectra, only minor differences are observed in the ^{23}Na MAS NMR spectra when the alkaline activator and curing times vary. The inference is that Na occupies similar sites in all the materials analysed. The ^{23}Na MAS NMR signal also broadens with increasing reaction time; however (see Fig. 6.10), a finding associated with the multi-site fixation of sodium in the N-A-S-H gel. These data have been corroborated by leaching test findings (Criado 2007). Figure 6.11 shows that the percentage of the sodium taken up by N-A-S-H gels and zeolites converges towards a common value as the reaction time increases. The percentage of sodium uptake is



6.10 Central component of ^{23}Na MAS NMR spectra for ash pastes activated with 8M NaOH and the solution specified in Fig. 6.5 (data from Criado 2007).



6.11 Variation in soluble sodium over time in all the systems analysed (data from Criado 2007).

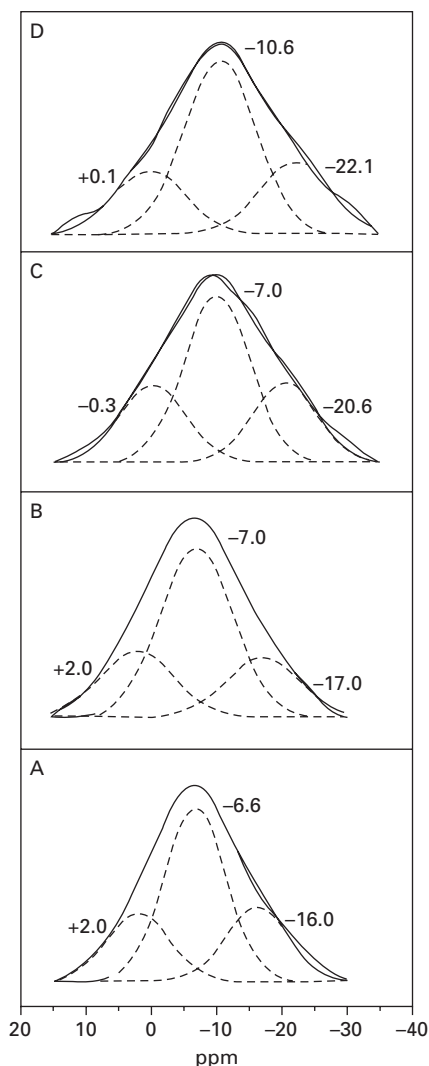
found by determining the amount of water soluble sodium as analysed by ion chromatography (Dionex model DX 500).

The aluminium content is the same in all materials studied here; only the silica content changes. Given that the sodium incorporated in these materials must be associated with the aluminium in the gel (N-A-S-H) or the zeolites (in a charge balancing capacity), the Na content fixed must be the same when the system reaches equilibrium (see Fig. 6.12).

Figure 6.12 also shows a slight shift in the most intense signal of the ^{23}Na spectra toward more negative values with rising soluble silica content in the alkaline solution. In materials activated with solutions A and B, the spectral centre of gravity appears at around -6.5 ± 0.5 ppm, while for materials activated with solutions C and D (high silica content) this area appears at around -10 ± 1 ppm (see Fig. 6.12), widening and growing more asymmetric. As in the ^{27}Al spectra, these variations in the ^{23}Na spectra may be associated primarily with variations in material composition due to the changing reaction kinetics.

The most intense signal in the ^{23}Na spectra systematically shifts to lower frequencies when the Si/Al ratio in the aluminosilicate glass rises, in all likelihood due to increases in Na-O distances or coordination numbers (Lee and Stebbins 2003). Where Na^+ shows a strong preference for sites surrounded by Si-O-Al instead of Si-O-Si or water molecules, the Si/Al ratio would be expected to show much less influence on the ^{23}Na MAS NMR spectra.

As in the foregoing, the addition of soluble silica affects the intermediate stages of the activation reaction (different types of zeolites). For instance, after 180 days some of the zeolites identified along with the 'zeolite precursor' (main reaction product) were: chabazite-Na (materials activated with solutions



6.12 Central component of the 180-day ^{23}Na MAS NMR spectra for activated ash pastes (data from Criado 2007).

A and B), phillipsite (solution C materials) and zeolite P (solution D materials), all having a Si/Al ratio of around 2.

Briefly, given the scant likelihood of Na occupying a single type of cage in zeolites (Lee and Stebbins 2003, Liang and Sherrif 1993), the most intense signal in all the materials studied is associated with rapid inter-site exchange. The sodium taken up in these materials is partially hydrated and must be in close proximity to aluminium ions to balance the charge deficit in the gel structure. In all the materials studied, Na^+ ion

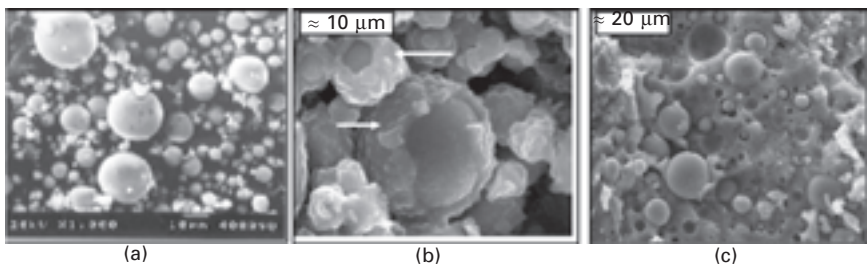
coordination is very similar and linked to oxygen and water molecules. Given the similarities in the Na ion environments only minor variations in shift values are observed. The small shift in materials with the highest Si/Al ratio is associated with the increasing Na-O distance in samples where the (N-A-S-H) gel content is higher than the zeolite content.

6.4 Microstructure of the fly ash geopolymer

The activation reaction rate as well as the microstructure and chemical composition of the reaction products depend on several factors, such as the particle size distribution and mineral composition of the initial fly ash, activator type and concentration and so on. Since, as has been indicated previously, the mechanisms controlling the general activation process are independent of the above variables, however, this section contains a summary of the microstructure of alkali activated fly ash pastes versus reaction time and the type of alkali activator used.

The characteristic morphology of the original fly ash is shown in the SEM image in Fig. 6.13(a), where it can be seen to consist of a series of spherical vitreous particles of different sizes (diameters ranging from 10 to 200 μm). Although usually hollow, some of these spheres may contain other particles of a smaller size in their interiors. Figures 6.13(b) and 6.13(c) show the changes detected in the fly ash microstructure after the alkaline attack and subsequent thermal curing. The primary reaction product resulting from that attack is a sodium silicate gel that consolidates with the gel formed by other particles during precipitation, giving rise to a cementitious matrix. In addition, in Fig. 6.14(b), a few small fly ash particles having already reacted with the alkali solution are observed to co-exist with some of the unreacted spheres and even with particles partially covered with reaction products. These spheres (more visible in Fig. 6.13(b)) will obviously react very slowly.

The figures also depict the full range of variation in fly ash particle reactivity, including no perceptible reaction, surface dimpling, particles inside



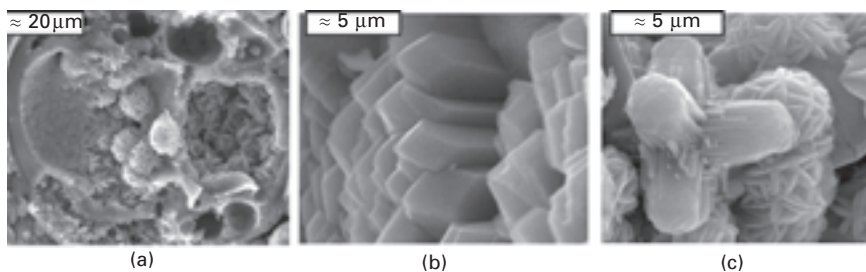
6.13 SEM images: (a) original fly ash; (b) fly ash activated with 8M NaOH for 20 hours at 85°C (showing reaction details for small spheres); (c) fly ash activated with sodium silicate. (data from Fernandez-Jimenez *et al.* 2005d).

shells (denoting reaction) and empty shells, indicative of full reaction. This variability, suggests either: (i) differences in the granular properties of the fly ash or (ii) limited exposure of some fly ash particles to alkaline attack.

Figure 6.14 shows the morphology of some of the types of zeolites that may form in these materials. The presence of small amounts of zeolites may have a beneficial effect on mechanical strength, for they normally appear in the hollows left by reacted ash. The formation of certain types of zeolites (hydroxysodalite, Na-chabazite, zeolite P, etc.) has been observed to enhance the durability of these materials (see Chapter 9). Since, however, zeolites largely form to the detriment of the gel, this decline also affects mechanical performance. When sodium silicate is used, the presence of silica normally retards the zeolite formation rate. As a result, higher initial strength values are obtained at lower degrees of reaction (Fernandez-Jimenez *et al.* 2005b, Palomo *et al.* 2004b, Criado *et al.* 2007c).

Finally, like the models proposed by other authors (Taylor 1990, Scrivener 1984) to explain the microstructure forming as a result of Portland cement hydration, a model has been proposed by Fernández-Jiménez *et al.* (2005d) to explain the reaction taking place during fly ash alkali activation (see Fig. 6.15). In the existing models for Portland cement, inasmuch as the particles are compact grains, the hydration reaction begins with a surface attack, after which the grains dissolve, a layer of hydration products forms around each one, particle diameter increases and tiny isolated clusters form. As hydration progresses the particles continue to grow and consolidate and what was initially a suspension becomes a porous solid (Brouwers and van Eijk 2002).

The model for the alkali activation of fly ash, by contrast, is illustrated in Fig. 6.15. As Fig. 6.15(a) shows, the initial chemical attack begins at one point on the surface of a particle and then expands to form a larger hole, exposing smaller particles, whether hollow or partially filled with other yet smaller ashes, to bi-directional alkaline attack: i.e., from the outside in and from the inside out (see Fig. 6.15(b)). Consequently, reaction product

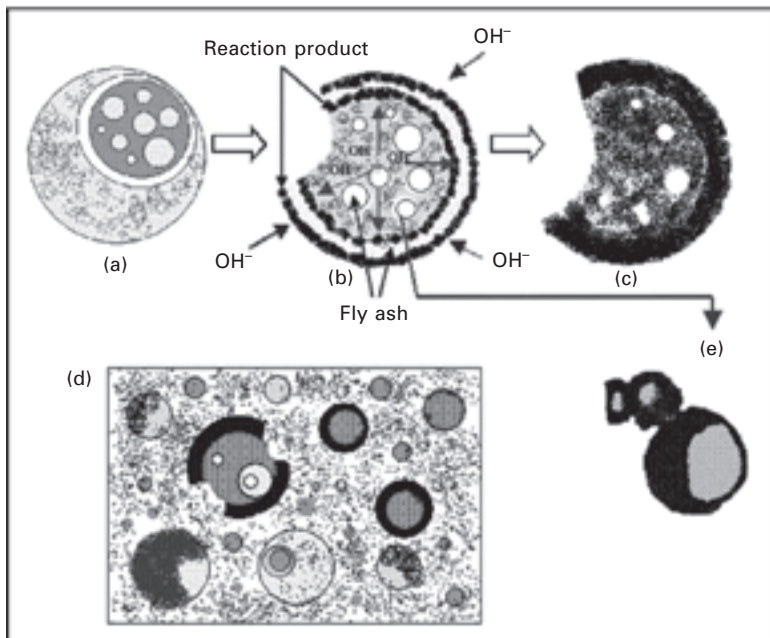


6.14 SEM images of zeolites forming in alkali activated fly ash as secondary reaction products, by curing conditions and the alkali activator used: (a) Na-chabazite; (b) Zeolite P; (c) Zeolite.

is generated both inside and outside the shell of the sphere, until the ash particle is completely or almost completely consumed (Fig. 6.15(c)). The mechanism involved at this stage of the reaction is dissolution. At the same time, as the alkaline solution penetrates and contacts the smaller particles housed inside the larger spheres, the interior space of the latter starts to fill up with reaction product, forming a dense matrix.

One of the consequences of the massive precipitation of reaction products is that a layer of these products covers certain portions of the smaller spheres. This crust prevents their contact with the alkaline medium (Fig. 6.15(e)). Ongoing reactions within the bulk of the matrix consolidate such crusts, with the concomitant effect on the pH gradient across the fly ash reaction product. As alkaline activation continues, the unreacted fly ash buried under reaction product may not be affected by the very high pH associated with the activator, thereby reducing the reaction rate. In this case activation is governed by a diffusion mechanism. The variation in the degree of reaction at different times may suggest variable permeability of the layers of hydration product.

Moreover, the processes described are not uniform throughout the gel but vary locally from one point in the matrix to another, depending on the distribution of particle size and the local chemistry (e.g. pH). Several



6.15 Alkali activation of fly ash. Descriptive model (data from Fernández-Jiménez *et al.* 2005d).

morphologies may co-exist in a single paste: unreacted particles, particles attacked by the alkaline solution but which maintain their spherical shape, reaction product and so on.

It should be stressed here that the presence of soluble silica in the activating dissolution plays an important role in the development of the microstructure in such cementitious systems, which resembles the very uniform, shapeless and scantily porous microstructure found in many types of glass. This uniformity is only interrupted by the presence of a few unreacted fly ash particles or traces of ash spheres. The Si and Na contents in this matrix are usually higher than in materials activated with NaOH. Nonetheless, the microstructure generated in the presence of soluble silica ions is essentially the same as obtained when the ash is activated with a NaOH solution and thermally cured for longer times.

6.5 Conclusions

Although a considerable and growing literature on alkali-activated systems has been emerging since the 1950s, assimilation of the information is difficult. Often interpretation of results has been rather empirical and sometimes poorly justified, and, in other cases, commercial interests have imposed restrictions on information dissemination. Clearly, fundamental studies have been reported but comparison from group to group has been often limited due to variations in experimental approaches. It is only relatively recently that a more consistent picture has begun to develop regarding the underlying chemistry behind phase development and product performance characterisation.

6.6 References

- Bakharev T., (2005) 'Geopolymeric materials prepared using Class F fly ash and elevated temperature curing', *Cem. Concr. Res.*, 35, 1224–1232.
- Barbosa V.F.F, Mackenzie K.J.D., (2003) 'Synthesis and thermal behaviour of potassium silicate geopolymers', *Mat. Lett.*, 57, 1477–1482.
- Barbosa V.F.F, MacKenzie K.J.D., Thaumaturgo C., (2000) 'Synthesis and characterisation of materials based on inorganic polymers of alumina and silica: sodium polysialate polymers', *Inter. J. Inorganic Mat.*, 2, 309–317.
- Barrer R.M., (1982) '*Hydrothermal chemistry of zeolites*', Academic, London, UK.
- Brouwers H.J.H., van Eijk R.J., (2002) 'Fly ash reactivity: Extension and application of a shrinking core model and thermodynamic approach', *J. Mater. Sci.*, 37(10) 2129–2141.
- Carman P.C., (1940) 'Constitution of colloidal silica', *Trans. Faraday Soc.*, 36, 964–972.
- Chen J.J., Thomas J.J., Taylor H.F.W., Jennings H.M., (2004) 'Solubility and structure of calcium silicate hydrate', *Cem. Concr. Res.*, 34, 1499–1519.
- Cong X., Kirkpatrick R.J., (1995) 'Effects of the temperature and relative humidity on the structure of C-S-H gel', *Cem. Concr. Res.*, 25, 1237–1245.

- Criado M., (2007) PhD Thesis. 'Nuevos materiales Cementantes basados en la activación alcalina de cenizas volantes. Caracterización de geles N-A-S-H en función del contenido de sílice soluble. Efecto del Na_2SO_4 ', Universidad Autónoma de Madrid, Madrid, Spain.
- Criado, A. Palomo, A. Fernández-Jiménez (2005) 'Alkali activation of fly ashes. Part I: Effect of curing conditions on the carbonation of the reaction products', *Fuel*, 84, 2048–2054.
- Criado M., Fernández-Jiménez A., Palomo A., (2007a) 'Alkali Activation of fly ash. Effect of the $\text{SiO}_2/\text{Na}_2\text{O}$ ratio. Part I: FTIR study', *Microp. Mesop. Mat.*, 106, 180–191.
- Criado M, Fernández-Jiménez A., Palomo A., Sobrados I., Sanz J., (2007b) 'Effect of the $\text{SiO}_2/\text{Na}_2\text{O}$ ratio on the alkali activation of fly ash. Part II: ^{29}Si MAS-NMR Survey', *Microp. Mesop. Mat.*, 109, 525–534.
- Criado M., Fernández-Jiménez A., de la Torre A.G., Aranda M.A.G., Palomo A., (2007c) 'An XRD study of the effect of the $\text{SiO}_2/\text{Na}_2\text{O}$ ratio on the alkali activation of fly ash', *Cem. Concr. Res.*, 37, 671–679.
- Davidovits J., (1988) 'Geopolymer properties and chemistry', 1st European Conference on Soft Mineralogy. Geopolymer'88. Compiègne (France) 25–48.
- Davidovits J., (1994) 'Properties of Geopolymer Cements', Proceedings of 1st International Conference on Alkaline Cements and Concretes, 1, 131–149, VIPOL Stock Company, Kiev, Ukraine, (1994).
- Davidovits J., (2008) '*Geopolymer. Chemistry and Applications*', Institute Gèopolymère, Saint-Quentin, France.
- De Silva P., Sagoë-Crenstil K., Sirivivatnanon V., (2007) 'Kinetics of geopolymerization: Role of Al_2O_3 and SiO_2 ', *Cem. Concr. Res.*, 37, 512–518.
- Duxson P., Lukey G.C., Separovic F. van Deventer J.S.J., (2005) 'Effect of alkali cations on aluminium incorporation in geopolymeric gels', *Ind. Eng. Chem. Res.*, 44, 832–839.
- Duxson P., Fernández-Jiménez A., Provis J.L., Lukey G.C., Palomo A., Van Deventer J.S.J., (2007a) 'Geopolymer technology: the current state of the art', *J. Mat. Sci.*, 42 (9) 2917–2933.
- Duxson P., Mallicoat S.W., Lukey G.C., Kriven W.M., van Deventer J.S.J., (2007b) 'The effect of alkali and Si/Al ratio on the development of mechanical properties of metakaolin-based geopolymers', *Colloids and Surfaces A: Physicochemical and Engineering Aspects*, 292, 8–20.
- Ejaz T., Jones A.G., Graham P., (1999) 'Solubility of Zeolite A and its amorphous precursor under synthesis conditions', *J. Chem. Eng. Data*, 44, 574–576.
- Engelhardt G. and Michel D., (1987) '*High-Resolution Solid-State NMR of Silicates and Zeolites*', John Wiley & Sons.
- Fernández-Jiménez A., Palomo A., (2003) 'Characterization of fly ashes. Potential reactivity as alkaline cements', *Fuel* 82, 2259–2265.
- Fernández-Jiménez A., Palomo A., Alonso M.M., (2005a) 'Alkali activation of fly ashes: Mechanisms of reaction', 2nd Inter. Symposium Non-Traditional Cement and Concrete, Brno, Czech Republic.
- Fernández-Jiménez A., Palomo A., (2005b). 'Composition and microstructure of alkali activated fly ash binder: Effect of the activator', *Cem. Concr. Res.*, 35, 1984–1992.
- Fernández-Jiménez A., Palomo A., (2005c) 'Mid-infrared spectroscopic studies of alkali-activated fly ash structure', *Microp. Mesop. Mat.*, 86, 207–214.
- Fernández-Jiménez A., Palomo A., Criado M., (2005d) 'Microstructure development of alkali-activated fly ash cement. A descriptive model' *Cem. Concr. Res.*, 35, 1204–1209.

- Fernández-Jiménez A., Palomo A., Sobrados I., Sanz J., (2006a) 'The role played by the reactive alumina content in the alkaline activation of fly ashes', *Microp. Mesop. Mater.*, 91, 111–119.
- Fernández-Jiménez A., Vallepu R., Terai T., Palomo A., Ikeda K., (2006b) 'Synthesis and thermal behaviour of different aluminosilicates', *J. Non-Cryst. Sol.*, 352, 2061–2066.
- Fernández-Jiménez A., Palomo A., López-Hombrados C., (2006c) 'Some engineering properties of alkali activated fly ash concrete', *ACI Materials Journal*, 103 (2) 106–112.
- Fernández-Jiménez A., Palomo A., Criado M., (2006d) 'Alkali activated fly ash binders. A comparative study between sodium and potassium activators', *Mater. Construct.*, 56, 51–65.
- Fernández-Jiménez A., de la Torre A. G., Palomo A., López-Olmo G., Alonso M. M. and Aranda M.A.G., (2006e) 'Quantitative determination of phases in alkaline activation of fly ashes. Part II: the degree of reaction', *Fuel*, 85, 1960–1969.
- Gasteiger H.A., Frederick W.J., Streisel R.C., (1992) 'Solubility of aluminosilicates in alkaline solutions and a thermodynamic equilibrium model', *Ind. Eng. Chem. Res.*, 31 1183–1190.
- Glasser L.S.D., Harvey G., (1984) 'The gelation behaviour of aluminosilicate solutions containing Na^+ , K^+ , Cs^+ , and Me_4N^+ ', *J. Chem. Soc., Chem. Commun.*, 13, 1250–1252.
- Glasser F.P., Hong S. Y., (2003) 'Thermal treatment of C-S-H gel at 1 bar H_2O pressure up to 200°C', *Cem. Con. Res.*, 33, 271–279.
- Glukhovskiy V.D., (1967) '*Soil Silicate Articles and Structures (Gruntosilikatnye vyrobki I konstruktsii)*', Budivelnyk Publisher, Kiev, Ukraine.
- Hannus I., Kónya Z., Nagy J.B., Lentz P., Kiricsi I., (1998) 'Solid state MAS NMR investigation of Y-type zeolites reacted with chlorofluorocarbons', *Applied Catalysis B: Environmental*, 17, 157–166.
- Hannus I., Kiricsi I., Lentz P., Nagy J. B., (1999) 'Characterisation of alkali ions in the Y-type zeolites by multi MAS NMR studies', *Colloids and Surfaces A*, 158, 29–34.
- Ikeda K., (1997) 'Preparation of fly ash monoliths consolidated with a sodium silicate binder at ambient temperature' *Cem. Concr. Res.*, 27, 657–663.
- Iler R. K., (1955) '*The Chemistry of Silica*', Wiley, New York.
- Krivenko V., (1992) 'Fly-ash- alkaline cements and concretes', Proceedings of the Fourth CANMET-ACI Int. Conference on Fly Ash, Silica Fume, Slag and Natural Pozzolans in Concrete (Supplementary Volume) Istanbul, Turkey (1992) 721–734.
- Lee S.K. and Stebbins J.F., (2003) 'The distribution of sodium ions in aluminosilicate glasses: A high-field Na-23 MAS and 3Q MAS NMR study', *Geochimica et Cosmochimica Acta*, 67, 1699–1709.
- Liang J.J. and Sherrif B.L., (1993) 'Lead exchange into zeolite and clay minerals: A ^{29}Si , ^{27}Al , ^{23}Na solid-state NMR study', *Geochimica et Cosmochimica Acta*, 57, 3885–3894.
- Palomo A., Glasser F.P., (1992) 'Chemically-bonded cementitious materials based on metakaolin', *Br. Ceram. Trans. J.*, 91, 107–112.
- Palomo A., Grutzeck M.W., Blanco M.T., (1999) 'Alkali-activated fly ashes – A cement for the future', *Cem. Concr. Res.*, 29, 1323–1329.
- Palomo A., Alonso S., Fernández-Jiménez A., Sobrados I., Sanz J., (2004a) 'Alkali activated of fly ashes. A NMR study of the reaction products'. *J. Am. Ceramic. Soc.*, 87, 1141–1145.

- Palomo A., Fernández-Jiménez A., López-Hombrados C., Lleyda J.L., (2004b) 'Precast elements made of alkali-activated fly ash concrete', International Conference on Fly Ash, Silica Fume, Slag and Natural Pozzolans in Concrete. Ed. V.M. Malhotra.
- Palomo A., Fernández-Jiménez A., Criado M., Alonso M.M., (2005a) 'The alkali activation of fly ashes: from macro to nanoscale', 2nd International Symposium on Nanotechnology in Construction, Bilbao, Spain (2005).
- Palomo A., Fernández-Jiménez A., Kovalchuk G., (2005b) 'Some key factors affecting the alkali activation of fly ash', 2nd Inter. Symposium Non-Traditional Cement & Concrete, Brno, Czech Republic.
- Patra A., Ganguli D., (1994) 'Role of dopant cations in the gelation behaviour of silica sols', *Bull. Mater. Sci.*, 17, 999–1004.
- Phair J.W., Smith J.D., Van Deventer J.S.J., (2003) 'Characteristics of aluminosilicate hydrogels related to commercial Geopolymers', *Material Letters*, 57, 4356–4367.
- Radnai T., May P.M., Hefter G.T., Sipos P., (1998) 'Structure of aqueous sodium aluminate solutions: A solution X-ray diffraction study', *J. Phys. Chem. A*, 102 (40) 7841–7850.
- Richardson I.G., (2000) 'The nature of the hydration products in hardened cement pastes', *Cem. Concr. Composites*, 22, 97–113.
- Richardson I.G., Brough A.R., Brydson R., Groves G.W., Dobson C.M., (1993) 'Location of aluminium in substituted calcium silicate hydrate (C-S-H) gels as determined by ^{29}Si and ^{27}Al NMR and EELS', *J. Am. Ceram. Soc.*, 76 (1993) 2285–2288.
- Rowles M.R., Hanna J.V., Pike K.J., Smith M.E., O'Connor B.H., (2007) ' ^{29}Si , ^{27}Al , ^1H and ^{23}Na MAS NMR study of the bonding character in aluminosilicate inorganic polymers', *Appl. Magn. Reson.*, 32, 663–689.
- Scrivener K.L. (1984) PhD Thesis, University of London, UK.
- Sharara A.M., El-Didamony H., Ebied E., Abd El-Aleem, (1994) 'Hydration characteristics of $\beta\text{-C}_2\text{S}$ in the presence of some pozzolanic materials' *Cem. Concr. Resear.*, 24, 966–974.
- Shi C., Krivenko P.V., Roy D., (2006) '*Alkali-activated cements and concretes*' Taylor & Francis, London, UK.
- Sofi M., van Deventer J.S.J., Mendis P.A., Lukey G.C., (2007) 'Engineering properties of inorganic polymer concretes (IPCs)', *Cem. Concr. Res.*, 37, 251–257.
- Taylor H. F. W., (1986) 'Proposed Structure for Calcium Silicate Hydrate Gel' *J. Amer. Ceram. Soc.*, 69, 464–467, DOI: 10.1111/j.1151-2916.1986.tb07446.x
- Taylor H.F.W., (1990) '*Cement Chemistry*'. Academic Press London, UK.
- Taylor H.F.W., (1992) 'Tobermorite, jennite, and cement gel', *Zeitschrift für Kristallographie*, 202, 41–50.

J L PROVIS and C A REES, University of Melbourne,
Australia

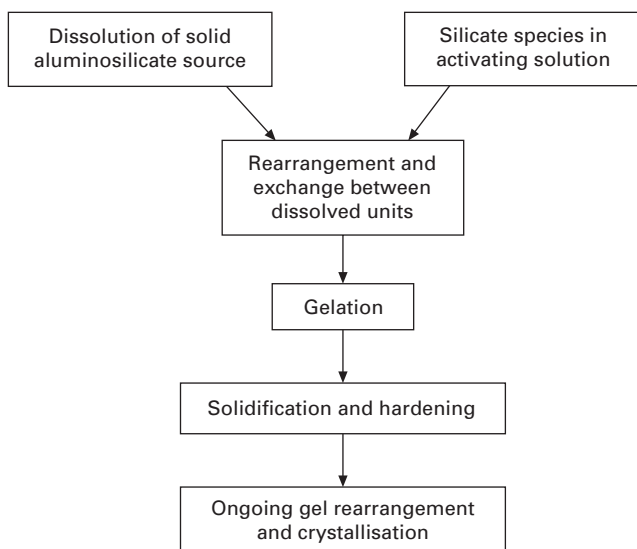
Abstract: The development of a detailed understanding of reaction kinetics is critical to the accurate control and tailoring of geopolymer setting rates, and to the nature of the products formed. Because geopolymerisation is a multistep reaction sequence by which one X-ray amorphous material (fly ash, metakaolin and/or slag) is converted into another X-ray amorphous material (geopolymer gel), many standard analytical techniques can provide only limited information. The application of less-standard techniques such as in situ infrared spectroscopy or in situ energy dispersive X-ray diffractometry provides valuable nanoscale information, and rheological and calorimetric analysis can bring additional insight. For any problem as complex as this, the development of an accurate mathematical model will be essential to the presentation of a holistic understanding of the chemical processes taking place, and initial steps have been made towards providing a basis for such a model incorporating empirical description of various factors which impact geopolymerisation kinetics.

Key words: geopolymer, aluminosilicate, kinetics, infrared spectroscopy, diffraction, kinetic modelling.

7.1 Introduction

The study of geopolymerisation kinetics has been the topic of significant discussion over the past decade. This work has a very practical application, as the mechanisms which govern the rates of reaction must be well understood before the setting processes can be adequately controlled, allowing these materials to be used in a wide variety of applications. Figure 7.1 presents a highly simplified overview of the chemical steps involved in the formation of a geopolymer binder, entirely aside from any physical processes (sorption on particle surfaces, gel drying, etc.) which occur concurrently. Various techniques are able to give insight into different aspects of this process, but it is immediately clear that there is no one technique which can provide a unified and all-encompassing description of this complex process.

Understanding reaction rates necessitates the development of analytical techniques capable of measuring the rate of geopolymer gel network growth, which is far from a trivial task. Reacting geopolymers are corrosive, sometimes sticky and tend to bond to most surfaces, meaning that if reactions are to be viewed up to the point of hardening, reaction cells must either be lined with a non-stick surface (PTFE is known to be effective), or else be sufficiently



7.1 Schematic depiction of the reaction steps taking place during geopolymerisation.

inexpensive to be replaced after each sample is tested. The fact that many geopolymer formulations react very rapidly necessitates short measurement time per point if detailed information is to be obtained. The fact that the key phases in both the reactants (metakaolin, fly ash and/or slag) and products (alkali aluminosilicate and/or calcium (alumino)silicate hydrate gels) are all lacking in long-range order means that the application of diffraction-based techniques is challenging. The presence of iron in fly ash, the slow relaxation times of key nuclei (^{29}Si in particular), and the tendency of geopolymers to stick to ceramic rotor surfaces mean that it is very difficult to apply NMR techniques to this problem.

This chapter will briefly discuss the application of various experimental and computational techniques to the study of geopolymerisation kinetics, in particular in the determination of aluminosilicate gel network growth rates and elucidation of some of the many factors affecting geopolymer kinetics. It is not possible to provide detailed coverage of all aspects of such a broad and diverse research area in a chapter such as this; rather, the focus will be on a few recently-developed techniques which find particular applicability to the study of geopolymers.

7.2 In situ infrared spectroscopy

Infrared spectroscopy is known to provide a particularly sensitive probe of the structure of the geopolymer binder, and has formed the basis of numerous

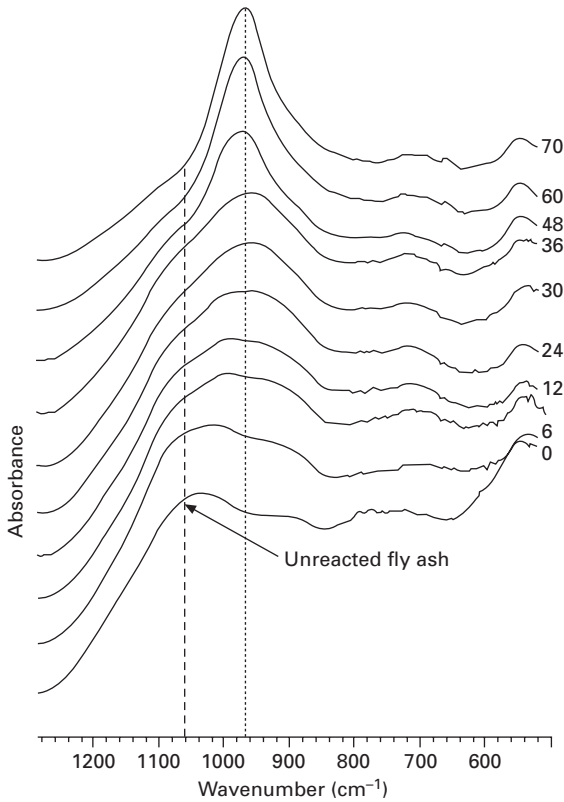
studies conducted on an *ex situ* basis (i.e., investigating hardened geopolymer products) (Lee and van Deventer 2003, Fernández-Jiménez and Palomo 2005, Criado *et al.* 2007, Rees *et al.* 2007a, and references cited therein). Recently, an *in situ* reaction cell was developed which enables the use of Attenuated Total Reflectance-Fourier Transform Infrared Spectroscopy (ATR-FTIR) to measure the relative concentration changes of the main functional groups involved in the early stages of geopolymer gel formation. In the initial demonstration of this apparatus, spectra were obtained at 1 minute intervals, over a 3 day period (Rees *et al.* 2007b).

The first stage of developing the *in situ* technique required a system-specific method of calibration. This involved the study of geopolymer gel ageing over a wide composition range using *ex situ* ATR-FTIR. Use of the ATR geometry allowed the direct analysis of the different phases at the surface of partially reacted geopolymer slurries and gels. The position of the asymmetric stretching vibration of the Si-O-T bonds (T: tetrahedral Si or Al; this band is often called the 'main band'), attributed primarily to the geopolymer gel network structure, was monitored for all samples at different time intervals over a period of 200 days. The position of the main band for each sample was therefore identified.

It should be noted that the *in situ* ATR-FTIR technique as applied here is problematic for geopolymers with concentrated silicate activating solutions. Dissolved silicate species exhibit strong stretching vibrations around the same region as the final geopolymer network (Rees 2007), making it difficult to distinguish between the two chemical groups. This violates the initial assumption that the peak intensity being quantified relates specifically to the vibrations of the of geopolymer gel network. The work presented in this section therefore relates specifically to the activation of fly ash by sodium hydroxide solutions.

An FTIR reaction profile for a fly ash geopolymer activated with sodium hydroxide, reacting at 30°C in a sealed reaction cell, is shown in Fig. 7.2 (Rees 2007). Although spectra were collected at 1 minute intervals, the times shown in this figure were selected to reflect only major spectral changes. The shoulder in the geopolymer spectra at approximately 1055 cm⁻¹, due to the main Si-O-T asymmetric stretching band for unreacted fly ash, reduced in intensity only slightly between 6 and 36 hours. A more significant reduction in this band was observed between 36 and 48 hours. Simultaneously, the band attributed to the geopolymer gel network, at approximately 960 cm⁻¹, began to increase in intensity. It can be seen from Fig. 7.2 that the band attributed to the geopolymer network begins to grow after a lag period, and then increases in intensity over time. The rate of intensity change for these bands is proportional to the amount of fly ash and geopolymer gel network present in the sample (Rees *et al.* 2007a, 2007b).

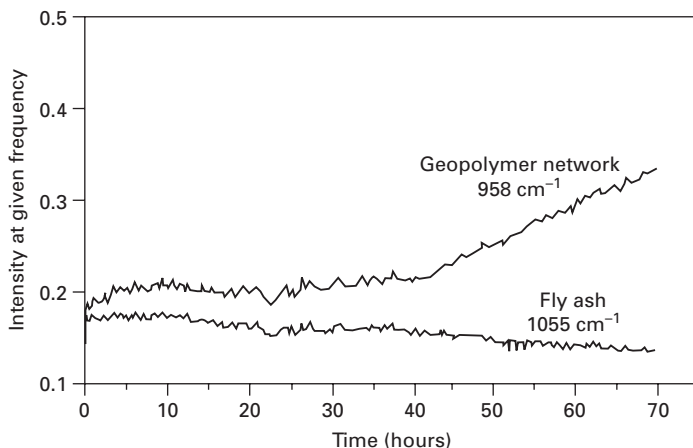
In order to quantify the time-dependence of the FTIR spectral changes,



7.2 FTIR spectra of geopolymer development for samples activated with 6M NaOH. Numbers represent time in hours. Data from Rees *et al.* (2007b).

the intensity of vibrational bands associated with the unreacted fly ash (1055 cm^{-1}), and the newly formed geopolymer network (960 cm^{-1}), may be plotted as a function of time (Fig. 7.3). Little change in the intensity of the main band (960 cm^{-1}) occurs from 0 to 42.5 hours. At 42.5 hours, the intensity of the 960 cm^{-1} band begins to increase, and this continues approximately linearly until the end of the 70-hour experiment.

The shoulder band due to unreacted fly ash reduces slightly in intensity between 0 and 42.5 hours, and the rate of decrease in this period appears to be approximately linear. Between 42.5 and 70 hours, the gradient becomes steeper, indicating that the rate of fly ash breakdown has increased during this period, but appears linear in this regime also. As predicted from Fig. 7.2, an intensity increase of the band at 960 cm^{-1} is accompanied by a reduction in intensity of the shoulder at 1055 cm^{-1} . During the lag phase, referred to as the ‘induction period’, the reagents are in contact; however, no coherent geopolymer network gel is formed. This is also observed in the fact that the

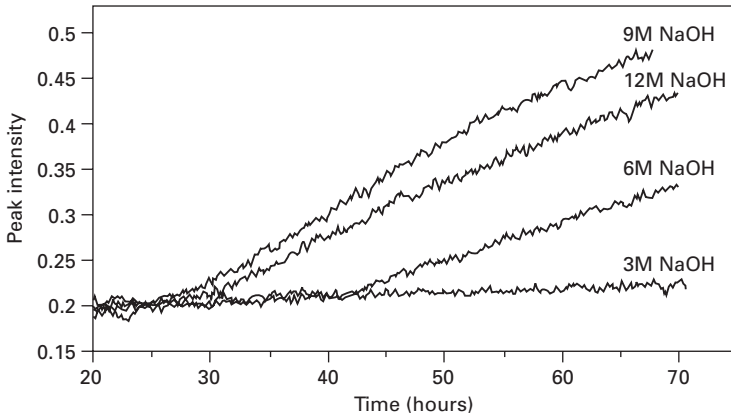


7.3 Kinetic analysis for a geopolymer sample activated with 6M NaOH. Data from Rees *et al.* (2007b).

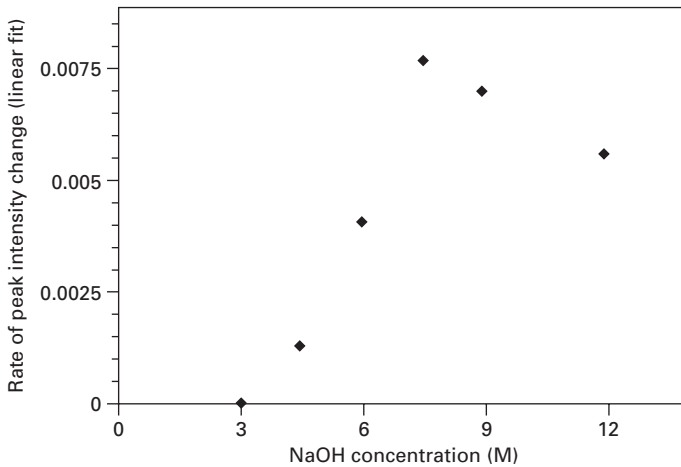
samples formed in this time period, although apparently solid, disintegrate rapidly when soaked in water (Rees *et al.* 2007a); there is some form of hardened gel phase forming, but it lacks sufficient structural integrity to genuinely be described as a crosslinked geopolymer binder.

Rates of geopolymer network growth were further investigated using lower and higher sodium hydroxide activating solution concentrations; a direct comparison of reaction rates for these samples is shown in Fig. 7.4. Intensities were normalised to the same starting point at $t = 20$ hours, for the purpose of comparing gradients. The sample activated with 3M NaOH shows little or no change in intensity over the entire 72 hours, indicating that the induction period was longer than the experiment. All geopolymer samples activated with higher sodium hydroxide concentrations exhibit a linear rate from immediately following the induction period until the end of the experiment. Linear functions were fitted to the data from the end of the activation period, with the relative network growth rates summarised in Fig. 7.5.

The activating solution sodium hydroxide concentration was found to have a profound effect on both the length of the induction period and the rate of network formation. Figure 7.5 illustrates the relationship between NaOH concentration ratio and the rate of geopolymer gel growth. There is an increase in the rate of geopolymer formation for increasing sodium hydroxide concentrations, until a maximum is reached, after which the rate is reduced by additional sodium hydroxide. Sodium hydroxide is known to speed the dissolution of silica (and thus aluminosilicate) in water (Brady and Walther 1989). Faster dissolution releases higher concentrations of silicate, aluminate, and/or aluminosilicate species into solution. This may appear to imply faster geopolymer network formation, due to rapid fly ash



7.4 Kinetic analysis for samples activated with different concentrations of sodium hydroxide as marked. Data from Rees *et al.* (2007b).



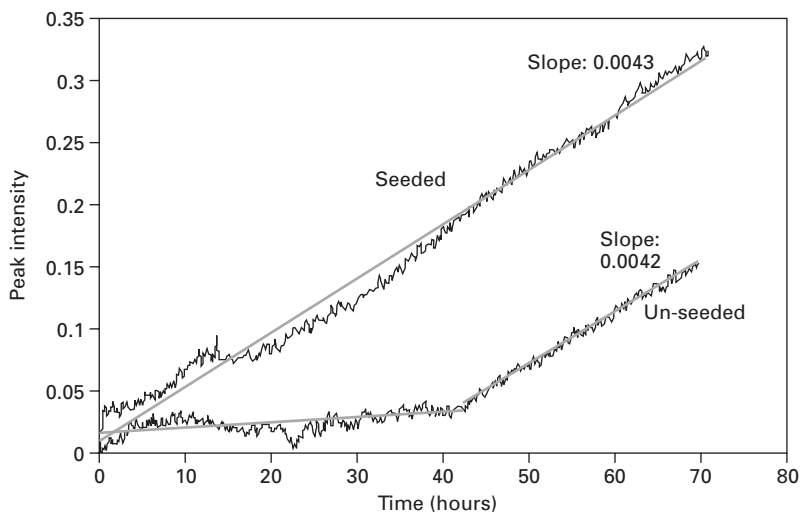
7.5 Rate of peak intensity change for the main band with for samples activated with varying concentrations of sodium hydroxide. Data from Rees *et al.* (2007b).

destruction; however, this is not necessarily the case. Although the increase in sodium hydroxide did shorten the induction period, the rate of network formation after this period was not always increased. This indicates that the rate determining step is likely to be geopolymer network formation rather than fly ash hydrolysis, and network formation is less favoured at high pH due to redissolution of gel components.

The well-developed understanding of zeolite synthesis kinetics can be used to explain some geopolymer kinetic phenomena. A recent review by Cundy and Cox (2005) presented a unified model for zeolite synthesis from

precursor gels, describing the formation of two different gel phases in the system prior to the appearance of zeolite crystals. The first gel formed is inhomogeneous and amorphous. Over time, the gel approaches equilibrium with the surrounding solution through depolymerisation-repolymerisation reactions, transforming into the ‘second gel’. Within the second gel, small, more highly ordered regions develop, which are later able to be released and act as nuclei (Cundy and Cox 2005, Antonić Jelić *et al.* 2007); when sufficient order is present and given sufficient mobility of nutrient species, these regions begin to grow into zeolite crystals. To accelerate crystal formation, mixtures are often seeded with small crystals which act as nucleation centres, eliminating the induction period (i.e., the time taken to produce stable crystal nuclei).

Similarly, the lag observed initially in geopolymer systems activated with sodium hydroxide could be identified as the time taken to form stable ‘gel nuclei,’ around which the geopolymer gel grows. These may be located on ash particle surfaces or elsewhere in the system; based on analysis of related zeolite syntheses it appears unlikely that homogeneous nucleation from the solution phase will occur (Bronić and Subotić 1995), meaning that it is likely that nucleation sites will be associated with the surfaces of solid particles. Therefore, the introduction of additional high-surface area solid particles to provide nucleation sites during synthesis would be expected to eliminate the initial lag period (Rees *et al.* 2008). To test this hypothesis, nucleation sites were added to geopolymer synthesis mixtures and in situ ATR-FTIR was used (Fig. 7.6). The lag period observed in the un-seeded geopolymer



7.6 Changes in intensity at 960cm^{-1} as a function of time for geopolymers activated with 6M NaOH. Straight lines have been graphically fitted. Data from Rees *et al.* (2008)

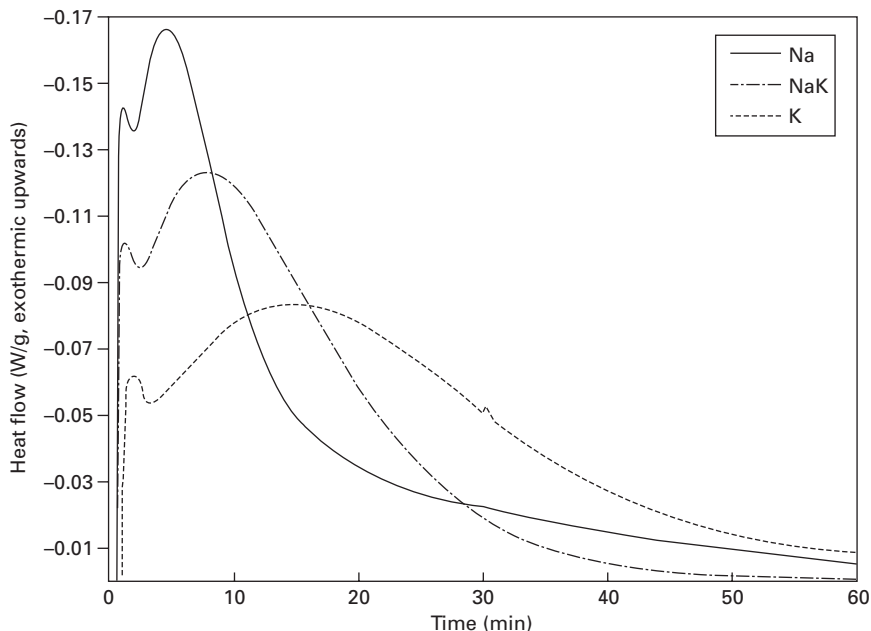
did not occur in the seeded sample; however, the rate of network growth, after onset, was the same in both systems.

Similar growth rates in the two systems indicate network growth mechanisms are similar; however, the addition of alumina nanoparticles (0.01g dose in a 60g sample) has removed the lag associated with nucleation in the unseeded system (Rees *et al.* 2008). There are also nanostructural changes induced by the addition of nanoparticles; different zeolitic crystallites are observed after an extended period of curing (including a phase not previously observed within geopolymers), and there are distinctive bands in the infrared spectra associated with the segregation of gel phases immediately surrounding the nucleation sites (Rees *et al.* 2008). These effects are not observed when a similar quantity of soluble alumina is added to a geopolymerisation system, meaning that they have not been induced by dissolution of the seed particles and must therefore be a true seeding effect. This highlights the importance of kinetic issues in controlling geopolymer structure formation and properties, and therefore the necessity to better understand and analyse these issues.

7.3 Calorimetry

Palomo and co-workers have studied the effect of various parameters including reaction temperature and calcium addition via isothermal conduction calorimetry (ICC) (Granizo *et al.* 2000, Alonso and Palomo 2001a, 2001b). Rahier *et al.* pioneered the use of quasi-isothermal modulated differential scanning calorimetry (DSC) as a means of simultaneously observing changes in heat flow and heat capacity during geopolymeric setting, and coupled these data with rheological measurements to correlate heat flow with the onset of gel crosslinking (Rahier *et al.* 1996a, 1996b, 2003). Both groups provided links between heat release data and the final mechanical strength of the geopolymeric products. However, little additional analysis of the underlying causes of the observed trends in the heat flow signals has yet been undertaken. In particular, it is clear from the multiple heat flow peaks observed during geopolymerisation that there are multiple chemical steps occurring, with Rahier *et al.* (2003) commenting that the reaction appears to have at least two steps – dissolution and polymerisation – and that the second step ‘seems to be autocatalytic.’ Comparison with calorimetric data was utilised in the early stages of the development of the reaction kinetic model to be discussed in detail in Section 7.8 (Provis *et al.* 2005d, Provis 2006, Provis and van Deventer 2007c); however, the identification of reaction enthalpies for the individual model steps proved problematic (Provis 2006).

Figure 7.7 shows an example of the data that can be obtained by the use of quasi-isothermal DSC to monitor geopolymerisation kinetics. This plot shows the reaction progress at 40°C of metakaolin-based geopolymer mixes with $\text{Si}/\text{Al} = 1.5$ and $\text{M}^+/\text{Al} = 1.0$, where M is either Na, K or an



7.7 Quasi-isothermal DSC data for the reaction of alkali silicate solutions with metakaolin at 40°C, for different alkalis as marked. Unpublished data supplied by P. Duxson.

equimolar mixture of the two. Two distinct exothermic peaks are observed in each case, and there is no significant mixed-alkali effect observed (i.e., the mixed Na-K system falls directly between the two endmember systems). It can also be observed that the total heat released (i.e., the area under the curve) is not dramatically different between the three systems, regardless of the differences in reaction rate. This correlates well with the observation that the overall extent of reaction in metakaolin-based geopolymerisation systems depends only to a limited degree on the identity of the alkali cations present in the case of Na, K, and mixtures thereof (Duxson *et al.* 2005c, Provis *et al.* 2005a).

7.4 Rheology

Various researchers have used rheological techniques to monitor the setting kinetics of geopolymers based on fly ash and on metakaolin. Rahier and colleagues (Rahier *et al.* 1996b, Swier *et al.* 1998) described the geopolymer gel as a ‘low-temperature inorganic polymer glass’, and observed that the reaction as measured by DSC continued for a significant period of time after the system ‘vitrified’ (i.e., hardened) according to rheology. Microstructural

confirmation of similar behaviour in fly ash geopolymers has recently been presented by Lloyd (2008). Phair *et al.* (2003) studied dilute hydrogels obtained from clear solutions as a proxy for understanding the early-age rheology of geopolymers, although it is not clear exactly to what extent the much lower degree of crosslinking present in these model systems will generate differences in observed behaviour. Strength development has also been used as a direct probe of geopolymerisation kinetics (De Silva *et al.* 2007); however, most of the chemically ‘interesting’ aspects of the geopolymerisation process take place prior to the development of measurable compressive strength and so this technique does not provide detailed mechanistic information.

By far the most detailed study of the rheology of fly ash geopolymers published to date is the work presented by Palomo *et al.* (2005), who found that a fly ash-based geopolymer paste is relatively well described by the Bingham visco-plastic fluid model, similar to a hydrating Portland cement. They also commented that the most significant parameter in determining the rheology of their samples, formulated by NaOH activation of different fly ashes, was the Fe_2O_3 content of the ash. This is potentially a very important observation, particularly in the light of subsequent discussions of the role played by the iron in fly ash in determining geopolymer reaction kinetics and properties (van Deventer *et al.* 2007, Keyte 2008, Lloyd 2008, Yong 2009).

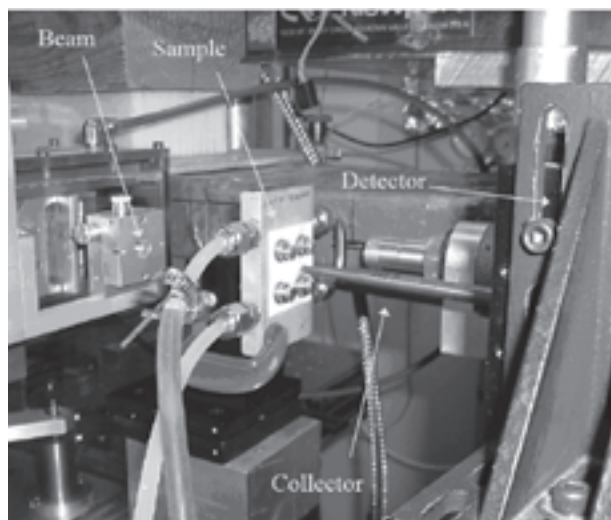
An important aspect of the observation of Bingham fluid behaviour in geopolymers is that a Bingham fluid has a history-dependent rheological profile; i.e., shearing a geopolymer paste can induce either temporary or lasting changes in its physical properties. This may be attributed to the disruption of the partially-formed network structure by the application of a shearing force, effectively retarding the rate of solidification. Similar behaviour in Portland cements is utilised widely in the application of ready-mixed concrete technology, where the application of shear forces in a drum on the back of a mixer truck means that the concrete remains sufficiently fluid to be poured once it reaches its destination. The shear-dependent rheology of geopolymers provides the basis for their use as a Portland cement replacement in this application also; geopolymer concretes may be kept fluid by shearing during transport, then solidify and gain strength at an acceptable rate upon pouring, when the shear force disrupting the growing gel network is no longer applied.

7.5 Diffraction techniques

The use of diffractometry to analyse geopolymerisation kinetics is greatly complicated, as noted in Section 7.1, by the fact that this reaction process involves conversion from one X-ray amorphous phase into another. X-ray diffraction analysis of the formation of crystalline zeolites within geopolymers

has been used as a probe of the reaction progress in systems synthesised or cured at higher temperatures (Olanrewaju 2002, Lloyd 2008), but gives limited information regarding the early stages of the reaction. A technique capable of distinguishing the two different disordered phases (precursor and geopolymer) from each other will depend on the use of a high-energy, high brilliance X-ray source and a low-angle detector to give sufficient d -spacing resolution as well as rapid data collection. Using such a setup (Fig. 7.8) with a white-light synchrotron beam, energy dispersive X-ray diffractometry (EDXRD) has been carried out in situ on a laboratory-sized (12mm thickness) geopolymer sample, characterising the rate of geopolymerisation during the first three hours of the reaction process (Provis and van Deventer 2007b, 2007a).

By carrying out the reactions at a temperature (40°C) where the geopolymer completes the solidification step shown in Fig. 7.1 during this period, the rate of formation of the initial geopolymeric gel phase by conversion of metakaolin is able to be described. It must be noted that this phase will differ structurally from the final geopolymer gel observed after extended curing, as the presence of moisture and heat will allow the gel to continue rearranging into a more thermodynamically favourable form, involving very high degrees of crosslinking (Duxson *et al.* 2005a) and also the formation of nanosized crystallites (Provis *et al.* 2005c). These two stages of gel evolution, denoted 'Gel I' and 'Gel II' (Fernández-Jiménez *et al.* 2006, Duxson *et al.* 2007), are represented in a general sense by the 'Solidification and hardening'



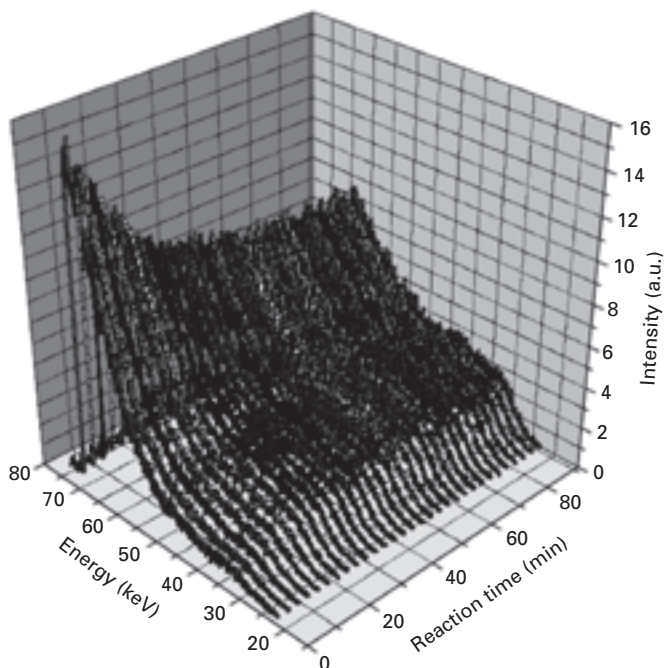
7.8 Apparatus used for the EDXRD experiments of Provis and van Deventer (2007a, 2007b) at the NSLS synchrotron, Brookhaven National Laboratory, USA.

and ‘Ongoing gel rearrangement and crystallisation’ boxes in Fig. 7.1. The regime measurable by EDXRD corresponds roughly to the first of these. A sample set of EDXRD data is given in Fig. 7.9; full experimental details and discussion of data processing issues are given by Provis and van Deventer (2007a, 2007b).

Quantification of the data obtained by EDXRD provides a measure of the relative extent of formation of the initial gel phase, subject to certain assumptions regarding processes occurring in the ~ 5 minute period before obtention of the first data point in each system.

7.6 Nuclear magnetic resonance (NMR)

Rahier *et al.* (2007) used ^{27}Al MAS NMR to probe kinetics in the very early stages of geopolymer formation, observing marked changes in the NMR-observable Al concentrations during reaction which was correlated with the release of Al from highly strained sites in the metakaolin precursor. They also conducted ^{29}Si MAS NMR experiments on the reacting mixture, but commented that accurate quantification of those data was ‘impossible’. They also combined these data with their rheological and calorimetric data



7.9 EDXRD data for the potassium silicate/metakaolin geopolymer system with $\text{SiO}_2/\text{Al}_2\text{O}_3 = 3.0$, at 40°C . Data from Provis (2006).

to propose a kinetic model for geopolymerisation, which gives a heuristic description of some of the phenomena taking place but provides little chemical detail due to its simplified nature.

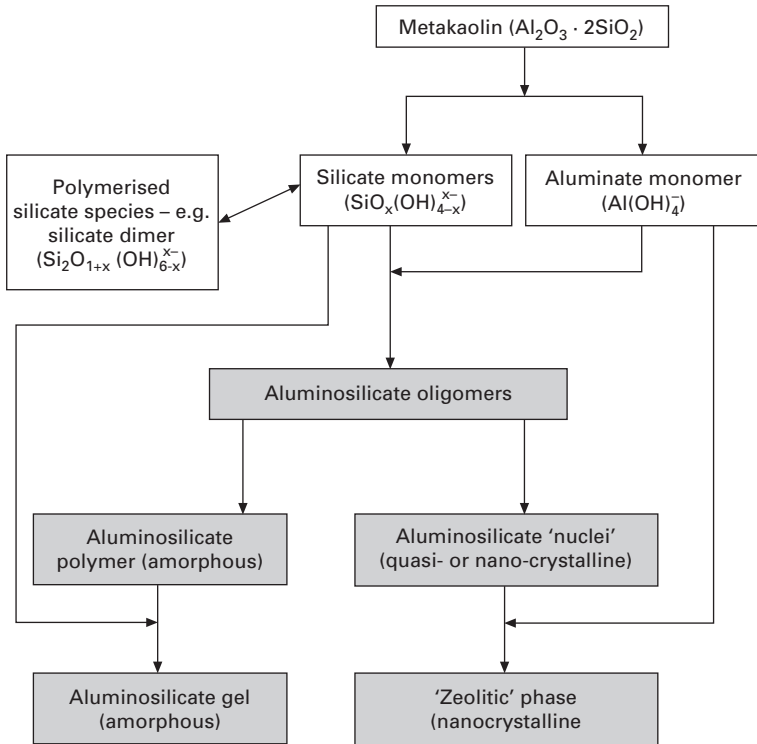
7.7 Microscopy

Environmental scanning electron microscopy (ESEM) has also been used to observe the morphological changes in geopolymers during the early stages of reaction (Wei *et al.* 2004, Zhang *et al.* 2005a, 2005b, 2007). In this technique the samples are held under high humidity in the microscope, at a pressure that is low enough to permit the electron beam to pass through the gas largely undisturbed (Donald 2003). However, the images that are produced show a largely featureless spongy gel structure, and the extraction of kinetic data from such images is fraught with difficulty. Additionally, the large sampling volume associated with X-ray microanalysis of geopolymers at higher electron energies (Lloyd 2008), and the inherent complications in microanalysis introduced by the gas environment (Donald 2003), mean that 'local' Si/Al ratios obtained by this method in an attempt to plot changes in chemistry as a function of reaction time (Wei *et al.* 2004, Zhang *et al.* 2005a, 2005b, 2007) are unlikely to be particularly instructive.

7.8 Modelling

The development of a reaction kinetic model for the early stages of geopolymerisation has been detailed by Provis and van Deventer (2007c). Briefly, the kinetics of aluminosilicate raw material dissolution, rearrangement of the monomeric $\text{Al}(\text{OH})_4^-$ and $\text{SiO}_x(\text{OH})_{4-x}^-$ species released from the solid source into various different aluminosilicate oligomers, and the combination of these oligomers to form amorphous and/or zeolite precursor gel networks, were described analytically. A schematic diagram of the reaction process modelled is shown in Fig. 7.10; this is essentially a more detailed form of the simplified process shown in Fig. 7.1. Each reaction step is modelled by assuming that the kinetics of a reaction are determined by its stoichiometry; this is clearly an oversimplification of reality, but does appear to give a good description of the processes taking place.

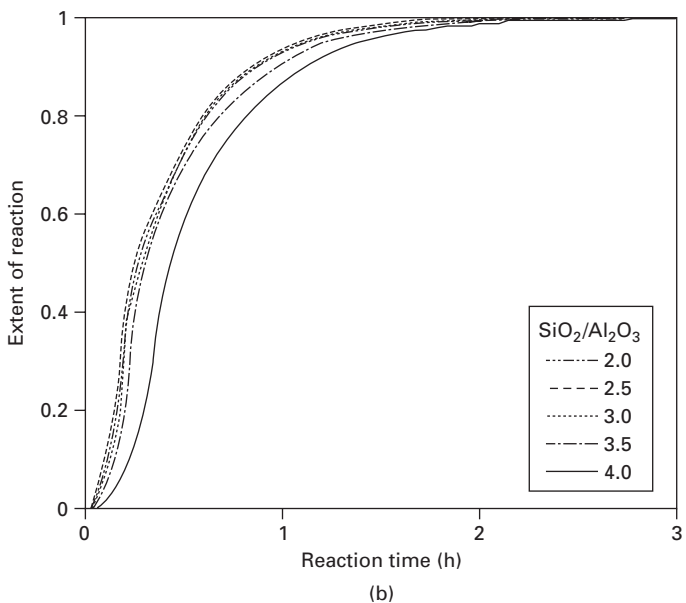
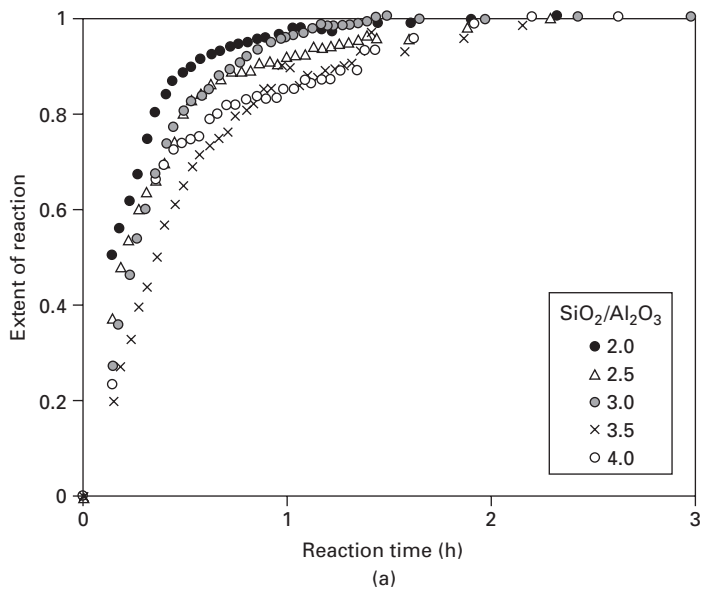
The computed variations in Si/Al ratio within each type of species present as the reaction progresses were monitored, with the oligomeric and larger species all being formed with Si/Al ratios determined by the concentrations of Si and Al monomers in solution. The extent and effect of silicate oligomerisation in solution was also described based on experimental data (Provis *et al.* 2005b), and the influences of other factors including the alkali cation content and the generation and consumption of water during reaction were incorporated into the model. A global measure of the extent



7.10 Reaction processes described by the reaction kinetic model of Provis and van Deventer (2007c). Shaded boxes are those that are categorised as 'reaction products' for the purpose of comparison with experimental data.

of reaction was obtained by summing the fraction of Si and Al included in the aluminosilicate oligomeric and/or solidified gel species, as shown shaded in Fig. 7.10. Figure 7.11 shows a comparison of selected model predictions with corresponding experimental 'extent of reaction' values obtained from EDXRD.

Figure 7.11 shows that the model, even as a very simplified description of the full multistep, heterogeneous process that is geopolymerisation, provides a relatively accurate description of some of the phenomena influencing the rate of geopolymer formation. The model predicts a general decrease in reaction rate with addition of silicate to the activating solution, corresponding well to the majority of the experimental results shown in Fig. 7.11a, with the exception of the highest $\text{SiO}_2/\text{Al}_2\text{O}_3$ ratio depicted. This sample has significant limitations imposed on the achievable extent of reaction by the high degree of connectivity in the initial activating solution (Duxson *et al.* 2005b), and also due to mass transport hindrance by the very high viscosity of the solution phase present even in the initial stages of reaction. This latter



7.11 Comparison of (a) experimental EDXRD data and (b) model predictions for the rate of geopolymerisation of potassium silicate/metakaolin geopolymer systems with $\text{SiO}_2/\text{Al}_2\text{O}_3$ ratios as shown. Data from Provis and van Deventer (2007c).

effect in particular is not described by the reaction kinetic model. However, it is notable that the model is able to predict the shape of the reaction extent-time curves, as well as describing most of the trend in reaction rate with $\text{SiO}_2/\text{Al}_2\text{O}_3$ variation. Recent work has also shown that the variations in species concentrations computed by the model correspond very well to changes in conductivity as observed by impedance spectroscopy (Provis *et al.* 2008), providing further validation for this modelling approach.

7.9 Conclusions

Geopolymerisation is a highly complex process, and so a combination of a number of different experimental techniques will be required to provide a detailed understanding of the mechanistic steps involved in the conversion of aluminosilicate precursors to geopolymers. In situ analysis of reacting geopolymer slurries by infrared spectroscopy and high-energy X-ray diffractometry provides valuable information on the nanoscale, which is complemented well by bulk measurements using calorimetry and rheology. Mathematical modelling provides additional insight into the progress of the reactions. To provide a fully detailed understanding of geopolymerisation kinetics, careful application of existing techniques as well as the development of new techniques will be required, as the reaction process is an immensely complex one with processes taking place on a variety of length scales. Such an understanding will provide the opportunity to control and tailor the setting rate of geopolymers, which would also provide a significant degree of control over the geopolymeric products thus formed.

7.10 References

- Alonso, S. and Palomo, A. (2001a) Alkaline activation of metakaolin and calcium hydroxide mixtures: Influence of temperature, activator concentration and solids ratio. *Materials Letters*, 47, 55–62. doi:10.1016/S0167-577X(00)00212-3.
- Alonso, S. and Palomo, A. (2001b) Calorimetric study of alkaline activation of calcium hydroxide-metakaolin solid mixtures. *Cement and Concrete Research*, 31, 25–30. doi:10.1016/S0008-8846(00)00435-X.
- Antonić Jelić, T., Bronić, J., Hadžija, M., Subotić, B. and Marić, I. (2007) Influence of the freeze-drying of hydrogel on the critical processes occurring during crystallization of zeolite A – A new evidence of the gel ‘memory’ effect. *Microporous and Mesoporous Materials*, 105, 65–74. doi:10.1016/j.micromeso.2007.05.023.
- Brady, P. V. and Walther, J. V. (1989) Controls on silicate dissolution rates in neutral and basic pH solutions at 25°C. *Geochimica et Cosmochimica Acta*, 53, 2823–2830. doi:10.1016/0016-7037(89)90160-9.
- Bronić, J. and Subotić, B. (1995) Role of homogeneous nucleation in the formation of primary zeolite particles. *Microporous Materials*, 4, 239–242. doi:10.1016/0927-6513(94)00087-C.
- Criado, M., Fernández-Jiménez, A. and Palomo, A. (2007) Alkali activation of fly ash.

- Effect of the $\text{SiO}_2/\text{Na}_2\text{O}$ ratio. Part I: FTIR study. *Microporous and Mesoporous Materials*, 106, 180–191. doi:10.1016/j.micromeso.2007.02.055.
- Cundy, C. S. and Cox, P. A. (2005) The hydrothermal synthesis of zeolites: Precursors, intermediates and reaction mechanism. *Microporous and Mesoporous Materials*, 82, 1–78. doi:10.1016/j.micromeso.2005.02.016.
- De Silva, P., Sagoe-Crentsil, K. and Sirivivatnanon, V. (2007) Kinetics of geopolymerization: Role of Al_2O_3 and SiO_2 . *Cement and Concrete Research*, 37, 512–518. doi:10.1016/j.cemconres.2007.01.003.
- Donald, A. M. (2003) The use of environmental scanning electron microscopy for imaging wet and insulating materials. *Nature Materials*, 2, 511–516. doi:10.1038/nmat898.
- Duxson, P., Provis, J. L., Lukey, G. C., Separovic, F. and Van Deventer, J. S. J. (2005a) ^{29}Si NMR study of structural ordering in aluminosilicate geopolymer gels. *Langmuir*, 21, 3028–3036. doi:10.1021/la047336x.
- Duxson, P., Provis, J. L., Lukey, G. C., Mallicoat, S. W., Kriven, W. M. and Van Deventer, J. S. J. (2005b) Understanding the relationship between geopolymer composition, microstructure and mechanical properties. *Colloids and Surfaces A – Physicochemical and Engineering Aspects*, 269, 47–58. doi:10.1016/j.colsurfa.2005.06.060.
- Duxson, P., Lukey, G. C., Separovic, F. and Van Deventer, J. S. J. (2005c) The effect of alkali cations on aluminum incorporation in geopolymeric gels. *Industrial and Engineering Chemistry Research*, 44, 832–839. doi:10.1021/ie0494216.
- Duxson, P., Fernández-Jiménez, A., Provis, J. L., Lukey, G. C., Palomo, A. and Van Deventer, J. S. J. (2007) Geopolymer technology: The current state of the art. *Journal of Materials Science*, 42, 2917–2933. doi:10.1007/s10853-006-0637-z.
- Fernández-Jiménez, A. and Palomo, A. (2005) Mid-infrared spectroscopic studies of alkali-activated fly ash structure. *Microporous and Mesoporous Materials*, 86, 207–214. doi:10.1016/j.micromeso.2005.05.057.
- Fernández-Jiménez, A., Palomo, A., Sobrados, I. and Sanz, J. (2006) The role played by the reactive alumina content in the alkaline activation of fly ashes. *Microporous and Mesoporous Materials*, 91, 111–119. doi:10.1016/j.micromeso.2005.11.015.
- Granizo, M. L., Blanco-Varela, M. T. and Palomo, A. (2000) Influence of the starting kaolin on alkali-activated materials based on metakaolin. Study of the reaction parameters by isothermal conduction calorimetry. *Journal of Materials Science*, 35, 6309–6315. doi:10.1023/A:1026790924882.
- Keyte, L. M. (2008) PhD Thesis, Department of Chemical and Biomolecular Engineering, University of Melbourne, Australia.
- Lee, W. K. W. and Van Deventer, J. S. J. (2003) Use of infrared spectroscopy to study geopolymerization of heterogeneous amorphous aluminosilicates. *Langmuir*, 19, 8726–8734. doi:10.1021/la026127e.
- Lloyd, R. R. (2008) PhD Thesis, Department of Chemical and Biomolecular Engineering, University of Melbourne, Australia.
- Olanrewaju, J. (2002) PhD Thesis, College of Earth and Mineral Sciences, Pennsylvania State University, USA.
- Palomo, A., Banfill, P. F. G., Fernández-Jiménez, A. and Swift, D. S. (2005) Properties of alkali-activated fly ashes determined from rheological measurements. *Advances in Cement Research*, 17, 143–151. doi:10.1680/adcr.2005.17.4.143.
- Phair, J. W., Smith, J. D. and Van Deventer, J. S. J. (2003) Characteristics of aluminosilicate hydrogels related to commercial ‘Geopolymers’. *Materials Letters*, 57, 4356–4367. doi:10.1016/S0167-577X(03)00325-2.

- Provis, J. L. (2006) PhD Thesis, Department of Chemical and Biomolecular Engineering, University of Melbourne.
- Provis, J. L. and Van Deventer, J. S. J. (2007a) Geopolymerisation kinetics. 1. In situ energy dispersive X-ray diffractometry. *Chemical Engineering Science*, 62, 2309–2317. doi:10.1016/j.ces.2007.01.027.
- Provis, J. L. and Van Deventer, J. S. J. (2007b) Direct measurement of the kinetics of geopolymerisation by in-situ energy dispersive X-ray diffractometry. *Journal of Materials Science*, 42, 2974–2981. doi:10.1007/s10853-006-0548-z.
- Provis, J. L. and Van Deventer, J. S. J. (2007c) Geopolymerisation kinetics. 2. Reaction kinetic modelling. *Chemical Engineering Science*, 62, 2318–2329. doi:10.1016/j.ces.2007.01.028.
- Provis, J. L., Duxson, P., Lukey, G. C. and Van Deventer, J. S. J. (2005a) Statistical thermodynamic model for Si/Al ordering in amorphous aluminosilicates. *Chemistry of Materials*, 17, 2976–2986. doi:10.1021/cm050219i.
- Provis, J. L., Duxson, P., Lukey, G. C., Separovic, F., Kriven, W. M. and Van Deventer, J. S. J. (2005b) Modeling speciation in highly concentrated alkaline silicate solutions. *Industrial and Engineering Chemistry Research*, 44, 8899–8908. doi:10.1021/ie050700i.
- Provis, J. L., Lukey, G. C. and Van Deventer, J. S. J. (2005c) Do geopolymers actually contain nanocrystalline zeolites? – A reexamination of existing results. *Chemistry of Materials*, 17, 3075–3085. doi:10.1021/cm050230i.
- Provis, J. L., Duxson, P., Van Deventer, J. S. J. and Lukey, G. C. (2005d) The role of mathematical modelling and gel chemistry in advancing geopolymer technology. *Chemical Engineering Research and Design*, 83, 853–860. doi:10.1016/S0263-8762(05)72773-8.
- Provis, J. L., Walls, P. A. and van Deventer, J. S. J. (2008) Geopolymerisation kinetics. 3. Effects of Cs and Sr. *Chemical Engineering Science*, 63(18), 4480–4489. doi:10.1016/j.ces.2008.06.008.
- Rahier, H., Van Mele, B., Biesemans, M., Wastiels, J. and Wu, X. (1996a) Low-temperature synthesized aluminosilicate glasses. 1. Low-temperature reaction stoichiometry and structure of a model compound. *Journal of Materials Science*, 31, 71–79. doi:10.1007/BF00355128.
- Rahier, H., Van Mele, B. and Wastiels, J. (1996b) Low-temperature synthesized aluminosilicate glasses. 2. Rheological transformations during low-temperature cure and high-temperature properties of a model compound. *Journal of Materials Science*, 31, 80–85. doi:10.1007/BF00355129.
- Rahier, H., Denayer, J. F. and Van Mele, B. (2003) Low-temperature synthesized aluminosilicate glasses. Part IV. Modulated DSC study on the effect of particle size of metakaolin on the production of inorganic polymer glasses. *Journal of Materials Science*, 38, 3131–3136. doi:10.1023/A:1024733431657.
- Rahier, H., Wastiels, J., Biesemans, M., Willem, R., Van Assche, G. and Van Mele, B. (2007) Reaction mechanism, kinetics and high temperature transformations of geopolymers. *Journal of Materials Science*, 42, 2982–2996. doi:10.1007/s10853-006-0568-8.
- Rees, C. A. (2007) PhD Thesis, Department of Chemical and Biomolecular Engineering, University of Melbourne.
- Rees, C. A., Provis, J. L., Lukey, G. C. and Van Deventer, J. S. J. (2007a) Attenuated total reflectance Fourier transform infrared analysis of fly ash geopolymer gel ageing. *Langmuir*, 23, 8170–8179. doi:10.1021/la700713g.
- Rees, C. A., Provis, J. L., Lukey, G. C. and Van Deventer, J. S. J. (2007b) In situ ATR-

- FTIR study of the early stages of fly ash geopolymer gel formation. *Langmuir*, 23, 9076–9082. doi: 10.1021/la701185g.
- Rees, C. A., Provis, J. L., Lukey, G. C. and Van Deventer, J. S. J. (2008) Geopolymer gel formation with seeded nucleation. *Colloids and Surfaces A – Physicochemical and Engineering Aspects*, 318, 97–105. doi:10.1016/j.colsurfa.2007.12.019.
- Swier, S., Van Assche, G., Van Hemelrijck, A., Rahier, H., Verdonck, E. and Van Mele, B. (1998) Characterization of reacting polymer systems by temperature-modulated differential scanning calorimetry. *Journal of Thermal Analysis*, 54, 585–604. doi:10.1023/A:1010150711172.
- van Deventer, J. S. J., Provis, J. L., Duxson, P. and Lukey, G. C. (2007) Reaction mechanisms in the geopolymeric conversion of inorganic waste to useful products. *Journal of Hazardous Materials*, A139, 506–513. doi:10.1016/j.jhazmat.2006.02.044.
- Wei, S., Zhang, Y.-S., Wei, L. and Liu, Z.-Y. (2004) In situ monitoring of the hydration process of K-PS geopolymer cement with ESEM. *Cement and Concrete Research*, 34, 935–940. doi:10.1016/j.cemconres.2003.10.026.
- Yong, S. L. (2009) PhD Thesis, Department of Chemical and Biomolecular Engineering, University of Melbourne.
- Zhang, Y., Sun, W. and Li, Z. (2005a) Hydration process of interfacial transition in potassium polysialate (K-PSDS) geopolymer concrete. *Magazine of Concrete Research*, 57, 33–38. doi:10.1680/macr.57.1.33.57865.
- Zhang, Y., Sun, W., Jin, Z., Yu, H. and Jia, Y. (2007) In situ observing the hydration process of K-PSS geopolymeric cement with environment scanning electron microscopy. *Materials Letters*, 61, 1552–1557. doi:10.1016/j.matlet.2006.07.077.
- Zhang, Y. S., Sun, W. and Li, Z. J. (2005b) Hydration process of potassium polysialate (K-PSDS) cement. *Advances in Cement Research*, 17, 23–28. doi:10.1680/adcr.17.1.23.58388.

Abstract: In this chapter the stability of amorphous geopolymer gels is examined, in particular through the use of accelerated ageing tests. Some assumptions regarding the persistence of the amorphous gel and the effect of conversion to crystalline phases are examined. Amorphous geopolymer gels synthesised from metakaolin, previously thought to be stable, are found to form crystalline zeolites upon ageing, accompanied by major restructuring of the gel and a dramatic loss of performance. Physically, the process bears some similarity to the well-known conversion phenomenon in calcium aluminate cements. Although some of the same reactions are observed in fly ash based geopolymer gels, they do not result in major strength regression, possibly due to the overlap between primary gel formation and crystallisation reactions. The presence of calcium appears to suppress crystallisation of zeolites.

Key words: durability, zeolites, hydrothermal stability, ageing.

8.1 Introduction

As commercial implementation of geopolymer technology draws nearer, a significant gap in the knowledge of the performance of these materials is evident. While various parameters of formulation, microstructure and chemical resistance have now been explored, there exist no data on long-term stability of these materials. As academic research in the field has commenced relatively recently, the situation is somewhat understandable; nevertheless, it is cause for concern.

Despite the vast amounts written about the lack of durability of Portland cement concrete in sulphate ground waters, exposed to biogenic acids, in marine spray zones, exposed to high temperatures and so-on, undisturbed Portland concrete is remarkably stable (Zivica and Bajza 2002; Glasser *et al.* 2008). Lifetimes of 100 years or more are virtually assured for concrete structures as long as precautions are taken to prevent environmentally induced degradation. The cement itself, in the undisturbed state, must therefore maintain its strength.

Is the stability of Portland cement a good measure of what to expect of other cements? Not necessarily. Calcium aluminate cement (CAC) was developed for improved durability, particularly in sulphate rich environments. Its rapid strength development was later exploited by the precast concrete industry, especially in the United Kingdom (Fu *et al.* 1996). Despite this it

has been abandoned in all but niche applications. The reason is a drastic loss of integrity that occurs as the concrete ages. The phases that form initially upon hydration are metastable; over time they convert to denser phases and strength is severely reduced (Revay and Wagner 1979). The process was not well understood during the 1950s and 1960s when the material was in vogue, with catastrophic failure of structural concrete in several buildings the result (Dunster and Holton 2000).

The lesson for geopolymers, and indeed any new cement, is clear: long-term stability cannot be taken for granted. Furthermore, resistance to various aggressive environments is not necessarily indicative of long-term stability of the undisturbed cement. It is generally accepted that the geopolymeric gel is amorphous; with a few exceptions (Navrotsky 2004), amorphous materials are thermodynamically unstable and will convert to some crystalline form over time. It is highly likely that amorphous geopolymers will convert to some crystalline form given sufficient time. Lack of crystallinity, however, is a poor measure of stability over the timescales relevant to the majority of concrete structures. The binding calcium silicate hydrate phases in hydrated Portland cement are generally amorphous or only weakly crystalline, yet they are stable enough for concrete construction; those of calcium aluminate cement are more clearly crystalline yet they are less stable. At present it is not known how rapidly crystallisation would occur in geopolymers, nor whether it would result in loss of performance. Clearly, then, establishing the likely crystallisation products of geopolymers, the rate of crystallisation, and the effect of crystallisation on material properties is of paramount importance in establishing confidence in geopolymers as an alternative cement system.

8.2 Crystallisation during synthesis of geopolymer gels

Although geopolymers are generally considered to be amorphous, numerous studies have shown that, under certain conditions, geopolymer syntheses result in the formation of crystalline zeolites. The amount of silica present in the activating solution dictates to a large extent whether or not X-ray diffracting crystals will form during geopolymerisation. In samples synthesised without dissolved silica, crystalline zeolites are abundant; these samples generally have lower strength than those activated in the presence of dissolved silica (Duxson *et al.* 2007). As the silica concentration in the activating solution increases, zeolite crystallisation appears to be suppressed. This effect has been observed in geopolymers synthesised from metakaolin (Duxson *et al.* 2007) and from fly ash (Fernández-Jiménez *et al.* 2006). The role of dissolved silica in the development of the microstructure of geopolymeric gel has been explored (Duxson *et al.* 2007; Lloyd 2008) and related to the physical properties of the binders formed.

The fate of crystalline zeolites, formed as the primary reaction product during geopolymer synthesis, can be predicted from current knowledge of zeolite chemistry. Essentially, zeolites transform to successively more thermodynamically stable forms in a process known as the Ostwald Law of Successive Transformations. Zeolites themselves can undergo further transformation, e.g. into feldspars (Bauer *et al.* 1998), so these are the probable ultimate products of the reaction; these reactions are likely to be very slow and of limited importance in the present context.

The fate of amorphous reaction products, which compose the binding phase in the majority of commercially interesting geopolymers, is less clear. Given the strong parallels between geopolymer formation and zeolite syntheses, it is plausible that crystallisation of amorphous geopolymer gel will result in zeolites. Some authors have referred to the geopolymeric gel as 'zeolite precursor' (Palomo *et al.* 2004), although a direct link remains to be established. It has also been suggested that the geopolymeric gel contains nanocrystalline zeolites too small to diffract X-rays coherently (Provis *et al.* 2005). As silicate-activated geopolymers have higher compressive strength they are of greater commercial interest; understanding to what they will crystallise, and how quickly, is therefore of significant interest.

8.3 Crystallisation during ageing of geopolymer gels

Given the general consensus that the binding phase in geopolymers is closely related to zeolite precursor gel, surprisingly little attention has been paid to the effects of ageing on geopolymers. Palomo *et al.* (1999) studied the effect of various aggressive solutions on metakaolin geopolymer mortar bars, exposed for up to 270 days at room temperature. Samples were cured for two hours at 85°C before exposure to deionised water, sea water, sodium sulphate solution or dilute sulphuric acid. Flexural strength was determined at various intervals; although significant fluctuations were observed, strength at 270 days was very similar to the initial strength. After 180 days traces of faujasite, a zeolite, were detected by XRD in all samples, to which the authors attributed an improvement in strength. It was suggested that faujasite formation occurred in the pore space and produced structural reinforcement akin to fibres cast into a cement matrix, however no supporting evidence was provided.

After examining ancient concretes, other authors have concluded not only that zeolites form in alkaline cements, but that zeolite formation is responsible for the excellent durability of ancient concretes (Krivenko 1999). It is understood that the binder for Roman *opus caementicium* consisted primarily of volcanic ash, activated with lime (Oleson *et al.* 2004); some structures produced using it still stand today, and testify to the durability of the cement.

The presence of zeolites in these materials is held to be both a significant contributor to their durability, and used as proof that zeolites are the stable final form of the amorphous intermediate reaction products (Krivenko 1999). While this theory initially seems reasonable, it is incomplete. Firstly, there are no records of the performance of ancient concretes when manufactured. Thus, it is not possible to say whether they have maintained performance, increased in strength or lost strength dramatically. The fact that a structure stands may indicate over-design as much as it indicates durable concrete. Clearly, the higher the level of over-design relative to the initial concrete strength, the larger the degree of strength loss that could be tolerated before the structure fails. Furthermore, the presence of zeolites in the concrete does not prove that they were formed *in situ*. In fact, volcanic ash (which is predominantly amorphous and thus likely to be thermodynamically unstable) is known to undergo metamorphism to produce zeolites. Novembre *et al.* (2004) examined volcanic ash from a site near Rome, and found it to contain the zeolites chabazite, phillipsite and analcite. Turriziani (1964) reports that pozzolanic tuffs from Italy, Spain and Germany were found to contain the zeolites phillipsite, chabazite, herschelite, clinoptilolite and analcite. Given that phillipsite and analcite are the particular zeolites that have been identified in ancient concretes (Krivenko 1999), it is quite possible that they are the unreacted remnants of the pozzolana initially used in the cement, rather than the final stable form of the binding phase. These arguments do not contradict the theory propounded by Krivenko (1999), rather they show that the theory remains unproven and that compelling evidence is lacking.

Contrary to other workers, De Silva and Sagoe-Crentsil (2008) reported crystallisation of zeolites from various metakaolin based geopolymers after prolonged warm (40°C) curing. This was associated with some loss of strength. Although some samples crystallised, the authors maintained that samples synthesised using a high concentration of dissolved silicate in the activating solution remained amorphous.

There remains significant uncertainty regarding the effects of ageing on geopolymers. The consensus appears to be that zeolites will form, in some time less than about 2000 years, and that the effects will probably be beneficial. Clearly this is not sufficient grounds for confident use of geopolymer concrete, and so further investigation is warranted.

8.4 Accelerated ageing tests of geopolymers

8.4.1 The need for accelerated ageing tests

A definitive answer to the question of long-term stability requires samples which have been aged for long periods. As academic research into geopolymers has commenced relatively recently, such samples are not available. Some

information might be obtained from alkali-activated slag concretes in service in Eastern Europe; however this must be assessed carefully due to the different binding phases present, specifically the predominance of C-S-H in activated slag (Wang and Scrivener 1995). An alternative to examining aged concrete is to accelerate the effects of ageing. Despite the attendant risks associated with the use of accelerated testing (Grattan-Bellew 1997), such tests are justified in this case due to the absence of alternatives. Well-designed and carefully performed tests will provide some insight into the processes occurring due to ageing, and provide an indication of whether geopolymer concrete may be used safely.

8.4.2 Considerations for ageing tests

Accelerated curing tests for Portland cement have garnered significant attention. They generally seek to predict 28-day strength based on one day of curing, and are essentially a quality control tool for the construction industry. Strength is of crucial importance and microstructure is largely ignored. ASTM C684 and BS 1881 describe accelerated curing regimes; these tests have been examined by various authors (Resheidat and Ghanma 1997; Ozkul 2001), and their validity discussed. The aim of an ageing test is somewhat different, and a distinction between curing and ageing tests must be made. Unlike curing tests, ageing tests are concerned with the stability of typical microstructure far into the future. Thus accelerated curing tests aim to minimise the time taken by fresh concrete to reach a 'well-cured' state, whereas accelerated ageing tests aim to take typical 'well-cured' cement and accelerate any subsequent autogenous transformations. This distinction is not trivial, as there is substantial evidence that accelerated curing of Portland cement results in microstructural differences when compared to normal curing (Skalny and Odler 1972; Kjellsen *et al.* 1991).

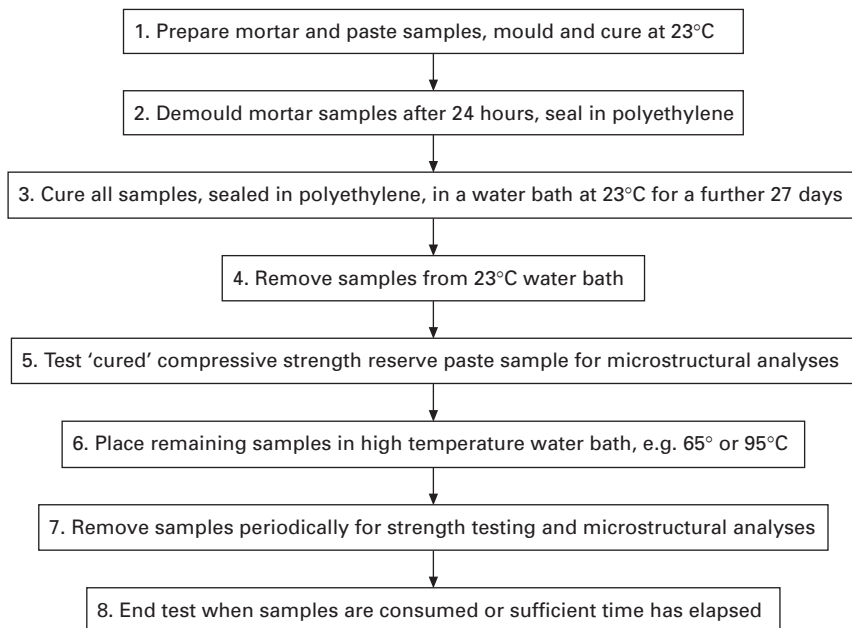
Accelerated ageing tests of hydrated Portland cement concrete are seldom performed. Well-aged Portland cement concrete is readily available, so there has been little need to develop accelerated tests to obtain material for analysis. Paul and Glasser (2000) performed one such test, in which a commercial Portland cement paste was aged at 85°C for 8.4 years and compared with paste aged at 20°C for the same duration.

In the development of an accelerated ageing test for geopolymers, it was considered important to minimise artefacts induced by the test procedure so as to provide the best representation of aged geopolymer binders in a short period of time. Several aspects were considered important to achieve this end:

- An initial period of regular curing should be carried out before beginning accelerated ageing, to allow normal microstructural development as far as possible.

- Relatively high temperatures should be used, so that ageing reactions are accelerated significantly and results can be obtained in a short period of time.
- The samples must be maintained as a closed system to prevent moisture loss, exposure to carbon dioxide, leaching of pore fluids, etc., all of which would lead to changes in the system other than those that would be experienced from purely autogenous processes.

A test to accelerate the effects of ageing on cements was proposed by Lloyd (2008). A flow chart of this procedure is presented in Fig. 8.1. Portland and calcium aluminate cements were used as negative and positive controls respectively in developing the test. Accelerated ageing demonstrated that Portland cement mortars retained their strength and underwent only minor microstructural change over the course of the experiment, which is representative of performance in the field. Calcium aluminate cement mortar demonstrated dramatic strength regression during ageing, consistent with field performance of CAC concrete. Conversion of cubic hydrates to hexagonal hydrates was followed by XRD, and correlated well with strength regression. There was no evidence of carbonation, decalcification, desiccation or other artefacts introduced by the test procedure (Lloyd 2008).



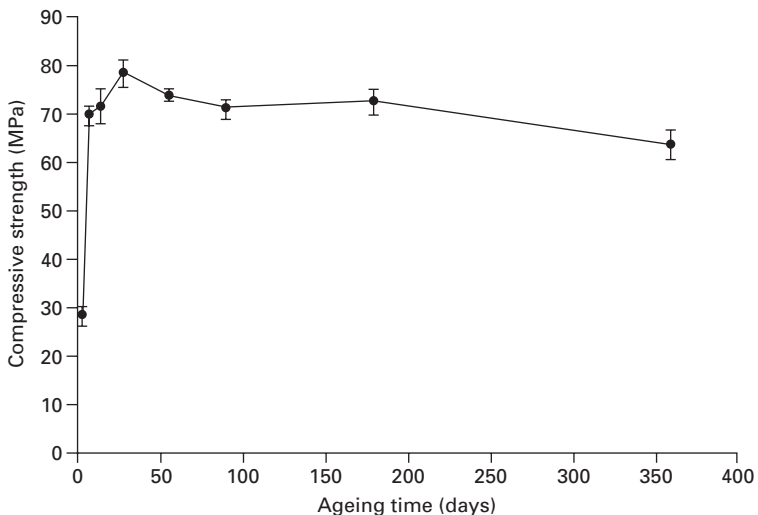
8.1 Accelerated ageing test procedure as proposed by Lloyd (2008).

8.5 Ageing of geopolymers synthesised from metakaolin

8.5.1 Ageing at ambient temperature

The development of compressive strength of a metakaolin-based geopolymer mortar, cured and aged at 23°C is shown in Fig. 8.2. Initial strength development was very rapid, achieving almost 70 MPa in 3 days. A modest but clear decline in strength can be observed after 28 days. Using a *t*-test the difference between compressive strength at 28 and 360 days is shown to be significant with greater than 99% confidence (*t*-Statistic of 6.83 versus a critical *t*-value of 3.71). This provides compelling evidence of strength regression in metakaolin geopolymers. As the samples were isolated from external environmental factors, any changes are due solely to autogenous processes.

Although these results appear to contradict those of Palomo *et al.* (1999), there are several confounding factors to consider. Firstly, the strength of the samples of Palomo *et al.* fluctuated considerably over the course of the experiment; as no measure of spread was provided it is difficult to assess their data objectively. Secondly, as the aim of their experiment was to examine the effect of various ionic species on the binder, rather than the binder in

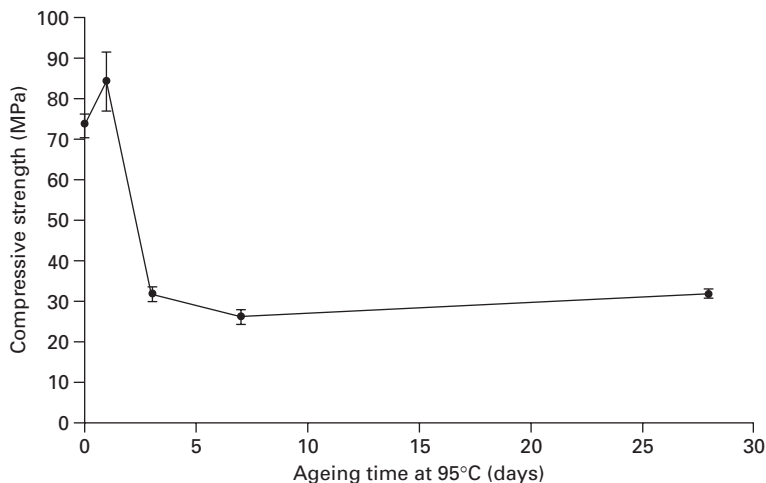


8.2 The compressive strength of metakaolin geopolymer mortar cubes during ageing at 23°C. Samples had the bulk composition $\text{Na}_2\text{O}:\text{Al}_2\text{O}_3:4\text{SiO}_2:13\text{H}_2\text{O}$. Samples were sealed in polyethylene bags to prevent any exchange with the surrounding environment during ageing. Mean of four replicates; error bars show ± 1 standard deviation.

isolation, all samples were immersed in solution. This makes it difficult to assess the effect of autogenous changes occurring within the binder.

8.5.2 Accelerated ageing at 95°C

Ageing at elevated temperature produces a dramatic acceleration of the ageing effects that are observed at 23°C. Figure 8.3 shows the compressive strength profile of a metakaolin-based geopolymer mortar after curing at 23°C for 28 days and subsequent aging at 95°C. The strength after completion of curing at 23°C was slightly lower than that reported by Duxson (2006) for samples of similar composition ($\text{Na}/\text{Al} = 1.0$, $\text{Si}/\text{Al} = 1.90$), which were cured for 7 days at 40°C. The compressive strength increased after one day of aging at 95°C to a value consistent with that reported by Duxson (2006). Between one and three days at 95°C a dramatic reduction in compressive strength was evident, following which strength remained relatively stable at approximately 30 MPa for the next 25 days of ageing at 95°C. The strength loss observed was approximately 60% of the cured value; this is comparable to the strength regression that occurs in calcium aluminate cements of high water/cement ratio (Robson 1964) and could lead to failure of concrete produced with this type of binder.

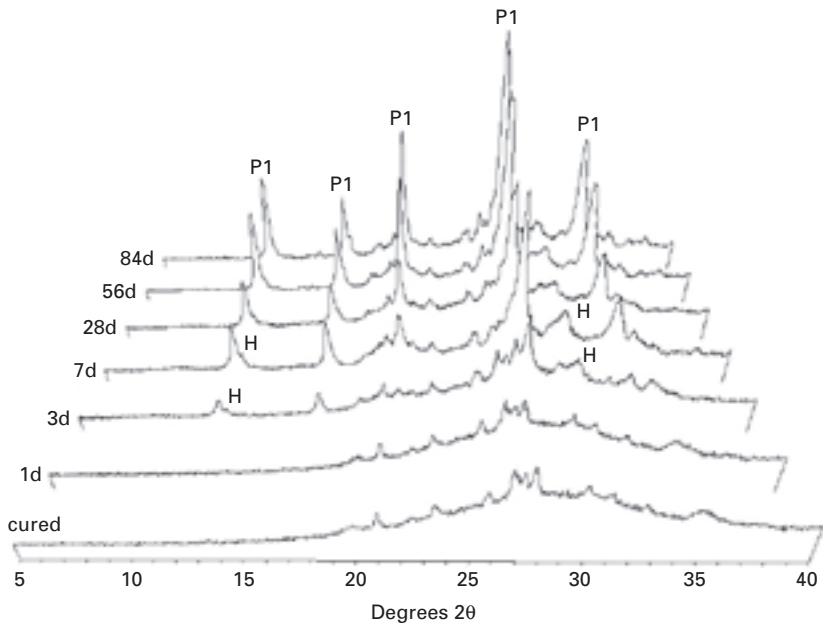


8.3 The compressive strength of metakaolin geopolymer mortar cubes during ageing at 95°C. The binder had the bulk composition $\text{Na}_2\text{O}:\text{Al}_2\text{O}_3:4\text{SiO}_2:13\text{H}_2\text{O}$, and was cured at 23°C for 28 days prior to the commencement of accelerated ageing at 95°C. Samples were sealed in polyethylene bags to prevent any exchange with the surrounding environment during ageing. Mean of three replicates; error bars show ± 1 standard deviation.

It is important to note that the geopolymer mortar in Fig. 8.3 was synthesised with a relatively high Si/Al ratio of 2, and thus represents the more stable end of the geopolymer compositional spectrum. It must be considered that loss of strength is likely in all metakaolin-based geopolymers with $\text{Si}/\text{Al} \leq 2$, and probably some of those with $\text{Si}/\text{Al} > 2$. This contradicts the assertion of De Silva *et al.* (2008) that metakaolin geopolymers synthesised with a high Si/Al ratio will remain stable during prolonged ageing. It is apparent that metakaolin-based geopolymers are not a suitable alternative to Portland cement for the production of concrete building materials, at least in their present state.

8.5.3 Phase changes during ageing

Figure 8.4 shows X-ray diffraction patterns of the metakaolin geopolymer after 28 days of curing at 23°C, and after ageing at 95°C for up to three months. The diffraction pattern of the cured sample is predominantly amorphous, with traces of crystalline material that were present in the metakaolin before reaction. After one day of ageing at 95°C no change can be discerned in the X-ray diffraction pattern. After three days, however, a new crystalline

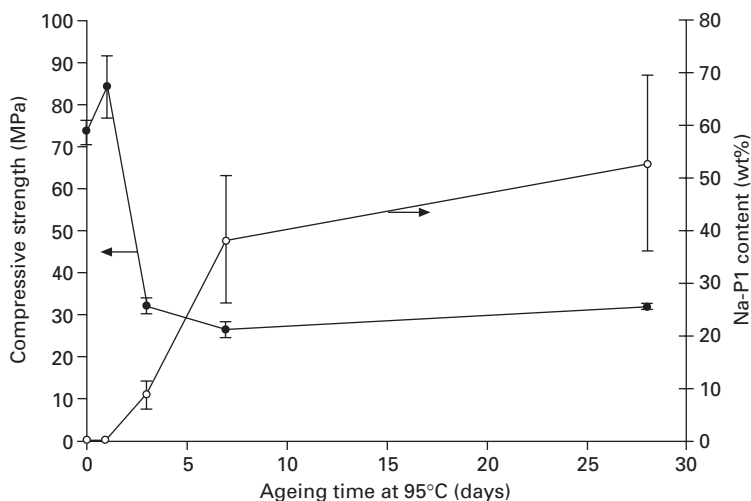


8.4 X-ray diffraction patterns ($\text{Cu K}\alpha$ radiation) of metakaolin geopolymer cured at 23°C for 28 days, then aged at 95°C for 1, 3, 7, 28, 56 and 84 days. Samples had the bulk composition $\text{Na}_2\text{O}:\text{Al}_2\text{O}_3:4\text{SiO}_2:13\text{H}_2\text{O}$. Reflections arising from the zeolites Na-P1 (P1) and sodium chabazite (H) are identified.

phase was evident, corresponding with the zeolite Na-P1 (Powder Diffraction File (PDF) # 044-0103), which has composition $\text{Na}_6\text{Al}_6\text{Si}_{10}\text{O}_{32}$ (Treacy and Higgins 2001) Traces of sodium chabazite (herschelite, $\text{NaAlSi}_2\text{O}_6 \cdot 3\text{H}_2\text{O}$, PDF# 019-1178) are also evident from the weak reflection at $12.84^\circ 2\theta$ and the diffuse peak at $30.65^\circ 2\theta$.

The amount of Na-P1 present increased up to 56 days of aging at 95°C . Na-chabazite content increased from three to seven days, then decreased and disappeared at subsequent ages. It appears that Na-chabazite is a metastable phase in the formation of zeolite P from the metakaolin geopolymer. Metastable phases are frequently seen in zeolite syntheses (Cundy and Cox 2005), and are predicted by the Ostwald Law of Successive Transformation. Zeolite P has been reported as succeeding from zeolite A (Rees and Chandrasekhar 1993), and from faujasite *via* hydroxysodalite (Katović *et al.* 1989).

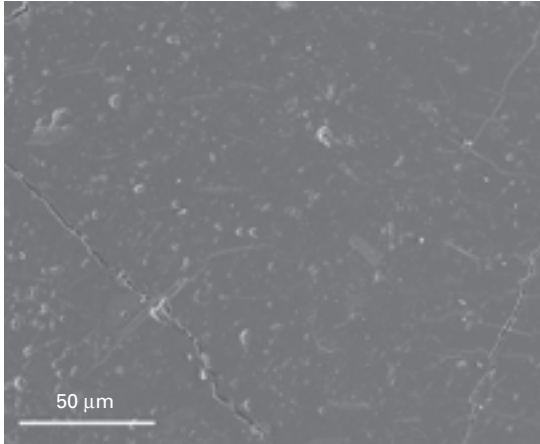
The correlation between compressive strength and Na-P1 content, determined by XRD, is shown in Fig. 8.5. The onset of zeolite crystallisation and strength loss clearly coincide, which contradicts the expectation (Krivenko 1999; Palomo *et al.* 1999) that zeolite crystallisation would be beneficial to the properties of geopolymer cements.



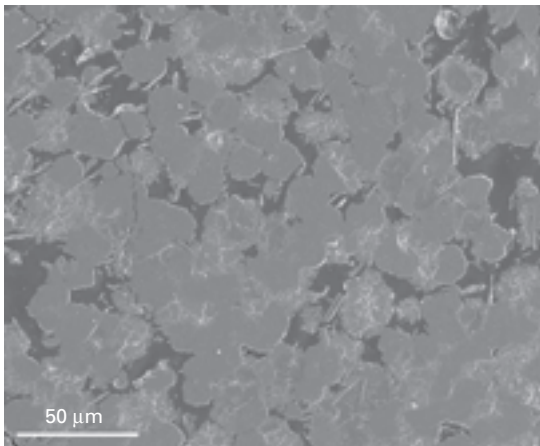
8.5 The correlation between compressive strength (●, left axis) and Na-P1 content (○, right axis) for metakaolin geopolymer cured for 28 days at 23°C , then aged at 95°C . The bulk composition of the samples was $\text{Na}_2\text{O}:\text{Al}_2\text{O}_3:4\text{SiO}_2:13\text{H}_2\text{O}$. Compressive strength values are the mean of three replicates, with error bars of one standard deviation. Na-P1 content was determined by XRD; error bars indicate relative error of $\pm 30\%$, based on values reported by Gualtieri (2000) for quantitative analysis without structural refinement.

8.5.4 SEM examination of aged geopolymer

Scanning electron microscopy is a useful tool for evaluating the changes that occur in the microstructure of geopolymers during ageing. Figure 8.6 shows the relatively featureless microstructure of a metakaolin geopolymer after curing but before the commencement of accelerated ageing. In Fig. 8.7



8.6 SEM image of a polished section of metakaolin geopolymer after curing for 28 days at 23°C. The binder appears relatively homogeneous and featureless.



8.7 SEM image of a polished section of metakaolin geopolymer after curing for 28 days at 23°C, then ageing at 95°C for 28 days. A dramatic restructuring of the binder has occurred, with segregation of the binder into dense regions (lighter grey) and pore space, shown here filled with epoxy resin (dark grey). The pore space consists of large, interconnected regions not apparent in the binder before ageing.

a dramatic restructuring of the geopolymer gel is apparent, coinciding with the formation of zeolites and loss of compressive strength. It is apparent that the ageing process results in the formation of very large, interconnected pore regions that are not apparent in the binder before ageing. As the external volume of the samples remained constant during ageing, the solid regions must be denser than those of the geopolymer gel before ageing.

8.5.5 The mechanism of strength loss during ageing

Given the similarity in the loss of performance of calcium aluminate cement and metakaolin geopolymers on ageing, it appears likely that a similar mechanism could be responsible in both cases. In CAC the initial hydrates formed are less dense than those to which they convert. The conversion process results in expulsion of water and aluminium hydroxide gel, and diminution of the volume occupied by calcium aluminate hydrate phases. During conversion the external dimensions of the system remain substantially the same, meaning that porosity must increase.

However, this explanation cannot be applied directly to the geopolymer system. Neither aluminosilicate gel nor zeolites contain large amounts of bound water, although some may be present in the gel as silanol groups. Thus, the total volume occupied by water will remain virtually constant during setting, curing and any subsequent ageing processes. The change from amorphous gel to crystalline zeolite cannot be linked directly to change in pore volume of the system as a whole, as it can with CAC. Furthermore, both gel and zeolite are porous, so the total pore space of the binder will be distributed between the two. The formation of zeolites could either increase or decrease the porosity of the remaining gel, depending on the specific pore volume of each.

As with CAC, the external dimensions of the samples tested did not change measurably during the experiment, meaning that the bulk density of the sample remained constant during ageing. The density of the metakaolin geopolymer paste examined was 1.76 g/cm^3 , while the density of the zeolite Na-P1 is approximately 2.17 g/cm^3 (determined by taking the mean of 2.21 g/cm^3 and 2.13 g/cm^3 , reported in PDF # 039-0219 and 044-0052 respectively). This clearly contradicts the assertion by Duxson (2006) that the density of zeolitic phases is lower than that of the geopolymeric gel, and that zeolite crystallisation must therefore be accompanied by mechanical work of expansion. The density of zeolitic phases is lower than the skeletal density of the gel, however the large volume of pores in the geopolymeric gel results in a lower density overall than that of zeolites. Therefore, no expansion is necessary to accompany crystallisation; in fact, the opposite is true.

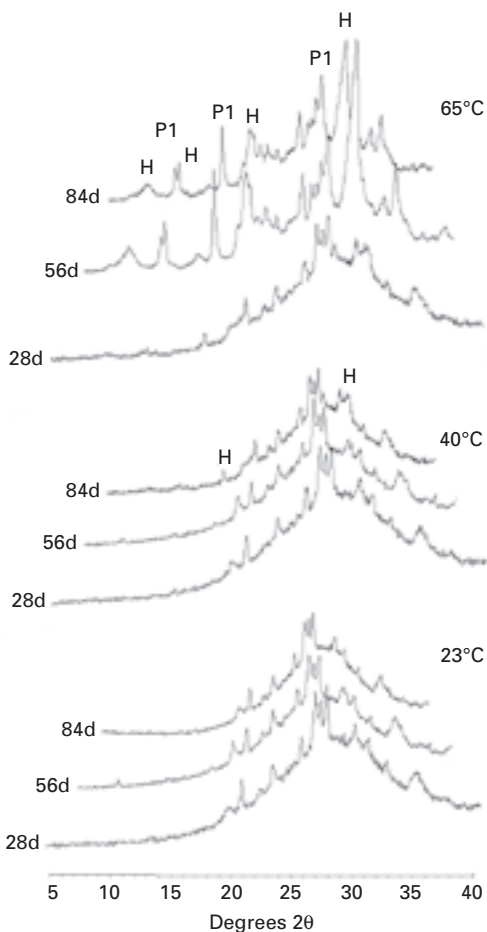
A more useful measure of density is the number of $(\text{Si,Al})\text{O}_4$ tetrahedra

(T) per unit volume. The difference in T density between gel and zeolite allows direct estimation of the change in volume that will occur during transformation from gel to zeolite. The metakaolin geopolymer has molecular formula $\text{NaAlSi}_2\text{O}_6$ and density of 1.76 g/cm^3 , which corresponds to a density of approximately 7.5 T/nm^3 . These tetrahedra are not dispersed evenly through the gel, rather they are globular 'skeletal' regions of high density, leaving the remaining volume of the gel occupied by pore space (Lloyd 2008). By comparison, zeolites of gismondine framework such as zeolite P contain approximately 15.3 T/nm^3 (Baerlocher *et al.* 2001), i.e. Na-P1 contains twice the density of tetrahedra of the geopolymer gel from which it formed (although lower density than the skeletal portion of the gel). As zeolite crystals grow larger than the colloidal particles of the framework of the gel they concentrate material, resulting in local densification and the formation of larger pores, which could explain strength loss.

The appearance of large pores during ageing corresponds well with strength loss, however the pore volume formed fails to correlate with the zeolite content determined by XRD (Lloyd 2008). It appears likely, therefore, that either another process occurs prior to the formation of zeolites, or that significantly more zeolite forms than is apparent by XRD. Such processes could be the formation of a secondary amorphous phase, more ordered than the initial geopolymeric gel, or the crystallisation of an intermediate zeolitic phase with crystallite size too small to diffract laboratory generated X-rays. Both processes are known to occur in conventional zeolite syntheses (Cundy and Cox 2005). Further studies, using techniques such as high-resolution transmission electron microscopy, may help elucidate the mechanisms of gel transformation in geopolymers.

8.5.6 The effect of temperature on geopolymer ageing

Temperature is known to affect the rate of crystallisation in zeolite syntheses (Tosheva and Valtchev 2005). It is to be expected that the rate of zeolite crystallisation from geopolymer gels is also strongly dependent on temperature. Figure 8.8 shows the significant decline in rate of zeolite crystallisation as ageing temperature is decreased. At 65°C and 40°C zeolites are seen after two and three months respectively, while at 23°C no crystallisation is observed within three months of ageing. Although the decrease in temperature results in slower crystallisation of zeolites, the same phases are observed at 65° and at 40° as are seen at 95°C , namely sodium chabazite and sodium P1. It is known that the effect of temperature on zeolite crystallisation in the range of interest here is primarily kinetic, and that after formation of viable nuclei during ambient temperature curing there are neither thermodynamic nor chemical considerations that prevent further growth of the crystallites (Tosheva and Valtchev 2005). Thus geopolymer samples cured and aged at



8.8 XRD diffractograms ($\text{Cu K}\alpha$ radiation) showing the effect of ageing temperature and time on zeolite crystallisation from metakaolin geopolymers. All samples had the bulk composition $\text{Na}_2\text{O}:\text{Al}_2\text{O}_3:4\text{SiO}_2:13\text{H}_2\text{O}$ and were cured for 28 days at 23°C prior to commencement of ageing at 23, 40 or 65°C for 28, 56 and 84 days. Reflections due to sodium chabazite (H) and sodium P1 (P1) are marked.

ambient temperature will result in the same products, eventually, as those aged at higher temperature. It is apparent, therefore, that the loss of strength observed in metakaolin-based geopolymers aged at elevated temperature will also occur in samples treated at ambient temperature. This is supported by the decline in strength of samples stored at 23°C for up to one year, shown in Fig. 8.2.

8.5.7 The effect of alkali type on geopolymer ageing

The choice of alkali cation – sodium, potassium or a mixture of the two – is known to control various properties of metakaolin geopolymers. During accelerated ageing, the alkali type present has been shown to control the zeolitic phase formed (Lloyd 2008). When potassium is the sole alkali present, potassium chabazite is the stable zeolitic phase; when an equimolar mixture of potassium and sodium is present, phillipsite is formed. In both cases conversion to zeolites is accompanied by loss of mechanical strength. Although the geopolymeric gel converts to zeolites irrespective of the alkali cation used, conversion occurs significantly slower when potassium alone is present.

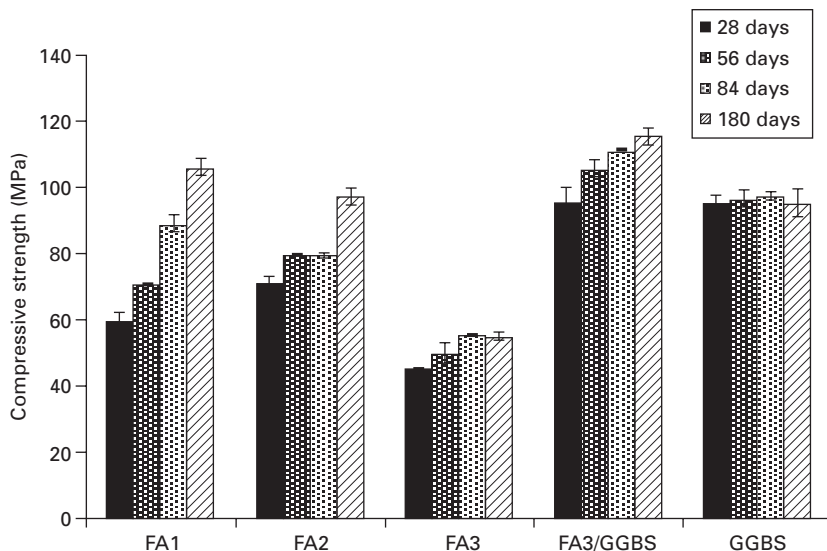
8.6 Ageing of geopolymers synthesised from fly ash

The prospects for use of metakaolin geopolymers in the construction industry are limited (Davidovits 2005); conversely, the beneficial properties and lower cost of fly ash-based geopolymers make them more promising. As there are clear similarities in the chemistry of metakaolin-based and fly ash-based geopolymers, the loss of strength that occurs as metakaolin geopolymers age makes a similar study of fly ash geopolymers imperative. Despite the similarities between the two systems, sufficient differences exist to suggest that the results are not a foregone conclusion.

Zeolites have been widely reported in fly ash-based IPC syntheses (Provis *et al.* 2005; Criado *et al.* 2007; Rees *et al.* 2007). In particular, syntheses which do not contain dissolved silicate in the activating solution have been shown to give rise to well crystallised zeolites, as has been studied extensively by the Palomo group in Madrid (Criado *et al.* 2007; Criado *et al.* 2008). As is the case with metakaolin, the activation of fly ash with alkaline silicate solution appears to suppress zeolite crystallisation and result in predominantly or entirely amorphous reaction products (Criado *et al.* 2007). Thus, the same questions must be asked of fly ash geopolymers as of their metakaolin equivalents: to what will the amorphous reaction products crystallise, how quickly will this occur and what will be the effect on the performance of the material?

8.6.1 The effect of ageing on strength

The ambient temperature strength development of geopolymer mortars, synthesised from fly ashes (FA), ground granulated blast-furnace slag (GGBS) or a mixture of the two, are shown in Figure 8.9. The composition of the binder materials is shown in Table 8.1. All the fly ash containing



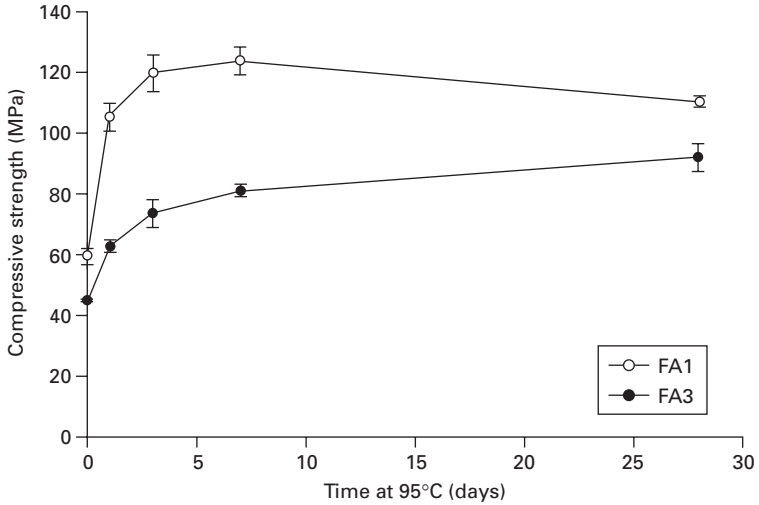
8.9 Strength development profiles of geopolymer mortars synthesised from fly ashes (FA1, FA2, FA3), ground, granulated blast-furnace slag (GGBS) and a blend of fly ash and slag (FA3+GGBS), stored at 23°C. All samples were activated with sodium silicate solution; solution was added to give 7% Na₂O and 7% SiO₂ by mass of binder (i.e. ash and/or slag), and water/binder ratio of 0.325, or 0.350 in the case of GGBS. Results are the mean of three replicates; error bars indicate one standard deviation either side of the mean.

Table 8.1 Elemental composition of fly ashes and GGBS, determined by fused bead XRF.

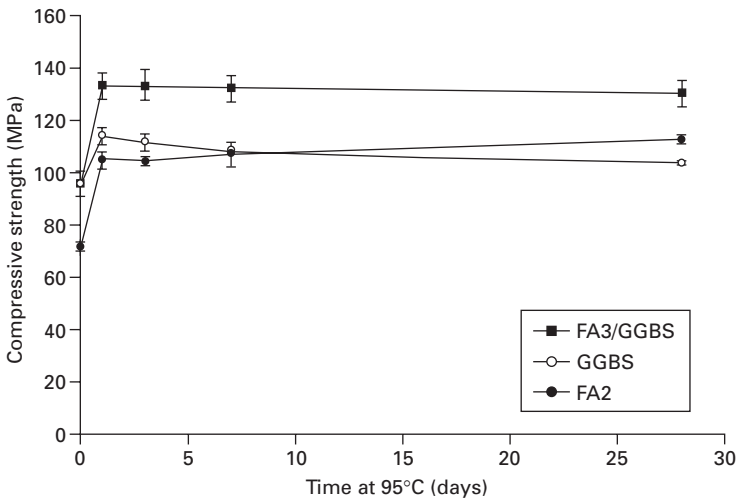
	Na ₂ O	MgO	Al ₂ O ₃	SiO ₂	K ₂ O	CaO	TiO ₂	Fe ₂ O ₃	Other
FA1	3.2	2.1	30.1	48.2	1.6	4.7	1.6	3.8	4.7
FA2	1.1	2.1	18.1	47.5	0.4	19.1	0.9	6.3	4.5
FA3	0.3	1.4	27.8	45.5	0.5	5.6	1.4	11.2	6.3
GGBS	0.3	6.0	13.2	32.9	0.3	40.1	0.7	0.3	6.2

mortars increased in strength over a six-month period, while the strength of the alkali-activated slag mortar remained constant over the test period. This is indicative of the relative rates of reaction of the binder materials – slag reacts quickly, while the more highly polymerised glass present in fly ash reacts more slowly.

Unlike their metakaolin-based counterparts, fly ash containing geopolymer mortars were found to be resistant to strength regression during accelerated ageing, as shown in Figs 8.10 and 8.11. In fact, the strength of all samples examined was higher after 28 days of ageing at 95°C than before ageing. Samples synthesised from fly ash FA1 demonstrated a small but statistically



8.10 The effect of accelerated ageing on low calcium fly ash geopolymer mortars, initially cured for 28 days at 23°C then aged at 95°C. Samples have the same composition as those in Fig. 8.9. Values are the mean of three replicates; error bars indicate one standard deviation either side of the mean.



8.11 The effect of accelerated ageing on high calcium content geopolymer mortars, synthesised from fly ash and/or GGBS, initially cured for 28 days at 23°C then aged at 95°C. Samples have the same composition as those in Fig. 8.9. Values are the mean of three replicates; error bars indicate one standard deviation either side of the mean.

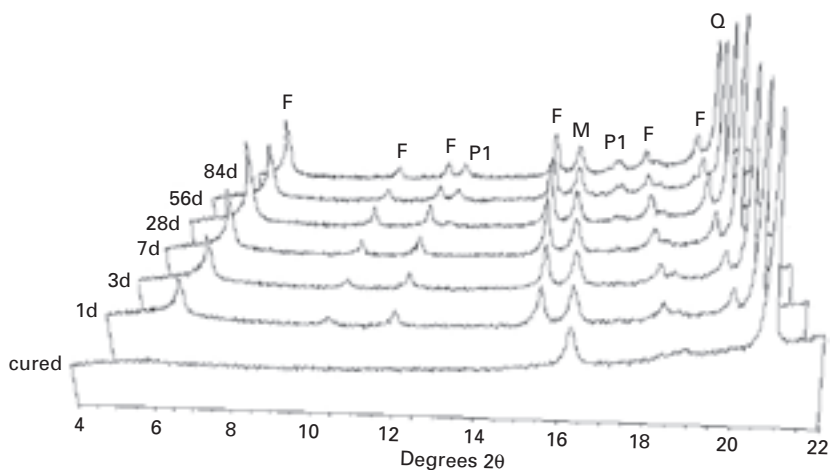
significant decline in strength between 7 and 28 days. Samples synthesised from neat GGBS also appeared to decline slightly in strength after the first day of ageing.

In general, samples with high calcium content showed a strength increase during the first day of ageing then very little change for the remainder of the ageing period. Samples with low calcium content displayed significantly more variation over the 28 days of ageing.

The ageing behaviour of fly ash-based geopolymers is clearly different to that of metakaolin-based geopolymers, which is of clear importance with regard to the use of geopolymers as construction materials. Furthermore, it appears that fly ash-based geopolymers show equivalent or better resistance to ageing when compared with alkali-activated slag mortar. The observed durability of alkali-activated slag concretes in Scandinavia and Ukraine, at least with regard to their ability to withstand ageing effects, may therefore provide some guide as to the future performance of fly ash-based geopolymers.

8.6.2 Phase changes during ageing

Samples synthesised from low calcium fly ashes, FA1 and FA3, showed some degree of crystallisation of zeolites during accelerated ageing. Figure 8.12 shows the development of the zeolites faujasite ($\text{Na}_2\text{Al}_2\text{Si}_{2.4}\text{O}_{8.8}$, PDF# 012-0246) and Na-P1 during ageing of FA1 geopolymers. The faujasite content increased during the first 28 days of accelerated ageing, then decreased



8.12 X-ray diffractograms ($\text{Cu K}\alpha$ radiation) showing the crystallisation of zeolites faujasite (F) and sodium P1 (P1) during 95°C ageing of geopolymer made with fly ash FA1. Reflections due to mullite (M) and quartz (Q) are marked; these were present in the ash before geopolymerisation.

as Na-P1 began to crystallise at later ages. This is consistent with the thermodynamics of zeolite crystallisation, and establishes a mechanistic link with the observed crystallisation of zeolites from metakaolin geopolymers. It is noteworthy that the same phase, zeolite Na-P1, appeared in both metakaolin-based and fly ash-based geopolymers, although it appeared much later, and at lower concentration, in the fly ash-based geopolymer than in the metakaolin-based samples; after 84 days of ageing at 95°C the Na-P1 content of the FA1 geopolymer was *ca.* 2 wt%, compared to *ca.* 50 wt% at 28 days for the metakaolin geopolymer. Only traces of faujasite were apparent after ageing of FA3 samples.

A difference in the crystallisation behaviour is in the formation of faujasite prior to Na-P1 in the fly ash geopolymer, rather than Na-chabazite. Faujasite appears earlier and persists much longer in the fly ash sample than does Na-chabazite in the metakaolin sample, indicating that transformation into Na-P1 is hindered in the fly ash-based sample. It is apparent from these results that similar reactions can occur in both fly ash- and metakaolin-based geopolymers. Zeolite formation in fly ash geopolymers, however, is not accompanied by major strength regression.

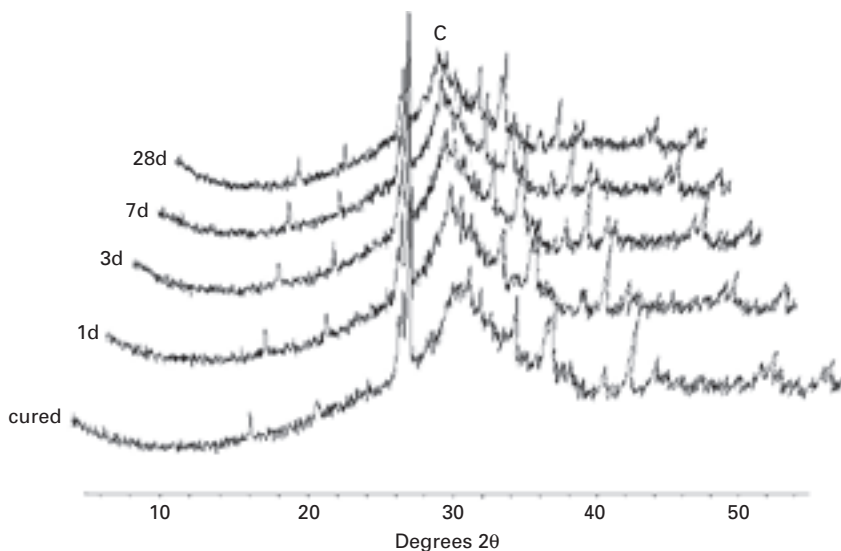
Samples synthesised with higher calcium content, whether derived from fly ash or GGBS, showed no trace of zeolites after ageing for up to 28 days at 95°C. During the first day of ageing an increase in hydrated calcium silicate, probably plombierite ($\text{Ca}_5\text{Si}_6\text{O}_{16}(\text{OH})_2 \cdot 6\text{H}_2\text{O}$, PDF# 029-0331, also known as 1.4 nm tobermorite) was observed, as shown for the mixed fly ash and GGBS binder in Fig. 8.13. No further increase in hydrated calcium silicate was observed at later ages. It appears, therefore, that the presence of calcium in geopolymer systems inhibits the crystallisation of zeolites. This could be the result of one or more of several factors, including:

- dilution of reactive aluminium as the calcium content of the binder increases
- competition for reactive silicate and aluminate species by calcium ions in solution
- hindered mass transfer due to the reduced porosity of the paste when calcium silicate hydrates are present.

8.6.3 SEM examination

Microscopic examination revealed the dramatic changes that occur within the structure of metakaolin geopolymer gel during ageing. It was proposed that this reorganisation, driven by the process of restructuring of the amorphous reaction gel to either intermediate gel or fully crystalline zeolites, was responsible for the dramatic loss of strength of the metakaolin mortar.

Contrary to the observed behaviour of metakaolin geopolymers, those

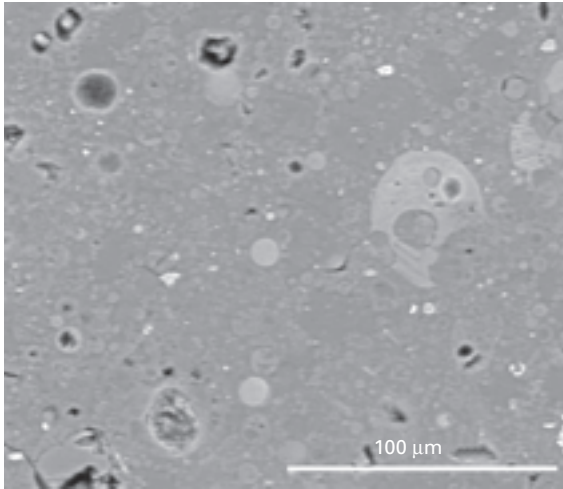


8.13 X-ray diffractograms (Cu K_{α} radiation) of geopolymer synthesised from FA3 and GGBS during ageing at 95°C. The location of the primary C-S-H peak is marked (C); other peaks are due to mullite, quartz and hematite and were present in the fly ash before geopolymerisation.

synthesised from fly ash gained significantly in strength during ageing, and little or no later strength regression was observed. The difference in ageing behaviour is clear when samples are examined microscopically, as shown for FA1 geopolymer in Fig. 8.14. When compared to the aged metakaolin-based geopolymer in Fig. 8.7, it is immediately apparent that the bulk restructuring of the geopolymer gel that is responsible for strength loss does not occur in the fly ash-based samples, at least over the time frame examined.

8.6.4 The effect of zeolite crystallisation on strength of fly ash geopolymers

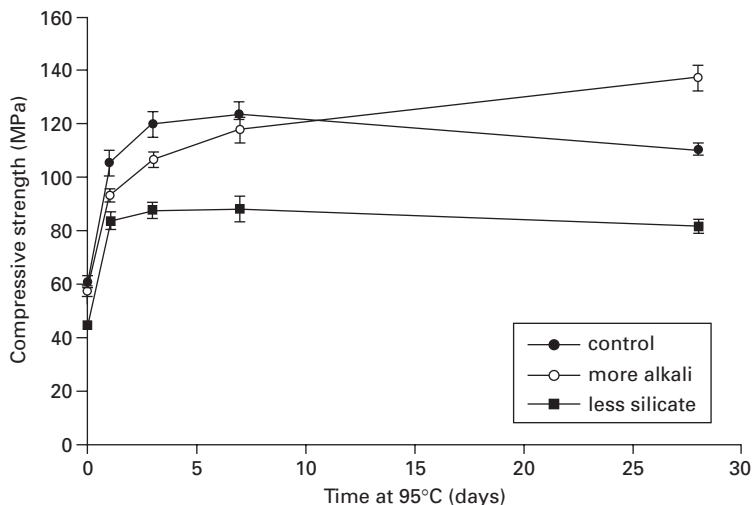
The samples examined thus far have demonstrated that zeolite crystallisation can occur in fly ash geopolymer pastes activated in the presence of dissolved silica, but that this is not accompanied by major strength loss. It is important to note, however, that the amount of zeolite formed in the fly ash-based geopolymer samples was minimal compared to that observed in metakaolin-based geopolymers. As relatively small amounts of zeolite were formed, it is not possible to rule out larger strength loss for systems in which more zeolite would crystallise. Previous work has shown that the amount of zeolite formed varies considerably as the composition of the activating solution is



8.14 SEM back-scattered electron image of a polished section of geopolymer synthesised from FA1, after curing for 28 days at 23°C then ageing at 95°C for 28 days. The binder appears dense and coherent, in stark contrast to the highly segregated metakaolin geopolymer paste after ageing.

changed (Criado *et al.* 2007). This allows the effect of zeolite formation on strength to be probed, by using activating solutions designed to enhance zeolite formation.

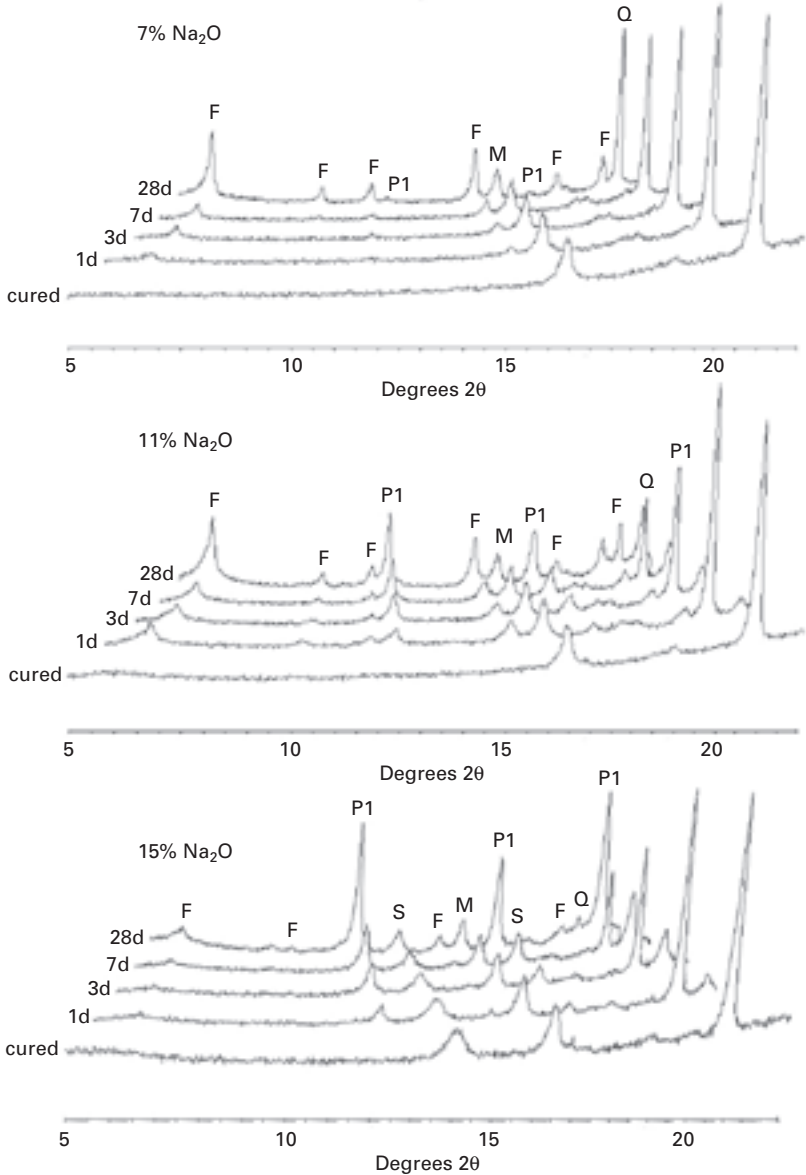
Figure 8.15 shows the effect of varying the composition of the activating solution on the strength development of geopolymer mortars synthesised from FA1. FA1 was chosen as it was the only fly ash tested that exhibited some degree of strength loss during ageing. Two major compositional factors were examined: decreasing the amount of silica dissolved in the activating solution while maintaining constant Na content, and increasing the amount of Na while maintaining constant dissolved silica content. Both factors increased the ratio of Na₂O to SiO₂ in the activating solution; the expected outcome was to promote the tendency to form zeolites (Duxson *et al.* 2007), and thus to exaggerate the effect of zeolite crystallisation on strength development during ageing. Decreasing the amount of silica dissolved in the activating solution decreased the strength of the products at all ages but had almost no effect on the course of strength development compared to the control samples. Conversely, increasing the amount of alkali present brought about a substantial change. The initial strength after curing at 23°C and the rate of strength gain during the first few days of ageing at 95°C were lowered; however, samples continued to gain strength at later ages, beyond the point at which slow decline was evident in the control samples. There was no indication of strength regression up to 28 days of ageing at 95°C.



8.15 The effect of changes in activator composition on ageing of FA1 geopolymer mortars at 95°C. The control (●) was activated with a solution containing 7% Na₂O and 7% SiO₂; the activating solution of the sample with more alkali (○) contained 11% Na₂O and 7% SiO₂; the activating solution of the sample with less silicate (■) contained 7% Na₂O and 3% SiO₂. Values reported are the mean of three replicates; error bars indicate ± 1 standard deviation.

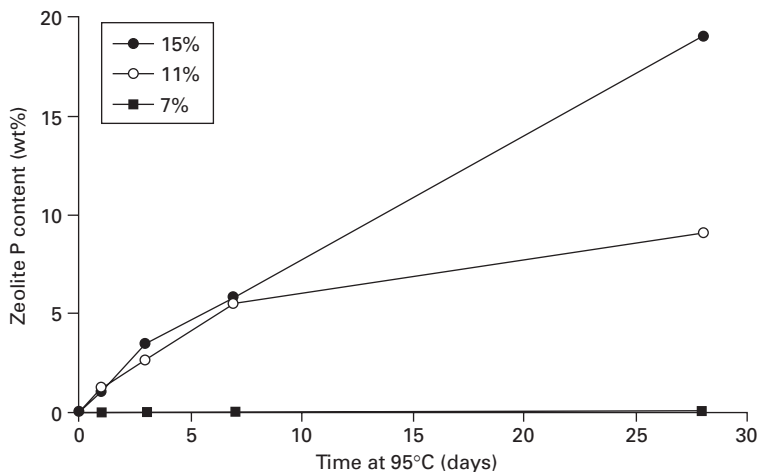
X-ray diffraction confirms that alkali content has a significant impact on zeolite crystallisation, as shown in Fig. 8.16. With 7% Na₂O by weight of fly ash, faujasite crystallisation was dominant and zeolite P reflections could be discerned only after 28 days. With an increase in alkali content to 11% Na₂O by weight of fly ash, crystallisation of zeolite P occurred much earlier and more extensively. Finally, with 15% Na₂O by weight of fly ash, zeolite P crystallisation was extensive and faujasite formation largely suppressed. Another phase, hydroxysodalite (Na₄Al₃Si₃O₁₂(OH), PDF# 011-0401), was evident immediately after curing and did not change in concentration during accelerated ageing. Estimates of the content of zeolite P, determined from the XRD patterns, are shown in Fig. 8.17. With 11% Na₂O present, the quantity of zeolite Na-P1 increased to a moderate level, while at 15% Na₂O almost 20 wt% of the zeolite had crystallised after 28 days at 95°C. Despite the large quantity of zeolite present, approaching half that present in the metakaolin-based samples, no evidence of strength regression was observed.

Figure 8.18 shows the development of regions of order not normally observed in fly ash-based geopolymers; these appear to be analogous to the regions formed in metakaolin-based geopolymers, although the shape is quite different. Despite their formation, the surrounding gel remained dense and strength increased monotonically with ageing. Given the steady

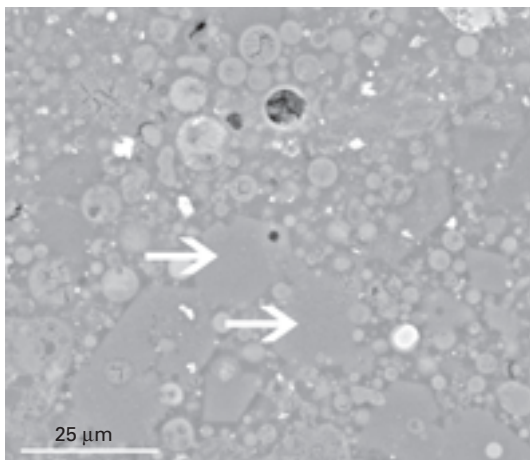


8.16 X-ray diffraction patterns for FA1 pastes activated with varying alkali content and constant dissolved silica. Reflections due to mullite (M), quartz (Q), faujasite (F), zeolite P (P1) and hydroxysodalite (S) are marked.

increase in strength despite the presence of significant amounts of zeolite P in samples activated with 11% Na₂O, the link between zeolite P crystallisation and strength loss apparent in metakaolin geopolymers must be rejected for



8.17 Zeolite P content of FA1 pastes activated with 7% (■), 11% (○) or 15% (●) Na₂O by weight of fly ash after various intervals of accelerated ageing at 95°C, determined by XRD. All samples were cured at 23°C for 28 days prior to ageing. Values may be considered accurate to ± 30% (Gualtieri 2000); error bars were omitted for clarity.



8.18 SEM back-scattered electron image of FA1 paste synthesised with 11% Na₂O in the activating solution, cured at 23°C for 28 days then aged at 95°C for a further 28 days. Regions of order not normally apparent in IPC are evident, highlighted in the by arrows.

fly ash-based geopolymers. There are strong parallels between the ageing behaviour of sodium aluminosilicate gel formed from metakaolin or from class F fly ash; there is sufficient difference, however, to ensure that fly ash-based products are much more durable. A plausible explanation for this difference

in behaviour is the difference in rate of reaction between metakaolin and fly ash. Metakaolin reacts much more quickly, due to both higher surface area (*ca.* 12 m²/g for metakaolin and 1 m²/g for fly ash used in this work) and the more unstable nature of the material, exemplified by the presence of highly strained five-coordinated aluminium (MacKenzie *et al.* 1985), which does not occur substantially in aluminosilicate glasses such as those present in fly ash (Schmücker *et al.* 1997). A large proportion of metakaolin will have reacted when gel restructuring occurs; as a consequence the highly segregated microstructure observed in the previous chapter develops, containing large void spaces. The slower reaction of fly ash, on the other hand, would result in a significant overlap between primary gel formation from fly ash dissolution, and gel restructuring. As a consequence the continued reaction of fly ash would replenish the gel as restructuring occurs.

This mechanism is able to explain the continued increase in strength on the one hand, with the observed gel restructuring and the development of crystallinity on the other. Clearly this cannot continue indefinitely; the reactive portion of fly ash would become depleted eventually, leaving no further material to fill the void space. Should this occur, however, the performance of fly ash-based geopolymer should be maintained. Evidence has been presented by Criado *et al.* (2007) that alkali-activated fly ash cements can have high compressive strength with high zeolite content. This is most likely due to the smaller amount of water necessary to make fly ash-based geopolymers than those made from metakaolin. The decreased pore volume that this confers reduces the amount of void space that must be filled by reaction products. Thus, even as the reaction gel forms zeolitic phases and becomes more dense, the void volume and the size of pores formed are not sufficiently large to degrade performance to an unacceptable level. It should be noted that these are general comments based on the materials tested here; it is certainly possible that detrimental reactions could occur in systems with very high water content or fly ash with poor reactivity. In either case the relative amount of material available to fill the pore volume would be lowered and degradation could be possible.

8.7 Conclusions

The value of accelerated tests for the examination of ageing effects in geopolymer gels has been demonstrated. Accelerated testing has shown that amorphous geopolymer gels are able to convert to crystalline zeolites upon ageing. The conversion process follows the processes known to occur in conventional zeolite syntheses, in which easily formed phases transform into more thermodynamically stable phases over time. This considerably strengthens the links between established zeolite chemistry and geopolymerisation.

Although crystallisation of amorphous gels is seen in geopolymers derived

from both fly ash and metakaolin, the effects are dramatically different. Metakaolin-based geopolymers undergo major microstructural reorganisation, resulting in densification of the binder and the formation of large pores. This is accompanied by large reduction in compressive strength, similar in extent to that observed during the conversion of calcium aluminate cement. For this reason, geopolymers based on metakaolin must be considered unsuitable for use in construction and building materials.

The effects of crystallisation in geopolymers derived from fly ash are more subtle. Much less of the binder is converted to zeolitic phases than is the case for metakaolin, and the conversion process occurs much more slowly. Furthermore, factors that enhance zeolite formation, such as increasing the alkali content present in the binder, increase strength and reduce any tendency towards strength loss, at least over the time period examined. It appears that the process which is so detrimental to geopolymers based on metakaolin has little or no negative effect on fly ash geopolymers. This may be a result of the slow reaction of fly ash, which causes a significant overlap between primary gel formation and zeolite crystallisation. The low water content necessary to synthesise geopolymers from fly ash, and thus the low pore volume of the system relative to metakaolin geopolymers, is also expected to contribute to the difference in the effects of zeolite formation. Geopolymers synthesised with a significant portion of reactive calcium present, whether it be in the fly ash or provided by GGBS, were resistant to strength regression during accelerated ageing. Zeolite formation appears to be hindered by the presence of calcium.

Based on the evidence provided by accelerated ageing tests, it is likely that geopolymers synthesised from fly ash could provide the basis for long-lasting materials for the building products and construction industries, assuming other aspects of durability are satisfied. Further work in this field is required to examine the degree of ageing promoted by accelerated tests, and to correlate the results of accelerated tests with samples aged under ambient conditions as these become available.

8.8 References

- Baerlocher, C., Meier W. M. and Olson D. H. (2001). *Atlas of Zeolite Framework Types*, Elsevier, 5th ed. 308pp.
- Bauer, A., Velder B. and Berger G. (1998). 'Kaolinite transformation in high molar KOH solutions.' *Applied Geochemistry*, **13**: 619–628.
- Criado, M., Fernández-Jiménez, A., de la Torre, A. G., Aranda M. A. G. and Palomo A. (2007). 'An XRD study of the effect of the $\text{SiO}_2/\text{Na}_2\text{O}$ ratio on the alkali activation of fly ash.' *Cement and Concrete Research*, **37**: 671–678.
- Criado, M., Fernández-Jiménez, A., Palomo, A., Sobrados I. and Sanz J. (2008). 'Effect of the $\text{SiO}_2/\text{Na}_2\text{O}$ ratio on the alkali activation of fly ash. Part II: ^{29}Si MAS-NMR survey.' *Microporous and Mesoporous Materials*, **109**: 525–534.

- Cundy, C. S. and Cox P. A. (2005). 'The hydrothermal synthesis of zeolites: Precursors, intermediates and reaction mechanism.' *Microporous and Mesoporous Materials*, **82**: 1–78.
- Davidovits, J. (2005). 'Geopolymer chemistry and sustainable development. The Poly(sialate) terminology: a very useful and simple model for the promotion and understanding of green-chemistry.' Geopolymer, Green Chemistry and Sustainable Development Solutions. Proceedings of the World Congress Geopolymer 2005. J. Davidovits (Ed.), Saint-Quentin, France. 30 June–1 July 2005. 9–15.
- De Silva, P. and Sagoe-Crentsil K. (2008). 'Medium-term phase stability of $\text{Na}_2\text{O}-\text{Al}_2\text{O}_3-\text{SiO}_2-\text{H}_2\text{O}$ geopolymer systems.' *Cement and Concrete Research*, **38**: 870–876.
- Dunster, A. and Holton I. (2000). 'Assessment of aging high alumina cement concrete.' *Structural Survey*, **18**(1): 16–21.
- Duxson, P. (2006). The Structure and Thermal Evolution of Metakaolin Geopolymers. PhD Thesis. *Department of Chemical and Biomolecular Engineering*, The University of Melbourne.
- Duxson, P., Mallicoat, S. W., Lukey, G. C., Kriven W. M. and van Deventer J. S. J. (2007). 'The effect of alkali and Si/Al ratio on the development of mechanical properties of metakaolin-based geopolymers.' *Colloids and Surfaces A: Physicochemical and Engineering Aspects*, **292**: 8–20.
- Fernández-Jiménez, A., de la Torre, A. G., Palomo, A., Lopez-Olmo, G., Alonso M. M. and Aranda M. A. G. (2006). 'Quantitative determination of phases in the alkaline activation of fly ash. Part II: Degree of reaction.' *Fuel*, **85**: 1960–1968.
- Fu, Y., Jian D. and Beaudoin J. J. (1996). 'Zeolite-based additives for high alumina cement products.' *Advanced Cement Based Materials*, **3**: 37–42.
- Glasser, F. P., Marchand J. and Samson E. (2008). 'Durability of concrete – Degradation phenomena involving detrimental chemical reactions.' *Cement and Concrete Research*, **38**: 226–246.
- Grattan-Bellew, P. E. (1997). 'A critical review of ultra-accelerated tests for alkali-silica reactivity.' *Cement and Concrete Composites*, **19**: 403–414.
- Gualtieri, A. F. (2000). 'Accuracy of XRPD QPA using the combined Rietveld-RIR method.' *Journal of Applied Crystallography*, **38**: 267–278.
- Katović, A., Subotić, B., mit I. and Despotović L. A. (1989). 'Crystallization of tetragonal (B8) and cubic (B1) modifications of zeolite NaP from freshly prepared gel. Part 1. Mechanism of the crystallization. *Zeolites*, **9**: 45–53.
- Kjellsen, K. O., Detwiler R. J. and Gjørsv O. E. (1991). 'Development of microstructures in plain cement pastes hydrated at different temperatures.' *Cement and Concrete Research*, **21**: 179–188.
- Krivenko, P. V. (1999). 'Alkaline cements and concretes: problems of durability.' Proceedings of the Second International Conference on Alkaline Cements and Concretes, Kiev, Ukraine. P.V. Krivenko (Ed.) 3–43, Oranta Ltd.
- Lloyd, R. R. (2008). The Durability of Inorganic Polymer Cements. PhD Thesis. *Department of Chemical and Biomolecular Engineering*, University of Melbourne.
- MacKenzie, K. J. D., Brown, I. W. M., Meinhold R. H. and Bowden M. E. (1985). 'Outstanding problems in the kaolinite-mullite reaction sequence investigated by ^{29}Si and ^{27}Al solid-state nuclear magnetic resonance: I, Metakaolinite.' *Journal of the American Ceramic Society*, **68**: 293–297.
- Navrotsky, A. (2004). 'Energetic clues to pathways to biomineralization: precursors, clusters, and nanoparticles.' *Proceedings of the National Academy of Sciences of the USA*, **101**: 12096–12101.

- Novembre, D., Di Sabatino, B., Gimeno, D., Garcia-Valles M. and Martinez-Manent S. (2004). 'Synthesis of Na-X zeolites from Tripolaceous deposits (Crotone, Italy) and volcanic zeolitised rocks (Vico volcano, Italy).' *Microporous and Mesoporous Materials*, **75**: 1–11.
- Oleson, J. P., Brandon, C., Cramer, S. M., Cucitore, R., Gotti E. and Hohlfelder R. L. (2004). 'The ROMACONS project: a contribution to the historical and engineering analysis of hydraulic concrete in roman maritime structures.' *The International Journal of Nautical Archaeology*, **33**: 199–228.
- Ozkul, M. H. (2001). 'Efficiency of accelerated curing in concrete.' *Cement and Concrete Research*, **31**: 1351–1357.
- Palomo, A., Blanco-Varela, M. T., Granizo, M. L., Puertas, F., Vazquez T. and Grutzeck M. W. (1999). 'Chemical stability of cementitious materials based on metakaolin.' *Cement and Concrete Research*, **29**: 997–1004.
- Palomo, A., Alonso, M. M., Fernández-Jiménez, A., Sobrados I. and Sanz J. (2004). 'Alkaline activation of fly ashes: NMR study of the reaction products.' *Journal of the American Ceramic Society*, **87**: 141–1145.
- Paul, M. and Glasser F. P. (2000). 'Impact of prolonged warm (85°C) moist cure on Portland cement paste.' *Cement and Concrete Research*, **30**: 1869–1877.
- Provis, J. L., Lukey G. C. and Van Deventer J. S. J. (2005). 'Do geopolymers actually contain nanocrystalline zeolites? A reexamination of existing results.' *Chemistry of Materials*, **17**: 3075–3085.
- Rees, C. A., Provis, J. L., Lukey G. C. and van Deventer J. S. J. (2007). 'Attenuated Total Reflectance Fourier Transform Infrared analysis of fly ash geopolymer gel aging.' *Langmuir*, **23**: 8170–8178.
- Rees, L. V. C. and Chandrasekhar S. (1993). 'Formation of zeolite from the system Na₂O-Al₂O₃-SiO₂-H₂O in alkaline medium (pH > 10).' *Zeolites*, **13**: 524–533.
- Resheidat, M. R. and Ghanma M. S. (1997). 'Accelerated strength and testing of concrete using blended cement.' *Advanced Cement Based Materials*, **5**: 49–56.
- Revay, M. and Wagner Z. (1979). 'Determination of the expected decrease in strength of high alumina cement concrete by derivatography.' *Thermochimica Acta*, **31**: 365–374.
- Robson, T. D. (1964). Aluminous Cement and Refractory Castables. *The Chemistry of Cements*, H. F. W. Taylor (Ed.). London, Academic Press. **2**: 3–35.
- Schmücker, M., MacKenzie, K. J. D., Schneider H. and Meinhold R. (1997). 'NMR studies on rapidly solidified SiO₂-Al₂O₃ and SiO₂-Al₂O₃-Na₂O-glasses.' *Journal of Non-Crystalline Solids*, **217**: 99–105.
- Skalny, J. and Odler I. (1972). 'Pore structure of calcium silicate hydrates.' *Cement and Concrete Research*, **2**: 387–400.
- Tosheva, L. and Valtchev V. P. (2005). 'Nanozeolites: Synthesis, crystallization mechanism, and applications.' *Chemistry of Materials*, **17**: 2494–2513.
- Treacy, M. M. J. and Higgins J. B. (2001). *Collection of Simulated XRD Powder Patterns for Zeolites*, Elsevier, 4th Ed. 586pp.
- Turriziani, R. (1964). Aspects of the chemistry of pozzolanas. In: *The Chemistry of Cements*. H. F. W. Taylor (Ed.), Academic Press. **2**: 69–86.
- Wang, S.-D. and Scrivener K. L. (1995). 'Hydration products of alkali activated slag cement.' *Cement and Concrete Research*, **25**: 561–571.
- Zivica, V. and Bajza A. (2002). 'Acidic attack of cement-based materials – a review. Part 2. Factors of rate of acidic attack and protective measures.' *Construction and Building Materials*, **16**: 215–222.

Chemical durability of geopolymers

A FERNÁNDEZ-JIMÉNEZ and A PALOMO,
Eduardo Torroja Institute, Spain

Abstract: This chapter discusses the durability of geopolymers obtained by alkali activation of aluminosilicate materials (i.e., metakaolin and fly ash). In general these inorganic polymer cements (IPC) are more durable than ordinary Portland cement (OPC). Pastes and mortars of IPC perform satisfactorily when exposed to sulphates, seawater attack, acidic media, alkali-silica reaction, steel corrosion, fire, and other potentially damaging environments. Since the mineralogical phases and characteristic microstructural elements of IPC pastes and mortars are very different from the properties of OPC mortars, the degradation processes differ in the two types of material.

Key words: chemical durability, sulphate attack, seawater attack, acidic media, alkali-silica reaction, corrosion, fire.

9.1 Introduction: general aspects

The deterioration of a material may occur through a variety of chemical or physical processes, especially when it is exposed to aggressive environments. The durability of a material has a significant influence on its service behaviour, design life and safety. In this chapter, emphasis is placed on the chemical processes in which inorganic polymer cement (IPC) is involved. Since the durability of any material is closely related to its mineralogical composition and microstructure, the significant differences found with regard to ordinary Portland cements (OPC) cannot be unexpected, given the substantial differences between the reactions products formed in each case. The main reaction product in IPC is an alkaline aluminosilicate gel with a three-dimensional structure (considered to be a zeolite precursor) (Davidovits 1994, Palomo *et al.* 1999a, 2004, Fernández-Jiménez and Palomo 2005a, Duxson *et al.* 2007), which is distinctly different from the C-S-H gel formed in OPC hydration. Also as secondary reaction product some crystalline zeolites can be formed.

In this type of material the presence of $\text{Ca}(\text{OH})_2$ is not usually detected. Given that many of the durability problems posed by OPC (Swamy 1992, Malek and Roy 1997, Taylor 1994, Taylor and Gollop 1997, Neville 1995) are associated in one way or another with the calcium content of its phases, it is normal to expect that in many cases the degradation processes will differ in the two types of materials.

The study described in the present chapter addresses the durability of alkaline inorganic polymer cement under different conditions: specifically, cement performance is measured in a number of aggressive environments (deionised water, ASTM seawater, sodium sulphate and acidic solutions), alkali-silica reaction-induced expansion, high temperature and fire resistance, frost attack, and other extreme environments. To determine the performance of IPC mortars and concretes, the chief parameters studied were: weight loss, compressive strength, variations in volume, presence of the products of degradation and microstructural changes, mechanism of attack, etc. Many of the results presented here are in agreement regarding the fact that the durability of IPC is in many aspects better than that of Portland cement concrete. However, there are still some gaps in the knowledge about the durability of these materials that also will be indicated.

9.2 Sulphate attack and sea water attack resistance

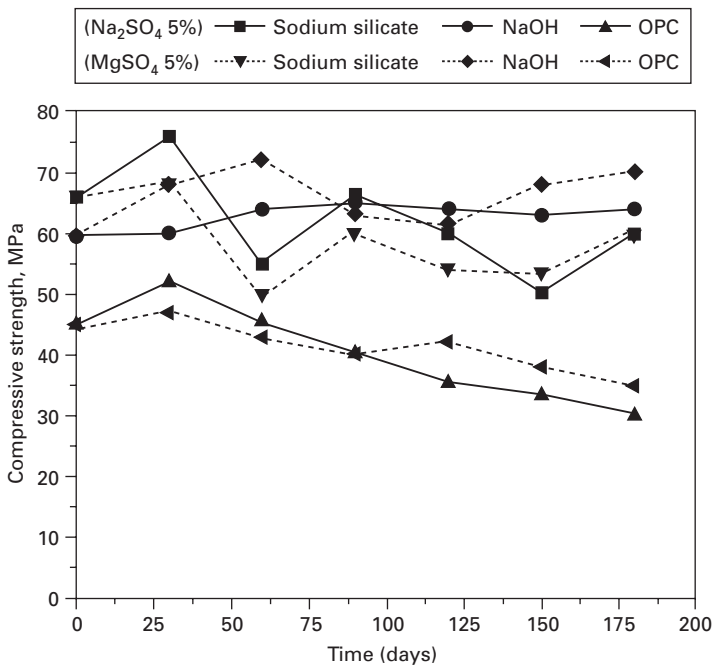
Sulphate attack can occur when cement is attacked by solutions containing sulphates, such as some natural or polluted ground waters. In OPC this type of attack can lead to strength loss, expansion, spalling of surface layers, and ultimately disintegration (Taylor 1994, Taylor and Gollop 1997, Neville 1995). However, in the case of alkaline inorganic polymer cements, including alkali activated metakaolin and fly ash; numerous references found in the literature show that this type of material displays very good resistance to conventional sulphate attack and sea water due to the absence of high-calcium phases.

Palomo *et al.* (1999b) reported that mortars made with alkali-activated metakaolin show very good stability when immersed in various types of aggressive solutions: deionised water, ASTM seawater, sodium sulphate solution (4.4% wt.) and sulphuric acid (0.001 M). It was observed that the nature of the aggressive solution had little negative effect on the evolution of microstructure and the strength of these materials. Only some fluctuations in flexural strength were observed between 7 days and 3 months of immersion (independent of the type of aggressive agent), which were considered to be due to a dissolution-precipitation phenomenon that occurs during this period. Clearly, this process has a negative influence on the development of mechanical strength. The transformation of the amorphous aluminosilicate network into a crystalline structure can be partly attributed to the duration of the treatment (immersion). While representing a relatively small proportion of these crystals, faujasites – which would appear to reinforce the cement matrix – account for the steady increase in its mechanical strength after 90 days of immersion.

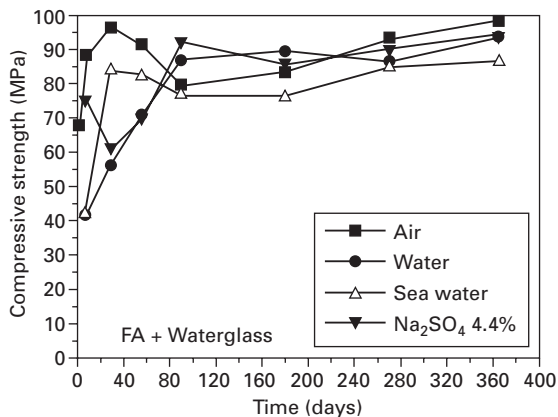
Bakharev (2005a), in turn, sustained that the stability of alkali-activated fly ash pastes in aggressive environments (5% solution of sodium sulphate, 5%

solution of magnesium sulphate and a mixture of both solutions) depended on the intrinsic ordering of the components within the aluminosilicate gel. She also observed some fluctuations of strength in all materials studied (see Fig. 9.1) that were linked to migration of alkalis from the geopolymer into solution. She found that geopolymer materials prepared with sodium hydroxide are more crystalline than when prepared with sodium silicate activators. The greater the crystallinity, the more stable were the geopolymers in aggressive environments. She attributed these findings to the formation of a more stable cross-linked aluminosilicate polymer structure when the activator used was sodium hydroxide. In any event, alkali-activated fly ash mortar was observed to perform better than ordinary Portland cement pastes and no visual signs of deterioration were observed.

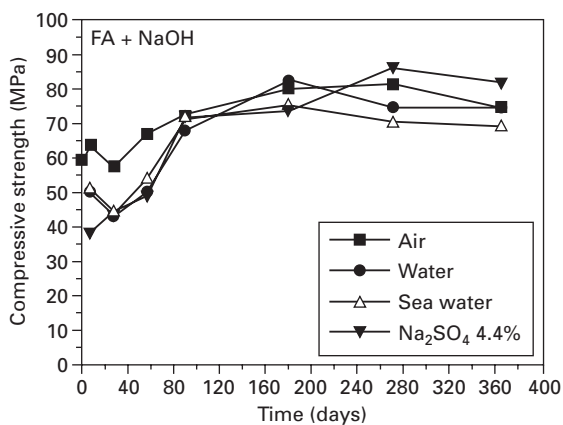
Similar behaviour was observed more recently by Fernández-Jiménez *et al.* (2007). They found that the materials did not deteriorate significantly, with mechanical strength increasing over time irrespective of the medium in which the specimens were immersed (air, water, 4.4% sodium sulphate solution, ASTM seawater), see Fig. 9.2. These results also show that mechanical strength fluctuated in the early ages in all media. Those authors considered



9.1 Compressive strength evolution of fly ash activated with NaOH and with sodium silicate solution, and Portland cement specimens, exposed to 5% sodium and magnesium sulphate solutions. Data obtained from Bakharev (2005a).



(a)



(b)

9.2 Compressive strength evolution of (a) fly ash mortars activated with an 8M NaOH solution, and (b) mortars activated with a sodium silicate solution (waterglass). Samples were held under laboratory conditions (air), and immersed in desionised water, 4.4% sodium sulphate solution, and ASTM seawater. Data obtained from Fernández-Jiménez *et al.* (2007).

that these fluctuations should not be solely attributed to the medium in which the samples were immersed, since they were also detected in the control specimens (cured under laboratory conditions, air). The reasons for such variations, also observed by the other authors, are not clear and will be addressed in greater detail in the near future.

All the results obtained by the different authors (Bakharev 2005a, Fernández-Jiménez *et al.* 2007) show that alkaline activated fly ash pastes and mortars perform satisfactorily when exposed to sulphates and seawater. No significant differences were observed in gel composition or microstructure after contact

with saline solutions. Nonetheless, the presence of sodium sulphate was detected in some cases, but this is associated less with the degradation of the matrix than with the inward migration of sulphate ions through its porous structure. Owing to the large amount of Na in the system, these sulphate ions precipitate into the gaps or pores in the matrix in the form of sodium sulphate. In the specimens immersed in seawater, magnesium ions in the solution also were observed to seep into the matrix. In this case, since the process appears to involve the exchange of Mg and Na ions, it introduces changes in gel composition and morphology. A silicon-rich gel with some magnesium was observed to appear sporadically in the specimens immersed in seawater. These reactions are very sporadic, however, and seem to have no significant effect on mechanical strength.

The performance differences in durability tests depending on the activator used (NaOH or sodium silicate) are due in part to the structural variations in the alkaline silicoaluminate gel formed as a result of the different Si/Al ratios induced in the system, as well as to the larger or smaller amounts of (zeolitic) crystalline phases in the matrix. It is known that the presence of soluble silicates in the activating solution generally reduces the degree of alkaline silicoaluminate crystallisation and retards zeolite crystallisation (Engelhardt and Michel 1987, Klinowski 1984). Moreover, the presence of silicate ions leads to the formation of more compact structures, with gels richer in Si (Duxson *et al.* 2005, Fernández-Jiménez and Palomo 2005b, Fernández-Jiménez *et al.* 2006, Criado *et al.* 2007). This would explain why mechanical strength is higher in mortars activated with sodium silicate solution than with NaOH.

Li *et al.* (2005) indicate that only a small extent of shrinkage was observed in prisms of geopolymer mortar (derived from metakaolin) immersed in 0.31 M Na₂SO₃ solution. However, in similar conditions, OPC mortar prisms displayed a large expansion.

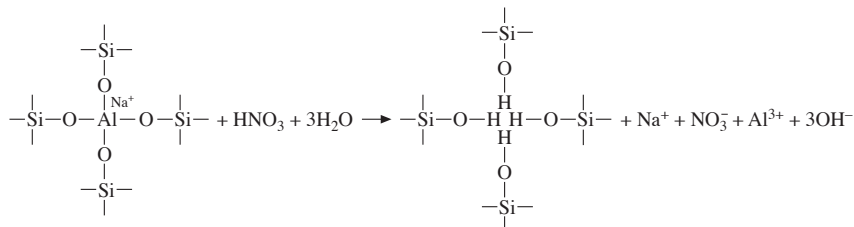
Sulphate attack in concrete or mortar based on Portland cement is generally attributed to the formation of expansive ettringite (AFt-phase) and gypsum. The sulphate ions intrude into the concrete and react with portlandite Ca(OH)₂ to generate gypsum. With the presence of sufficient sulphate, the metastable monosulphoaluminate transforms into ettringite. This ettringite then absorbs moisture to generate expansion and results in local disruption of the matrix. The more voluminous gypsum and ettringite formed as a result of sulphate attack are the cause of expansion cracking and spalling (Malek and Roy 1997, Taylor 1994, Taylor and Gollop 1997). Geopolymer products do not in general contain Ca(OH)₂ and monosulphoaluminate due to being formed from source materials containing little or no calcium. So, when these materials are exposed to sodium sulphate solution, there is no growth of gypsum and ettringite in the matrix to cause expansion, meaning that geopolymer mortar cannot be corroded by sulphate attack according to these mechanisms.

9.3 Acid attack

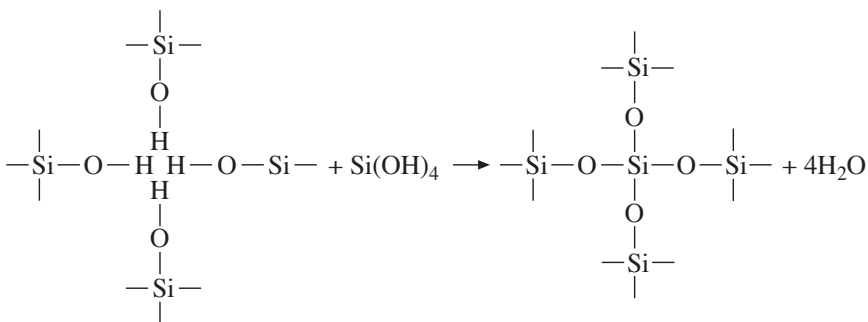
An interesting property of geopolymer cement is its relatively high resistance to acidic media. The resistance of alkali activated metakaolin or fly ash to chemical attack by acids such as nitric, sulphuric, or hydrochloric has been claimed to be far better than that of Portland cement mortar or concrete. Davidovits *et al.* (1999), for example, indicates that metakaolin-based geopolymer ‘K-PSS’ showed only 7% mass loss when samples were immersed in a 5% sulphuric acid solution for 4 weeks. According to Silverstrim *et al.* (1997), an alkali activated fly ash specimen exposed to 70 vol% nitric acid for 3 months retained its dense microstructure.

In 2001 Allahverdi and Skvara (2001) postulated that the mechanism of corrosion of hardened paste of geopolymer cement in solution of nitric acid involves two steps:

1. The first step involves a leaching process in which the alkali cations included in the aluminosilicate framework to charge-balance the tetrahedral aluminium are exchanged by H^+ or H_3O^+ ions from acidic solution. This occurs along with electrophilic attack by acid protons on framework Si-O-Al bonds, resulting in the ejection of tetrahedral aluminium from the aluminosilicate framework:



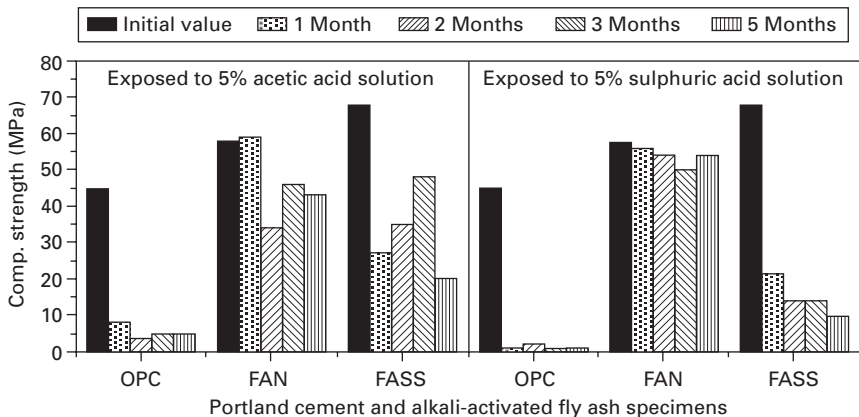
2. In the second step the framework vacancies are mostly re-occupied by silicon atoms resulting in the formation of an imperfect highly siliceous framework. The ejected aluminium, converted to octahedral coordination, mostly accumulates in the intra-framework space.



More recently Rostami and Brendley (2003) stated that alkali ash concrete has high acid resistance in terms of mass loss, and similar microstructure in SEM micrographs before and after acid testing. A class F fly ash based geopolymer concrete subjected to 10% sulphuric acid for 8 weeks was reported by Song *et al.* (2005) to show about 3% mass loss and 35% decrease in compressive strength. He found that sulphuric acid (pH=1.0) attacking geopolymer concrete is controlled by a diffusion mechanism. The diffusion depth is related to the immersion time. Most of the Na and some of the Al ions were leached from the corroded geopolymer matrix and the pH value in this region dropped from 10–11 to about 3. Simultaneously, sulphate and H^+ , supplied by sulphuric acid, diffuse into concrete. However, no obvious changes were observed between the corroded region and the unaffected one in SEM micrographs. Song *et al.* (2005) considered this to mean that geopolymer gel can exist in an acid environment with a pH value as low as 3 and still serve a bonding function to the surrounding aggregates.

Bakharev (2005b) studied the durability of geopolymer manufactured using fly ash and alkaline activators when exposed to 5% solutions of acetic (pH=2.4) and sulphuric acids (pH=0.8). In this case, as was the case in the presence of sodium sulphate solution, it was found that the best performance in both tests was achieved by samples activated with NaOH solution (see Fig. 9.3) instead of samples activated with sodium silicate solution or a mixture of sodium hydroxide and potassium hydroxide solution.

The deterioration observed was connected to the depolymerisation of aluminosilicate polymers with liberation of silicic acid, replacement of Na and K cations by hydrogen or hydronium ions, and dealumination of the



9.3 Compressive strength evolution of Portland cement and alkali activated fly ash (with NaOH (FAN) and sodium silicate (FASS)) specimens exposed to 5% acetic acid solution and 5% sulphuric acid solution. Data obtained from Bakharev (2005b).

geopolymer structure. It was also connected to condensation of siliceous polymers and zeolites, which in some cases led to a significant loss of strength.

The more crystalline geopolymer material prepared with sodium hydroxide was more stable in the aggressive environment of sulphuric and acetic acid solutions than was the amorphous geopolymer prepared with a sodium silicate activator. The chemical instability would also depend on the presence of active sites on the aluminosilicate gel surface, which appeared to increase in the presence of K ions.

Interaction of geopolymer with a concentrated weak acid (e.g., acetic acid) can cause replacement of the exchangeable cations (Na, K) in the geopolymer framework by hydrogen or hydronium ions. However, treatment of a geopolymer with a strong acid (e.g., sulphuric acid) results in a direct attack on the aluminosilicate framework and dealumination. This attack will cause breakage of Si-O-Al bonds, an increased number of Si-OH and Al-OH groups in geopolymer, and an increased amount of silicic acid ions and dimers in solution (precipitation of silica gel could be observed in one case). Therefore, this process leads to a mass loss in the geopolymer materials. Inorganic polymer structures with a Si/Al ratio of 1 are more subject to the attack by acid than more siliceous polymers. In other cases the dealumination process caused an increase in the Si/Al ratio and the polymer chain length in the gel (Bakharev 2005b).

OPC specimens did not perform well in either sulphuric or acetic acid solution, deteriorating completely within the first month of the test (Fig. 9.3). This severe deterioration of OPC samples in acidic environments is connected to the high calcium content of the material.

In acidic environments, high-performance geopolymer materials deteriorate via the formation of fissures in the amorphous polymer matrix, while low-performance geopolymers deteriorate through crystallisation of zeolites and formation of fragile grainy structures.

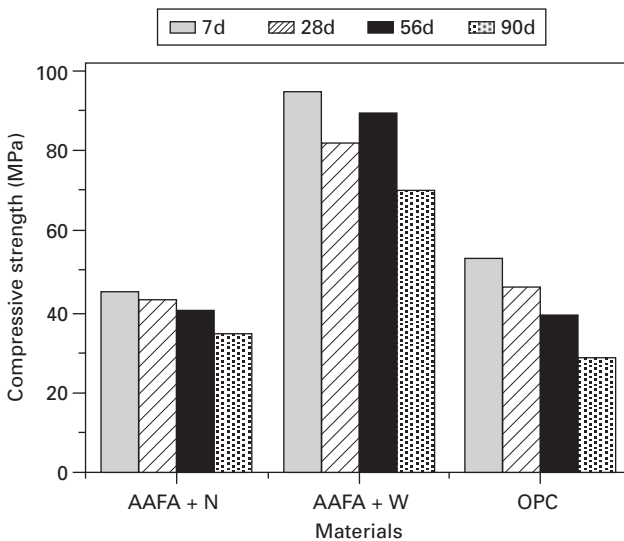
Wallah *et al.* (2005) indicated that geopolymer concrete (derived from alkali-activated fly ash) showed pitting and erosion on the surface of specimens soaked in sulphuric acid solution (2% concentration) after one year of exposure. Also, a significant decrease in the compressive strength was observed. However, the reduction in the compressive strength was significantly smaller in the case of 1% and 0.5% concentrations of sulphuric acid.

More recently, Fernandez-Jimenez *et al.* (2007) studied the behaviour of alkali-activated fly ash completely submerged in HCl solution (0.1N, pH=1.0). A visual examination of the specimens exposed to acid solutions showed that while the alkali activated fly ash specimens appeared to be healthy after 90 days, the OPC specimens were severely deteriorated after 56 days of immersion, with a conspicuous colour change and a loss of mass around the edges of the cubes. The compressive strength results obtained showed that

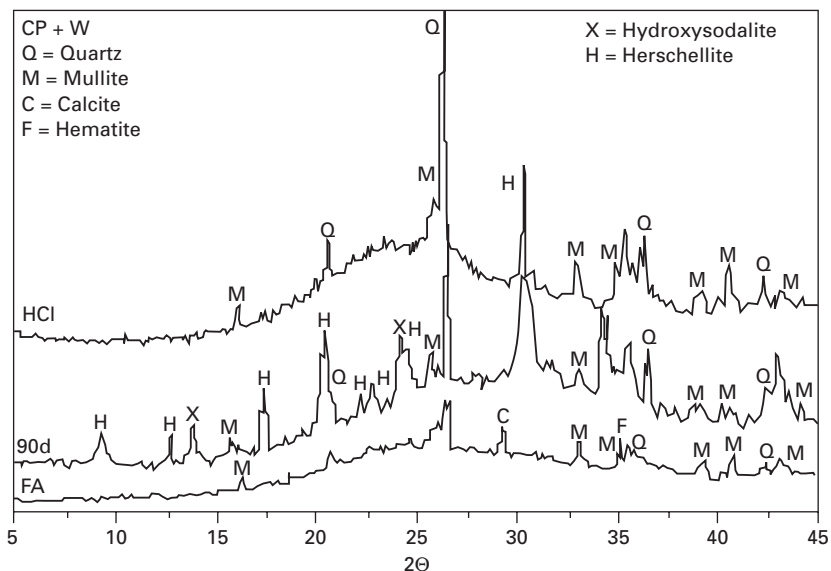
in fly ash mortars activated with sodium hydroxide (N) or sodium silicate (W) solutions, the strength declined approximately 23–25%, whereas in the OPC mortars strength dropped at nearly twice that rate (47%) (Fig. 9.4). This decline in strength values went hand-in-hand with a decrease in specimen mass: the 90-day weight loss in mortars made with solution N-activated fly ash came to 2.5%, compared to 4.2% for solution W-activated ash. The mass loss of OPC mortars was 9.8%.

The XRD results in this case revealed some changes in the mineralogy of mortars; in particular, the peaks associated with the zeolitic phases tended to disappear with time (see Fig. 9.5). At the same time, the area of the amorphous halo peak was observed to grow. In other words, HCl solution attack also leads to a dealumination process similar to that which occurs with nitric and sulphuric solution attack. This further reinforces the suggestion that the mechanism of interaction between the geopolymer reaction products and the acid solution used involved the replacement of exchangeable cations (Na, K) with hydrogen or hydronium ions.

In summary, the acid attack mechanism is very similar in all cases (Allahverdi and Skvara 2001, 2005, Bakharev 2005b, Davidovits 1991 and Fernandez-Jimenez *et al.* 2007), and the small differences between one investigation or another depends on: the strength of the acid selected, the solution concentration, the time of exposure, as well as the physico-chemical and mineralogical composition of the specimens. In general, fly ash alkali activated with NaOH solution has the best acid resistance. However, in any



9.4 Mechanical strength of AAFA and OPC mortars attacked with a 0.1N solution of HCl. Data obtained from Fernandez-Jimenez *et al.* (2007).



9.5 XRD diffractograms of fly ash, the same ash activated with sodium silicate solution and cured in the laboratory for 90 days, and the same material immersed in 0.1 N HCl for 90 days. Data obtained from Fernandez-Jimenez *et al.* (2007).

case the performance of geopolymers is still better than observed in OPC mortars.

Finally, the results obtained indicate that the alkali cation used also plays an important role in determining acid resistance. It has been reported (Weldes and Lange 1969) that K-containing silicates usually exhibit better resistance to sulphuric acid or carbon dioxide because of the tendency of Na to form hydrated salts with these acids, a property K does not have. However, as matrices containing K have a lower degree of crystallinity, this lends them an inherently lower resistance to attack by HCl (van Jaarsveld and van Deventer 1999).

9.4 Resistance to corrosion of steel reinforcement

In Portland cement concretes, the main reason for premature failure of reinforced concrete structures (RCS) is the corrosion of reinforcement. In this respect, RCS are being constructed today which will require costly repairs or even demolition in a very short period of time, resulting in a 10-year to 20-year lifetime. These risks are frequently associated with highly aggressive environments, or originate from the incorrect use of RCS know-how. The consequence of this is that approximately 40–60% of resources in the construction industry are dedicated to maintenance and repairs. The

economic and social importance of the construction sector makes RC failure – and specially RCS failure – the principal challenge facing civil engineering in developed nations.

Considering that reinforcement corrosion is the main cause of RCS failure, the capacity of activated fly ash mortars and concretes to passivate steel reinforcement is a very important property to guarantee the durability of RCS constructed using these new materials. There are only a few studies about reinforcement corrosion in geopolymer concrete available in the scientific literature.

Miranda *et al.* (2005), Fernández-Jiménez *et al.* (2009) and Bastidas *et al.* (2008) showed fly ash mortars to be able to passivate steel reinforcement, although the stability of the passive state in changing environmental conditions was found to depend heavily on the activating solution used. The main conclusions of this work were:

- (i) Activated fly ash mortars passivate steel reinforcement as rapidly and effectively as Portland cement mortars.
- (ii) Passive state longevity or stability depends heavily on the compounds used to activate the fly ash.
- (iii) The lower permeability of mortars activated with waterglass and caustic soda retards carbonation substantially, guaranteeing longer duration of the passive state in reinforcing steel in the absence of other depassivating factors such as chlorides.
- (iv) The presence of chlorides in activated fly ash mortars in concentrations higher than the critical depassivation threshold multiplies corrosion rates by approximately 100, i.e. practically the same factor as observed in traditional Portland cement mortars.

They studied the behaviour of electrodes embedded in Portland cement and alkali activated fly ash mortars with NaOH- and sodium silicate solutions by monitoring the corrosion potential (E_{corr}) and polarization resistance (R_p) over a period of 2.5 years. In this test the mortar specimens tested were moved from a very high initial relative humidity (RH \approx 95%) to a fairly dry atmosphere (RH \approx 30%) for several months, and then returned to the initial conditions through the end of the test period.

Figure 9.6 shows the variation in i_{corr} for the steel bars embedded in Portland cement mortars (a); alkali activated fly ash with NaOH solution (b) and alkali activated fly ash with sodium silicate solution (c); containing 0 and 2% chlorides (by cement weight). Points A and B mark the beginning and end of exposure to a dry laboratory atmosphere. Prior to A and after B, the environmental RH was kept at around 95%. In very humid environments the addition of chlorides multiplied the corrosion rate by a factor of nearly 100.

These results show that, as in the case of specimens made with Portland cement, activated fly ash rapidly passivates steel reinforcement, while chloride

ions have the same depassivating effect in these materials as identified many years ago in Portland cement products (Page *et al.* 1990, Slater 1983).

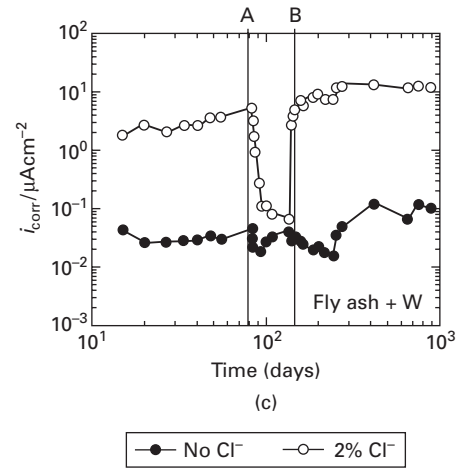
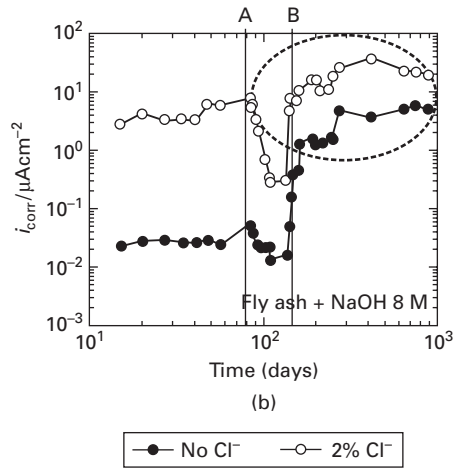
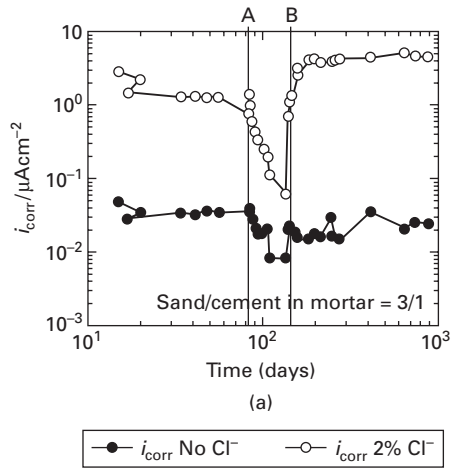
The wide fluctuations in relative humidity (and hence in the moisture content in the pore network) prevailing under environmental conditions, however, alter the passive state in 8M NaOH-activated fly ash mortar (Fig. 9.6(b)). By contrast, these changes do not affect passive state stability in Portland cement mortars or materials activated with a waterglass-caustic soda mix. The authors suggested that, for a better understanding of this process to be developed through future research, gravimetric study should be undertaken in parallel with electrochemical monitoring to ensure wholly reliable quantitative estimates of the corrosion rates deriving from R_p readings. Such reliability was verified for Portland cement mortars many years ago (Andrade and González 1978).

A very feasible reason explaining the steel depassivation observed in the chloride-free fly ash matrices activated with 8M NaOH but not in matrices activated with NaOH+waterglass is the formation of a sodium carbonate in the first set of samples. The precipitation of this compound in the system can provoke a pH decrease as confirmed by a phenolphthalein test. Consequently, the more intense carbonation of materials activated with 8M NaOH compared to those ashes activated with the mixture of caustic soda plus waterglass could be due to the fact that the latter are less porous and show smaller pore sizes. This is in good agreement with bibliographical references about the permeability of these materials (Criado *et al.* 2005 and Kovalchuk *et al.* 2007), which ultimately contributes to retarding the penetration of atmospheric CO_2 through the pore network.

The extension of the tests in the present study to a total of 2.5 years is a promising reference, given that recent research has shown that in addition to the type of alkali activator used to initiate the chemical reactions involved in geopolymerisation, the curing procedure for fresh pastes also plays an important role in the development of less porous and more carbonation resistant matrices (Criado *et al.* 2005, Kovalchuk *et al.* 2007).

Similar results were obtained by Yodmune and Yodsudjai (2006) in studying the corrosion of reinforcement in alkali activated fly ash concrete by accelerated corrosion testing, applying electrical direct current to the steel bar embedded in the concrete. They found that for materials of similar compressive strength, the geopolymer concrete has better resistance to steel bar corrosion than the conventional concrete. The higher compressive strength geopolymer concretes were also those which gave better resistance to steel bar corrosion.

With respect to the corrosion of other types of metal, Morris and Hodges (2001) found that a number of representative engineering metals embedded in a range of fly ash based geopolymers and mortars showed broadly similar electrochemical and corrosion behaviour to that expected in OPC concrete



9.6 Variation of i_{corr} vs time in (a) Portland cement mortars; (b) fly ash mortar with NaOH solution; (c) fly ash mortars with sodium silicate solution; with 2% of Cl^- by cement weight and without Cl^- .

systems. Steel, copper and Type 316 stainless steel were successfully embedded in alkali activated fly ash mortars, but severe corrosion of aluminium in contact with the uncured mix made it unsuitable for use in this system. The initial rapid corrosion of zinc in contact with uncured mixes raises questions over its suitability, although the corrosion rate decreased fast enough that stable bonding with the matrix was possible. Nevertheless, more studies in this area are necessary

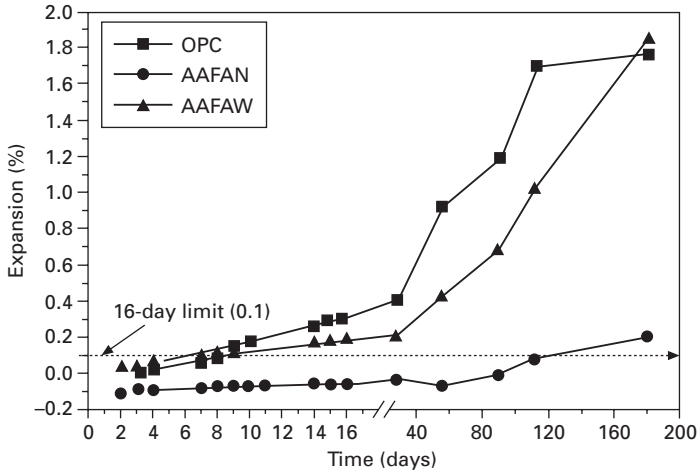
9.5 Alkali silica reaction

The alkali-silica reaction is a chemical process involving alkaline oxides generally derived from the alkalis in the cement, and certain forms of reactive silica present in the aggregate (Swamy 1992). This process depends on factors such as the presence of potentially reactive aggregate, the existence of alkalis in the medium (i.e., $\text{Na}_2\text{O}+\text{K}_2\text{O}$), Ca-rich phases, humidity, and so on. The absence of any of these factors reduces or may even prevent the alkali-silica reaction process and consequent damage due to expansion.

Alkali-activated fly ash mortars have a high alkali content but a very low Ca content. For this reason, with potentially non-reactive aggregates such as are normally used to manufacture OPC concrete, expansive sodium-calcium silicate gels are unlikely to form. Gourley and Johnson (2005) indicate that any alkali-silica reaction that is likely to occur in geopolymer mortars will take place during the original dissolution and condensation polymerisation process, while the material is still in gel form. Such reactions are beneficial as they provide paste-aggregate chemical bonding, which is believed to account for the substantial tensile strength exhibited by geopolymer concretes. Later age reactivity is not possible as a dense bond zone has formed around each aggregate particle during curing. In addition, pore water pH is lower at about 10 to 11, and the matrix contains a significant proportion of un-reacted fly ash.

In other studies, according to the accelerated test described in ASTM standard C1260-94, García-Lodeiro *et al.* (2007) and Fernández-Jiménez *et al.* (2007) found that alkali-activated fly ash mortars with sodium hydroxide or sodium silicate solution expanded less than the 0.1% limit stipulated in the standard after 16 days (see Fig. 9.7). The specimens tested appeared to be healthy, with no surface cracking and no typical ASR products were detected by SEM/EDX – only sodium aluminosilicate gel (N-A-S-H gel) and some crystalline zeolites were visible.

In fly ash-based systems, then, the alkalis were found to be able to interact in two competitive reactions. In the primary reaction, they are taken up to activate the vitreous component of the ash and convert it into a cementitious material, or even form zeolite crystals; but at the same time they may be involved in a second reaction that attacks the aggregate. In the fly ash systems

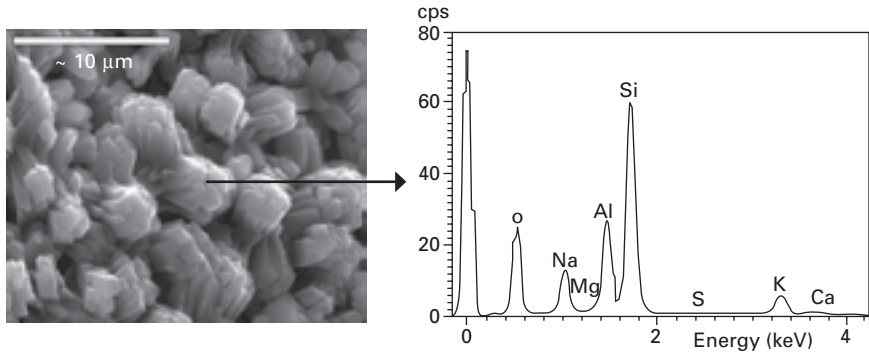


9.7 Alkali-silica reaction-induced expansion determined by an accelerated test based on ASTM standard C1260-94. Data obtained from Fernández-Jiménez *et al.* 2007).

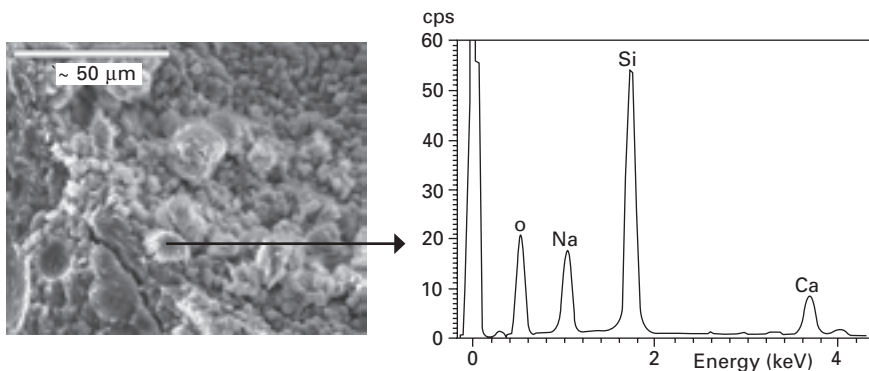
studied here, the primary reaction was clearly alkali activation that led to the formation of an inorganic polymer and a few zeolitic crystalline phases from the vitreous component of the original ash. The alkali-aggregate reaction also runs in parallel with this process. However, due to the lack of calcium in these systems, the AAR product is not expansive. Consequently, all the ash systems tested expanded less than the corresponding Portland cement systems, see Fig. 9.7.

However, at older ages (180 days), some expansion was observed regardless of the type of activating solution used. Such expansion was nonetheless less intense than in OPC mortars under similar conditions. According to the authors of this study the intrinsic characteristics of the ASTM C1260-94 accelerated test may cause an overlapping of two effects that may explain this expansion at older ages:

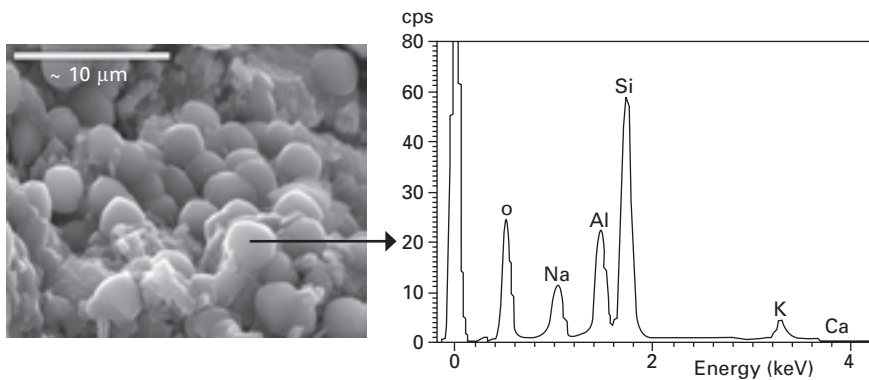
- (i) **Formation of expansive products by ASR.** The severe conditions of the test (specimens immersed in a 1M solution of NaOH at a temperature of 85°C) are known to substantially accelerate the formation of ASR expansive products in OPC systems. The same may occur in the alkali-activated fly ash materials, where an ASR product was detected, albeit in small amounts (see Fig. 9.8(b)).
- (ii) **Zeolite transformation.** After 180 days of storage in 1M NaOH at 85°C, a new zeolitic phase was detected, specifically analcime. This zeolite transformation is believed to be the cause of a certain amount of stress, which would contribute to the expansion detected.



(a)



(b)



(c)

9.8 Microanalysis of solution N-activated fly ash mortar subjected to the accelerated test (ASTM C1260-94): (a) zeolite P crystals observed after 16 days; (b) alkali-silica reaction product with pseudo-rossette crystals after 180 days; (c) analcime crystals after 180 days. Data obtained from Fernández-Jiménez *et al.* 2007.

The essential conclusion to be drawn from this research is that binders (mortars and concretes) formed by activating fly ash (with no Portland cement) with an alkaline solution are scantily susceptible to the expansive alkali-silica reaction. The expansion observed when the duration of the accelerated test is extended far beyond its standard duration may be explained by the combination of two effects: ASR and/or zeolite growth.

The second hypothesis, involving zeolite growth, is according with the results obtained by Sindhunata *et al.* (2008), who studied the effect of immersion in alkaline solutions on the gel structure and pore network of fly ash-based geopolymers. They found that immersion in carbonate (pH ~ 11) or hydroxide solutions (pH > 14) results in very little leaching of framework components (Si or Al) from the geopolymer gel, and a largely unchanged mesoporous gel structure. Higher alkalinity, up to 8 M NaOH, causes more damage to the gel framework as species are leached into solution and the pore network collapses. Crystallisation of small quantities of zeolites from the initially X-ray amorphous gel was also observed. The zeolitic products formed are in general the same products that are observed in geopolymers cured at elevated temperature for extended periods of time, suggesting that the reactions taking place during the alkaline immersion are to some extent a continuation of the initial geopolymerisation process. However, immersion in saturated Na₂CO₃ solution had very little effect, due predominantly to hindered mass transport, while immersion in water does not lead to a significant level of framework dissolution.

9.6 High temperature and fire resistance

With respect to the behaviour of the alkali-activated aluminosilicates at high temperature, different authors have studied this behaviour and there is general agreement that geopolymers show better resistance to fire than Portland cement mortars or concrete. Previous investigations by Davidovits *et al.* (1991, 1994, 1999) reported very good heat resistance properties of materials prepared using sodium silicate, potassium silicates and metakaolin, having thermal stability up to 1200–1400°C. Barbosa and MacKenzie (2003) found that increased amounts of water and/or sodium silicate could cause reduce the thermal resistance of geopolymer material when exposed to firing. They reported also very high thermal stability of ‘potassium silicate’ (Si/Al ~ 1) geopolymers up to 1300–1400°C, and in this investigation geopolymer specimens experienced re-crystallisation to feldspars, leucite and kalsilite at 1000°C.

For alkali-activated fly ashes Bakharev (2006) found that materials alkali activated with K-containing alkaline solution present better fire resistance than those activated with Na. Fly ash samples activated with Na-containing activators developed shrinkage cracking and rapid deterioration of strength

at 800°C, which was connected to a dramatic increase of the average pore size. Loss of strength on firing was possibly connected to the deterioration of aluminosilicate gel. Decomposition of the aluminosilicate gel freed sodium, silicon and aluminium, producing Na-feldspars. The melting point occurred at a lower temperature if the sodium content of the specimens increased. For materials activated with potassium silicate, compressive strength was significantly increased on heating, and deterioration of strength started only at 1000°C. This can be attributed to a higher diffusion coefficient of Na than K in the matrix upon firing (van Vlack 1964).

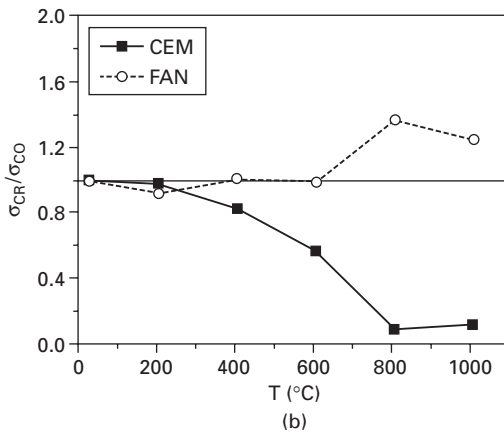
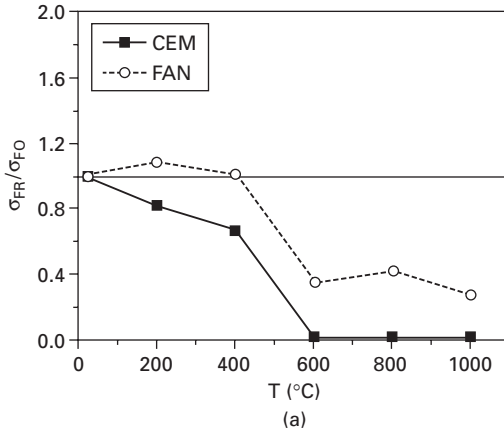
Comparing this with the results of other authors (Davidovits 1991, Barbosa and Mackenzie 2003), it can be deduced that the performance of alkali-activated fly ash materials with Na-containing activators was lower than that of materials prepared using metakaolin, possibly due to a lower degree of reaction of fly ash, incomplete polymerisation of geopolymers and because of impurities present in the fly ash, (i.e., iron content) which lowered the melting temperature of the materials.

Gourley and Johnson (2005) indicated that as geopolymer is a network structure similar to a glass, unlike OPC which is a hydrate, resistance to heat (and specifically to fire) is greatly improved. The absolute volume of water contained in the pore structure is low, and the pore structure is continuous. Thus, the mode of decomposition of geopolymers is to melt at temperatures in excess of 1000°C, rather than to explosively release water or dehydrate to a powder.

Skvara *et al.* (2005) also agree that the main problems of temperature resistance of alkali activated fly ash cement appear in the range 500–700°C, and could be caused by the occurrence of the melt that began to form. Different authors (Bakharev 2006, Barbosa and Mackenzie 2003, Krivenko and Kovalchuk 2002, 2007, Fernández-Jiménez *et al.* 2008, Skvara *et al.* 2005) agree that the compressive strength measured on cold samples after their firing shows a growing tendency; this behaviour can be attributed to the solidifying melt. Nevertheless, the residual strength of alkali-activated fly ash after heat treatment is relatively higher than that of the basis of Portland cement (see Fig. 9.9, from Fernández-Jiménez *et al.* 2008).

Krivenko and Kovalchuk (2002, 2007) show the influence of chemical composition of cement material, curing conditions, and some peculiarities of microstructure and properties on heat resistance at high temperature. Two different aluminosilicate components were studied by these authors: metakaolin and fly ash. The main conclusions of this work were:

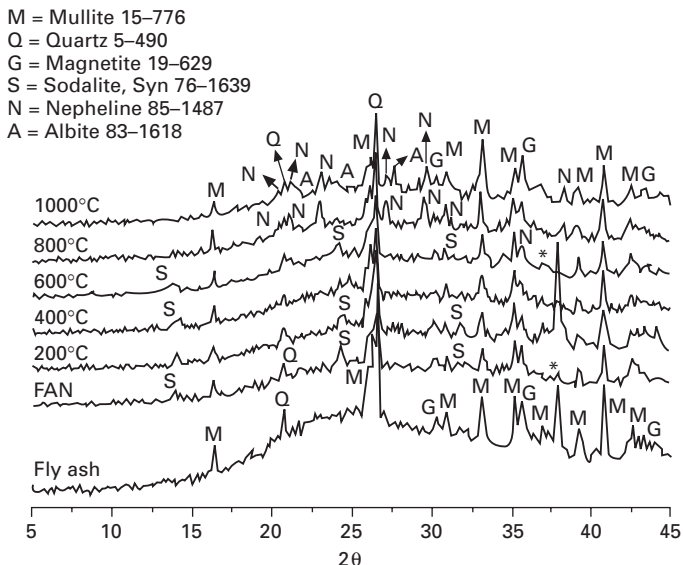
- (i) At low temperature (<250°C), the main reactions product is an aluminosilicate amorphous-semicrystalline gel (gel N-A-S-H), with inclusions of some crystalline zeolites. The gel composition and zeolite types depend on curing conditions, type and concentration of activator, raw materials (metakaolin, fly ash), etc. On the converse, when these



9.9 Variation in residual bending (a) and compressive (b) strength in cold samples (CEM = Portland cement paste; FAN = alkali-activated fly ash with sodium hydroxide) after one hour of exposition to high temperatures. Data obtained from Fernández-Jiménez *et al.* 2008.

materials are exposed to high temperature (750–1300°C), crystalline feldspathoid products are formed, the nature of which depends exclusively on the firing temperature and the initial chemical composition, and does not depend on the type of preliminary low temperature curing (see Fig. 9.10).

- (ii) The temperature of crystallisation of the anhydrous aluminosilicate depends on the initial composition, and most importantly on the alkali content. Normally in alkali-rich systems the crystallites appear in limited amounts at 600°C, whereas in low-alkali compositions the crystallisation process begins only at 1000°C
- (iii) Some shrinkage/expansion processes can occur during heating at high

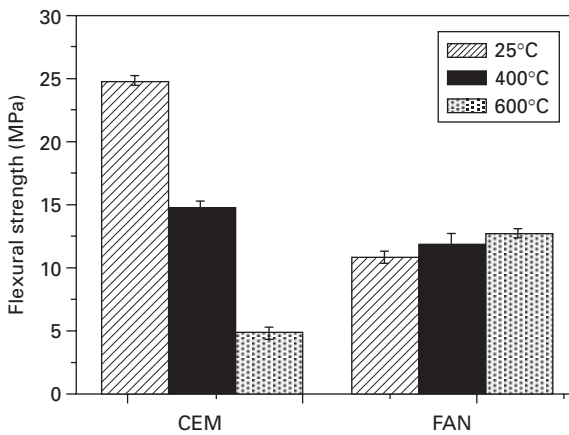


9.10 XRD diffractograms for the initial fly ash, a sample tested at ambient temperature (labelled FAN), and samples after testing at high temperature. Data obtained from Fernandez-Jimenez *et al.* 2008b.

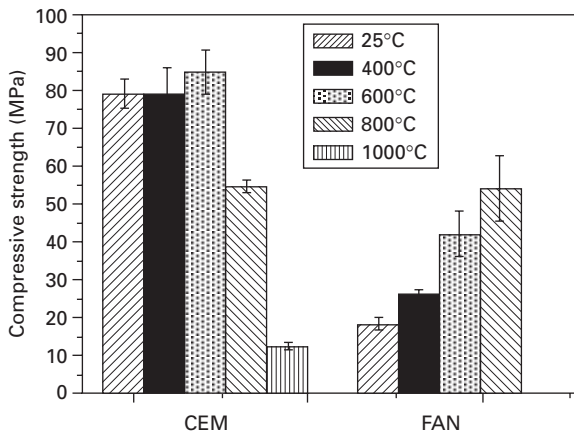
temperature. Materials with a moderate amount (from 2.5 to 10%) of thermo-stable zeolite-like products (i.e., analcine, hydroxysodalite, etc.) can show reduced contraction after firing. These phases are characterised by a smooth dehydration and subsequent re-crystallisation into stable anhydrous alkaline aluminosilicates such as nepheline and albite without destruction of the aluminosilicate framework. Also, the shrinkage/expansion process could be regulated by the selection of an optimal mix composition side by side with the addition of heat resistant filler (e.g., chamotte).

Another factor these investigations listed above share in common is that they each studied the material after being subjected to high temperatures, once the samples had cooled down. Fernandez-Jiménez *et al.* (2008) and Palomo *et al.* (2008) also studied the behaviour of the material when subjected to a load in situ at a high temperature. Different types of prismatic samples were used to determine the flexural and compressive strength (between 25°C and 600°C) in an Instron servomechanical machine, installed inside a furnace. The specimens were heated at a rate of 4°C/min. Once the target temperature was reached, the specimen was stabilised for 20 minutes before conducting the test. Also, in all cases the specimens were subjected to a 5 N preload during heating to fasten them securely to the testing device.

In Fig. 9.11, the results obtained for the flexural and compressive strengths of OPC (reference system) and alkali-activated fly ash with NaOH solution are shown. While the Portland cement control exhibited high bending and compressive strength at ambient temperature, these values declined with rising temperatures; at 600°C, the bending strength was just 20% of the initial figure. This decline was more visible and occurred at lower temperatures in the bending test due to its greater sensitivity to the presence of flaws or damage induced in the material. By contrast, the bending strength of the cement obtained from activated fly ash barely changed with temperature (and in fact rose slightly), while its compressive strength, surprisingly, climbed considerably at temperatures of over 400°C.



(a)



(b)

9.11 (a) Flexural and (b) Compressive strength versus temperature (Test 1). Data obtained from Palomo *et al.* 2008.

At 600 °C the Portland cement specimens (whose strength declined abruptly with rising temperatures) showed macroscopic cracks, and fragments of material were found in the furnace. This, together with the data presented in Fig. 9.11, explains the rapid deterioration of the strength of this sample at over 400 °C. However, alkali activated fly ash at 600 °C shows a very compact matrix, with no cracks observed. Nevertheless, at $T > 600^\circ\text{C}$ in flexural tests, the fly ash paste shows an interesting ‘pseudo-plastic’ behaviour. Applying a little load to the prisms (only 5N in order to keep the prism fixed to the testing device), a temperature of 600 °C is enough to provoke some deformation of the solid. In such a case, the prisms become broken around 800 °C.

Formation of a vitreous phase is expected to be responsible for the plastic behaviour observed, including possibly giving rise to local plastic behaviour that would initially lead to the sealing of cracks and pores. Both the un-reacted fly ash particles and the zeolite crystals formed would become embedded in the resulting matrix, which would be more compact. That in turn would increase the cross-sectional area of the material that is able to transmit loads. Consequently, despite a possible dip in intrinsic strength, macroscopic strength would grow as a result of this increase in area; i.e., σ_C would rise. These events also explain the higher strength observed at temperatures of over 500–600 °C, as the material would be more compact and the size of its flaws smaller. At the same time, these processes would account for the rapid deterioration of the material above 600 °C, with the spread of plasticity throughout the specimen, which would therefore exhibit deformation even under very light loads.

This particular characteristic confirms the fact that a melted phase component is forming part of the bulk material at high temperatures. The solidification of that melted phase during the cooling process may explain the excellent *ex situ* mechanical performance of thermally treated and cooled alkali activated fly ashes.

It can also be concluded that geopolymer materials compare favourably with organic polymers, as they are non-flammable, do not release toxic fumes and have very low weight loss of 5–12% as compared to 50–80% for fire-resistant polymer nanocomposites when heated up to 1000 °C (Bakharev 2006). The geopolymer materials were found superior to Portland cement concretes in their thermal properties when exposed to 700–1000 °C (Bakharev 2006). However according to the literature (Bakharev 2006, Krivenko and Kovalchuk 2002, 2007, Fernández-Jiménez *et al.* 2008, Palomo *et al.* 2008 Skvara *et al.* 2005), materials utilising class F fly ash are not suitable for refractory applications due to high shrinkage and large changes in compressive strength, which were possibly caused by the negative influence of the large amount of iron impurity present in the fly ash. However, in a fire-protection context, studies show that these materials have relatively good stability and strength after firing, which is indicative of good fire resistance. However,

more study is needed to determine heat conduction through a sample when exposed to the standard fire defined by ISO 834, as well as the relation between the thermal resistance of the protection layer and the thickness of an equivalent concrete protection.

9.7 Resistance to extreme environment: frost attack

It is known that for Portland cement mortars and concretes, the resistance to freezing and thawing mainly depends on its degree of saturation and the pore system of the hardened cement paste. If the concrete is never going to be saturated, there is no danger of damage from freezing and thawing. However, when as a consequence of freezing the dilation of the concrete exceeds its tensile strength, damage occurs. The extent of the damage varies from surface scaling to complete disintegration as ice is formed, starting at the exposed surface of the concrete and progressing through its depth. Also in some cases the salts used for de-icing road or bridge surfaces become absorbed by the upper part of the concrete. This produces a high osmotic pressure, with a consequent movement of water toward the coldest zone where freezing takes place, which aggravates the scaling condition of concrete.

With respect to the behaviour of geopolymer to frost attack, the available results are contradictory. Skvara (2007) indicated that geopolymer materials based on fly ash possess excellent frost resistance. For alkali-activated fly ash concrete with sodium silicate, the mass of the sample body did not change to any practical extent during the freezing and defrosting cycles taking place in an aqueous environment (i.e., no disintegration of the samples took place). The compressive strengths of the sample bodies after the freezing cycles were lower as compared with those obtained for samples after 28 days without any freeze-thaw cycling. No visible defects or deformation could be observed after 150 cycles. However, after 150 freezing cycles, the strength values dropped to about 70% of the strength measured in unexposed samples held at ambient conditions for the same period of time.

However, Puertas *et al.* (2003) show that the behaviour of alkali-activated fly ash mortars with NaOH solution is worse than the normal Portland cement, when both materials are exposed to 50 cycles of freezing/thawing. Similar results were obtained for wet/dry tests.

It is probable that the different results are related to with differences in the microstructures of the materials. The porosity and pore size have a significant influence in the resistance to frost, and as has been indicated earlier in this chapter and elsewhere in this book, the concentration and type of activator and the time and temperature of curing have a great influence on the microstructure of the materials. In any case, more studies of geopolymer

frost resistance are necessary in the future to enable the mechanisms to be better understood.

9.8 Conclusions

In this chapter a summary on the existing knowledge about durability of geopolymers (alkali-activated fly ashes or alkali-activated metakaolin) has been prepared. The authors are aware that the whole available information in bibliography on this particular topic has not been collected, but we honestly believe that we have included the most relevant data.

The main conclusion which can be extracted from a rational analysis of this chapter is that geopolymers have a durable behaviour similar to that of Portland cement. Even more, some durability characteristics of geopolymers are excellent; much better than in the case of OPC: resistance to acidic attack, behaviour at high temperatures, etc.

In any case, the authors consider that durability of geopolymers is a topic still needing much more investigation. We are still a long way from being able to establish accurate relationships between compositional-microstructural properties of the material and its response to different aggressive conditions.

Inevitably, long-term testing is the only certain method of investigation, but this approach is only rarely possible. Much effort is being extended to stabilise an appropriated standard procedure for this type of materials.

9.9 References

- Allahverdi A., Skvara F., (2001), 'Nitric acid attack on hardened paste of geopolymeric cements', *Ceramics-Silikaty*, 45, (4), 143–149.
- Allahverdi A., Skvara F., (2005), 'Sulfuric acid attack on hardened paste of geopolymer cements. Part 1. Mechanisms of corrosion at relatively high concentrations', *Ceram-Silik*, 49, 225.
- Andrade C. and González J.A., (1978), 'Quantitative measurements of corrosion rate of reinforcing steels embedded in concrete using polarization resistance measurements', *Werk. Korros.*, 29, 515–519.
- Bakharev T., (2005a), 'Durability of geopolymer materials in sodium and magnesium sulfate solutions' *Cem. Concr. Res.*, 35, 1233–1246.
- Bakharev T. (2005b), 'Resistance of geopolymer materials to acid attack' *Cement Concr. Res.*, 35, 658–670.
- Bakharev T., (2006), 'Thermal behaviour of geopolymers prepared using class F fly ash and elevated temperature curing', *Cem. and Concr. Res.*, 36, 1134–1147.
- Barbosa V.F.F., Mackenzie K.J.D., (2003), 'Thermal behaviour of inorganic geopolymers and composites derived from sodium polysialate', *Mater. Res. Bull.*, 38, 319–331.
- Bastidas D.M., Fernández-Jiménez A., Palomo A., González J.A., (2008), 'A study on the passive state stability of steel embedded in activated fly ash mortars', *Corrosion Science*, 50(4), 1058–1065.

- Criado M., Fernández-Jiménez A., and Palomo A., (2005), 'Alkali activation of fly ashes. Part 1: Effect of curing conditions on the carbonation of the reaction products', *Fuel*, 84, 2048–2054.
- Criado M., Fernández-Jiménez A., de la Torre A.G., Aranda M.A.G., and Palomo A., (2007), 'An XRD study of the effect of the SiO₂/Na₂O ratio on the alkali activation of fly ash', *Cem. Concr. Res.*, 37, 671–679.
- Davidovits, J., (1991), 'Geopolymer: inorganic polymeric new materials' *J. of Thermal Analysis*, 37 (8), 1633–1656.
- Davidovits J., (1994), 'Properties of geopolymer cements', Proceedings First Int. Conf. Alkaline Cements and Concretes, Vol.1, SRIBM, Kiev, Ukraine, 131–149.
- Davidovits J., Buzzi L., Rocher P., Gimeno D., Marini C., and Tocco S., (1999), Geopolymeric Cement based on Low Cost Geopolymer Materials. Results from the European Research Project GEOCISTEM, Geopolymer '99 Proceeding, 83–96.
- Duxson P., Provis J.L., Lukey G.C., Mallicoat S.W., Kriven W.M., and van Deventer J.S.J., (2005), 'Understanding the relationship between geopolymer composition, microstructure and mechanical properties' *Colloids and Surfaces A – Physicochemical and Engineering Aspects*, 269, (1–3), 47–58.
- Duxson P., Fernández-Jiménez A., Provis J.L., Lukey G.C., Palomo A., van Deventer J.S.J., (2007), 'Geopolymer technology: The current state of the art', *J. Materials Science*, 42, 2917–2933.
- Engelhardt G., and Michel D., (1987), *High-Resolution Solid-State NMR of Silicates and Zeolites*. John Wiley and Sons.
- Fernández-Jiménez A., and Palomo A., (2005a), 'Mid-infrared spectroscopic studies of alkali-activated fly ash structure', *Microporous and Mesoporous Materials*, 86, 207–214.
- Fernández-Jiménez A., and Palomo A., (2005b), 'Composition and Microstructure of alkali activated fly ash mortars. Effect of the activator', *Cem. Concr. Res.*, 35, 1984–1992.
- Fernández-Jiménez A., Palomo A., Sobrados I., and Sanz J., (2006), 'The role played by the reactive alumina content in the alkaline activation of fly ashes', *Microporous and Mesoporous Materials*, 91, 111–119.
- Fernández-Jiménez A., García-Lodeiro I., and Palomo A., (2007), 'Durability of alkali-activated fly ash cementitious materials', *J. Materials Science*, 42, 3055–3065.
- Fernández-Jiménez A., Palomo A., Pastor J.Y., Martín A. (2008), 'New binder material based in alkali activated fly ashes. Mechanical behaviour at high temperature' *J. Am. Ceramic Society*, 91, (10), 3308–3314.
- Fernández-Jiménez A., Miranda J.M., González J.A. and Palomo A. (2009), 'Steel passive state stability in activated fly ash mortars' *Cem Concr. Res.*, (in press).
- García-Lodeiro I., Palomo A., and Fernández-Jiménez A., (2007), 'The alkali-aggregate reactions in alkali activated fly ash mortars' *Cem. Concr. Res.*, 37, (2), 175–183.
- Gourley G., Johnson G.B., (2005), 'Developments in geopolymer precast concrete' World Congress Geopolymer 2005: Green chemistry and sustainable development solution, France, 139–143.
- Klinowski J, (1984), 'Nuclear magnetic resonance studies of zeolites', *Progress in NMR Spectroscopy*, 16, (3–4), 237–309.
- Kovalchuk G., Palomo A., and Fernández-Jiménez A., (2007), 'Alkali activated fly ashes. Effect of thermal curing conditions on mechanical and microstructural development – Part II', *Fuel*, 86, 315–322.
- Krivenko P.V., Kovalchuk G.Y., (2002), 'Heat-resistant fly ash based geocements'

- Proceedings of the Int. Conf. Geopolymer 28–29 October 2002, Melbourne, Australia, 2002.
- Krivenko P.V., Kovalchuk G.Y. (2007), 'Directed synthesis of alkaline aluminosilicate minerals in a geocement matrix', *J. Mater. Sci.*, 42, 2944–2952.
- Li K-L., Huang G-H, Chen J., Wang D. and Tang X.-S (2005), 'Early Mechanical Property and Durability of Geopolymer', *Geopolymer 2005*, Proceedings, 117–120.
- Malek R.I.A., Roy D.M. (1997), in: *Mechanisms of Chemical Degradation of Cement Based Systems*, p-83-89, Eds. Scrivener K.L. Young J.F., E & FN Spon, London 1997.
- Miranda J.M., Fernández-Jiménez A., González J.A., Palomo A., (2005) Corrosion resistance in activated fly-ash mortars, *Cem. Concr. Res.*, 35, 1210–1217.
- Morris J., Hodges S., (2001), 'Corrosion of metals in fly ash-based geopolymers' *Geopolymer, Green Chemistry and Sustainable Development Solutions*. Geopolymer Institute, France, 51–55.
- Neville, A. M. (1995), '*Properties of Concrete*', Longman, Essex.
- Page, C.L. Treadaway, K.W.J. and Bamforth P.B. (eds) (1990), *Corrosion of Reinforcement in Concrete*, Society of Chemical Industry, published by Elsevier Applied Science, London.
- Palomo A., Grutzeck M.W. and Blanco M.T., (1999a), 'Alkali-activated fly ashes. A cement for the future' *Cem. Concr. Res.*, 29, 1323–1329.
- Palomo A., Blanco-Valera M.T., Granizo M.L., Puertas F., Vázquez T. and Grutzeck M.W., (1999b), 'Chemical stability of cementitious materials based on metakaolin' *Cem. Concr. Res.*, 29, 997–1004.
- Palomo A., Alonso S., Fernández-Jiménez A., Sobrados I., and Sanz J., (2004), 'Alkali activated of fly ashes. A NMR study of the reaction products', *J. Am. Ceramic. Soc.*, 87, (6), 1141–1145.
- Palomo A., Fernández-Jiménez A., Pastor J.Y., Martín A., LLorca J., (2008), 'Alkali Activated Fly Ash: Mechanical Behaviour At High Temperatures' Non-Traditional Cement & Concrete (3rd International Symposium) Brno, Czech Republic, June 10–12, 2008, 525–534, ISBN: 978-80-214-3642-8.
- Puertas F., Amat T., Fernández-Jiménez A., Vazquez T., (2003), 'Mechanical and durable behaviour of alkaline cement mortars reinforced with polypropylene fibres' *Cem. Concr. Res.*, 33, 2031–2036.
- Rostami H., Brendley W., (2003), 'Alkali Ash Material: A Novel Fly Ash-Based Cement' *Environ Sci. Technol.*, 37, 3454.
- Silverstrim T., Rostami H., Clark J., Martin J., (1997), 'Microstructure and Properties of Chemically Activated Fly Ash Concrete', *Proc. 19th Int. Conf. Cem. Microsc.*, Int. Cement Microscopy Assoc. 355–373.
- Sindhunata, Provis J.L., Lukey G.C., Xu H., and van Deventer J.S.J., (2008), 'Structural Evolution of fly ash Based Geopolymers in Alkaline Environments' *Ind. Eng. Chem. Res.*, 47, 2991–2999.
- Skvara F., (2007), 'Alkali activated material-Geopolymer' Proceedings of 2007 Int. Conf. on Alkali Activated Materials. Research. Production and Utilization, Prague, Czech Republic, 661–676, ISBN 978-80-86742-19-9.
- Skvara F., Jilek T., Kopecky L., (2005), 'Geopolymer materials based on fly ash' *Ceramics-Silikáty*, 3, 195–204.
- Slater J.E., (1983), '*Corrosion of Metals in Association with Concrete*', ASTM STP 818. Philadelphia, PA.
- Song X-J., Marosszeky M., Brungs M., and Chang Z-T, (2005), 'Response of geopolymer concrete to sulphuric acid attack' *Geopolymer 2005 Proceedings*, 157–160.

- Swamy R.N., (1992), '*The Alkali-Silica Reaction in Concrete*' Chap.1 Blackie, New York 96–121.
- Taylor H.F.W., (1994), 'Delayed Ettringite Formation', in *Advances in Cement and Concrete* (M.W. Gruzdek & S.L. Sarkar, Eds.), American Society of Civil Engineers, 1994; see also: 'Sulfate Reactions – Microstructural and Chemical Aspects', in *Cement Technology, Ceramic Transactions* 40, (1994), 61–78.
- Taylor H.F.W., Gollop R.S. (1997), 'Some chemical and microstructural aspects of concrete durability,' in: K.L. Scrivener, J.F. Young (Eds), *Mechanisms of Chemical Degradation of Cement-Based Systems*, E. and FN Spon, London, 177–184.
- van Jaarsveld J.G.S. and van Deventer J.S.J. (1999), 'Effect of the alkali metal activator on the properties of fly ash-based geopolymers' *Ind. Eng. Chem. Res.*, 38, 3932–3941.
- Van Vlack H. (1964). '*Physical Ceramics for Engineering*, Addison-Wesley London, pp.94–102.
- Wallah S.E. Hardjito D., Sumajouw D.M.J. and Rangan B.V. (2005), 'Performance of fly ash-based geopolymer concrete under sulphate and acid exposure' *Geopolymer 2005, Proceedings*, 153–156.
- Weldes H.H., Lange K.R. (1969), 'Properties of soluble silicates.' *Ind. Eng. Chem.*, 65(14) 61–69.
- Yodmune S., Yodsudjai W., (2006), 'Study on corrosion of steel bar in fly ash-based geopolymer concrete' *International conference on Pozzolan, Concrete and Geopolymer, Khon Kaen, Thailand, May 24–25*, 189–194.

Life-cycle analysis of geopolymers

M WEIL, Institute for Technology Assessment and
Systems Analysis, Germany

K DOMBROWSKI, Technische Universität
Bergakademie Freiberg, Germany and

A BUCHWALD, Bauhaus University Weimar,
Germany

Abstract: Geopolymers as alternative binder systems are attracting increasing interest in research and development. They can display outstanding technical properties, such as high strength, high acid resistance, and/or high temperature resistance.

It has been documented by several investigations that good performance of geopolymers can also be obtained by the utilisation of secondary raw materials (industrial wastes like fly ash or slag). This explains the strong interest in this technology from countries with growing industrialisation. These countries accumulate large quantities of industrial wastes and do not have a developed recycling pathway. The use of waste for geopolymer production could not only solve a waste problem, but also reduce the consumption of primary raw materials.

Nevertheless, only limited knowledge exists about the ecological implications of geopolymer production. In this chapter, the effects of geopolymer production will be investigated from an environmental point of view. Furthermore, the predominant drivers of ecological impacts of geopolymers will be discussed to provide guidance for the development of geopolymer compositions for different applications.

Key words: life cycle assessment, geopolymer, concrete, cement, waste.

10.1 Introduction

According to the publications of Glukhovsky, geopolymers or inorganic polymer binder systems had already emerged in the late 1960s (Glukhovsky, 1959). In Russia and the Eastern part of Europe, some industrial applications of geopolymers (e.g., railway sleepers) were reported (Petrova *et al.*, 2005), but it seems that geopolymers were never in a state of mass production. Until today, only niche applications (e.g., fire-resistant glue, exhaust fume pipes, heat/fire barriers) have been established in Western Europe.

Owing to increased environmental concerns as well as increased costs of raw materials, however, research and development of geopolymers is currently experiencing a renaissance. Upcoming industrial nations, in particular China and India, are searching for a recycling option for increasing amounts of

industrial wastes to prevent large-scale dumping as well as to help resolve cement shortages.

Geopolymer systems are suitable, in principle, for the utilisation of industrial wastes (e.g., hard/soft coal fly ash, blast furnace slag, red mud) as a secondary resource. Hence, upcoming industrial nations are keenly interested in the development of geopolymers for mass applications.

Although production of applicable geopolymers on the basis of secondary resources has been demonstrated on laboratory and semi-industrial scales, very little knowledge exists about the ecological impact of geopolymer production, especially in comparison to competitive systems.

On a quantitative level, some estimations or rough calculations of single environmental aspects (without clear system boundaries) can be found in literature. Most of them refer to CO₂ emissions only and compare geopolymer (concrete) production with that of Portland cement (concrete). Estimated potential reductions of CO₂ emissions by geopolymer systems vary from a moderate 20% up to an ambitious 80% (Duxson *et al.*, 2007c; Komnitsas and Zaharaki, 2007; Nowak, 2008). But the assessment of new materials on the basis of CO₂ emissions alone is not sufficient. Other emissions and the consumption of resources should be taken into account to gain a more detailed impression.

The most common approach to assessing potential environmental impacts is the method of life cycle assessment (LCA). LCA is a cross-media approach and allows for a more holistic investigation of products and services. The goal of this study is to provide guidance to geopolymer designers for the development of ecologically more advantageous geopolymers.

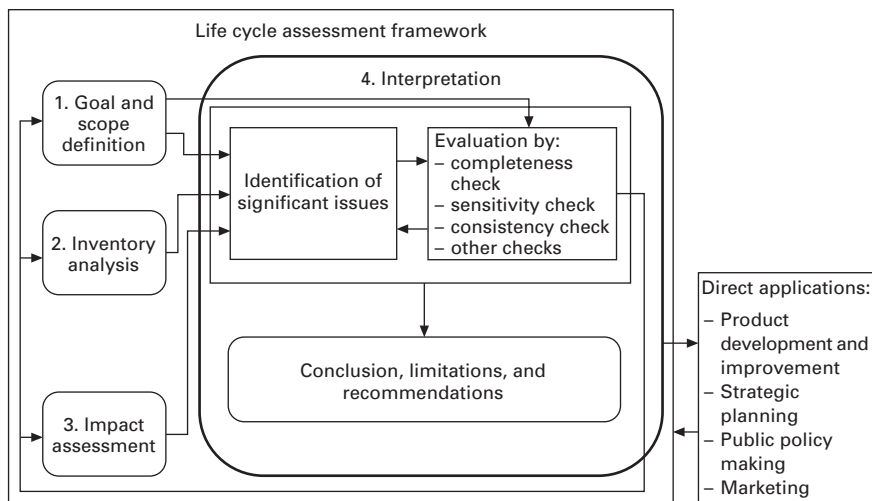
10.2 Life cycle assessment

10.2.1 Methodology of life cycle assessment

The production phase, the utilisation phase as well as the after-use phase (recycling, disposal) of every product is associated with the consumption of resources and emissions into air, water, and earth. To understand the complexity of the product, life cycle analysis methods as well as a quality-assured database are necessary.

Life cycle assessment (LCA) is an established method to evaluate the potential ecological impact of materials, products, or technologies. In LCA, an inventory of all material and energy flows of all processes relevant to an item is taken over the entire life cycle ('cradle to grave') to assess its environmental effects. The LCA methodology is described in the international ISO standards 14040 ff (ISO 14040, 2006). These standards represent a valid framework and permit consistent approaches.

A complete LCA generally comprises four major steps (Fig. 10.1):



10.1 LCA framework according to ISO Standard 14040 series (ISO 14040, 2006).

Goal and scope

The ‘goal and scope’ step defines the objective and intended application of the investigation. Life cycle assessment of a product will never be exhaustive. As a consequence, the ‘goal and scope’ determine the necessary degree of precision and correctness of a study and which part of the life cycle is modelled (e.g., cradle to gate, cradle to grave, or gate to gate). Closely related to the goal of the study is the determination of the functional unit which explicitly defines the functionality of a considered system. This is an important step, because careful definition of a functional unit prevents apples from being compared with oranges. The LCA results always refer to the functional unit.

Inventory analysis (LCI)

Inventory analysis (LCI) indicates the relevant inputs and outputs of a product or service system. On the input side, all energy and raw material consumption are considered, for instance, whereas products and emissions into air, water, and land are counted on the output side. LCI results represent an important information source for the LCA interpretation step.

Impact assessment (LCIA)

Impact assessment evaluates potential environmental impacts associated with the environmental inputs and outputs identified by the LCI.

By applying different models of environmental mechanisms (e.g., global warming due to the emission of greenhouse gases), the inventory (LCI) is translated into potential environmental impacts. For the ‘translation’, different methods are available with various strengths and shortcomings, (Dreyer *et al.*, 2003). A selection of often used impact categories (and indicators) is presented below:

- Depletion of resources (abiotic depletion potential – ADP)
- Climate change (global warming potential – GWP)
- Acidification (acidification potential – AP)
- Eutrophication (eutrophication potential – EP)
- Human toxicity (human toxicity potential – HTP)
- Ozone depletion (ozone depletion potential – ODP).

Interpretation

The final interpretation step identifies significant environmental impacts (e.g., energy use, greenhouse gases) as well as significant unit processes in the system. Both LCI and LCIA results are considered to identify the environmental drivers. In addition, this final step includes a consistency check, a sensitivity analysis, and a completeness check. Conclusions are drawn and recommendations are made, taking into account the assumptions, limits, and original goal and scope of the study.

10.2.2 Database

In the present study, LCIs were accomplished based on data from different sources. The most frequently used basic data for raw materials, auxiliary materials, and semi-finished products were taken from the Ecoinvent database (Ecoinvent, 2006). Ecoinvent provides scientifically sound, transparent, and quality-assured data sets. Nevertheless, suitability of a specific inventory of the database for a planned investigation remains to be proven in each case. For some inventories of specific raw materials (e.g., metakaolin), new and product-specific data sets had to be provided. In case of metakaolin, basic data (e.g., energy consumption) were obtained from a metakaolin producer/seller in Europe¹. In Table 10.1, all materials and processes utilised are displayed together with the data source and data quality. The estimated quality of the applied data ranks from very good to adequate. Adequate data quality means that there are some restrictions (e.g., in the form of data gaps, or different regional contexts), but the data are still acceptable for the investigation carried out.

¹BASF (formerly Engelhard) declare quite low CO₂ emissions for metakaolin production, cited in Duxson *et al.* (2007c), which cannot be confirmed by our data.

Table 10.1 Utilised inventories with data source and estimated data quality

Process	Data source	Data quality
silicate solution	ecoinvent, literature	very good
NaOH solution	ecoinvent	good
blast furnace slag	industry, literature	adequate (particle emissions into air from grinding are not included)
metakaolin	industry	good (particle emissions into air are not included)
hard/soft coal fly ash	estimation, literature	adequate
Portland cement	ecoinvent	good
gravel/sand	ecoinvent	good
water	ecoinvent	good
HDPE	ecoinvent	good (human and ecotoxicity assessment is severely limited)
auxiliary materials	ecoinvent	good
mixing	industry	adequate (particle emissions into air are not included)
plastic forming	ecoinvent	good
transportation lorry/ship	ecoinvent	very good

10.2.3 Impact assessment method

For this study, the CML method is applied (Guinée *et al.*, 2001) and the cumulative energy demand (CED, [MJ]) is also considered. The CML method comprises several environmental sectors with the related indicators. Two important environmental indicators are analysed:

- Global warming potential (GWP, [kg CO₂ equivalent])
- Abiotic resource depletion potential (ADP, [kg antimony equivalent]).

It would also be interesting to analyse the indicator of human toxicity, but unfortunately the database does not allow for the calculation of potential impacts. Basic data for particle emissions (dust), which have a great impact on human health, are lacking in particular for the mineral processing processes (e.g., grinding of slag).

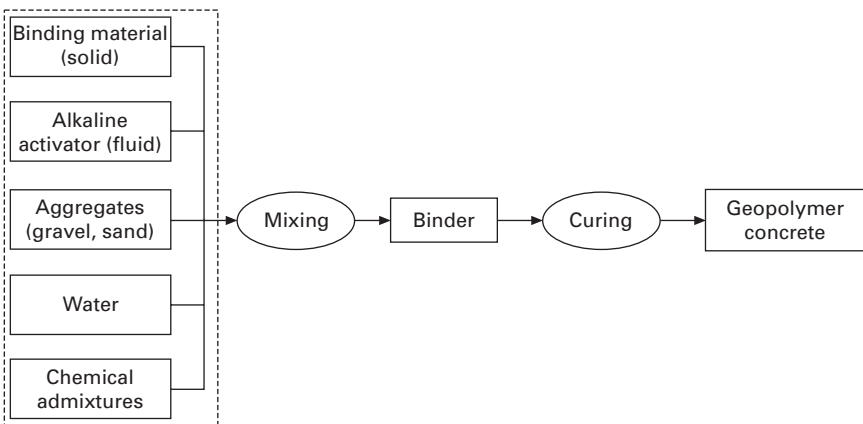
10.3 Influence of the geopolymer composition on environmental impacts

Geopolymers can be produced from a broad range of solid and fluid raw materials of significantly different qualities. Apart from the processing conditions, the raw materials selected are the important parameters, which determine the setting behaviour, the workability, and the chemical as well as the physical properties of geopolymeric products (Duxson *et al.*, 2007a). Furthermore, the environmental profiles depend largely on the raw materials used. There are significant differences between resource-intensive primary

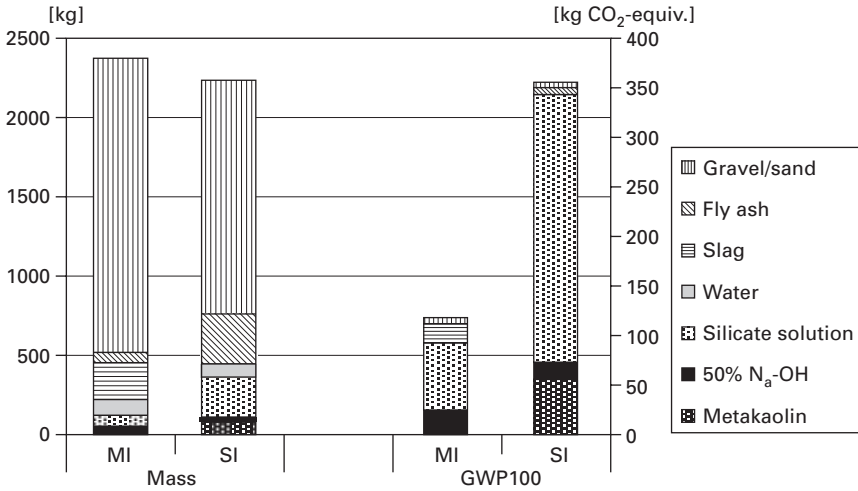
solid raw materials (e.g., metakaolin) and less resource-intensive secondary solid raw materials (e.g., fly ash) and between resource-intensive primary fluid raw materials (e.g., NaOH solution, silicate solution) and less resource-intensive primary fluid raw materials (e.g., water). The system boundaries for a comparison of different geopolymer (raw material) compositions are demonstrated in Fig. 10.2, whereby transportation processes are not being included. A comparison of the ratio of raw material mass (Fig. 10.3, left) to the share of environmental impacts represented by the indicator GWP 100 (Fig. 10.3, right) of two different geopolymer compositions reveals the following important aspects:

- Despite their high mass proportion, sand and gravel contribute only a little to the GWP.
- Fly ash (hard coal fly ash or soft coal fly ash) does not significantly contribute to the GWP.
- Slag (only a composite in mixture MI, Fig. 10.3) contributes noticeably to the GWP.
- The provision of water does not noticeably contribute to the GWP.
- Silicate solution contributes significantly to the GWP and dominates the environmental profile of both mixtures.
- Moderate use of NaOH solution (50%) in both mixtures causes a significant contribution to the GWP.
- Moderate usage of metakaolin (only in mixtures SI) contributes significantly to the GWP.

Some general conclusions can be drawn for geopolymer mixtures, which do not consider the influence of composition changes on the technical performance of the final geopolymers. As far as possible, the application



10.2 System boundaries for the comparison of different geopolymer compositions.



10.3 Comparison of mass balances and GWP results of two different geopolymer compositions (MI, SI).

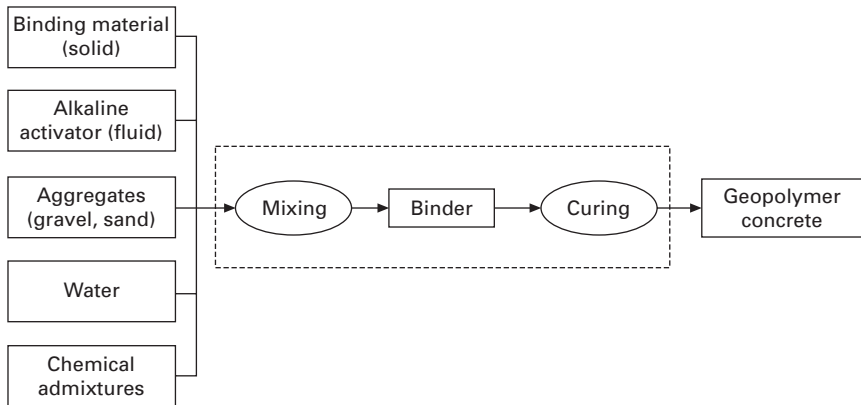
of silicate solution and NaOH solution should be reduced to a minimum, or these materials should be replaced by a more environmentally friendly activator. This is also true for metakaolin which should be replaced by alternatives in order to reduce the environmental load. It has to be stated that the applied (commonly available) quality of metakaolin is very high (in terms of purity). It should therefore be checked whether a lower quality would be more adequate for a broad application in geopolymer systems. Utilisation of secondary raw materials, such as fly ashes (no grinding and no thermal activation necessary) or blast furnace slag from iron production (only grinding necessary), is more favourable, provided that these secondary resources (wastes) are available and environmental limit values are not exceeded.

10.4 Influence of the geopolymer production process on environmental impacts

The geopolymer production process (Fig. 10.4) can be divided into the following major production steps:

- mixing of components
- heat curing.

An additional compaction process (by using a vibration table) during casting is not considered, but its contribution to the environmental impacts is known to be insignificant in other cases (common use). This is also true



10.4 System boundary for the identification of relevant production processes.

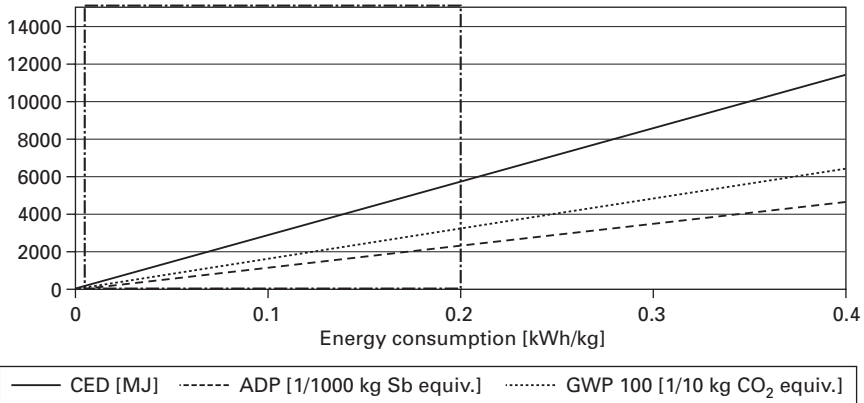
for the mixing process, which contributes less than 1% to the environmental effects (geopolymer production).

In contrast to this, the heat curing process may change the environmental profile of geopolymers significantly. It must be noted that not every geopolymer composition needs the heat curing step. Especially slag-rich geopolymer compositions achieve the desired technical properties within a few hours or days at room temperature without any heat curing (Duxson *et al.*, 2007b; Bakharev *et al.*, 1999).

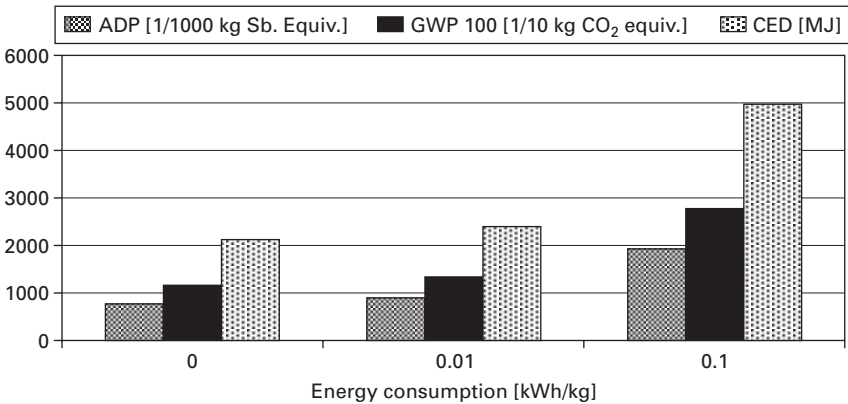
Mixtures containing predominantly fly ash (or other slowly reacting raw materials) require a heat treatment to enhance the maturity of the geopolymers. The moderate temperature ranges usually between 20°C and 80°C. Heat curing within a similar temperature range is also quite common in the pre-cast concrete industry, where the strength development of the concrete elements is accelerated.

The energy consumption for concrete production of common pre-cast companies ranges between 20 and 500 kWh/m³ (Menzel, 1991), or approximately 0.01–0.2 kWh/kg. For the assumption that an electric conditioning cabinet (<100 kW) is used, the effects of energy consumption on the environmental indicators (CED, GWP, ADP) are highlighted in Fig. 10.5. A simple linear relationship between the energy consumption and the environmental indicators becomes evident. In addition, the normal range of energy consumption for heat curing is indicated (dashed line, Fig. 10.5).

The effect of heat curing on the environmental impacts of geopolymer production is demonstrated in Fig. 10.6. In this specific case, all indicator values are more than doubled, if heat curing consumes a moderate amount of energy (0.1 kWh/kg). If a gas fan burner is used instead of an electric conditioning cabinet, the increase of the environmental indicator values



10.5 Effects of heat curing (consumption of electric energy) on the environmental impact indicators.



10.6 Effect of heat curing on the environmental impacts of geopolymer production.

would be less dramatic, but still significant. From a process perspective, the application of heat curing should therefore be reduced to a minimum. Another option to reduce the environmental impact may exist in the use of waste heat from other processes.

10.5 LCA comparison of geopolymers to other product systems

The understanding of the interdependence of composition, processing, technical performance and ecological/economic effects is essential to develop

competitive geopolymers for different application fields (Weil *et al.*, 2006; Dombrowski *et al.*, 2008). Research tends to focus on the improvement of one or two properties to produce so-called high-performance materials. In fact, the market needs a product of suitable technical performance (broad requirement profile, minimum properties are specified in guidelines and/or standards) at moderate costs (competitive to existing technologies) that preferably have low environmental impacts. A comparative LCA, i.e. a comparison with existing traditional systems, already during the development phase of geopolymers is very helpful to identify optimisation potentials or issue warnings from an environmental perspective. As geopolymers have not yet reached product character in many application fields, the comparison with traditional systems is subject to some restrictions. Whereas long-term experience (e.g., durability) exists for traditional systems, information on geopolymers are often limited (Gruskovnjak *et al.*, 2006).

Nevertheless, the utilisation period of materials (including maintenance) has a significant influence on the total environmental performance. To deal with this problem, comprehensible assumptions have to be applied or the results obtained have to be discussed in the light of the known restrictions.

Focusing on two quite different applications, an approach towards an adequate comparison will be presented.

10.5.1 Geopolymer versus cement concrete

In industrialised countries, cement may be considered a cheap product suitable for concrete mass production. To compete with such an optimised system, cheap raw materials, such as blast furnace slag and coal fly ash, may be used for geopolymer production.

The use of secondary raw materials also reduces the environmental impact of the geopolymer system. Nevertheless, the question arises of whether the geopolymer system is competitive to a cement-based system from an environmental point of view. For comparison, a concrete complying with increased requirements is considered (functional unit): freeze-thaw-resistant concrete of exposition class XF2 and XF4 according to DIN EN 206-1/DIN 1045-2. The system boundaries are shown in Fig. 10.7.

After use, geopolymer concrete and cement concrete might be crushed and used for different applications in civil engineering. Thus there is no evidence of geopolymer concrete having major ecological advantages or drawbacks in comparison to cement concrete as far as the 'recycling/disposal' phase is concerned. Hence, both after-use phases may be considered comparable. This conclusion may only be drawn, however, if both the raw materials and the product meet the environmental threshold values existing (e.g., for heavy metals).

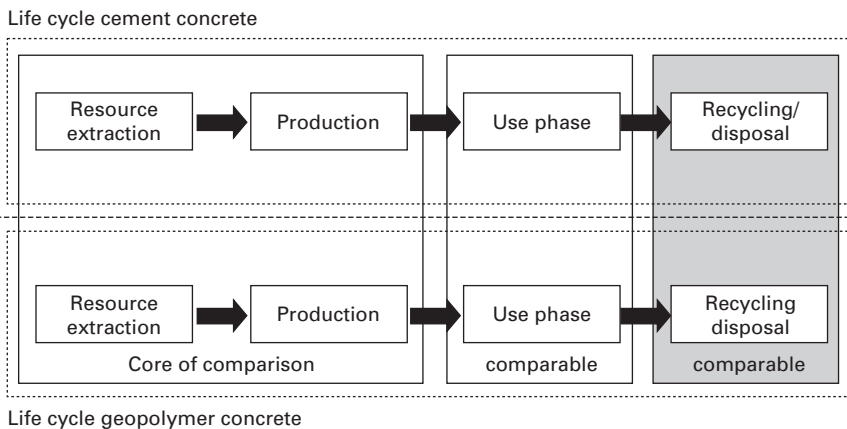
Comparability of the utilisation phase of both materials is ensured

by fulfilling minimum requirements of the functional unit (freeze-thaw-resistant concrete of exposition class XF2 and XF4). The necessary investigation basically covers strength development and freeze-thaw tests -CDF- (Dombrowski *et al.*, 2008), according to which geopolymer concrete is comparable to cement concrete or even better (as far as major technical properties are concerned).

The life cycle phase that is comparable for both materials may be excluded in a comparative LCA. The investigation will therefore focus on the production phase and the related pre-chains of resource extraction (Fig. 10.7). Although the transport of raw materials contributes at least noticeably to the environmental profile, it is not included in the system boundaries, because the efforts needed to transport the raw materials needed are quite different worldwide. The impact of transportation processes should only be assessed in a specific regional context.

The compositions of the compared systems are shown in Table 10.2. All mixtures have an identical content of gravel/sand and the concretes are produced without any chemical admixtures (e.g., superplasticisers). The Portland cement concrete mixture contains 340 kg cement/m³, which is 20 kg above the minimum cement content for freeze-thaw-resistant concrete (XF2-XF4) according to DIN EN 206-1/DIN 1045-2. The already optimised geopolymer concrete (Dombrowski *et al.*, 2008) with a slag/fly ash ratio of approximately 80:20 does not need any heat curing and hardens at room temperature (20°C).

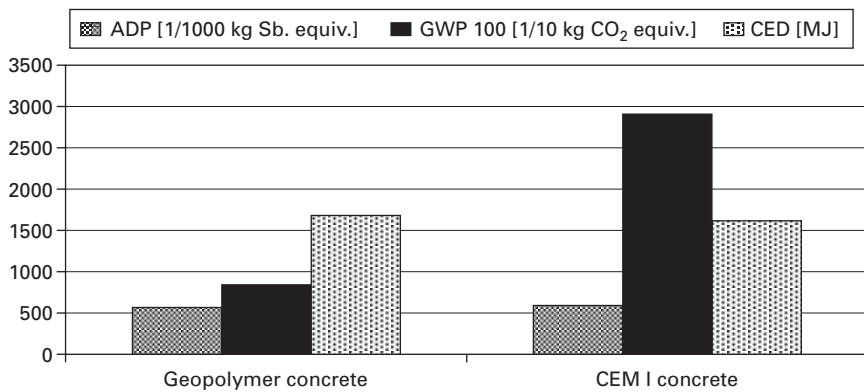
In the case where the utilisation phase and the recycling/disposal phase are considered to be equal, the results in Fig. 10.8 exhibit comparable environmental impacts in terms of ADP and CED of the geopolymer system



10.7 System boundaries for the comparison of geopolymer concrete and cement concrete production.

Table 10.2 Composition of geopolymer and cement concrete [kg/m³]

Material	Cement concrete	Geopolymer concrete
cement CEM I 32.5R	340	
slag		230
fly ash		57
reactive waste		83
silicate solution/Na silicate (37%)		33
NaOH (50%)		24
de-ionised water	170	99
gravel/sand (0-16mm)	1878	1878
kg/m ³	2388	2404



10.8 LCA results of geopolymers and cement concrete.

for this specific application (freeze-thaw-resistant concrete). In contrast to this, the geopolymer concrete contributes much less to the global warming potential (GWP). In comparison to the Portland cement concrete, the GWP of geopolymer concrete is approximately 70% lower.

Compared to cement concrete, two aspects have to be considered critical:

- the cement content used exceeded the prescriptive minimum cement content (DIN EN 206-1/DIN 1045-2) by 20 kg per m³
- Portland cement (with the highest energy and resource requirements of all known cement types) is used instead of blended cements, such as CEM II or even CEM III, which may be also be applied for class XF2-XF4 according to DIN EN 206-1/DIN 1045-2.

In fact, both mentioned aspects would improve the environmental profile of cement concrete. The reduction of the cement content to the required minimum (320 kg) will reduce the indicator values by 3–5%, use of a slag-rich CEM II cement will reduce the indicator values by 11–16%. In such a best

case assumption for cement concrete and provided that such mixtures have the technical performance required, the cement concrete mixture will have noticeable advantages in terms of ADP and CED. But still, the geopolymer would have a considerably lower impact on the global warming potential (GWP indicator). To facilitate decision, the regional transport efforts have to be taken into account.

The utilisation phases of both systems are considered to be comparable, as the requirements according to DIN EN 206-1/DIN 1045-2 are fulfilled. Owing to its different carbonation performance, varying durability of reinforced cement and geopolymer concrete should be investigated from a technical point of view. By means of a durability model considering complex environmental conditions, the lifetime of each system could be assessed more detailed. Such lifetime predictions would be an important input for a more holistic LCA comparison of geopolymers and cement concrete.

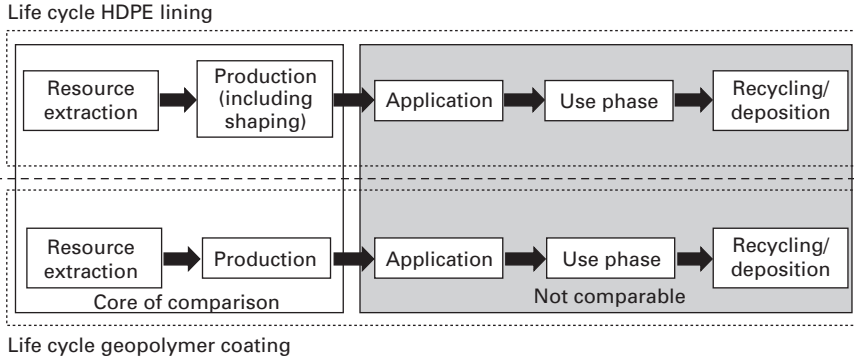
10.5.2 Comparison of geopolymer coating with HDPE liner systems in sewage sludge pipes

Geopolymers may exhibit remarkable technical performance, such as a high strength, high heat resistance, and high acid resistance. The latter property is used to design an acid-resistant coating for sewage sludge pipes. Unprotected concrete pipes are usually used for domestic wastewater transport. If increased resistance against acid is requested and/or a longer life cycle is desired, concrete pipes are often lined with high-density polyethylene (HDPE). Sewage sludge pipes with an HDPE lining are well protected against chemical and mechanical corrosion (Guerhazi *et al.*, 2008).

In principle, geopolymer coatings are also qualified to protect a concrete surface against chemical attack (Bakharev, 2005; Bakharev *et al.*, 2003) and mechanical abrasion.

The system boundaries for a comparative investigation of both protection systems are shown in Fig. 10.9. The concrete pipe (the protected item) may be assumed to be identical and will not be considered within the system boundaries. The shaped HDPE 'pipe' is applied to the inner part of the tube directly after stripping the moulds of the concrete pipe without using additional adhesive components. In contrast to the HDPE lining, the geopolymer coating must be applied by a spray technique. There is no evidence of either application technique causing a considerable environmental impact.

Owing to the use of different materials in both systems (Fig. 10.9), the utilisation phase and the recycling/disposal phase might be different as well. In this case, the utilisation phase (including maintenance) probably contributes decisively to the environmental profile. The recycling/disposal phase is estimated to be of small importance. Since data on the application, use, and recycling/disposal phases are lacking, in a simplification the investigation



10.9 System boundaries for the comparison of geopolymers coating and HDPE lining.

focuses solely on the production phase. But it must be kept in mind that the significance of the results gained is limited, especially due to the exclusion of the utilisation phase.

The functional unit of the comparative assessment is a 100 m² protective layer:

- HDPE lining of 5 mm thickness (density 0.97 kg/dm³)
- geopolymer coating of 10 mm thickness (density 2.23 kg/dm³).

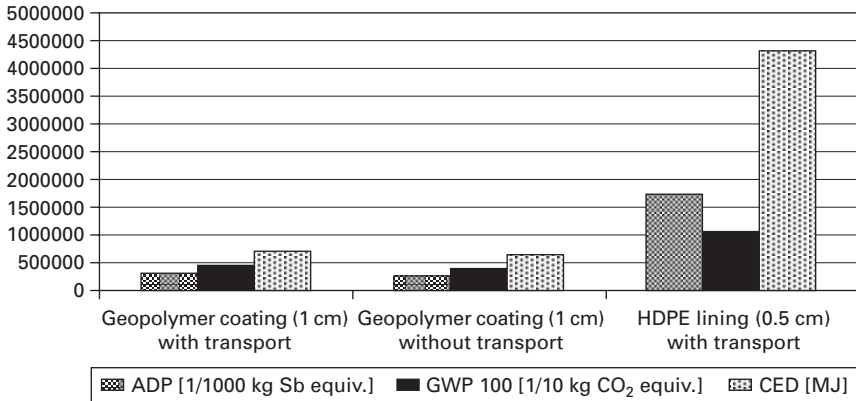
A suitable geopolymer mixture with very promising technical properties for this application has been designed by Anja Buchwald. The mixture contains:

- 14.3% soft coal fly ash (lorry transport distance 300 km)
- 6.1% metakaolin (lorry transport distance 300 km, ship transport distance 6000 km)
- 11.8% silicate solution (lorry transport distance 300 km)
- 2.2% NaOH solution (lorry transport distance 300 km)
- 3.9% water (no transport)
- 61.7% sand/fine sand (lorry transport distance 10 km).

To compare the HDPE lining (which includes already the transport of the raw materials) and the geopolymer coating system in a consistent way, a transportation scenario for the geopolymer-based system (focused on central Europe) is considered in addition (Fig. 10.10). The assumed transport distances for the raw materials are given above and are rather high (worst case assumption).

The geopolymer coating reaches much lower values for all environmental impact indicators considered. This is true for the geopolymer coating with and without consideration of raw material transportation.

The GWP of the HDPE system is higher by a factor of 2.3, the CED by



10.10 LCA results for geopolymers coating (with and without transport) and HDPE lining.

a factor of 5.9. As mentioned above, the use phase presumably contributes decisively to the environmental profile. Hence, the results presented do not favour one option, unless comparable information exists with respect to the durability of both systems.

However, the discussion may also be reversed. Although the geopolymer coating reaches only half of the lifetime of the HDPE lining and hence needs in-situ maintenance (recoating with geopolymer), it might have environmental advantages. The geopolymer coating might also be an attractive compromise between an uncoated concrete pipe and an expensive HDPE-protected concrete pipe for a moderately aggressive environment.

10.6 Geopolymers and the utilisation of secondary resources

A geopolymer composition can be optimised in terms of environmental impacts (and costs) by replacing primary raw materials with secondary resources. This kind of optimisation is recommended by the LCA results, but in practice is associated with several problems when good technical performance is desired. Secondary raw materials tend to have a greater variety of chemical compositions compared to primary raw materials. Consequently, technical performance of geopolymers also varies considerably, which is quite problematic for an industrial application. Some secondary raw materials also contain heavy metals, hence the use of such materials for industrial production might be restricted by environmental threshold values.

Another problem is the availability of secondary resources, especially these with a desirable low variation in chemical composition and a low content of heavy metals or impurities. Even if the availability varies a lot worldwide,

the problem remains the same, as other traditional or new systems compete for these secondary resources. For instance, blast furnace slag is already used in traditional cement-based systems in Germany. Competition with a traditional utilisation of the same secondary resource does not facilitate market introduction of a new technology. Thus, the development of geopolymer mixtures for different applications should preferentially favour secondary resources which are not already used as raw materials to a large extent in other industrial sectors.

10.7 Conclusions

The environmental impact of products should be reduced to a minimum. To develop more environmentally friendly materials, the material designer needs some knowledge about the environmental drivers of new material systems, but also knowledge of the environmental impacts of competitive traditional material systems. Geopolymers can be produced from different raw materials at variable process conditions to achieve different properties which make them suitable for a variety of applications. Hence, the issue of environmental implications of geopolymers is a rather complex one.

This investigation reveals that a careful raw material selection should focus on both the solid and fluid components. To improve the environmental profile of geopolymers, the replacement of silicate solution and Na-OH solution shows great potential. Furthermore, the application of heat curing for geopolymer production should be reduced to a minimum level, or waste heat from other processes should be utilised in order to reduce the accompanied environmental burdens.

A comparative assessment shows clearly the competitiveness of geopolymer systems with cement based systems from an environmental point of view. It will depend on the exact composition (in both systems), for a specific application field, to favour one option (assumed that the technical performance is comparable). The comparison of geopolymer pipe coating with an HDPE lining demonstrates a quite different picture. In this specific case the geopolymer system exhibits considerable environmental advantages as far as the production phase is considered. In general there is a great need to understand the durability and lifetime performance of geopolymer systems in comparison with traditional systems. Only with this important information can a final conclusion on the environmental impacts of geopolymer products be drawn.

10.8 Acknowledgement

This research work was made possible by the financial support provided by the foundation Volkswagen Stiftung.

10.9 References

- Bakharev, T. (2005). Resistance of geopolymer materials to acid attack. *Cement and Concrete Research*, 35(4), 658–670.
- Bakharev, T., Sanjayan, J.G., and Cheng, Y.-B. (1999). Effect of elevated temperature curing on properties of alkali-activated slag concrete. *Cement and Concrete Research*, 29(10), 1619–1625.
- Bakharev, T., Sanjayan, J.G., and Cheng, Y.-B. (2003). Resistance of alkali-activated slag concrete to acid attack. *Cement and Concrete Research*, 33(10), 1607–1611.
- Dombrowski, K., Weil, M., and Buchwald, A. (2008). Geopolymer binders. *ZKG International*, 61(3), 70–80.
- Dreyer, L.C., Niemann, A.L., and Hauschild, M.Z. (2003). Comparison of three different LCIA methods: EDIP97, CML2001 and Eco-indicator 99 – Does it matter which one you choose? *International Journal of Life Cycle Assessment*, 8(4), 191–200.
- Duxson, P., Fernandez-Jimenez, A., Provis, J.L., Lukey, G.C., Palomo, A., and van Deventer, J.S.J. (2007a). Geopolymer technology: the current state of the art. *Journal of Materials Science*, 42(9), 2917–2933.
- Duxson, P., Mallicoat, S.W., Lukey, G.C., Kriven, W.M., and van Deventer, J.S.J. (2007b). The effect of alkali and Si/Al ratio on the development of mechanical properties of metakaolin-based geopolymers. *Colloids and Surfaces A: Physicochemical and Engineering Aspects*, 292(1), 8–20.
- Duxson, P., Provis, J.L., Lukey, G.C., and Van Deventer, J.S.J. (2007c). The role of inorganic polymer technology in the development of 'green concrete'. *Cement and Concrete Research*, 37(12), 1590–1597.
- Ecoinvent (2006). Database. *Ecoinvent Version v 1.3*.
- Glukhovskiy, V.D. (1959). *Soil Silicates*. Gosstroyizdat Ukrainy Publishing, Kiev.
- Gruskovnjak, A., Lothenbach, B., Holzer, L., Figi, R., and Winnefeld, F. (2006). Hydration of alkali-activated slag: comparison with ordinary Portland cement. *Advances in Cement Research*, 18(3), 119–128.
- Guermazi, N., Elleuch, K., Ayedi, H.F., Zahouani, H., and Kapsa, P. (2008). Susceptibility to scratch damage of high density polyethylene coating. *Materials Science and Engineering: A*, 492(1–2), 400–406.
- Guinée *et al.* (2001). Life cycle assessment. An operational guide to the ISO standards. Part 1: LCA in perspective. Part 2a: Guide. Part 2b: Operational annex. Part 3: Scientific background. Ministry of Housing, Spatial Planning and the Environment (VROM) and Centre of Environmental Science, Leiden Nederlande.
- ISO 14040 (2006). *Environmental management – life cycle assessment – principles and framework*. International Organization for Standardization (ISO).
- Komnitsas, K. and Zaharakis, D. (2007). Geopolymerisation: A review and prospects for the minerals industry. *Minerals Engineering*, 20(14), 1261–1277.
- Menzel, U. (1991). Heat treatment of concrete. *Concrete plant + precast technology*, 12, 92–96.
- Nowak, R. (2008). Geopolymer concrete opens to reduce CO₂ emissions. *The New Scientist*, 197(2640), 28–29.
- Petrova, T., Dzhashi, N., and Poletaev, A. (2005). Durability of Slag-Alkaline Concretes. In: Bilek, V., Keršner, Z. (Eds.), *Proceeding of the 2nd International Symposium Non-Traditional Cement and Concrete*, Brno, 14–16 June, 61–68.
- Weil, M., Buchwald, A., and Dombrowski, K. (2006). Sustainable Design of Geopolymers – Integration of Economic and Environmental Aspects in the Early Stages of Material Development. *GDCH-Monograph*, 36, 297–306.

Engineering properties of geopolymer concrete

B V RANGAN, Curtin University of Technology, Australia

Abstract: This chapter deals with fly ash-based geopolymer concrete. The mixture design, production, and curing of geopolymer concrete are briefly given. The behaviour and the short-term properties in compression and tension are then described. The chapter also includes an account of the drying shrinkage and creep properties of geopolymer concrete. Excellent resistance offered by the fly ash-based geopolymer concrete to sulfate and acid attacks is also demonstrated.

Key words: acid attack, compressive strength, creep, drying shrinkage, elastic modulus, fly ash, geopolymer concrete, sulfate resistance, tensile strength.

11.1 Introduction

Demand for Portland cement concrete, one of the most widely used construction materials, is on the increase. The cement industry is held responsible for some of the CO₂ emissions that cause climate change, because the production of one ton of Portland cement emits approximately one ton of CO₂ into the atmosphere. In this respect, geopolymers show considerable promise for application in the concrete industry as an alternative binder to Portland cement (Duxson *et al.*, 2007). In terms of global warming, geopolymer technology could significantly reduce CO₂ emission to the atmosphere caused by the cement industries as shown by the detailed analyses of Gartner (2004).

The chemical composition of geopolymers has been explained by several researchers (Davidovits, 1994; van Jaarsveld *et al.*, 1997), and in other parts of this book. With regard to the engineering properties of geopolymer concrete, it must be noted that water is released during the chemical reaction that occurs in the formation of geopolymers. This water, expelled from the geopolymer matrix during the curing and further drying periods, leaves behind discontinuous nano-pores in the matrix, which provide benefits to the performance of geopolymer concrete. The water in a geopolymer concrete mixture, therefore, plays no role in the chemical reaction that takes place; it merely provides the workability to the mixture during handling. This is in contrast to the chemical reaction of water in a Portland cement concrete mixture during the hydration process.

This chapter describes the engineering properties of heat-cured low-calcium fly ash-based geopolymer concrete. Low-calcium (ASTM Class F) fly ash is preferred as a source material than high-calcium (ASTM Class C) fly ash. The presence of calcium in high amounts may interfere with the polymerisation process and alter the microstructure (Gourley, 2003, Gourley and Johnson, 2005).

11.2 Geopolymer concrete

Geopolymer concrete can be manufactured by using the low-calcium (ASTM Class F) fly ash obtained from coal-burning power stations. Low-calcium fly ash has been successfully used to manufacture geopolymer concrete when the silicon and aluminum oxides constituted about 80% by mass, with the Si-to-Al ratio of about 2. The content of the iron oxide usually ranged from 10 to 20% by mass, whereas the calcium oxide content was less than 5% by mass. The carbon content of the fly ash, as indicated by the loss on ignition by mass, was as low as less than 2%. The particle size distribution tests revealed that 80% of the fly ash particles were smaller than 50 μm (Gourley, 2003, Hardjito and Rangan, 2005, Wallah and Rangan 2006, Sumajouw and Rangan 2006, Fernandez-Jimenez *et al.* 2006a, Sofi *et al.* 2007a). The reactivity of low-calcium fly ash in geopolymer matrix has been studied by Fernandez-Jimenez *et al.* (2006b).

Coarse and fine aggregates used by the concrete industry are suitable to manufacture geopolymer concrete. The aggregate grading curves currently used in concrete practice are applicable in the case of geopolymer concrete (Hardjito and Rangan, 2005, Wallah and Rangan, 2006, Sumajouw and Rangan, 2006, Gourley, 2003).

A combination of sodium silicate solution and sodium hydroxide (NaOH) solution can be used as the alkaline liquid. The sodium silicate solution A53 with SiO_2 -to- Na_2O ratio by mass of approximately 2, i.e., $\text{SiO}_2 = 29.4\%$, $\text{Na}_2\text{O} = 14.7\%$, and water = 55.9% by mass, and the sodium hydroxide solids with 97–98% purity dissolved in water were used in laboratory studies (Hardjito and Rangan, 2005, Wallah and Rangan, 2006, Sumajouw and Rangan, 2006). The concentration of sodium hydroxide solution can vary in the range between 8 Molar and 16 Molar. Note that the mass of water is the major component in the alkaline liquid.

In order to improve workability, a high range water reducer super plasticiser and extra water may be added to the mixture.

11.3 Mixture design, production, and curing

11.3.1 Mixture design

The primary difference between geopolymer concrete and Portland cement concrete is the binder. The silicon and aluminum oxides in the low-calcium fly ash reacts with the alkaline liquid to form the geopolymer paste that binds the loose coarse aggregates, fine aggregates, and other un-reacted materials together to form the geopolymer concrete.

As in the case of Portland cement concrete, the coarse and fine aggregates occupy about 75 to 80% of the mass of geopolymer concrete. This component of geopolymer concrete mixtures can be designed using the tools currently available for Portland cement concrete.

The compressive strength and the workability of geopolymer concrete are influenced by the proportions and properties of the constituent materials that make the geopolymer paste. Experimental results (Hardjito and Rangan, 2005) have shown the following:

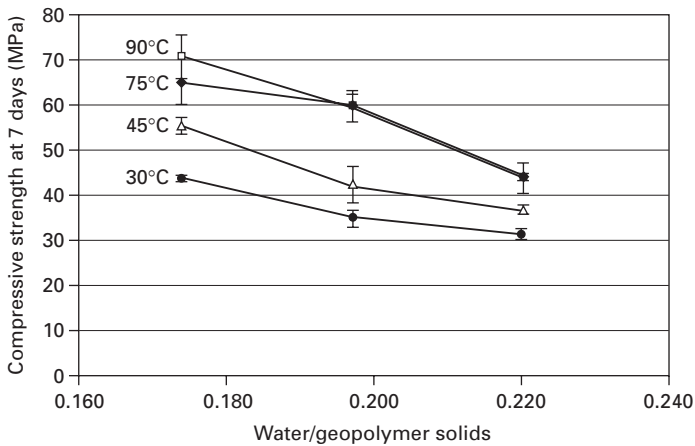
- Higher concentration (in terms of molar) of sodium hydroxide solution results in higher compressive strength of geopolymer concrete.
- The higher the ratio of sodium silicate solution-to-sodium hydroxide solution ratio by mass the higher the compressive strength of geopolymer concrete.
- The addition of naphthalene sulfonate-based super plasticiser, up to approximately 4% of fly ash by mass, improves the workability of the fresh geopolymer concrete; however, there is a slight degradation in the compressive strength of hardened concrete when the super plasticiser dosage is greater than 2%.
- The slump value of the fresh geopolymer concrete increases when the water content of the mixture increases.
- As the H_2O -to- Na_2O molar ratio increases, the compressive strength of geopolymer concrete decreases.

As can be seen from the above, the interaction of various parameters on the compressive strength and the workability of geopolymer concrete is complex. In order to assist the design of low-calcium fly ash-based geopolymer concrete mixtures, a single parameter called 'water-to-geopolymer solids ratio' by mass was devised. In this parameter, the total mass of water is the sum of the mass of water contained in the sodium silicate solution, the mass of water in the sodium hydroxide solution, and the mass of extra water, if any, added to the mixture. The mass of geopolymer solids is the sum of the mass of fly ash, the mass of sodium hydroxide solids, and the mass of solids in the sodium silicate solution (i.e., the mass of Na_2O and SiO_2).

Tests were performed to establish the effect of water-to-geopolymer solids ratio by mass on the compressive strength and the workability of geopolymer

concrete. The test specimens were 100 × 200 mm cylinders, heat-cured in an oven at various temperatures for 24 hours. The results of these tests, plotted in Fig. 11.1, show that the compressive strength of geopolymer concrete decreases as the water-to-geopolymer solids ratio by mass increases (Hardjito and Rangan, 2005). This test trend is analogous to the well-known effect of water-to-cement ratio on the compressive strength of Portland cement concrete. Obviously, as the water-to-geopolymer solids ratio increased, the workability increased as the mixtures contained more water.

The proportions of two different geopolymer concrete mixtures used in laboratory studies are given in Table 11.1 (Wallah and Rangan, 2006). The details of numerous other mixtures are reported elsewhere (Hardjito and Rangan, 2005; Sumajouw and Rangan, 2006).



11.1 Effect of water-to-geopolymer solids ratio by mass on compressive strength of geopolymer concrete (Hardjito and Rangan, 2005).

Table 11.1 Geopolymer concrete mixture proportions

Materials	Mass (kg/m ³)	
	Mixture 1	Mixture 2
Coarse aggregates:		
20 mm	277	277
14 mm	370	370
7 mm	647	647
Fine sand	554	554
Fly ash (low-calcium ASTM Class F)	408	408
Sodium silicate solution (A53)	103	103
Sodium hydroxide solution	41 (8 Molar)	41 (14 Molar)
Super plasticiser	6	6
Extra water	None	22.5

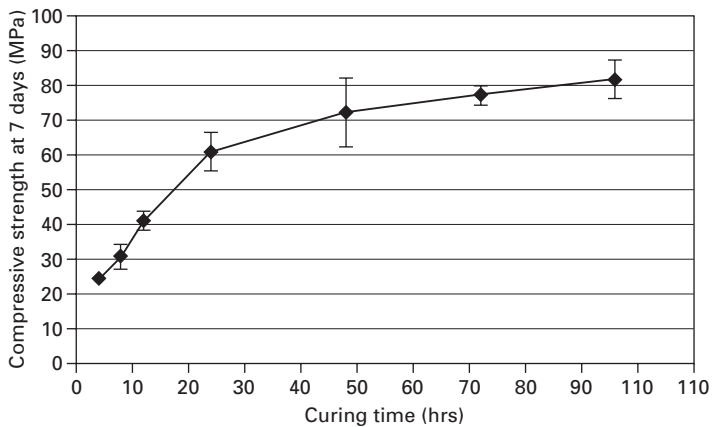
11.3.2 Production

Geopolymer concrete can be produced by adopting the conventional techniques used in the manufacture of Portland cement concrete. In the laboratory, the fly ash and the aggregates were first mixed together dry in an 80-litre capacity pan mixer for about three minutes. The alkaline liquid was mixed with the super plasticiser and the extra water, if any. The liquid component of the mixture was then added to the dry materials and the mixing continued for another four minutes. The fresh concrete could be handled up to 120 minutes without any sign of setting and without any degradation in the compressive strength. The fresh concrete was cast and compacted by the usual methods used in the case of Portland cement concrete (Hardjito and Rangan, 2005; Wallah and Rangan, 2006; Sumajouw and Rangan, 2006). The compressive strength and workability of geopolymer concrete are also influenced by the wet-mixing time (Hardjito and Rangan, 2005). As the wet-mixing time increased, the compressive strength of hardened geopolymer concrete increased with a slight loss in the workability of the fresh concrete.

11.3.3 Curing

Although low-calcium fly ash-based geopolymer concrete can be cured in ambient conditions, heat-curing is generally recommended. Heat-curing substantially assists the chemical reaction that occurs in the geopolymer paste.

Both curing time and curing temperature influence the compressive strength of geopolymer concrete. The effect of curing time is illustrated in Fig. 11.2 (Hardjito and Rangan, 2005). The test specimens were 100×200



11.2 Effect of curing time on compressive strength of geopolymer concrete (Hardjito and Rangan, 2005).

mm cylinders heat-cured at 60°C in an oven. The curing time varied from 4 hours to 96 hours (4 days). Longer curing time improved the polymerisation process resulting in higher compressive strength. The rate of increase in strength was rapid up to 24 hours of curing time; beyond 24 hours, the gain in strength is only moderate. Therefore, heat-curing time need not be more than 24 hours in practical applications. The effect of curing temperature on the compressive strength is indicated by the test data shown in Fig. 11.1.

Heat-curing can be achieved by either steam-curing or dry-curing. Test data show that the compressive strength of dry-cured geopolymer concrete is approximately 15% larger than that of steam-cured geopolymer concrete (Hardjito and Rangan, 2005).

The required heat-curing regime can be manipulated to fit the needs of practical applications. In laboratory trials, precast products were manufactured using geopolymer concrete; the design specifications required steam curing at 60°C for 24 hours. In order to optimise the usage of moulds, the products were cast and steam cured initially for about 4 hours. The steam curing was then stopped for some time to allow the release of the products from the moulds. The steam curing of the products then continued for another 21 hours. This two-stage steam curing regime did not produce any degradation in the strength of the products (Hardjito and Rangan, 2005).

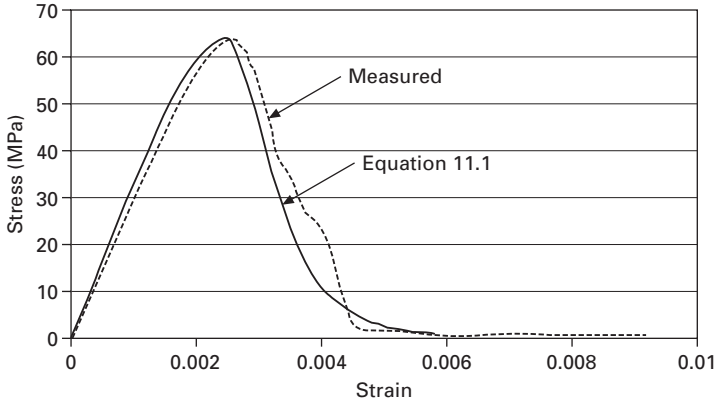
Also, the start of heat curing of geopolymer concrete can be delayed for several days. Tests have shown that a delay in the start of heat curing up to five days did not produce any degradation in the compressive strength. In fact, such a delay in the start of heat-curing substantially increased the compressive strength of geopolymer concrete (Hardjito and Rangan, 2005). This may be due to the geopolymerisation that occurs prior to the start of heat curing.

The above flexibilities in the heat curing regime of geopolymer concrete can be exploited in the production of prototype products in practical applications.

11.4 Short-term properties of geopolymer concrete

11.4.1 Behaviour in compression

The behaviour and failure mode of fly ash-based geopolymer concrete in compression is similar to that of Portland cement concrete. Figure 11.3 shows a typical stress-strain curve of geopolymer concrete. Test data show that the strain at peak stress is in the range of 0.0024 to 0.0026 (Hardjito and Rangan, 2005). Collins *et al.* (1993) have proposed that the stress-strain relation of Portland cement concrete in compression can be predicted using the following expression:



11.3 Stress-strain relation of geopolymer concrete in compression (Hardjito and Rangan, 2005).

$$\sigma_c = f_{cm} \frac{\epsilon_c}{\epsilon_{cm}} \frac{n}{n - 1 + (\epsilon_c/\epsilon_{cm})^{nk}} \quad 11.1$$

where f_{cm} = peak stress, ϵ_{cm} = strain at peak stress, $n = 0.8 + (f_{cm}/17)$, and $k = 0.67 + (f_{cm}/62)$ when $\epsilon_c/\epsilon_{cm} > 1$ or equal to 1.0 when $\epsilon_c/\epsilon_{cm} \leq 1$. Figure 11.3 shows that the measured stress-strain curve of geopolymer concrete correlates well with that calculated using Equation 11.1.

Table 11.2 gives the measured values of modulus of elasticity (E_c) of geopolymer concrete in compression. As expected, the modulus of elasticity increased as the compressive strength of geopolymer concrete increased (Hardjito and Rangan, 2005).

For Portland cement concrete, the draft Australian Standard AS3600 (2005) recommends the following expression to calculate the value of the modulus of elasticity within an error of plus or minus 20%:

$$E_c = \rho^{1.5} \times (0.024 \sqrt{f_{cm}} + 0.12) \quad (\text{MPa}) \quad 11.2$$

where ρ is the unit-weight of concrete in kg/m^3 , and f_{cm} is the mean compressive strength in MPa.

American Concrete Institute (ACI) Committee 363 (1992) has recommended the following expression to calculate the modulus of elasticity:

$$E_c = 3320 \sqrt{f_{cm}} + 6900 \quad (\text{MPa}) \quad 11.3$$

The average unit-weight of fly ash-based geopolymer concrete was 2350 kg/m^3 . Table 11.2 shows the comparison between the measured values of modulus of elasticity of fly ash-based geopolymer concrete with the values calculated using Equation 11.2 and Equation 11.3.

It can be seen from Table 11.2 that the measured values were consistently lower than the values calculated using Equation 11.2 and Equation 11.3. This

Table 11.2 Modulus of elasticity of geopolymer concrete in compression

f_{cm}	E_c (measured) (GPa)	E_c [Eq. 11.2] (GPa)	E_c [Eq.11.3] (GPa)
89	30.8	39.5 ± 7.9	38.2
68	27.3	36.2 ± 7.2	34.3
55	26.1	33.9 ± 6.8	31.5
44	23.0	31.8 ± 6.4	28.9

is due to the type of coarse aggregates used in the manufacture of geopolymer concrete.

The type of the coarse aggregate used in the test programme was of granite-type. Even in the case of specimens made of mixture with $f_{cm} = 44$ MPa, the failure surface of test cylinders cut across the coarse aggregates, thus resulting in a smooth failure surface. This indicates that the coarse aggregates were weaker than the geopolymer matrix and the matrix-aggregate interface (Hardjito and Rangan, 2005).

For Portland cement concrete using granite-type coarse aggregate, Aitcin and Mehta (1990) reported modulus of elasticity values of 31.7 GPa and 33.8 GPa when $f_{cm} = 84.8$ MPa and 88.6 MPa, respectively. These values are similar to those measured for geopolymer concrete given in Table 11.2.

Sofi *et al.* (2007a) used low-calcium fly ash from three different sources to manufacture geopolymer mortar and concrete specimens. The measured values of modulus of elasticity reported in that study showed a trend similar to that observed in the results given in Table 11.2.

Experimental studies have shown that the aggregate-binder interfaces are stronger in geopolymers than in the case of Portland cement (Lee and van Deventer, 2004). This may lead to superior mechanical properties and long-term durability of geopolymer concretes (Provis *et al.* 2007).

The Poisson's ratio of fly ash-based geopolymer concrete with compressive strength in the range of 40 to 90 MPa falls between 0.12 and 0.16. These values are similar to those of Portland cement concrete.

11.4.2 Indirect tensile strength

The tensile strength of fly ash-based geopolymer concrete was measured by performing the cylinder splitting test on 150 × 300 mm concrete cylinders. The test results are given in Table 11.3. These test results show that the tensile splitting strength of geopolymer concrete is only a fraction of the compressive strength, as in the case of Portland cement concrete (Hardjito and Rangan, 2005).

The draft Australian Standards for Concrete Structures AS3600 (2005) recommends the following design expression to determine the characteristic principal tensile strength (f_{ct}) of Portland cement concrete:

Table 11.3 Indirect tensile splitting strength of geopolymer concrete

Mean compressive strength (MPa)	Mean indirect tensile strength (MPa)	Characteristic principal tensile strength, Equation 11.4 (MPa)	Splitting strength, Equation 11.5 (MPa)
89	7.43	3.77	5.98
68	5.52	3.30	5.00
55	5.45	3.00	4.34
44	4.43	2.65	3.74

$$f_{ct} = 0.4 \sqrt{f_{cm}} \quad (\text{MPa}) \quad 11.4$$

Neville (2000) recommended that the relation between the tensile splitting strength and the compressive strength of Portland cement concrete may be expressed as:

$$f_{ct} = 0.3 (f_{cm})^{2/3} \quad (\text{MPa}) \quad 11.5$$

The calculated values of f_{ct} using Equations 11.4 and 11.5, given in Table 11.3, show that the measured indirect tensile strength of fly ash-based geopolymer concrete is larger than the values recommends by the draft Australian Standard AS3600 (2005) and Neville (2000) for Portland cement concrete. This trend of results is similar to that observed in the case of Portland cement concrete.

Sofi *et al.* (2007a) also performed indirect tensile tests on geopolymer mortar and concrete specimens made using three different sources of low-calcium fly ash. The trend test results observed in that study is similar to that observed in the results given in Table 11.3.

11.4.3 Unit-weight

The unit-weight of concrete primarily depends on the unit mass of aggregates used in the mixture. Tests show that the unit-weight of the low-calcium fly ash-based geopolymer concrete is similar to that of Portland cement concrete. When granite-type coarse aggregates were used, the unit-weight varied between 2330 and 2430 kg/m³ (Hardjito and Rangan, 2005).

11.5 Long-term properties of geopolymer concrete

11.5.1 Compressive strength

Numerous batches of Mixture 1 and Mixture 2 (Table 11.1) were manufactured during a period of four years. For each batch of geopolymer concrete made, 100 × 200 mm cylinders specimens were prepared. At least three of these cylinders were tested for compressive strength at an age of seven days after casting. The unit-weight of specimens was also determined at the same

time. For these numerous specimens made from Mixture 1 and Mixture 2 and heat-cured at 60°C for 24 hours after casting, the average results are presented in Table 11.4 (Wallah and Rangan, 2006).

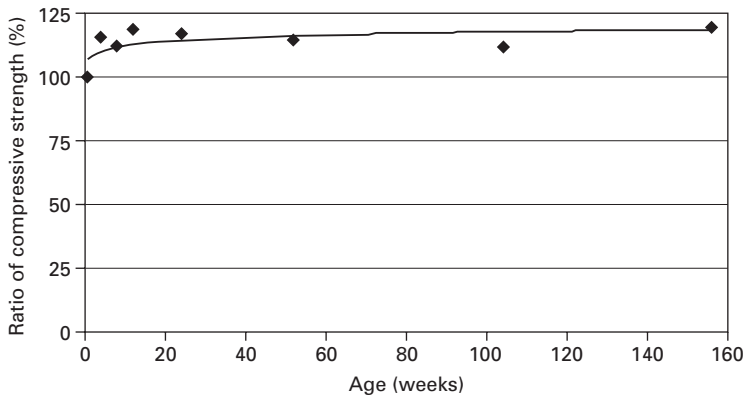
In order to observe the effect of age on compressive strength of heat-cured geopolymer concrete, 100 × 200 mm cylinders were made from several batches of Mixture 1 given in Table 11.1. The specimens were heat-cured in the oven for 24 hours at 60°C, and tested in compression at different age up to three years. These test data, shown in Fig. 11.4, indicate that the compressive strength increased with age in the order of 10 to 20 percent when compared to the 7th day compressive strength (Wallah and Rangan, 2006).

The above test data demonstrate the consistent quality, reproducibility, and long-term stability of low-calcium fly ash-based geopolymer concrete.

In order to study the effect of age on the compressive strength of fly ash-based geopolymer concrete cured in laboratory ambient conditions, three batches of geopolymer concrete were made using Mixture 1 given in Table 11.1. The test specimens were 100 × 200 mm cylinders. The first batch, called

Table 11.4 Mean compressive strength and unit-weight of geopolymer concrete

Mixture	Curing type	7th Day compressive strength (heat-curing at 60°C for 24 hours), MPa		Unit-weight, kg/m ³	
		Mean	Standard deviation	Mean	Standard deviation
Mixture 1	Dry curing (oven)	58	6	2379	17
	Steam curing	56	3	2388	15
Mixture 2	Dry curing (oven)	45	7	2302	52
	Steam curing	36	8	2302	49



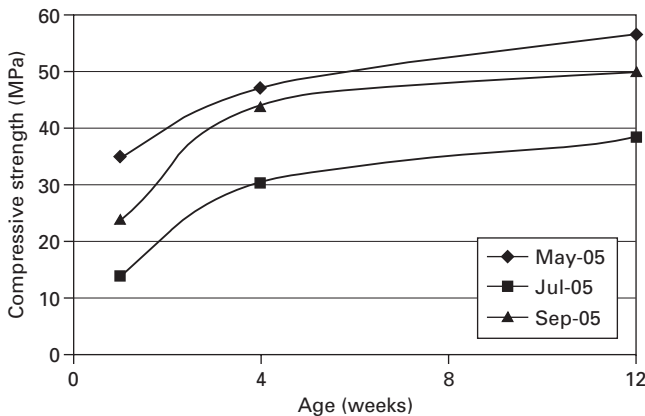
11.4 Change in compressive strength of heat-cured geopolymer concrete with age (Wallah and Rangan, 2006).

May 05, was cast in the month of May 2005, while the second batch (July 05) was cast in the month of July 2005 and the third batch (September 05) in September 2005. The ambient temperature in May 2005 during the first week after casting the concrete ranged from about 18 to 25°C, while this temperature was around 8 to 18°C in July 2005 and 12 to 22°C in September 2005. The average humidity in the laboratory during those months was between 40% and 60%. The test cylinders were removed from the moulds one day after casting and left in laboratory ambient conditions until the day of test.

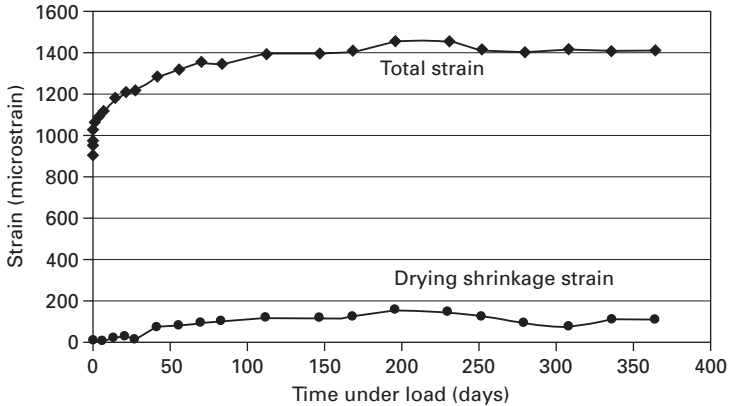
The test results plotted in Fig. 11.5 show that the compressive strength of ambient-cured geopolymer concrete significantly increased with the age (Wallah and Rangan, 2006). This test trend is in contrast to the effect of age on the compressive strength of heat-cured geopolymer concrete mentioned earlier.

11.5.2 Creep and drying shrinkage

The creep and drying shrinkage behaviour of heat-cured low-calcium fly ash-based geopolymer concrete was studied for a period of one year (Wallah and Rangan, 2006). The geopolymer concrete mixture proportions used in that study were Mixture 1 and Mixture 2, as given in Table 11.1. The test specimens were 150 × 300 mm cylinders, heat-cured at 60°C for 24 hours. The creep tests commenced on the 7th day after casting the test specimens and the sustained stress was 40% of the compressive strength on that day. The test results obtained for specimens made using Mixture 1 and heat-cured in an oven are shown in Fig. 11.6 (Wallah and Rangan, 2006). The test trends were similar for both Mixture 1 and Mixture 2, heat-cured either in an oven or steam-cured.



11.5 Compressive strength of geopolymer concrete cured in ambient condition (Wallah and Rangan, 2006).



11.6 Total strain and drying shrinkage strain of heat-cured geopolymer concrete (Wallah and Rangan, 2006).

Test results show that heat-cured fly ash-based geopolymer concrete undergoes very little drying shrinkage in the order of about 100 micro strains after one year. This value is significantly smaller than the range of values usually experienced by Portland cement concrete.

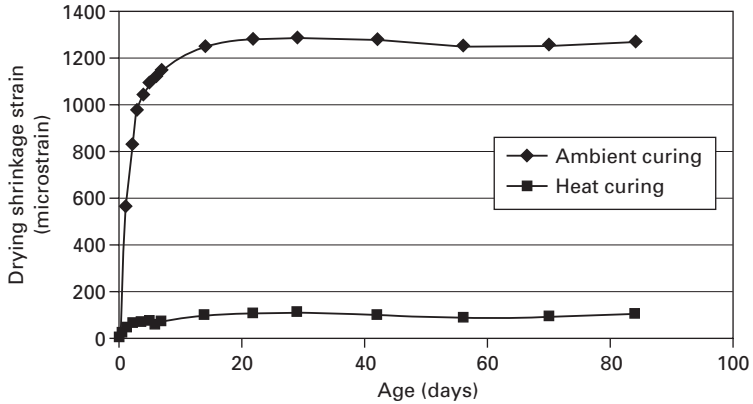
The creep coefficient, defined as the ratio of creep strain-to-elastic strain, after one year of loading for heat-cured geopolymer concrete with compressive strength of 40, 47 and 57 MPa is between 0.6 and 0.7, while for geopolymer concrete with compressive strength of 67 MPa this value is between 0.4 and 0.5. These values are about 50% of the values recommended by the draft Australian Standard AS3600 (2005) for Portland cement concrete.

The low drying shrinkage and the low creep of heat-cured geopolymer concrete offer benefits to the long-term performance of concrete structures.

The drying shrinkage strains of geopolymer concrete cured in ambient conditions are many folds larger than those experienced by the heat-cured specimens (Fig. 11.6). As mentioned earlier, water is released during the chemical reaction process of geopolymers. In the specimens cured in ambient conditions, this water may evaporate over a period of time causing significantly large drying shrinkage strains especially in first two weeks as can be seen in Fig. 11.7 (Wallah and Rangan, 2006).

11.5.3 Sulfate resistance

Tests were performed to study the sulfate resistance of heat-cured low-calcium fly ash-based geopolymer concrete. The test specimens were made using Mixture 1 (Table 11.1) and heat-cured at 60°C for 24 hours after casting; they were immersed in 5% sodium sulfate solution for various periods of



11.7 Drying shrinkage strain of heat-cured and ambient-cured geopolymer concrete (Wallah and Rangan, 2006).

exposure up to one year. The sulfate resistance was evaluated based on the change in mass, change in length, and change in compressive strength of the specimens after sulfate exposure. The test specimens were 100×200 mm cylinders for change in mass and change in compressive strength tests and $75 \times 75 \times 285$ mm prisms for change in length test (Wallah and Rangan, 2006).

Test results showed that heat-cured low-calcium fly ash-based geopolymer concrete has an excellent resistance to sulfate attack. The visual appearances of test specimens after soaking in sodium sulfate solution up to one year revealed that there was no change in the appearance of the specimens compared to the condition before they were exposed. There was no sign of surface erosion, cracking or spalling on the specimens. The specimens soaked in tap water also showed no change in the visual appearance.

Test results also showed that there were no significant changes in the mass and the compressive strength of test specimens after various periods of exposure up to one year. The change in length was extremely small and less than 0.015% (Wallah and Rangan, 2006).

The deterioration of Portland cement concrete due to sulfate attack is attributed to the formation of expansive gypsum and ettringite which causes expansion, cracking, and spalling in the concrete. Low-calcium fly ash-based geopolymer concrete undergoes a different mechanism to that of Portland cement concrete and the geopolymerisation products are also different from hydration products. The main product of geopolymerisation is not susceptible to sulfate attack like the hydration products. Because there is generally no gypsum or ettringite formation in the main products of geopolymerisation, there is no mechanism of sulfate attack in heat-cured low-calcium fly ash-based geopolymer concrete. However, presence of high calcium either in

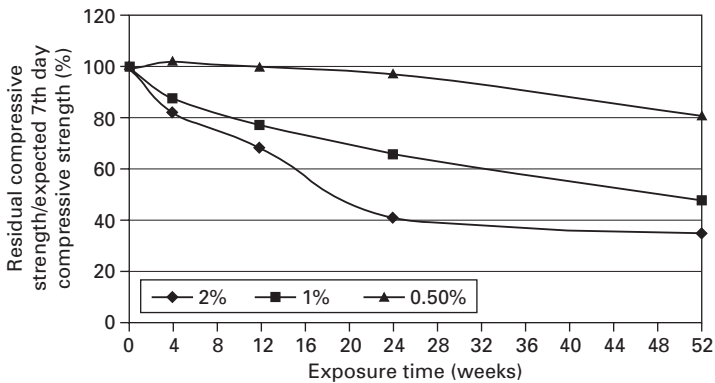
the fly ash or in the aggregates could cause the formation of gypsum and ettringite in geopolymer concrete.

11.5.4 Sulfuric acid resistance

Tests were performed to study the sulfuric acid resistance of heat-cured low-calcium fly ash-based geopolymer concrete. The concentration of sulfuric acid solution was 2%, 1% and 0.5%. The sulfuric acid resistance of geopolymer concrete was evaluated based on the mass loss and the residual compressive strength of the test specimens after acid exposure up to one year. The test specimens, 100 × 200 mm cylinders, were made using Mixture 1 (Table 11.1) and heat-cured at 60°C for 24 hours after casting (Wallah and Rangan, 2006).

The visual appearances of the geopolymer concrete specimens after soaking in various concentrations of sulfuric acid solution for a period of one year showed the erosion of the specimen surface. The damage to the surface of the specimens increased as the concentration of the acid solution increased.

The maximum mass loss of test specimens of about 3% after one year of exposure is relatively small compared to that for Portland cement concrete as reported in other studies (Gourley and Jonson, 2005). As shown in Fig. 11.8, exposure to sulfuric acid caused degradation in the compressive strength; the extent of degradation depended on the concentration of the acid solution and the period of exposure (Wallah and Rangan, 2006). The visual inspection of the broken pieces of concrete cylinders after the compression test revealed that the acid damage of the specimens, soaked in 2% sulfuric acid solution for one year, seems to have occurred in the outer 20 mm shell of the 100 mm diameter test cylinders.



11.8 Acid resistance of heat-cured geopolymer concrete (Wallah and Rangan, 2006).

11.6 Conclusions

The chapter presented information on the engineering properties of heat-cured fly ash-based geopolymer concrete. Low-calcium fly ash (ASTM Class F) is used as the source material, instead of the Portland cement, to make concrete.

Low-calcium fly ash-based geopolymer concrete has excellent compressive strength and is suitable for many applications. The salient factors that influence the properties of the fresh concrete and the hardened concrete have been identified.

The elastic properties of hardened geopolymer concrete are similar to those observed in the case of Portland cement concrete. Heat-cured low-calcium fly ash-based geopolymer concrete also shows excellent resistance to sulfate attack, good acid resistance, undergoes low creep, and suffers very little drying shrinkage.

Several studies have been carried out on reinforced geopolymer concrete members (Sumajouw and Rangan, 2006, Fernandez-Jimenez *et al.*, 2006a, Sofi *et al.*, 2007b, Gourley and Johnson, 2005). These studies demonstrate that the design provisions contained in Codes (ACI Committee 318, 2002) and Standards (Committee BD-002 Standards Australia 2005) currently available for reinforced Portland cement concrete are applicable for reinforced geopolymer concrete members. Therefore, geopolymer concrete has considerable potential to be used as a construction material in many applications.

11.7 References

- ACI Committee 363 (1992), State-of-the-Art Report on High-Strength Concrete, ACI 363R-92, Farmington Hills, MI.
- ACI Committee 318 (2002), *Building Code Requirements for Structural Concrete*, American Concrete Institute, Farmington Hills, MI.
- Aitcin, P C and P K Mehta (1990), 'Effect of coarse-aggregate characteristics on mechanical properties of high-strength concrete' *ACI Materials Journal* 87(2), 103-107.
- Collins, M P, Mitchell D and MacGregor J G (1993), 'Structural design considerations for high strength concrete' *ACI Concrete International* 15(5), 27-34.
- Committee BD-002 Standards Australia (2005), *Concrete Structures: Draft Australian Standard AS3600-200x*, Standards Australia.
- Davidovits J (1994), 'High-Alkali Cements for 21st Century Concretes'. In *Concrete Technology, Past, Present and Future*, in Metha P K (ed.), *Proceedings of V. Mohan Malhotra Symposium*, ACI SP-144, American Concrete Institute, Detroit, 383-397.
- Duxson P, Provis J L, Lukey G C and van Deventer J S J (2007), 'The role of inorganic polymer technology in the development of Green concrete', *Cement and Concrete Research*, 37(12), 1590-1597.
- Fernández-Jiménez A M, Palomo A, and López-Hombrados C (2006a), 'Engineering properties of alkali-activated fly ash concrete' *ACI Materials Journal*, 103(2), 106-112.

- Fernández-Jiménez A M, de la Torre A G, Palomo A, López-Olmo G, Alonso M M, and Aranda M A G (2006b), 'Quantitative determination of phases in the alkali activation of fly ash. Part I. Potential ash reactivity', *Fuel*, 85(5–6), 625–634.
- Gartner E (2004), 'Industrially interesting approaches to 'low-CO₂' cements' *Cement and Concrete Research*, 34(9), 1489–1498.
- Gourley J T (2003), 'Geopolymers; Opportunities for Environmentally Friendly Construction Materials' in *Materials 2003 Conference: Adaptive Materials for a Modern Society*, Sydney.
- Gourley J T and Johnson G B (2005), 'Developments in Geopolymer Precast Concrete' in *Proceedings of the International Workshop on Geopolymers and Geopolymer Concrete*, Perth.
- Hardjito D and Rangan B V (2005), *Development and Properties of Low-Calcium Fly Ash-based Geopolymer Concrete*, Research Report GC1, Faculty of Engineering, Curtin University of Technology, Perth, available at espace@curtin.
- Lee W K W and van Deventer J S J (2004), 'The interface between natural siliceous aggregates and geopolymers' *Cement and Concrete Research*, 34(2) 195–206.
- Neville A M (2000), *Properties of Concrete*, Prentice Hall.
- Provis J L, Muntingh Y, Lloyd R R, Xu H, Keyte L M, Lorenzen L, Krivenko P V, and J.S.J. van Deventer J S J (2007), 'Will geopolymers stand the test of time?', *Ceramic Engineering and Science Proceedings*, 28(9), 235–248.
- Sofi M, van Deventer J S J, Mendis P A and Lukey G C (2007a), 'Engineering properties of inorganic polymer concretes (IPCs)' *Cement and Concrete Research*, 37(2), 251–257.
- Sofi M, van Deventer J S J, Mendis P A and Lukey G C (2007b), 'Bond performance of reinforcing bars in inorganic polymer concrete (IPC)', *Journal of Materials Science*, 42(9), 3007–3016.
- Sumajouw M D J and Rangan B V (2006), *Low-Calcium Fly Ash-Based Geopolymer Concrete: Reinforced Beams and Columns*, Research Report GC3, Faculty of Engineering, Curtin University of Technology, Perth, available at espace@curtin.
- van Jaarsveld, J G S, van Deventer J S J and Lorenzen L (1997), 'The potential use of geopolymeric materials to immobilise toxic metals: Part I. Theory and applications', *Minerals Engineering*, 10(7), 659–669.
- Wallah S E and Rangan, B V. (2006), *Low-Calcium Fly Ash-Based Geopolymer Concrete: Long-Term Properties*, Research Report GC2, Faculty of Engineering, Curtin University of Technology, Perth, available at espace@curtin.

Producing fire- and heat-resistant geopolymers

G KOVALCHUK and P V KRIVENKO,
Kyiv National University for Civil Engineering
and Architecture, Ukraine

Abstract: Alkaline activated aluminosilicate cements are suggested to be a prospective solution for making concretes and building composite materials resistant to elevated temperatures. When the structure formation is appropriately directed, thermally resistant zeolite-like products (hydroxysodalite, analcime, chabazite, faujasite-type) dominate in the microstructure, and these products re-crystallize to crystallochemically similar anhydrous aluminosilicates (feldspathoids and feldspars) during heating, remaining a stable and durable matrix. These materials might be used for making both fire-resistant and heat-resistant concretes and composites.

Key words: alkali activated materials, heat resistance, fire resistance, structure formation, alkaline aluminosilicate minerals.

12.1 Introduction

The problem of making cement and concretes more and more resistant to high temperatures has become a vital need nowadays. Generally speaking, there are two important areas for these materials to be applied in, namely: (1) making concrete constructions with improved fire resistance and (2) making non-fired concretes for masonries for high-temperature equipment instead of ceramic refractory materials.

Experience of catastrophic fires in important or potentially dangerous buildings all around the world has shown a vital need to search for new fire-resistant materials to be applied in highly responsible construction of tunnels, underground structures, skyscrapers, strategic objects, etc. These constructions should warrant stability of functional properties in case of extensive fire. However, traditional OPC-based structures lose mechanical strength at high temperature, resulting in damage. This can restrict evacuation and rescue operations.

From the other side, there is a constantly increasing interest for concrete application in masonries. Compared to traditional refractory materials, heat-resistant concrete does not require firing. It makes for 1.5–2 times lower fuel consumption and 30–50% lower cost per unit of masonry material, improved productivity and increased durability (Inamura, 1984).

Traditional Portland cement-based concrete is not structurally stable when exposed to high temperatures, even when other factors affecting concrete's behaviour at high temperatures are chosen appropriately (i.e., size, load, humidity, reinforcement, type of aggregate, etc.). The main reason for OPC-based materials to fail after firing is instability of microstructural elements during heating caused by dehydration and destruction of CSH-gel and other crystalline hydrates. Crystallochemically speaking, microstructure phases after firing have nothing to do with initial hydrated products. The most dangerous phase in this respect is calcium hydroxide: during firing it converts to calcium oxide, and the latter re-hydrates after subsequent cooling with the atmosphere's humidity; resulting in serious volume expansion and almost complete destruction of a matrix. That is why residual strength of OPC-based concrete after firing at 800–1000°C does not exceed 20–30% normally (Nekrasov, 1972; Diederichs *et al.* 1989).

The traditional approach to improve thermal properties of OPC is to use additives capable of binding calcium hydroxide, i.e. to use pozzolanic additives. However, this technology does not completely eliminate the problem; it just extends the temperature of application up to 700–800°C, but these systems have lower initial mechanical strength and continue losing mechanical strength after firing, too. Other cements used for application at high temperatures (Nekrasov, 1988) are expensive and have additional disadvantages: strength variations for aluminat cements, high viscosity and no water resistance for waterglass, short setting time and environmental impact for phosphate binders.

Pushkarova (1994) demonstrated an opportunity to create heat-resistant slag alkaline cements in system $\text{Na}_2\text{O}-\text{CaO}-\text{Al}_2\text{O}_3-\text{SiO}_2-\text{H}_2\text{O}$ and $\text{Na}_2\text{O}-\text{CaO}-\text{MgO}-\text{Al}_2\text{O}_3-\text{SiO}_2-\text{H}_2\text{O}$. It was found that thermal properties of alkali/alkali-earth activated slag cements improved for the reasons listed below:

- hydraulic products should be able to re-crystallize topotactically into anhydrous ones
- anhydrous products produced during firing should accrete epitaxially as a result of their crystallochemical similarity
- eutectic fusion liquid should be present in quantity of 5–10%, providing for the process of self-reinforcement of a matrix
- the matrix should be well fragmented; there should be an optimal ratio between glassy and crystalline phases of a conglomerate.

These principles allow heat-resistant slag alkaline cements with application temperatures up to 1000–1600°C (depending upon slag composition and ratio between main oxides). Depending upon the composition of the initial system, products of dehydration after firing were represented mainly by garnets ($\text{C}_3\text{AS}_3-\text{C}_3\text{FS}_3$), calcium silicates (α - and β -CS), nepheline (NAS_2), magnesium silicates (CMS_2 and MS). Alkaline Portland cement, a mix of

OPC clinker, aluminosilicate modifier (fly ash or metakaolin) and alkaline activator, was also found to be a prospective system for heat-resistant concrete (Krivenko *et al.*, 2005, 2007).

However, all the above-mentioned studies dealt with Class II alkaline cements (Krivenko, 1995, 1997), that is to say, only binary sodium+calcium activation was applied. In these systems, alkaline aluminosilicate structures represented by N-A-S-H gel ('zeolite precursor') play a secondary role in structure formation at both normal and high-temperature conditions. In contrast to that, in geocements/geopolymers the above-mentioned compounds are the only phases responsible for genesis of mechanical strength, both after low-temperature and high-temperature curing. It means that the structure formation process in these systems proceeds in a completely different way, tailoring different properties and, subsequently, different fields of application.

12.2 Phase composition of alkaline aluminosilicate cements after curing at normal and elevated temperature

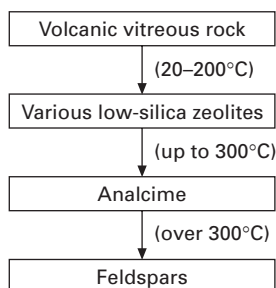
12.2.1 Transformation of alkaline aluminosilicate minerals in geological process

Alkalis are known to be excellent fluxes; that's why their content in refractory materials is strongly restricted. However, nature has shown us a good example of how alkaline compounds can form heat-resistant minerals such as nepheline (NAS_2), with a melting point of 1257°C or albite (NAS_6), with a melting point of 1118°C (Schairer and Bowen, 1956). The ultimate condition for alkalis to form a durable heat-resistant mineral is to be covalently-bonded in a three-dimensional aluminosilicate network.

Nature is known to be the best judge of durability, and nothing is more durable than natural minerals. This should be taken into account when durability becomes a cornerstone in developing new cements. However, a phase composition of the ordinary Portland cement (OPC) is represented by the compounds not having analogies to natural minerals. It results in some problems connected with durability of OPC concretes which are currently discussed. At the same time, the excellent durability of ancient cements is believed to be explained by peculiarities of their chemical composition (that is, by the increased content of alkalis) which led to formation of the analogies to natural zeolites in the reaction products of such cements (Malinowski, 1979, Davidovits, 1987, Krivenko, 1999). Glukhovskiy (1959, 1967, 1989) was the first who assumed that since the geological process of transformations of some volcanic rocks into zeolites takes place during formation of the sedimentary rocks at low temperatures and pressure, it might be modelled and carried out in the cementitious systems.

The alkalis play an important role in mutual transformations and circulation of minerals in the earth's crust. It should be also mentioned that the alkaline aluminosilicates (first of all, feldspars), are known to be stable and durable compared to the calcium ones (Glukhovskiy, 1967). Predominance of one or other mineral may be taken as an indication of the mineral's durability. The zeolites, natural alkaline or alkali-earth hydrated aluminosilicates with a porous structure of framework, are supposed to be one of the most important groups of the sedimentary minerals. Usually, they are formed as a result of transformation of the aluminosilicate volcanic rocks in the presence of alkaline solutions at low temperatures (below 200–300°C, depending on zeolite type). The increase in temperature to 400°C promotes their re-crystallization into more stable high-silica structures (first of all, analcime) and then into secondary feldspars which are the dominant minerals of the Earth's crust. In particular, transformation of a primary volcanic glass in the salt lakes or open hydrological formations might be represented as it is shown in Fig. 12.1 (Breck, 1974, Barrer, 1982, Dyer, 1988).

The type of aluminosilicate phase formed depends on cation type, too (Table 12.1). Note: the family of zeolites is extremely varied; however, there are only certain corresponding anhydrous phases (feldspathoids and feldspars). Additionally, there is a persistent continuous line of mixed sodium/



12.1 Transformations of natural alkaline aluminosilicates in a geological process.

Table 12.1 Transformation of alkaline aluminosilicate minerals depending on a cation type

Mineralogical group	Cation type		
	Sodium (Na)	Calcium (Ca)	Potassium (K)
Zeolites (example)	analcime NAS ₄ H ₂	chabazite CAS ₄ H _{7.5}	phillipsite KAS _{4.4} H ₄
Feldspathoids	nepheline NAS ₂		leucite KAS ₄
Feldspars	Plagioclases: albite (NAS ₆) → anorthite (CAS ₂)		orthoclase KAS ₆

calcium feldspars called plagioclases ($\text{Na}_2\text{O}-\text{CaO}-\text{Al}_2\text{O}_3-\text{SiO}_2$, from albite to anorthite, which give almost equal XRD reflection and thus may not be analyzed using XRD method), depending on Na/Ca ratio. However, potassium feldspar orthoclase ($\text{K}_2\text{O}-\text{Al}_2\text{O}_3-6\text{SiO}_2$) in nature do not normally mix with either sodium or potassium analogues (the only exception, a mixed sodium/potassium feldspar anorthoclase, is a rarer mineral compared to orthoclase or plagioclases).

It is clearly seen that all these transformations take place at relatively low temperatures, which may be modelled in the process of hardening of the cementitious systems. Since the geological processes require a lot of time in real natural conditions, these processes should be accelerated in the construction industry by applying high-intensive technologies such as easily reactive starting materials, high initial alkalinity, high curing temperatures, etc. A directed synthesis of the alkaline aluminosilicate minerals in the phase composition of such cementitious systems may ensure excellent durability of an artificial stone formed side by side with a set of useful new properties since the structures and properties of the zeolites vary within a wide range.

12.2.2 Phase transformation at low temperatures: a key for future heat resistance

Three-dimensional-polymeric hydrated alkaline aluminosilicates in crystalline or semi-crystalline state are the main products of structure formation of geocements at low temperatures (usually below 200°C). Correspondingly, they are called 'zeolites' or 'zeolite precursors'. Thermal stability of these phases depend on their structure: some zeolite structures are known to be resistant to heating, and some of them tend to be destroyed during heating. Among various zeolites able to crystallize in geocement compositions, only certain zeolites maintain their structure until $700-800^\circ\text{C}$. Thermally stable structures are: sodalite network (hydroxysodalite), analcime, chabazite structures (zeolite R, herschelite), faujasite family (zeolites Na-X and Na-Y), mordenite (Breck, 1974). When these phases (or N-A-S-H gels of a similar structure) are synthesized in a geocement stone, they improve their crystallinity during heating until $200-400^\circ\text{C}$, and then maintain their structure up to approx 800°C and then recrystallize to structurally similar nepheline or albite (Skurchinskaya, 1973; Krivenko and Kovalchuk, 2002). Other zeolite structures, for example zeolites Na-A or P, are destroyed at different temperatures in the range of $120-300^\circ\text{C}$, making utilization of such materials at high temperatures impossible.

That is why phase composition after low-temperature curing ('pre-curing') is essential from the point of view of future thermal properties. In fact, directed formation of a heat resistant matrix marks the beginning at the stage

of a low-temperature structure formation by directed formation of certain zeolite products in crystalline or semi-crystalline form.

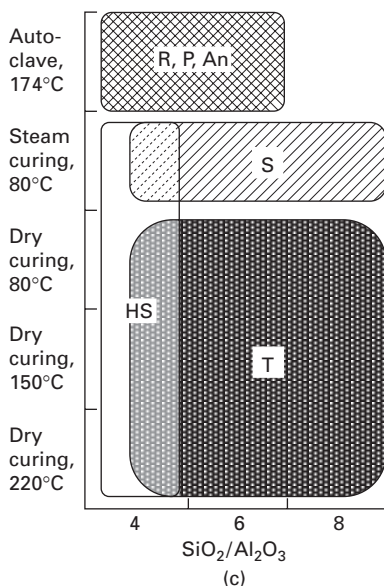
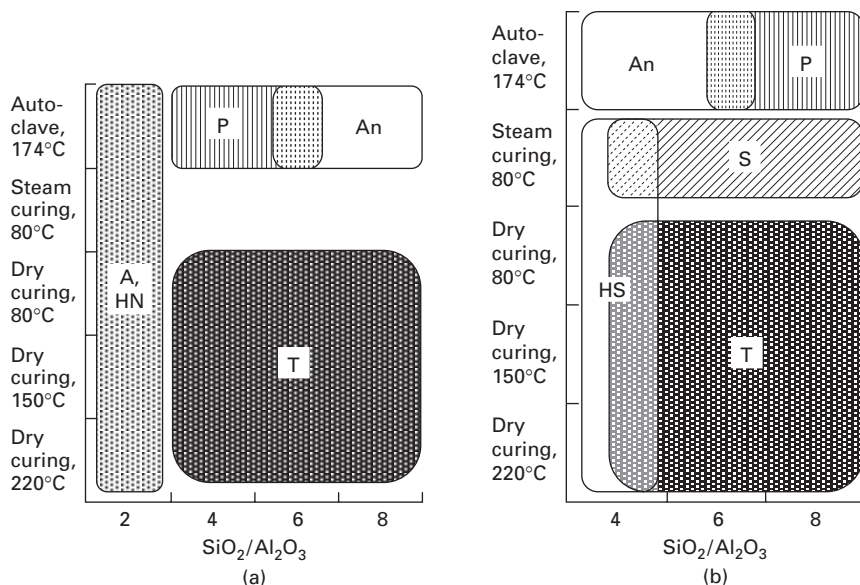
There is a principal similarity of the phase composition of the hydration products of the alkali activated metakaolin and fly ash (Table 12.2, Fig. 12.2). Thus, a phase composition of the autoclave-cured alkali activated fly ash is represented mainly by the analcime, zeolite – and zeolite R (chabazite/herschelite family). Being dependent on high content of the caustic soda due to peculiarities of the mix formulations, a synthesis of hydroxysodalite in steam cured and dry cured fly ash- based compositions with $\text{SiO}_2/\text{Al}_2\text{O}_3 = 4$ correlates well with the results obtained on similar systems with high alkali concentrations and normal pressure of treatment. When using the low-alkali compositions with $\text{SiO}_2/\text{Al}_2\text{O}_3 = 6\text{--}8$ simultaneously with a low-intensity treatment such as steam or dry curing, standard exposition time is not enough for the zeolite crystallization. However, the DTA patterns allowed assuming the formation of a 3d-aluminosilicate gel.

The rate of zeolite formation measured by height of the XRD peaks was much higher in the fly ash-based geocements compared to that in the metakaolin-based ones. Besides, the application of the fly ash 1 (total $\text{SiO}_2+\text{Al}_2\text{O}_3$ content is 73.8%, Table 12.2) made for a synthesis of rather large amounts of plain zeolite-like products, whereas the application of the less pure fly ash 2 (total $\text{SiO}_2+\text{Al}_2\text{O}_3$ content is 67.9%, Table 12.2) resulted in the formation of the more diverse composition of less crystallized zeolites.

After dry curing of both metakaolin- and fly ash-based geocements, irrespectively of a composition, the weak XRD peaks (0.493, 0.323, 0.308, 0.264, 0.245, 0.211, 0.204 nm) were fixed. This minor phase was marked at first as a ‘phase Z’, but recent studies on carbonation finally showed that these peaks could be identified as a mineral trona ($\text{Na}_2\text{CO}_3\cdot\text{NaHCO}_3\cdot 2\text{H}_2\text{O}$, JCPDS # 29-1447, 75-1195, 76-0739, 76-1105, 78-1064). In case of steam curing, another minor sodium carbonate, $\text{Na}_2\text{CO}_3\cdot\text{H}_2\text{O}$ (JCPDS # 08-0037, 70-0845, 70-2148, 76-0910), with main peaks at 0.276, 0.237 nm, was synthesized. The reason for carbonation is an insufficient rate of sodium bound into insoluble zeolite-like products. Recent studies have also shown that these two phases may coexist sometimes, although a synthesis of the trona tended to increase at the higher initial W/S ratio, and a synthesis of the sodium carbonate hydrate took place only in the mixes with low W/S ratio and with the increased alkalinity under hydrothermal conditions (steam curing, curing in an air tight mould). It means that these two phases appeared under a different mechanism. Further investigations on the carbonation are required as these two carbonate phases mentioned above have different chemical properties and, according to the preliminary results, the formation of the sodium carbonate hydrate is undesirable from the point of view of durability.

Table 12.2 Chemical composition of raw materials

Constituent	Chemical composition (% by mass)												Blaine fineness, m ² /kg
	SiO ₂	TiO ₂	Al ₂ O ₃	Fe ₂ O ₃	FeO	MnO	MgO	CaO	R ₂ O	P ₂ O ₅	LOI	In total	
Kaolin clay	48.17	0.62	36.33	0.36	–	–	0.30	0.62	–	–	13.63	100.03	1000
Fly ash 1	50.27	1.20	23.55	9.60	0.70	0.15	1.75	2.30	3.24	0.45	6.05	100.06	360
Fly ash 2	48.20	0.89	19.65	4.50	3.15	0.11	1.36	2.18	3.82	0.02	16.02	99.92	380
Chamotte	60.2	–	35.3	0.8	–	–	0.31	0.29	2.13	–	0.22	99.25	410



12.2 Composition of hydration products vs. the geocement compositions (aluminosilicate component: a – metakaolin, b – fly ash 1, c – fly ash 2) and curing conditions. An – analcime, A – zeolite Na-A, P – zeolite P, R – zeolite R, HN – nepheline hydrate, HS – hydroxysodalite; T – trona, S – sodium carbonate hydrate Taken from (Krivenko and Kovalchuk, 2007).

12.2.3 Phase transformation of alkaline aluminosilicate cements during heating

After firing, the zeolite-like products in geocement structures recrystallize into anhydrous aluminosilicates. Genesis of microstructure may be represented as follows:

- formation of zeolite-type structures (crystalline or semi-crystalline)
- intensification of its synthesis up to approx. 400°C
- amorphization or not (depending on the composition)
- crystallization of stable anhydrous phases (nepheline, albite or cristobalite, depending on mix composition and curing temperature), beginning from 600–800°C.
- melting (sintering) leading to destruction.

The last two stages lead to quasi-ceramic structure synthesized, with excellent service properties, compressive strength above all.

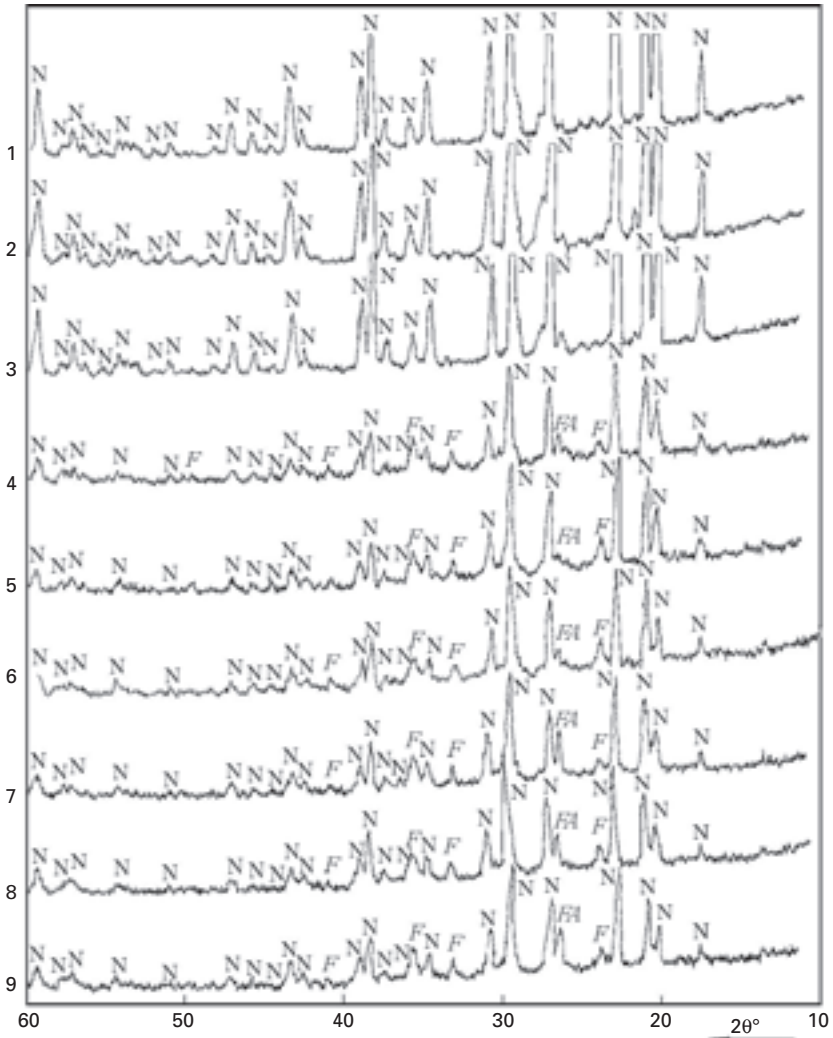
The above-mentioned is a general rule; however, there are some peculiarities of the geocements' phase transformations at high temperatures affected by various factors. Among them, the most important ones are:

- temperature of curing, reactive silica content ($\text{SiO}_2/\text{Al}_2\text{O}_3$ ratio);
- initial alkalinity ($\text{Na}_2\text{O}/\text{Al}_2\text{O}_3$ ratio);
- cation type (Na or K, as well as additives of Ca).

All these factors also influence the thermal properties of the geocement-based materials; however, initial microstructure (the one formed after curing at low temperatures, hereinafter called 'pre-curing') is also an important factor. Thus, type of pre-curing, as well as type of initial aluminosilicate component (kaolin, metakaolin or fly ash), have very little influence on the essence of phase transformations at high temperatures, but it does influence thermal properties.

Role of a pre-curing mode

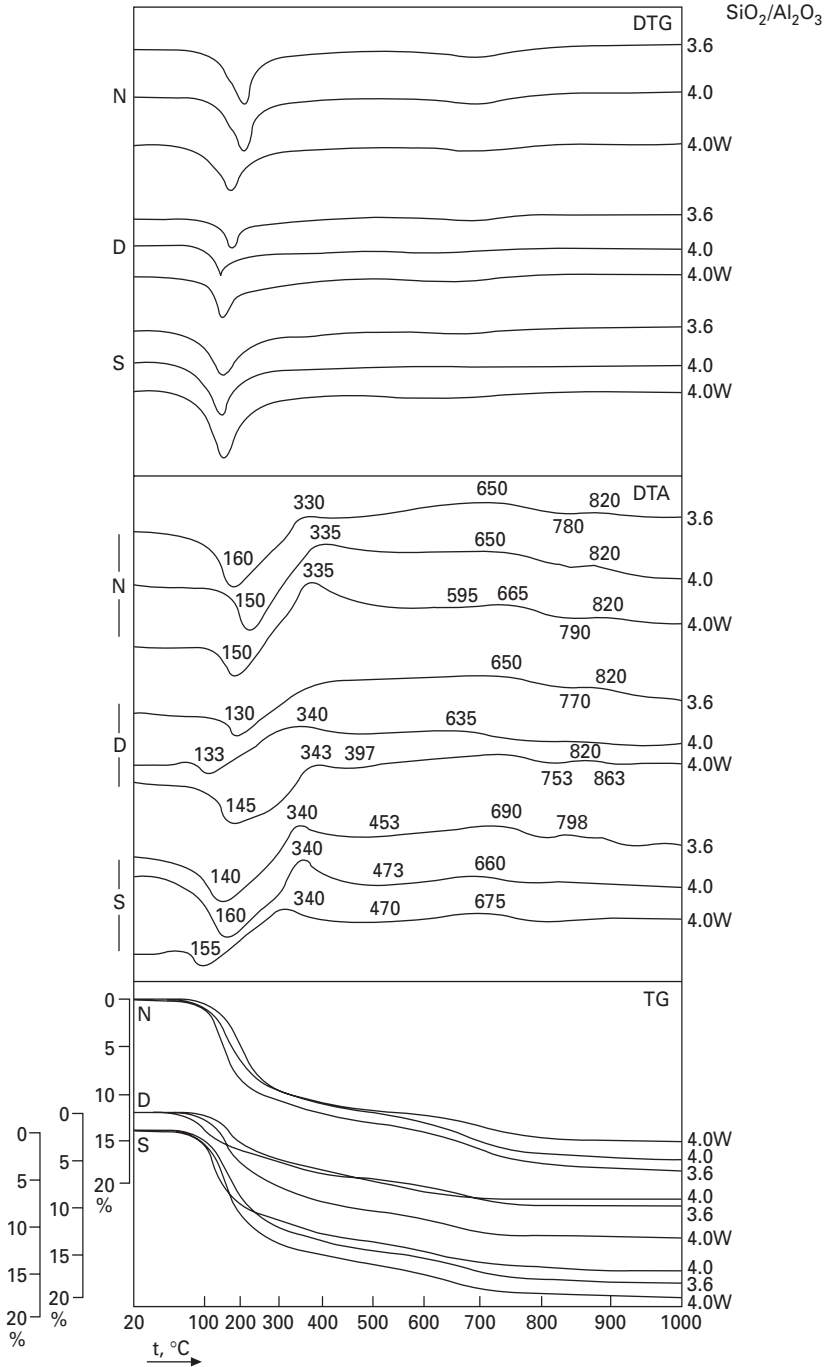
Contrary to the phase composition after hydration, which is dependent above all on a type of low temperature curing, the phase composition after dehydration at 800°C depends only on the geocement composition and does not depend on the type of the preliminary low temperature curing. Thus, a phase composition of the geocements with $\text{SiO}_2/\text{Al}_2\text{O}_3 = 4$, irrespective of the type of preliminary low temperature curing, is represented by a nepheline (Fig. 12.3), and the rest of SiO_2 is probably present as either amorphous silica or zeolite precursor which do not give XRD reflections. The degree of crystallization of the crystalline products formed does not depend on the type of preliminary low temperature curing as well, and with other conditions being



12.3 XRD patterns of geocements with $\text{SiO}_2/\text{Al}_2\text{O}_3 = 4$, after firing at 800°C . Aluminosilicate component: metakaolin (1–3), fly ash 1 (4–6), fly ash 2 (7–9). Pre-curing mode: steam curing (1, 4, 7), dry curing (2, 5, 8), without pre-curing (3, 6, 9).

equal depends on a type of the aluminosilicate component: a maximal value was observed when the metakaolin, the most chemically pure component, was used. The impurities from the fly ash resulted in the reduced content of the anhydrous aluminosilicates formed and in the formation of additional amount of a hematite.

Figure 12.4 presents typical DTA patterns of fly ash-based geocements, divided by $\text{SiO}_2/\text{Al}_2\text{O}_3$ molar ratio, initial water/solid ratio and a curing



12.4 DTA patterns of fly ash-based geocements. Curing mode: N – curing in a sealed mould, D – dry curing, S – steam curing. W – increased water/solid ratio (0.36 vs. 0.18).

mode. The DTA curves are typical for these systems: they reveal thermal effects as listed below:

- Endothermic one: 125–160°C, related to the evaporation of the water adsorbed by N-A-S-H structures and evaporation of hydrates from carbonation products. Shape, intensity and temperature of these effects depend on the composition and pre-curing conditions.
- Exothermic one: approx. 330°C, related to the structural transformations of iron oxide from fly ash composition (transformation hematite → magnetite).
- Weak exothermic effect: 630–690°C, related to the burning coal residuum from fly ash composition.
- Weak exothermic effect: 820°C, related to crystallization of nepheline.

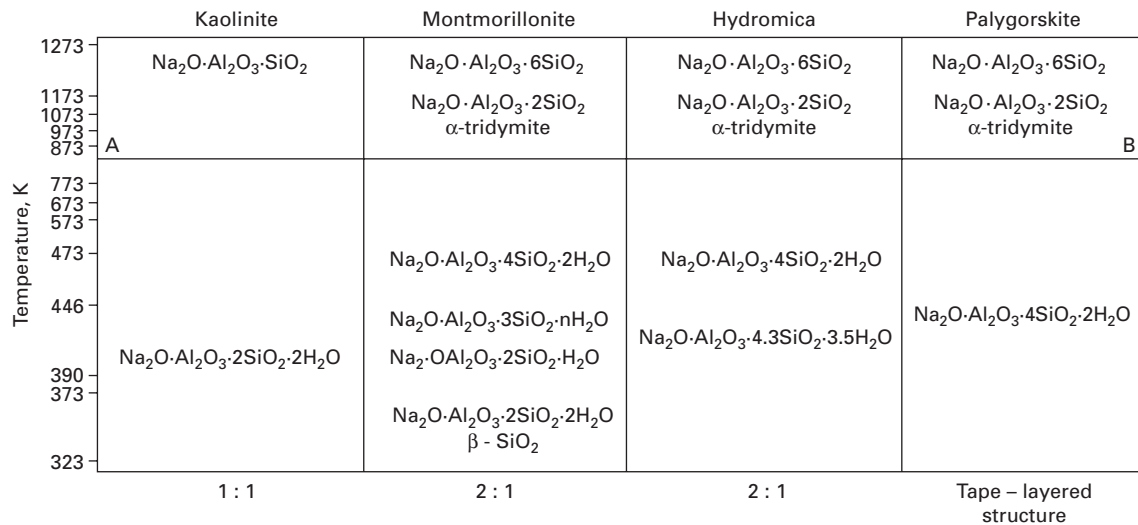
The rest of the effects are very weak and cannot be identified.

There is no principal difference in thermal behaviour of studied systems depending upon pre-curing conditions. The main difference is an amount of bounded water lost within 120–170°C which shows that the amount of hydrated products tends to increase in the order of: dry curing < curing in a sealed mould < steam curing. Thus, pre-curing conditions do not influence a process of thermal transformation of geocement-based systems; however, some differences in bounded water content may be reflected in differences in thermal properties such as residual compressive strength, thermal shrinkage, etc.

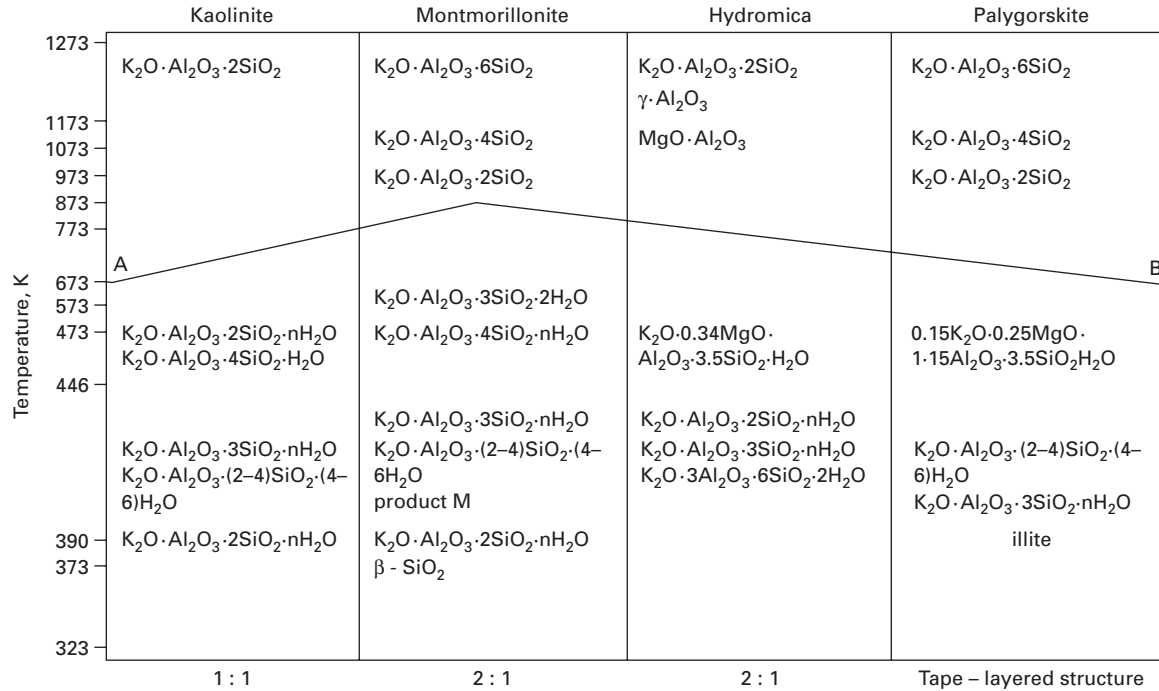
Role of aluminosilicate component type and $\text{SiO}_2/\text{Al}_2\text{O}_3$ ratio

Metakaolin and fly ash are the most useful aluminosilicate components used for making geocements/geopolymers. Clay minerals (kaolin first of all) were also used in earlier studies. Despite some structural peculiarities, there is no significant difference in the structure-forming processes of cementitious materials based on them. All these materials, when alkali activated and properly cured at mild temperatures, represent a microstructure based on three-dimensional alkaline aluminosilicates in amorphous or semi-crystalline state ('zeolite precursors') with some inclusions of crystalline zeolites depending on curing mode. When cured at high temperatures, both metakaolin- and fly ash-based alkali activated materials reveal recrystallization of initial zeolite-like structures into anhydrous alkaline aluminosilicates.

Peculiarities of phase transformations of clay-based alkaline aluminosilicate cements depend on $\text{SiO}_2/\text{Al}_2\text{O}_3$ ratio in initial clay mineral and type of activator (Skurchinskaya, 1973, Krivenko, 1994). Thus, feldspathoid nepheline and feldspar albite appear in clays activated with sodium carbonate after 600°C; feldspathoid leucite and feldspar orthoclase are the main products in clays activated with potassium carbonate after 400–600°C (Fig. 12.5).



12.5 Phase transformations in alkali activated clays during heating depending on clay mineral (in the top) and type of activator: sodium carbonate (a) or potassium carbonate (b).



12.5 Cont'd

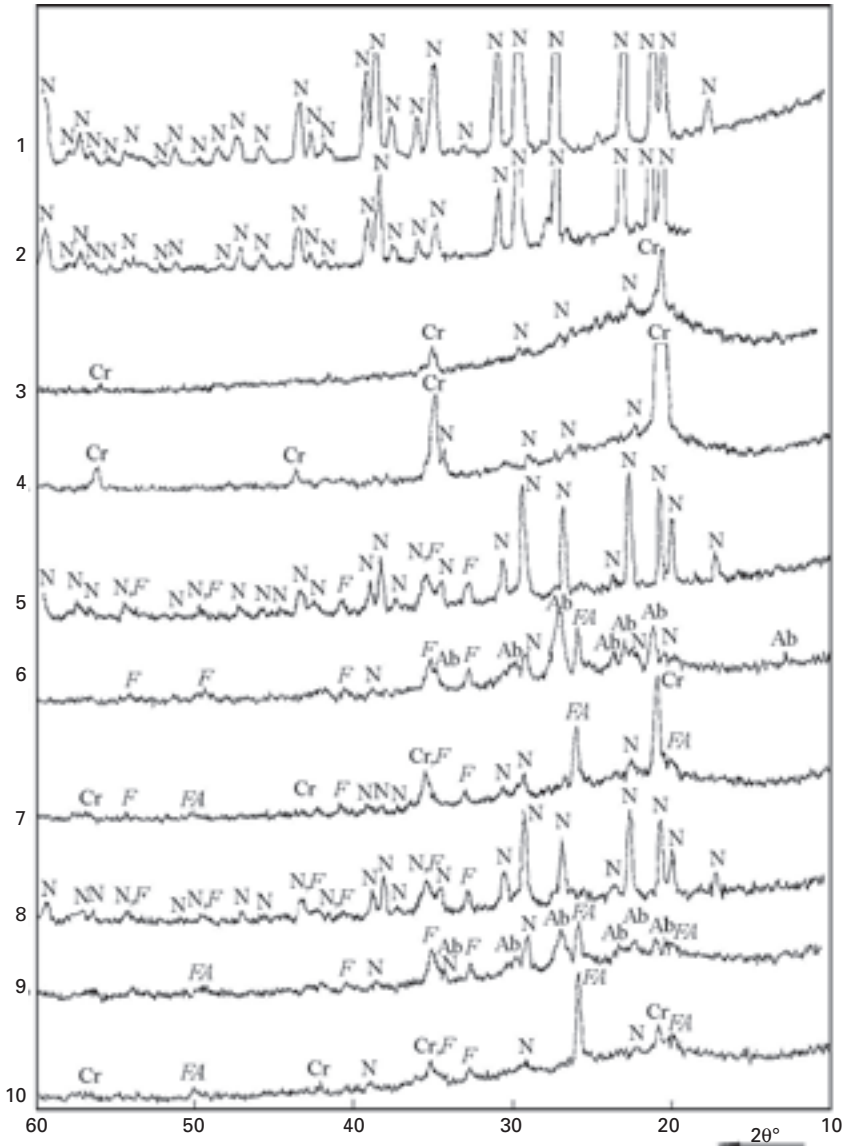
In studying the influence of the mix composition of alkali activated metakaolin and fly ash on phase composition after its dehydration (Krivenko and Kovalchuk, 2007), it was determined that a correlation exists between the $\text{SiO}_2/\text{Al}_2\text{O}_3$ molar ratio in the initial geocements and their dehydration products (Table 12.3, Fig. 12.6). With increase in this ratio from 2 to 8, the dehydration products change in the direction as follows: nepheline ($\text{Na}_2\text{O}\cdot\text{Al}_2\text{O}_3\cdot 2\text{SiO}_2$) – albite ($\text{Na}_2\text{O}\cdot\text{Al}_2\text{O}_3\cdot 6\text{SiO}_2$) – cristobalite (SiO_2). Thus, a phase composition of the geocements with $\text{SiO}_2/\text{Al}_2\text{O}_3 = (2-4)$, irrespective of type of the aluminosilicate component used, is represented by a feldspathoid nepheline ($\text{SiO}_2/\text{Al}_2\text{O}_3 = 2$ in the aluminosilicate framework). It should be mentioned that a quantity of the synthesized nepheline measured by the XRD method was found to reach a maximum degree in case when the stoichiometric nepheline composition was used. The increase in the $\text{SiO}_2/\text{Al}_2\text{O}_3$ ratio up to (6–8) in the metakaolin-based geocements resulted in crystallization of the amorphous silica into the -cristobalite ($d = 0.411; 0.252; 0.206; 0.163$ nm). It coincides with the data of hydrothermal chemistry (Barrer, 1982) on the crystallization of amorphous silica in the alkaline systems through a metastable phase (cristobalite) instead of a stable one (quartz), in accordance with Ostwald's rule of successive transformations. The speed of cristobalite formation tends to increase sharply with an increase in the amorphous silica content; it testifies to insufficient reaction of the amorphous silica introduced in a form of the silica fume in comparison with that introduced in a form of the soluble sodium silicate (water glass).

In contrast to the metakaolin-based geocements, an increase in the $\text{SiO}_2/\text{Al}_2\text{O}_3$ ratio in the fly ash-based composition up to six results in the formation of the high-silica feldspar albite side by side with the smaller amounts of the nepheline (Fig. 12.6). The formation of the albite, in this case, is explained by high content of impurities, which can also be regarded as oxide-mineralizers. Additionally, the albite formation may also depend on the peculiarities of

Table 12.3 Correlation between $\text{SiO}_2/\text{Al}_2\text{O}_3$ molar ratio of initial geocements and their products of dehydration at 800°C (high temperature structure formation). Taken from (Krivenko and Kovalchuk, 2007)

Aluminosilicate component	$\text{SiO}_2/\text{Al}_2\text{O}_3$ molar ratio	
	Initial geocements	Products of dehydration (corresponding phase)
Metakaolin	2	2 (nepheline)
	4	2 (nepheline)
	6	∞ (cristobalite), 2 (nepheline)
	8	∞ (cristobalite), 2 (nepheline)
Fly ash	4	2 (nepheline)
	6	6 (albite) , 2 (nepheline)
	8	∞ (cristobalite), 2 (nepheline)

*Dominating phases are given in bold



12.6 XRD patterns of geocements (Tables 12.2, 12.3) with after firing at 800°C. Aluminosilicate component: metakaolin (1–3), fly ash 1 (4–6), fly ash 2 (7–9). N – nepheline, Ab – albite, Cr – cristobalite, F – hematite, FA – residuums of crystalline impurities of fly ash.

kinetic of alkaline dissolution of silica and alumina from the initial metakaolin and fly ash. With an increase in the SiO₂/Al₂O₃ ratio up to 8, the composition of the dehydrated products of the fly ash-based geocements tends to become similar to that of the metakaolin-based one, but a quantity of the cristobalite

is smaller than that in the metakaolin-based compositions. This may depend on some quantities of the silica contained in the fly ash-based compositions in a form of non-active compounds such as quartz and mullite, which decrease the real $\text{SiO}_2/\text{Al}_2\text{O}_3$ ratio in the fly ash-based systems.

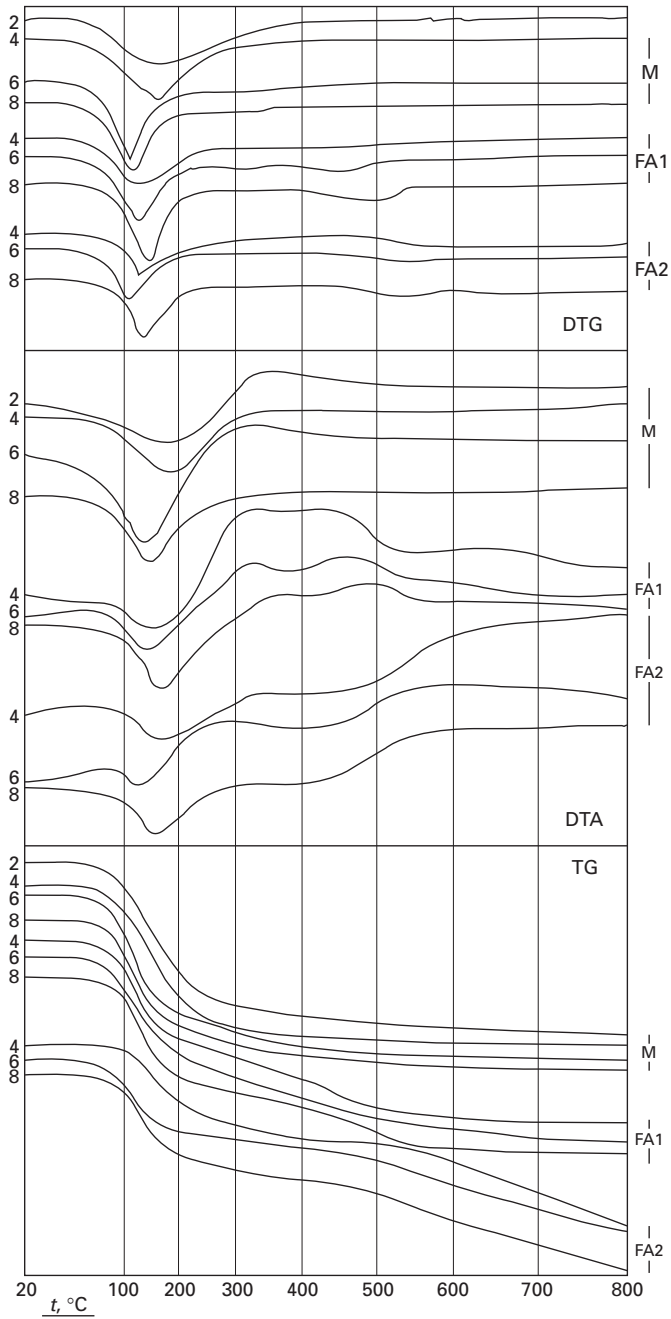
As mentioned above, the type of aluminosilicate component used (metakaolin or fly ash) does not affect the differences in general. It can be seen from Fig. 12.7 (Kovalchuk, 2002), that the shape of DTA curves is approximately equal for above-mentioned alkali activated metakaolin and fly ash cements at equal $\text{SiO}_2/\text{Al}_2\text{O}_3$ ratio (compare mixes M4, B4 and T4, with $\text{SiO}_2/\text{Al}_2\text{O}_3 = 4$). However, it differs notably when this ratio is different because DTA curve reflect differences in hydrated products synthesized.

Once heated to high temperatures (600–1000°C), all the geocements tend to have the high-thermal microstructure based on stable new formations. In contrast to OPC-based materials, there is no unstable phase fixed. However, metakaolin, a more pure aluminosilicate component, makes for higher purity and higher content of high-temperature phases formed (compare, for example, intensity of a nepheline peak for metakaolin- and fly ash-based geocements, # 2, 5 and 8 on Fig. 12.6). At the same time, fly ash makes for synthesis of lower quantity of products, which have, however, more variable composition (for example, albite, a more high-temperature phase in comparison with nepheline, appears at 800°C only in fly ash-based systems). It may be caused both by differences in solubility of silica and alumina from metekaolin and fly ash, on the one hand, and by higher content of additional oxides in fly ash composition (these oxides, such as Fe_2O_3 , may influence reactions which take place at high temperatures).

Duxson *et al.* (2007a,b) found that, irrespective of the cation type (Na, K or mixed Na/K), the higher $\text{SiO}_2/\text{Al}_2\text{O}_3$ ratio, the higher onset temperature of crystallization of anhydrous phases in metakaolin-based geopolymers, and the lower overall percentage of corresponding crystalline phases observed. Thus, at $\text{SiO}_2/\text{Al}_2\text{O}_3 = 2.3$ the percentage of crystalline phases (nepheline or kaliophilite) reached (65–90)% at 1000°C and the crystallization began from 600°C. However, at $\text{SiO}_2/\text{Al}_2\text{O}_3 = 4.3$ the crystalline anhydrous aluminosilicates represented only (30–40)%, and their crystallization was observed to start at 800°C.

Role of initial alkalinity ($\text{Na}_2\text{O}/\text{Al}_2\text{O}_3$ ratio)

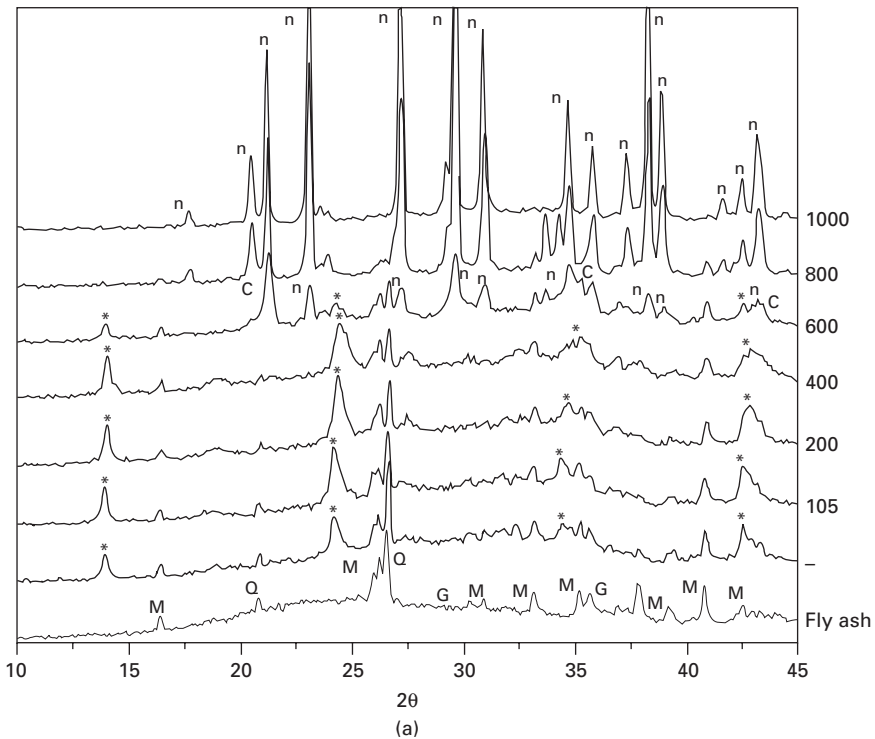
It is a well-known fact that the alkalis are very good flushing agents, that's why their content in refractory materials is extremely limited. However, in alkaline cements, the alkalis play a very important role at all the stages of structure formation. In particular, the content of alkalis determines velocity and rate of activation of initial substance, for example fly ash (Glukhovskiy *et al.*, 1969; Krivenko, 1994; Palomo and Fernández-Jiménez, 2003; Kovalchuk



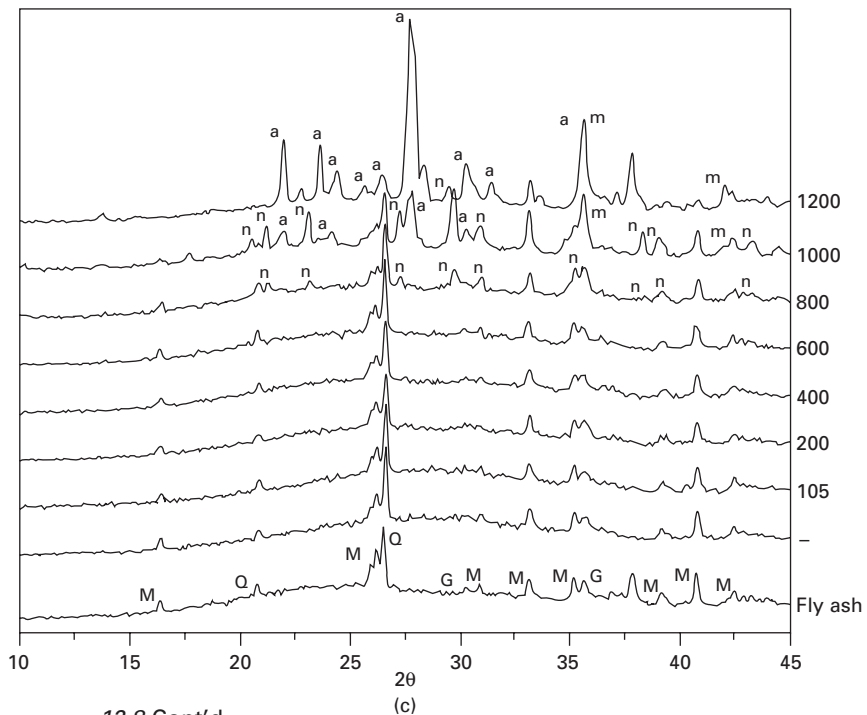
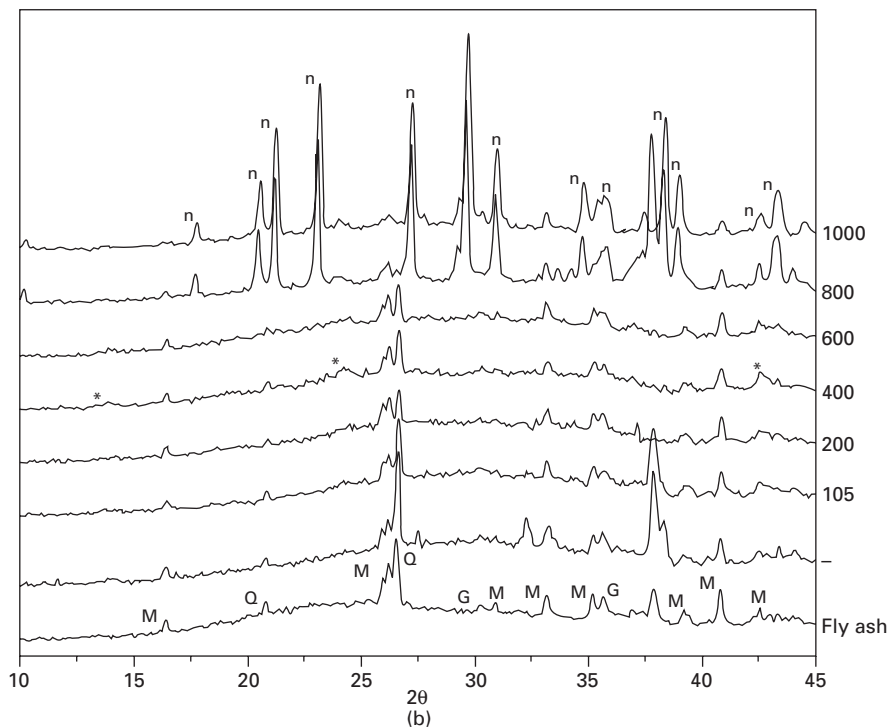
12.7 DTA curves of alkali activated metakaolin (M) and two different fly ashes (FA1, FA2), after steam curing. The numbers represent $\text{SiO}_2/\text{Al}_2\text{O}_3$ ratio.

et al., 2007a), thus, limitation of alkali content affects low initial strength (before high temperature curing). From this point of view, an optimal content of alkalis should be found in order to achieve sufficient initial strength together with limited thermal shrinkage after heating to the working temperature.

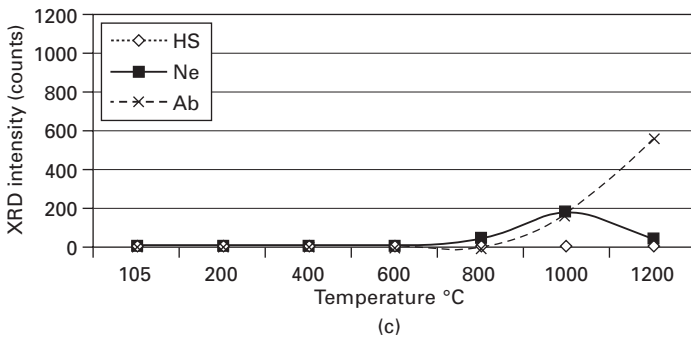
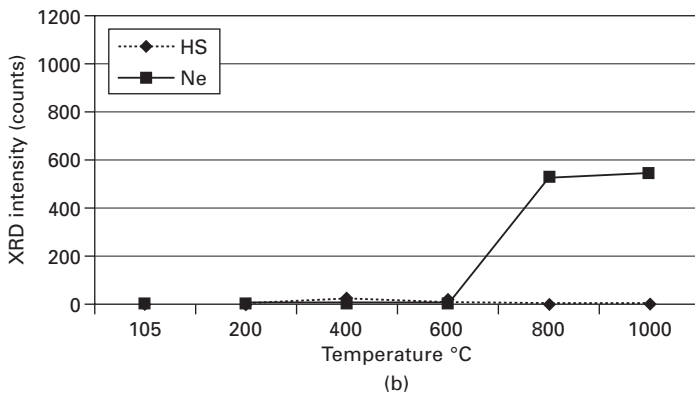
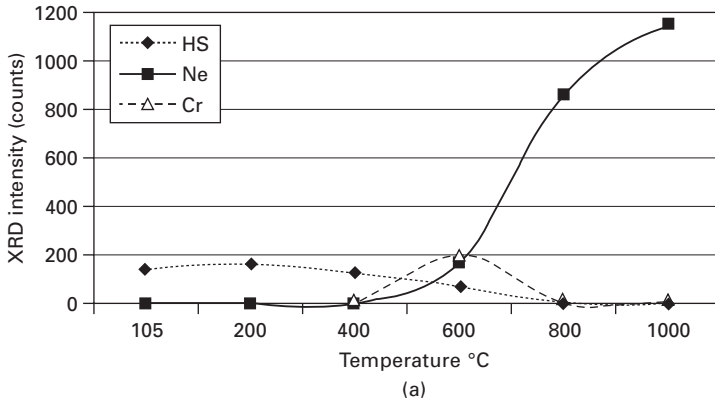
Temperature of crystallization of the anhydrous aluminosilicates depends on the initial composition, and first of all, on the alkali content. In the alkali-rich systems ($\text{Na}_2\text{O}/\text{Al}_2\text{O}_3 = 1.0$, $\text{SiO}_2/\text{Al}_2\text{O}_3 = 3.6$) they appear in limited amounts at 600°C , in the slightly less alkaline mix ($\text{Na}_2\text{O}/\text{Al}_2\text{O}_3 = 1.0$, $\text{SiO}_2/\text{Al}_2\text{O}_3 = 4.0$) they appear at 800°C , whereas in the low-alkaline compositions ($\text{Na}_2\text{O}/\text{Al}_2\text{O}_3 = 0.5$, $\text{SiO}_2/\text{Al}_2\text{O}_3 = 4.0$) the crystallization only begins at 1000°C (Figs 12.8, 12.9) (Krivenko *et al.*, 2006, Kovalchuk *et al.*, 2007b), probably, it is because a lower amount of liquid (sintering) phase appeared at an equal temperature. Correspondingly, the higher amount of anhydrous phases crystallized due to temperature growth, the lower amount of initial hydrated products (in this case, hydroxysodalite) remained.



12.8 XRD patterns of the compositions $\text{Na}_2\text{O}\cdot\text{Al}_2\text{O}_3\cdot 3.6\text{SiO}_2\cdot x\text{H}_2\text{O}$ (a), $\text{Na}_2\text{O}\cdot\text{Al}_2\text{O}_3\cdot 4.0\text{SiO}_2\cdot x\text{H}_2\text{O}$ (b), and $0.5\text{Na}_2\text{O}\cdot\text{Al}_2\text{O}_3\cdot 4.0\text{SiO}_2\cdot x\text{H}_2\text{O}$ (c). Fly ash crystalline impurities: Q – quartz, M – mullite, G – gematite. New formations: * and # - hydroxysodalite or sodalite, n – nepheline, a – albite, m – magnetite. (Krivenko *et al.* 2006).



12.8 Cont'd



12.9 XRD intensities of the phases formed in alkali activated fly ash cements depending on initial composition: $\text{Na}_2\text{O}\cdot\text{Al}_2\text{O}_2\cdot 3.6\text{SiO}_2\cdot x\text{H}_2\text{O}$ (a), $\text{Na}_2\text{O}\cdot\text{Al}_2\text{O}_3\cdot 4.0\text{SiO}_2\cdot x\text{H}_2\text{O}$ (b), and $0.5\text{Na}_2\text{O}\cdot\text{Al}_2\text{O}_3\cdot 4.0\text{SiO}_2\cdot x\text{H}_2\text{O}$ (c). Calculated values from Fig. 12.8.

That is to say, that theoretically, the lower the amount of initial alkalinity, the higher the thermal resistance. However, initial alkalinity should warrant a sufficient mechanical strength of conglomerate before firing, since it is known that initial alkalinity in alkali activated materials regulates a velocity of alkaline activation and, subsequently, it regulates strength growth. That's why a mix design of alkali activated materials for high-temperature application should be a compromise between sufficient initial mechanical strength and target properties after firing.

Role of a cation type and the direction of phase transformations

Sodium-based geocements have become the most applied geocements due to their lowest price from the possible alkaline aluminosilicate binding systems. However, in some special cases potassium-based geocements may give better results. In particular, potassium aluminosilicates are known to be more thermally resistant than sodium ones: for example, the temperature of thermal destruction (fusion) of orthoclase ($K_2O \cdot Al_2O_3 \cdot 6SiO_2$) is higher than that of albite ($Na_2O \cdot Al_2O_3 \cdot 6SiO_2$) – 1170 vs 1118°C. But it is to be underlined that binary systems (for example, sodium/potassium) are significantly less thermally resistant than pure systems: it is a well-known fact that eutectic solutions form in such systems and these mixed systems fuse at significantly lower temperatures (Eitel, 1954). The same situation occurs in other binary systems (Na/Ca or K/Ca) and a ternary system (Na/K/Ca). This is important in view of the wide application of Ca-containing compounds as modifiers of geocements: this technology solves many problems in ordinary geocements (Krivenko *et al.*, 2000) but, once applied for heat-resistant materials, an increased content of Ca may cause low temperature of sintering and high thermal shrinkage. It is to be noted that this rule is only effective at a limited content of calcium oxide (approximately up to 10%), because at higher calcium content the system begins revealing other behaviour and, in fact, is not a pure geocement/geopolymer. At high calcium content, calcium compounds begin playing a separate role and their behaviour becomes similar to that of Class II alkaline cements (Krivenko, 1997), in particular, slag-alkaline cements.

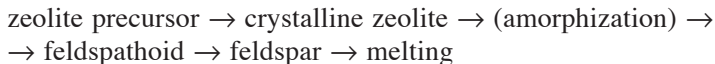
Despite these differences, there was a general regularity founded in all alkali activated cements independently on a type of cation and a type of aluminosilicate component used: the first phases which appear during heating (at approx. 600–900°C) are low-silica feldspathoids (nepheline for sodium-based geocements and leucite for potassium-based ones), whereas high-silica feldspars appear at higher temperatures (900–1200°C). Thus, earlier results from the alkaline activation of various clays (Fig. 12.5) which showed that a phase composition of the alkaline aluminosilicates synthesized might also be regulated by changing a temperature of high-thermal curing. Thus, independent of clay type and type of preliminary low-thermal curing,

a nepheline was found to be a main product of the system ‘clay + sodium alkaline component’ after firing at 750–900°C, and an albite appeared after firing at 900–1000°C. Alkali activated fly ash showed similar behaviour (Table 12.4). When clays were activated by potassium compounds, leucite was the main product after firing (Skurchinskaya, 1994).

Since there are no corresponding feldspathoid-type phases in ternary systems, only a mix of sodium and potassium feldspathoids may appear at (600–800)°C. At higher temperatures, potassium remains in system as a leucite, but sodium and calcium compounds result in synthesis of plagioclases (binary sodium-calcium feldspars such as labradorite). Results were obtained in the potassium (KOH)⁻ and calcium (OPC clinker)-modified geocements (Kovalchuk, 2002), in which a leucite (a potassium feldspathoid) and labradorite (a sodium-calcium feldspar) were found to be the main phases after firing (Fig. 12.10). This mixed compound composition, N-K-C-A-S-H, had an amorphous structure after firing at 800°C, whereas strong XRD peaks of leucite and labradorite were identified after firing at 1000°C. Temperature of their crystallization measured by a DTA method was about 900°C (Fig. 12.11). Being fired at 1300°C, the system demonstrates redistribution of shares of the products mentioned, in accordance with their thermodynamic stability at this temperature: quantity of the labradorite increases, whereas that of the leucite decreases.

In pure potassium-activated metakaolin (Duxson *et al.*, 2007b), kaliophilite was observed to begin crystallizing at approx. 600°C, and after 800°C it begins substituting with leucite. At the same time, mixed sodium/potassium nepheline, kaliophilite or leucite were observed to be the principal crystalline phases after heating when mixed sodium/potassium activation was applied.

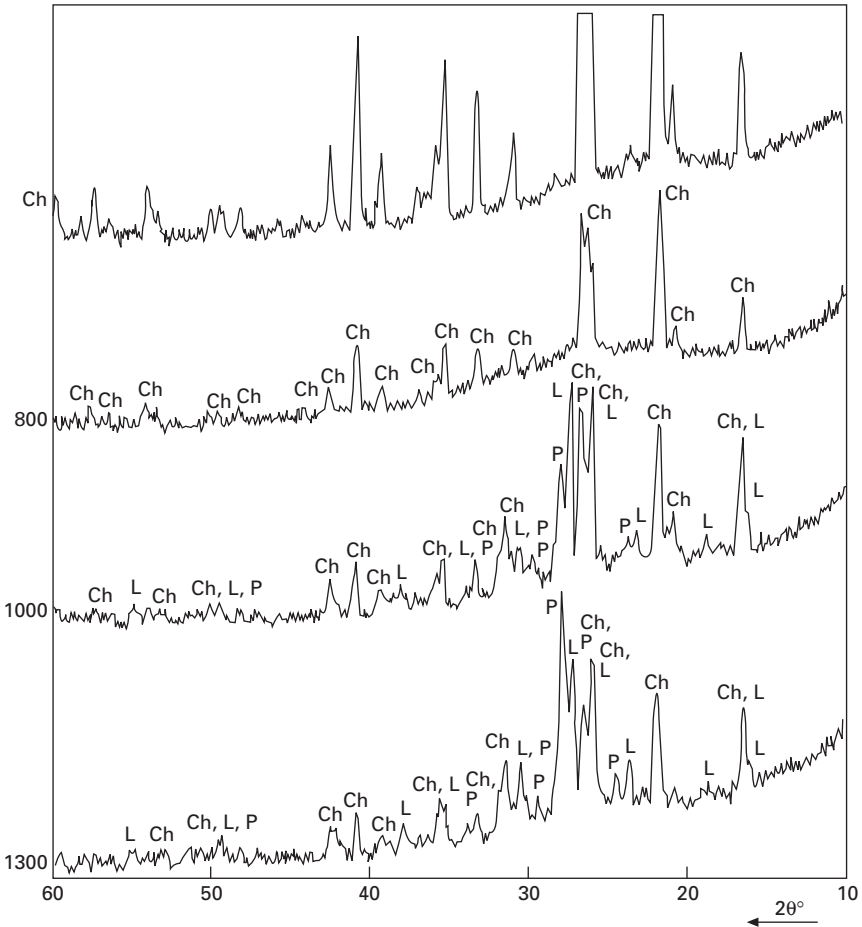
Concluding the above-mentioned information, it is to be stated that formation of microstructure of geocements may normally be expressed by a scheme:



Amorphization does not take place when thermally stable zeolites are

Table 12.4 Phase composition of the alkali activated cements after firing vs. cation type

Temperature range (°C)	Products after heating, for geocement system		
	N-A-S-(H)	K-A-S-(H)	N-K-C-A-S-(H)*
(400–600)	none	–	–
(600–900)	nepheline	kaliophilite, then	–
900...	albite	leucite	leucite, then plagioclase

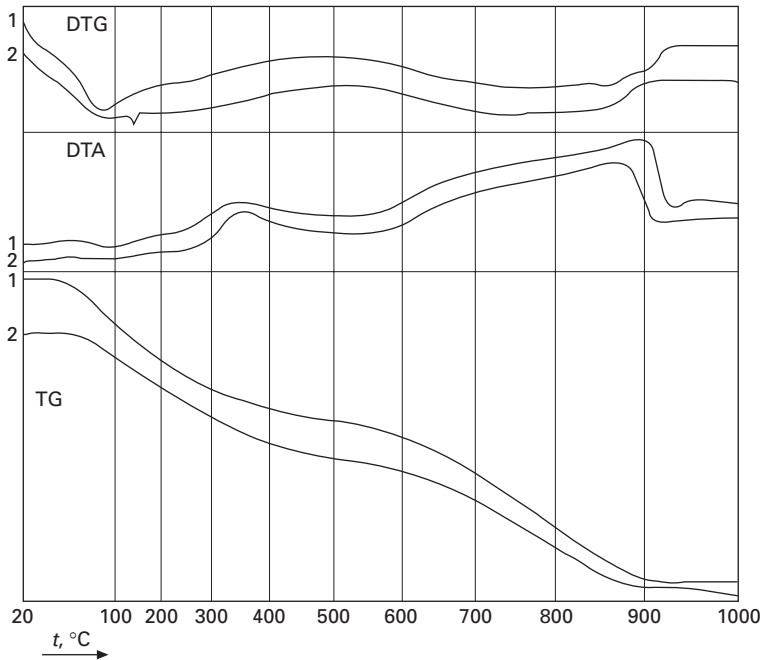


12.10 XRD patterns of the system Na-K geocement – OPC clinker (below 10%), after firing at 800°C (1), 1000°C (2) and 1300°C (3). Geocements were filled with a chamotte (Ch). L-Leucite, P – plagioclase, Ch – crystalline phases from chamotte composition.

synthesized at low temperatures. Type of feldspathoids or feldspars depends on both geocement composition and heating temperature.

12.3 Interrelation between mix proportion, phase composition after hydration and dehydration, and properties

It is to be emphasized that low residual strength, which is the main problem of making heat-resistant materials based on OPC, is not a problem in the majority of alkaline cements, including alkali activated metakaolin or fly ash



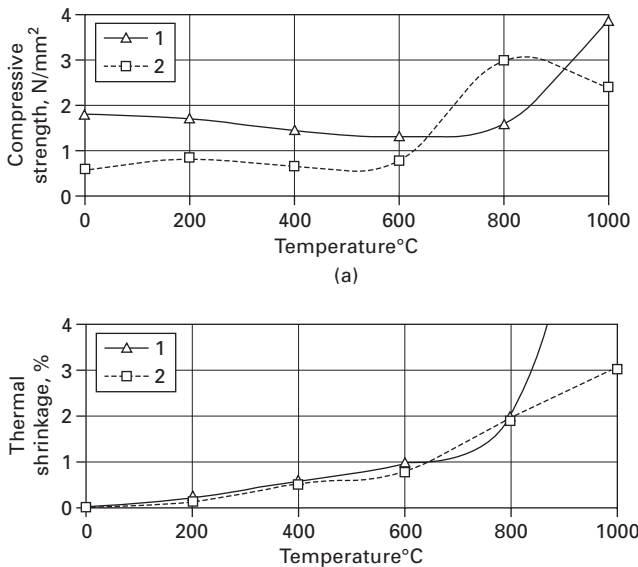
12.11 XRD patterns of the system Na-K geocement – OPC clinker (below 10%). Geocements were filled with a chamotte. Breakpoint on the DTA curves after 900°C probably corresponds to formation of anhydrous aluminosilicates.

because almost all of these systems demonstrate high strength after firing at (800–1000)°C. Taking into account traditionally high compressive strength of alkaline cements at standard conditions, the problem of making heat-resistant geocements is to achieve stability of properties within (200–600)°C, when a particular or complete amorphization of microstructure occurs, which may result in reduced strength. Another problem is high thermal shrinkage caused by increased amount of melting liquid phase appearing due to high alkali content. That's why some studies dealing only with residual strength after firing/heating without mentioning thermal shrinkage are incorrect. Thus, the principal target is to regulate a structure formation process at low and high temperatures for both preventing significant strength variations during heating and controlling thermal shrinkage. Other characteristics of particular interest in some cases are cracking, thermal resistance (evaluated in cycles heating/cooling) and temperature of deformation (4 and 40%) under a load.

The majority of researchers (Davidovits, 1988; Xu and Van Deventer, 1999; Van Jaarsveld and Van Deventer, 1999; Palomo and Fernández-Jiménez, 2003) concluded that an amorphous structure of the geocement/geopolymer artificial stone synthesized was preferable in order to achieve optimal mechanical

strength. However, a crystalline or semi-crystalline structure seems to be more suitable for some special applications. In particular, as crystals are more resistant to acid attack or to thermal shock, the improved crystallinity of the artificial stone is expected to be more resistant to the above-mentioned factors (Krivenko *et al.*, 2000; Kovalchuk, 2002). Moreover, since the zeolite family is extremely diverse, different zeolites, once synthesized in the geocement composition, are thought to secure different target properties. In particular, Gonchar (2000) reported that the metakaolin-based geocements, in which the analcime is formed as a hydration product, are suitable for making low-temperature ceramic materials; the zeolite P ensures high strength within the temperature range of 20–250°C; the zeolites R, NaX, NaY provide for stability of mechanical strength during heating up to 800°C. That’s why properties of the alkali activated material should be studied vs. peculiarities of microstructure (phase composition, crystallinity, etc.).

Compressive strength and thermal shrinkage undergo significant changes during heating. When thermally stable zeolite-like phases are the main products, compressive strength tends to decrease slowly within 200–600°C (sometimes up to 800°C) step-by-step with a slowly increasing thermal shrinkage. After that, some amount of sintering liquid phase appears, it makes for a sharp increase in strength but also for sharp increase in shrinkage (Fig. 12.12). Once thermal shrinkage reaches some established value (normally



12.12 Compressive strength (a) and thermal shrinkage vs. heating temperature. Material: heat-resistant aerated concrete made with geocements: 1 – based on metakaolin, 2 – based on fly ash.

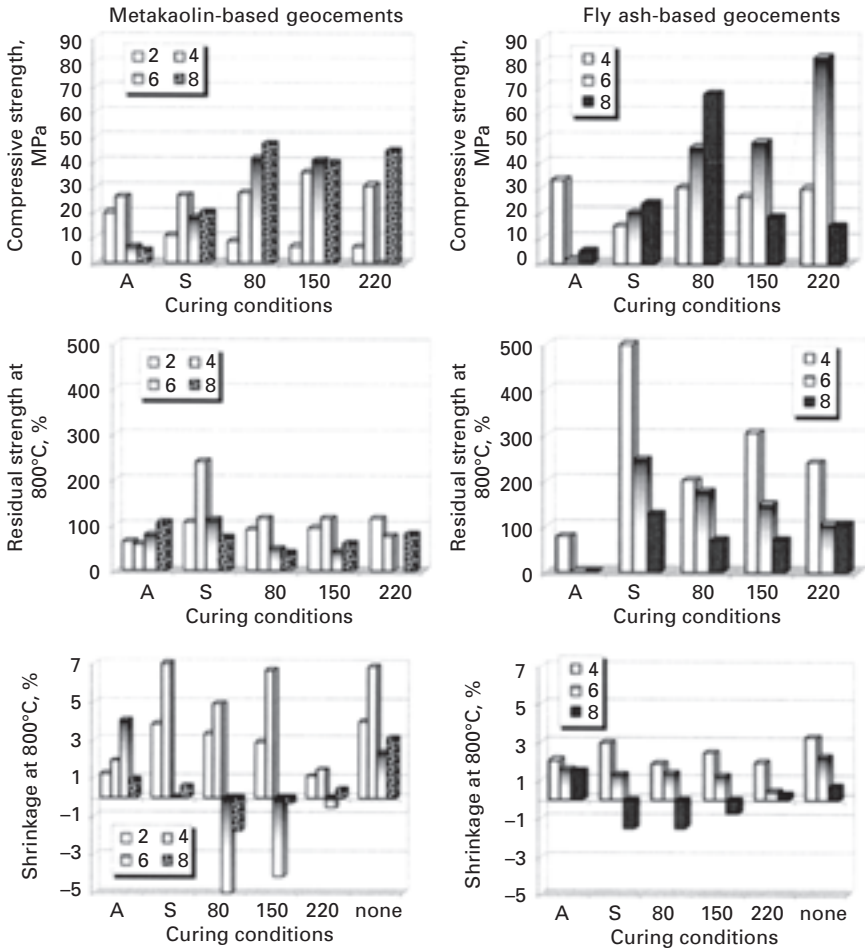
1–2%), materials based on them may not remain functioning because of the cracking, instability of volume and shape, etc., despite still keeping good mechanical strength. So in major cases, the temperature of reaching the limited value of thermal shrinkage is a maximum exploitation temperature for this material. But if the material is kept heating, each geocement composition has a temperature when it becomes soft. This temperature depends mainly upon alkalinity and cation type. The best heat-resistant geocement-based materials may resist up to 1300°C (some special slag-alkaline cements up to 1600°C).

Thermal shrinkage of alkali activated materials has two maximums (Duxson *et al.*, 2006): the first one, at nearly 150–200°C belongs to losses of physically bounded water (drying), and the second one, at 700–900°C, belongs to sintering, and the latter is much more dangerous.

In order to control the shrinkage, some possible solutions are listed below:

- Directed structure formation resulted in a synthesis of an optimal amount of thermally stable crystalline zeolites which act as centres of a skeleton resistant to mechanical stress during heating.
- Introducing some values of heat-resistant filler. This filler should be of an aluminosilicate nature, should resist well against high temperatures and should not contain calcium or magnesium additives. The best fillers for heat-resistant geocements are chamotte, mullite-silica materials (powdered refractories, fibres), corundum and fly ash (for metakaolin-based systems).
- Introducing some amounts of above-mentioned materials as fine aggregates (up to 2 mm in size) decreases mechanical strength but improves other properties.
- Introducing heat-resistant fibres.
- Introducing materials which support the system with silica at high temperatures (not at low ones!).
- Introducing some natural or artificial zeolites which may act as centres of crystallization and centres of improved resistance to thermal shock.

The heat-resistant composite materials require a stability of volume changes within a wide temperature range. The study showed that a shrinkage/expansion process during heating should be regulated by a selection of optimal geocement mix composition side-by-side with the addition of heat-resistant filler. A chamotte was found to be the rational one (Gonchar, 2000; Kovalchuk, 2002). The study of interrelation between a mix composition, curing conditions, phase composition of microstructure and properties of the geocement-based artificial stone was carried out on the compositions modified by the ground chamotte taken in a quantity of 1:1 by mass (Fig. 12.13). Additionally, an interrelation between relative intensity of the crystalline



12.13 Compressive strength (a), residual strength after firing (b) and shrinkage after firing at 800°C (c) vs. geocement composition and pre-curing conditions (A – autoclave curing; S – steam curing, 80–220°C – dry curing at corresponding temperature). The legend represents $\text{SiO}_2/\text{Al}_2\text{O}_3$ molar ratio. Negative values in the diagrams of shrinkage correspond to expansion of the specimens. Taken from (Krivenko and Kovalchuk, 2007).

phases formation and key properties was studied: the maximum peak height in the XRD patterns in this experiment (fixed for the analcime’s main peak at 0.343 nm in the XRD pattern of the autoclaved fly ash 1- based geocement with $\text{SiO}_2/\text{Al}_2\text{O}_3 = 4$) was taken as 100%.

The study of interrelation between mix composition, curing conditions, phase composition of microstructure and properties of geocement-based artificial stone was carried out on compositions modified by milled chamotte

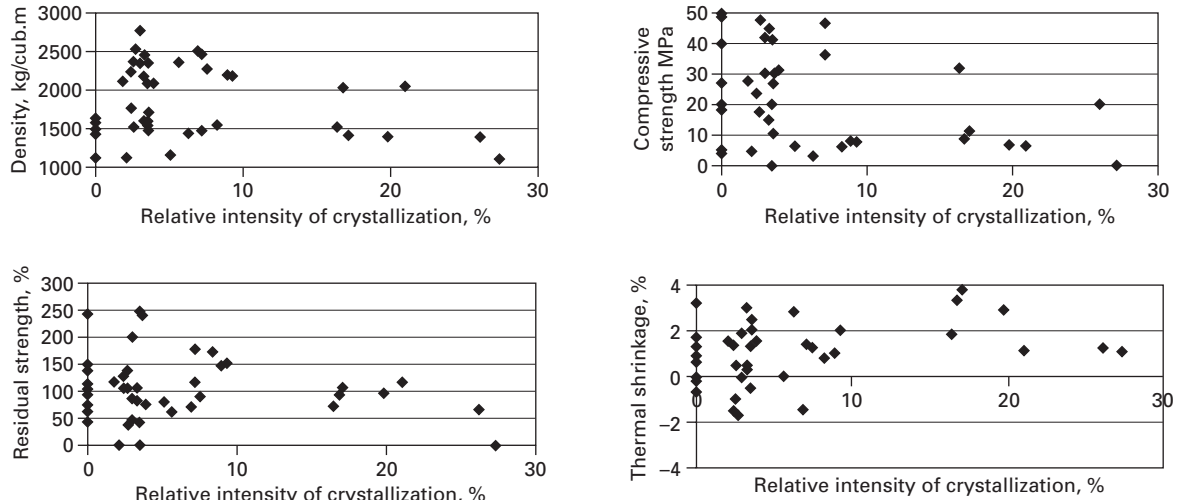
in 1:1 ratio. It was also found that the 1:1 ratio for the composition of 'fly ash-based geocement – milled chamotte' was optimal for the heightened requirements of setting time and compressive strength at normal or high temperature. Increased filler content results in worsening of these properties. Besides, high-replacement (up to 1:3) compositions can be recommended to limit binder content for economic reasons or to control high thermal expansion/contraction.

For complex investigations of interrelation between peculiarities of structure formation processes and properties of the composition to determine fields of optimal mixes, interrelation between relative intensity of formation of crystalline phases and main properties was studied. The maximum peak height on XRD patterns in the whole experiment was taken to be 100%. Search for correlation was done in the relative crystallization range of 0–30%, which includes 94% of experimental data (Fig. 12.14).

It was revealed that optimal thermo-mechanical properties such as high density and mechanical strength along with low contraction after firing was achieved in the mixes with a microstructure composition presented by an average amount (from 2.5 to 10%) of the thermo-stable zeolite-like products such as analcime, hydroxysodalite and zeolite R (Krivenko, Kovalchuk, 2002). These phases are characterized by a smooth dehydration and subsequent recrystallization into stable anhydrous alkaline aluminosilicates such as nepheline and albite) without destruction of the aluminosilicate framework. High intensity of the crystal formation (higher than 10%) in the autoclave-cured compositions as well as insufficient rate of crystallization of the high-silica geocements (from 0 to 2.5%) was found to result in a sharp deterioration of service properties. In case of a high-crystalline structure, it may be caused by the increase in stresses in the already hardened cement stone during intensive recrystallization taking place at high temperature. At the same time, in case of low-crystalline structure it is caused by the absence of a hard crystalline framework. Heat resistance of the fly ash-based geocements is higher than that of the metakaolin-based ones.

Taking into account higher activity of metakaolin on initial stages of hydration in comparison with fly ash, two systems of heat resistant compositions were suggested to be optimal (Table 12.5). These optimal compositions have setting time at 80°C up to 4 hours, compressive strength – up to 89 MPa, residual strength after firing – up to 245% and contraction after firing – in 4.2% limit. Such compositions are to be used for elaboration of a wide area of unfired heat-resistant composites.

In cementitious systems and concretes, melting means shrinkage. Correspondingly, the lower the temperature of initial liquidization, the higher the thermal shrinkage. Phase diagrams of mixed systems also show that monocomponent systems always have higher sintering temperature compared to any mixed system. That is why more than one cation additionally introduced



12.14 Correlation between relative intensity of crystallization and properties of 'geocement-chamotte' compositions: density, compressive strength after low-temperature treatment, residual strength and contraction after firing at 800°C.

Table 12.5 Optimal mixes of heat resistant Na-based geocement-based composites

Geocement mix		
aluminosilicate source	SiO ₂ /Al ₂ O ₃	Heat-resistant filler
metakaolin	4.0	fly ash 1
metakaolin	4.0	fly ash 2
fly ash 1	4.5	ground chamotte
fly ash 2	5.0	ground chamotte

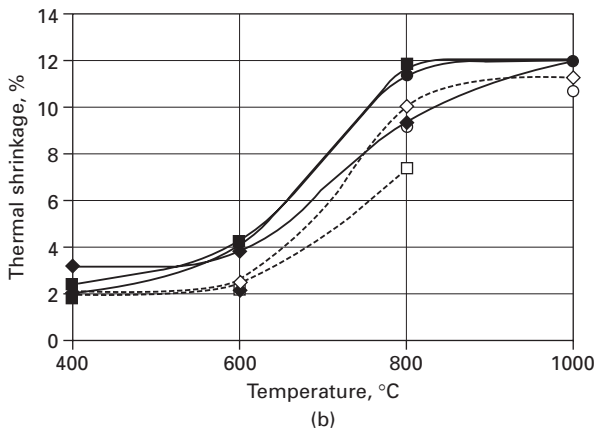
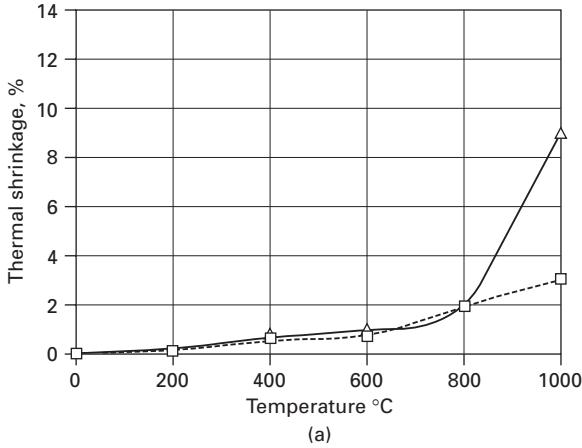
to the mix makes for increased thermal shrinkage (Fig. 12.15). Isoparametric diagrams of thermal shrinkage of geocement-based aerated concrete (Fig. 12.16) also show that thermal shrinkage is inversely proportional to the content of Ca-containing clinker additive (see that the areas of a minimal shrinkage, below 2%, lay at minimal content of a clinker additive presented at the vertical axis X2).

Potassium-based geopolymers always reveal lower shrinkage than sodium-based analogues. At the same time, thermal shrinkage of mixed sodium/potassium geopolymers lay between pure sodium and potassium analogues only for low-silica mixes (up to SiO₂/Al₂O₃ = 2.8), and at higher silica content mixed geopolymers have higher thermal shrinkage than that of either potassium or sodium mixes (Duxson *et al.*, 2006). Thermal shrinkage, started at 600–800°C is accompanied by sharp collapse of porosity, which always drops towards zero beginning from 800°C (Duxson *et al.*, 2007a).

12.4 Experience of application

Remaining a stable structure at high temperatures, alkali activated metakaolin or fly ash represent an excellent base for various materials to be applied at 800°C and more, such as heat-resistant and/or fire-resistant concrete, high-temperature adhesives, composite materials for civil engineering, metallurgic, marine and automotive industry, protective coatings, ceramic application, etc. (Shi *et al.* 2006).

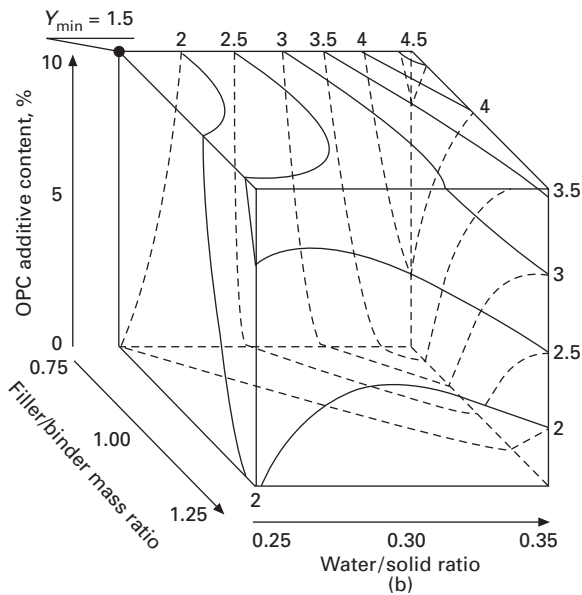
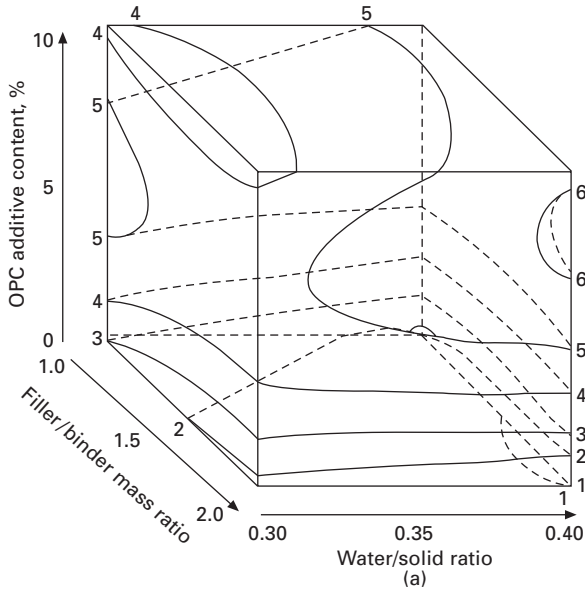
Despite there being no data on industrial-scale application of heat-resistant heavy concretes based on alkali activated metakaolin or fly ash, it seems that the above-mentioned properties make this direction very promising. However, there is an experience of application of heat-resistant lightweight concretes. Heat-resistant aerated concrete with a maximal use temperature of 800°C was developed using the fly ash-based geocements and an aluminium powder as a gas producing agent (Kovalchuk, 2002; Krivenko *et al.*, 2005). The material is intended for thermal insulation of high-temperature equipment, such as furnaces, conduits, chimneys, boilers, fireplaces, etc. The development of process parameters and mix proportions allowed production of heat-resistant aerated concretes of density varying within 300–1200 kg/m³, compressive strength up to 16 MPa, thermal resistance up to 34 cycles in the air, residual



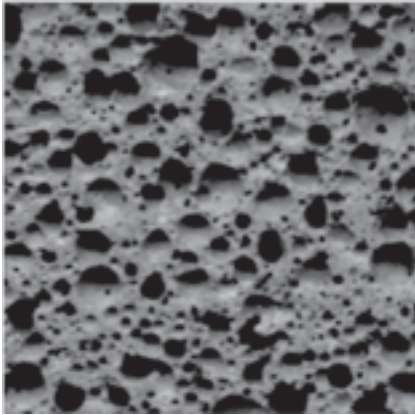
12.15 Thermal shrinkage vs. heating temperature for geocement-based materials with a composition N-A-S-H (a) and N-K-C-A-S-H (b).

strength after firing at 800°C of 75–537% and shrinkage of 0.94–1.97%. The manufacture of this material does not require high temperatures, and thus its manufacture is cheaper, more energy saving and environmentally friendly in comparison with the manufacture of traditional lightweight refractory materials. A commercial scale application of this material as heat insulation of a furnace lining took place in the glassware plant (Kiev, Ukraine). Heat-resistant tiles made from the aerated concrete were glued using specially designed geocement-based heat-resistant adhesive directly to a hot furnace surface (up to 700°C) without interruption of the furnace operation (Fig. 12.17). After six months in service, no destruction of the heat-resistant aerated concrete products was seen.

Fire-resistant concretes based on geocements/geopolymers might be a promising solution for highly responsible constructions of tunnels, underground



12.16 Isoparametric diagrams of thermal shrinkage (%) of geocement-based heat-resistant aerated concretes after firing at 800°C. Geocements were prepared using metakaolin (a) and fly ash (b).



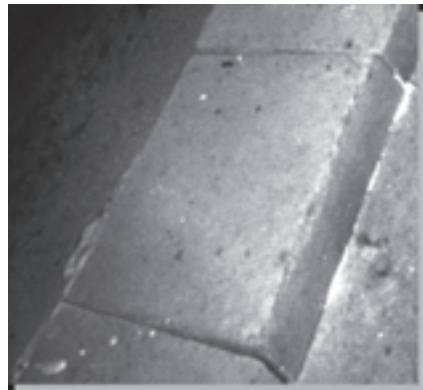
(a)



(b)



(c)



(d)

12.17 Pilot-scale application of the geocement-based heat resistant aerated concrete: structure of the heat-resistant aerated concrete (a); testing of heat-resistant adhesive in a laboratory oven (b); fragments of a glassware furnace lining insulated with the developed material (c, d) Taken from Krivenko and Kovalchuk (2007).

structures, skyscrapers, strategic objects, etc. The most important properties from this point of view are high heat-resistant (stability of mechanical strength at high temperatures) and good endothermic properties (i.e. low temperature conductivity) due to high content of $[-OH]-$ groups in initial structure (Davidovits, 1999).

Alkali activated materials filled with heat-resistant fibres (carbon or aluminosilicate) are used for making composite materials for automotive/aviation industry (Davidovits, 1999; Davidovits, 2002), marine construction in order to improve fire resistance (Tailing, 2002; Van Deventer, 2002), metallurgic industry for making tubes for a liquid metal (Vozniuk, 1999)

and high-temperature heat insulation (Krivenko *et al.*, 2002). Alkaline aluminosilicate matrix has a similar coefficient of thermal expansion to that of carbon or aluminosilicate fibres, providing for successful joint work in the wide temperature range.

Composite materials based on alkaline aluminosilicate binders filled with dispersed fine aggregate (chamotte, corundum, silicon carbide) were successfully used for making abrasive and heat-resistant industrial instruments (cutting and whetting wheels, etc.) (Gonchar, 2000). From the other side, composites filled with lightweight filler (vermiculite or perlite) demonstrate good thermal resistance and might also be used for heat insulation of high-temperature equipments (Krivenko *et al.*, 1999b).

Full-scale application of geocements for fireproof doors of elevators was realized as a joint project of V.D.Glukhovskiy Institute (Ukraine) and OTIS Company (Fig. 12.18). In this project, heat-resistant adhesive was used for joining heat-resistant layers with a metal construction of the door. The doors prepared this way met all the requirements for fireproof doors (Krivenko *et al.*, 2002). Heat-resistant adhesive was also successfully used for installing heat-resistant aerated concrete tiles to the hot surface of a stove (Krivenko and Kovalchuk, 2002; Kovalchuk, 2008).

Alkali-activated materials with high silica content expand when being heated up to 300–600°C. It was used for creation of bloating coatings for fire protection of steel and wooden constructions (Krivenko *et al.*, 1999a). The mix is to be placed onto the surface of the construction to be protected, and in case of fire this layer may bloat (expand) making good heat insulation and extending the time till the construction is damaged. This additional time is needed for fire squad in order to evacuate personal and localize a fire.

Finally, the technology of directed structure formation of anhydrous aluminosilicates in the matrix is used for various ceramic applications.

12.5 Conclusions

After firing, the zeolite-like products in geocement structures recrystallize into anhydrous aluminosilicates. Genesis of microstructure may be represented as follows:

- formation of zeolite-type structures (crystalline or semicrystalline)
- intensification of its synthesis up to approx. 400°C
- amorphization or not (depending on the composition)
- crystallization of stable anhydrous phases (nepheline, albite or cristobalite, depending on mix composition and curing temperature), beginning from 600–800°C
- melting (sintering) leading to destruction.

Fly ash-based geocements generally increase in strength after drying



(a)



(b)



(c)

12.18 Experience of making fireproof doors for elevators: preparing a geocement adhesive (a), placing the adhesive to the door (b), completely door storage (c).

at 150°C, but lose in strength after dehydration/amorphization up to the point of formation of new crystalline structure based on anhydrous alkaline aluminosilicates (nepheline or albite 600–800°C depending on the composition). Formation of above-mentioned structure results in slight increasing in strength (until destruction by melting begins), but also results in increased volume changes due to appearance of liquid phase. Depending on the composition, the lesser alkali content and the higher thermo-mechanical properties.

Phase composition after low-temperature curing ('pre-curing') is essential from the point of view of future thermal properties. In fact, directed formation of a heat-resistant matrix marks the beginning at the stage of a low-temperature structure formation by directed formation of certain zeolite products in crystalline or semi-crystalline form. Direct synthesis of thermo-stable zeolite-like products (such as analcime, zeolite R and hydroxysodalite) characterized by smooth dehydration and subsequent recrystallization into stable anhydrous alkaline aluminosilicates (nepheline and albite) allows heat-resistant composites.

Remaining a stable structure at high temperatures, alkali activated metakaolin or fly ash represent an excellent base for various materials to be applied at 800°C and more. There is positive experience of industrial application of these materials for making heat-resistant and/or fire-resistant concrete, high-temperature adhesives, composite materials for civil engineering, metallurgic, marine and automotive industry, protective coatings, ceramic application, etc.

12.6 References

- Barrer R (1982), *Hydrothermal chemistry of zeolites*, London, Academic Press.
- Breck D (1974), *Zeolite molecular sieves*, New York, J. Wiley & Sons.
- Davidovits J (1987), 'Ancient and modern concretes: what is the real difference', *Concrete Intern.: Design and Construction*, 9, No. 12:23.
- Davidovits J (1988), 'Geopolymer chemistry and properties', in Davidovits J (ed.), *Proceedings of the 1st European Conf. on Soft Mineralogy 'Geopolymer'88*, Saint-Quentin, 25–48.
- Davidovits J (1999), 'Fire proof geopolymeric cements', in Davidovits J (ed.), *Proceedings of the Second International Conf. on Geopolymers 'Geopolymer'99*, Saint-Quentin, 165–169.
- Davidovits J (2002), '30 years of successes and failures in Geopolymer application', in Lukey G C (ed.), *Proceedings of the international conference 'Geopolymer-2002'*, Melbourne.
- Diederichs U, Jumppanen U-M, and Penttala V (1989), '*Behavior of high strength concrete at high temperatures*', Report 92, Julkaisu.
- Duxson P, Lukey G C, and Van Deventer J S J (2006), 'The thermal evolution of metakaolin geopolymers: Part 2 – Physical evolution', *Journal of Non-Crystalline Solids*, 352, 5541–5555.
- Duxson P, Lukey G C, and Van Deventer J S J (2007a), 'Physical evolution of Na-geopolymer derived from metakaolin up to 1000°C', *J Mater Sci*, 42, 3044–3054.

- Duxson P, Lukey G C, and Van Deventer J S J (2007b), 'The thermal evolution of metakaolin geopolymers: Part 2 – Phase stability and structural development', *Journal of Non-Crystalline Solids*, 353, 2186–2200.
- Dyer A (1988), *An Introduction to Zeolite Molecular Sieves*, New York, J. Wiley & Sons.
- Eitel W (1954), *The Physical Chemistry of the Silicates*, The University of Chicago Press.
- Glukhovskiy V (1959), *Soil Silicates*, Kiev, Gosstroyizdat USSR.
- Glukhovskiy V (1967), *Soil Silicate Articles and Constructions*, Kiev, Budivel'nik.
- Glukhovskiy V (1989), 'Ancient, modern and future concretes', in *Durability of concrete. Aspects of Admixtures and Industrial By-Products*, Goteborg, 53–62.
- Glukhovskiy V, Starchevskaya E, and Krivenko P (1969), 'Studies on formation of silicates in mixes of clays, quartz sand and sodium carbonate', *Ukrainian Chemical Journal*, T. 35, V. 4, 65–68.
- Gonchar V (2000), *Abrasive and Thermoresistant Composite Materials Based on Alkaline Aluminosilicate Binders*, PhD Thesis, Kyiv National Univ. on Civil Eng. and Architecture.
- Inamura (Ed.) (1984), *Refractory Materials and their Applications*, Moscow, Metallurgia.
- Kovalchuk G (2002), *Heat Resistant Gas Concrete Based on Alkaline Aluminosilicate Binder*, PhD Thesis, Kyiv National Univ. on Civil Eng. and Architecture.
- Kovalchuk O (2008), 'Experience of industrial application of foamed concrete with improved thermo-mechanical properties based on alkaline Portland cement', in *Construction of Ukraine*, 1'2008, 18–19.
- Kovalchuk G, Palomo A, and Fernandez-Jimenez A. (2007a), 'Alkali Activated Fly Ash. Mechanical strength development as a function of the composition of the starting system', *Mater. Construcc.*, 58, 291, 35–52.
- Kovalchuk G, Palomo A, and Fernandez-Jimenez A. (2007b), 'Alkali Activated Fly Ash. Part II: Mechanical strength development as a function of the thermal curing conditions', *Fuel*, Vol. 86, Issue 3, 315–322.
- Krivenko P (1994), 'Alkaline cements', in Krivenko P (ed.), *Proceedings of the 1st Intern. Conf. 'Alkaline Cements and Concretes'*, Kyiv, Oranta, 11–129.
- Krivenko P (1995), 'Alkaline cements: Terminology, classification, fields of application', *Building materials and constructions*, 1, 23–24.
- Krivenko P (1997), 'Alkaline Cements: Terminology, Classification, Aspects of Durability', in *Proceedings of the 10th ICCC, Goteborg*, 4iv046–4iv050.
- Krivenko P (1999), 'Alkaline cements and concretes: Problems of durability', in Krivenko P (ed.), *Proceedings of the 2nd Intern. Conf. 'Alkaline Cements and Concretes'*, Kyiv, Oranta, 3–43.
- Krivenko P, and Kovalchuk G (2002), 'Heat-resistant fly ash-based geocements', in Lukey G C (ed.), *Proceedings of the international conference 'Geopolymer-2002'*, Melbourne.
- Krivenko P, and Kovalchuk G (2007), 'Directed synthesis of alkaline aluminosilicate minerals in a geocement matrix', *J Mat Sci*, 42, No. 9, 2944–2952.
- Krivenko P, Pushkarova K, and Sukhanevich M (1999a), 'Concrete Coatings to Improve Fire-Resistance of Building Structures', in Dhir R K (ed.), *Proceedings of the International Conference on Creating with Concrete (Concrete Durability and Repair Technology)*, Dundee, 415–422.
- Krivenko P, Petropavlovskiy O, Mokhort M, and Resenchuk V (1999b), 'Heat insulating

- and constructive materials based on alkaline aluminosilicate binders and expanded natural materials', in *Proceedings of the seminar 'Effective heat and hydro insulation of buildings and constructions, and their fire protection'*, Kyiv, NDIBK, 26–32.
- Krivenko P, Mokhort M, and Popel G (2000), 'Durability of protective coatings for concrete on Geocement base', in *Proceedings 5th CANMET/ACI Internat. Conf. on Durability of Concrete*, Barcelona, 719–735.
- Krivenko P, Mokhort M, and Petropavlovskii O (2002), 'Industrial uses of Geocement-based materials in construction and other industries', in Lukey G C (ed.), *Proceedings of the international conference 'Geopolymer-2002'*, Melbourne.
- Krivenko P, Kovalchuk G, and Kovalchuk O (2005), 'Heat-resistant cellular concretes based on alkaline cements', in Dhir R K (ed.), *Proceedings of the Intern. Congress 'Global Construction: Ultimate Concrete Opportunities'*, University of Dundee, 97–104.
- Krivenko P, Kovalchuk G, Palomo A, and Fernández-Jiménez A (2006), 'Fly Ash Based Geocement: Genesis of Microstructure and Properties in Hydration-Dehydration Process', in *Proceedings of the International Congress BMC-8*, Warsaw, 55–64.
- Krivenko P, Kovalchuk O, and Kovalchuk G (2007), 'Directing the Hydration/Dehydration Structure Formation of Alkaline Portland Cement: A Perspective Way for Obtaining a High Temperature Concrete', in *Proceedings of the International Conf. 'Alkali Activated Materials – Research, Production and Utilization'*, Prague, Agentura Action M, 369–378.
- Malinowski R (1979), 'Concretes and Mortars in Ancient Aqueducts', in *Concrete Intern.: Design and Construction*, 1.
- Nekrasov K (ed.) (1972), *Heavy concrete in the increased temperature conditions*, Moscow, Stroyizdat.
- Nekrasov K (1988), 'Development of heat resistant concretes' production', in *Cement-free heat resistant concretes based on natural and waste raw materials*, Makhachkala, Academy of Science USSR, 5–15.
- Palomo A, and Fernandez-Jimenez A (2003), 'Alkali Activated Fly Ash: Properties and Characteristics', in *Proceedings of the 11th Intern. Congress on the Chemistry of Cement*, Durban, 1332–1340.
- Pushkarova E (1994), 'Heat resistant alkaline binders', in Krivenko P (ed.), *Proceedings of the 1st Intern. Conf. 'Alkaline Cements and Concretes'*, Kyiv, Oranta, 245–256.
- Schairer J, and Bowen N (1956) 'The system $\text{Na}_2\text{O}-\text{SiO}_2-\text{Al}_2\text{O}_3$ ', *American Journal of Science*, 254(3), 129–195.
- Shi C, Krivenko P, and Roy D (2006), *Alkali Activated Cements and Concretes*, Taylor & Francis.
- Skurchinskaya Zh (1973), Synthesis of natural minerals' analogs in order to obtain an artificial stone, PhD Thesis, Kiev Institute for Civil Engineering.
- Skurchinskaya Zh (1994), Progress in alkaline cements', in Krivenko P (ed.), *Proceedings of the 1st Intern. Conf. Alkaline Cements and Concretes'*, Kyiv, Oranta, 271–298.
- Tailing B (2002), 'Geopolymers give firesafety to passengers cruise ships', in Lukey G C (ed.), *Proceedings of the international conference 'Geopolymer-2002'*, Melbourne.
- Van Deventer J S J (2002), 'Opportunities and Obstacles in the Commercialization of Geopolymers', in Lukey G C (ed.), *Proceedings of the international conference 'Geopolymer-2002'*, Melbourne.
- Van Jaarsveld G S, and Van Deventer J S J (1999), 'Effect of the alkali metal activator on the properties of fly ash based geopolymers', *Ind. Eng. Chem. Res.*, 38 3932–3941.

- Vozniuk G (1999), 'Environmentally friendly composite materials based on geocements for foundry application (moulding and core mixes)', in Krivenko P (ed), *Proceedings of the 2nd International Conference on Alkaline Cements and Concretes*, Kyiv, Oranta, 237–247.
- Xu H, and Van Deventer J (1999), 'The geopolymerisation of natural aluminosilicates', in Davidovits J (ed.), *Proceedings of the Second International Conf. on Geopolymers "Geopolymer '99"*, Saint-Quentin, 43–64.

Utilization of mining wastes to produce geopolymer binders

F PACHECO-TORGAL and S JALALI,
University of Minho, Portugal and
JP CASTRO GOMES,
University of Beira Interior, Portugal

Abstract: This chapter discusses the utilization of mining wastes to produce geopolymeric binders. It includes the influence of calcination operations in the reactivity of mine wastes; in what way mix design parameters influence strength gain; it covers physical and mechanical properties and also durability and environmental performance.

Key words: mine wastes, geopolymeric binders, properties, durability, adhesion.

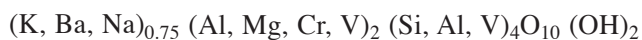
13.1 Introduction

Mineral waste can be defined as the ‘residues, tailings or other non-valuable material produced after the extraction and processing of material to form mineral products’ (Harrison *et al.*, 2002). Nevertheless there is no universally recognized classification of mineral wastes. For the past fifteen years many countries have carried out surveys about mining waste materials (Mitchell *et al.*, 2004). The main reasons for undertaking such surveys are the need to conserve scarce natural resources, reduce environmental pollution and to conserve energy (Hammond, 1988). Not very long ago the failure cases of Aznalcollar mine in Spain (1998) which affected 2656 ha of Donana Nature Park with pyrite sludge, Baia Mare mine (2000) in Romania clearly showed that in the short-term and environmentally speaking, mine wastes represent a clear and present danger as important as greenhouse gas emissions (BRGM, 2001; Puura *et al.*, 2002). Mining and quarrying wastes represent 15% of total wastes in Western Europe and 31% in Eastern Europe (Eurostat, 2003). Western Europe’s mining and quarrying sector is the most concentrated and active in the world. Furthermore it makes a highly significant contribution to Europe’s economy. Overall the extractive industry has an output of some 3 billions tonnes, with a value of about €50 billion, and employs around 500 000 people. It is estimated that over 20% of European Union’s Gross Domestic Product is dependent in some form or other on the extractive industry (Brodskom, 2000). Therefore significant efforts must be made by the scientific community to find alternative uses for mining and quarrying

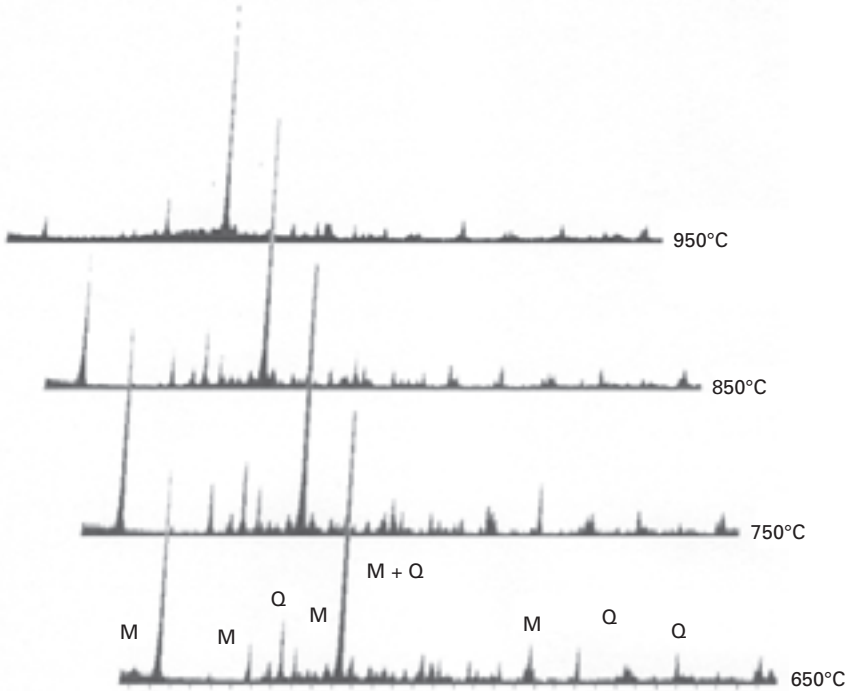
wastes, but also ways of stabilizing them to prevent them from spreading, and polluting surrounding areas in order to preserve natural biodiversity, as well as to protect drinking water supply and urban environments. Since alumino-silicate minerals are the most abundant in the Earth's crust, most mining wastes are likely to be of this kind. Therefore alumino-silicate wastes might become sources of geopolymerization. This chapter analyses the utilization of mining wastes to produce geopolymeric binders. It includes the influence of calcination operations in the reactivity of mine wastes; in the way mix design parameters influence strength gain; it covers some physical and mechanical properties particularly the adhesion between the mine waste binders and ordinary Portland cement concrete; it describes durability performance from abrasion and acid resistance and also assesses environmental performance from leaching tests. A more detailed coverage about the geopolymerization of mine wastes is presented elsewhere (Torgal *et al.*, 2007a, 2007b, 2007c, 2008).

13.2 Influence of calcination operations in the reactivity of mine wastes

The thermal treatment of aluminosilicate materials causes changes in their structure with an increase in the amorphous phase. Therefore, the mechanical strength of alkali-activated binders depends on the structural conditions of the alumino-silicate materials, as natural materials lead to lower mechanical performance. Higher mechanical strength is associated with materials submitted to calcination like metakaolin or formed as by-products of high-temperature processes such as fly ashes, blast furnace slag. As happens in pozzolanic reactivity, alkali-activation reactivity depends on the amorphous content of silica and aluminium. The reactivity is linked to the material structure, being higher for higher amorphous content. Recent authors' investigations have focussed on alumino-silicate wastes from a tungsten mine. Geochemistry of Portuguese tungsten deposits is composed of blue schist formations with some quartz veins (Neiva, 1987). Schist is a very common metamorphic rock formed by dynamic high-temperature, high-pressure metamorphism that involves a lot of strain. For tungsten mine wastes the authors report that thermal treatment is responsible for increase reactivity. XRD patterns (Fig. 13.1) indicated that mine wastes used consisted mainly of muscovite and quartz which were identified by their characteristic patterns using the Materials Data JADE 6.0. software as follows: muscovite (card 46 – 1409) and quartz (card 46 – 1045). The chemical formula of muscovite is as follows:



The chemical composition and specific surface of the mine waste mud are shown in Table 13.1. Phase transformations on calcination were monitored by



13.1 XRD patterns of mine waste treated at different temperatures (M – muscovite; Q – quartz).

Table 13.1 Chemical composition and specific surface

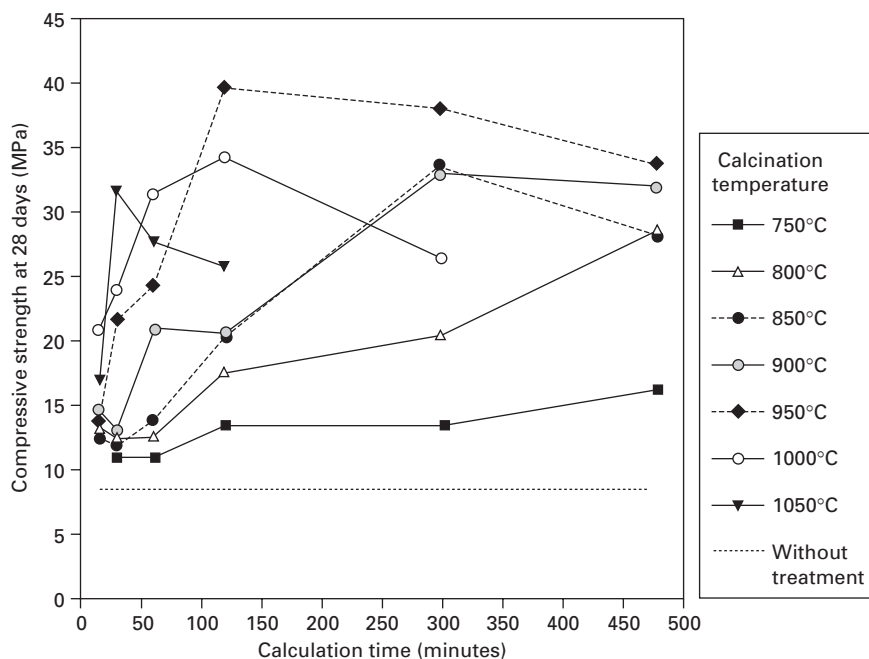
Constituents (mass %)	Mine waste mud
SiO ₂	53.48
Al ₂ O ₃	16.66
Fe ₂ O ₃	12.33
K ₂ O	7.65
Na ₂ O	0.62
MgO	1.27
SO ₄	3.10
TiO ₂	1.39
As	1.28
Other minor oxides	2.22
Blaine fineness (m ² /kg)	357

XRD of waste powder quenched to room temperature to avoid crystallization of amorphous muscovite. Samples were placed in the static furnace only after the temperature treatment had been reached. After thermal treatment, the static furnace was opened to remove the samples. Results show that calcination leads to formation of an amorphous phase, causing an increase in the general background (BG) of XRD patterns and dominantly taking

place in the calcination interval from 850 to 950°C (Table 13.2), with a thermal behaviour similar to other phyllosilicate clay minerals (He *et al.*, 1995). The main muscovite peak ($2\theta = 8.8^\circ$) persisted even after the sample had been heated at 950°C, although it decreased considerably. Peak area measurements revealed that about 12% of muscovite survived calcination at 950°C. Compressive strength of mine waste mortars was used to evaluate dehydroxylation degree, $50 \times 50 \times 50$ mm cubes were cast to study the compressive strength and their development with curing time. The mass ratio of sand: waste: activator was 1:1:1. An activator with sodium hydroxide (12M) and sodium silicate solution was used with a mass ratio of 1:2.5. Compressive strength results of mortars made with waste mud calcined during 30, 60, 120, 300 and 480 minutes are shown in Fig. 13.2. Calcination temperature below

Table 13.2 Calcination effects on XRD diffraction of mine waste

XRD	Calcination temperature (°C)			
	650	750	850	950
2θ	8.845	8.807	8.803	8.806
Main muscovite peak area (%)	51	47.4	40.8	11.5
BG (%)	33.5	33.7	40.5	58.3



13.2 Compressive strength of mine waste mortars according to the thermal treatment of the waste.

750°C does not contribute to the compressive strength of alkali-activated waste mud-based mortars, which means it has no effect whatsoever in the reactivity of the waste. Increasing calcination temperature to 800°C shows some reactivity, although only after a long calcination time. Calcination at 850°C and 900°C leads to a very similar compressive strength after 5 hours of calcination but underperform against a calcination temperature at 950°C for 2 hours, which clearly shows a structural change in the calcined material. Calcination of waste powder at 950°C for 120 min considerably increases compressive strength at 28 days of curing due to the structural dehydroxylation process which leads to an amorphous product of dehydration of muscovite. This result is consistent with XRD results previously shown in Table 13.2. Furthermore increased calcination time and temperature does not lead to higher compressive performances due to possible formation of crystalline phases like mullite and reported by Mazzucato *et al.* (1999). Compressive strength data related to alkali-activated mine waste mortars made with, raw waste mud and calcined waste mud respectively showed an increase of more than 300% (Table 13.3) justifying the thermal treatment. Although calcination of mine waste mud in a static furnace, as happens in this study, may be expensive, some authors had already developed flash calciner industrial 800 Kg/h production units, capable of reducing calcination time to a few seconds and with the additional advantage of no further grinding operations (Salvador, 1995, 2000) which will cut down the cost of down mine waste mud thermal treatment.

13.3 Strength gain and mix design parameters

13.3.1 Influence of $\text{Ca}(\text{OH})_2$ and sodium hydroxide concentration

Previous investigations showed that mine waste mixtures without calcium hydroxide have a very low compressive strength performance. The mortar mixtures (Table 13.4) with a 10% calcium hydroxide percentage present the maximum compressive strength, almost 30 MPa, for a sodium hydroxide

Table 13.3 Compressive strength of alkali activated mine waste mud mortars

Curing (days)	Compressive strength (MPa)	
	Raw mine waste	Waste calcined at 950°C for 2 h
7	8.4 (1.2)	28.4 (1.8)
14	9.3 (4.3)	37.0 (1.1)
28	11.2 (1.8)	39.6 (1.8)

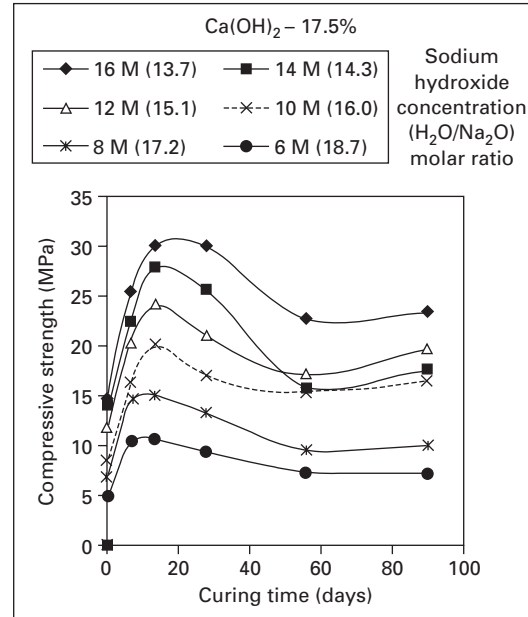
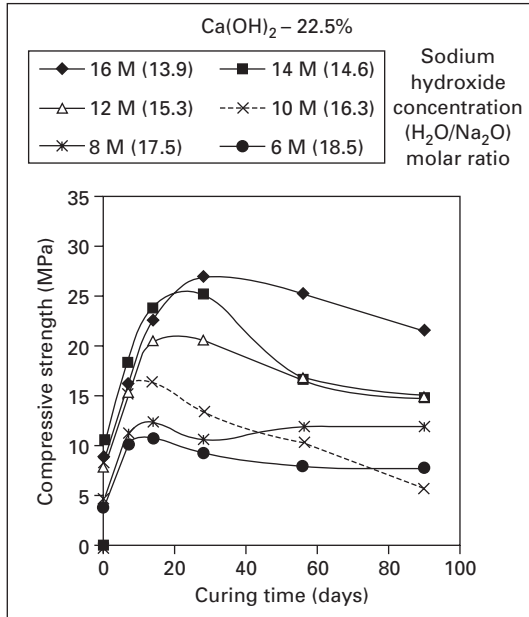
Bracketed values are the standard deviation

Table 13.4 Mortar composition (C105–C116)

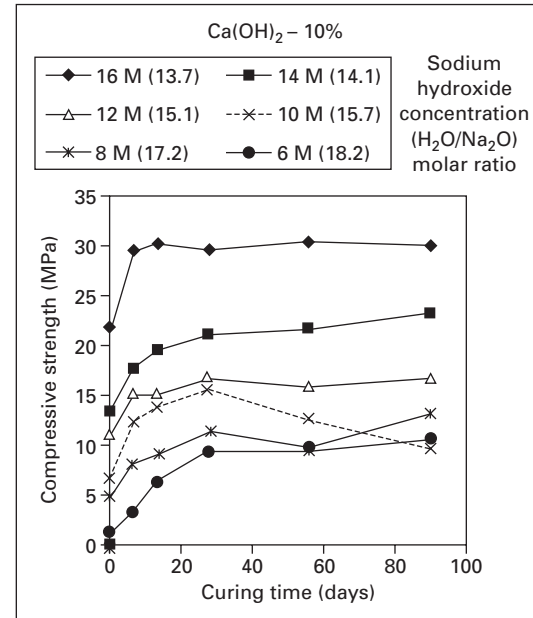
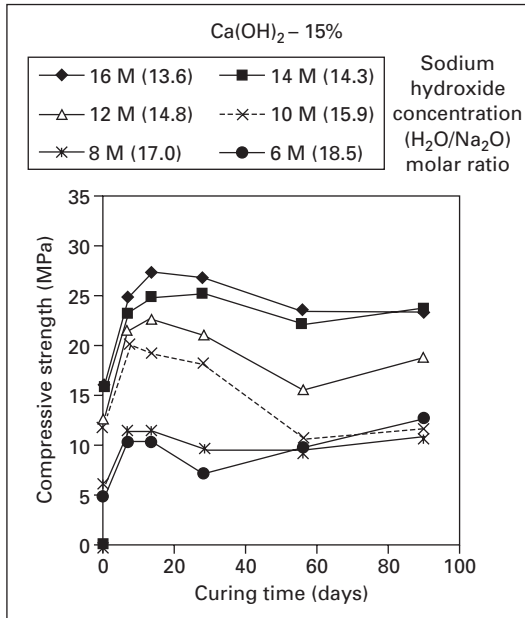
Comp.	Conc. hydroxide	Waterglass: hydroxide	Ms (silica modulus)	H ₂ O/Na ₂ O Molar r.	Calcium hydrox.(%)
C105	16M	2.5:1	1.34	13.7	17.5
C106				13.9	22.5
C107	14M		1.41	14.3	17.5
C108				14.6	22.5
C109	12M		1.49	15.1	17.5
C110				15.3	22.5
C111	10M		1.59	16.0	17.5
C112				16.3	22.5
C113	8M		1.72	17.2	17.5
C114				17.5	22.5
C115				18.7	17.5
C116	6M			19.1	22.5

concentration of 16M, (to which correspond a H₂O/ Na₂O molar ratio of 13.4 (Fig. 13.3)). The total mass of water used to determine the water-binder ratio is the sum of water contained in the sodium hydroxide solution, the water contained in waterglass and the mass of extra water added to the mixture. These results are consistent with the ones obtained by Alonso and Palomo (2001a, 2001b). These authors, using metakaolin/calcium hydroxide mixtures, reported the influence of the sodium hydroxide concentration on the nature of the final reaction product formed. The results help to explain the importance of calcium in geopolymer binders and also why the composition of the geopolymer cement PZ-Geopoly[®] patent has a content of 11.1% of calcium oxide (Davidovits, 1999). Apart from the explanation that positive ions such as Ca²⁺ need to be present in the framework cavities to balance the negative charge of the aluminate group, it is still not clear why calcium hydroxide plays such a significant role in the strength of alkali-activated binders.

The mixtures in which calcium hydroxide percentage is higher than 10%, show strength decrease after 14 days curing. This strength loss related behaviour has been confirmed by others (Yip *et al.*, 2005). The explanation for that is related to the formation of two different phases, geopolymeric gel and calcium silicate hydrates, being that the former acts as microaggregates. These authors believe that strength loss with curing time is maybe due to the fact that CSH reaction and the geopolymeric reaction will compete against each other for soluble silicates, giving rise to a binder composed of two porous phases that leads to strength loss. More recently Yip *et al.* (2008) studied the



13.3 Compressive strength versus sodium hydroxide concentration according to calcium hydroxide percentage (22.5; 17.5; 15 and 10%).

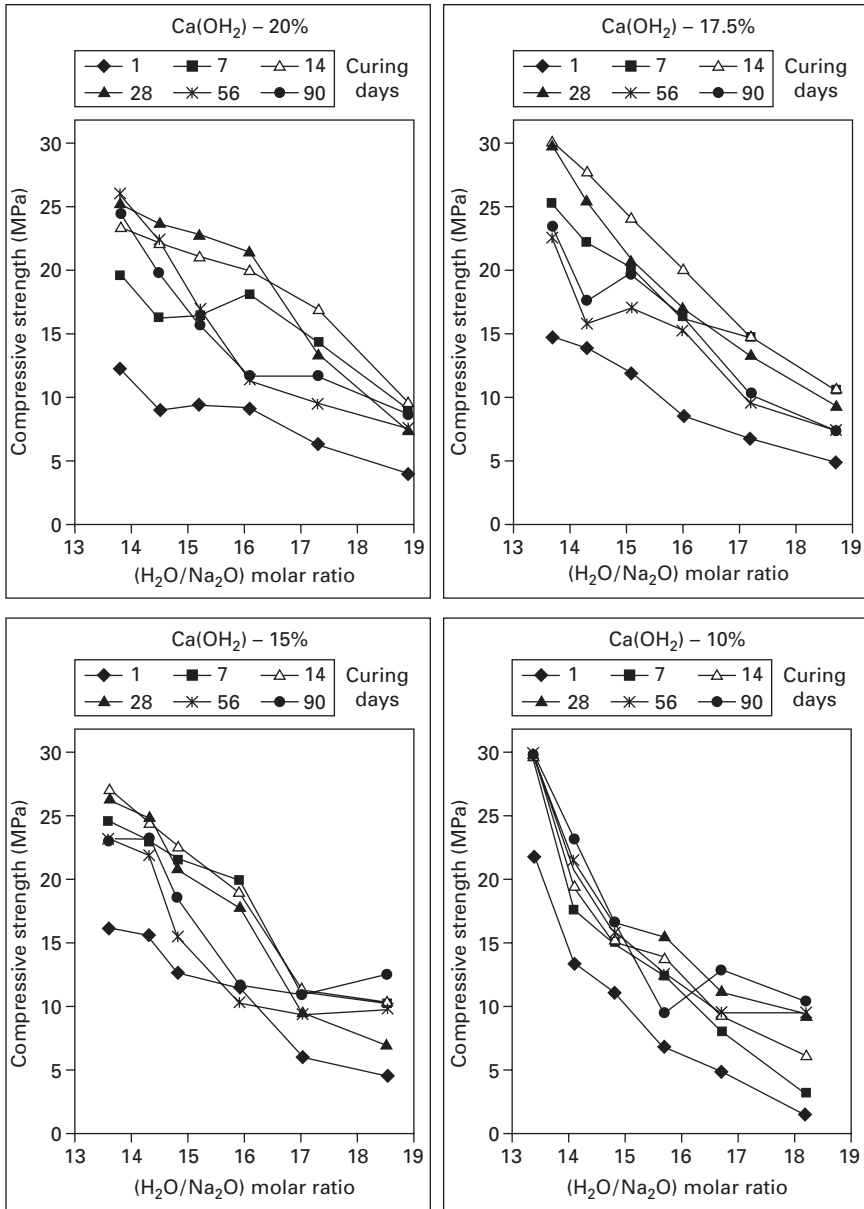


13.3 Cont'd

effect of calcium sources on the geopolymerization stating that lower strengths were due to the unreacted mineral particles that disrupt the geopolymeric gel network. An alternative explanation is related to the possibility of the occurrence of shrinkage cracking near the aggregates, originating a clear tensile strength reduction, that could only be confirmed when shrinkage and tensile strength were studied. Results show a compressive strength increase with the H_2O/Na_2O molar ratio decrease Fig. 13.4. It is clearer for mixtures with a 10% calcium hydroxide percentage a H_2O/Na_2O molar ratio lower than 15 and higher curing ages. The rest of the mixtures with higher calcium hydroxide percentages sometimes show a strength increase for H_2O/Na_2O molar ratio decreases that occurs from 14 days curing forward. However, sometimes they also present a strength decrease when H_2O/Na_2O molar ratio decreases. This behaviour has to do with calcium hydroxide solubility in high alkaline environment and with the formation of calcium hydroxide and CNSH precipitates (Stade, 1989; Macphee, 1989).

13.3.2 Influence of H_2O/Na_2O molar ratio

A major strength increase, with 30MPa after just 1 day, reaching almost 70MPa after 28 days curing (Fig. 13.5) is noticed. This performance is mainly related to the use of less aggregates and thus less extra water (Table 13.5). The use of mixtures containing 5% calcium hydroxide leads to lower strength after long curing time than when 10% calcium hydroxide mixtures were used. The strength differences are much higher for the initial curing days, after just 1 day the mixtures with 5% calcium hydroxide have just half the strength of the 10% calcium hydroxide mixtures. The extraordinary strength increase is due to the use of a low H_2O/Na_2O molar ratio, which influences strength development. When the alkaline concentration rises, that implies a higher amount of dissolved aluminosilicate species, meaning more cementitious material available to react. Results show that compressive strength is influenced by the percentage of calcium hydroxide: the highest strength is achieved for 10% calcium hydroxide percentage. However the use of 5% calcium hydroxide percentage leads to similar strength results for long curing times. This means that for this mixing condition compressive strength is not so influenced by calcium hydroxide percentage. An explanation for such behaviour may rely in the fact that aluminosilicate (geopolymeric) compounds are being formed. The use of 16.7% and 25% calcium hydroxide percentages, although associated with a strength rise due to the use of a 24M concentration, achieved a far lower strength than the 10% calcium hydroxide percentage. This behaviour can be explained by the use of less aluminosilicate mine waste (replaced by calcium hydroxide) as well as from the increase of unreacted particles, due to less setting time, because calcium hydroxide shortens setting time.

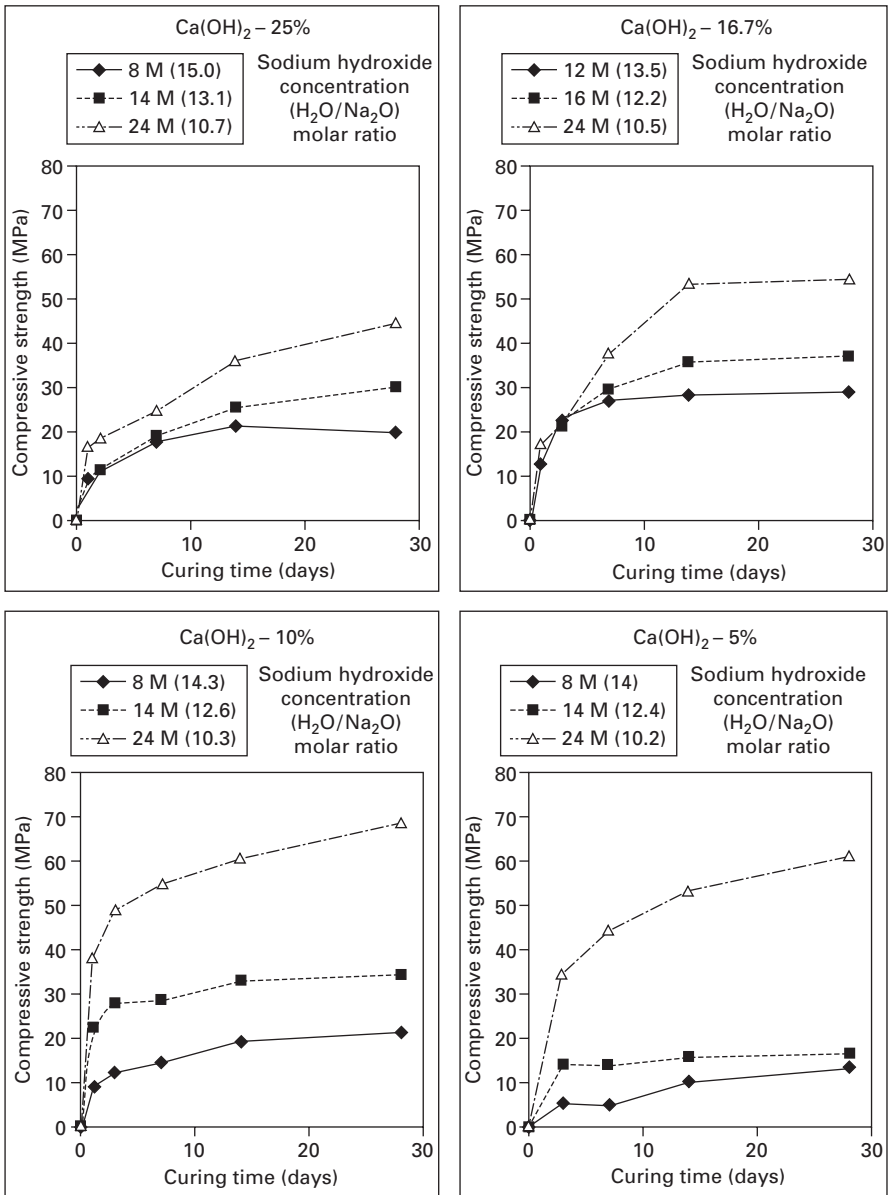


13.4 Compressive strength versus H₂O/Na₂O molar ratio according to calcium hydroxide concentration (10, 15, 17.5 and 20%).

13.4 Physical and mechanical properties

13.4.1 Workability

Workability is a property of a freshly mixed binder (mortar or concrete) that determines the ease with which it can be mixed, placed, consolidated



13.5 Compressive strength according to curing time for several calcium hydroxide percentages and waterglass/sodium hydroxide mass ratios.

and finished (Neville and Aitcin, 1998). Neville (1997) also mentioned the flowability capacity as an important property related to workability. It was not possible to evaluate the workability of mine waste mortars using the ‘flow table’ device, due to the adhesiveness of the waterglass which is responsible

Table 13.5 Mortar composition (C126–C128)

Comp.	Conc. hydroxide	Waterglass: hydroxide	Ms (silica modulus)	H ₂ O/Na ₂ O molar r.	Calcium hydrox.(%)
C126				10.3	10
C127	24M	2.5:1	1.17	10.7	25
C128				10.2	5

for the bonding behaviour between the mortar and the metallic surfaces of the device. Not even the use of a grease coat has been sufficient to prevent that behaviour. The use of extra water (water added to the mixture after all components have been properly mixed) leads to an increase in the ease of placing operations (without strength loss if the molar ratio water/sodium remain the same by using a higher sodium concentration in the first place). When mine waste mortar is placed inside the conic mold of the ‘flow table’, it remains bonded to their metallic faces when the mould is lifted, preventing the test being carried out. This behaviour was not overcome not even when a superplasticizer (SP) was used in the mixtures.

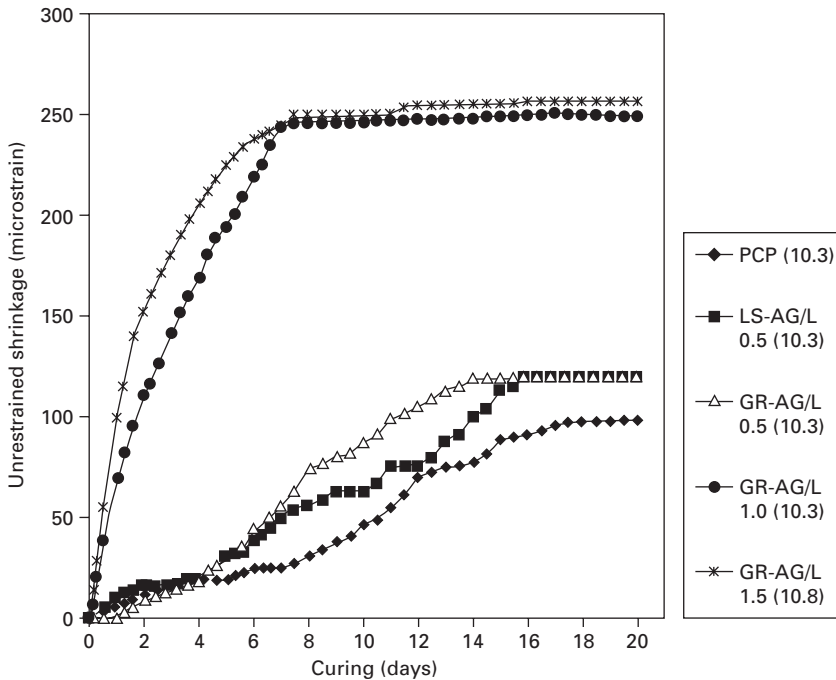
13.4.2 Setting time

The setting time of a binder material is linked to the loss of consistency when the binder changes from a fluid to a rigid state. For practical purposes that time must not be less than the time required to place the binder material. The setting time (ST) was evaluated using the Vicat needle device. For a mine waste paste with a percentage substitution of waste mud for 10% calcium hydroxide, a waterglass/sodium hydroxide mass ratio of 2.5 and a sodium hydroxide concentration of 24 M was respectively 125 and 145 minutes for initial and final setting time. This ST is rather higher than the one reported by Pinto (2004), who mentioned an initial ST of 28 minutes for alkali activated metakaolin with the same percentage of calcium hydroxide. However, one must consider the fact that metakaolin is a more reactive aluminosilicate material due to its high geologic purity and also higher reactive aluminosilicate phases. That explains why the alkali activation of tungsten mine waste mud (TMWM) can only be possible by the use of soluble silica (waterglass) and with high concentration of sodium hydroxide. Besides, the use of extra water to increase the workability of the mixtures may explain part of the ST delay. Furthermore, the ST may also be influenced by the moment when the extra water is added to the mixture. Depending on that particular time, different amount of dissolved aluminosilicate particles will be in the mixture. This means that contrary to OPC binders for which the paste ST gives a good estimation of ST for concrete mixtures, in the case of alkali activated based binders such estimation is not possible.

13.4.3 Unrestrained shrinkage

Unrestrained shrinkage (US) for mine waste geopolymeric binders is shown in Fig. 13.6. The mass ratio of water/dry solid binder content was 3.6% in most of the samples, except for samples with an aggregate/binder mass ratio of 1.5 or 1.7 in those cases, the extra water percentages were respectively 7 and 10%. TMWM binders using schist (SC) fine aggregates with an aggregate/binder ratio of 1.5 was named SC – AG/B 1.5. Similarly when limestone (LS) or granite (GR) aggregates were used were named respectively LS – AG/B 1.5 and GR – AG/B 1.5. TMWM mixtures made with 2% superplasticizer by mass of binder lime and mine waste mud, were named respectively SC/SP, GR/SP and LS/SP. Unrestrained shrinkage used prismatic specimens measuring $40 \times 40 \times 160 \text{ mm}^3$ and was determined according to Portuguese Standard LNEC E398-1993. Unrestrained shrinkage readings were performed every hour in the first 10h, every 3 h in the next 6 days and twice a day in the remaining days.

Unfortunately, as the apparatus only measures shrinkage 24 hours after the mixtures were cast, it misses an important part of US deformation, that may take place between the time when setting occurs until the specimens were removed from the moulds and place in the device. That hypothesis can



13.6 Unrestrained shrinkage.

only be confirmed using a test device that could measure US deformation since the beginning of setting, something that cannot be done with the Vicat penetration test which is currently used for OPC technology, where the shrinkage deformation in the first 24 h is disregarded (Aitcin, 2001). The US data shows a different behaviour for mine waste mortars with an aggregate/binder mass ratio between 1.0 and 1.5 and the ones with the equivalent 0.5, which have higher shrinkage than the pastes. As the aggregates percentage used in the mortars is much lower than for concretes, i.e mortar aggregate/binder mass ratio is below 2.0 versus between 4 and 5 for concrete, it follows that aggregates act as a set of inclusions trapped in a continuous paste matrix and do not form a rigid skeleton which help to diminish US deformation (Aitcin, 2001; Tazawa and Myazawa, 1995). So increasing aggregate content in terms of aggregate/binder mass ratio from 0.5 to 1.5 is not enough to achieve a US reduction. Besides the volume change associated to the shrinkage behaviour is also dependent on the mass of specimens, i.e the US will be higher for lower mass and higher porosity.

13.4.4 Water absorption

The capillarity water absorption coefficients (CWAC) in terms of (g/cm^2) are shown in Table 13.6. It can be seen that several mixtures have similar CWAC, which makes sense since they have the same mass of aggregates, which have much lower CWAC. Torgal and Castro Gomes (2006) reported CWAC between 0.005 and 0.0007 g/cm^2 for granitic and limestone rocks, so it means capillarity water absorption of the TMWM specimens is mainly influenced by the capillarity water absorption of the paste. Besides if a porous and permeable aggregate-paste interface exists, it would be expected that the mixture (SC/SP – AG/B 1.5) would present a much higher CWAC due to their lower dimension aggregates. As for the (GR/SP – AG/B 1.5) mixture which presents the highest CWAC that is of difficult explanation because, having been made with a superplasticizer and, therefore, having better compressive strength than the equivalent without that additive (GR – AG/B 1.5) due to higher packing, it should have lower CWAC.

Table 13.6 Capillarity water absorption coefficients (CWAC)

Mixture	CWAC ($\text{g}.\text{cm}^2$)	Coefficient of variation C.V (%)
SC/SP – AG/B 1.5	0.012	0.9
GR – AG/B 1.5	0.013	0.8
LS/SP – AG/B 1.5	0.012	1.2
GR/SP – AG/B 1.5	0.015	1.6

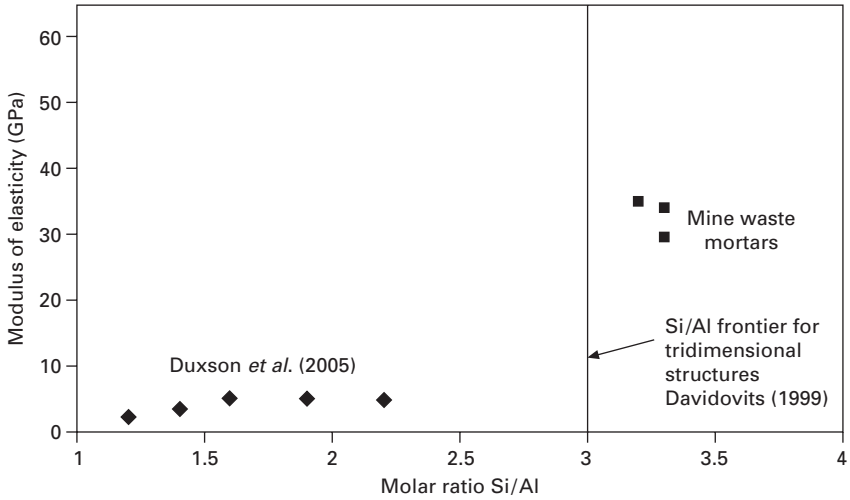
13.4.5 Static modulus of elasticity (SME)

The SME allows separation of the elasticity behaviour of the mixture with granitic aggregates (GR) from the ones with schist (SC) (Table 13.7). From the same mass amount of aggregates different static modulus of elasticity were obtained (the SME of mixture with granitic aggregates is 85% of mixture with schist aggregates). That is probably related to aggregate dimension, as a higher dimension and a lower volume led to lower SME. For mixtures with granitic aggregates, an increase of 100% in aggregate amount lead to 14.5% higher SME. The SME data are similar to that obtained by others (Pinto, 2004; Hardjito *et al.*, 2004; Duxson *et al.*, 2005; Wang *et al.*, 2005; Kirschner and Harmuth, 2004). That can be explained by the influence of the aggregates. In fact some authors considered aggregates to be the most important parameter concerning OPC modulus of elasticity (Teychenné, 1978; Zhou *et al.*, 1995; Rashid *et al.*, 2002). While Hardjito *et al.* (2004) and Pinto (2004) measured SME in concrete specimens, Duxson *et al.* (2005), Wang *et al.* (2005) and Kirschner and Harmuth (2004) evaluated the SME for pastes, which may explain their strangely lower results. Previous investigations on mine waste binders with SEM/EDS microanalysis led to the following data; Si/Al = 3.3 for (GR – AG/B 1.5) and Si/Al = 3.2 for (XS – AG/B 1.5). The investigations done by Davidovits (1999) using high purity alkali activated metakaolin show a decrease in SME, for increase Si/Al molar ratio above 3. This has some confirmation in the work of Fletcher *et al.* (2004), who also used alkali activated metakaolin and stated that decrease only happens to an increase in Si/Al molar ratio above 24. The SME data obtained for mine waste binders do not confirm the Si/Al limits proposed by Davidovits (1999) for tridimensional structures (Fig. 13.7). It is believed that such behaviour is due to the different aluminosilicate materials used in this work, which may generate different hydration products and different structure formation. On the other hand, since not even Fletcher confirms those Si/Al limits, it seems that they must be considered just as information data.

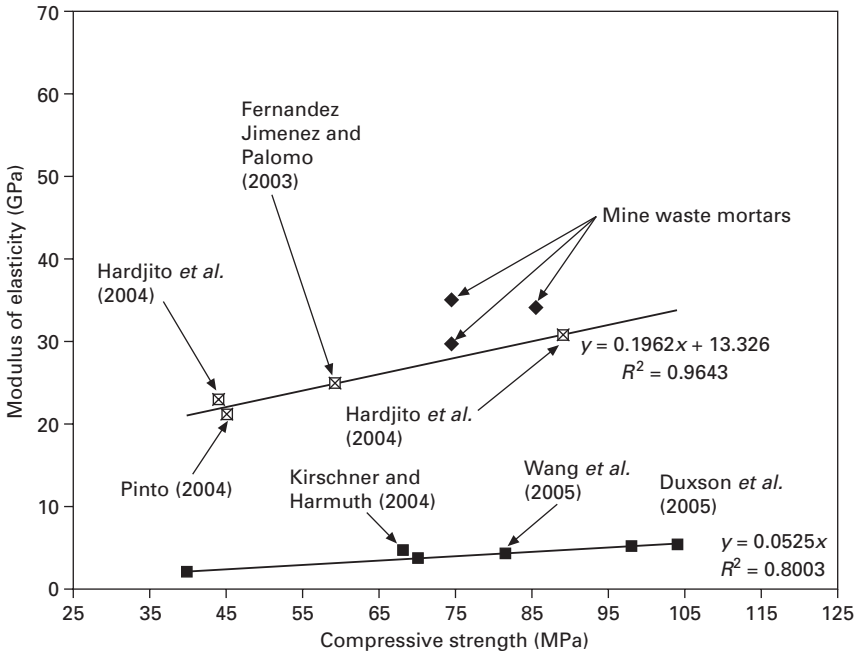
Concerning the statistical relationship between SME and compressive strength (Fig. 13.8), it can be seen that literature data related to alkali activated binder pastes are located as a family group in which SME changes very little with increase compressive strength. On the other hand, the literature data for alkali activated concretes is located as a second family near the data obtained for mine waste binders. The former has higher SME which may be due to a coarser microstructure originated by the use of aluminosilicate material with lower Blaine fineness.

Table 13.7 Static modulus of elasticity (SME)

Mixture	SC – AG/B 0.75	GR – AG/B 0.75	GR – AG/B 1.5
SME (GPa)	34.9	29.7	34.0



13.7 Modulus of elasticity versus molar ratio Si/A.



13.8 Relationships between compressive strength and modulus of elasticity.

13.4.6 Adhesion characterization of mine wastes geopolymeric binders

The failure modes were characterized by the location of the failure in the slant specimens. An adhesive failure is defined when the plane of failure is along the interface surface. Figure 13.9 shows a slant shear specimen failed in a monolithic failure mode. The values of bond strength in slant specimens with a monolithic failure mode are a lower estimate. The specimens were named after the name of repair material and the concrete substrate surface treatment. Specimens using concrete substrate repaired with commercial product R1 with and without surface treatment were named respectively, R1 – ES (Etched surface) and R1 – NTS (No treatment surface). Similarly when TMWM geopolymer binder was used to bond the two halves they were named respectively GP – ES and GP – NTS. Slant specimens with substrate surface treatment as cast against metallic formwork, and as cast against wood formwork were also used repaired with TMWM geopolymeric binder and

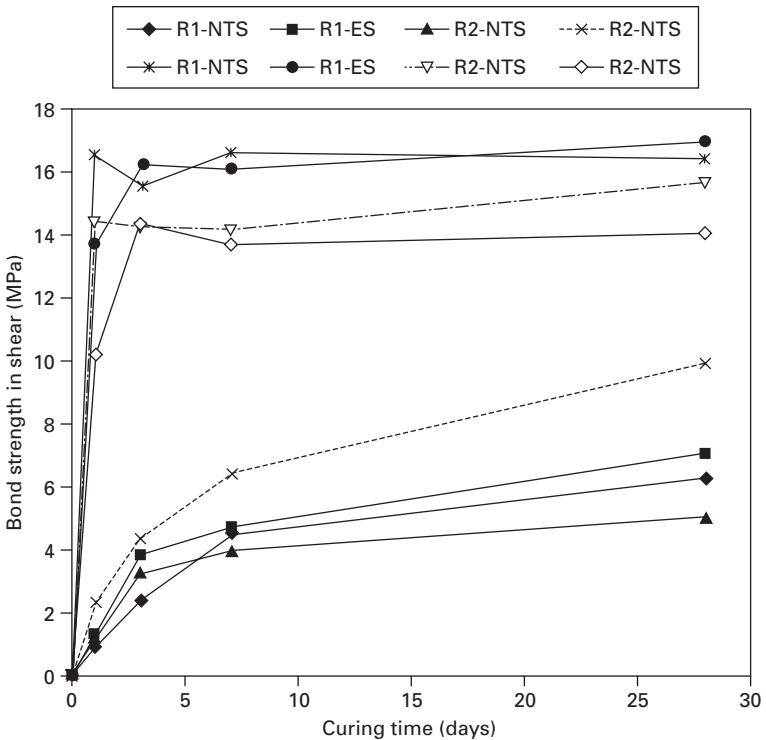


13.9 Slant specimen with a monolithic failure.

were respectively, GP-MF and GP-WF. It can be seen that specimens repaired with mine waste geopolymeric binder present the high bond strength even at early ages (Fig. 13.10). Specimens repaired with geopolymer binder with 1 day curing have higher bond strength than specimens repaired with current commercial products even after 28 days curing. Specimens repaired with mine waste geopolymeric binder are influenced not by chemical treatment in sawn concrete surface substrate, but by the use of concrete surfaces as cast against formwork. Those kinds of surfaces are rich in calcium hydroxide but lack exposed coarse aggregates which could contribute to improve bond strength due to silica dissolution from aggregate surface.

Commercial repair products used in the investigation were supplied as pre-packed blend of graded aggregates with a maximum size 2 mm, Portland cement, silica fume, fibres and other additives. The typical density of the fresh material is 2100 kg/m³. The repair products are ready for on-site mixing and use, requiring only the addition of clean water.

The strength performance of commercial repair products is very dependent on the curing time and that constitutes a serious setback when early bond strength is required. Results show that bond strength when using repair product R2 are clear influenced by surface treatment.



13.10 Slant shear test results.

Table 13.8 shows the number of the specimens that had an adhesive failure. As can be seen, only the slant specimens repaired with geopolymeric binder and saw concrete substrates present monolithic failures due to its high bond strength. The failure mode for specimens repaired with current commercial repair products R1 and R2 are identical and occurs in the interface section, independently of the concrete substrate surface treatment. Table 13.9 shows the coefficient of variation (COV) of bond strength results according to curing age. The results show that in all cases COV decreases with curing age and shear strength increase except in the case of specimens repaired with mine waste geopolymeric binder and with chemical surface treatment (GP-ES). Specimens repaired with current commercial repair products R1 and R2 present very high COV at early ages. However, after 28 days curing this factor show acceptable values. For both commercial repair products COV results are clearly influenced by surface treatment. Specimens repaired with mine waste geopolymeric binder shows low COV values even at early ages which are not influenced by the chemical treatment. When comparing COV results in specimens repaired with current commercial repair products and geopolymeric binder it seems clear that the last repair solution is much more reliable. The explanation to that behaviour relies on the fact that OPC

Table 13.8 Specimens with an adhesive failure

		Repair material and substrate surface treatment							
		R1		R2		GP			
		ES	NTS	ES	NTS	ES	NTS	MF	WF
Curing days	1	4	4	4	4	2	0	4	4
	3	4	4	4	4	0	0	4	4
	7	4	4	4	4	0	0	4	4
	28	4	4	4	4	0	0	4	4

ES (etched surface)

NTS (no treatment surface)

MF (metallic formwork)

WF (wood formwork)

Table 13.9 Coefficient of variation of bond strength (%)

		Repair material and substrate surface treatment							
		R1		R2		GP			
		ES	NTS	ES	NTS	ES	NTS	MF	WF
Curing days	1	23.0	33.3	21.7	27.3	6.7	6.7	12.5	14.8
	3	13.1	20.8	20.4	24.2	5.6	6.4	8.4	6.3
	7	8.5	17.7	14.1	20.0	5.6	6.0	7.7	5.8
	28	10.0	16.1	12.1	16.0	6.0	6.1	7.0	1.4

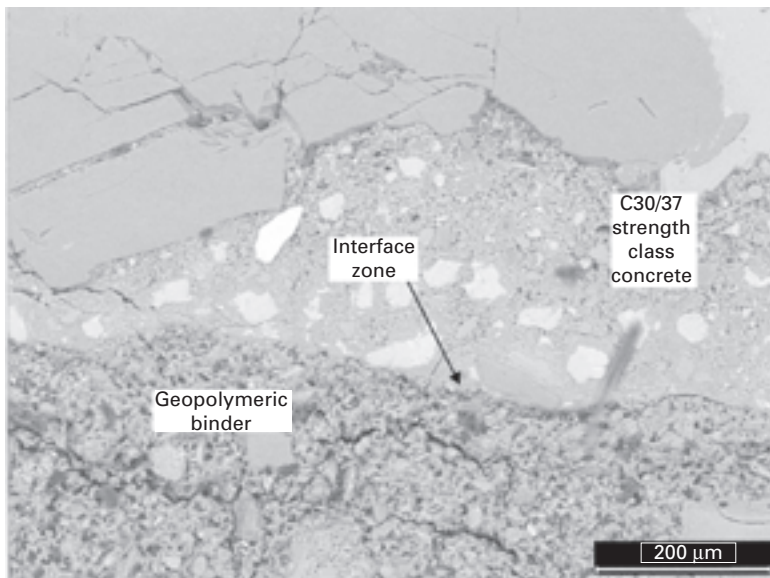
concrete substrate surfaces are rich in calcium hydroxide that will react to geopolymeric based binder due to the need of positive ions such as Ca^{2+} to be present in the framework cavities to balance the negative charge of AlO_4 groups and also to the mechanical interlock yield by silica ions release from aggregate surface when subject to the high alkaline activator. Therefore concrete substrates will chemically bonds to the geopolymeric phase as it can be seen by the absence of a clear interfacial transition zone in a microstructural level (Fig. 13.11).

13.5 Durability and environmental performance

For the durability performance, abrasion and acid resistance were assessed for mine waste geopolymeric mixtures and comparable OPC binders. The environmental performance was assessed with leaching tests.

13.5.1 Abrasion resistance

The abrasion resistance was evaluated using the Los Angeles abrasion apparatus (ASTM C 131-06), which consists of a metal cylinder, where eight $50 \times 50 \times 50 \text{ mm}^3$ cubic specimens have been placed together with eight steel spheres. The cylinder is then submitted to 1000 full rotations,

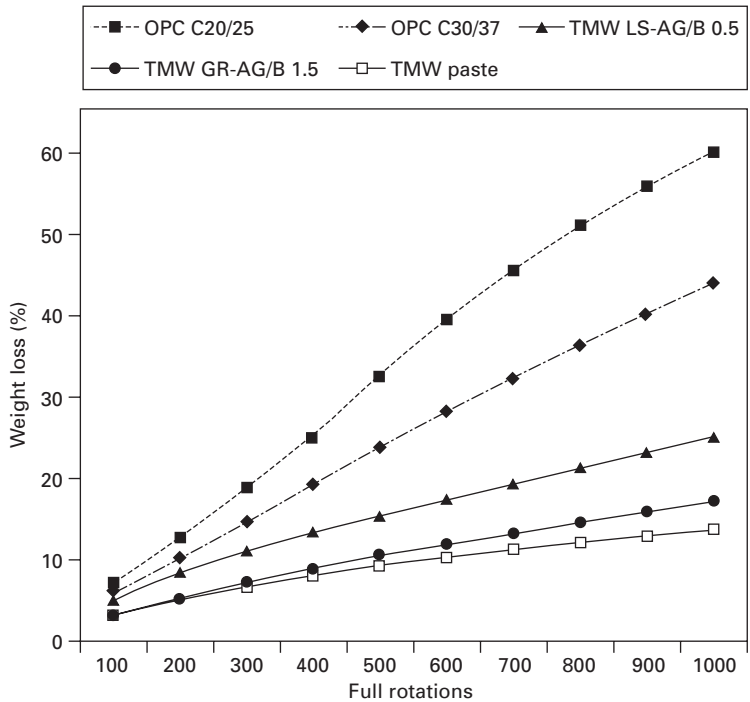


13.11 SEM micrograph of interfacial transition zone between concrete substrate and mine waste geopolymeric binder.

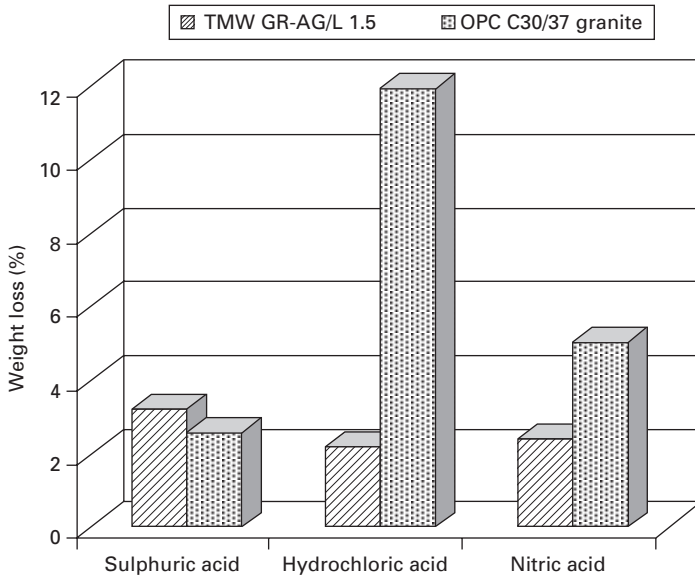
and after every 100 full rotations the specimens are weighed to detect the weight change. Mine waste binder specimens show a low level of weight loss while in OPC specimens a severe weight loss was observed. For mine waste binders the higher abrasion resistance was achieved in paste specimens (Fig. 13.12). This result is related to the fact that mine waste paste had the highest compressive strength. As for OPC specimens, abrasion resistance seems to be more influenced by the compressive strength than for the aggregates used in the mix.

13.5.2 Acid resistance

Acid resistance of OPC C30/37 concrete and mine waste binders as weight loss is shown in Fig. 13.13. The resistance to acid attack was tested by immersion of the mine waste binders and OPC concrete $50 \times 50 \times 50 \text{ mm}^3$ specimens in 5% sulphuric, hydrochloric and nitric acid solutions during 28 days. To keep a constant pH, acid solutions were replaced after 14 days. After 28 days the specimens were oven-dried to achieve constant weight, and detachable particles were removed. The acid resistance was assessed by the differences



13.12 Abrasion resistance with the Los Angeles test for OPC and tungsten mine waste mud binders (TMWM).



13.13 Weight loss after acid attack.

in weight of dry specimens before and after acid attack, since compressive strength of specimens immersed in acid media could not be evaluated. With the exception of specimens immersed in sulphuric acid solutions, the OPC resistance to acid attack is rather poor, the weight loss of these specimens is due to the reaction between calcium hydroxide present at the surface of the specimens and the acid. The worst case scenario takes place when OPC specimens are subjected to hydrochloric acid. This type of acid reacts with calcium compounds leading to the formation of calcium chloride, which has extremely high solubility (46,1wt%) (Zivica and Baja, 2001). Weight loss results for mine waste binders are not very dependent on the type of acid. Other authors report different results for geopolymers based on fly ash and blast furnace slag (Allahverdi and Skvára; 2001a, 2001b, 2005). For mine waste geopolymeric specimens the weight loss is low; this behaviour may be due to the low water absorption of these binders and also to their low content in calcium hydroxide. Geopolymeric mine waste binders have low acid resistance performance when compared to geopolymeric binders based on metakaolin (Palomo *et al.*, 1999). These authors report compressive strength increase for geopolymer specimens immersed in acid.

13.5.3 Environmental assessment

The use of new binder as a building material requires the assessment of its environmental performance. For that, leaching tests have been carried

out according to DIN 38414 – S4. Leaching results show that all chemical parameters are below the limits established by the standard and can be considered an inert material (Table 13.10). As to the limits for water contamination set by the Portuguese Decree 236/98 (Table 13.11), it can be stated that although some chemical parameters are above the limits for drinkable water, all limits are met concerning water for irrigation purposes.

13.6 Future research trends

Further investigations about geopolymeric mine waste based binders are needed in order to clarify several aspects that current knowledge does not, such as:

- Since water content influences the amorphous nature of reaction products, it means that mine waste binders with low water level must be studied.
- The workability of mine waste mortars lacks the knowledge of which additives can overcome some stiff behaviour.
- In OPC binders the setting time is evaluated using pastes and the Vicat needle. Since the setting time for mine waste binders is influenced by the volume and nature of the aggregates, other ways to evaluate this property must be studied.
- The evaluation of shrinkage behaviour of mine waste binders does not assess the total shrinkage deformation, therefore shrinkage deformation must be assessed using cells placed inside the specimens.
- Mine waste binders present in some mixtures cause flexural strength loss. Several hypotheses have been raised to explain that behaviour but further research is needed to clarify that issue.
- Paste aggregate interface investigations performed so far are not enough to understand the contribution of coarse aggregates species dissolution

Table 13.10 Contaminant concentration in the wastewater by leaching process standard DIN 38414 – S4

Contaminant	Test results (mg/l)	Limits (DIN 38414 – S4)	
		Max.	Min.
Zinc	0.011	2	5
Arsenic	< 0.002	0.1	0.5
Lead	0.197	0.5	1.0
Copper	0.062	2	5
Manganese	0.019	–	–
Iron	0.203	–	–
Potassium	123.75	–	–
Sodium	3792.5	–	–
Magnesium	0.163	–	–
Sulphates	< 0.003	500	1500

Table 13.11 Water quality according to the Portuguese Decree 236/98 (mg/l)

Constituents	Appendix I						Drinkable water Appendix VI		Irrigation water Appendix XVI	
	A1		A2		A3		VMR	VMA	VMR	VMA
	VMR	VMA	VMR	VMA	VMR	VMA				
Zinc	0.5	3.0	1.0	5.0	1.0	5.0	(*)	–	2	10
Arsenic	0.01	0.05	–	0.05	0.05	0.1	–	0.05	0.1	10
Lead	–	0.05	–	0.05	–	0.05	–	0.05	50	20
Copper	0.02	0.05	0.05	–	1.0	–	(**)	–	0.2	5.0
Manganese	0.05	–	0.1	–	1.0	–	0.02	0.05	0.2	1.0
Iron	0.1	0.3	1.0	2.0	1.0	–	0.05	0.2	5.0	–
Potassium	–	–	–	–	–	–	0.01	0.01	–	–
Sodium	–	–	–	–	–	–	0.02	0.15	–	–
Magnesium	–	–	–	–	–	–	0.03	0.05	–	–
Sulphates	150	250	–	–	150	250	0.03	0.25	575	–

VMR – Maximum recommended value

VMA – Maximum value

* – After standard treatment (0.1×10^{-3})

** – After standard treatment (0.1)

A1 – Physical treatment and disinfection

A2 – Physical and chemical treatment and disinfection

A3 – Physical and chemical treatment of control and disinfection

and how these species influence reaction mechanisms involved in the hardening of these new binders. So, further investigations are needed using aggregates with different sizes and different porosity levels.

13.7 References

- Aitcin, P.C. (2001), *High performance concrete. Modern Concrete Technology 5 E & FN Spon.*
- Allahverdi, A., Škvára, F. (2001a), 'Nitric acid attack on hardened paste of geopolymeric cements – Part 1.' *Ceramics-Silikaty*, 45, 81–88.
- Allahverdi, A., Škvára, F. (2001b), 'Nitric acid attack on hardened paste of geopolymeric cements – Part 2.' *Ceramics-Silikaty*, 45, 143–149.
- Allahverdi, A., Škvára, F. (2005), Sulfuric acid attack on hardened paste of geopolymer cements. Part 1. Mechanism of corrosion at relatively high concentrations. *Ceramics-Silikaty*, 49, 225–229.
- Alonso, S., Palomo, A. (2001a), 'Calorimetric study of alkaline activation of calcium hydroxide metakaolin solid mixtures.' *Cement and Concrete Research*, 31, 25–30. doi:10.1016/S0008-8846(00)00435-X.
- Alonso, S., Palomo, A. (2001b), 'Alkaline activation of metakaolin and calcium hydroxide mixtures: Influence of temperature, activator concentration and solids ratio.' *Materials Letters* 47, 55–62. doi:10.1016/S0167-577X(00)00212-3.
- BRGM (2001), 'Management of mining, quarrying and ore-processing waste in the European Union.' European Commission, DG environment, 50319–FR.
- Brodtkom, F.(2000), '*Good Environmental Practice in the European Extractive Industry: A reference guide.*' Centre Terre & Pierre, 88.
- Davidovits, J. (1999), 'Chemistry of geopolymeric systems. Terminology.' Proceedings of 99 Geopolymere Conference (1)9–40. France.
- Duxon, P., Provis, J.L., Lukey, G.C., Mallicoat, S., Kriven, W., van Deventer, J.S.J. (2005), 'Understanding the relationship between geopolymer composition, microstructure and mechanical properties.' *Colloids and Surfaces A*, 269, 347–58. doi:10.1016/j.colsurfa.2005.06.060.
- Eurostat, Theme 8 Environment and Energy (2003), 'Waste generated and treated in Europe.' Data 1990–2001.
- Fernandez-Jimenez, A., Palomo, A. (2003), 'Characterisation of fly ashes. Potential reactivity as alkaline cements.' *Fuel*, 82, 2259–2265. doi:10.1016/S0016-2361(03)00194-7.
- Fletcher, R. A., Mackenzie, K.J.D., Nicholson, C., Shimada, S. (2004), 'The composition range of aluminosilicate geopolymers.' *Journal of European Ceramic Society*, 25, 1471–1477. doi:10.1016/j.jeurceramsoc.2004.06.001.
- Hammond, A. (1988), 'Mining and quarrying wastes: a critical review.' *Engineering Geology*, 25, 17–31. doi:10.1016/0013-7952(88)90016-6.
- Hardjito, D., Wallah, S. E., Sumajouw, D., Rangan, B. V. (2004), 'Fly ash based geopolymer concrete, Construction material for sustainable development.' *Concrete World: Engineering & Materials*, American Concrete Institute, India.
- Harrison, D. J., Bloodworth, A. J., Eyre, J. M., Macfarlane, M., Mitchell, C. J., Scott, P. W., Steadman, E. J. (2002), '*Utilisation of mineral waste:cases studies.*' BGS Commissioned Report CR/02/227 N.
- He, C., Makovic, E., Osbaeck, B. (1995), 'Thermal stability and pozzolanic activity of raw and calcined illite.' *Applied Clay Science*, 9, 337–354. doi:10.1016/S0169-1317(00)00011-9.

- Kirschner, A., Harmuth, H. (2004), 'Investigation of geopolymer binders with respect to their application for building materials.' *Ceramics – Silikaty*, 48, 117–120.
- Macphee, D. E. (1989), 'Solubility and aging of calcium silicate hydrates in alkaline solutions at 25°C.' *Journal of the American Ceramic Society*, 72, 646–654. doi:10.1111/j.1151-2916.1989.tb06189.x.
- Mazzucato, E., Artioli, G., Gualtieri, A (1999), 'High temperature dehydroxylation of muscovite 2M.' *Physics and Chemistry of Minerals*, 26, 375–381.
- Mitchell, C. J., Harrison, D. J., Robinson, H. L., Ghazireh, N. (2004), 'Minerals from waste: recent BGS and Tarmac experience in finding uses for mine and quarry waste.' *Minerals Engineering*, 17, 279–284. doi:10.1016/j.mineng.2003.07.020.
- Neiva, A. M. R. (1987), 'Geochemistry of white micas from Portuguese tin and tungsten deposits.' *Chemical Geology*, 63, 299–317. doi:10.1016/0009-2541(87)90168-9.
- Neville, A. M. (1997), '*Properties of concrete*.' Fourth and Final Edition (1997). J. Wiley.
- Neville, A., Aitcin, P. (1998), 'High performance concrete-An overview.' *Materials and Structures/ Materiaux et Constructions*, 31, 111–117.
- Palomo, A., Blanco-Varela, M. T., Granizo, M.L., Puertas, F., Vazquez, T., Grutzeck, M. W. (1999), 'Chemical stability of cementitious materials based on metakaolin.' *Cement and Concrete Research*, 29, 997–1004. doi:10.1016/S0008-8846(99)00074-5.
- Pinto, A. T. (2004), *Metakaolin alkali-activated based binders*. PhD Thesis, University of Minho. Portugal. [in Portuguese].
- Puura, E., Marmo, L., Marco, A. (2002), 'Mine and quarry waste – the burden from the past.' Directorate General Environment of the European Commission, Italy.
- Rashid, M. A., Mansur, M. A., Paramasivam, P. (2002), 'Correlations between mechanical properties of high strength concrete.' *Journal of Materials in Civil Engineering*, 230–238. doi:10.1061/(ASCE)0899-1561(2002)14:3(230).
- Salvador, S. (1995), 'Pozzolanic properties of flash-calcined kaolinite. A comparative study with soak-calcinated products.' *Cement and Concrete Research* 25, 102–112. doi:10.1016/0008-8846(94)00118-1.
- Salvador, S. (2000), 'A semi-mobile flash dryer/calciner unit manufacture pozzolana from raw clay soils – application to soil stabilization.' *Construction and Building Materials*, 14, 109–117. doi:10.1016/S0950-0618(00)00005-2.
- Stade, H. (1989), 'On the reaction of CSH with alkali hydroxides.' *Cement and Concrete Research* 19, 802–810 doi:10.1016/0008-8846(89)90051-3.
- Tazawa, E., Myazawa, M. (1995), 'Experimental study on mechanism of autogenous concrete shrinkage of concrete.' *Cement and Concrete Research*, 25, 1633–1638. doi:10.1016/j.cemconres.2004.05.050.
- Teychenné, D. C. (1978), '*The used of crushed rock aggregates in concrete*.' Building Research Establishment, Garston.
- Torgal, F. P., Castro Gomes, J. P. (2006), 'Influence of physical and geometrical properties of granite and limestone aggregates on the durability of a C20/25 strength class concrete.' *Construction and Building Materials*, 20, 1079–1088. doi:10.1016/j.conbuildmat.2005.01.063.
- Torgal, F. P., Castro Gomes, J. P., Jalali, S. (2007a), 'Investigations on mix design of tungsten mine waste geopolymeric binder.' *Construction and Building Materials*, 22, 9, 1939–1949. doi:10.1016/j.conbuildmat.2007.07.015.
- Torgal, F. P., Castro Gomes, J. P., Jalali, S. (2007b), 'Properties of tungsten mine waste geopolymeric binder.' *Construction and Building Materials*, 22, 6, 1201–1211. doi:10.1016/j.conbuildmat.2007.01.022.

- Torgal, F. P., Castro Gomes, J. P., Jalali, S. (2007c), 'Investigations about the effect of aggregates on strength and microstructure of geopolymeric mine waste mud binders.' *Cement and Concrete Research*, 37, 933–941 doi:10.1016/j.cemconres.2007.02.006.
- Torgal, F. P., Castro Gomes, J. P., Jalali, S. (2008), 'Adhesion characterization of tungsten mine waste geopolymeric binder. Influence of OPC concrete substrate surface treatment.' *Construction and Building Materials*, 22, 154–161. doi:10.1016/j.conbuildmat.2006.10.005.
- Wang, H., Li, H., Yan, F., Yan (2005), 'Synthesis and mechanical properties of metakaolinite-based geopolymer.' *Colloids and Surfaces A*, 268, 1–6. doi:10.1016/j.colsurfa.2005.01.016.
- Yip, C. K., Lukey, G. C., van Deventer, J. S. J. (2005), 'The coexistence of geopolymeric gel and calcium silicate hydrate gel at the early stage of alkaline activation.' *Cement and Concrete Research*, 35, 1688–1697. doi:10.1016/j.cemconres.2004.10.042.
- Yip, C. K., Lukey, G. C., Provis, J. L., van Deventer, J. S. J (2008), 'Effect of calcium silicate sources on geopolymerisation.' *Cement and Concrete Research*, 38, 554–564. doi:10.1016/j.cemconres.2007.11.001.
- Zhou, F. P., Lydon, F. D., Barr, B. I. (1995), 'Effect of coarse aggregate on elastic modulus and compressive strength of high performance concrete.' *Cement and Concrete Research*, 25, 177–186. doi:10.1016/0008-8846(94)00125-I.
- Zivica, V., Bazja, A. (2001), 'Acid attack of cement based materials – a review. Part 1. Principle of acid attack.' *Construction and Building Materials*, 15, 331–340. doi:10.1016/S0950-0618(01)00012-5.

Utilisation of non-thermally activated clays in the production of geopolymers

K J D MACKENZIE, Victoria University of Wellington,
New Zealand

Abstract: This chapter discusses the structural effects of the thermal pre-treatment of clays, as required in conventional synthesis of aluminosilicate geopolymers from metakaolin. It then considers alternative methods of pre-treatment for producing similar effects on clays, to synthesise lower-energy geopolymers. The alternative pre-treatments include mechanochemical processing (energetic grinding) of the raw clay and treatment with acid or alkali. The chapter also briefly discusses solid-state methods suitable for producing unusual geopolymers, and a soft chemical synthesis that eliminates the need for the solid aluminosilicate source.

Key words: thermal pre-treatment of clays, acid and alkali pre-treatment of clays, solid-state geopolymer synthesis, soft chemical geopolymer synthesis.

14.1 Introduction

The conventional method of producing aluminosilicate geopolymers as originally proposed by their inventor, Joseph Davidovits, involved the reaction of fully dehydroxylated kaolinitic clay (known as metakaolinite) with an alkaline silicate solution such as sodium or potassium silicate, or a mixture of both, under strongly alkaline conditions (Davidovits and Davidovics, 1988; Davidovits, 1991).

Dehydroxylation of kaolinite occurs at temperatures as low as 500–550°C, but the thermal treatment temperature of 800°C recommended in the original Davidovits literature clearly indicates the perception that the dehydroxylation reaction should be fully complete. Since one of the main advantages of geopolymer materials is the energy saving resulting from their ability to set at ambient temperatures, this advantage is offset by the expenditure of energy required to pre-process the principal solid reactant, and any reduction in this requirement (without compromising the properties of the product) would be of great benefit.

It should be noted that the Davidovits invention is not the first use of alkali-treated clays to produce useful products such as building materials. Earlier workers, including Gluchovskii (1959) and Berg *et al.* (1970) treated a variety of aluminosilicate raw materials with alkaline compounds to produce useful products. In particular, Berg *et al.* (1970) reacted undehydroxylated

kaolinite clay with NaOH at 140–170°C, under which conditions 30–50% of the kaolinite was transformed to the zeolite mineral hydroxysodalite, $\text{Na}_2\text{Al}_2\text{Si}_2\text{O}_8 \cdot \text{H}_2\text{O}$ by the reaction



The resulting hydroxysodalite strongly binds other mineral particles such as quartz sand or brick wastes and was used to form building materials with high abrasion resistance and frost resistance. The addition of synthetic or natural colouring pigments enabled the products to be used as decorative claddings (Berg *et al.*, 1970). The recommended production process involved blending raw kaolinite with NaOH solution and sand, pressing to the required shape then heating at 140–170°C for 2hr.

A seemingly related application of geopolymerisation of unheated soil clays is the stabilisation of pozzolanic soils by reaction with strong NaOH solution or an alkaline solution of NaAlO_2 , setting to give a strong material with the XRD and NMR characteristics of a conventional geopolymer (Verdolotti *et al.*, 2008). However, the pozzolanic soils in this case are unusual in having already been subjected to elevated temperatures by volcanic action and therefore are not strictly comparable with the undehydroxylated clays from which it would be energetically advantageous to be able to synthesise geopolymers.

Although there are similarities between these products and the geopolymers of Davidovits, they bring into focus the question addressed by Škvára (2007) as to how geopolymers are related to other alkali-activated materials. It has been suggested (Škvára, 2007) that reaction mixtures containing a high proportion of the solid phase form the predominantly X-ray amorphous solid products described by Davidovits as geopolymers; other reaction conditions and/or raw materials can produce a range of zeolitic cementing compounds or gels (Škvára, 2007). This raises questions about the effect of reaction conditions (alkali type, concentration, water content, reaction temperature, etc.), all of which have been extensively studied but are outside the scope of this chapter.

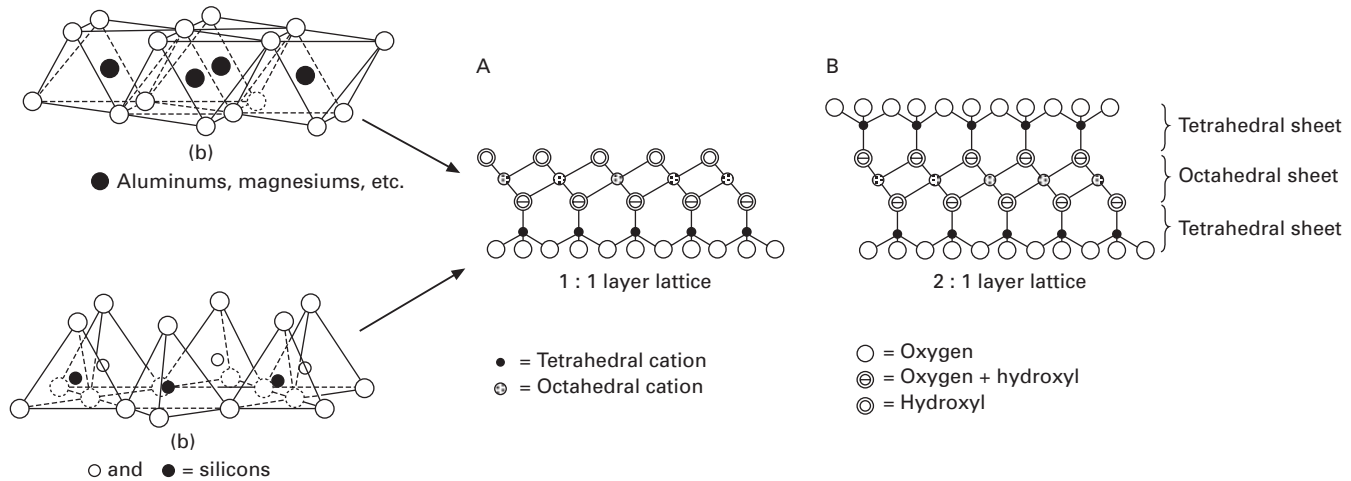
Here, the influence of the structure and composition of the aluminosilicate clay minerals on the formation of Davidovits-type geopolymers will be considered, and in particular, to what extent thermal pre-treatment modifies the initial structure, making the minerals more reactive to alkali and thus more amenable to geopolymer formation. This leads to a consideration of other possible pre-treatments that might have the same effect on the mineral structure and reaction mechanism. The discussion is also briefly extended to other methods for forming geopolymer precursors, by either solid-state reactions of undehydroxylated clays or by the elimination of the clay altogether, utilising the soluble components that in conventional clay-based syntheses are derived from the clay minerals themselves.

14.2 Dehydroxylation of 1:1 layer-lattice aluminosilicate minerals

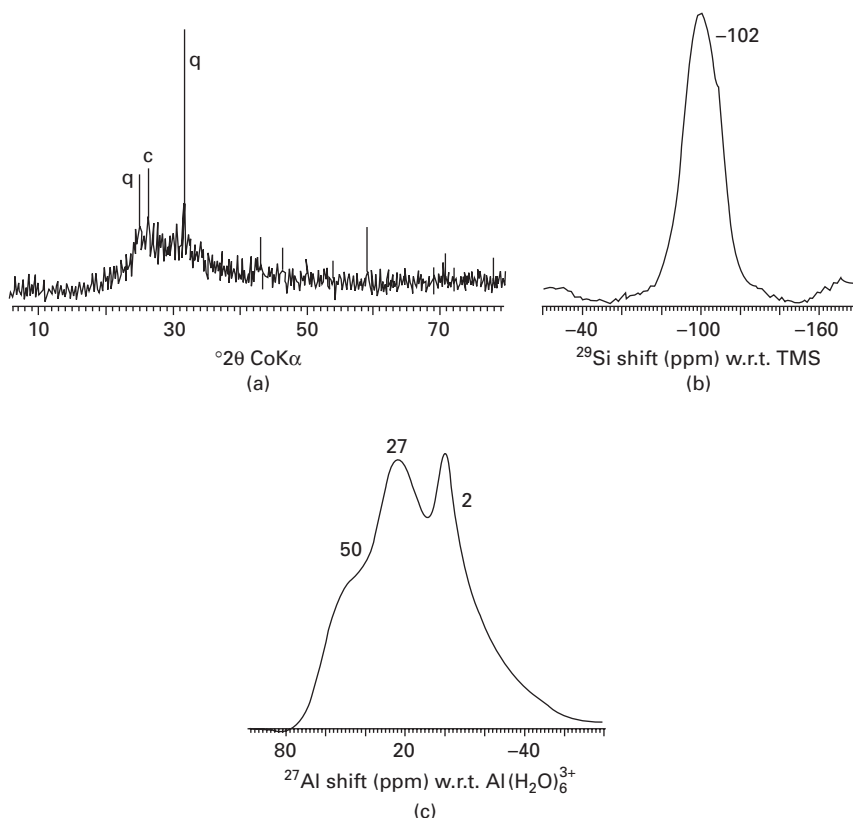
As a starting point, it is necessary to understand the effect of conventional thermal dehydroxylation on the structure and reactivity of the 1:1 layer-lattice aluminosilicate clay minerals, since this is the method for producing metakaolin, the most commonly used starting material in conventional Davidovits-type geopolymer synthesis.

14.2.1 Kaolinite dehydroxylation

The best-known representative of the 1:1 layer-lattice aluminosilicates is kaolinite, $\text{Al}_2\text{Si}_2\text{O}_5(\text{OH})_4$. This has a structure consisting of silicate sheets made up of silicon-oxygen tetrahedra joined by their basal apical oxygens to form a hexagonal network (Fig. 14.1A). These tetrahedral layers (a) are interspersed with sheets formed from aluminium-oxygen octahedra (b) joined by sharing their octahedral edges to form an ab ab ab repeating stacking sequence. To balance the charge in this structure, some of the oxygens in the layer common to both silica and alumina units are hydroxyl groups, as are all the octahedral oxygen positions facing away from the common oxygen layer. Thus, it is the aluminium atoms that are intimately associated with the hydroxyl groups, and are most influenced by their thermal removal as hydroxyl water, an endothermic process that occurs at approximately 500–600°C with a mass loss of approximately 14% (Deer *et al.*, 1962). The product of this heating, called metakaolinite (or kaolinite dehydroxylate), is extremely disordered and amorphous to X-rays (Fig. 14.2a). Radial distribution functions calculated from X-ray scattering experiments (Gualtieri and Bellotto, 1998) show that the loss of long-range order reflects the disorder of the original kaolinite. The ^{27}Al solid-state MAS NMR spectrum of metakaolinite (Fig. 14.2c) contains typically three broad resonances at about 53, 28 and 4 ppm corresponding to Al in 4, 5 and 6-fold coordination with oxygen (MacKenzie and Smith, 2002). The disordered nature of this material is confirmed by its ^{29}Si MAS NMR spectrum (Fig. 14.2b), in which the sharp kaolinite resonance at –92 ppm broadens and shifts to about –102 ppm in metakaolinite, consistent with a range of Si-O environments and a flattening of the Si-O layers (MacKenzie and Smith, 2002). These gross distortions of the kaolinite structure upon thermal dehydroxylation, first investigated by solid-state MAS NMR spectroscopy (MacKenzie *et al.*, 1985), explain the increased reactivity of metakaolinite in the geopolymerisation reaction, and also help to shed light on the reasons for the different behaviour of the 2:1 layer lattice aluminosilicate minerals (see below).



14.1 Structures of the layer-lattice aluminosilicate minerals, showing the octahedral Al-O and tetrahedral Si-O sheets and the way in which these are stacked in (A) 1:1 layer lattice aluminosilicates (e.g., kaolinite) and (B) 2:1 layer lattice aluminosilicates (e.g. pyrophyllite).



14.2 (a) XRD powder pattern of dehydroxylated halloysite. The sharp peaks superimposed on the broad baseline hump result from the crystalline impurities quartz (q) and cristobalite (c). (b) 11.7T ^{29}Si MAS NMR spectrum. (c) 11.7T ^{27}Al MAS NMR spectrum.

14.2.2 Halloysite dehydroxylation

Halloysite is of similar chemical composition to kaolinite, but of different morphology, being composed of kaolinite plates rolled up into tubes inside which additional water is located. Thus, on heating, the water is lost in two endothermic events, the first, at about 150°C, corresponding to a 2.6% loss of the internal hydration water, and the second, at about 550°C corresponding to normal dehydroxylation. From the point of view of geopolymerisation, halloysite dehydroxylate behaves identically to metakaolin in every respect, but has been the raw material of preference for some fundamental studies (MacKenzie *et al.*, 2007) because of its availability in a highly pure form.

14.3 Dehydroxylation of 2:1 layer-lattice aluminosilicate minerals

The 2:1 layer-lattice aluminosilicate minerals form a class in which geopolymerisation is much more difficult, even starting from the dehydroxylated material. To understand this difference in reactivity, it is necessary to consider the structure of these minerals (Fig. 14.1B), and how this structure is changed by dehydroxylation. The representative 2:1 aluminosilicate mineral is pyrophyllite, $\text{Al}_4\text{Si}_8\text{O}_{20}(\text{OH})_4$ but other 2:1 layer-lattice minerals structurally related to pyrophyllite are montmorillonite, in which varying degrees of substitution of octahedral aluminium by magnesium occur, and muscovite mica, in which the octahedral sites are exclusively occupied by aluminium but there is extensive substitution of the tetrahedral silicon sites by aluminium (Deer *et al.*, 1962).

14.3.1 Pyrophyllite dehydroxylation

The structure of pyrophyllite, $\text{Al}_4\text{Si}_8\text{O}_{20}(\text{OH})_4$ consists of an octahedral Al-O layer (b) sandwiched between two tetrahedral Si-O layers (a) (Fig. 14.1B), with a stacking sequence of aba aba aba. The silica tetrahedra point inwards and, as in kaolinite, there is little or no tetrahedral substitution of silicon by aluminium and the hydroxyl ions are associated with the Al-O units. On heating to the dehydroxylation temperature (about 550–900°C) pyrophyllite dehydroxylate is formed. This is a phase with a sharp XRD pattern only slightly different from the unheated mineral (Wardle and Brindley, 1972). This X-ray powder pattern is consistent with a structure in which the Al-O configuration has changed from 4-fold to 5-fold trigonal bipyramidal (Wardle and Brindley, 1972), confirmed by the ^{27}Al NMR spectrum that shows a sharp quadrupolar lineshape consistent with 5-fold coordinated Al in a single well-defined site (Fitzgerald *et al.*, 1989). The crystallinity of pyrophyllite dehydroxylate and the protection of its octahedral layers by the enclosing tetrahedral Si-O layers of the 2:1 structure suggests that geopolymerisation of either the raw or dehydroxylated mineral will be difficult, as proves to be the case (MacKenzie *et al.*, 2008). On the basis of this structural reasoning, similar difficulties might be encountered in geopolymer formation from the other 2:1 layer-lattice minerals montmorillonite, muscovite and the fully magnesium analogue talc, $\text{Mg}_6\text{Si}_8\text{O}_{20}(\text{OH})_4$. However, as shown below, the reactivity of some of these layer-lattice silicate minerals to alkali is also influenced by the degree and type of substitution in the tetrahedral and octahedral layers. This aspect will be addressed next.

14.4 Reactions of thermally dehydroxylated clays with alkali

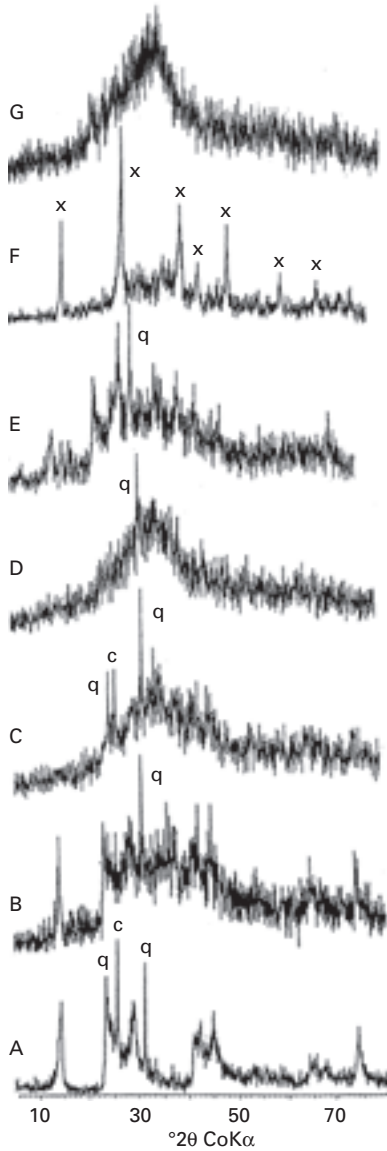
Since the geopolymerisation reaction involves the interaction of dehydroxylated clays with strong alkali, it is of interest to briefly review the plentiful experimental data on this aspect. Considerable information has been accumulated (see the references in Okada and MacKenzie, 2006), mostly from the point of view of the formation of nanoporous structures by selectively leaching out the octahedral or tetrahedral layers of the clay mineral. The conclusions most relevant to geopolymerisation are:

- Undehydroxylated clays are generally unreactive to both alkali and acid attack, but are rendered much more reactive by dehydroxylation.
- Both Al-O and Si-O are soluble in highly alkaline conditions, but the relative rates of dissolution of the two species are considerably different.
- The reactivity of a clay mineral is influenced by the degree of substitution in its tetrahedral layers, minerals containing a higher degree of tetrahedral Al-for-Si substitution showing higher leaching rates in acid (MacKenzie *et al.*, 2004). The crystallinity and particle size of the clay also influences its reactivity towards leaching.

Applying these conclusions to the specific case of geopolymer synthesis from metakaolin, alkali would be expected to have much less effect on the dehydroxylated clay than acid, which can be used to selectively leach away the octahedral sheet, leaving a framework of nanoporous silica (Okada *et al.*, 1998; Madhusoodana *et al.*, 2006). Significant reaction with alkali only occurs in kaolinite heated to 980°C, well above the dehydroxylation temperature, at which point the silica and alumina begins to separate (Okada *et al.*, 1995).

The relationship between the degree of thermal dehydroxylation of a clay and its ability to form a geopolymer has been studied for the 1:1 kaolinite-type mineral halloysite (MacKenzie *et al.*, 2007). In this and related studies, several criteria have been adopted to determine successful geopolymer synthesis, namely, (a) setting and hardening at ambient temperatures (up to 60°C), (b) formation of an X-ray amorphous compound, (c) conversion of essentially all the aluminium to tetrahedral coordination (as determined by ²⁷Al solid-state MAS NMR), (d) appearance of a single broad ²⁹Si MAS NMR resonance at about -90 ppm corresponding to a range Al-substituted Si units, predominantly Q⁴(2Al) or Q⁴(3Al) (Barbosa *et al.*, 2000).

These studies confirmed the inability of undehydroxylated halloysite to form a viable geopolymer although some degree of reaction was observed; the samples set to some extent but did not achieve the texture and hardness of a well-formed geopolymer, the original halloysite XRD powder pattern (Fig. 14.3A) became more diffuse (Fig. 14.3B) but was not destroyed, and



14.3 XRD powder patterns of geopolymers synthesised from starting materials subjected to various pretreatments. A. Raw halloysite. B. Geopolymer from raw halloysite. C. Geopolymer from halloysite dehydroxylated at 550°C. D. Geopolymer from halloysite ground in a vibratory mill for 15 min. E. Geopolymer from halloysite leached with 0.1M HCl for 24 hr. F. Geopolymer from halloysite leached with 0.1M NaOH for 24 hr. G. Geopolymer from silica fume and sodium aluminate solution (Brew and MacKenzie, 2007). Key: q = quartz (ICDD no. 33-1161), c = cristobalite (ICDD no. 11-695), x = $6\text{NaAlSiO}_4 \cdot \text{Na}_2\text{CO}_3$ (ICDD no. 24-1045).

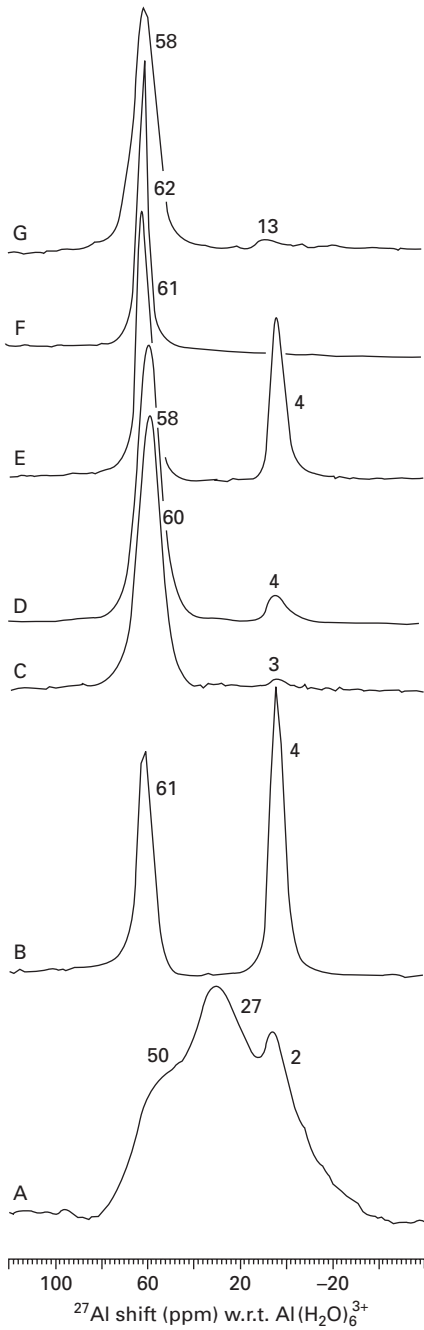
the sample retained approximately 60% of the original octahedral aluminium (Fig. 14.4B) (MacKenzie *et al.*, 2007). Thermal dehydroxylation for 2h at 550°C removed 77% of the hydroxyl water and produced a geopolymer with typical X-ray amorphous characteristics and only a small amount of residual octahedral aluminium (Fig. 14.4C). Thus, dehydroxylation at temperatures considerably lower than the previously recommended 800°C produced well-formed geopolymers from this particular clay, but the optimum temperature will depend on the clay, since Pinto and Vieira (2006) report the optimum thermal pre-treatment for geopolymer formation from a Portuguese kaolin is 750°C for 2 hr. There are indications that much higher thermal pre-treatment temperatures (1000°C) are deleterious, producing less-well hardened geopolymers containing an increased amount of octahedral Al (MacKenzie *et al.*, 2007). Although the high-temperature phase mullite, $\text{Al}_6\text{Si}_2\text{O}_{13}$, has not yet formed at this temperature, its incipient crystallisation to stable columns of octahedral AlO_6 units may render its transformation to a tetrahedral geopolymer framework increasingly difficult, despite the increased reactivity to alkali of the silicate units in clays heated to these temperatures.

In the case of the 2:1 layer-lattice aluminosilicate clay pyrophyllite, dehydroxylation at 800°C converts most of the octahedral aluminium to tetrahedral coordination and produces changes in the ^{29}Si MAS NMR spectrum (MacKenzie *et al.*, 2008; Sanchez-Soto *et al.*, 1997), but does not produce a viable hardened geopolymer. This has been attributed to the lack of a disordered, X-ray amorphous dehydroxylate formed by this clay and to the protection of the aluminate sheet from alkaline attack by its enclosure between two silicate sheets in each repeating layer (MacKenzie *et al.*, 2008).

Since in geopolymer synthesis additional soluble silica is added in the form of an alkali silicate solution, these results suggest that the most important role of thermal dehydroxylation is to render the aluminium portion of the clay mineral more soluble under the alkaline synthesis environment. It is now necessary to examine possible alternative methods for achieving this effect.

14.5 Methods for reproducing the effects of thermal dehydroxylation in clays

Thermal dehydroxylation results in: (a) the loss of structural water, (b) the destruction of the crystal structure of the clay (in 1:1 aluminosilicate clays), and (c) conversion of the octahedral aluminium to a mixture of 4, 5 and 6-fold coordination. Of these, (b) and (c) are probably the most important, and it might be expected that any other method for securing a similar effect in the mineral structure would have a beneficial effect on the geopolymerisation reaction.

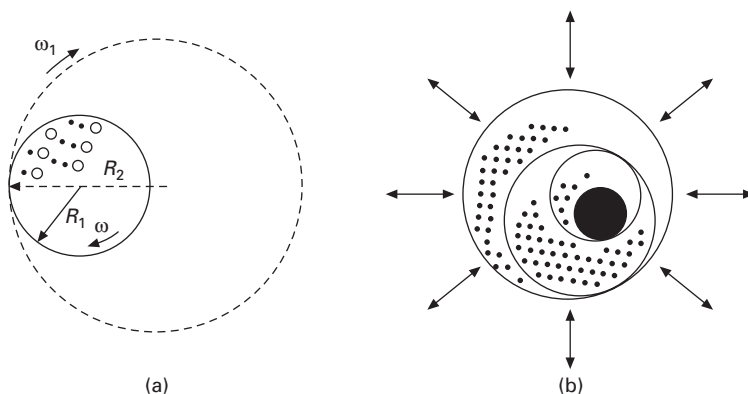


14.4 11.7T ^{27}Al MAS NMR spectra of geopolymers synthesised from starting materials subjected to various pretreatments. A. Raw halloysite. B. Geopolymer from raw halloysite. C. Geopolymer from halloysite dehydroxylated at 550°C. D. Geopolymer from halloysite ground in a vibratory mill for 15 min. E. Geopolymer from halloysite leached with 0.1M HCl for 24 hr. F. Geopolymer from halloysite leached with 0.1M NaOH for 24 hr. G. Geopolymer from silica fume and sodium aluminate solution (Brew and MacKenzie, 2007).

14.5.1 Mechanochemical processing (high-energy grinding)

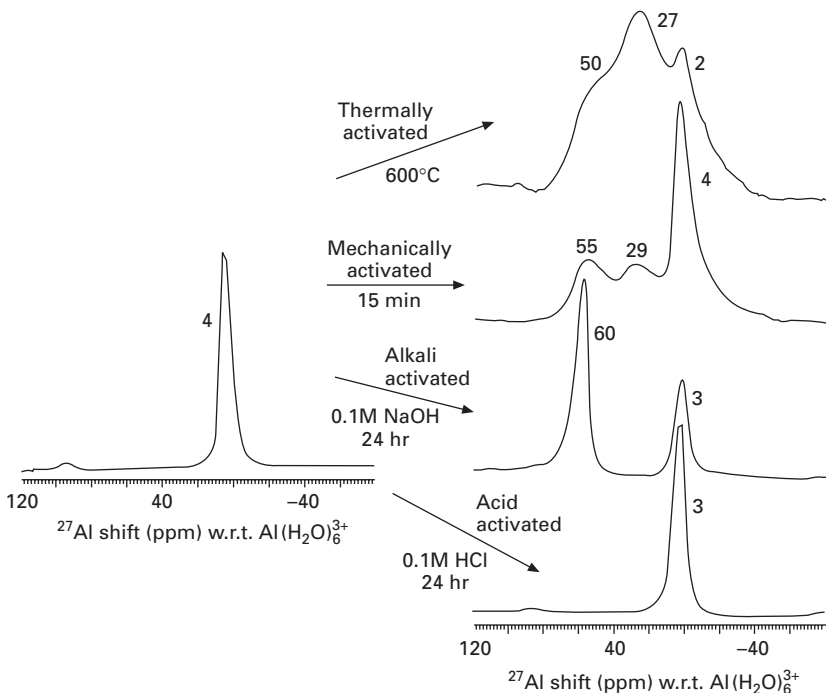
High-energy grinding is well known to disrupt the crystal structure of clay minerals, rendering them X-ray amorphous and making them more reactive to chemical treatment and solid-state reactions (Avvakumov *et al.*, 2001). Various forms of grinding mill are available for this purpose, ranging from ball mills in which the sample is rotated in a hard ceramic pot containing ceramic grinding balls to vibratory mills, in which the sample is rapidly vibrated between heavy concentric grinding rings. A variation of the ball mill is the planetary mill (Fig. 14.5a), in which the rotating grinding pot of radius R_1 is simultaneously rotated in the opposite direction at the end of an arm of radius R_2 , imparting an additional centrifugal force to the grinding balls (Avvakumov *et al.*, 2001). The theoretical power W of a planetary ball mill is a complex function of the mass of the grinding media, the pot diameter, the rotation frequency ω of the pot and the ratio of the radii R_1 and R_2 (Golosov and Molchanov, 1966).

Theoretical studies have identified the processes by which energy is transferred to a sample during grinding as friction, particle deformation and crack formation/cominution (Boldyrev and Avvakumov, 1971; Boldyrev, 2006). The interaction and charge-transfer chemistry of basic and acidic surface groups present on the surface of the reactants has also been investigated (Senna, 1993), as has the effect of residual liquid on soft mechanochemical reactions and possible mechanochemically-induced hydrothermal reactions (Temuujin *et al.*, 1998).



14.5 Schematic plan view of: (a) Planetary ball mill, showing the toughened ceramic grinding media (larger open circles and the sample grains (small black dots). (b) Vibratory mill, showing the heavy concentric grinding rings, the central grinding puck and the sample grains (small black dots).

Mechanochemical treatment in air of kaolinite reduces its particle size, causing it to become X-ray amorphous and rupturing the Al-OH and Al-O-Si bonds with the formation of molecular water (Avvakumov *et al.*, 2001). This bond rupture has been confirmed by IR spectroscopy (Klevtsov *et al.*, 1986) and is accompanied by a change in the aluminium coordination from 6-fold to a mixture of 4, 5 and 6-fold (Fig. 14.6) (MacKenzie, 2000). Thus, mechanochemical activation of sufficient energy has an effect on the kaolinite structure not unlike that of thermal dehydroxylation. There is considerable variation in the amount of energy transferred to the sample by the different mills, the most energetic being the vibratory type (Fig. 14.5b). A grinding study of halloysite clay (MacKenzie *et al.*, 2007) showed that grinding for 20h in a planetary ball mill reduced the X-ray crystallinity of the clay but did not change the aluminium coordination from octahedral to a lower coordination number, whereas grinding for 15 min. in a vibratory mill completely destroyed the X-ray crystallinity and produced a similar structural effect to thermal dehydroxylation (Fig. 14.6). When subjected to a geopolymer synthesis reaction, the clay ground in the planetary mill behaved similarly to the unground clay, but the product contained slightly more tetrahedral aluminium, reflecting a slight disruption of the structure. By contrast, the clay



14.6 The effect of various pre-treatments on the 11.7T ^{27}Al MAS NMR spectra of halloysite (left-hand spectrum).

ground for 15 min in the vibratory mill behaved in a similar manner to that dehydroxylated at 550°C, hardening to form a geopolymer containing only a small amount of residual octahedral aluminium (MacKenzie *et al.*, 2007). Thus, in the case of 1:1 aluminosilicates, grinding of sufficiently high energy to completely disrupt the clay structure could be a viable alternative to thermal dehydroxylation, but since both pre-treatment methods involve supplying energy to the clay, a comparison of the relative energy consumption is needed to determine the advantage, if any, of mechanochemical processing.

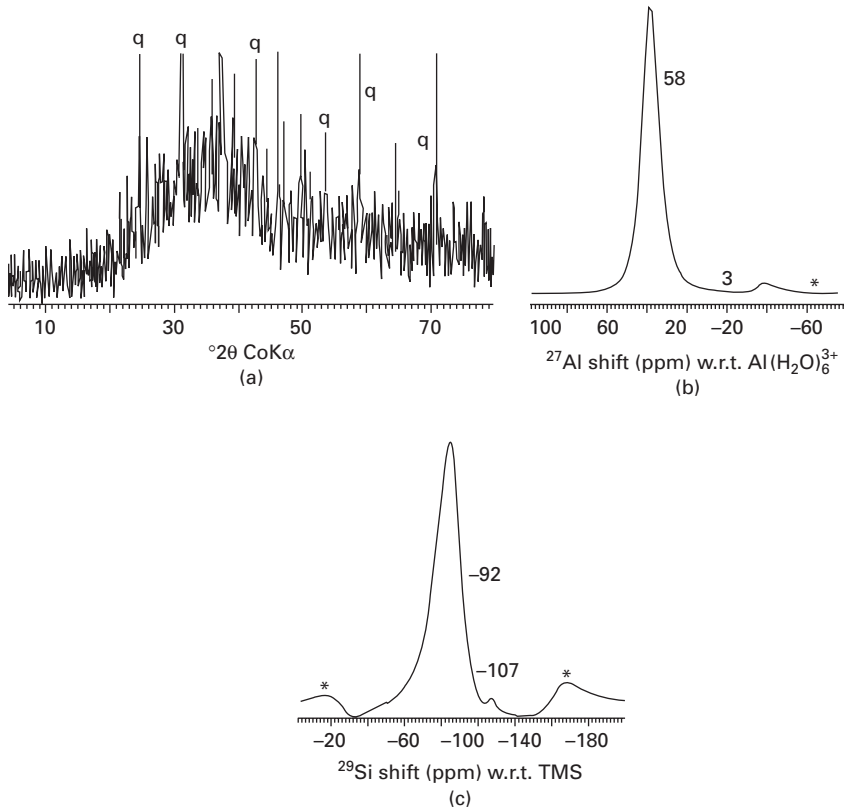
In the case of the 2:1 layer-lattice aluminosilicates typified by pyrophyllite, disruption of the mineral structure by high-energy milling has been reported to partially destroy the crystal structure and convert some of the 6-coordinate aluminium to 4 and 5-coordinated (Sanchez-Soto *et al.*, 1997). Grinding brings about the formation of an amorphous Al-O-Si phase, facilitating leaching of the aluminium (Temuujin *et al.*, 2003). The ^{27}Al NMR spectra of pyrophyllite samples ball-milled for 60hr are similar to those ground in a vibratory mill for 15 min, and, when subjected to a geopolymerisation reaction, set and harden well and show ^{27}Al and ^{29}Si MAS NMR spectra consistent with well-formed geopolymers (Fig. 14.7) (Mackenzie *et al.*, 2008). Unlike geopolymers from the 1:1 clay minerals, these products are not fully X-ray amorphous, and show traces of crystalline zeolites (MacKenzie *et al.*, 2008).

14.5.2 Chemical pre-treatment

Methods of rendering the clay mineral more reactive to geopolymer synthesis without the expenditure of additional energy are of even greater interest. Chemical treatment of clays has long been used to produce porous materials (Okada and MacKenzie, 2006), but this process is generally combined with thermal dehydroxylation or heating to even higher temperatures to make the clay sufficiently reactive to chemical treatment, thereby offsetting the possible energy advantage of chemical treatment alone. For this reason, geopolymer synthesis experiments have been carried out on unheated 1:1 aluminosilicate clays pre-treated with acid or alkali with the aim of rendering them more reactive (MacKenzie *et al.*, 2007).

Acid treatment (including phosphoric acid treatment)

Pre-treatment of halloysite clay with 0.1M HCl for up to 24 hr had no effect on the XRD pattern or the ^{27}Al (Fig. 14.6) or ^{29}Si MAS NMR spectra (MacKenzie *et al.*, 2007). When subjected to a geopolymer synthesis reaction, the product was similar to that from untreated halloysite, showing very poor strength and hardness and retaining the XRD pattern of the clay (Fig. 14.3E). However, the ^{27}Al MAS NMR spectrum (Fig. 14.4E) showed the presence

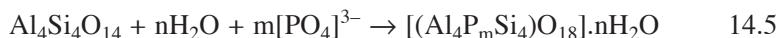


14.7 (a) XRD powder pattern, (b) 11.7T ^{27}Al MAS NMR spectrum and (c) 11.7T ^{29}Si MAS NMR spectrum of a geopolymer prepared from the undehydroxylated 2:1 layer-lattice aluminosilicate pyrophyllite ground in a vibratory mill for 15 min. Key: q = quartz, unmarked XRD peaks are from pyrophyllite. Asterisks denote spinning side bands.

of about 65% tetrahedral aluminium, suggesting that the acid treatment may have disrupted the octahedral layer to a slight extent, but not sufficiently to form a viable product (MacKenzie *et al.*, 2007). On this basis, it is possible that leaching with more concentrated acid may produce a better result, but in view of the known acid solubility of the octahedral layer, this may have the undesired effect of removing aluminium from the system.

The reaction of phosphoric acid with kaolinite and metakaolinite has been utilised to form geopolymers containing phosphorus in the tetrahedral network (Cao *et al.*, 2005). These materials differ from conventional geopolymers in being formed in acid rather than alkaline conditions, with no monovalent charge-balancing cations being required if the numbers of tetrahedral $[\text{PO}_4]^{3-}$ and $[\text{AlO}_4]^{5-}$ units are equal. The XRD diffractograms of the products indicate a lack of long-range atomic order characteristic of geopolymers

but the ^{27}Al MAS NMR spectra indicate the presence of predominantly octahedral aluminium, with two small tetrahedral resonances at 51 and 46 ppm, corresponding to $\text{Al}[\text{OSi}(\text{P})]_4$ and $\text{Al}[\text{OP}(\text{Si})]_4$ units respectively (Cao *et al.*, 2005). The suggested geopolymerisation reaction is:



Although this reaction proceeds well with metakaolin, as would be expected from the preceding discussion, undehydroxylated kaolinite gave a product without strength or hardness; a minimum dehydroxylation temperature of 450°C was required (Cao *et al.*, 2005). Thus, this is not a viable method for producing geopolymers from raw clay.

Alkali treatment

Since the geopolymerisation reaction is conducted under highly alkaline conditions, another potentially useful chemical approach is to pre-treat the clay with alkali. Studies in which halloysite was pre-soaked for up to 24 hr in 0.1M NaOH showed that this treatment resulted in the formation of significant amounts of the crystalline zeolite LTA ($\text{Na}_{12}\text{Al}_{12}\text{Si}_{12}\text{O}_{48}\cdot 27\text{H}_2\text{O}$), with the conversion of a significant amount of the original octahedral aluminium to tetrahedral (Fig. 14.6) (MacKenzie *et al.*, 2007). This process has begun even after only 3hr treatment. Although it might be expected that the formation of tetrahedral aluminium would significantly facilitate subsequent geopolymer synthesis, this appears to be offset by the presence of the crystalline zeolite phase, since although the product of geopolymer synthesis sets, it contains the XRD peaks of a crystalline sodium aluminium silicate carbonate (Fig. 14.3F). In this compound the carbonate is a guest species included in a sodalite cage during hydrothermal synthesis from kaolinite in the presence of sodium carbonate (Barrer and Cole, 1970). In the present case, its formation probably results from atmospheric carbonation of the excess alkali present (MacKenzie *et al.*, 2007). Both the ^{27}Al and ^{29}Si MAS NMR spectra are consistent with a normal geopolymer, but their resonances are uncharacteristically narrow (Fig. 14.4F), consistent with a crystalline product. Nevertheless, this approach is one of the more promising for reducing the energy required to render a 1:1 aluminosilicate clay mineral sufficiently reactive, and deserves further investigation.

14.6 Other methods for forming aluminosilicate geopolymers

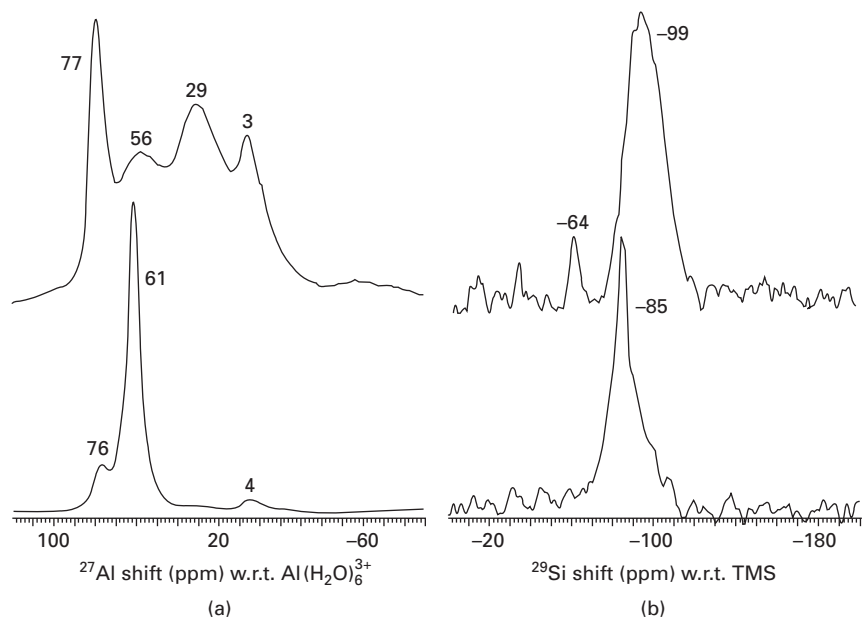
In addition to the conventional Davidovits geopolymer synthesis in which a thermally activated clay provides the labile aluminium and additional soluble silica is derived from an alkali silicate solution, two other proposed synthesis

methods will now be discussed. One of these utilises undehydroxylated clay in a solid-state reaction, while the other eliminates the need for the clay mineral altogether.

14.6.1 Solid-state synthesis

In this approach, undehydroxylated 1:1 aluminosilicate clay (low-grade kaolin) was reacted at 550°C for 4 hr with a mixture of sodium and potassium hydroxides in the weight ratio kaolin:NaOH:KOH = 6.5:1:1 at 550°C (Kolousek *et al.*, 2007). The product of this reaction was largely X-ray amorphous, with aluminium in predominantly tetrahedral coordination and SiO₄ units in predominantly Q⁴(4Al) and Q⁴(3Al) environments. Addition of sufficient water to this material to form a paste causes it to set and harden in 1 day to a product with XRD, ²⁷Al and ²⁹Si MAS NMR characteristics of a conventional geopolymer (Kolousek *et al.*, 2007). The mechanical strength of these materials is low (about 1 MPa), but can be increased significantly to 12-10 MPa by hydrothermal treatment for 1 day at 140°C resulting in the formation of zeolites (chabazite and phillipsite) (Koulosek *et al.*, 2007). In this respect, the product is not unlike that of Berg *et al.* (1970) in which the strength was developed by the formation of zeolites under hydrothermal treatment.

From an energy conservation point of view, the solid state synthesis offers no advantage, since, although it utilises an undehydroxylated starting material, the solid-state reaction is carried out at a typical dehydroxylation temperature. Nevertheless, this process represents a synthetic route to geopolymers that are difficult to make by the conventional Davidovits method. For example, the synthesis of lithium geopolymers from metakaolinite, lithium hydroxide and lithium silicate solution is difficult because of the low alkalinity and poor solubility of lithium hydroxide, but solid-state reaction at 550°C between undehydroxylated halloysite and lithium hydroxide produces a product that sets on the addition of water (O'Connor and MacKenzie, unpublished). The unhydrated product of the solid-state reaction has ²⁷Al and ²⁹Si NMR spectra similar to halloysite dehydroxylate, with an additional tetrahedral ²⁷Al resonance at 77 ppm (Fig. 14.8). The hardened material shows solid-state NMR features (Fig. 14.8) typical of a geopolymer (O'Connor and MacKenzie, unpublished). Likewise, the solid-state route has been successfully used to synthesise a gallium-germanium analogue of an aluminosilicate geopolymer from precursors formed by reaction of Ga₂O₃ and GeO₂ with an alkali hydroxide in the solid state (Durant and MacKenzie, unpublished). Thus, this synthesis technique is most appropriate to geopolymers that are difficult to prepare by other methods.



14.8 (a) 11.7T ^{27}Al and (b) ^{29}Si MAS NMR spectra of lithium geopolymer precursor prepared by solid state reaction at 550°C of halloysite with LiOH (upper spectra) and the hardened hydrated geopolymer (lower spectra).

14.6.2 Soft chemical synthesis

Bearing in mind that the soluble components, in particular the aluminium species, are derived in the conventional Davidovits-type geopolymer synthesis from clay minerals that have been rendered more reactive by the processes described above, a logical step might be to eliminate the need for the clay mineral altogether. This has been achieved by the use of a solution of sodium aluminate as the aluminium source, and a solution of sodium silicate prepared *in situ* by reaction of fine silica fume with NaOH (Brew and MacKenzie, 2007). The resulting products exhibit all the properties of geopolymers, curing and hardening at 40°C to an X-ray amorphous material (Fig. 14.3G) (provided the $\text{H}_2\text{O}:\text{Na}_2\text{O}$ ratio is <10), with all the aluminium in tetrahedral coordination (Fig. 14.4G). The ^{29}Si spectrum is better resolved than a typical geopolymer, containing three resonances. One, at -109 ppm is from the original silica fume, indicating the presence of some unreacted silica. The other two resonances, at -97 and -87 ppm correspond to $\text{Q}^4(1\text{Al})$ (or $\text{Q}^4(2\text{Al})$) and $\text{Q}^4(4\text{Al})$ units respectively (MacKenzie and Smith, 2002), and fall in the range normally under the envelope of the broad geopolymer Si spectrum (Duxson *et al.*, 2005). The crushing strength of the product, determined in triplicate on 4 cm cubes, was 26.3 MPa. Thus, provided the

$\text{H}_2\text{O}:\text{Na}_2\text{O}$ ratio is maintained below 10, this material satisfies the criteria of a conventional aluminosilicate geopolymer, but at higher water contents, the product contains increasing amounts of the crystalline zeolite LTA (Brew and MacKenzie, 2007).

14.7 Conclusions

The formation of viable aluminosilicate geopolymers from the 1:1 clay minerals kaolinite and halloysite (judged by the criteria of strength attainment at ambient temperatures, lack of long-range X-ray crystallinity and tetrahedral aluminium coordination) proceeds readily if the minerals are thermally dehydroxylated at temperatures of at least 550°C . The reaction does not proceed in undehydroxylated clays, although higher temperatures and hydrothermal conditions can render undehydroxylated kaolinite sufficiently reactive to form crystalline zeolites by reaction with alkali, producing strong materials.

Thermal dehydroxylation destroys the mineral crystallinity and changes the aluminium coordination from 6-fold to a mixture of 4, 5 and 6-fold, rendering the aluminium reactive to alkali under the ambient conditions of geopolymer synthesis. A similar effect can be secured by subjecting the clay to mechanochemical processing with sufficient energy to destroy the crystalline structure and convert the aluminium coordination to a mixture of 4, 5 and 6. Halloysite clay treated in this way produces viable geopolymers according to the above criteria, but this method of pre-treatment requires an input of energy and, in terms of convenience, may not present a significant advantage over thermal pre-treatment.

Chemical treatment of undehydroxylated halloysite clay with 0.1M mineral acid does not disrupt the crystal structure or change the aluminium coordination, and even the reaction of clay with more concentrated H_3PO_4 to form phosphate geopolymers occurs only with thermally dehydroxylated kaolinite. By contrast, pre-treatment of halloysite with 0.1M NaOH for 3 hr produces a significant amount of tetrahedral aluminium, reflecting the conversion to the crystalline zeolite LTA. This mixture sets and hardens, but contains crystalline material and its solid-state NMR spectra are abnormally narrow for a geopolymer. Nevertheless, pre-treatment of the clay with alkali solution seems to represent the best of these methods for reducing the energy consumption of geopolymerisation.

By contrast with the 1:1 aluminosilicate clays, it is much more difficult to increase the reactivity of the corresponding 2:1 clays sufficiently to form geopolymers, probably due to the protection of the aluminium in the octahedral layer by the enclosing silica sheets. Thermal treatment of pyrophyllite up to 900°C produces a crystalline dehydroxylate phase in which the aluminium occupies well-defined 5-coordinated sites; this dehydroxylate is no more reactive to geopolymerisation than the parent clay. However, high-energy

grinding destroys the crystal structure sufficiently to permit the synthesis of a geopolymer-like material that sets and hardens satisfactorily and has the NMR characteristics of a well-formed geopolymer, but is not fully X-ray amorphous, containing traces of zeolite.

Other methods of producing geopolymers include solid-state reaction of an undehydroxylated 1:1 clay at 550°C with a mixture of alkali hydroxides to form a powder that sets when water is added. Although there is no energy saving in this method, it can be used to prepare lithium geopolymers and unusual compounds such as gallio germanates analogous to aluminosilicate geopolymers.

Another low-energy method for producing aluminosilicate geopolymers utilises a solution of alkali aluminate as the labile aluminium source for reaction with sodium silicate, produced by reaction of silica fume with alkali hydroxide. The product has all the characteristics of a conventional aluminosilicate geopolymer.

14.8 References

- Avvakumov E, Senna M and Kosova N (2001), *Soft mechanical synthesis*, Massachusetts, Kluwer.
- Barbosa V F F, MacKenzie K J D and Thaumaturgo C (2000), 'Synthesis and characterisation of materials based on inorganic polymers of alumina and silica: sodium polysialate polymers', *Int. J. Inorg. Mater.*, 2, 309–17.
- Barrer R.M. and Cole J.F (1970), 'Chemistry of soil minerals. Part VI. Salt entrainment by sodalite and cancrinite during their synthesis', *J. Chem. Soc. A*, 1516–23.
- Berg L G, Demidenko B A, Remiznikova V A and Nizamov M S (1970), 'Unfired finishing building materials based on kaolin'. *Stroitel'nye Materialy*, 10, 22.
- Boldyrev V V (2006), 'Mechanochemistry and mechanical activation of solids', *Russ. Chem. Rev.*, 75, 177–89.
- Boldyrev V V and Avvakumov E (1971), 'Mechanochemistry of inorganic solids', *Russ. Chem. Rev.*, 40, 847–59.
- Brew D R M and MacKenzie K J D (2007), 'Geopolymer synthesis using silica fume and sodium aluminate', *J. Mater. Sci.*, 42, 3990–3.
- Cao D, Su, D, Lu B and Yang Y (2005), 'Synthesis and structure characterization of geopolymeric material based on metakaolinite and phosphoric acid', *J. Chinese Ceram. Soc.*, 33, 1385–9.
- Davidovits J (1991), 'Geopolymers: inorganic polymeric new materials', *J. Thermal Analysis* 37, 1633–56.
- Davidovits J and Davidovics M (1988), '*Ceram. Eng. Sci. Proc.*', 9, 835–42.
- Deer W A, Howie R A and Zussman J (1962), *Rock-forming minerals Vol. 3*, London, Longmans.
- Duxson P, Provis, J L, Lukey G C, Separovic F and van Deventer J S J (2005), '²⁹Si NMR study of structural ordering in aluminosilicate geopolymer gels', *Langmuir* 21, 3028–36.
- Fitzgerald J J, Dec S F and Hamza A I (1989), 'Observation of five-coordinated Al in pyrophyllite dehydroxylate by solid state ²⁷Al NMR spectroscopy at 14T', *Amer. Mineral.*, 74, 1405–8.

- Gluchovskii V D (1959), *Gruntosilikaty*, Kiev, Gosstroizdat.
- Golosoov S I and Molchanov V I (1966), *Physicochemical changes of minerals during fine grinding*, Novosibirsk, Institute of Geology and Geophysics.
- Gualtieri A and Bellotto M (1998), 'Modelling the structure of the metastable phases in the reaction sequence kaolinite-mullite by X-ray scattering experiments', *Phys. Chem. Mineral.*, 25, 442–52.
- Klevtsov D P, Mastikhin V M and Krivoruchko O P (1986), 'Investigation of the mechanism of solid-phase transformations during thermal treatment of aluminosilicate systems. II. Investigation of the effect of mechanical activation on kaolinite', *Izv. So An SSSR ser. khim, nauk*, 3, 62–70.
- Koloušek D, Brus J, Urbanová M, Andertová J, Hulínský V, and Vorel J (2007), 'Preparation, structure and hydrothermal stability of alternative (sodium silicate-free) geopolymers', *J. Mater. Sci.*, 42, 9267–75.
- MacKenzie K J D (2000), 'Mechanochemical processing of ceramics studied by multinuclear magnetic resonance spectroscopy (MAS NMR)', *Proc. 1st Int. Conf. Adv. Mater. Processing*, 45–50.
- MacKenzie K J D and Smith M E (2002), *Multinuclear solid-state NMR of inorganic materials*, Oxford, Pergamon-Elsevier.
- MacKenzie K J D, Brown I W M, Meinhold R H, and Bowden M E (1985), 'Outstanding problems in the kaolinite-mullite reaction sequence investigated by ^{29}Si and ^{27}Al solid-state nuclear magnetic resonance. I. Metakaolinite'. *J. Amer. Ceram. Soc.*, 68, 293–7.
- MacKenzie K J D, Okada K and Temuujin J (2004), 'Nanoporous inorganic materials from mineral templates', *Current Appl. Phys.*, 4, 167–70.
- MacKenzie K J D, Brew D R M, Fletcher R A and Vagana R (2007), 'Formation of aluminosilicate geopolymers from 1:1 layer-lattice minerals pre-treated by various methods: a comparative study', *J. Mater. Sci.*, 42, 4667–74.
- MacKenzie K J D, Komphanchai S, and Vagana R (2008), 'Formation of inorganic polymers (geopolymers) from 2:1 layer lattice aluminosilicates', *J. Eur Ceram. Soc.*, 28, 177–81.
- Madhusoodana C D, Kameshima Y, Nakajima A, Okada K, Kogure T and MacKenzie K J D (2006), 'Synthesis of high surface area Al-containing mesoporous silica from calcined and acid-leached kaolinite as the precursors', *J. Colloid Interface Sci.*, 297, 724–31.
- Okada K and MacKenzie K J D (2006), 'Nanoporous materials from mineral and organic templates', in *Nanomaterials from research to applications*, Oxford, Elsevier, p. 349–79.
- Okada K, Kawashima H, Saito Y, Hayashi S and Yasumori A (1995), 'New preparation method for mesoporous γ -alumina by selective leaching of calcined kaolin minerals', *J. Mater. Chem.*, 5, 1241–4.
- Okada K, Shimai A, Takei T, Hayashi S, Yasumori A, and MacKenzie K J D (1998), 'Preparation of microporous silica from metakaolinite by selective leaching method', *Microporous Mesoporous Mater.*, 21, 289–96.
- Pinto A T and Vieira E (2006), 'Optimised conditions for the obtaining of metakaolin', *Mater. Sci. Forum*, 514–516, 1536–40.
- Sanchez-Soto P J, Perez-Rodriguez J L, Sobrados I and Sanz J (1997), 'Influence of grinding in pyrophyllite-mullite thermal transformation assessed by ^{29}Si and ^{27}Al MAS NMR spectroscopies', *Chem. Mater.*, 9, 677–84.
- Senna M (1993), 'Incipient chemical interaction between fine particles under mechanical

- stress – Feasibility of producing advanced materials via mechanochemical routes’, *Solid State Ionics*, 63–65, 3–9.
- Škvára F (2007), ‘Alkali activated materials or geopolymers?’, *Ceram.-Silikary* 51, 173–7.
- Temuujin J, Okada K and MacKenzie K J D (1998), ‘Role of water in the mechanochemical reactions of MgO-SiO₂ systems’, *J. Solid State Chem.*, 138, 169–77.
- Temuujin J, Okada K, Jadambaa T S, MacKenzie K J D and Amarsanaa J (2003), ‘Effect of grinding on the leaching behaviour of pyrophyllite’, *J. Eur. Ceram. Soc.*, 23, 1277–82.
- Verdolotti L, Iannace S, Lavorgna M and Lamanna R (2008), ‘Geopolymerization reaction to consolidate incoherent pozzolanic soil’, *J. Mater. Sci.*, 43, 865–73.
- Wardle R and Brindley G W (1972), ‘The crystal structure of pyrophyllite 1Tc and of its dehydroxylate’. *Am. Mineral.*, 57, 732–50.

Thermal properties of geopolymers

A VAN RIESSEN and W RICKARD,
Curtin University of Technology, Australia and
J SANJAYAN, Monash University, Australia

Abstract: The thermal properties of metakaolin and fly ash geopolymers with comparisons to ordinary Portland cement (OPC) are reviewed. The role and presence of secondary phases and aggregates are also discussed. The chapter explores the following characteristics of geopolymers upon exposure to high temperature: thermal expansion, weight loss, thermodynamics, thermal conductivity, fire resistance and mechanical strength. Merits and pitfalls of various high temperature applications of geopolymers are also discussed.

Key words: geopolymer, fly ash, metakaolin, thermal properties, fire resistance.

15.1 Introduction

This chapter reviews the thermal properties of metakaolin and fly ash geopolymers and compares them to existing cements such as OPC. Geopolymers have been shown to have huge potential for use in high temperature applications, which is why many researchers have studied their behaviour during high temperature exposure.

Owing to their inorganic framework, geopolymers exhibit excellent thermal stability, far in excess of that of traditional cements [1]. These characteristics allow geopolymers and geopolymer composites to be considered for use in high temperature applications such as furnace linings, thermal insulation and wall panels.

Macroscopic characteristics critical in assessing a cement's suitability for high temperature applications include: thermal expansion, thermal conductivity, strength retention, spalling and melting point. Microstructural characteristics relevant to the thermal analysis of geopolymers are phase stability, morphology changes, dehydration and thermodynamics. This chapter will review the literature concerning these properties of geopolymers including expected results and influencing factors.

Throughout this chapter reference is made to the Si:Al ratio of geopolymers as a compositional variable influencing a range of properties including thermal properties. Unfortunately, it is difficult to ascertain the exact Si:Al of geopolymer binder unless careful analysis is undertaken in a SEM with

x-ray detector. Papers tend to quote the Si:Al ratio of geopolymer even if they are aware that some of the precursor material has not been dissolved. Thus there is an overall Si:Al ratio and the actual Si:Al ratio of the binder. The difference could be substantial and creates an uncertainty in determining correct trends in geopolymer research.

15.2 Thermal expansion

Thermal expansion/shrinkage of geopolymeric materials can be measured in-situ through dilatometry or ex-situ through dimensional measurements. Dilatometry is the most common method as it can be performed in real time and logged electronically. Dilatometry measurements can be measured directly with a 'push rod' or indirectly using a laser measurement system [2]. Repeated thermal cycling can give an indication as to the permanency or reversibility of dilation changes.

The thermal expansion/shrinkage of geopolymers is of particular interest when assessing their potential for high temperature applications. Shrinkage or expansion during heating causes both internal and external stresses, which potentially weakens or damages the structure. In a refractory context, minimal thermal dilation is desired to retain structural integrity.

The influence on the thermal expansion of the water-to-cement (w/c) ratio¹, source material type, alkali type and compositional ratios are explored. In addition, the thermal expansion of geopolymer concrete is reviewed to establish the effect the differential thermal expansion of the aggregate and paste has on the composite.

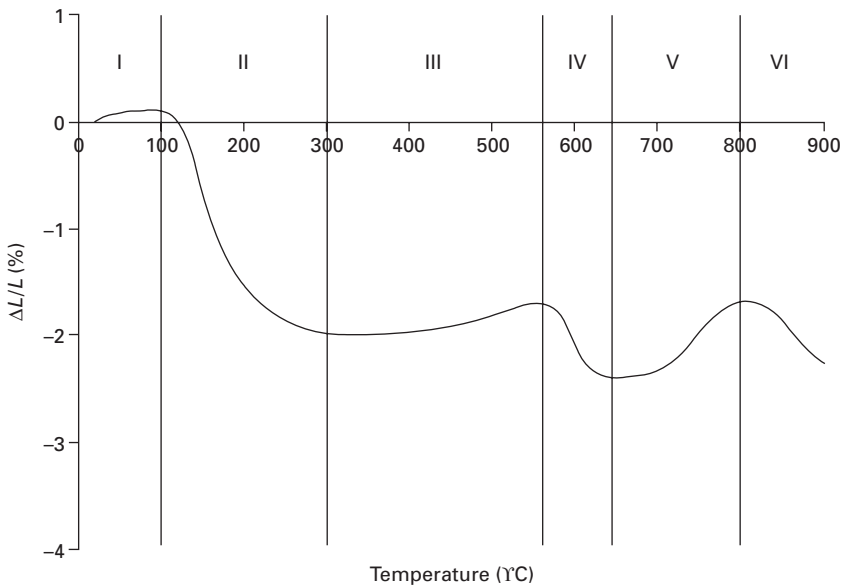
Thermal expansion of geopolymers is isotropic due to their amorphous structure; however, non-uniform expansion can occur in regions of the sample due to local variations in composition and temperature which cause thermal stresses to arise, leading to cracking, spalling, etc. The thermal expansion characteristics common to all geopolymers are listed in Table 15.1. A regional breakdown first proposed by Duxson *et al.* [3] and expanded on by Rickard *et al.* [4] is included in the table and shown in Fig. 15.1. The temperature range of each region is variable and dependent on sample composition and testing conditions. It should be noted that not all geopolymers will exhibit all the regions defined in Table 15.1 and Fig. 15.1.

Geopolymers, like most solid materials, expand upon heating (Region I). However, geopolymers contain a high proportion of water that exists either adsorbed in the pores or chemically bound in the structure. Nuclear magnetic resonance (NMR) and thermogravimetric analysis (TGA) show that most of the water is physically rather than chemically bound, at least in relatively

¹The w/c ratio refers to the total amount of water including that arising from the activating solution.

Table 15.1 Thermal shrinkage/expansion characteristics of geopolymers

Region	Temperature range (°C)	Description	Effect	Factors
I	0–150	Resistive dehydration	Slight expansion	Young's modulus of sample. Heat rate
II	100–300	Dehydration of free water	Significant shrinkage	Water content. Heat rate
III	250–600	Dehydroxylation	Minimal shrinkage	Abundance of hydroxyl groups and chemically bound water
IV	550–900	Densification by viscous sintering	Significant shrinkage	Residual water content. Si:Al ratio
V	Above densification temperature	Crystallisation in the geopolymer paste	Moderate expansion	Compositional ratio. Concentration and type of impurities
VI	Above densification temperature	Further densification	Large shrinkage	Compositional ratio



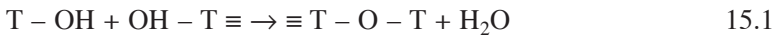
15.1 Thermal expansion of a fly ash geopolymer showing regional breakdown (see text for details). Si:Al = 2.3, w/c 0.2 [5].

well-reacted samples. Upon heating, the water dehydrates at various stages depending on the energy required to free the water. Dehydration of water results in a shrinkage event and as such the total thermal expansion of the geopolymer paste is a convolution of the expansion of the solids and the shrinkage of the pores (Region II). Other reactions such as crystallisation

(paste and secondary phases), oxidation (secondary phases only), sintering and melting affect the thermal expansion at high temperatures.

The extent of the dehydration shrinkage is dependent on the water content of the material. For example, Rickard *et al.* [4] found that fly ash geopolymers with a pre-curing water content of 15.2 wt% ($w/c = 0.2$) experienced a 2% dehydration shrinkage between 100°C and 300°C (Fig. 15.1). The nature of the dehydration shrinkage, such as onset temperature and duration, is dependent on the structure of the geopolymer and the heat rate during measurement. Duxson *et al.* [3] proposed that geopolymer resistance to dehydration shrinkage is proportional to the Young's modulus of the sample. Geopolymers with a greater Young's modulus can withstand the capillary strain forces developed during dehydration for longer [3] and as such the onset temperature of the initial shrinkage is increased. The rate of dehydration is affected by the rate of diffusion of the water through the structure. Thus the pore structure has an influence on the dehydration rate. Duxson *et al.* [3] found that increasing the heating rate increased the onset temperature and duration of the dehydration shrinkage event in metakaolin geopolymers.

Dehydroxylation occurs between 25°C and 400°C and is associated with a small mass loss. The dehydroxylation reaction in geopolymers can be generalised by the following reaction [3]:



where T is an aluminium or silicon atom.

The slight thermal shrinkage that occurs in region III, (generally occurring between 300°C and 600°C) is due to the physical contraction of the geopolymer paste as the hydroxyl groups are released, creating shorter T–O–T linkages [3]. However, the small amount of shrinkage in this region can be masked by the expansion of secondary phases as shown in Fig. 15.1. This is more often the case in fly ash geopolymers due to the relatively high concentration of impurities.

The second major shrinkage event occurs between 550°C and 900°C (region IV) due to the densification of the geopolymer as the paste sinters and viscous flow fills the voids of the material. Rahier *et al.* [6] proposed that the shrinkage in this region is an indication of the glass transition temperature (T_g) of the geopolymer. Duxson *et al.* [3] found that the onset temperature of the densification reduced with increasing Si:Al ratio. The same study also noted that residual water in the material after dehydration reduces the activation energy for viscous flow.

Beyond the densification region (region V), no consistent trend of thermal expansion has been reported in the literature. Rickard *et al.* [4] and Rahier *et al.* [6] measured a thermal expansion, Duxson *et al.* [3] and Dombrowski *et al.* [7] measured a sharp thermal shrinkage and Barbosa [1] measured the

geopolymer to be dimensionally stable. The differences in thermal expansion in this region are believed to be due to differences in composition and the presence of secondary phases (introduced as impurities from the source material). The nature of thermal dilation in this region is dependent on the degree of crystal growth in the geopolymer paste and secondary material, the heat rate and the melting temperature of the sample.

Growth of feldspar-based crystal phases such as kaliophilite (K-activated), leucite (K-activated) and nepheline (Na-activated) has been observed to occur in geopolymers at high temperatures [1, 8]. These phases crystallise from the amorphous geopolymer paste and their concentration is dependent on Si:Al ratio [8]. Barbosa and MacKenzie [1] observed that off-stoichiometric geopolymers exhibited increased feldspar growth due to the presence of unbound alkali cations. The Duxson [8] study found that the magnitude of thermal dilation at temperatures above the densification region was influenced by the degree of crystal growth, which is an expansion event. Further details on crystallisation in geopolymers can be found in Section 15.7.

Other factors which are believed to influence thermal expansion in region V are crack formation and an increase in porosity. Section 15.8 discusses pore structure evolution in more detail. Rickard *et al.* [4] also found that the thermal expansion in this region beyond the densification is dependent on sample size, with larger samples exhibiting greater thermal expansion.

The last characteristic region of thermal expansion is region VI and is identified by large and usually rapid shrinkage. This is often the failure point of the material. Subaer [9] reported a sharp shrinkage leading to the failure of the material, whereas Duxson *et al.* [3] observed a slower shrinkage though the magnitude for both cases was the same. The cause for the shrinkage in this region is due to one or more of the following; continued densification (similar to region IV), destruction of crystalline phases formed in region V, collapse of the pore structure formed in region V, or melting of the sample.

15.2.1 Factors influencing the thermal expansion of geopolymers

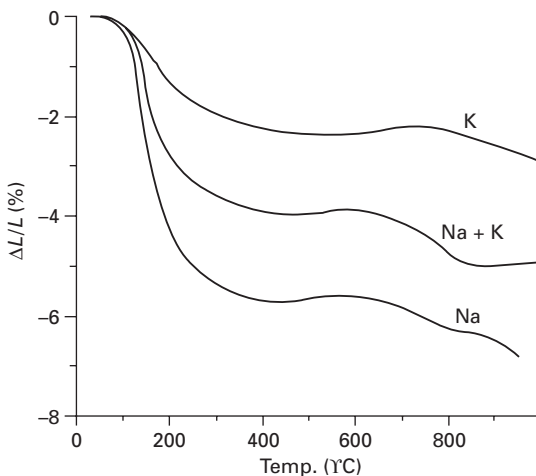
Water content (w/c ratio)

The nature of the thermal expansion of geopolymer paste is strongly influenced by the water-to-cement ratio (can also be expressed as the water/binder, water/cementitious material or water/solid ratio). The higher the water content the greater the amplitude of the shrinkage due to dehydration of the water. Typical w/c ratios for geopolymers range between 0.15 and 0.4. Geopolymers synthesised for high temperature applications are designed with minimal water content; however, they are restricted by the need for the pre cured mix to

be workable. Kong *et al.* [10] reported that with fly ash-based geopolymers a lower w/c ratio can be achieved than with metakaolin geopolymers whilst maintaining a workable mixture. This is due to the spherical shape of fly ash particles allowing for a more workable paste than the platy shape of metakaolin particles. Bakharev [11] was able to achieve lower w/c ratio by compacting the mixture with forces up to 10 MPa prior to curing. Walls *et al.* [2] used a high speed centrifugal mixer to reduce water content (from 15% to 5%) in processing fly ash-based geopolymers and observed a concomitant increase in cold crushing strength and Young's modulus.

Alkali activator

Duxson *et al.* [12] investigated the effect the alkali cation (Na, K or a mix) had on the thermal expansion of metakaolin geopolymers of $1.15 < \text{Si:Al} < 2.15$. The study found that the choice of alkali had a significant effect on the thermal expansion (see Fig. 15.2). Thermal shrinkage of the various alkali based geopolymers was measured to be in the order $\text{Na} > \text{Na} + \text{K} > \text{K}$. The magnitude and the rate of dehydration shrinkage (region II) were most affected by the change in alkali source. This effect was more significant in geopolymers of $\text{Si:Al} \leq 1.4$. The onset temperature of region IV also changed with alkali source in the order $\text{K} > \text{Na} + \text{K} \approx \text{Na}$.



15.2 Thermal shrinkage of Na-, Na+K- and K-activated geopolymers with Si:Al ratio of 1.15 [12].

Compositional ratio

Duxson *et al.* [3, 12] investigated the effect that varying the Si:Al ratio had on the thermal expansion of metakaolin geopolymers over the range $1.15 \leq \text{Si:Al} \leq 2.15$. The study found that the total shrinkage upon heating to 1000°C increases with Si:Al. The amplitude of dehydration and dehydroxylation shrinkage was not observed to be influenced by Si:Al ratio. The onset temperature for densification of the geopolymer paste (region IV) was found to reduce with increasing Si:Al ratio. It was proposed by Duxson that the reduced onset temperature is due to the incomplete incorporation of aluminium from the source material, leaving free sodium atoms in the system, which reduces the T_g of aluminosilicates.

Source material type

The following section describes the effect of source material on the thermal expansion of geopolymers.

15.2.2 Thermal expansion/shrinkage of metakaolin geopolymers

The thermal properties of metakaolin geopolymers have been studied extensively in the literature [1, 3, 6, 9, 12, 20]. The trend observed in each study is similar, though the amplitude and temperature of the thermal shrinkage vary between studies. Differences in alkali sources and water content are believed to be the main causes for the observed differences in thermal shrinkage between studies.

15.2.3 Thermal expansion of fly ash geopolymers

Fly ash-based geopolymers have been observed to have similar thermal shrinkage character to metakaolin geopolymers though the magnitude of the shrinkage is typically less due to the lower water content used to process fly ash geopolymers [5, 7, 11, 13]. The other difference in the shrinkage/expansion character is caused by the impurities introduced via the fly ash. Common impurities in fly ash geopolymers are crystalline silica (quartz), residual carbon, iron and calcium oxides.

Rickard *et al.* [4] studied the effect of high iron and quartz content in fly ash-based geopolymers. The study found that a quartz content of 20 wt% had only minimal effect on the thermal expansion (most notably a small increase in thermal expansion in region III). Increasing the quartz content to 40 wt% reduced the thermal shrinkage by over 50% at 500°C . Iron oxides were found to have a strong influence on the thermal expansion character

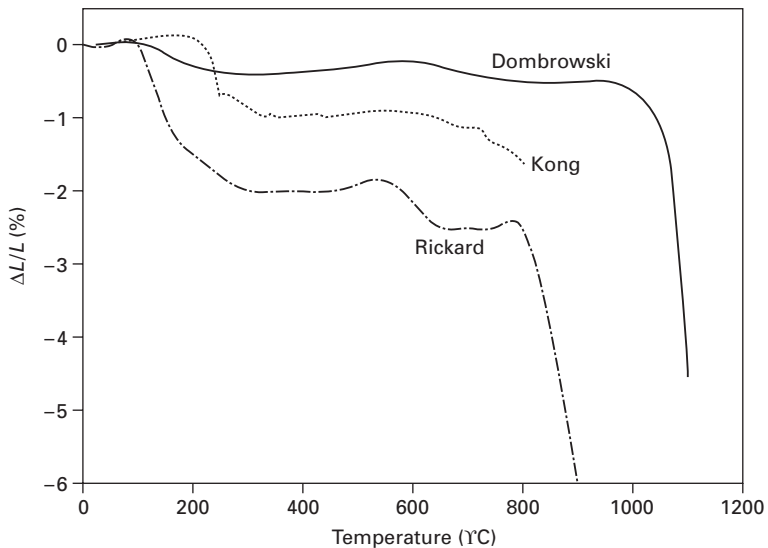
at temperatures above 500°C. A thermal expansion event was observed to occur at approximately 800°C (Fig. 15.1). The expansion in this region was determined to be due to oxidation and crystallisation of the iron oxides in the geopolymer.

Dombrowski *et al.* [7] studied the effect of calcium content on the thermal expansion of fly ash geopolymers and found that 8% $\text{Ca}(\text{OH})_2$ was the optimum amount for reduced shrinkage to 1050°C (Figure 15.3).

15.2.4 Comparison with the thermal expansion of OPC

Thermal expansion data for OPC paste and concrete is widely available in the literature, a thorough investigation can be found at [14]. However, like geopolymers, there is no one thermal expansion curve that is representative for all OPC products. This makes a direct comparison with geopolymers difficult and somewhat subjective.

High temperature (>300°C) thermal expansion is more significant for comparison between OPC and geopolymer products as the dehydration of free water is common to both materials. No noticeable trend in the magnitude of the thermal shrinkage was determined from the literature when comparing OPC and geopolymers. However, it was noticed that OPC continues to shrink throughout the heating cycle [15], whereas geopolymers in many cases exhibited a region of dimensional stability.



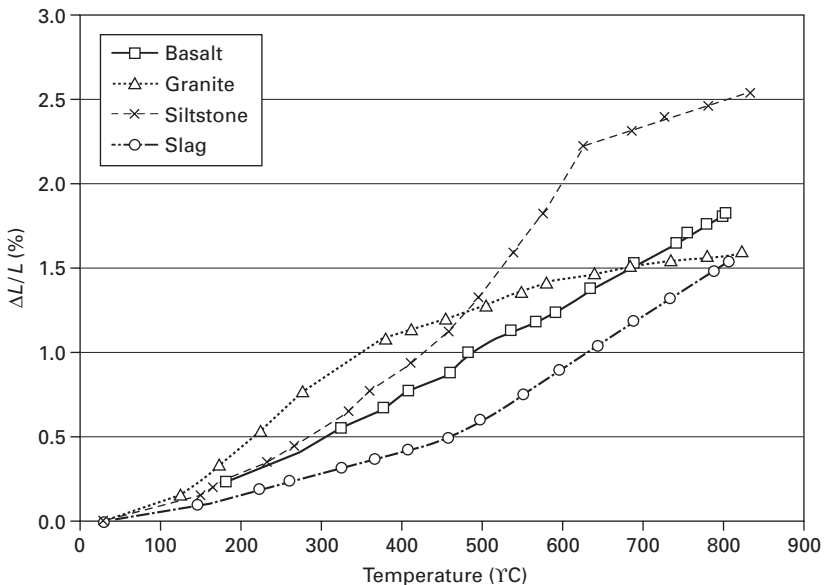
15.3 Thermal shrinkage of fly ash geopolymers. Rickard [4], Dombrowski [7], Kong [13].

15.2.5 Thermal expansion of geopolymer concrete

The thermal expansion of concrete, whether Portland or geopolymer cement based, is dominated by the thermal expansion of the aggregates as they usually comprise between 65 and 80% of the volume [14]. In general, the cement paste shrinks and the aggregate expands during high temperature exposure. The differential expansion of the aggregate and the paste has implications for the mechanical strength after high temperature exposure.

Thermal expansion of geopolymer concrete varies with factors such as aggregate type (Fig. 15.4), cement content and w/c ratio. Of these, aggregate type has the greatest influence [13, 14]. Aggregates suitable for use in geopolymer concrete are the same as used in OPC. It is important to note that concretes made with high-quartz aggregates are strongly affected by the rapid expansion in the vicinity of the α - β quartz phase change occurring at 573°C (as can be seen the thermal expansion of siltstone in Fig. 15.4).

A definitive study on the thermal expansion of geopolymer concrete has not yet been published, though studies on geopolymer mortars have been reported. Subaer and van Riessen [16] investigated the thermal expansion of metakaolin geopolymer mortars containing fine quartz and granite aggregates. The study found that the introduction of fine aggregate reduced the thermal shrinkage of the mortar to less than 1%, half that of the paste only specimen. It was noted that the phase change in the quartz aggregate set the upper value of the dimensionally stable temperature range.



15.4 Thermal expansion of common coarse aggregates [13].

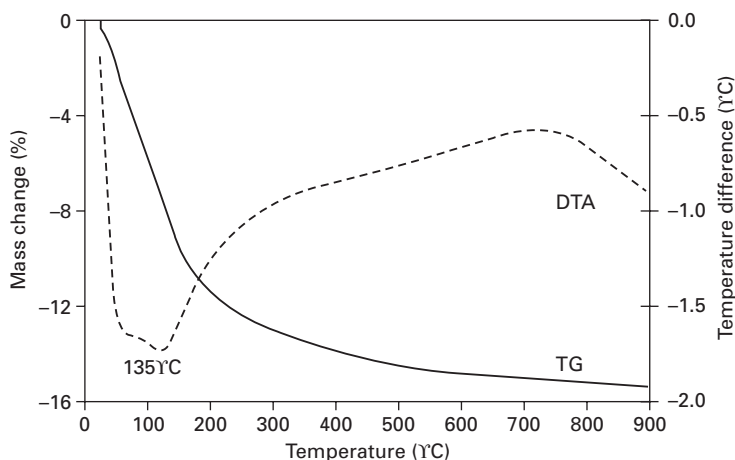
15.3 Thermoanalysis

Thermodynamic processes in geopolymer cements have been measured using differential temperature analysis (DTA) and differential scanning calorimetry (DSC) [1, 3, 4, 16, 17]. Weight loss during high temperature exposure has been measured using thermogravimetric analysis (TGA) (often simultaneously with DTA) [1, 3, 4, 10, 11, 16]. These testing techniques, as with dilatometry, usually allow a choice of atmosphere during testing. Inert atmospheres such as nitrogen or argon can be used to eliminate secondary atmospheric reactions such as oxidation.

15.3.1 TGA/DTA

Figure 15.5 contains a typical TGA/DTA result from a metakaolin geopolymer. Weight loss, due to the dehydration of adsorbed water, begins above ambient temperatures and the percentage mass loss is proportional to the initial water content of the sample. Water continues to evaporate until approximately 300°C, where the bulk of the free water has been liberated. A number of studies have shown that at least 80% of the weight loss occurs below 200°C [1, 3, 4, 18], though this dehydration period can be extended when fast heat rates are applied.

Dehydration is an endothermic event, which is evident in the minima in the DTA thermograms of Fig. 15.5. The temperature of the endothermic minimum and the temperature range of the event has been observed to reduce with increasing Si:Al ratio [3]. Beyond the dehydration endotherm geopolymers become thermodynamically stable, though slightly exothermic. Geopolymer

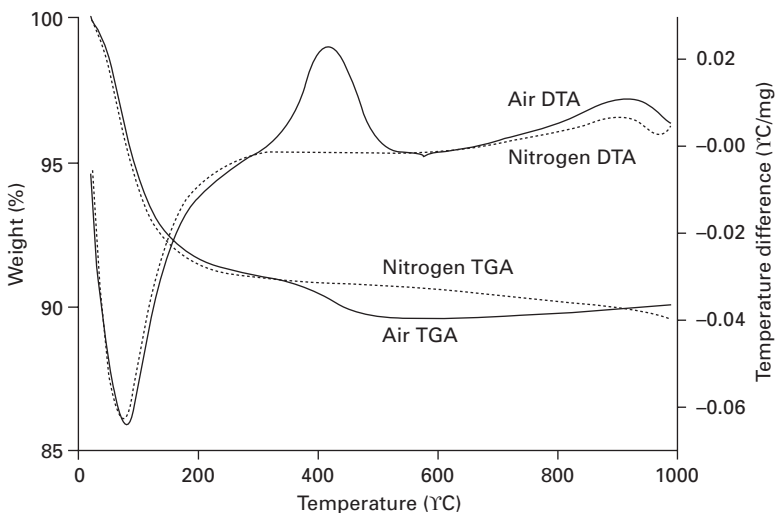


15.5 TGA–DTA curves for a metakaolin geopolymer prepared with Si:Al = 1.5, Na:Al = 0.6 [16].

pastes with compositions conducive to promotion of crystallisation may exhibit high temperature endothermic/exothermic activity as the phases form and collapse with increasing temperature. Duxson *et al.* [3] observed an exotherm at approximately 700 °C in metakaolin geopolymers of Si:Al = 1.15 which was attributed to the collapse of a faujasite phase formed at a lower temperature.

Above 300 °C, the weight loss in TGA data is attributed to the dehydroxylation of the chemically bound water. The densification of geopolymers at temperatures >600 °C observed in thermal expansion results does not correspond to any mass loss in observed TGA thermograms.

TGA/DTA results are more complicated in fly ash geopolymers due to the presence of impurities. Figure 15.6 displays the simultaneous TGA/DTA results from a fly ash geopolymer, where the fly ash contained 20 wt% quartz and 15 wt% iron oxide. Rickard *et al.* [4] observed an exothermic spike at approximately 400 °C in the DTA results and a simultaneous weight loss in the TGA results (Fig. 15.6). The exotherm was caused by energy release as the poorly ordered iron oxide (possibly ferrihydrite) from the fly ash, crystallised to hematite. The weight loss resulted from the loss of hydroxyl groups during the phase change. The same study also observed mass gain in fly ash geopolymers heated above 600 °C in air while no mass gain was observed in geopolymer samples heated in flowing nitrogen. The mass gain was attributed to the oxidation of the iron oxides and was exothermic in nature.



15.6 TGA/DTA results for a fly ash geopolymer, Si:Al = 2.3, Na:Al = 0.85, H₂O:SiO₂ = 2.0 [4].

15.4 Thermophysical properties

Thermal conductivity, thermal diffusivity and the specific heat are all properties of interest to scientists studying geopolymers. These characteristics can be determined by analysing data from hot plate or transient line experiments. Details on the hot plate test method and subsequent data analysis can be found elsewhere [19]. The transient line method can be performed by either embedding a thermocouple and a heat source into the sample or using a commercially available thermal analysis probe.

15.4.1 Thermal conductivity

The thermal conductivity of geopolymers is measured to assess their potential application as an insulating product or a concrete building material. Insulators require a low thermal conductivity because they are designed to reduce the conduction of heat whereas concretes require a relatively high thermal conductivity, as this reduces expansion stresses within the material [9].

Low density geopolymer foams designed as thermal insulators have been produced with a thermal conductivity of $0.037 \text{ Wm}^{-1}\text{K}^{-1}$ [20]. Duxson *et al.* [21] reported the thermal conductivity of metakaolin geopolymers as approximately $0.8 \text{ Wm}^{-1}\text{K}^{-1}$. Subaer and van Riessen's [16] results were slightly lower than the Duxson study, ranging between 0.55 and $0.65 \text{ Wm}^{-1}\text{K}^{-1}$. The thermal conductivity values reported by Subaer and Duxson are higher than that of OPC paste which has a thermal conductivity of $0.53 \text{ Wm}^{-1}\text{K}^{-1}$ [22]. The Subaer study found that the addition of 40 wt% quartz aggregate increased the thermal conductivity by 40% relative to metakaolin geopolymers (Table 15.2). This is in good agreement with density dependency hypothesis as the addition of aggregate increases the sample's bulk density. The higher thermal conductivity of quartz (11.1 and $5.9 \text{ Wm}^{-1}\text{K}^{-1}$ for the c-axis and a-axis, respectively [43]) will also result in an overall increase of the thermal conductivity of the geopolymer-quartz composite.

Table 15.2 Density and thermal conductivity of metakaolin geopolymers of various compositions [16]

Sample ID	Density (g cm^{-3})	Thermal conductivity ($\text{Wm}^{-1}\text{K}^{-1}$)
Si:Al = 1.5, Na:Al = 0.6	1.68 ± 0.09	0.65 ± 0.04
Si:Al = 1.5, Na:Al = 0.8	1.62 ± 0.05	0.64 ± 0.03
Si:Al = 2.0, Na:Al = 1.0	1.43 ± 0.01	0.55 ± 0.03
Si:Al = 1.5, Na:Al = 0.6 (+40 wt% quartz aggregate)	1.89 ± 0.02	0.91 ± 0.07

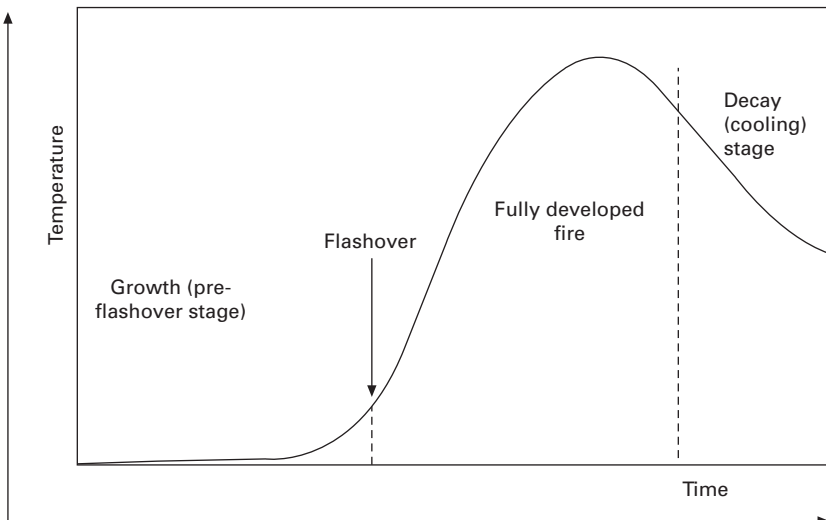
15.5 Fire resistance

Unlike other construction materials, some geopolymers have been shown to increase their strength after elevated temperature exposure [10, 18, 23]. However, superior performance of a material in an elevated temperature exposure does not necessarily translate into good performance in a fire. In a fire, the materials not only get exposed to elevated temperatures, but also certain rate of temperature increase with time that needs to be accommodated. The time versus temperature variation of a fire depends on the type of fire and where it occurs.

15.5.1 Standard fire curves

There is considerable debate and differences in opinions as to what should constitute a standard fire. A typical sequence of a room fire can be expressed in terms of the average air temperature in the room. Figure 15.7 illustrates three stages of such fire:

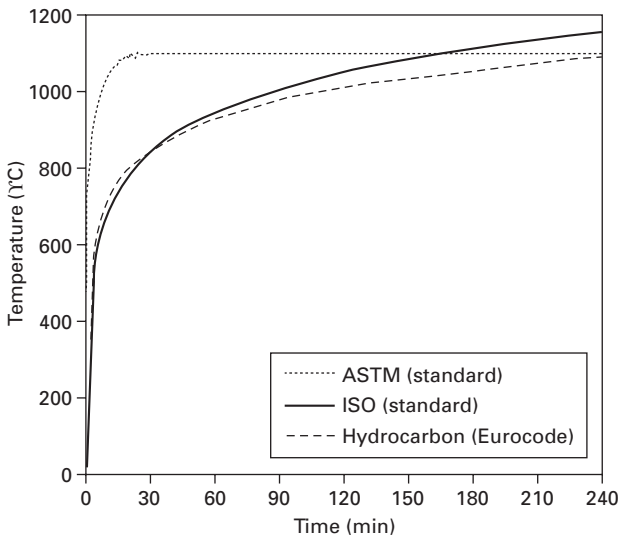
- (1) the growth or pre-flashover stage, in which the average temperature is low and the fire is localised in the vicinity of its origin;
- (2) the fully-developed or post-flashover fire, during which all combustible items in the room are involved and flames appear to fill the entire volume; and
- (3) the decay or cooling period.



15.7 Time versus temperature curve of a typical room fire (this was developed based on the concepts from [36]).

Building and structural components are generally required to be shown to withstand an accidental fire. For this purpose, it is necessary to adopt a standard fire curve so that there is a common benchmark test to compare different options for the building components. The most commonly adopted fire curve is the ISO 834, while the ASTM E119 fire curve is also commonly used which differs slightly from the ISO curve. The ISO 834 curve is based on cellulose fire, and is also adopted by the Australian (AS1530.4), Norwegian (Nordtest NT Fire 046) standards and Eurocode (EN1991-1-2:2002). The time versus temperature relationship of the standard (cellulose) fire is shown in Fig. 15.8. The standard fire curves (Fig. 15.8) aim to simulate the temperature versus time curve of Fig. 15.7, starting from the flash over stage. Pre-flashover stage of the fire is normally ignored, as it has insignificant impact on building components.

For many materials, the performance of the material in a fire can be determined by knowing the maximum temperature exposure of the material. However, materials which are relatively brittle, such as geopolymers and Portland cement-based concretes, are also affected by the thermal gradient developed in the material and building component. One significant parameter that affects the thermal gradient is the rate of temperature rise of the fire during the initial stages. As compared to standard fire which is modelled based on cellulose fire, hydrocarbon fire results in rapid rise of temperature at the beginning. In situations where the probability of occurrence of a hydrocarbon fire exposure is significant, such as road and railway tunnels, offshore and petrochemical industries, the response of the building component to such



15.8 Temperature versus time relationship of a standard fire. (ASTM E119 [38], ISO 834 [39], Eurocode EN1991-1-2 [40]).

fire should also be considered in the design. Eurocode (EN1991-1-2 [40]) provides a curve for this purpose and is also shown in Fig. 15.8.

Hydrocarbon fire is particularly damaging for materials such as Portland cement concrete, because the rapid temperature rise causing steep thermal gradients and steam pressure build up in the pores can lead to explosive spalling. Therefore, unlike materials such as steel where the actual temperature and duration of exposure are the primary factors that influence the fire response, in relatively brittle materials, rate of temperature rise is an important factor.

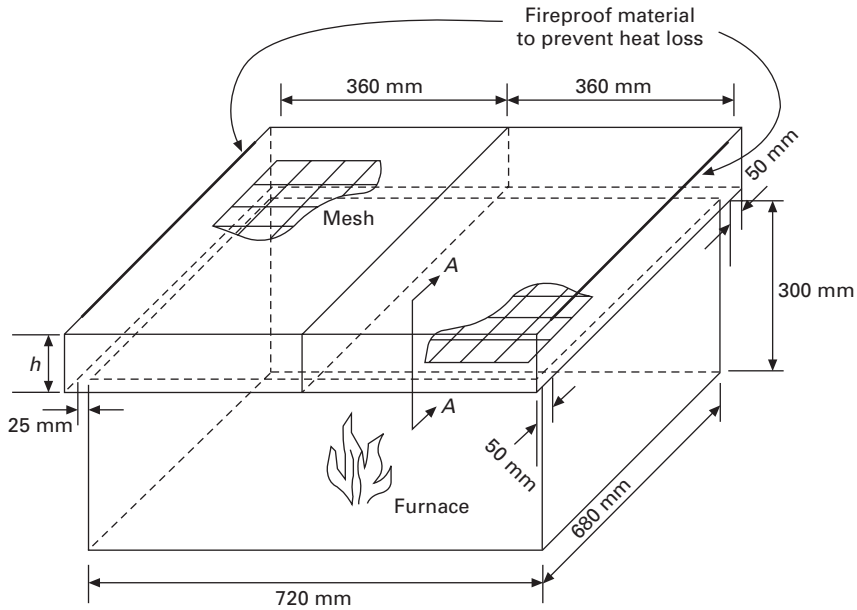
15.5.2 Fire test results

Portland cement concrete, in particular high strength concrete, is highly susceptible to spalling in a fire [37]. High strength concretes are generally defined as concretes with compressive strengths above 50 MPa, and are widely used in construction since the late 1980s. Spalling of high strength concrete, first reported in 1993 [37], is an explosive dislodgement of pieces from the surface of concrete in a fire. The high risk of spalling of high strength concretes is believed to be due to the reduced permeability and increased brittleness, compared to normal strength concretes. The risk of spalling is further exacerbated when the concretes are exposed to rapid rise of temperatures, such as in hydrocarbon fires.

A comparative test of geopolymer concrete and high strength concrete was carried out at Monash University, and is presented below. The specimens tested were rectangular slabs of 780 mm long and 360 mm wide with a thickness of 200 mm. The specimens were reinforced with 100 mm × 100 mm steel mesh with a bar diameter of 6 mm. All the concretes investigated were approximately the same compressive strength of 75 MPa at the time of the test date which is considered a high strength concrete. The mixture proportions of the Portland cement concrete and geopolymer concretes are shown in Table 15.3. The specimens were exposed to hydrocarbon fire on one side (underside). Figure 15.9 shows the test set up. The one-sided exposure to fire is considered to be worse case scenario than fire exposure

Table 15.3 Mixture proportions of Portland cement concrete and geopolymer concretes tested in hydrocarbon fire

Materials (kg/m ³)	Portland cement concrete	Geopolymer concrete
Fly ash		420
Portland cement	420	
Water	170	
Sodium silicate		150
Potassium hydroxide		60
Fine aggregate	750	750
Coarse aggregate	1125	1125



15.9 Schematic showing concrete slabs being tested for hydrocarbon fire exposure.

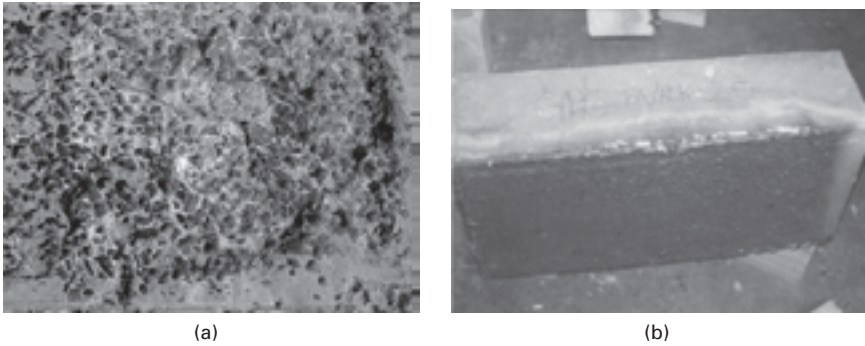
to all sides since the thermal gradient is higher in one sided exposure, and is commonly encountered in walls and doors preventing fire from spreading and in underside of floor slabs.

Furnace temperature followed the temperature time curve prescribed for hydrocarbon fire in Eurocode EN1991-1-2 [40] as shown in Fig. 15.8. Explosive spalling noises were heard after about 30 minutes from the beginning of the test. Observation of the specimens after the fire test revealed that moderate to severe spalling on the underside of Portland cement concrete. The geopolymer concrete specimen did not have any spalling. Figure 15.10 shows the underside of both Portland cement and geopolymer concrete specimens after the fire test.

The reasons for the contrasting behaviour of these two different concretes are not very well understood. Further tests to obtain greater understanding of the behaviours are currently underway.

15.6 Mechanical strength evolution

Thermal exposure affects the mechanical strength of geopolymers, the extent of which can be used as an indication of the material's thermal resistance. Mechanical strength is commonly measured ex-situ (away from the heating environment) by unconfined compressive strength measurements. Young's



15.10 Specimens after fire test: (a) Spalling of portland cement concrete specimen (b) geopolymer concrete specimen.

modulus, splitting and flexural strength measurements can also give an indication as to the change in strength with temperature. Standard testing techniques used for decades on OPC materials are applied in the same way for geopolymers. Testing that involves thermal cycling can demonstrate the long-term mechanical performance of the material.

Changes in the mechanical strength, both during and after thermal exposure, are critical in assessing the high temperature performance of geopolymers, especially for materials intended for use in structural applications. Most reported mechanical strength results are derived from *ex-situ* experiments due to the difficulties of *in situ* mechanical testing at high temperatures.

Mechanical strength of geopolymers changes due to high temperature induced structural and phase composition changes in the material. Structural changes include sintering, densification, melting, cracking and pore size/volume/interconnectivity changes. Phase composition changes include crystal growth, crystal destruction, dehydration and geopolymer paste decomposition to release free Si, Al and alkali. Thermal dilation of secondary phases such as crystalline impurities or aggregates during exposure will also affect the mechanical strength [9]. Not all of these changes are detrimental to the mechanical strength.

Densification of the geopolymer results in fewer voids and allows for more uniform stress gradients during an applied load, enabling greater mechanical strength. Sintering of the un-reacted material, such as crystalline fly ash particles, provides increased mechanical strength due to stronger bonding between the particles. This is especially important in geopolymers containing aggregates. The temperature of the densification and sintering is dependent on the sample's composition and the type of secondary phases.

Pore structural changes have a mixed effect on the mechanical strength of geopolymers. Pores act as defects, and in general, mechanical strength decreases as pore size and volume increases. However, this is not always the case. Increased pore interconnectivity allows for greater water mobility

during heating, which reduces structural damages caused by vapour pressure on the pore walls [10]. Thus geopolymers with a more interconnected pore structure will experience a lower strength loss than a comparable geopolymer sample with an isolated pore structure. Pore structure is known to vary in geopolymers during thermal exposure [3, 11, 24, 25] (see Section 15.8 for further details) which cause non linear variations in mechanical strength during heating.

Kong [10, 13, 18] compared the mechanical strength evolution of metakaolin geopolymers to fly ash geopolymers. The study found that fly ash geopolymers retained greater compressive strength after thermal exposure when compared to metakaolin geopolymers. It was reported that this is due to the fact that fly ash geopolymers have large numbers of interconnected pores which facilitate the escape of moisture when heated, causing minimal damage to the geopolymer matrix; whereas metakaolin geopolymers possess a more isolated pore structure which forces escaping water during heating to damage the structure. The study also found that the strength increase in fly ash geopolymers is partially attributed to sintering of un-reacted fly ash particles [10]. As expected the strength of geopolymer concrete degraded after temperature exposure due to the thermal expansion mismatch between binder and aggregate.

Geopolymers with high shrinkage will tend to have lower mechanical strength after heating due to crack formation. Cracking increases in samples with high water content. The higher water content of metakaolin geopolymers makes them more prone to cracking due to heating.

Geopolymers prepared with different alkali activators perform differently when exposed to elevated temperatures. Bakharev [11] found that geopolymers prepared with a potassium activator exhibited increased compressive strength after heating to 800 °C, whereas geopolymers prepared with sodium activator exhibited a greatly reduced compressive strength after heating to 800 °C.

Dombrowski [7] found that the addition of a small amount of calcium to fly ash geopolymers increased the initial compressive strength, however it reduced the amount of strength gain upon heating to 1000 °C when compared to samples without added calcium. Zuda *et al.* [25] found increased compressive strength in slag geopolymers (39 wt% CaO) which revealed crystal growth in the XRD pattern when compared to a similar sample tested prior to the onset of crystallisation at 1200 °C.

15.6.1 Comparison to OPC

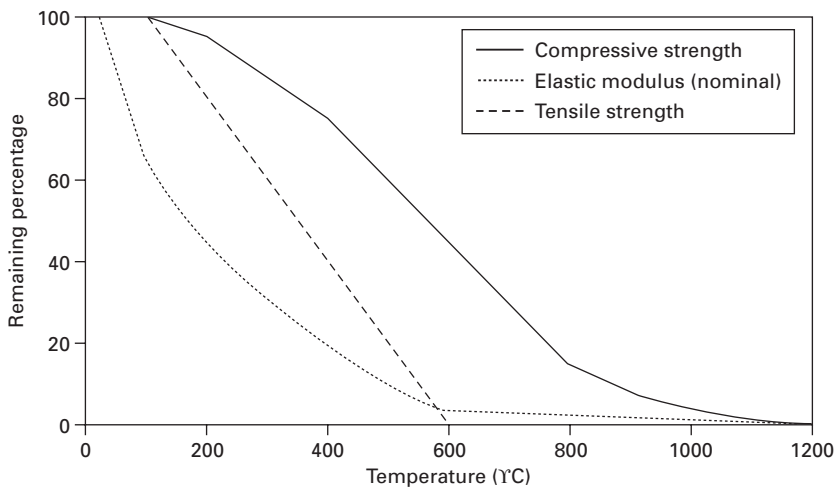
Unexposed compressive strengths of geopolymers can be tailored to be analogous to the strengths of OPC products, including high strength concrete. The significant comparable property between the two materials is the evolution of the mechanical strength during and after high temperature

exposure. Globally valid comparisons are difficult as there are many variations of geopolymer concretes and OPC concretes, all of which perform differently at high temperatures. Figure 15.11 shows an example of the loss of mechanical strength of Portland cement-based concrete upon elevated temperature exposure.

The strength loss in OPC concretes is mainly due to the decomposition of calcium hydroxide, beginning at 400 °C [26]. OPC concretes can also lose strength due to explosive spalling (as discussed in Section 15.5) at temperatures of 200 °C. There are, however, specialist cements such as calcium aluminate cement, which exhibit enhanced thermal resistance, though they are much more expensive to produce (up to four times more than standard OPC) [27]. Geopolymers have the potential to out perform even specialist OPC products due to their intrinsic thermal resistance.

15.7 Phase changes at elevated temperatures

Crystallisation and phase changes have been observed to occur in geopolymers exposed to elevated temperatures [1, 4, 7, 8, 11, 17]. Phase identification is usually conducted by analysis of x-ray diffraction (XRD) data, though electron diffraction data can also be used for single crystals in small samples. The analysis can be performed qualitatively (peak identification) or quantitatively (Rietveld refinement or relative intensity ratio method). Synchrotron x-ray sources provide high resolution, low noise data, though for most cases laboratory x-rays are sufficient.



15.11 Degradation of mechanical properties of Portland cement-based concrete (the graph plotted is based on the information provided by Eurocode EN 1992-1-2, 2004 [41]).

Geopolymers designed for high temperature applications may be exposed to temperatures in excess of 1400°C. The high temperatures provide the energy to induce a wide range of changes in the crystal structure and phase abundance in geopolymers. The three main changes are crystal formation, crystal destruction and crystal structural changes. The changes can occur in the geopolymer paste or in the secondary phases such as quartz. Crystal growth in geopolymers can either enhance the thermal resistance of geopolymers by increasing the melting temperature [28], or reduce the thermal resistance by increasing the amount of thermal expansion.

15.7.1 Phase changes in the geopolymer paste (formation and destruction)

Geopolymer paste is well known to have only short range order and appear amorphous under Bragg diffraction conditions. During heating to high temperatures, decomposition of the geopolymer paste frees Na, Si and Al species to crystallise to various zeolitic phases and alkali feldspars. The temperature for the onset of crystal growth in the paste is variable, for example, Barbosa and MacKenzie [1] found that geopolymers remain totally amorphous up to 1200°C, whereas Duxson observed crystallisation to begin as low as 600°C [29].

Mineral phases nepheline ($\text{NaAlSi}_3\text{O}_8$), leucite (KAlSi_2O_6) and kaliophilite ($\text{KAl}_4\text{Si}_4\text{O}_{16}$), have been observed to crystallise from the geopolymer paste in geopolymers exposed up to 1000°C [1, 8, 11, 17]. Bell *et al.* [42] formed pollucite ($\text{CsAlSi}_2\text{O}_6$) from a Cs-geopolymer heated to above 1000°C. Higher temperature studies by Barbosa and MacKenzie [1] observed corundum (Al_2O_3) and mullite ($\text{Al}_6\text{Si}_2\text{O}_{13}$) forming in metakaolin geopolymers at temperatures greater than 1100°C. Duxson [8] found that initially amorphous geopolymers can contain greater than 80% crystalline material after heating to 1000°C.

The degree and type of crystallisation in geopolymers depends on sample composition and heating conditions. Poorly reacted geopolymers have additional Na or K, Si or Al monomers not incorporated in the geopolymer paste and consequently exhibit higher crystal growth during heating [1, 11]. Sodium based geopolymers have been observed to be more prone to crystallisation than potassium geopolymers [8, 11] which has been attributed to sodium's higher diffusion coefficient [11].

The Si:Al ratio is once again a strong influence on the behaviour of geopolymers at high temperatures. It has been observed that the extent of crystallisation (the amount of amorphous content that crystallises) decreases with increasing Si:Al ratio [8, 28]. Coupled with this is the onset temperature of crystallisation increases with Si:Al ratio [8]. In general terms, the higher the Si:Al ratio, the greater the phase stability of the geopolymer paste during high temperature exposure.

Crystallisation in geopolymers has been observed to be time dependant [8, 17]. Rahier *et al.* [17] analysed the diffraction pattern of metakaolin geopolymers held at 1000 °C and found that the small amount of nepheline initially present at 1000 °C increased significantly over the period of 2.5 hours. Similarly, Duxson *et al.* [8] demonstrated that increased heat rates during testing, reduced that amount of crystal growth of some phases.

15.7.2 Phases formed from secondary material

Geopolymers are a composite material with crystalline phases present amongst the amorphous paste. The crystalline material initially present in the geopolymers can either come from the source material or the aggregate. This material is subject to phase changes during high temperature exposure which can affect the bulk thermal properties of the geopolymer.

Rickard *et al.* [4] observed increased hematite (Fe_2O_3) in XRD data of fly ash geopolymers after heating to 900 °C. The hematite phase evolved from the amorphous iron oxides (commonly ferrihydrite) initially present in the fly ash. The ferrihydrite-hematite phase change is reported to be kinetic in the literature [30], however it was observed to be oxygen dependant in geopolymers. Bakharev [11] observed a similar increase in hematite peak intensity in fly ash geopolymers after exposure to 1200 °C.

Quartz is commonly found in geopolymers, not only as part of the aggregate but as a fine impurity in the source material (common in fly ashes). Quartz undergoes a phase change at 573°C from low to high quartz [31], which is observable in DTA thermograms and dilatometry curves of geopolymers [4]. The phase change, as previously mentioned, is accompanied by a volume change which adversely influences the bulk properties such as mechanical strength. There may be other crystalline phases of silica in fly ash geopolymers (formed during the high temperature coal combustion process) such as cristobalite or tridymite which will undergo phase changes upon heating.

Gehlenite ($\text{Ca}_2\text{Al}_2\text{SiO}_7$) has been observed to form at 800°C in geopolymer samples containing lime ($\text{Ca}(\text{OH})_2$) and is produced by the decomposition of calcium-silicate-hydrates (C-S-H) phases [7, 24].

OPC is made up of several crystalline phases and is thus more structured than the amorphous geopolymers. However, the crystalline phases in OPC, such as C-S-H, are not stable at high temperature and consequentially breakdown, resulting in poor thermal resistance. From a phase stability standpoint alone, geopolymers are intrinsically more thermally resistant than OPC products.

15.8 Microstructural changes

Changes in geopolymer microstructure have been observed to affect the bulk thermal properties and as such are important to study and characterise.

Electron microscopy has been widely used to analyse the microstructure of geopolymers due to its high resolution. Electron microscopy can be performed using a scanning electron microscope (SEM) or a transmission electron microscope (TEM). Pore analysis is of interest to researchers to understand the implications for mechanical strength and thermophysical properties. There are a wide range of pore analysis techniques including mercury intrusion porosimetry (MIP), nitrogen adsorption/desorption and x-ray computed tomography (XCT).

Thermal exposure alters the microstructure of geopolymers in a number of ways. Sintering, crystallisation and eventual melting alter the morphology of the paste at high temperatures, whilst dehydration and densification affect the size and distribution of the pore structure.

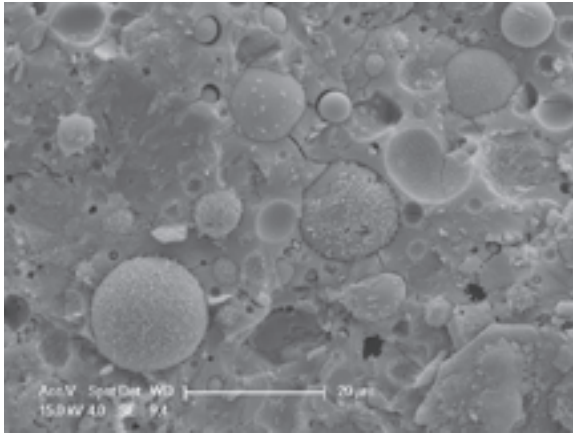
Dehydration causes the first microstructural change, beginning at just above ambient temperature and continuing to above 200°C. Vapour pressure from the escaping water causes damage to the geopolymer structure and alters the pore interconnectivity by creating pathways to the surface of the material. Kong *et al.* [10] reported that metakaolin geopolymers experience more damage to the microstructure during evaporation than fly ash geopolymers due to the lower interconnectivity of the pore structure.

At higher temperatures, sintering and densification of the geopolymer paste alter the morphology (Fig. 15.12). The post exposure geopolymer paste has fewer inclusions and exhibits a smoother texture than the unexposed geopolymer. This is caused by the viscous sintering of the paste during the high temperature exposure which also leads to crack healing. This was also observed by Duxson *et al.* [12] in metakaolin geopolymers. Note the partially dissolved fly ash particles are seen to have a porous internal structure. It is the opinion of the authors that all the amorphous aluminosilicate material has melted into the surrounding geopolymer paste and only the inert crystalline material remains. Similar observations were made in investigations by Bakharev [11] and Kong *et al.* [10].

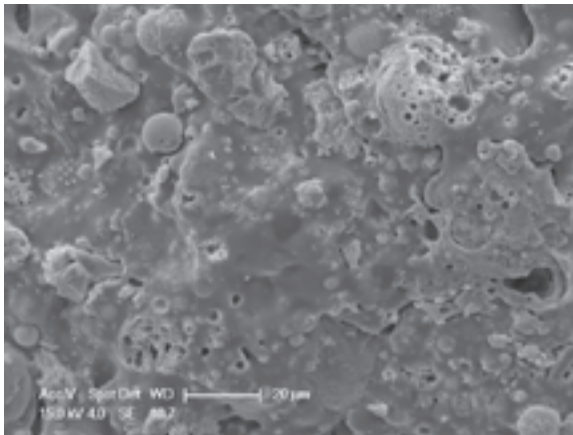
Geopolymers containing aggregates undergo additional microstructural changes during high temperature exposure. Differential thermal dilation of geopolymer and the aggregate (especially aggregates containing quartz) cause a separation at the interface. After sintering, viscous flow of the paste may re-establish contact with the aggregate [25].

15.8.1 Pore structure evolution

Fly ash geopolymers exhibit quite different changes in pore structure compared to metakaolin geopolymers during heating. Fly ash geopolymers have smaller, more connected pores than metakaolin geopolymers which better allows water to permeate to the surface (Fig. 15.13). Fly ash geopolymers also contain unreacted fly ash particles that can also contain pores.



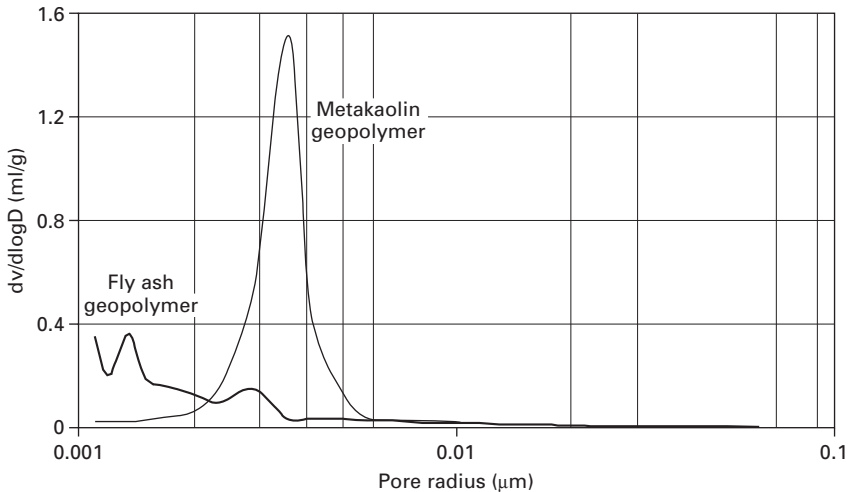
(a)



(b)

15.12 SEM micrographs of the fracture surface of a fly ash geopolymer before and after high temperature exposure. (a) Unexposed. (b) After exposure to 900°C.

During heating, the pore volume of all geopolymers increases initially as voids once filled with water are emptied. At higher temperatures, multiple factors influence the size and distribution of the pores. Melting of the amorphous material from fly ash particles during heating exposes additional pores from within the unreacted fly ash particles [10]. This can be seen in Fig. 15.12. The additional porosity from the unreacted fly ash particles increases the total interconnected porosity of the geopolymer composite. Metakaolin geopolymers do not experience such an effect and as such do not in general exhibit as great an increase in pore volume after heating as fly ash geopolymers.



15.13 Mercury intrusion porosimetry data showing pore size distributions of metakaolin and fly ash geopolymers at the age of 3 days [10].

Bakharev [11] found that in fly ash geopolymers the cumulative pore volume, when compared to unheated samples, increased by 26% and 29% after exposure to 800 and 1000°C, respectively. The same study also found that the average pore size increased significantly from 37.6 nm in initial specimen to 121 and 1835 nm after exposure to 800 and 1000°C, respectively [11]. Duxson *et al.* [3] found that the pore volume of metakaolin geopolymers decreases slightly after the initial increase due to dehydration. Above the sintering temperature, the pore structure in metakaolin geopolymers was inaccessible to nitrogen absorption and as such could not be measured.

Degeneration and subsequent crystallisation in the geopolymer paste has also been attributed to an increase in porosity [11] in geopolymers as the freed monomers pack more densely into an ordered structure. Thus, geopolymers that experience greater crystallisation, such as low Si:Al samples, will exhibit a greater increase in pore volume after high temperature exposure, all else being constant.

Microstructural investigations on OPC reveal a clear deformation of well-developed calcium hydroxide crystals and C-S-H gel beyond 600°C [32]. This is much more extensive than the microstructural variations in geopolymers and is the main reason for the large loss of strength in OPC after high temperature exposure.

15.9 High temperature applications of geopolymers

The fire-resistant character of geopolymers has led them to be suggested for use in applications where fire damage can be critical for the structure

or its occupants. Geopolymer products have the benefit over OPC of significantly reduced spalling and mechanical strength loss after exposure to fire. Example applications for fire-resistant geopolymer products include tunnels, high rise buildings and ships. The structure can be insulated or protected by a geopolymer coating, or built entirely from geopolymer concrete. Geopolymer coatings may be sprayed (either as shotcrete or gunnite) or precast during the construction phase. This application is especially useful for protecting metallic structures such as I-beams from melting during a fire. Structures built entirely from geopolymer concrete provide the best fire protection by removing lamina effects caused by the differential thermal expansion of the coating and the structure. Tunnels built from geopolymer concrete will be significantly safer in the event of a fire than ones built just from OPC.

Geopolymers composites have been trialled, for use in aircraft due to their fire resistance and comparatively low density [33]. This technology is still in its infancy however it has shown great potential. Geopolymer composites have also been used as thermal insulation on the exhaust pipes of Formula 1 race cars [34].

Specialised geopolymer formulations are suitable for refractory applications. Low water content and highly pure geopolymers suit industrial refractory applications where the material may be subjected to temperatures in excess of 1200°C.

Kriven *et al.* [35] demonstrated that Cs- and K-based geopolymers could be used as precursors to form the ceramic phases pollucite and leucite, respectively. This is quite an alternative application, but novel and exciting none the less.

High temperature geopolymer products are on the cusp of production and with further research and development will one day enhance the suite of materials available to society.

15.10 References

1. Barbosa, V.F.F. and MacKenzie, K.J.D. Thermal behaviour of inorganic geopolymers and composites derived from sodium polysialate *Materials Research Bulletin*, 2003. **38**(2): p. 319–331.
2. Walls, P.A. *Optimising the Processing of Geopolymer Cements*. in *26th Conference on Cement and Concrete Science*. 2006. Sheffield University, UK.
3. Duxson, P., Lukey, G.C. and van Deventer, J.S.J. Physical evolution of Na-geopolymer derived from metakaolin up to 1000°C., *Journal of Materials Science*, 2007. **42**(6): p. 3044–3054.
4. Rickard, W.D.A., Van Riessen, A. and Walls, P.A. Thermal character of geopolymers synthesised from class F fly ash containing high concentrations of iron and α -quartz. *International Journal of Applied Ceramic Technology*, 2008. doi:10.1111/j.1744-7402.2008.02328.x.

5. Rickard, W.D.A. *Thermal properties of Geopolymers*. 2007. Curtin University of Technology, Perth. Honours Thesis.
6. Rahier, H., Simons, W. van Mele, B. and Biesemans, M. Low-temperature synthesized aluminosilicate glasses. Part III Influence of the composition of the silicate solution on production, structure and properties. *Journal of Materials Science*, 1997. **32**: p. 2237–2247.
7. Dombrowski, K., Buchwald, A. and Weil, M. The influence of calcium content on the structure and thermal performance of fly ash based geopolymers. *Journal of Materials Science*, 2007. **42**: p. 3033–3043.
8. Duxson, P., Lukey, G.C. and van Deventer, J.S.J. Thermal evolution of metakaolin geopolymers: Part 2 – Phase stability and structural development. *Journal of Non-crystalline Solids*, 2007. **353**: p. 2186–2200.
9. Subaer, *Influence of Aggregate on the Microstructure of Geopolymer*. 2005. Curtin University of Technology, Perth. PhD Thesis.
10. Kong, D., Sanjayan, J. and Sagoe-Crentsil, K. Comparative performance of geopolymers made with metakaolin and fly ash after exposure to elevated temperatures. *Cement and Concrete Research*, 2007. **37**: p. 1583–1589.
11. Bakharev, T., Thermal behaviour of geopolymers prepared using class F fly ash and elevated temperature curing. *Cement and Concrete Research*, 2006. **36**: p. 1134–1147.
12. Duxson, P., Lukey, G.C. and van Deventer, J.S.J. Thermal evolution of metakaolin geopolymers: Part 1 – Physical evolution. *Journal of Non-crystalline Solids*, 2006. **352**(22–23): p. 2186–2200.
13. Kong, D., Sanjayan, J.G. and Sagoe-Crentsil, K. *The behaviour of Geopolymer Paste and Concrete at Elevated Temperatures*. in *Proceeding of the International Conference on Pozzolan, Concrete and Geopolymer*. 2005. Khon Kaen.
14. Bazant, Z.P. and Kaplan, M.F. *Concrete at High Temperatures*. 1996, Essex: Longman Group Limited. pp. 39–58.
15. Cruz, C.R. and Gillen, M. Thermal Expansion of Portland Cement Paste, Mortar and Concrete at High Temperatures. *Fire and Materials*, 1980. **4**(2): p. 66–70.
16. Subaer and van Riessen, A. Thermo-mechanical and microstructural characterisation of sodium-poly(silicate-siloxo) (Na-PSS) geopolymers. *Journal of Materials Science*, 2006. **42**(9): p. 3117–3123.
17. Rahier, H., Wastiels, J. Biesemans, M. Willem, R. van Assche, G. and van Mele., B Reaction Mechanism, kinetics and high temperature transformations of geopolymers. *Journal of Materials Science*, 2007. **42**: p. 2982–2996.
18. Kong, D., Sanjayan, J. and Sagoe-Crentsil, K. Factors affecting the performance of metakaolin geopolymers exposed to elevated temperatures. *Journal of Materials Science*, 2008. **43**: p. 824–831.
19. Gustafsson, S.E. Transient plane source techniques for thermal conductivity and thermal diffusivity measurements of solid materials. *Review of Scientific Instruments*, 1991. **62**(3): p. 797–804.
20. Liefke, E. *Industrial applications of foamed inorganic polymers*. in *Geopolymere '99*. 1999. Saint-Quentin, France.
21. Duxson, P., Lukey, G.C. and van Deventer, J.S.J. Thermal Conductivity of Metakaolin Geopolymers Used as a First Approximation for Determining Gel Interconnectivity. *Industrial and Engineering Chemistry Research*, 2006. **45**: p. 7781–7788.
22. Demiborga, R. Thermo-mechanical properties of sand and high volume mineral admixtures. *Energy and Buildings*, 2003. **35**: p. 435–439.

23. Kong, D. and Sanjayan, J.G. Damage behavior of geopolymer composites exposed to elevated temperatures. *Cement and Concrete Composites*, (in print), available online, <http://dx.doi.org/10.1016/j.cemconcomp.2008.08.001>, 2008.
24. Perera, S. and Trautman, R.L. Geopolymer with the Potential use as Refractory Castables. *AZojomo (Journal of Materials online)*, 2006. **2**: p. 1–5.
25. Zuda, L., Pavlik, Z., Rovnanikova, P., Bayer, P. and Cerny, R. Properties of Alkali Activated Aluminosilicate Materials after Thermal Load. *International Journal of Thermophysics*, 2006. **27**(4): p. 1250–1263.
26. Neville, A.M. *Properties of Concrete*. 4th Edition ed. 1995, Essex: Addison Wesley Limited. pp. 385–387.
27. Scrivener, K.L., Cabiron, J. and Letourneux, R. High-performance concretes from calcium aluminate cements *Cement and Concrete Research*, 1999. **29**(8): p. 1215–1223.
28. Barbosa, V.F.F. and MacKenzie, K.J.D. Synthesis and thermal behaviour of potassium silicate geopolymers. *Materials Letters*, 2003. **57**: p. 1477–1482.
29. Duxson, P., Lukey, G.C. and van Deventer, J.S.J. Evolution of Gel Structure during Thermal Processing of Na-Geopolymer Gels. *Langmuir*, 2006. **22**: p. 8750–8757.
30. Cornell, R.M. and Schwertmann, U. *The Iron Oxides: Structure, Properties, Reactions, Occurrence and Uses*. 1996, Weinheim: VCH.
31. Deer, W.A., Howie, R.A. and Zussman, J. *An Introduction to The Rock Forming Minerals. 2nd Edition*. 1996, Essex, England.
32. Handoo, S.K., Agarwal, S. and Agarwal, S.K. Physicochemical, mineralogical, and morphological characteristics of concrete exposed to elevated temperatures. *Cement and Concrete Research*, 2002. **32**(7): p. 1009–1018.
33. Giancaspro, J., Balaguru, P.N. and Lyon, R.E. Use of Inorganic Polymer to Improve the Fire Response of Balsa Sandwich Structures. *Journal of Materials in Civil Engineering*, 2006. **18**(3): p. 390–397.
34. Geopolymer Institute, Geopolymer composite material for structural or protective applications, temperature range 300°C to 1000°C. 2008. Accessed on 3/8/2008; Available from: <http://www.geopolymer.org/applications/fire-proof-heat-resistant-composites>.
35. Kriven, W.M. *From Geopolymers to Ceramics*, Proceedings of International Conference, Materials and Austceram, Sydney, Australia, 2007.
36. Working Party on Fire Engineering, The National Committee on Structural Engineering, *Fire Engineering for Building Structures and Safety*, Institution of Engineers Australia, 1989, 205 p.
37. Sanjayan, G. and Stocks, L. Spalling of High-Strength Silica Fume Concrete in Fire, *ACI Materials Journal, American Concrete Institute*, **90** (2), March-April, 1993, pp. 170–173.
38. ASTM E119-05a, *Standard Test Methods for Fire Tests of Building Construction Materials*, ASTM International, 32 p.
39. ISO 834: 1999, *Fire-resistance tests – Elements of building construction – Part 1: General requirements*, International Organization for Standardization, 1999.
40. EN1991-1-2, Eurocode 1: *Actions on Structures – Part 1-2: General Actions – Actions on structures exposed to fire*, European Standard, 2004.
41. EN1992-1-2, Eurocode 2: *Design of concrete structures – Part 1-2: General rules – Structural fire design*, European Standard, 2004.

42. Bell, J.L., Sarin, P. Provis, J.L. Haggerty, R.P. Dreimeyer, P.E. Chupas, P.J. van Deventer J.S.J. and Kriven, W.M. Atomic structure of a cesium aluminosilicate geopolymer: A pair distribution function study, *Chem. Mater*, **20**, 4768–4776.
43. Weast, R.C. (editor) *CRC Handbook of Chemistry and Physics*, 65th edition, 1986, p E6. CRC Press, Inc. Boca Raton, Florida.

Utilisation of low-calcium slags to improve the strength and durability of geopolymers

K KOMNITSAS and D ZAHARAKI,
Technical University of Crete, Greece

Abstract: The present chapter discusses the main factors affecting the compressive strength of geopolymers produced from low-calcium ferronickel slag, namely paste composition, activator concentration, pre-curing, thermal conditions and presence of additives. Durability and structural integrity of geopolymers immersed in various aquatic and acidic solutions or subjected to freeze-thaw cycles over a period of 9 months as well as to high temperature heating are also investigated. XRD, SEM, FTIR and TG were used to identify new phases and subsequently elucidate to a certain extent the mechanisms involved.

Key words: low-calcium slag, alkali, compressive strength, durability.

16.1 Introduction

Millions of tons of metallurgical slags, consisting mainly of silicate and glassy phases, are produced every year from several types of furnaces during non ferrous, ferrous metal and steel production. In steelmaking, the generation of slags reaches almost 15% of the quantity of metal produced (Wang and Scrivener, 1995; Viklund-White and Ye, 1999; Wang, 2000). Molten slags are usually fast cooled with water so that fine grained and often brittle material is produced.

Slags were considered as non toxic and have been used widely in the past in several applications, e.g. harbour and, road construction, etc. (Kontopoulos *et al.*, 1996). Today, blast furnace slag is mainly used in Portland cement production, whereas the small reactivity of steel slag restricts its large scale use as additive in the concrete and cement industry (Zhang *et al.*, 2007; Hu *et al.*, 2008). Large quantities of slags are still disposed of in surface dumps or under the sea in several countries (Komnitsas *et al.*, 2007; Zhang *et al.*, 2007).

Mining and metallurgical waste disposal practices must comply with environmental regulations enabling among others immobilisation of hazardous elements. Under specific environmental conditions solubilisation and subsequent migration of some of these elements may endanger the quality of surface- and groundwater causing thus severe damage to affected ecosystems (Kontopoulos *et al.*, 1996). In addition, the implementation in

most countries of new strict environmental regulations through the adoption of recent European Commission (EC) and other waste management directives necessitates the development of an integrated management scheme that prohibits disposal of metallurgical slags without prior detailed environmental characterisation and toxicity assessment (EC – IPPC Bureau, 2002).

The need for the development of new-low cost technologies that utilise these by-products for the development of high added value materials is soon expected to increase. Establishment of geopolymerisation as a feasible technology for the management of metallurgical wastes, such as slags, is anticipated to offer considerable savings in disposal costs and reduce greenhouse gas emissions. Mining and metallurgical wastes could serve as potential source materials for the synthesis of geopolymers characterised by less porous microstructure, advanced mechanical and thermal properties and good resistance to attack by aggressive solutions (Phair and Van Deventer, 2002; Xu and Van Deventer, 2002; Phair *et al.*, 2004; Bakharev, 2005a; Buchwald *et al.*, 2007; Komnitsas and Zaharaki, 2007).

Alkali-activation of high-calcium slags has been investigated over the last years and the resulting products have been used in large-scale construction applications in Europe (Glukhovskiy, 1994; Cheng and Chiu, 2003; Van Deventer *et al.*, 2007). Astutiningsih and Liu (2005) produced geopolymers using Australian milled slag with a CaO content of almost 40%; the paste was cured at 60 °C for 24 h and the final products exhibited compressive strength of 30 MPa. Cheng and Chiu (2003) used granulated blast furnace slag as active filler for the production of geopolymers and the compressive strength acquired reached 79 MPa. Similar results were obtained when blast furnace slag was mixed with metakaolinite and heated at 80 °C for 8 hours (Buchwald *et al.*, 2007; Zhang *et al.*, 2007). Furthermore, geopolymers synthesised using low-calcium slag exhibited maximum compressive strength of almost 60 MPa (Zaharaki *et al.*, 2006; Komnitsas *et al.*, 2007; 2009; Zaharaki and Komnitsas, 2008). Excessive content of CaO in slags is often undesirable since Ca²⁺ substitutes Na⁺, affects charge balance and deteriorates the properties of the final products (Yip and Van Deventer, 2003; Astutiningsih and Liu, 2005; Buchwald *et al.*, 2007).

The present chapter discusses the main factors affecting the compressive strength of geopolymers produced from low-calcium ferronickel slag, namely paste composition, activator concentration, pre-curing, thermal conditions and presence of additives. Durability and structural integrity of geopolymers immersed in various aquatic and acidic solutions or subjected to freeze-thaw cycles over a period of 9 months as well as to high temperature heating are also investigated. XRD, SEM, FTIR and TG were used to identify new phases and subsequently elucidate to a certain extent the mechanisms involved.

16.2 Materials and methodology

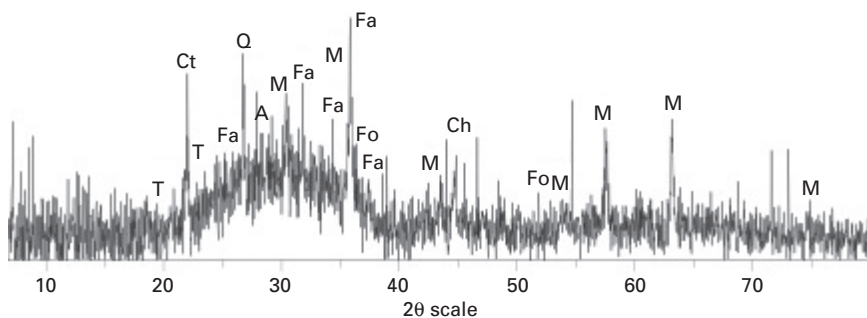
Electric arc slag produced at LARCO S.A Larymna ferronickel plant, Greece, was used for the synthesis of geopolymers. The annual slag production is about 1,700,000 t of which approximately 450,000 t are used by the cement industry. Disposal cost of the remaining quantities reaches € 650,000/year. The particle size of the brittle slag varies between 0.075 and 4 mm (most of it is seen in the 0.1–1.5 mm fraction). Slag was dried and crushed (91% $-50\ \mu\text{m}$, 47% $-10\ \mu\text{m}$) using a FRITSCH pulveriser in order to increase surface area and improve the compressive strength of the produced geopolymers (Zaharaki, 2005; Zaharaki and Komnitsas, 2005; Zaharaki *et al.*, 2006). Additives used include kaolinite (Fluka), metakaolinite (derived by calcining kaolinite at 600°C for 4 hours), CaO (Alfa Aesar), silica sand as well as pozzolan, fly ash, red mud and glass.

Table 16.1 shows the chemical analysis of the slag and the additives used in the form of oxides and trace elements. The iron content in slag is shown as Fe_2O_3 , but a significant fraction of ferrous iron is also present. Trace elements are seen in elemental form. The main mineralogical phases present in slag, namely fayalite, anorthite, quartz, tridymite, cristobalite, magnetite, forsterite and chromite are seen in the XRD pattern of Fig. 16.1. From the shape of the pattern it is estimated that the amorphous content exceeds 50%.

Silica sand, purchased in a granular form, consists of quartz. Pozzolan, obtained from Milos island, Greece, is a very cheap material and when used in Portland cement concrete increases its long-term compressive strength. Fly ash was obtained from Ptolemais, N.W. Greece, thermal power station and is classified according to ASTM as type C; its main mineralogical phases

Table 16.1 Chemical analysis of raw material and additives

%	Ferronickel slag	Pozzolan	Fly ash	Red mud	Commercial glass
Fe_2O_3	43.83	1.09	5.60	45.48	–
SiO_2	32.74	72.22	33.40	6.96	74.00
Al_2O_3	8.32	17.73	13.10	15.65	1.30
CaO	3.73	0.95	35.31	14.84	10.50
Cr_2O_3	3.07	–	–	–	–
MgO	2.76	1.10	3.67	–	–
Mn_3O_4	0.44	0.19	0.19	–	–
Na_2O	–	3.30	0.46	3.26	13.00
K_2O	–	3.05	0.76	–	–
P_2O_5	–	0.56	–	–	–
TiO_2	–	0.14	0.71	4.80	–
SO_3	–	–	6.58	–	–
S	0.18	–	–	–	–
C	0.11	–	–	–	–
Ni	0.10	–	–	–	–
Co	0.02	–	–	–	–



16.1 XRD pattern of slag (Fa: Fayalite, A: Anorthite, Q: Quartz, T: Tridymite, Ct: Cristobalite, M: Magnetite, Fo: Forsterite, Ch: Chromite).

are quartz SiO_2 , calcite CaCO_3 , anhydrite CaSO_4 , gehlenite $\text{Ca}_2(\text{Al}(\text{AlSi})\text{O}_7)$, albite $\text{NaAl}_4\text{Si}_3\text{O}_8$, lime CaO and portlandite $\text{Ca}(\text{OH})_2$. Red mud was obtained from 'Aluminum of Greece' S.A. and consists of quartz SiO_2 , hematite Fe_2O_3 , gibbsite $\text{Al}(\text{OH})_3$, diaspore $\text{AlO}(\text{OH})$, calcite CaCO_3 , cancrinite $\text{Na}_6\text{Ca}_2\text{Al}_6\text{Si}_6\text{O}_{24}(\text{CO}_3)_2$ and katoite $\text{Ca}_3\text{Al}_2(\text{SiO}_4)(\text{OH})_8$. Commercial glass is an amorphous material consisting mainly of silicon, calcium and sodium oxides. Glass and silica sand were pulverised prior to use.

Slag and additives were mixed and added slowly in the activating solution prepared by dissolving sodium or potassium hydroxide anhydrous pellets (ACS-ISO for analysis) in distilled water and mixing with sodium silicate solution (Merck, $\text{Na}_2\text{O}:\text{SiO}_2 = 0.3$, $\text{Na}_2\text{O} = 7.5\text{--}8.5\%$, $\text{SiO}_2 = 25.5\text{--}28.5\%$). Under continuous mechanical mixing a reactive and homogeneous paste was obtained. The wt% addition of slag and additives varies and depends on the reagents used in each case to produce a workable paste. Several control specimens were synthesised using slag and activating solution in each experimental series.

The paste was cast in plastic cubic moulds (5 cm each side) which were vibrated for five minutes to remove trapped air. Some specimens were pre-cured at room temperature for a maximum period of 4 days and then heated in a laboratory oven (MMM GmbH) at the required temperature for 24 or 48 hours. After de-moulding, aging took place at room temperature for either 7 or 28 days in order to enhance the development of structural bonds. The compressive strength was then measured using an MTS 1600 load frame. All experiments were carried out in duplicate. Only in a few cases, when deviation in the experimental results was higher than 10%, additional specimens were prepared.

In order to study the geochemical stability of the produced geopolymers, specimens synthesised using slag and kaolinite under the conditions 80°C , 48 h, 28 d were immersed in solutions containing distilled, seawater and 0.5N HCl and left for a maximum period of 9 months. Initially, 400 mL of

each solution were used, while fresh solutions were added when required to account for evaporation losses. Liquid samples were collected monthly and analysed for pH, oxidation-reduction potential (Hanna 211 pH/Eh meter) and electrical conductivity (Hanna EC215 conductivity meter). Seawater was considered as a lixiviant to assess the integrity of geopolymers when used in coastal or under water construction works. HCl solution was used to assess their behaviour in extremely aggressive/corrosive industrial environments.

Specimens were subjected to freeze-thaw cycles (using -15°C and 20°C as temperature extremes) for a period of 9 months as well as to high temperature heating (up to 800°C) for 6 hours to assess their structural integrity; no kaolinite was added during geopolymer synthesis when the effect of high temperature heating was studied.

XRD analysis was performed by a Siemens D500 diffractometer using a Fe tube and a scanning range from 3° to $70^{\circ} 2\theta$, with a step 0.03° and 4 sec/step measuring time. Qualitative analysis was carried out using the *Diffrac_{plus}* Software (Bruker AXS) and the PDF database. Imaging of the geopolymer microstructure was carried out using a JEOL JSM-5400 scanning electron microscope equipped with an Oxford energy dispersive X-ray spectrometer (EDS). The samples were coated with carbon prior to analysis to increase conductivity of the surface. FTIR analysis was carried out by the FTIR Spectrometer Model 1000 (Perkin-Elmer) using the KBr pellet technique (1.5 mg powder sample mixed with 150 mg of KBr). TG analysis was performed using a Perkin Elmer Thermogravimetric Analyser TGA 6 (maximum heating temperature was 950°C at a rate of $10^{\circ}\text{C min}^{-1}$ using a nitrogen purge rate of 60 mL min^{-1}).

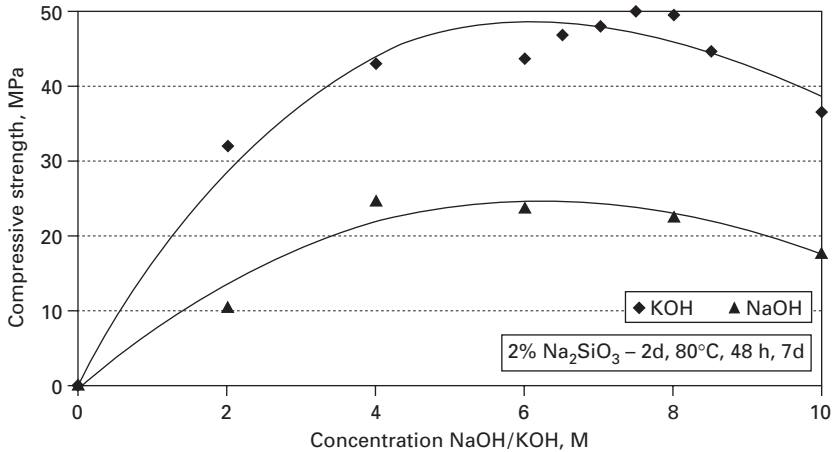
16.3 Factors affecting compressive strength

16.3.1 Alkali hydroxide/alkali silicate concentration

In order to examine the effect of NaOH/KOH concentration on the compressive strength, geopolymers were synthesised using slag and activating solution. Pre-curing took place for 2 days at room temperature and then the specimens heated at 80°C for 48 hours and cured at room temperature for 7 days.

Figure 16.2 shows that the use of KOH solution is more beneficial and the maximum compressive strength reaches 50 MPa. The optimum strength is acquired for KOH concentration close to 8M; it is underlined though that when the concentration of KOH varies between 4M and 8M the strength of the specimens exceeds 40 MPa whereas when higher concentration is used the strength decreases. It is seen from the experimental results that excess KOH does not accelerate geopolymerisation reactions while it assists the formation of carbonates reducing thus strength.

On the other hand, when NaOH is used, the compressive strength

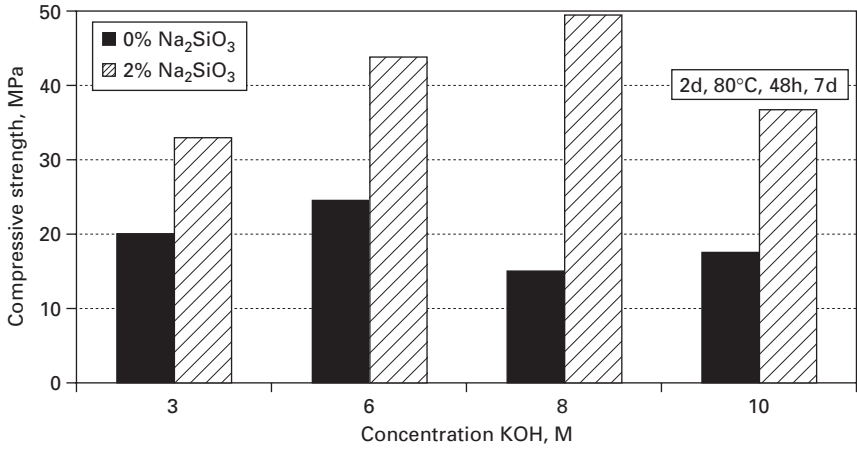


16.2 Evolution of compressive strength of slag-based geopolymers vs. alkali hydroxide concentration.

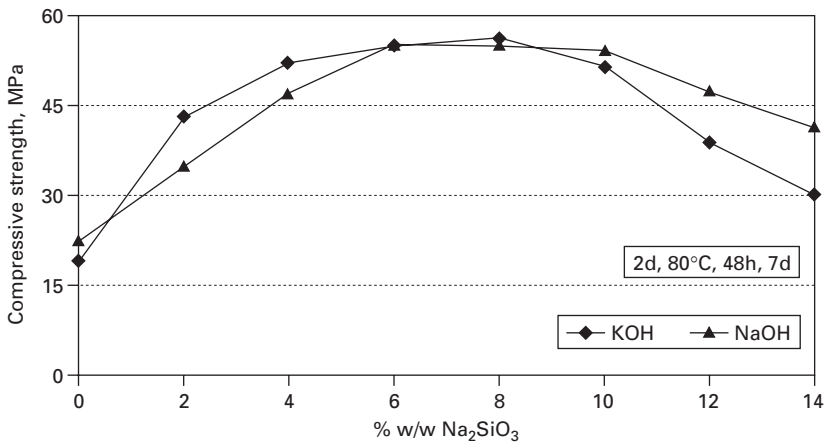
acquired is much lower and does not exceed 25 MPa; the optimum range of NaOH concentration is similar to that of KOH. Alkali hydroxide causes partial solubilisation of Si and Al from the raw materials enhancing thus the development of geopolymeric bonds (Paniias *et al.*, 2007; Komnitsas *et al.*, 2009). It has to be mentioned though that when no alkali hydroxide solution is used, the paste becomes too viscous, cannot solidify and the specimens acquire practically no strength (0.22 MPa).

Figure 16.3 shows the evolution of the compressive strength of slag-based geopolymers vs. KOH concentration in the presence and absence of Na_2SiO_3 . It is seen from this data that when no alkali silicate solution (Na_2SiO_3) is added during synthesis, the paste requires longer time to solidify and the final strength does not exceed 25 MPa. Addition of 2% w/w Na_2SiO_3 improves paste properties and the maximum compressive strength acquired reaches 50 MPa when the concentration of KOH is 8M. It is concluded therefore that sodium silicate solution provides extra soluble silicates, acts as binder or plasticiser thus resulting in denser structures, enhances the development of Si-O-Al bonds and improves the workability of the mixture (Douglas *et al.*, 1991; Van Jaarsveld *et al.*, 1997; Phair, 2001).

Figure 16.4 shows the evolution of the compressive strength of slag-based geopolymers vs. the % w/w addition of Na_2SiO_3 , varying between 0 and 14%. In each case, water percentage was adjusted accordingly, affecting thus also alkali hydroxide concentration, so that a workable paste was obtained. It is seen from this figure that the optimum percentage addition of sodium silicate is close to 8% w/w when either KOH (8.7M) or NaOH (12.2M) is used. The maximum compressive strength acquired is 56.2 MPa which decreases when higher percentages of alkali silicate are used.



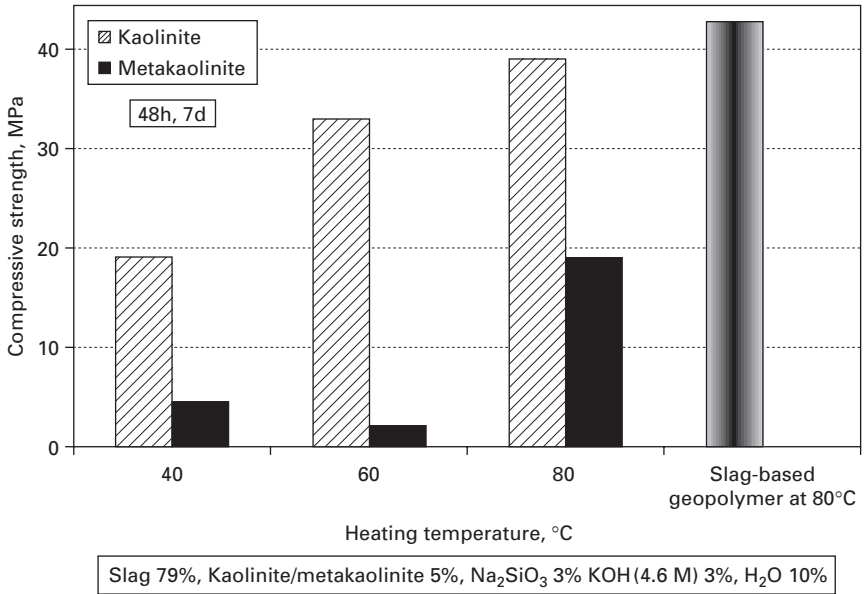
16.3 Evolution of compressive strength of slag-based geopolymers vs. KOH concentration in the presence and absence of Na₂SiO₃.



16.4 Evolution of compressive strength of slag-based geopolymers vs. the % w/w addition of Na₂SiO₃ when either KOH or NaOH is used.

16.3.2 Additives

Several experiments were carried out by mixing slag and various additives so that additional Al and Si ions were provided in the geopolymeric paste. The effect of aluminosilicate fillers, such as kaolinite or metakaolinite, on the compressive strength of geopolymers over a temperature range 40–80°C, is shown in Fig. 16.5. It is seen that increase in temperature results in higher compressive strength for slag-kaolinite geopolymers, which at 80°C reaches almost 40 MPa. When metakaolinite is used the compressive strength is much lower and only at 80°C reaches almost 20 MPa.

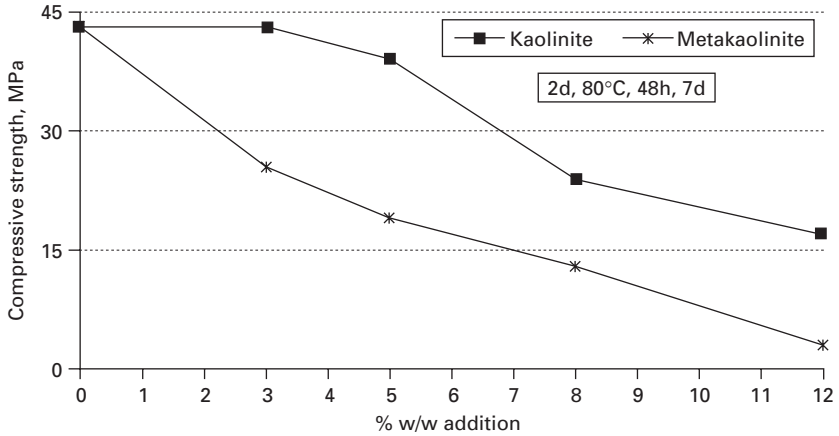


16.5 Evolution of compressive strength vs. temperature when either kaolinite or metakaolinite is added in the starting mixture.

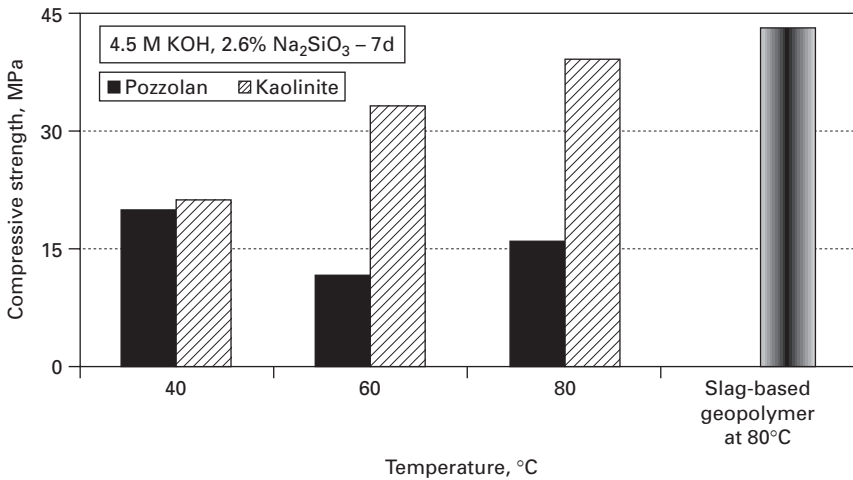
Figure 16.6 shows the evolution of the compressive strength of geopolymers synthesised under the optimum conditions (48 hours heating at 80°C) vs. the % w/w addition of kaolinite or metakaolinite, varying between 0% (control specimen) and 12%. It is seen again that none of the additives used improves the compressive strength; increased percentages of kaolinite or metakaolinite in the initial mixture result in decreased compressive strength, reaching 17 and 3 MPa respectively for the maximum addition percentage of 12% w/w.

Similar results were derived for alkali activated metakaolinite-blast furnace slag mixtures (Buchwald *et al.*, 2007); pure slag geopolymers acquired strength of about 35 MPa whereas pure metakaolinite geopolymers acquired very low strength (5 MPa). On the contrary, metakaolinite-fly ash geopolymers synthesised at room temperature acquired much higher compressive strength compared to fly ash-based geopolymers (Jirasit *et al.*, 2006). Addition of either kaolinite or metakaolinite in fly ash-based geopolymers may also affect the propensity of the matrix to immobilise effectively heavy metals (Van Jaarsveld *et al.*, 2004).

The effect of pozzolan addition on the compressive strength of geopolymers was studied by mixing 5% w/w of pozzolan with slag while the alkali-activated specimens were heated for 48 hours at 40, 60 and 80°C. Figure 16.7 shows the evolution of the compressive strength of geopolymers vs. temperature when either pozzolan or kaolinite were added. Addition of pozzolan results



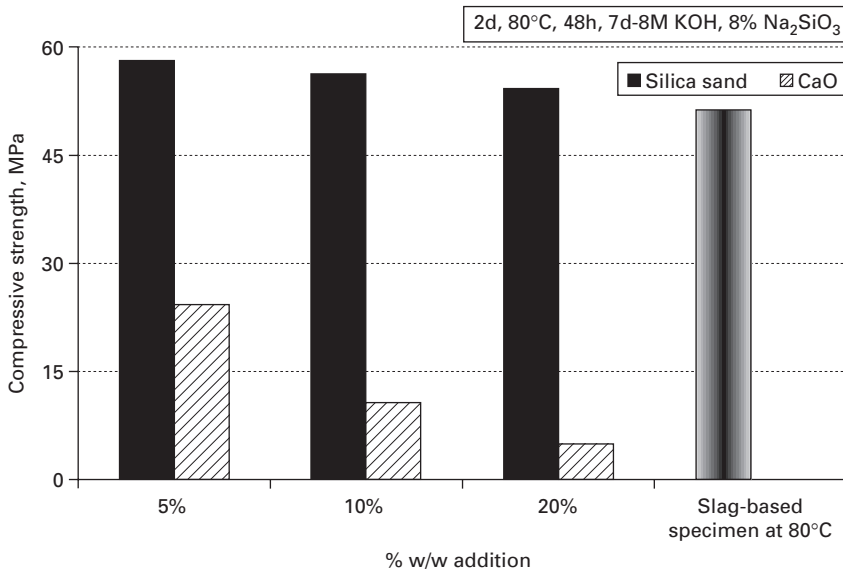
16.6 Evolution of compressive strength vs. the % w/w addition of kaolinite or metakaolinite.



16.7 Evolution of compressive strength vs. temperature when either 5% w/w pozzolan or kaolinite is added.

in decrease of compressive strength by more than 50% compared to the control specimen over the temperature range studied; strength acquired varies between 12 and 20 MPa. On the other hand, addition of kaolinite results in higher compressive strength reaching at 80°C the values obtained for the control specimen.

Figure 16.8 shows the evolution of the compressive strength vs. the % w/w addition of silica sand or CaO in the starting mixture. Silica sand addition improves in all cases the compressive strength that reaches almost 60 MPa. The compressive strength drops slightly when the % w/w silica sand

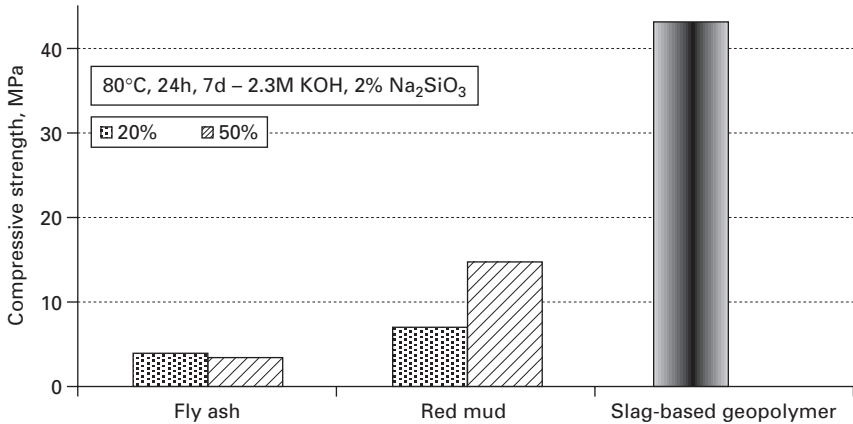


16.8 Evolution of compressive strength vs. % w/w addition of silica sand or CaO.

addition increases from 5% to 20%; this is probably due to the fact that the activating solution used is not sufficient to react with the entire quantity of silica sand and form strong bonds. On the other hand, CaO addition results in low strength which decreases gradually when higher percentages are used; in this case the excess calcium provided in the system cannot react to form more C-S-H gel and therefore the geopolymeric network is disrupted (Zaharaki *et al.*, 2007; Yip *et al.*, 2008).

The effect of fly ash or red mud addition on the compressive strength is shown in Fig. 16.9; these tests were carried out to explore the possibility of co-utilisation of mining and metallurgical wastes. It is seen from this figure that very low strength is obtained for both additives when addition percentages vary between 20 and 50 % w/w. Slag as well as both additives used consist of various oxides exhibiting different degree of solubilisation and therefore the number of Si and Al ions added in the system in each case cannot be easily assessed.

It is therefore seen that addition of kaolinite, metakaolinite, pozzolan, CaO, fly ash or red mud does not further contribute to the formation of stronger geopolymeric bonds. Most of Si and Al ions dissolved from the additives remain practically un-reacted, as also seen in XRD studies (Section 16.5.1) and therefore limited strength is obtained. The high Fe_2O_3 content of slag may also play an important role during geopolymer synthesis, since it may react with the solutions used forming thus strong bonds (Zaharaki *et*



16.9 Effect of fly ash/red mud addition on the compressive strength.

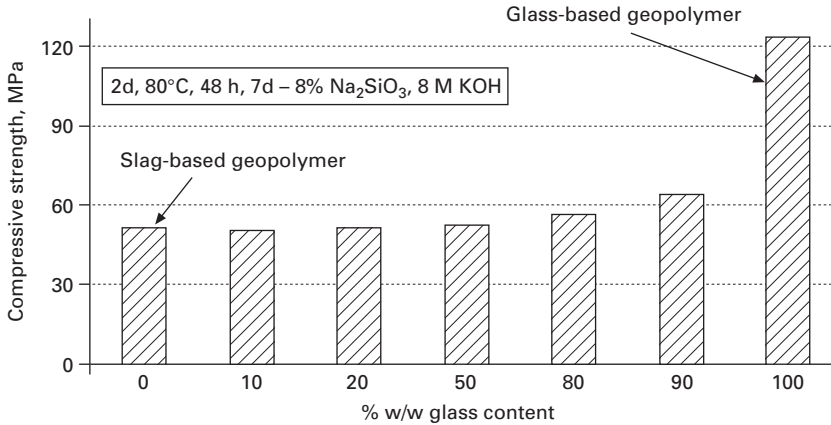
al., 2007); it should be mentioned though that iron does not take part in the formation of geopolymeric gel tetrahedral networks.

Figure 16.10 shows the evolution of the compressive strength vs. the % w/w glass addition; the compressive strength of pure slag and pure glass specimens (used as controls) is also seen. Addition of glass up to 50% w/w in the starting mixture does not practically improve strength which remains close to 52 MPa. When the percentage of glass increases to 90% w/w the acquired strength reaches 64 MPa. When only glass is used as raw material the compressive strength acquired is extremely high and reaches almost 125 MPa. In this case stronger bonds are developed in the amorphous microstructure, which is typical for three dimensional alumino-silicates. It is mentioned that addition of kaolinite in glass-based geopolymers synthesised at 80°C results in much lower strength, barely exceeding 35 MPa (Zaharaki and Komnitsas, 2008).

16.3.3 Paste composition

In order to study the effect of paste composition on the compressive strength several specimens were prepared, as seen in Table 16.2. C is the control specimen while in all other specimens the percentages (% w/w) of kaolinite, KOH and Na_2SiO_3 were modified accordingly. The water content varied slightly in each case so that a workable paste was obtained, but remained close to the optimum value of 12% w/w. Geopolymers were pre-cured for 2 days and then heated at 80°C for 48 hours; aging took place for 7 days.

As seen in Fig. 16.11 when the percentages of the three additives are low ($1/3 \times C$, $1/2 \times C$), the compressive strength acquired is limited and does not exceed 15 MPa. When, on the other hand, these percentages increase



16.10 Evolution of compressive strength of geopolymers vs. the % w/w glass content.

Table 16.2 Composition (% w/w) of slag-kaolinite geopolymers

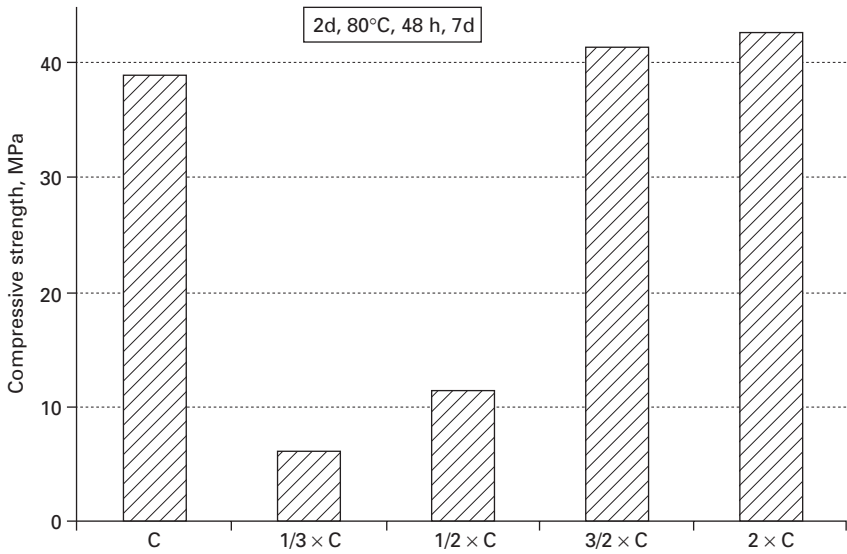
	C	$\frac{1}{3} \times C$	$\frac{1}{2} \times C$	$\frac{3}{2} \times C$	$2 \times C$
Slag	76.60	83.09	81.52	71.78	67.10
H ₂ O	12.45	13.27	13.00	11.80	11.00
Kaolinite	5.43	1.80	2.72	8.14	10.86
KOH	2.97	0.99	1.48	4.46	5.94
Na ₂ SiO ₃	2.55	0.85	1.28	3.82	5.10
Total	100	100	100	100	100

substantially ($\frac{3}{2} \times C$, $2 \times C$) the compressive strength increases only slightly. It is therefore concluded that the composition of the control specimen is considered as optimum.

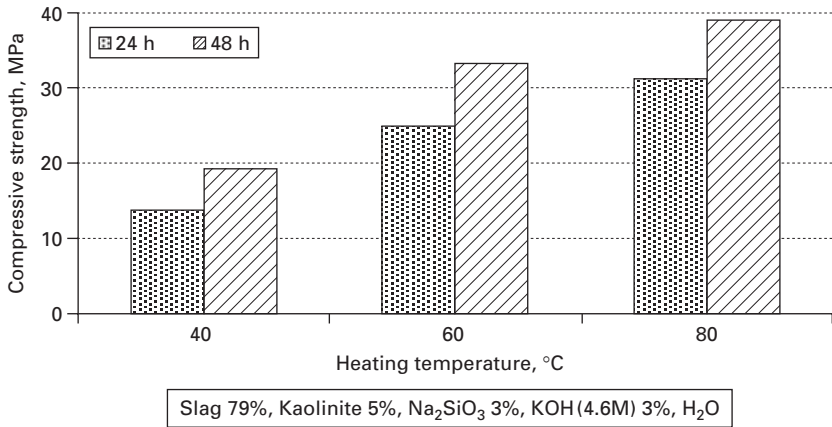
16.3.4 Thermal treatment

In order to examine the effect of heating time and temperature on the compressive strength, slag-kaolinite geopolymers were heated at 40, 60 and 80°C for 24 or 48 hours. Aging took place at room temperature for 7 days. The experimental results are shown in Fig. 16.12. It is seen from this data that when the duration of heating increases from 24 to 48 hours the increase in the compressive strength varies between 26 and 39% over the temperature range examined. On the other hand, the compressive strength increases substantially with temperature, regardless of the heating time, and reaches almost 40 MPa at 80°C after 48 hours heating.

Figure 16.13 shows the effect of pre-curing period, varying between 0 and 4 days, on the compressive strength of slag-kaolinite specimens heated

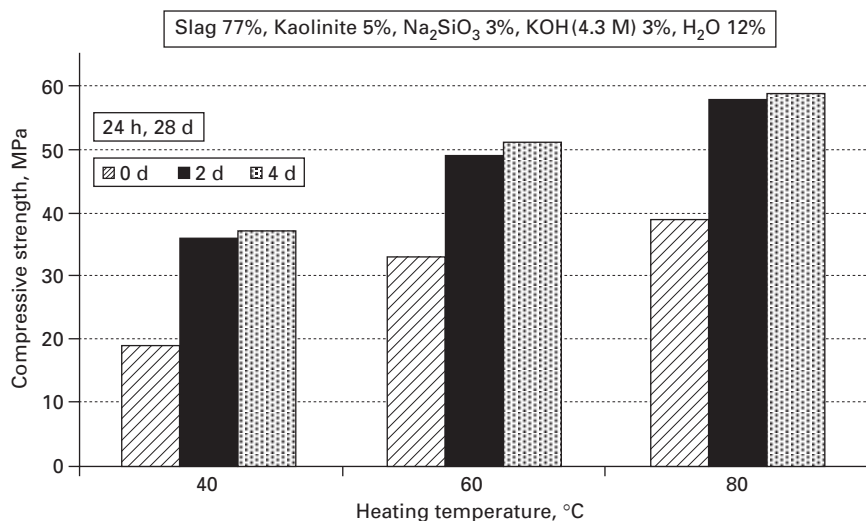


16.11 Effect of paste composition on the compressive strength of slag-kaolinite geopolymers.



16.12 Evolution of the compressive strength vs. temperature and heating time.

at 40, 60 and 80°C for 24 hours and aged at room temperature for 28 days. As seen from the experimental data the compressive strength increases substantially, between 48 and 88% over the temperature range examined, when the paste is pre-cured for 2 days. No further improvement is seen when a longer pre-curing period (4 days) is used. If the paste is not pre-cured but heated immediately the final strength acquired is in general low since most



16.13 Effect of pre-curing period on the compressive strength of slag-kaolinite geopolymers.

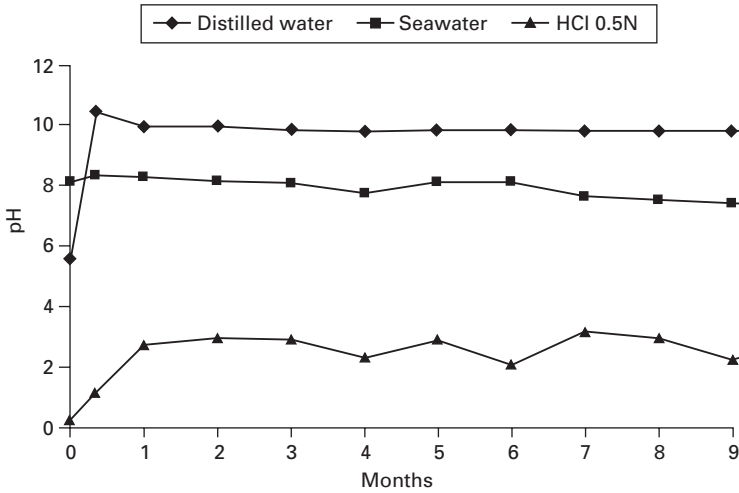
of the water contained in the reactive mixture evaporates fast and cannot participate in reactions involved in strength development.

16.4 Durability studies

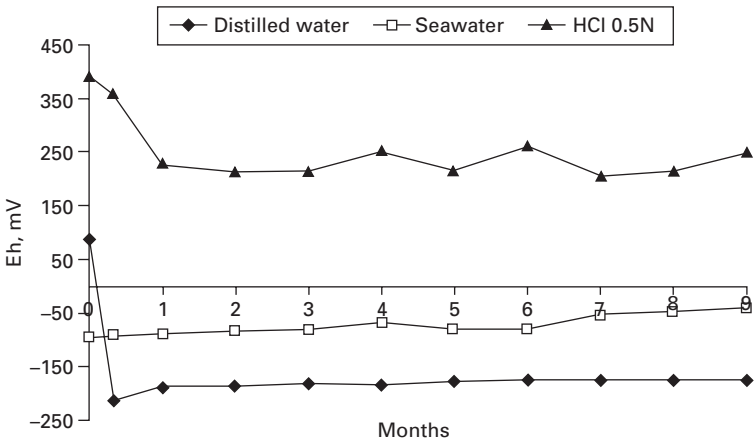
The durability of slag-kaolinite geopolymers was tested by immersing specimens in various aquatic solutions (distilled, seawater, 0.5N HCl) or subjecting them to freeze-thaw cycles over a period of 9 months. Figure 16.14 shows the evolution of pH vs time. In distilled water pH values after an initial increase from 5.6 to 10.5 during the first 10 days drop slightly and remain stable at around 9.9 over the entire experimental period. When geopolymers are immersed in seawater pH values remain practically unchanged at around 8. Immersion for one month in 0.5N HCl solution results in an increase of pH from 0.27 to 2.9; values then fluctuate around this level for the remaining period.

Figure 16.15 shows the evolution of Eh vs. time. Eh values of distilled water decrease from 90 to -215 mV after 10 days of immersion, while for the remaining period remain stable at around -185 mV. When geopolymers are immersed in seawater a slight increase of Eh over time, from -50 mV to -80 mV, is seen. Eh values of 0.5N HCl solution drop from 390 to 230 mV during the first three months and fluctuate around this level for the remaining period.

Figure 16.16 shows the evolution of conductivity vs. time. Conductivity values are in line with pH and Eh measurements; they are extremely low in



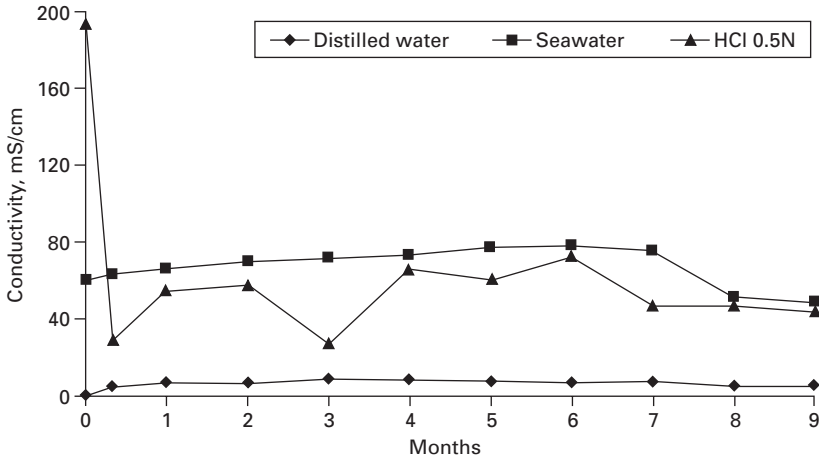
16.14 Evolution of pH vs. time when geopolymers are immersed in various solutions.



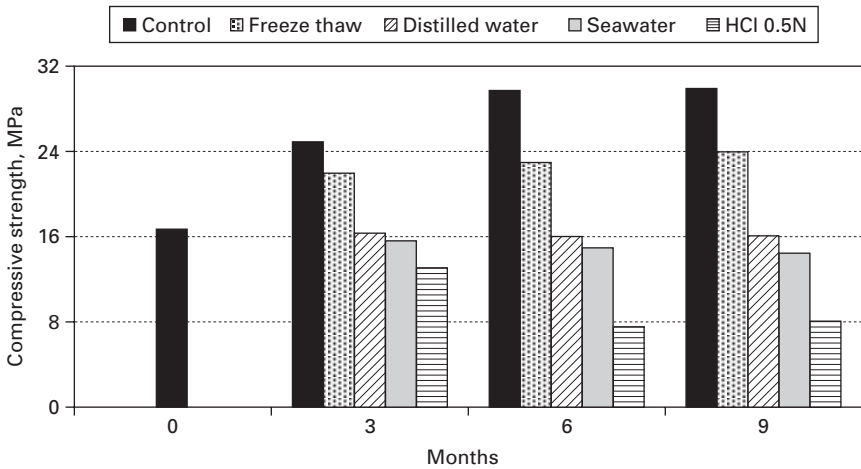
16.15 Evolution of Eh (mV) vs. time when geopolymers are immersed in various solutions.

distilled water and do not exceed 9 mS/cm during the entire experimental period. Higher conductivity values are seen when specimens are immersed in seawater; they increase slowly up to 78 mS/cm until month 6 and then gradually drop to 50 mS/cm. Conductivity values in 0.5N HCl solution after a sharp drop from 193 to 29 mS/cm during the first 10 days of immersion fluctuate between 27 and 73 mS/cm.

The evolution of the compressive strength of geopolymers immersed in various solutions or subjected to freeze-thaw cycles is shown in



16.16 Evolution of conductivity (mS/cm) vs. time when geopolymers are immersed in various solutions.



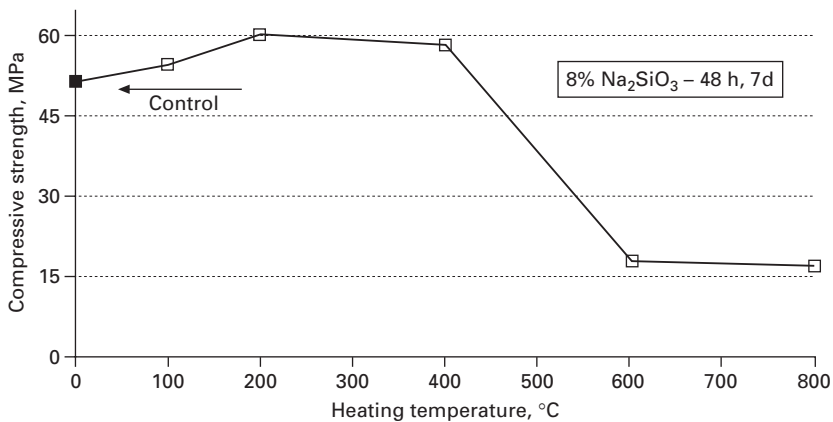
16.17 Evolution of compressive strength of slag-based geopolymers immersed in various solutions or subjected to freeze-thaw cycles.

Fig. 16.17. It has to be underlined at this stage that specimens with lower initial strength were used in order to better assess the effect of the factors investigated. The compressive strength of the control specimen increases significantly with time and reaches 30 MPa after 9 months; no further increase in strength is seen, though, after 6 months. A slight increase in strength is seen for specimens subjected to freeze-thaw cycles; it is therefore concluded that specimens can sustain temperature variations and maintain their structural integrity under conditions exhibiting temperature extremes. Immersion in distilled and seawater over a period of 9 months does not

practically affect compressive strength, indicating that geopolymers can be used in outdoor or coastal applications. On the contrary, a continuous decrease of the compressive strength is seen for specimens immersed in 0.5 N HCl; almost 50% of the compressive strength is lost after 9 months. It is important to underline that the outer surface of specimens immersed in 0.5N HCl solution, which is considered quite aggressive, is eroded and softened, geopolymeric bonds disintegrate and a gel like phase consisting of amorphous silica is formed.

Allahverdi and Škvára (2001a; 2001b; 2005) have also shown that blast furnace slag-fly ash geopolymers were corroded when immersed in nitric acid solution for a period of one month. Corrosion was due to ion exchange reactions between the charge compensating cations of the framework (i.e., sodium, potassium or calcium) and the H^+ ions present in solution as well as due to the electrophilic attack of polymeric Si–O–Al bonds by acid protons, causing thus ejection of tetrahedral aluminum from the aluminosilicate framework.

The structural integrity of specimens was further examined by subjecting them to high temperature heating; slag-based geopolymers produced after heating at 80°C for 48 hours were used since they acquire much higher strength compared to slag-kaolinite geopolymers (Komnitsas *et al.*, 2009). Figure 16.18 shows the evolution of the compressive strength. It is seen from these data that strength increases gradually up to 200°C reaching the maximum value of 60 MPa, whereas a sharp drop is noticed when heating temperature exceeds 400°C; heating at high temperatures accelerates evaporation of lattice water, causing disintegration of Si–O–Al bonds and pore development.



16.18 Evolution of the compressive strength of slag-based geopolymers subjected to high temperature heating.

16.5 Mineralogical studies

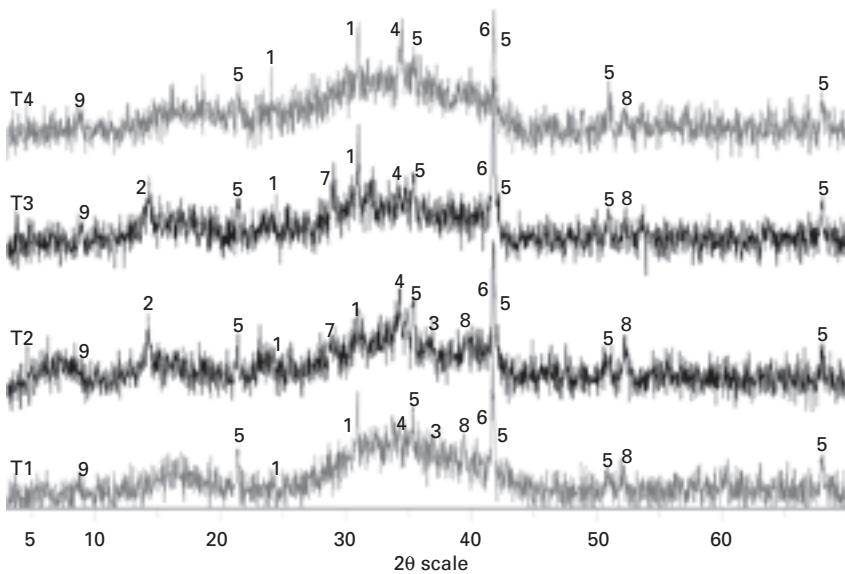
16.5.1 XRD

Despite the substantial amorphous nature of geopolymers, XRD is often used to identify new formed phases, define the degree to which starting materials have reacted and assess the level of amorphicity of the final products. XRD patterns of geopolymers T1, T2, T3 and T4 synthesised under the experimental conditions shown in Table 16.3, are presented in Fig. 16.19.

XRD patterns reveal the presence of kaolinite, fayalite, quartz, magnetite and the formation of new phases, such as hydroxysodalite, maghemite, calcite,

Table 16.3 Experimental synthesis conditions of T1, T2, T3 and T4 geopolymers

Specimen	Composition	Experimental conditions	Compressive Strength (MPa)
T1	Slag 77%, Metakaolinite 5%, NaOH 3%, Na ₂ SiO ₃ 3%, H ₂ O 12%	60°C, 24 h, 7 d	1.5
T2	Slag 77%, Kaolinite 5%, NaOH 3%, Na ₂ SiO ₃ 3%, H ₂ O 12%	60°C, 48 h, 7 d	18
T3	Slag 77%, Kaolinite 5%, KOH 3%, Na ₂ SiO ₃ 3%, H ₂ O 12%	60°C, 24 h, 28 d	53
T4	Slag 75%, Metakaolinite 5%, KOH 6%, Na ₂ SiO ₃ 3%, H ₂ O 12%	80°C, 48 h, 7 d	7

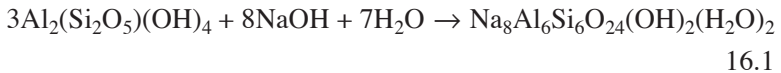


16.19 XRD patterns of geopolymers T1, T2, T3 and T4 (1: Quartz, 2: Kaolinite, 3: Fayalite, 4: Calcite, 5: Magnetite, 6: Maghemite, 7: Hydroxysodalite, 8: Trona, 9: Calcium silicate hydrate).

calcium silicate hydrate and trona. The broad peak seen between 25° and 40° 2θ indicates that specimens T1 and T4 are characterised by a higher level of amorphicity.

The presence of remaining kaolinite in specimens T2 and T3 indicates that the initial amount added has not fully reacted (Van Jaarsveld *et al.*, 2004; Komnitsas *et al.*, 2007). The remaining fayalite, Fe₂SiO₄, seen in lesser quantities in the XRD patterns of specimens T1 and T2, indicates that silicates of the olivine group are easily weathered.

Hydroxysodalite, Na₈Al₆Si₆O₂₄(OH)₂(H₂O)₂, detected only in T2 and T3 slag-kaolinite geopolymers that exhibit higher strength, is formed according to reaction [16.1] between NaOH and kaolinite, when OH⁻ replace Cl⁻ ions in the framework of sodalite Na₄Al₃(SiO₄)₃Cl (Komnitsas *et al.*, 2007):



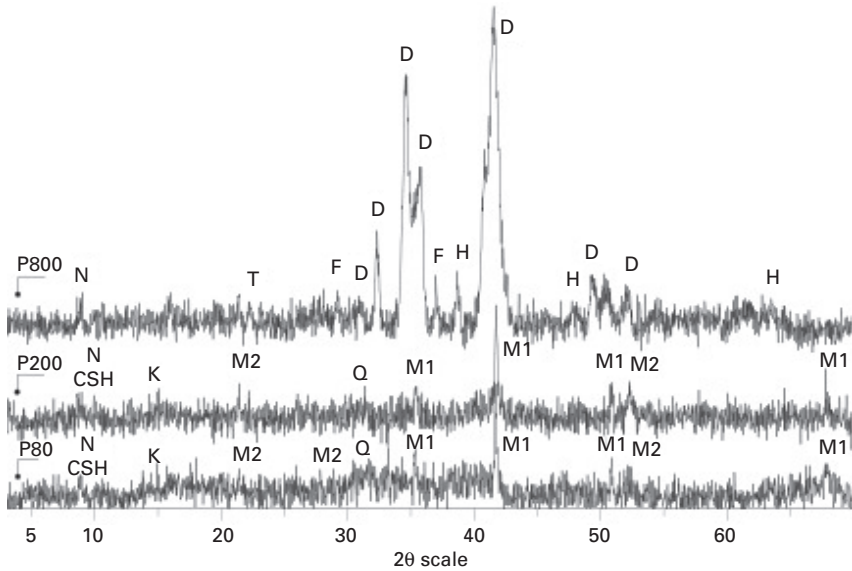
Engelhardt *et al.* (1992) and Dombrowski *et al.* (2007) mention that the dissolution of kaolinite provides OH⁻ and accelerates reaction [16.1], whereas the dissolution of metakaolinite which is a dehydroxylation product does not contribute to hydroxysodalite formation. However, the formation of sodalite under low-temperature hydrothermal conditions has been reported in other studies when either kaolinite or metakaolinite were present in the starting mixture (Barrer *et al.*, 1968; Barrer and Mainwaring, 1972a; 1972b).

Maghemite, γ-Fe₂O₃, may be formed during low-temperature oxidation of ferrous iron phases present in the raw slag (Gadsden, 1975). Calcite, CaCO₃, is formed when calcium hydroxide reacts with atmospheric carbon dioxide; it is well known that the solubility of calcium decreases at elevated pHs due to the formation of unstable calcium hydroxide. Calcium silicate hydrate and trona, Na₃(CO₃)(HCO₃)·2(H₂O), are also seen in all specimens.

The XRD patterns of the surface of geopolymers immersed in aquatic solutions or subjected to freeze-thaw cycles reveal the presence of kaolinite, quartz and magnetite. Maghemite and calcite were detected in all specimens. Hydroxysodalite is detected only at the surface of specimens immersed in seawater and HCl solution when as mentioned earlier OH⁻ substitute Cl⁻ ions.

XRD patterns of slag-based geopolymers subjected to high temperature heating are shown in Fig. 16.20. It is seen that the patterns of specimens heated at 80 °C (P80) and 200 °C (P200) are almost identical, thus no new phases are formed in detectable quantities during heating at temperatures up to 200 °C. When specimens are heated at 800 °C (P800) diopside (CaO + 2SiO₂ + MgO → CaMgSi₂O₆) and hematite, Fe₂O₃, are formed.

Sodium aluminum oxide, NaAl₁₁O₁₇, coexists with calcium silicate hydrate in P80 and P200 specimens. When heating temperature reaches 800 °C, water



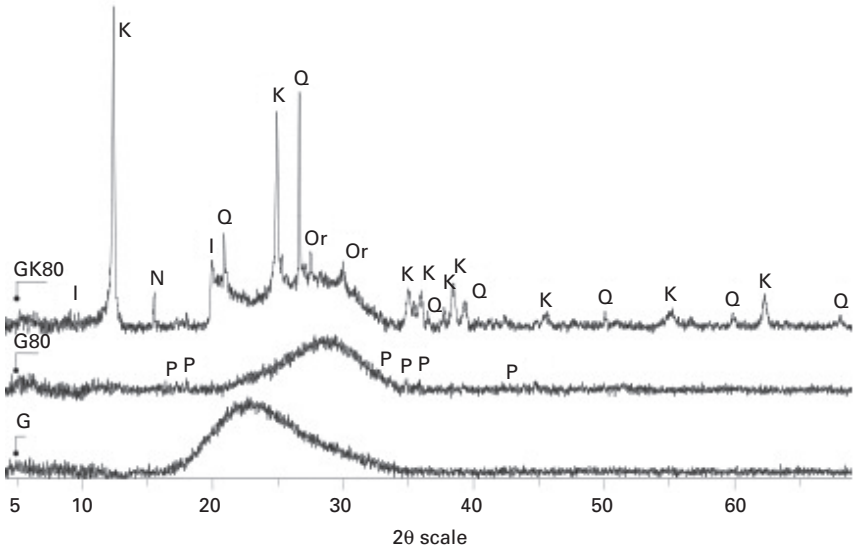
16.20 XRD patterns of geopolymers P80, P200 and P800 (Q: Quartz, K: Kaolinite, M1: Magnetite, M2: Maghemite, F: Fayalite, CSH: Calcium Silicate Hydrate, D: Diopside, T: Tridymite, H: Hematite, N: Sodium aluminum oxide).

evaporates from the system and therefore no calcium silicate hydrates are formed. Fayalite and tridymite initially present in slag are also seen in the pattern of P800 specimen.

XRD patterns of glass-kaolinite (GK80) and glass (G80) geopolymers as well as of raw glass (G), are seen in Fig. 16.21. The broad peak seen for raw glass between 17° and 32° 2θ is typical for its amorphous nature; this peak is slightly shifted to the right (between 23° and 34° 2θ) for G80 and GK80 specimens. Pirssonite, $\text{CaNa}_2(\text{CO}_3)_2(\text{H}_2\text{O})_2$, which is an evaporite formed by atmospheric carbonation is detected in G80 specimen due to the high calcium content (10.5% w/w) of glass. Phases such as kaolinite and quartz present in the raw materials are also detected in GK80 geopolymer. New phases such as illite, $\text{K}(\text{Al}_4\text{Si}_2\text{O}_9(\text{OH})_3)$, orthoclase, $\text{K}_{0.58}\text{Na}_{0.42}\text{AlSi}_3\text{O}_8$ and natrolite, $\text{Na}_2\text{Al}_2\text{Si}_3\text{O}_{10}$, which belongs to zeolite group, are formed when kaolinite reacts with KOH and Na_2SiO_3 . Salt like phases consisting of synthetic thermonatrite $\text{Na}_2\text{CO}_3 \cdot \text{H}_2\text{O}$ and trona $\text{Na}_3(\text{CO}_3)(\text{HCO}_3) \cdot 2(\text{H}_2\text{O})$ are also formed on the surface of the products.

16.5.2 SEM

Selected specimens exhibiting high compressive strength were examined under the microscope in order to define their microstructure and elucidate



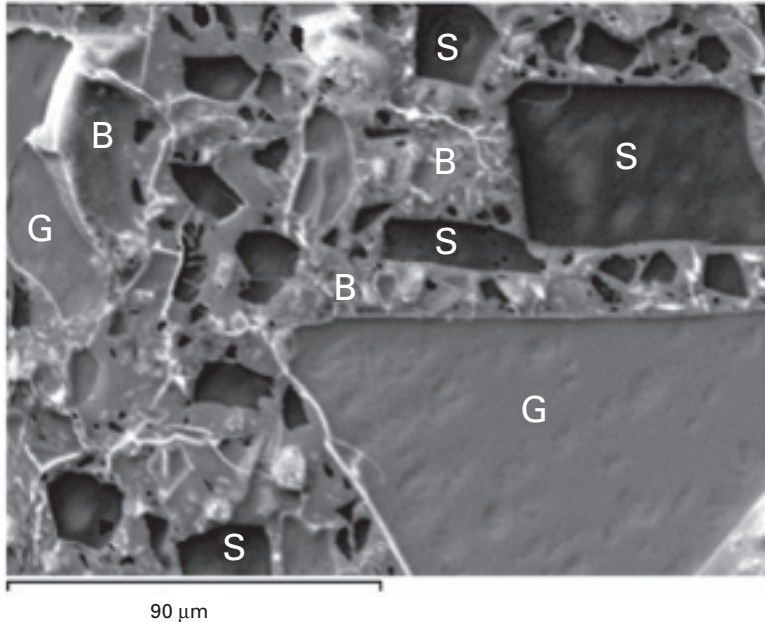
16.21 XRD patterns of glass-kaolinite (GK80) and glass (G80) geopolymers produced under various conditions, as well as of raw glass (G) (Q: Quartz, K: Kaolinite, I: Illite, Or: Orthoclase, N: Natrolite, P: Pirssonite).

to a certain degree the mechanisms involved during geopolymer synthesis. A backscattered electron image (BSI) displaying the microstructure of a 50% w/w slag-glass geopolymer is seen in Fig. 16.22. It is seen in this micrograph that the matrix is quite heterogenous; slag and glass grains are pointed out (slag grains are darker). The binder formed by the geopolymeric gel is seen between slag and glass grains.

Figure 16.23 shows the element mapping of Fig. 16.22; brighter areas indicate the presence of potassium, iron, silicon and aluminum. Potassium, provided by the KOH solution used during geopolymer synthesis, is seen scattered within the binder (Fig. 16.23a). Iron is detected only in slag grains as shown in Fig. 16.23b. Figures 16.23c and 16.23d show the distribution of silicon and aluminum solubilised from both slag and glass; silicon is also provided by the alkali silicate solution. Aluminum is mostly concentrated in slag grains and is widely scattered over the entire geopolymer matrix.

Figures 16.24, 16.25 and 16.26 show the element spectrum for slag and glass grains as well as for the binder. The Si/Al ratio in slag, which also contains calcium and chromium, is 2.5. Glass grains consist mainly of silicon (Si/Al ratio of 21.6) while some calcium and magnesium are also seen. The binder contains silicon and aluminum solubilised from the raw materials; silicon is also provided from the sodium silicate solution used during synthesis.

The Si/Al ratio (~13) in the binder is higher than the respective ratio in slag (2.5) and lower than that in glass (21.6) and is affected by the potassium

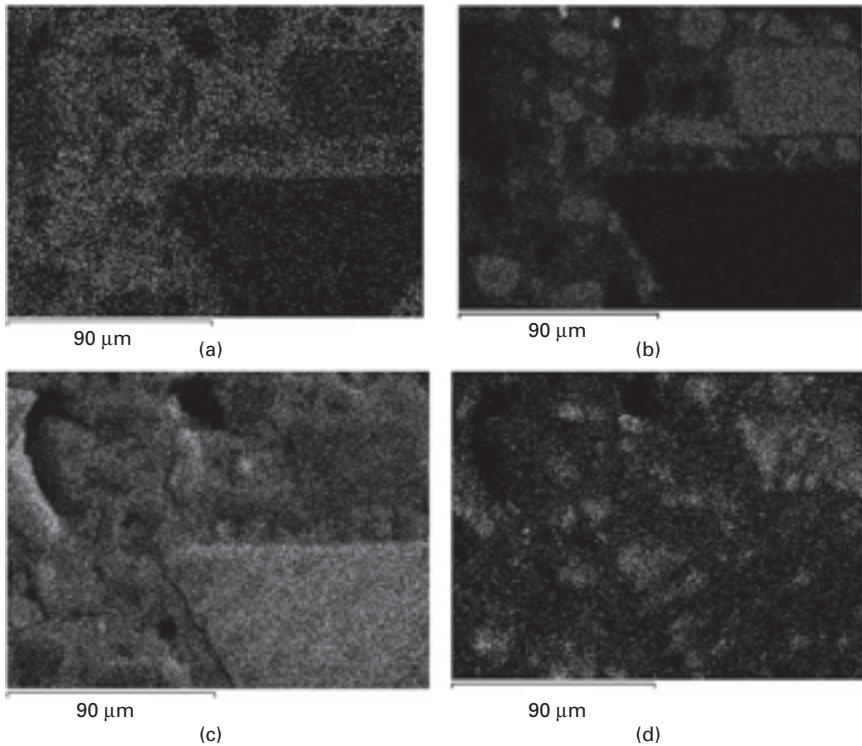


16.22 Backscattered image of slag-glass geopolymer (S: slag grains, G: glass grains, B: binder).

hydroxide concentration (Schneider *et al.*, 2001). Considering that Si and Ca are the main elements present in the binder (the content of Na and Al is much lower), it is believed that calcium silicate hydrates (CSH) may be also formed (Zhang *et al.*, 2007). However, it is assumed that these CSHs differ from those formed during hydration of Portland cement that has a higher Ca content; the Ca/Si ratio (0.25) in the binder is much lower compared to the respective ratio (1.6) seen in Portland cement (Gani, 1997; Yip *et al.*, 2005).

As reported in literature (Richardson, 2000; Richardson and Cabrera 2000; Brough and Atkinson, 2002) the presence of some aluminum atoms in CSH phases in geopolymeric systems is due to substitution of silicon atoms. The calculated Al/Ca ratio in the binder (~ 0.3) is lower than the K/Ca ratio (~ 0.9) and therefore the amount of potassium present is higher than the one required to play a charge-balancing role in the geopolymeric structure (Yip *et al.*, 2005).

Considerable amounts of iron and lesser amounts of chromium solubilised from slag are also seen in Fig. 16.26. This implies that both elements are solubilised even when heating takes place in relatively low temperature ($<80^\circ\text{C}$) and bound in the formed binder. The Fe/Cr ratio is almost identical in slag and the binder, 7.1 and 6.9 respectively, indicating that the solubilisation rate of iron and chromium phases present in the raw material is equal.



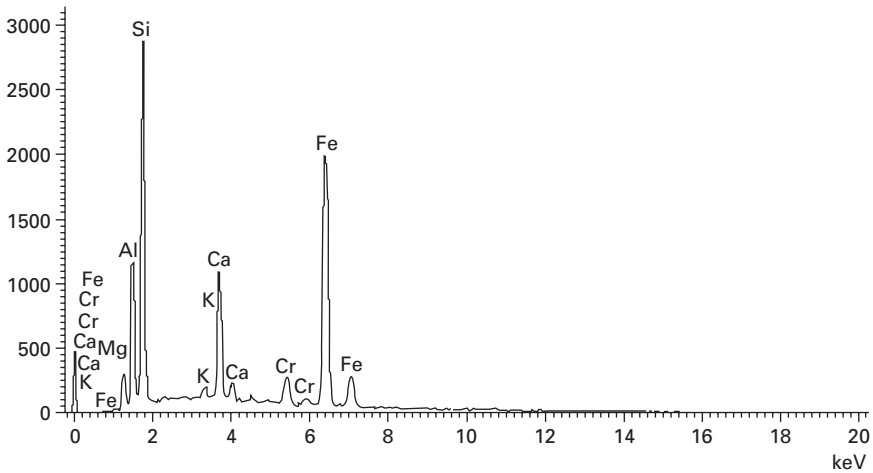
16.23 Element mapping of slag-glass geopolymers for (a) potassium, (b) iron, (c) silicon and (d) aluminum.

Similar mechanisms may be also prevail in the geopolymeric matrix during encapsulation and subsequent immobilisation of hazardous heavy metals (Van Jaarsveld *et al.*, 1998; 1999; Perera *et al.*, 2005; Shi and Fernández-Jiménez, 2006; Zhang *et al.*, 2008).

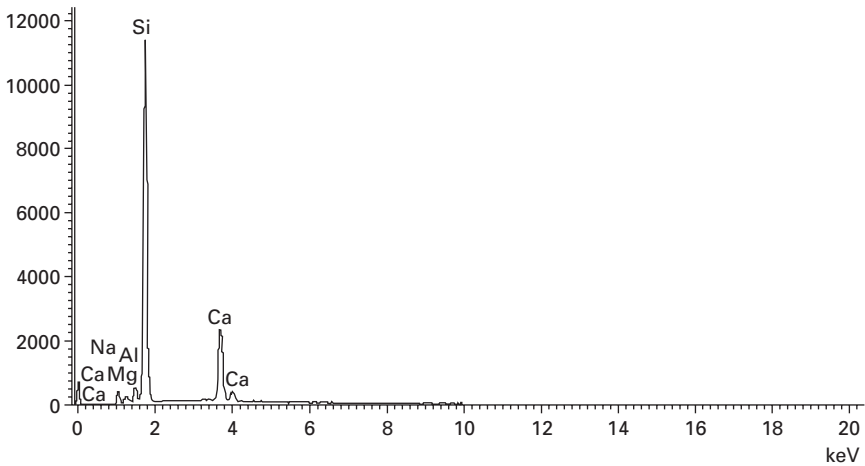
16.5.3 FTIR

FTIR analysis is considered as an appropriate method to study the structural evolution of amorphous aluminosilicates exhibiting high heterogeneity (Lee and Van Deventer, 2002). Infrared absorption bands enable identification of specific molecular components and structures. The difference in absorption frequencies between slag and geopolymers identifies transformations taking place during synthesis. The FTIR spectra of slag and geopolymers T1, T2, T3 and T4 are shown in Fig. 16.27. The noise seen in some parts of the curves is due to instrumental difficulties.

The bands at $460\text{--}465\text{ cm}^{-1}$ seen for specimens T2, T3 and T4 are due to in plane Si – O bending and Al–O linkages (Van Jaarsveld *et al.*, 2002).



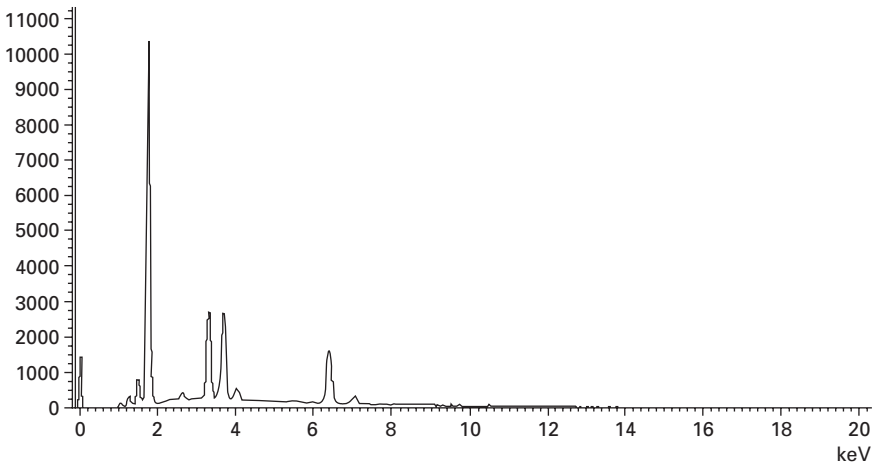
16.24 Element spectrum of slag grains.



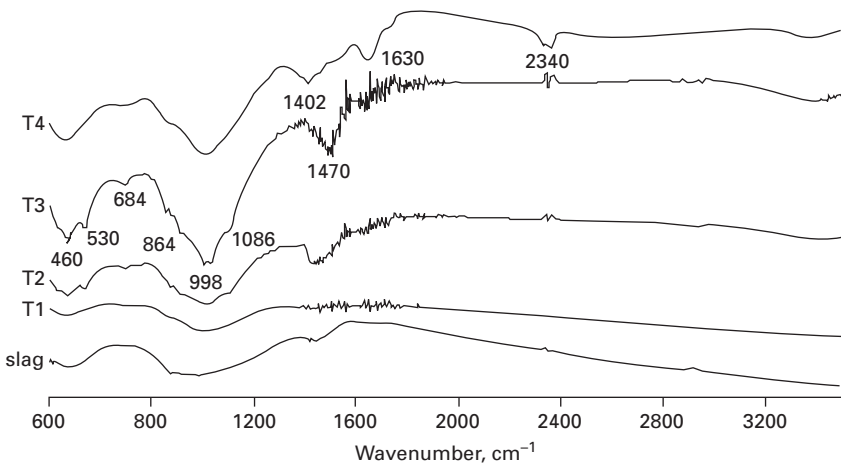
16.25 Element spectrum of glass grains.

The small band seen at $\sim 530 \text{ cm}^{-1}$ only for T2 and T3 specimens is mainly due to out of plane Si – O bending; it may be also overlapped by hematite absorption exhibiting a strong peak between 520 and 610 cm^{-1} . The bands at approximately 680 cm^{-1} represent the functional group of AlO_2 (Socrates, 2001). The very small peak seen at 864 cm^{-1} for all geopolymers corresponds to dissolved silicate and/or aluminosilicate species indicating that partial dissolution of raw materials takes place (Bass and Turner, 1997; Rees *et al.*, 2007).

The band at around 850 cm^{-1} is assigned to T–OH (T: Si or Al) stretching modes (Bakharev, 2005b), while the one at around 965 cm^{-1} may be due to



16.26 Element spectrum of binder.



16.27 FTIR spectra of slag and geopolymers T1, T2, T3 and T4.

T–O–Si asymmetric stretching vibration ($950\text{--}1200\text{ cm}^{-1}$) as a result of TO_4 reorganisation that takes place during synthesis (Gadsden, 1975; Rees *et al.*, 2007). The position of the main T–O–Si stretching band indicates the length as well as the angle of the bonds in a silicate network (Rees *et al.*, 2007); shifting to lower wavenumbers hints lengthening of T–O–Si bonds, reduction in the bond angle and therefore decrease of the molecular vibrational force constant (Sweet and White, 1969; Roy, 1990; Innocenzi, 2003). All bands at around 1088 cm^{-1} are a major fingerprint of the geopolymeric matrix and define the extent of polysialation or aluminum incorporation (Gadsden, 1975).

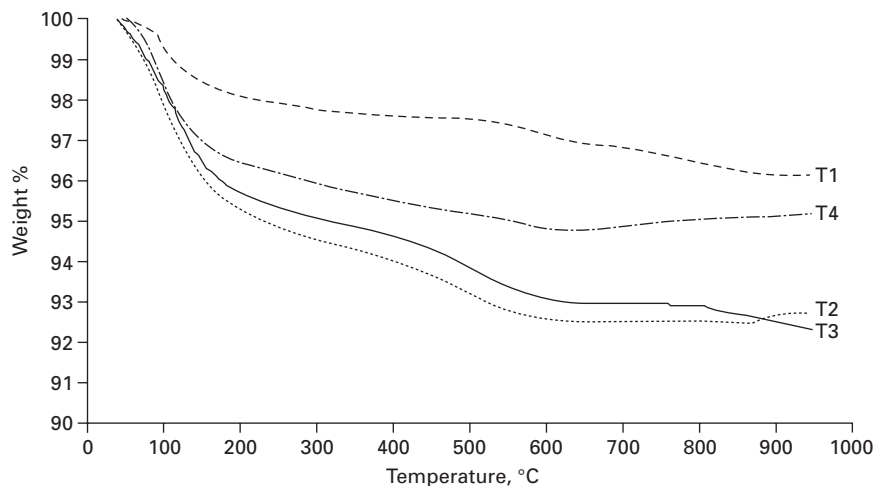
Atmospheric carbonation is reflected in the infrared spectral region of 1410–1570 cm^{-1} (Mollah *et al.*, 1993; Barbosa *et al.*, 2000); part of the excess Na is carried to the surface where it reacts (Barbosa *et al.*, 1999). The band seen at 1630 cm^{-1} for specimen T4 is attributed to bending vibrations (H–O–H) and is typical for polymeric structures including aluminosilicate networks (Bakharev, 2005b). The small bands seen at around 2504 cm^{-1} are probably due to the infrared band position of HCO_3^- ions (Socrates, 2001).

16.5.4 TG

Thermogravimetric analysis (TG) may be used to define water evaporation mechanisms causing losses of material weight as a result of controlled heating (Joo and Yong, 2007). Figure 16.28 shows TG curves for geopolymers T1, T2, T3 and T4; the total water loss was calculated as 4%, 7%, 6.5% and 5% w/w for each specimen respectively.

The absorbed water is lost at temperatures lower than 200°C. The remaining water is either bound tightly or is less able to diffuse to the surface (Subaer and Van Riessen, 2007) and continues to evaporate slowly at higher temperatures. The continuous weight loss up to about 550°C is due to evaporation of hygroscopic water or water residing in the channels (Perraki *et al.*, 2005). The water loss at around 550°C is probably due to dehydroxylation of kaolinite.

It is therefore concluded that an optimum water content should be present in the initial reactive paste so that an adequate compressive strength is acquired;



16.28 TG plot of weight % vs. temperature for geopolymers T1, T2, T3 and T4.

this is why pre-curing period is considered beneficial during synthesis; specimen T3 reaches 53 MPa, while specimen T1 only 1.5 MPa.

16.6 Prospects for industrial applications

The need for the development of new low-cost technologies that utilise mining and metallurgical wastes for the production of new high added value products, such as geopolymers or geopolymeric cements, is expected to increase in the following years. It is seen therefore that geopolymerisation may be considered as a feasible alternative for the management of several industrial wastes, including slag, fly ash and red mud.

The main barrier that geopolymerisation has to overcome is the quite conservative perspective of the industry to adopt new technologies and products that will replace existing ones. In order to overcome the entrenched position of Ordinary Portland Cement (OPC) more intensive efforts regarding the study of the compatibility between C–S–H and geopolymer gels are required by the research community (Goretta *et al.*, 2004; Yip *et al.*, 2005; Duxson *et al.*, 2007). It is also underlined that the cost for the synthesis of geopolymers is as low as for Portland cement production (~0.05–0.08 USD/kg, base year 2006) (Sofi *et al.*, 2007).

Acceptance of geopolymerisation by the industry may be also enhanced if state action is taken for issues associated with greenhouse gas emissions and control (e.g., ratification of the Kyoto protocol, introduction of carbon trading schemes as well as taxes and levies on greenhouse gas emitting materials). It should be also stated that geopolymerisation is in line with the principles of sustainable development and may offer solutions to problems such as energy loss and CO₂ emissions due to OPC manufacture (Yip *et al.*, 2004; Van Deventer *et al.*, 2006).

16.7 Conclusions

The present chapter discusses the factors affecting the compressive strength of geopolymers synthesised using low Ca ferronickel slag. Pre-curing for a short period (e.g. two days) is required to initiate geopolymeric reactions by taking advantage of the paste moisture, so that the final products acquire high compressive strength; if excess water is present, non-reacting water will diffuse or evaporate during heating thus causing the development of pores and cracks. Heating temperature and time as well as aging period also affect the properties of the final products. Substantial strength is acquired when the paste is heated at 80°C for 48 hours and the hardened specimens are then aged for 7 days.

The concentration of alkali hydroxide and alkali silicate also affects the properties of the geopolymers produced. KOH seems to have a more

beneficial effect compared to NaOH; the optimum molarity varies between 4 and 8M. The use of sodium silicate solution that acts as a binder improves the compressive strength of the final products.

The presence of certain additives in the initial mixture has a detrimental effect on the final compressive strength. More specifically, the presence of kaolinite decreases compressive strength by almost 60%. When metakaolinite, produced from calcination of kaolinite, is used, the final compressive strength decreases further, probably due to the increased porosity of the new structure as a result of thermal processing. Addition of pozzolan, CaO, fly ash or red mud in the starting mixture also has an adverse effect on the properties of the final products. Pozzolan addition decreases compressive strength by more than 50% over the temperature range studied. CaO addition also results in very low strength, which decreases further when higher addition percentages are used. Very low strength is obtained when 20 to 50%w/w fly ash or red mud are added, probably due to solubilisation of additional silicon, aluminum and calcium that affects the respective ratios in the geopolymeric gel. On the contrary silica sand or glass addition improves the compressive strength of the final products.

Durability studies show that slag-kaolinite geopolymers exhibit quite good behaviour in various aggressive environments. Application of several freeze-thaw cycles or immersion of specimens in distilled water and seawater over a period of 9 months does not practically affect their structural integrity. On the other hand, a continuous decrease of strength that reaches 50% is noticed for specimens immersed in 0.5N HCl solution. It is believed that the presence of Cl^- and H^+ ions accelerates deterioration of geopolymer structure. Furthermore, the compressive strength of slag-based geopolymers heated up to 400°C is very satisfactory and reaches almost 60 MPa; heating at higher temperatures, up to 800°C, results in substantial strength loss to almost 15 MPa.

XRD, SEM, TG and FTIR techniques may be used to identify new phases formed, determine the level of amorphicity of the final products and elucidate to a certain degree the mechanisms involved during synthesis. Hydroxysodalite is identified in slag-kaolinite geopolymers exhibiting higher compressive strength, as well as in the surface of specimens immersed in seawater or HCl. Phases such as diopside and hematite are identified in slag-based geopolymers heated at temperatures up to 800°C. Pirssonite, $\text{CaNa}_2(\text{CO}_3)_2(\text{H}_2\text{O})_2$, is an evaporite formed in geopolymers made of pure high calcium glass due to atmospheric carbonation.

The morphology of slag-glass geopolymers was also investigated using backscattered SEM; unreacted particles present in the raw materials as well as calcium silicate hydrates (CSH) were identified. Element mapping analysis shows clearly the distribution of potassium, iron, silicon and aluminum in the geopolymeric matrix.

FTIR analysis reveals the transformations taking place during geopolymer synthesis corresponding mainly to Si–O bending and Al–O bonds. Thermogravimetric analysis shows that the absorbed water is lost at temperatures lower than 200°C. An optimum water content should be maintained in the geopolymeric paste so that an adequate compressive strength is acquired.

Additional research is required to assess the optimum synthesis conditions, elucidate the mechanisms involved and establish geopolymerisation as a feasible option for the management of potentially hazardous mining and metallurgical wastes, such as low calcium ferronickel slags. This innovative technology, when fully established, may contribute to considerable savings in disposal costs and substantial reduction of greenhouse gas emissions.

16.8 Sources of further information and advice

- Buchwald A, Hilbig H and Kaps Ch (2007), ‘Alkali-activated metakaolin slag blends—performance and structure in dependence of their composition’, *J Mater Sci*, 42, 3024–3032.
- Cheng TW and Chiu JP (2003), ‘Fire-resistant geopolymer produced by granulated blast furnace slag’, *Miner Eng*, 16, 205–210.
- Komnitsas K and Zaharaki D (2007), ‘Geopolymerisation: A review and prospects for the minerals industry’, *Miner Eng*, 20, 1261–1277.
- Komnitsas K, Zaharaki D and Perdikatsis V (2007), ‘Geopolymerisation of low calcium ferronickel slags’, *J Mater Sci*, 42, 3073–3082.
- Komnitsas K, Zaharaki D and Perdikatsis V (2009), ‘Effect of synthesis parameters on the compressive strength of low-calcium ferronickel slag inorganic polymers’, *J Hazard Mater*, 161(2–3), 760–768.
- Zhang Y, Sun W, Chen Q and Chen L (2007), ‘Synthesis and heavy metal immobilization behaviors of slag based geopolymers’, *J Hazard Mater*, 143 (1–2), 206–213.
- Proceedings of the 1st European Conference Geopolymere ’88 on Soft Mineralurgy (eds. Davidovits J and Orlinski J), Compiègne, France, June 1–3, 1988.
- Proceedings of the 2nd International Conference Geopolymere ’99 (eds. Davidovits J, Davidovits R and James C), Saint-Quentin, France, June 30–July 2, 1999.
- Proceedings of the International Conference Geopolymers 2002 – Turn potential into profit (eds. Lukey GC, in CD-ROM), Melbourne, Australia, October 28–29, 2002.

16.9 References

- Allahverdi A and Škvára F (2001a), ‘Nitric acid attack on hardened paste of geopolymeric cements – Part 1’, *Ceram-Silikaty*, 45, 81–88.

- Allahverdi A and Škvára F (2001b), 'Nitric acid attack on hardened paste of geopolymeric cements – Part 2', *Ceram-Silikaty*, 45, 143–149.
- Allahverdi A and Škvára F (2005), 'Sulfuric acid attack on hardened paste of geopolymer cements. Part 1. Mechanism of corrosion at relatively high concentrations', *Ceram-Silikaty*, 49, 225–229.
- Astutiningsih S and Liu Y (2005), 'Geopolymerisation of Australian slag with effective dissolution by the alkali', Proceedings of the World Congress on Geopolymer, Green chemistry and sustainable development solutions, Saint Quentin, France, 69–73.
- Bakharev T (2005a), 'Geopolymeric materials prepared using Class F fly ash and elevated temperature curing', *Cement Concrete Res*, 35, 1224–1232.
- Bakharev T (2005b), 'Resistance of geopolymer materials to acid attack', *Cement Concrete Res*, 35 (4), 658–670.
- Barbosa V F F, Mackenzie K J D and Thaumaturgo C (1999), 'Synthesis and characterisation of sodium polysialate inorganic polymer based on alumina and silica', Proceedings of the 2nd International Conference Geopolymere '99, Saint-Quentin, France, 65–77.
- Barbosa V F F, MacKenzie K J D and Thaumaturgo C (2000), 'Synthesis and characterisation of materials based on inorganic polymers of alumina and silica: sodium polysialate polymers', *Int J Inorg Mater*, 2, 309–317.
- Barrer R M and Mainwaring D E (1972a), 'Chemistry of soil minerals. Part XI. Hydrothermal transformations of metakaolinite in potassium hydroxide', *J Chem Soc Dalton*, 12, 1254–1259.
- Barrer R M and Mainwaring D E (1972b), 'Chemistry of soil minerals. Part XIII. Reactions of metakaolinite with single and mixed bases', *J Chem Soc Dalton*, 22, 2534–2546.
- Barrer R M, Cole J F and Sticher H (1968), 'Chemistry of soil minerals. Part V. Low temperature hydrothermal transformations of kaolinite', *J Chem Soc A*, 2475–2485.
- Bass J L and Turner G L (1997), 'Anion distributions in sodium silicate solutions. Characterization by ^{29}Si NMR and infrared spectroscopies, and vapor phase osmometry', *J Phys Chem B*, 50, 10638–10644.
- Brough A R and Atkinson A (2002), 'Sodium silicate-based, alkali-activated slag mortars: Part 1. Strength, hydration and microstructure', *Cement Concrete Res*, 32, 865–879.
- Buchwald A, Hilbig H and Kaps Ch (2007), 'Alkali-activated metakaolin-slag blends—performance and structure in dependence of their composition', *J Mater Sci*, 42, 3024–3032.
- Cheng T W and Chiu J P (2003), 'Fire-resistant geopolymer produced by granulated blast furnace slag', *Miner Eng*, 16, 205–210.
- Dombrowski K, Buchwald A and Weil M (2007), 'The influence of calcium content on the structure and thermal performance of fly ash based geopolymers', *J Mater Sci*, 42, 3033–3043.
- Douglas E, Bilodeau A, Brandstetr J and Malhotra V M (1991), 'Alkali activated ground granulated blast-furnace slag concrete: preliminary investigation', *Cement Concrete Res*, 21, 101–108.
- Duxson P, Fernández-Jiménez A, Provis J L, Lukey G C, Palomo A and Van Deventer J S J (2007), 'Geopolymer technology: the current state of the art', *J Mater Sci*, 42, 2917–2933.
- Engelhardt G, Felsche J and Sieger P (1992), 'The hydrosodalite system $\text{Na}_{6+x}[\text{SiAlO}_4]_6(\text{OH})_x \cdot n\text{H}_2\text{O}$: Formation, phase composition, and de- and rehydration studied by ^1H , ^{23}Na , and ^{29}Si MAS-NMR spectroscopy in Tandem with Thermal Analysis, X-ray Diffraction, and IR Spectroscopy', *J Am Chem Soc*, 114, 1173–1182.
- European Commission – IPPC Bureau of 2002, Draft reference document on best available

- techniques for management of tailings and waste-rock in mining activities, <http://eippcb.jrc.es/pages/Fmembers.htm>.
- Gadsden A (1975), *Infrared spectra of minerals and related inorganic compounds*, London, Butterworths.
- Gani M S J (1997), *Cement and Concrete*, 1st edn., London, Chapman and Hall.
- Glukhovskiy V D (1994), 'Ancient, modern and future concretes', Proceedings of the 1st International Conference on Alkaline Cements and Concretes, VIPOL Stock Company, Kiev, Ukraine, 1–9.
- Goretta K C, Nan Chen, Gutierrez-Mora F, Routbort J L, Lukey G C and Van Deventer J S J (2004), 'Solid-particle erosion of a geopolymer containing fly ash and blast-furnace slag', *Wear*, 256 (7–8), 714–719.
- Hu S, Wang H, Zhang G and Ding Q (2008), 'Bonding and abrasion resistance of geopolymeric repair material made with steel slag', *Cement Concrete Comp*, 30 (3), 239–244.
- Innocenzi P (2003), 'Infrared spectroscopy of sol-gel derived silica-based films: A spectral-microstructure overview', *J Non-Cryst Solids*, 316 (2–3), 309–319.
- Jirasit F, Rüscher C H and Lohaus L (2006), 'A study on the substantial improvement of fly ash-based geopolymeric cement with the addition of metakaolin', Proceedings of the International Conference on Pozzolan, Concrete and Geopolymer, Khon Kaen, Thailand, 247–261.
- Joo H H and Yong H C (2007), 'Physico-chemical properties of protein-bound polysaccharide from *Agaricus blazei* Murill prepared by ultrafiltration and spray drying process', *Int J Food Sci Technol*, 42, 1–8.
- Komnitsas K and Zaharaki D (2007), 'Geopolymerisation: A review and prospects for the minerals industry', *Miner Eng*, 20, 1261–1277.
- Komnitsas K, Zaharaki D and Perdikatsis V (2007), 'Geopolymerisation of low calcium ferronickel slags', *J Mater Sci*, 42, 3073–3082.
- Komnitsas K, Zaharaki D and Perdikatsis V (2009), 'Effect of synthesis parameters on the compressive strength of low-calcium ferronickel slag inorganic polymers', *J Hazard Mater*, 161 (2–3), 760–768.
- Kontopoulos A, Komnitsas K and Xenidis A (1996), 'Environmental Characterisation of the lead smelter slags in Lavrion', Proceedings of the IMM Minerals Metals and the Environment II Conference, Prague, 405–419.
- Lee W K W and Van Deventer J S J (2002), 'The effects of inorganic salt contamination on the strength and durability of geopolymers', *Colloids Surf A*, 211 (2–3), 115–126.
- Mollah Y M, Hess T R, Tsai Y-N and Cocke D L (1993), 'FTIR and XPS investigations of the effects of carbonation on the solidification/stabilization of cement-based system – Portland type V with zinc', *Cement Concrete Res*, 23 (4), 773–784.
- Panias D, Giannopoulou I P and Perraki T (2007), 'Effect of synthesis parameters on the mechanical properties of fly ash-based geopolymers', *Colloid Surf A*, 301 (1–3), 246–254.
- Perera D S, Aly Z, Vance E R and Mizumoz M (2005), 'Immobilization of Pb in a geopolymer matrix', *J Am Ceram Soc*, 88 (9), 2586–2588.
- Perraki T, Kakali G and Kontori E (2005), 'Characterization and pozzolanic activity of thermally treated zeolite', *J Therm Anal Calorim*, 82, 109–113.
- Phair J W (2001) 'Compositional effects and microstructure of fly ash based geopolymers', PhD Thesis, Department of Chemical Engineering, University of Melbourne, Victoria, Australia.
- Phair J W, Van Deventer J S J (2002), 'Effect of the silicate activator pH on the

- microstructural characteristics of waste-based geopolymers', *Int J Miner Process*, 66 (1–4), 121–143.
- Phair J W, Van Deventer J S J and Smith J D (2004), 'Effect of Al source and alkali activation on Pb and Cu immobilisation in fly-ash based geopolymers', *Appl Geochem*, 19 (3), 423–434.
- Rees C A, Provis J L, Lukey G C and Van Deventer J S J (2007), 'Attenuated total reflectance fourier transform infrared analysis of fly ash geopolymer gel aging', *Langmuir*, 23, 8170–8179.
- Richardson I G (2000), 'The nature of the hydration products in hardened cement pastes', *Cement Concrete Comp*, 22, 97–113.
- Richardson I G and Cabrera J G (2000), 'The nature of C–S–H in model slag cements', *Cement Concrete Comp*, 22, 259–266.
- Roy BN (1990), 'Infrared spectroscopy of lead and alkaline-earth aluminosilicate glasses', *J Am Ceram Soc*, 73 (4), 846–855.
- Schneider J, Cincotto M A and Panepucci H (2001), '²⁹Si and ²⁷Al high-resolution NMR characterization of calcium silicate hydrate phases in activated blast-furnace slag pastes', *Cement Concrete Res*, 31 (7), 993–1001.
- Shi C and Fernández-Jiménez A (2006), 'Stabilization/solidification of hazardous and radioactive wastes with alkali-activated cements', *J Hazard Mater*, B137, 1656–1663.
- Socrates G (2001), *Infrared and Raman Characteristic Group Frequencies*, England, John Wiley & Sons Ltd, 3rd edition.
- Sofi M, Van Deventer J S J, Mendis P A and Lukey GC (2007), 'Engineering properties of inorganic polymer concretes (IPCs)', *Cement Concrete Res*, 37, 251–257.
- Subaer and Van Riessen A (2007), 'Thermo-mechanical and microstructural characterisation of sodium-poly(sialate-siloxo) (Na-PSS) geopolymers', *J Mater Sci*, 42 (9), 3117–3123.
- Sweet J R and White W B (1969), 'Study of sodium silicate glasses and liquids by infrared reflectance spectroscopy', *Phys Chem Glasses*, 10 (6), 246–251.
- Van Deventer J S J, Provis J L, Duxson P and Lukey G C (2006), 'Technological, environmental and commercial drivers for the use of geopolymers in a sustainable materials industry', Proceedings of the 2006 TMS Fall Extraction and Processing Division: Sohn International Symposium, San Diego, California, vol. 3, 241–252.
- Van Deventer J S J, Provis J L, Duxson P, Lukey G C (2007), 'Reaction mechanisms in the geopolymeric conversion of inorganic waste to useful products', *J Hazard Mater*, 139 (3), 506–513.
- Van Jaarsveld J G S, Van Deventer J G J and Lorenzen L (1997), 'The potential use of geopolymeric materials to immobilise toxic metals: Part I. Theory and applications', *Minerals Engineering*, 10 (7), 659–669.
- Van Jaarsveld J G S, Van Deventer J S J and Lorenzen L (1998), 'Factors affecting the immobilisation of metals in geopolymerised fly ash', *Metall Mater Trans B*, 29, 283–291.
- Van Jaarsveld J G S, Van Deventer J S J and Schwartzman A (1999), 'The potential use of geopolymeric materials to immobilize toxic metals: part II. Material and leaching characteristics', *Miner Eng*, 12 (1), 75–91.
- Van Jaarsveld J G S, Van Deventer J S J and Lukey G C (2002), 'The effect of composition and temperature on the properties of fly ash- and kaolinite-based geopolymers', *Chem Eng J*, 89 (1–3), 63–73.
- Van Jaarsveld J G S, Van Deventer J S J and Lukey G C (2004), 'A comparative study of

- kaolinite versus metakaolinite in fly ash based geopolymers containing immobilized metals', *Chem Eng Commun*, 191, 531–549.
- Viklund-White C and Ye G (1999), 'Utilization and treatment of steelmaking slags', Proceedings of the TMS Fall Extraction and Processing Conference 1, San Diego, California, 337–345.
- Wang S D (2000), 'Alkali-activated slag: hydration process and development of microstructure', *Adv Cem Res*, 12 (4), 163–172.
- Wang S D and Scrivener KL (1995), 'Hydration products of alkali activated slag cement', *Cement Concrete Res*, 25 (3), 561–571.
- Xu H and Van Deventer J S J (2002), 'Geopolymerisation of multiple minerals', *Miner Eng*, 15, 1131–1139.
- Yip C K and Van Deventer J S J (2003), 'Microanalysis of calcium silicate hydrate gel formed within a geopolymeric binder', *J Mater Sci*, 38, 3851–3860.
- Yip C K, Lukey G C and Van Deventer J S J (2004), 'Effect of blast furnace slag addition on microstructure and properties of metakaolinite geopolymeric materials', *Ceram Trans*, 153, 187–209.
- Yip C K, Lukey G C and Van Deventer J S J (2005), 'The coexistence of geopolymeric gel and calcium silicate hydrate at the early stage of alkaline activation', *Cement Concrete Res*, 35 (9), 1688–1697.
- Yip C K, Lukey G C, Provis J L and Van Deventer J S J (2008), 'Effect of calcium silicate sources on geopolymerisation', *Cement Concrete Res*, 38 (4), 554–564.
- Zaharaki D (2005), 'Optimisation of synthesis of geopolymers synthesised using electric arc furnace ferronickel slag', MSc Thesis, Department of Mineral Resources Engineering, Technical University Crete.
- Zaharaki D and Komnitsas K (2005), 'Use of factorial design in environmental applications and in waste management', Proceedings of the International Workshop in Geoenvironment and Geotechnics, Milos island, Greece, 261–268.
- Zaharaki D and Komnitsas K (2008), 'Effect of additives on the compressive strength of slag-based inorganic polymers', Proceedings of the 2nd International Conference on Engineering for Waste Valorisation (in CD ROM), Patras, Greece.
- Zaharaki D, Komnitsas K and Perdikatsis V (2006), 'Factors affecting synthesis of ferronickel slag based geopolymers', Proceedings of the 2nd International Conference on Advances in Mineral Resources Management and Environmental Geotechnology, Chania, Crete, Greece, 63–68.
- Zaharaki D, Komnitsas K and Perdikatsis V (2007), 'Factors affecting the performance of waste-based geopolymers', Proceedings of the VI International Congress on Valorisation and recycling of Industrial Waste (in CDROM), L'Aquila, Italy.
- Zhang Y, Sun W, Chen Q and Chen L (2007), 'Synthesis and heavy metal immobilization behaviors of slag based geopolymers', *J Hazard Mater*, 143 (1–2), 206–213.
- Zhang J, Provis J L, Feng D and Van Deventer J S J (2008), 'Geopolymers for immobilization of Cr^{6+} , Cd^{2+} , and Pb^{2+} ', *J Hazard Mater*, 157, 587–598.

Commercialization of geopolymers for construction – opportunities and obstacles

P DUXSON and J S J VAN DEVENTER,
The University of Melbourne, Australia

Abstract: This chapter presents a discussion of the factors influencing the commercial uptake of geopolymer (or, more broadly, alkaline activation) technology in the construction industry: why it has historically not been achieved on a large scale, the factors in the current global environment which are generating massively increased interest at present, and the likely future role of these materials in the global economy.

Key words: geopolymer, commercialisation alkaline activation, concrete, greenhouse emission reduction.

17.1 Introduction

Concrete made from Ordinary Portland Cement (OPC) is second only to water as the commodity most used by mankind today. Global OPC production in 2008 is estimated to be 2.6 billion tons per annum in a thorough market analysis,¹ while other sources² mention 1.5 billion tons p.a., which is a huge variation. This \$150 billion³ industry contributes conservatively 5–8% of global carbon dioxide (CO₂) emissions,⁴ mainly as a result of the decomposition of limestone during the energy intensive cement making process. With rapid development in infrastructure in China, India, the Middle East and elsewhere in Asia, the cement and concrete industries are expected to expand significantly. Already there are shortages of cement in many locations. As a result of established infrastructure, market dominance and no significant driver to utilize alternative binders, OPC has become accepted technically and commercially as the only viable binder to make concrete. Therefore, alternative binder systems such as alkali activated materials (AAM), including geopolymers, despite significant reduction in CO₂ emissions, have not been taken up on a commercial scale as CO₂ has not been a driver historically. Usually the driver for competition has been cost reduction, in which case AAM starting from a low volume basis can never compete against large scale OPC production. The recent focus on global warming, public and consumer preference for ‘green’ products, and the associated market in carbon credits, have all made AAM a viable proposition in the conservative cement and concrete industry. This chapter outlines a brief history of AAM from a commercial perspective, and analyses

the historical barriers to introduction, as well as the barriers to entry and adoption in a modern pane of reference.

17.2 Alkaline activation: is this a new idea?

It is well known that the Egyptians and Romans produced concrete that is far more durable than modern OPC concrete; in fact, repair work to ancient structures using OPC has not lasted at all. In the popular literature it is often said that these ancient concretes look and behave the same as modern OPC. This view is even held by cement and concrete experts today, as the books say that the composition of raw materials used by the Romans, i.e. volcanic ash, lime, clay, other pozzolans and natural rock, is about the same as is now used in OPC manufacturing.

Studies of ancient Roman, Syrian and Jordanian concretes have shown significant crystalline analcite and analcime zeolitic phases, the stability of which would explain the superior durability of these ancient concretes. Aluminosilicate calcium hydrates similar to the ones in OPC concrete were also found. However, it appears that it is the combination of amorphous and crystalline zeolitic phases, together with the OPC-like hydrates, that rendered the ancient concretes their durability. It is precisely these phases and chemistry that are associated with a well prepared AAM concrete.

In the mid-1950s Prof Victor Glukhovsky of Kiev, Ukraine, investigated the binders used in ancient Roman and Egyptian structures.⁵ Based on these observations he developed binders called ‘soil-cement’, combining aluminosilicate waste such as slag with alkali industrial waste. In the 1960s when there was a shortage of OPC in the former Soviet Union, the Kiev team was involved in the construction of apartment buildings, railway sleepers, road sections, pipes, drainage and irrigation channels, flooring for dairy farms, pre-cast slabs and blocks, using alkali activated blast furnace slag.⁶ Subsequent studies have shown that these structures have high durability.⁷ It is relevant to note that the earlier work by the Kiev team was all based on slag and that their work on fly ash is more recent. A vast number of patents and standards were produced on the earlier slag mixes, but this documentation has been largely inaccessible to the West.

In late 1970s Prof Joseph Davidovits⁸ of Saint Quentin, France, coined the term ‘geopolymer’ for a range of alkali-activated metakaolinite binders that did not involve OPC-like phases in its chemistry. Controversially, he has claimed that the internal blocks in the Egyptian pyramids were cast in-situ from geopolymer-like material instead of hewn limestone. Davidovits holds a large number of patents on geopolymers, with only a few having found industrial application in niche areas. Davidovits has contributed substantially to the field, as today the term ‘geopolymer’ is used generically for AAM in the same way as OPC is used for a variety of cement types.

Recent advances in the technology have been driven by two core groups of Prof. Jannie van Deventer and Prof. Angel Palomo. Jannie van Deventer started working on geopolymer-type materials in 1993 in South Africa and continued this work when he accepted a chair at the University of Melbourne, Australia in 1995. The geopolymer research group at the University of Melbourne⁹ is arguably today the world's leading academic research group on AAM, judged by numbers of journal papers and impact criteria. Prof. Angel Palomo of the Eduardo Torroja Institute (CSIC) in Madrid, Spain, is a cement chemist who has been working on AAM since the mid 1990s, shortly after the group of Prof Della Roy at the Pennsylvania State University started working on AAM. Palomo's group continues to contribute substantially to the science of AAM and besides the Melbourne group, is arguably the top contributor to the research literature in this field. Palomo has co-edited a journal special issue with the Melbourne geopolymer group.

Since the late 1990s and particularly in the past five years there has been an explosion in the number of research institutes and universities with an active interest in the field of geopolymer technology. In 2007 a special edition of the *Journal of Materials Science* was dedicated to geopolymer technology, indicating the generic level of interest in the material. Yet, despite the level of academic and research interest in the field, the amount of commercial activity utilizing the fruits of this work was effectively nil.

17.3 Why has AAM technology not been commercialized before now?

17.3.1 Brief history of R&D and commercial efforts

Geopolymer and alkali-activation technology has been known to the cement and concrete industry for approximately fifty years, yet the commercial uptake of the technology to date has been effectively non-existent. The reasons for this range from technical capacity of the technology to commercial barriers and regulatory issues.

The ground work on alkali-activation was completed in the 1950s by Prof Victor Glukhovsky and co-workers in the Ukraine. The key driver for this research was the chronic shortage of OPC cement in post-World War II Eastern Europe. The short-term answer was utilization of blast furnace slag. A vast range of concretes were utilized in a broad range of applications in the former USSR in the 1960s. These structures were built from slag activated mainly with carbonate instead of alkali silicate as in most other AAM mixtures. Nevertheless, the chemistry of the carbonate system is sufficiently close to the alkali silica activated system to demonstrate long-term durability of AAM as a general class of material. These materials have shown outstanding durability over decades under highly aggressive environments,

where comparative structures of Portland-based cements disintegrated entirely within a few years. Samples of these old concretes have been analyzed recently proving that these materials are extremely durable.⁷ From these early beginnings it could be concluded that the technology was a success. And yet, despite this, once cement production capacity was restored the technology was effectively sidelined and lay dormant for another twenty years until it became popularized and re-invented in France by Prof Joseph Davidovits. Glukhovsky and co-workers utilized simple, empirical and yet extremely effective scientific techniques to gain deep insight into the system.

Joseph Davidovits, the so-called father of geopolymers, reinvigorated the area in the 1970s. Davidovits was prolific both scientifically and commercially, publishing numerous papers and registering a list of world-wide patents on the technology. At the time the key commercial driver for this work was related to fire-resistance and the rapid gain of strength development profiles, although these systems were very expensive relative to cementitious systems. Scientifically, Davidovits brought a fresh and scientifically sophisticated edge to the area, which was a major positive step forward from the more empirical work of the Glukhovsky era that has been treated with skepticism. His work has unfortunately left the field with the liability of a widely confusing nomenclature. Davidovits, while naming the material, also named what he thought were the 'building blocks' of geopolymers. These 'polymer' constructs originated from his training as an organic chemist and look like carbon polymers with silicon and aluminium replacing the carbon atoms. He continues to name these polymers poly-sialate, poly-sialate-siloxo, and poly-sialate-di-siloxo for the ratio of silicon to aluminum being one, two and three respectively.¹⁰ This is a seriously flawed description, as has been demonstrated by fundamental research and not only leads to confusion in the market about what a geopolymer is, but has also hindered scientific advancement. Davidovits attempts to regulate all description of geopolymer work, including denunciation of Wikipedia for its entries on geopolymers. This attitude has historically turned interested researchers and companies away from the field.

Davidovits was also associated with several commercial entities in this 1970–1990s period, the most notable being Lone Star with their product Pyrament. Pyrament was a blended cement alkali-activated system. Basic ingredients included fly ash and admixtures – including calcium nitrite accelerator – that were all inter-ground. The technology of blending not only cements but admixtures was new in the late 1980s. What attracted Lone Star was the high performance characteristics including fast set and strength gain, very low permeability (as low as 8 to 10% micro silica fume concrete) and high freeze-thaw durability.

Pyrament was and is a great idea, but Lone Star did not know how to market such a product. Bagged powder sold very well but trying to get a ready-mix

supplier to dedicate a silo or to put Pyrament into an agitator concrete truck was practically impossible. Industry sources in the USA knew of at least three cement agitator drums in which Pyrament flash set, which damaged the on-the-ground credibility dramatically. Lone Star had the opportunity to sell the marketing rights to Master Builders, which may have been a way to gain a wider industry player interest and acceptance, but declined. Finally, there was also a great deal of organizational instability. This business related instability in tandem with some highly visible technical troubles effectively killed the product, and indeed the technology for the next decade.

Since the late 1990s the field of geopolymer technology has seen an explosion of interest. Previous work, including that of Davidovits, was largely empirical and commercially driven by small groups of workers. The latter period of research brought a more in-depth analytical and systematic approach to the technology, and with this a greater level of scientific, but not industry, acceptance. In this period Palomo (Spain) and Van Deventer (Australia) were the key researchers and provided the bulk of the published literature in the field from 1997–2007. The research has been targeted towards providing a more fundamental science base to the technology, and has resulted in numerous highly cited publications, cover articles, all in leading journals. It is fair to say that most technical queries were solved in this period, with the ‘science’ now to a large extent proven, though still there has not been fundamental acceptance of the technology in industry.

The most advanced commercial entity of this period was Siloxo Pty. Ltd. Siloxo began operation in 1997 and operated on a business model that revolved around developing intellectual property and then licensing this to preferably large concrete users and cement producers. Siloxo was dependent on external funds for operating capital, and therefore sold IP to clients to survive. There is publicly available knowledge suggesting that Siloxo had substantial ability to produce both ready-mix concrete and a range of pre-cast products from both Class F and Class C fly ashes. In 2003 Fletcher Building Ltd of New Zealand bought a 40% stake and effective control in Siloxo. Fletcher has a cement production facility in New Zealand (Golden Bay Cement). This move ensured operating capital for Siloxo but made it difficult to control the destiny of its intellectual property. Furthermore, this move appeared to stifle the ability of the company to make timely commercial decisions independently of a cement producer’s perspective, and probably inhibited Siloxo from progressing commercial agreements with what Fletcher rightly saw as their competitors. It can be questioned whether it was in the best interest of a cement producer at the time to hold a vision for alkali-activated materials in parallel or separate from OPC, or if they were simply hedging their risk against future uncertainty of OPC production in view of carbon costing. Internal tension seemed to build and led to the company being shelved.

17.3.2 Barriers overcome

The research, development and commercial efforts described above achieved many goals and did overcome substantial barriers. For instance, in traditional OPC culture, ‘alkali’ is a dirty word. Most cement standards have, for example, limits of alkali in terms of compositions. Therefore, in utilizing an alkali-based binder, this provided a substantial barrier. The reason behind the fear of alkali in OPC chemistry comes from the alkali-aggregate reaction (AAR), also known as the Alkali-silica reaction (ASR).¹¹

Alkali-silica reaction (ASR) can cause serious expansion and cracking in OPC-based concrete, resulting in major structural problems. ASR is caused by a reaction between the hydroxyl ions in the alkaline cement pore solution in the concrete and reactive forms of silica in the aggregate (examples: chert, quartzite, opal, strained quartz crystals), generally over the medium to long term. A hydrated alkali silicate gel is produced, which increases in volume as it hydrates and so exerts an expansive pressure, resulting in failure of the concrete. In alkali-activated concrete, the reactive medium is alkaline and contains silicon. In fact, the ASR is to some extent the basis of geopolymer chemistry. To affect a flip-change in mentality from a situation where one problem becomes the fundamental requirement of another system has taken time. This has been achieved through rigorous academic work and interfacing with the industry through conferences and workshops. This message has been in part accepted by the community as it provides for a major opportunity to utilize a class of aggregates that have been shown to be susceptible to ASR.

The trail-blazing industrial-scale trial work of Glukhovsky and co-workers over 50 years, Palomo and co-workers over the past decade and Siloxo have demonstrated to the world that it is possible to make AAM concrete products, including ambient curing high-strength ready-mix, despite the fact that this knowledge is concentrated in a small number of individuals at this time.

17.3.3 Remaining barriers

Recent commercial history has proven that an obvious issue in the introduction of a new material into the construction industry is (1) the need for standards in each governmental jurisdiction and (2) the unanswerable question on durability of concrete given a standard requirement for structural concretes to last for at least several decades.

In the developed world, there are very specific standards for what is considered ‘acceptable’ performance for a cementitious binder. These have clearly been developed over many years in collaboration with input from the cement manufacturing companies with the chemistry and behaviour of OPC-based concretes either specifically or intrinsically in mind. Despite

this, standards containing constraints such as ‘minimum cement content’ are beginning to be seen as prohibitive, even for cement-based systems. High cement content essentially allows and encourages mix-design favouring poor quality aggregates and high water content. Products such as geopolymer or AAM concrete, or other non-cementitious and even high-performance cementitious based systems, may not simply be an evolution of existing OPC technology but instead may require an entirely different chemical paradigm to understand their behaviour, and may perform entirely acceptably but without conforming exactly to the established regulatory standards – particularly with regard to rheology and chemical composition.¹² This was thought to be a significant hindrance to the acceptance of AAM or geopolymer technology in these markets. However, by working with all stakeholders to explain the product, these barriers can be overcome, so long as the intent of regulatory standards is met.

Provided that a practical mechanism can be put in place to achieve regulatory acceptance of geopolymer concrete in the market, the question still remains over durability. A material that has been subjected to detailed investigation only recently cannot possibly have decades’ worth of durability data to prove its long-term stability. Most standard methods of testing cement and concrete durability involve exposing small samples to very extreme conditions – like highly concentrated acid or salt solutions – for short periods of time. These results are then used to predict how the material will perform in normal environmental conditions over a period of decades or more. The major problem with this approach to ‘prove’ durability is that it can only ever give indications of the expected performance, rather than definitive proof. Therefore, there has been a process of very slow adoption of new materials, as one may need to wait up to 20–30 years for real-world verification. Adoption of fly ash and slag in concretes is the prime example, where the use of these supplementary materials was resisted for decades.

17.4 How the standards and regulations framework is addressed

The regulatory framework for concrete utilized in various applications relies on a typical cascade of standards, with application standards referring to concrete standards, and concrete standards referring to standards covering cement and other concrete raw materials. Therefore in looking at the regulatory framework for a concrete binder system such as alkali activated (AAM) cement, most of the regulatory aspects are focused on the cement standards, although some aspects of concrete standards need to be considered also.

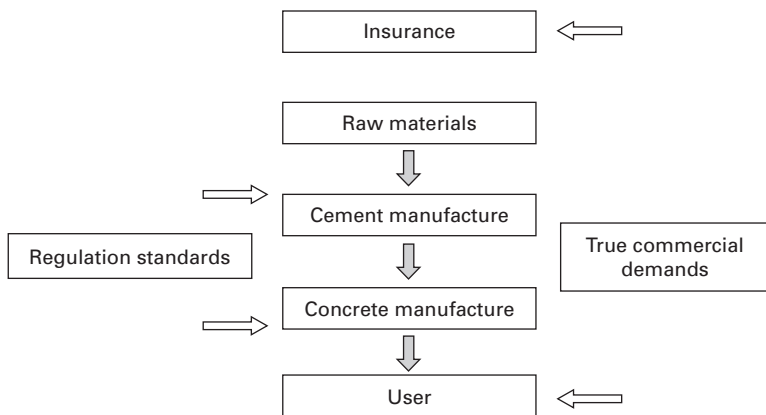
In general, all of the world’s concrete application, concrete and cement standards are based on two ‘super’ standards, which are those of the European Union (EN 197) and the United States (ASTM C150/C595/C1157). Essentially

all of the main cement-consuming markets in the world derive their standards from the standards of these two major jurisdictions. For instance, Chinese cement and concrete standards are based heavily on European Union Standards, while Canadian and Australian standards are based heavily on the American standards.

17.4.1 Drivers for standards development

The existing standards for cement and concrete have been developed and refined effectively over the past century. In fact, the world’s first quality control system was created by Joseph Bazelgette during the construction of the sewer system for London in 1859–1865, which was the first major project to utilize OPC. In solving problems of variability Bazelgette developed a system to control the water-to-cement ratio – a method which is still engrained in the heart of both the EU and US standards – and one which does not necessarily have any meaning for AAM.

Over the years these unofficial standards have become official, and now represent a system of market supply regulation rather than driving safety and maintaining technical performance. To exemplify this, Fig. 17.1 shows the material flow for cement from raw material through to concrete in place. As shown, the regulatory environment has been fundamentally shaped by the bodies involved in cement and concrete manufacture, whereas the bodies that purchase the product and take the risk by insuring the product have traditionally been left out of this process despite the fact they are the only stakeholders who actually stand to lose. For example, many of the criteria written into cement standards exist for the purpose of controlling material



17.1 Schematic diagram of supply chain for cement and concrete with bodies of regulatory influence and commercial risk takers shown.

flows, particularly the ability to reduce cement content of concrete (or what is also known as clinker levels in cement) regardless of technical performance. Such standards are known as ‘prescriptive’.

17.4.2 Prescription versus performance standards

As the business in supplementary cementitious materials (SCMs: mainly fly ash, slag, metakaolin, silica fume and pozzolans) has grown, to the benefit of the SCM suppliers, these standards have proved to be a major hindrance to business growth and market access. Over the past two decades, the SCM suppliers have inserted themselves into the standards boards and have begun to alter the standards to allow for greater flexibility to incorporate their products, namely fly ash and slag, into cement via a lower clinker level, or concrete via OPC replacement. Again, this drive has been made by companies that are now effectively owned by, and in some cases are, existing OPC cement manufacturers. The result of this change in standards in practical terms is termed ‘performance’ standards. Performance standards rely more heavily on tests that measure the qualities of cement and concrete in their hardened or ‘in-service’ forms, and not on their make-up in terms of OPC cement content. This was seen as the opening of the door for greater amounts of fly ash and slag in cement and concrete, as these concretes can meet all of the performance criteria of OPC concrete (or exceed them), but do so with less cement and products of different composition.

In shifting the focus of standards towards performance and away from prescription, the door has opened to utilize binders that do not rely on OPC. For instance, in Australia there are two types of cement: GP, consisting of 95% OPC, and GB, which contains more than 5% fly ash and slag. There is still the prescription for ‘some’ OPC in both types, but clearly there is only a small step to be taken from GB towards a zero OPC cement. Nonetheless, anyone would be able to make an AAM concrete that is able to fit within the existing Australian cement standards by adding a teaspoon of cement to each agitator load of concrete. While this is possible, it would be (1) disingenuous and (2) ineffectual.

A shift towards truly performance-based standards was envisaged in the Appendix of Australian Standard AS3972:

‘For many years cement standards all over the world have been to a large degree prescriptive. Prescription-based specifications are convenient: the tests needed to police prescriptions are usually simple and quick to carry out. However this convenience is achieved at the expense of innovation and being able to easily incorporate new or advanced knowledge. With prescriptive specifications only a narrow range of solutions to any one problem is acceptable even though many other solutions may be available

which would give equal or better performance.’¹³ Further in the Appendix of AS3972, the basis for performance standards development is given: ‘The following three elements are essential for the development of a performance-based Standard:

- (a) Performance parameter – Usually the property or properties that best relate to the desired performance;
- (b) Criteria Quality – Level(s) of the required property that yield the desired performance;
- (c) Test Method – A clear, reliable, easy-to-use method of test which determines compliance with the criteria.’

17.4.3 Long-term global standards development

In January 2007 a Technical Committee (TC) on Alkali Activated Materials was initiated within Réunion Internationale des Laboratoires et Experts des Matériaux, systèmes de construction et ouvrages (RILEM).¹⁴ The primary aim of this TC is to develop performance-based specifications and recommendations for the development of standards that are specifically applicable to these classes of materials. The TC contains three Working Groups which are:

- (a) Working Group I. Survey of research and commercialization progress.
- (b) Working Group II. Survey of existing standards regime and development of recommendations for new standards.
- (c) Working Group III. Testing methodologies and philosophies to underpin the standards recommendations in Working Group II.

17.4.4 Short-term regulatory barriers

While the RILEM TC provides a long-term mechanism for legitimately and globally creating an ideal regulatory environment for AAM, there remain short term hurdles and barriers for AAM to be used in the concrete industry today. As mentioned above as a case study, AS3972 does require all ‘cements’ to contain OPC. While this can be achieved under the designation of GB (General Blended) cement by addition of *some* OPC, this then invalidates the claim of *no cement*, which is both the unique and most saleable one point of distinction for AAM compared with other cement blends and systems. Therefore, to utilize AAM in Australia one would need to involve all of the risk-taking and concrete purchasing and specifying stakeholders in the material flow in Fig. 17.1 into the process. Zeobond, a small AAM concrete company in Australia, has completed exactly this process and has found that insuring bodies, construction companies, designers, architects and the ultimate customers of concrete are willing to accept a concrete product (E-Crete™)

that contains no cement as long as it meets performance standards of OPC concrete. The motivation of each stakeholder for doing this is different and will be discussed below.

Customers are looking for innovative solutions, particularly if they can generate very high reductions in CO₂. This is particularly strong in large infrastructure projects and private projects where 'greenness' has a premium from both a political and image perspective. While in the longer term as the product becomes more widely adopted these drivers will necessarily become reduced, it is a significant driver for uptake in the coming years.

The next most influential group is the consulting engineering firms. If one is not able to get these firms to use one's product, then it is immaterial whether or not the customer or architect specifies AAM, as the engineer must sign off on the design structurally. However, this hierarchy also provides an opportunity in two ways. Firstly, in the current environment ecological factors play an important role in the design and construction of buildings. Furthermore, it also plays an important role in the tendering process for design firms. While the customer is not in a position to require a company to utilize certain materials, it is in a position to drive demand for innovation. Indeed this is the situation that has evolved, with consulting engineers now looking for an environmental edge in the market to provide a point of difference with their competitors, or simply to maintain equal footing and not lose market share. Architects are in a similar situation to consulting engineers, but without the aspect of professional indemnity in terms of structural elements. Therefore, these stakeholders are also looking for new and innovative environmental aspects to incorporate in designs to both make them relevant in terms of general innovation in architecture, but also for market gains.

17.4.5 Insurance and risk assessment

As alluded to above, the ability to insure projects utilizing AAM is critical to adoption of the material. Insurance companies have always been considered to be even more conservative than consulting engineers; after all it is the insurance companies that provide cover for the engineers. However, more so than any other business sector, insurance companies manage long term risk. While the 'untried' and 'unproven' status of alternative binder systems for concrete still exists, and will do so for some time regardless of their use in large iconic projects, insurance companies also understand that the nature of risk has changed. Environmental awareness and the need to shift to a low-carbon economy mean that the weighting of different factors in providing an overall risk profile for construction has changed substantially. Previously, long-term track-record and cost were amongst the top weighted factors. While these have not been diminished, carbon cost has been elevated substantially,

both for AAM and OPC. In the thinking of insurance companies, the cost of carbon means that its usage as a proportion of the total market must be reduced in the future, even if for demand and application reasons that in real tonnes per annum its usage does not decline. How much of the market AAM or other binder systems are able to penetrate is the risk factor, not *if*. The only certainty as far as they are concerned is that OPC usage will be one of many binder systems used regularly. Therefore, to manage and determine a price for their exposure to the risk of these materials, they must become involved in a way that does not hinder their usage relative to the incumbent (OPC) until such a time as the track record is generated to price the risk properly. While this presents itself as a business risk to them, it is balanced by the probability that alternative products replace OPC and they are not able to maintain their market share as they have no understanding of the risk profile. Similar to the consulting engineers and architects, there is an initial opportunity for companies to grow their business through innovation, but ultimately it is a risk minimization strategy also against a future in which the lowest risk factor is that change will occur.

17.5 Analysis of the cement market

17.5.1 Size of the cement market

Cement manufacture accounts for two-thirds of total energy use in the production of non-metallic minerals. In terms of CO₂ emissions, cement production is by far the most important activity in this category. Global cement production grew from 594 Mt in 1970 to 2,284 Mt in 2005, and is approximately 2,500 Mt today. The vast majority of the growth in the past decades has occurred in developing countries, especially China. In 2005, China produced 1,064 Mt (47% of world cement production), while India, Thailand, Brazil, Turkey, Indonesia, Iran, Egypt, Vietnam and Saudi Arabia accounted for another 394 Mt (17%) (Table 17.1).

17.5.2 Drivers for cement demand

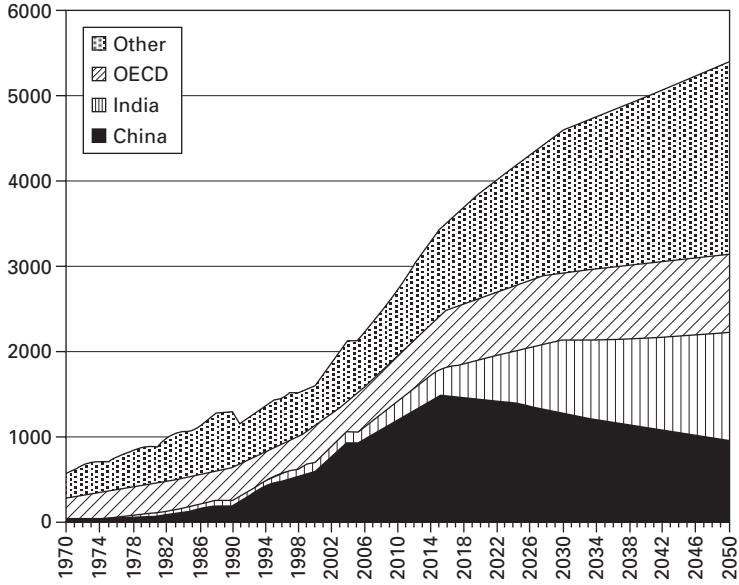
Global GDP is expected to grow by 2.9% per year between 2003 and 2050, resulting in a global production around 3.6 times larger in 2050 than it is today. There has been little change in the absolute demand in Europe and North America since 1970, with virtually all of the growth in cement demand coming from developing countries. More specifically, China's demand for cement has exploded, and between 1998 and 2004 it accounted for around two-thirds of the global growth in cement demand (USGS). Current cement demand projections have been developed by the International Energy Agency, which assume a peak in the intensity of cement demand per unit of GDP

Table 17.1 Cement production in 2005, adapted from¹⁵

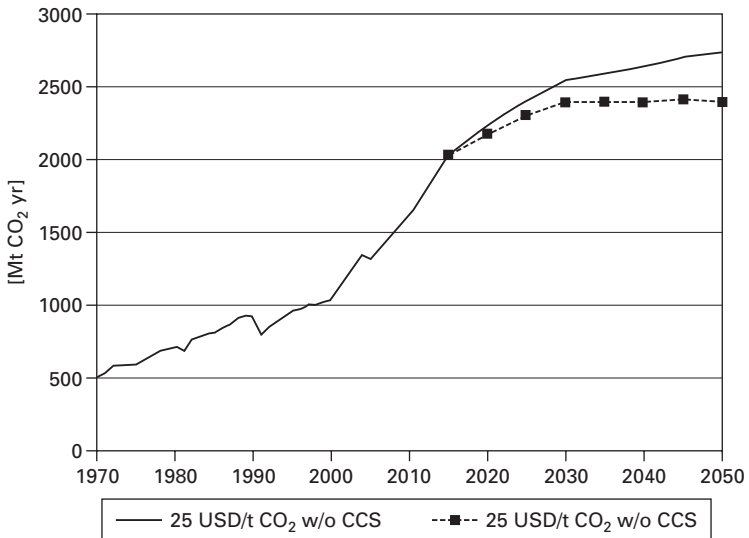
Country	Production Mt/yr	Share,%
China	1064	46.6
India	130	5.7
United States	99	4.3
Japan	66	2.9
Korea	50	2.2
Spain	48	2.1
Russia	45	2.0
Thailand	40	1.8
Brazil	39	1.7
Italy	38	1.7
Turkey	38	1.7
Indonesia	37	1.6
Mexico	36	1.6
Germany	32	1.4
Iran	32	1.4
Egypt	27	1.2
Vietnam	27	1.2
Saudi Arabia	24	1.1
France	20	0.9
Other	392	17.2
World	2284	100.0

between 2015 and 2045 for developing countries. The resulting cement demand is shown in Fig. 17.2. China and India account for around half of global cement production.

Linked with global cement demand is the growth in CO₂ emissions associated with cement production, and importantly the ability of the cement industry to reduce emissions with efficiency and reductions in cement content of concrete. The general assumptions used to determine the projected annual CO₂ output of the cement production industry by the International Energy Agency (IEA)¹⁵ include that the world average clinker production fuel intensity declines to what is now a world's best practice level of 3 GJ/t clinker, the electricity use also declines to world's best practice 100 kWh/t cement, the shares of coal, gas and alternative fuels are 70%, 5% and 25% by 2050, and the clinker/cement ratio declines to 0.7, all of which are world's best practice. The results of this work are shown in Fig. 17.3. Despite these assumptions of industry wide world's best practice, the CO₂ emissions almost double from today's level to 2.4–2.7 Gt CO₂/yr. This compares to IEA predicted total world CO₂ emissions of about 28 Gt by 2050. This figure means that 9–10% of the world CO₂ emissions will be attributed to cement production. Almost 2 Gt of CO₂ (70% of the total cement industry CO₂ emission) is process emission which cannot be reduced through energy efficiency measures of any kind. This is an intrinsic feature of OPC chemistry.



17.2 Global cement demand by region and country (1970–2050), adapted from.¹⁵



17.3 Direct CO₂ emissions from cement production (1970–2050), adapted from.¹⁵

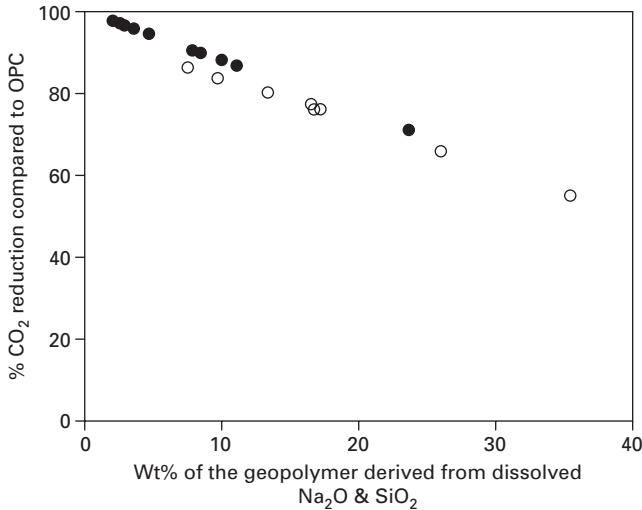
17.6 How climate change and carbon trading create opportunities

The aim of global emission reduction schemes is environmental, i.e. to reduce emissions of greenhouse gas and thereby slow global warming. As cement manufacture is one of the world's most energy intensive and intrinsically CO₂ emitting industries, it is central to world emission reduction schemes. A great deal of effort is focused on minimizing the impact of carbon abatement schemes on OPC as a product. The approach adopted by all cement-related parties is to focus attention on energy savings made to date, and to emphasize the absolute reliance of construction and economic development on OPC cement. Consequently, the absolute limit of energy savings is set by the intrinsic chemistry of cement making, which yields 0.61 ton CO₂ per ton cement. This ensures that the message of cement manufacture's impact on CO₂ emissions is kept quiet. Pressure is put on governments to accept this 'inevitability' of cement chemistry. The politics of denial have been largely successful as there has been genuine progress with respect to emission reduction, on the one hand, relative to the theoretical minimum (that the cement manufacturers set themselves), but also because there has not been a viable and proven alternative like AAM that could provide a new lower carbon footprint.

17.6.1 Lifecycle analysis

As highlighted in this chapter, the compelling reason why AAM are now being considered for commercial application is a result of a perceived significant reduction in carbon emissions and energy embodiment of the material relative to OPC. The method developed for investigating the energy and emissions of materials for determining their carbon footprint is called Life Cycle Analysis (LCA). Several different attempts were made to complete informal LCAs by Weil *et al.*¹⁶ and Duxson *et al.*¹⁷ Duxson *et al.* showed that the tCO₂e (tonnes CO₂ equivalent) associated with producing a geopolymer binder is highly dependent on the activator content (Fig. 17.4). This is because the energy associated with the manufacturing of alkali sources is several orders of magnitude higher than that of either fly ash, slag or metakaolin. Therefore, the energy embodied in manufacturing AAM is effectively linearly dependent on the activator content, as shown in Fig. 17.1. Most interestingly, the source of aluminosilicate has little effect on the energy embodiment, indicating that alternative sources of aluminosilicate than fly and slag can produce binders of very low energy embodiment from even virgin raw materials.

Such academic analyses of AAM binders though do not necessarily have the same weight as an independent audit of a commercially viable system,



17.4 Total estimated CO₂ emission of geopolymer binders as a function of dissolved component content. Compositions are taken from the literature, for fly ash (solid points) and metakaolin (open circles) geopolymers. Calculations include 72 kg CO₂/tonne metakaolin production. Adapted from¹⁷.

such as that completed by Zeobond Pty Ltd in Melbourne, Australia. The LCA conducted by an independent firm expert in LCA in the cement industry found that the tCO₂e savings from AAM were in line with the calculations made by Duxson et al. Apparently, the binder system applied by Zeobond produces 80% less tCO₂e than cement in Australia utilizing actual concrete mix-designs from VicRoads (the Victorian Government road authority) to compare like with like performance in place. This is an even more interesting claim as the comparison with ‘cement’ used in the LCA was a binder comprised of fly ash, slag and OPC with a tCO₂e value per ton of 0.67. Therefore, compared to neat ground OPC clinker the commercial implementation of AAM utilized by Zeobond performs exceptionally well in terms of CO₂ abatement.

17.6.2 Different emission reduction instruments

Emission abatement and reduction schemes can be implemented by taxing emissions of CO₂ directly (called a price instrument) or by a market-based approach such as carbon cap-and-trade system (called a quantity instrument). Direct taxation has the benefit of being easily understood and can be popular with the public if the tax is earmarked to fund environmental projects. A price is set on emissions of CO₂, which thereby provides a price advantage to low carbon products, which should drive emission reductions. Trading schemes are based on government-controlled limits or caps on the amount

of CO₂ that can be emitted. Companies or other groups are issued emission permits and are required to hold an equivalent number of allowances (or credits) which represent the right to emit a specific amount. The total amount of allowances and credits cannot exceed the cap, limiting total emissions to that level. Companies that need to increase their emissions must buy credits from those who pollute less. The transfer of allowances is referred to as a trade. In effect, the buyer is paying a charge for polluting, while the seller is being rewarded for having reduced emissions by more than was needed. Thus, in theory, those that can easily reduce emissions most cheaply will do so, achieving the pollution reduction at the lowest possible cost to society. Over time, the size of permits (and the cap) can be reduced, thereby reducing emissions. Clearly, a quantitative instrument based trading scheme is more complex than a price instrument scheme.

Despite superficial differences in relative complexity of each scheme, there has been longstanding debate on the relative merits of price versus quantity instruments to achieve emission reductions. An emission cap and permit trading system is a quantity instrument because it fixes the overall emission level (quantity) and allows the price to vary. One problem with the cap-and-trade system is the uncertainty of the cost of compliance as the price of a permit and the method of its allocation are not always known in advance and will vary over time according to market conditions. In contrast, emission taxes are a price instrument because it fixes the price while the emission level is allowed to vary according to economic activity. A major drawback of such emission taxes is that the environmental outcome (e.g., the amount of emissions) is not guaranteed.

A third option, known as a safety valve, is a hybrid of the price and quantity instruments. The system is essentially an emission cap and tradable permit system but the maximum (or minimum) permit price is capped. Emitters have the choice of either obtaining permits in the marketplace or purchasing them from the government at a specified trigger price (which can be adjusted over time). The system is sometimes recommended as a way of overcoming the fundamental disadvantages of both systems by giving governments the flexibility to adjust the system as new information comes to light. It can be shown that by setting the trigger price high enough, or the number of permits low enough, the safety valve can be used to mimic either a pure quantity or pure price mechanism.

Currently all three methods are being used as policy instruments to control greenhouse gas emissions: the European Union Emission Trading Scheme (EU-ETS) is a quantity system using the cap-and-trading system to meet targets set by National Allocation Plans, the UK's Climate Change Levy is a price system using a direct carbon tax, while China uses the CO₂ market price for funding of its Clean Development Mechanism projects, but imposes a safety valve of a minimum price per ton of CO₂. Therefore, as each of

the three different mechanisms operates in substantial cement consuming markets, it is important to have a business model for AAM manufacture that functions amongst all emission instruments.

17.6.3 Tax, trade and permit allocation

Carbon tax systems are viewed by the cement industry as a very simple and easy to deal with application of emission reduction. Simply, their strategy is to maintain the denial of alternatives to OPC, to continue to lobby government about reducing emissions by (1) clinker substitution by fly ash and slag at the lowest practicable rate, (2) use of alternative fuels and technologies, and (3) to emphasize financial loss owing to carbon leakage from less regulated markets through importation, and to pass on the majority of the carbon tax to the consumer to maintain EBITDA margins. For the cement industry carbon trading is a more complex and difficult mechanism to apply their strategy. By solely aiming at the cap it makes reduction in emissions unavoidable without the possible avenues of compromises to lobby groups that often accompany carbon tax methods.

Perhaps the most critical design element in an emissions trading system is the mechanism by which companies first obtain emission allowances. One simple way to allocate allowances is to give them away for free (also referred to as grandfathering) to companies based on past emissions, energy consumption, output or other criteria. Another way to allocate allowances is for the government to sell them in an auction, the revenues from which can be recycled through reductions in marginal tax rates in order to provide a boost to the economy that can offset, in part, the cost of the control programme (this system is to be applied in Canada). Because allowances can have significant asset value, the question of how they are distributed is of massive importance in the cement industry. As cement manufacturers have high historic emissions they politically and naturally prefer grandfathering based on past emissions. Such an allocation can compensate them for the costs they may incur as a participant in the trading system.

On the other hand, a new company without historic emissions and technology significantly lower in emissions prefers that allowances be allocated based on the efficiency of output, assuming the new company has relatively new and efficient equipment. In this case, the new company would receive more allowances (i.e., more assets) than an older competitor with less efficient technology. In practice, the real allocation methods used by EU Member States for example, stand somewhere between the two polar extremes of grandfathering and output-based allocations due to 5-yearly updating and the special provisions for new cement plants and plant closings.

The carbon reduction mechanism used in each market is critical in determining the strategy of adoption of AAM in those jurisdictions. Further,

in a quantity instrument environment the method of permit allocation will also have a massive effect on the value proposition of AAM. For each implementation there are different costs associated with the extraction of value. For instance to access Certified Emission Reductions (CERs) through the Clean Development Mechanism (CDM) of the United Nations, it is necessary to go through a complex process of assessment and the creation of a methodology. This is a costly and expensive process, and is best done only once the technology is ubiquitous.

17.6.4 Carbon trading market

The European Union Emission Trading Scheme (EU-ETS) is the largest multi-national, greenhouse gas emissions trading scheme in the world and was created in conjunction with the Kyoto Protocol. It is currently the world's only mandatory carbon trading programme. Therefore, it provides the best and only true model for future global carbon reduction schemes.

After voluntary trials in the UK and Denmark, Phase I commenced operation in January 2005 with all 15 (now 25 of the 27) Member States of the European Union participating. The programme caps the amount of carbon dioxide that can be emitted from large installations, including cement manufacturing plants and covers almost half of the EU's carbon dioxide emissions. Phase I permits participants to trade amongst themselves and in validated credits from the developing world through Kyoto's Clean Development Mechanism. The first phase (2005–2007) received much criticism due to oversupply of allowances and the distribution of allowances via grandfathering rather than auctioning. Phase II links the ETS to other countries participating in the Kyoto trading system. The European Commission has been tough on Member States' Plans for Phase II, dismissing many of them as being too loose again. In addition, the first phase has established a strong carbon market. Compliance was high in 2006, increasing confidence in the scheme, although the value of allowances dropped when the national caps were met.

Carbon emissions trading has been steadily increasing in recent years. According to the World Bank's Carbon Finance Unit, 374 million metric tons of carbon dioxide equivalent (tCO₂e) were exchanged through projects in 2005, a 240% increase relative to 2004 (110 mtCO₂e) which was itself a 41% increase relative to 2003 (78 mtCO₂e). The current spot price of CERs in June 2008 is about € 27/ton.

Most published reports forecast an increase in carbon price, as carbon trading increases and the true environmental cost of the carbon driven economy becomes better quantified. With the pressure growing to become carbon neutral, it can be expected that the demand for CERs will exceed the offer of CERs into the market, with a concomitant increase in price. The extent to which the carbon markets remain local or open to international trading will

have a substantial impact on price patterns and price differentials between trading markets. It is inevitable that the carbon markets must ultimately become international and open, otherwise large market discrepancies in carbon pricing will cause major shifts in industry between jurisdictions, which will not be sanctioned politically. If the premise of carbon trading is successful, new low CO₂ technologies like AAM will enter the market and gradually replace existing technologies. The outcome of such substitution should be decreased demand for CERs and hence lower carbon prices. It can be expected that the US and ultimately China and India will invest significantly in low CO₂ technologies, which will remove demand from the CER market. In summary, the CER market could offer a substantial medium-term incentive to AAM producers to enter the cement and concrete market that usually has very high entry barriers. However, as AAM becomes the norm rather than the exception in a market previously dominated by OPC, CERs will no longer provide any competitive advantage to AAM. At that stage, AAM will become a commodity market and like today with OPC, competitive advantage will be secured through market share.

17.7 Opportunities for AAM

17.7.1 Focus on climate change

High level awareness campaigns such as that by Al Gore¹⁸ and increasing press coverage have focused the minds of the public, policy makers and buyers on climate change, with the result that 'green' technologies and businesses enjoy a rare, once-in-a-lifetime opportunity to get new products into established and conservative markets, like construction materials.

17.7.2 'Green' as a competitive advantage in the market

Increasingly, construction materials companies, property and infrastructure developers, architects, engineering consultants, city and shire councils all want to demonstrate innovation, a commitment to 'doing the right thing' and environmental responsibility by incorporating 'green' construction materials, even if it is initially of mere symbolic significance. Key performance indicators for major projects now often include environmental innovativeness, so that a low CO₂ concrete is in demand even before a carbon trading system is in place. Market research has shown that world-wide a 'green' alternative cement or concrete will be preferred, but the market is prepared to pay a premium only in the more 'green' jurisdictions. Such a premium is a temporary necessity resulting from a lack of scale, only until such time as a larger scale supply chain is in place for AAM.

17.7.3 Carbon trading opportunities

It can be expected that a carbon trading or tax system will impact negatively on the OPC cement industry. However, CER approval through the UN's CDM is an expensive process but once completed it will benefit of all AAM producers. As CER carbon trading increases in volume, this approval will add substantial value to the technology.

17.7.4 Overcoming regulatory obstacles

The RILEM technical committee on AAM will play a key role to influence standard committees with the aim to widen performance standards to non-OPC binders and concretes. At the same time, local authorities and regulatory bodies are now more open than ever to new binders due to climate change concerns. Academic work is answering key questions about AAM durability and engineering properties, with the aim to enhance the level of confidence in AAM materials. All this work is very important, as a strong scientific base is essential to support AAM as a high technology material. Nevertheless, none of these activities has the same impact as quality concrete in the ground paid for by customers, in terms of convincing the market, technical experts and regulatory authorities. The fact that some companies have now placed AAM in various ready-mix and precast applications has substantially de-risked the material. At this stage the AAM community can use only research results and references to the durability of alkali activated slag concrete in the former USSR and Roman cements to provide comfort about long term durability.

17.8 Conclusions

Despite the long history of academic and industrial development of AAM over the past half century, there has been until very recently no significant commercialization of the technology. The lack of commercial development has been largely a result of no significant driver for uptake. The incumbent technology, OPC, has been until recently viewed by the market as being essentially without fault. This image has been recently altered as the cost of energy in the form of carbon footprint has become a steadily more important factor motivating the uptake of alternative materials. Until such drivers were established, there was no rapid need for the tangible barriers from technical to regulatory to be addressed. Now the cost of carbon will have both a commercial and a social cost attached to it over the coming decades,

With this commercial impetus the main barriers that need to be overcome in the path towards broad adoption of AAM for regular concrete use are now being addressed in earnest. These primarily involve getting examples of AAM concrete in place for monitoring and demonstration, which is then

used as a basis, in collaboration with technical experts, to formulate a set of recommendations for standards to be applied in different regulatory regimes around the world.

17.9 References

1. <http://www.freedoniagroup.com/World-Cement.html>
2. http://www.wbcdcement.org/about_cement.asp
3. <http://www.freedoniagroup.com/World-Cement.html>
4. Scrivener, K.L. and Kirkpatrick, R.J. Innovation in use and research on cementitious material, *Cement and Concrete Research*, vol. 38, 2008, pp. 128–136.
5. Pacheco-Torgal, F. Castro-Gomes J. and Jalali S. Alkali-activated binders: A review. Part 1. Historical background, terminology, reaction mechanisms and hydration products, *Construction and Building Materials*, vol. 22, 2008, pp. 1305–1314.
6. Rostovskaya, G. Illyin V. and Blazhis A. The service properties of the slag alkaline concretes, *Proceedings of 2007 International Conference on Alkali Activated Materials*, Česká Rozvojová Agentura O.P.S., Prague, 21–22 June 2007, pp. 725–734.
7. Xu, H. Provis, J.L. Van Deventer J.S.J. and Krivenko P.V. Characterization of aged slag concretes, *ACI Materials Journal*, vol. 105, 2008, pp. 131–139.
8. www.geopolymer.org
9. <http://www.chemeng.unimelb.edu.au/geopolymer/>
10. Davidovits, J. *Geopolymer Chemistry and Applications*, www.geopolymer.org, 2008.
11. Helmuth, R. Stark, D. Diamond S. and Moranville-Regourd M. (1993) *Alkali-Silica Reactivity: An Overview of Research*. Strategic Highway Research Program Report C-342, Washington, DC.
12. Hooton R.D. Bridging the gap between research and standards, *Cement and Concrete Research*, vol. 38, 2008, pp. 247–258.
13. Australian Standard AS3972, Portland and Blended Cements, 1997 (amended 2007).
14. <http://www.rilem.net/tcDetails.php?tc=AAM>
15. Taylor, M. Tam C. and Gielen D. *Energy efficiency and CO₂ emissions from the global cement industry*, International Energy Agency, 2006.
16. Weil, M. Jeske, U. Dombrowski K. and Buchwald A. (2007) Sustainable design of geopolymers – evaluation of raw materials by the integration of economic and environmental aspects in the early phases of material development. *Advances in Life Cycle Engineering for Sustainable Manufacturing Businesses*, Tokyo, Japan, Takata, S. and Umeda, Y. (Eds.), 279–283.
17. Duxson, P. Provis, J.L. Lukey, G.C. and van Deventer J.S.J. (2007) The role of inorganic polymer technology in the development of ‘Green concrete’. *Cement and Concrete Research*, 37, 1590–1597.
18. A. Gore, *An Inconvenient Truth*, Documentary film, Paramount, 2006.

Geopolymers for nuclear waste immobilisation

E R VANCE and D S PERERA,
Institute of Materials Engineering, Australia

Abstract: The usefulness of geopolymers for immobilisation of low-level and intermediate-level nuclear waste is considered. While the aqueous dissolution behaviour of geopolymers is a key feature, other important parameters are flash-set and set-inhibition; radiolytic hydrogen formation, fire resistance, freeze-thaw behaviour and all these are discussed. Geopolymers are argued to have advantages over candidate materials for low- and intermediate-level nuclear waste immobilisation. Future work necessary to follow up these advantages is detailed, particularly in the area of understanding the fundamentals of the reaction between geopolymers and water.

Key words: geopolymers, nuclear waste immobilisation, aqueous dissolution.

18.1 Nuclear wastes around the world

Before discussing the role of geopolymers in nuclear waste immobilisation, we need to discuss nuclear waste on a worldwide basis. There are over 440 operating nuclear power reactors around the world and spent nuclear fuel accumulates at around 30 t/yr for a 1 GW plant, so since nuclear power currently runs at ~ 400 GW worldwide, ~ 12000 t/yr of spent fuel is produced (Herbert and Hopley, 2007, p33). The spent fuel is mostly solid UO_2 and contains a few wt% of fission products and transuranic elements, many of which are highly radioactive. Table 18.1 shows some of the more important fission products and transuranic elements formed while the fuel is in the reactor and which persist for extended periods after removal of the fuel from the reactor.

Worldwide only a relatively small fraction of spent fuel is currently reprocessed by chemical treatment to extract U and Pu for further nuclear fuel production. However, with climate change as a strong driver for additional construction of nuclear power plants, there is presently a lot more interest in reprocessing (commonly referred to as recycling) to (a) utilise the residual U and actinides in once-through spent fuel to make fresh fuel and (b) minimise the volumes of waste for final disposition. In addition, high-level wastes (HLW) from Pu production for atomic weapons during the Cold War between Russia and the US constitute many millions of litres. This production involved relatively short (< 1 yr) in-reactor times to maximise ^{239}Pu production,

Table 18.1 Halflives and principal decay modes of some of the more important fission products and actinides in nuclear wastes derived from the nuclear fuel cycle

Beta* emitters	Halflife (yr)	Alpha emitters	Halflife (yr)
¹³⁷ Cs	30	²³⁷ Np	2.1×10^6
⁹⁰ Sr	30	²³⁵ U	7.0×10^8
⁹⁹ Tc	2.1×10^5	²³⁸ U	4.5×10^9
¹³⁵ Cs	2.3×10^6	²³⁸ Pu	88
¹²⁹ I	1.7×10^7	²³⁹ Pu	2.4×10^4
⁷⁹ Se	6.5×10^4	²⁴⁰ Pu	6.5×10^3
¹⁵¹ Sm	90	²⁴¹ Pu	14
		²⁴¹ Am	430
		²⁴³ Am	7.4×10^3
		²⁴⁴ Cm	18

followed by various means of chemical reprocessing to extract the Pu from the irradiated fuel.

The categories of radioactive wastes around the world range from (a) HLW consisting of fission products, minor actinides and process chemicals from reprocessing of spent fuel from nuclear power plants or Pu production operations, and spent fuel itself; (b) intermediate level waste (ILW) from nuclear reactor operations to (c) low level wastes (LLW) from radioisotope production, contaminated laboratory apparatus, used radioactive sources, etc. ILW and particularly LLW have much larger volumes than HLW but only a few percent of the total radioactivity. LLW is normally stored in metal drums (see Fig. 18.1) before permanent disposal. Radioactive mine tailings from ore production are normally exempt from radioactive controls because of their relatively low radioactivity but they may be chemically toxic.

The radioactivities of nuclear wastes decrease with increasing time after their production and are not precisely dependent on the class of waste but they range from roughly 10000–1 Ci/L for HLW, 10 – 10^{-3} Ci/L for ILW and 10^{-3} – 10^{-6} Ci/L for LLW (1 curie (Ci) = 3.7×10^{10} becquerels (decays/second)).

The most important fission products in nuclear wastes are not the ones with the highest specific activity, as these are very short-lived (halflives of a few days or less) and decay quickly to zero activity during the several years of storage of spent nuclear fuel in water-cooled ponds or, later, in dry storage. Rather, it is the isotopes which have halflives of several tens of years which create the main problems in the context of human lifetimes and potential for human exposure, as these have high specific activities and take several hundred years to decay to harmless levels. The radioactive species with very long halflives are an obvious concern but their specific activities (inversely proportional to the decay half-life) are correspondingly less. It is noted in passing that nonradioactive toxic inorganic elements such as Pb and As have essentially infinitely long decay half-lives.



18.1 Drums containing LLW stored at ANSTO.

The disposition of HLW has been studied worldwide for > 50 years and work up to the mid-1980s is dealt with in Lutze and Ewing (1988). It is commonly, but not universally, agreed that these wastes should be ultimately disposed of in deep (> 0.5 km) geological repositories in the Earth after a period of retrievable above ground storage while much of the radioactivity decreases with time. Retrievable storage both allows the radioactivity to decay somewhat, making the final disposal easier, and gives the option of reworking the waste form if a significantly better waste form technology is developed in the future. Such repositories are envisaged to be constructed in clay deposits or crystalline rocks.

Liquid HLW from reprocessing would be converted to water-resistant glasses or ceramics (generally called waste forms) by the addition to the waste of glass- or ceramic-forming chemicals, followed by mixing and appropriate heat-treatment to consolidate and immobilise these wastes. Canisterised spent fuel from some nuclear countries – notably North America – is targeted to be disposed of in the repository without further treatment.

Glass waste form production rates of up to tonnes/day can be envisaged, and new facilities for this purpose are under construction at Hanford in the state of Washington, USA (Duncan, 2005). The baseline properties of glasses and ceramic alternatives for immobilised HLW can be summarised as follows: (a) loadings of ~10–50 wt% of waste in the glass or ceramic on a dry oxide basis; (b) production temperatures of 1000–1300°C via Joule- or cold-crucible for melting or sintering/hot-pressing; (c) normalised leach rates in cold or warm

water using a low waste form surface area to liquid volume (SA/V) of $< 1 \text{ g/m}^2/\text{day}$, corresponding to fractions of a micron/day. Normalised leach rates relate to the fractional inventory of the species being studied so that leach rates are defined as

$$LR = w / (SA \cdot c \cdot t) \quad 18.1$$

where w = weight of leached species, SA = geometrical surface area of sample, c = concentration of species of interest in the waste form, and t = leaching time. These rates are typically $0.001\text{--}1 \text{ g/m}^2/\text{day}$, the usual unit of leaching rate in the context of radioactive waste immobilisation.

The dimensions of large solid bodies are simply measured to obtain the geometrical surface areas. For reasons of conservatism, geometrical surface areas of powders in measured particle size distributions are taken assuming the particles are cubes or spheres. These areas are used rather than surface areas of powders derived from Brunauer-Emmett-Teller (BET) measurements. It has been found in practice that BET surface areas of powders of solid materials are ~ 7 times the geometrical surface areas. However the N_2 BET areas of porous materials such as cement might be tens of m^2/g (Odler, 2003), whereas the geometrical surface areas will be much smaller, depending on the particle size. Of course, the potential overall radionuclide extraction by water is minimised if the waste can be consolidated as large bodies of preferably non-porous material. The significant point about Equation (18.1) is that, unlike in the TCLP test (EPA, 1992) for hazardous waste testing, dilution of the waste radionuclide into a larger body of material not only has economic penalties but does not in first order change the leach rate, insofar as the gross leach rate is divided by the concentration of the element in question.

There is still widespread debate about whether glasses or ceramics are the most appropriate for given types of HLW, but generally speaking, both are within the zone of acceptability, as defined by national regulators and the IAEA (IAEA, 1996), and the main part of the debate is which approach has a smaller footprint and better economics.

The protection of the biosphere after insertion of the HLW glasses or ceramics into the geological repository is further assured by the use of engineered barriers, which consist of resistant metal containers for the waste forms, possible surrounding of the containerised waste by clay to sorb any nuclides released from the containers, and finally concrete linings of the repository plus rock backfills if and when the repositories are to be finally sealed off.

No country has yet constructed a geological repository for HLW, though substantial progress is being made in Finland and Sweden. The selection by the US Congress in 2002 of Yucca Mountain in the US as a national HLW repository is also noteworthy, but legal and technical challenges are expected to persist for at least several more years.

18.2 Cementitious LLW/ILW waste forms

The costs of producing glass and ceramics by high temperature technologies for the vast volumes (millions of m³ in the USA alone (Ewing, 2008)) of extant LLW/ILW waste would be huge, so there is a compelling driver to utilise 'cheap' low-temperature processes such as cementation and bitumenisation to immobilise these wastes. While ordinary Portland cements (OPC) have been examined for possible candidacy as immobilising agents for HLW, the normalised leach rates (USDOE, 1982) when referred to geometrical surface areas rather than those derived from BET measurements, are deemed as excessive for this purpose. For elements which do not form highly insoluble hydroxides (such as Cs), leach rates are in the order of 10–100 g/m²/day (corresponding to ~ 10–100 µm/day) in short term HLW regulatory tests of a few days (see Section 18.2.2), although they decrease with increasing leaching time.

However, regulatory criteria for dealing with LLW/ILW are far less stringent than those applicable to HLW. So it is reasonable that OPC and variants thereof are being used around the world for immobilising LLW/ILW, and cementation should be considered as a baseline technology for this purpose.

As groundwater is a key medium for the transport of waste radioactivity to the human domain – the biosphere – LLW/ILW radioactive wastes for immobilisation need to be devoid of free water in the first instance. Such dewatering would also remove substantial fractions of organic material. They can then be incorporated in cementitious materials and metal drums, according to international standard practice.

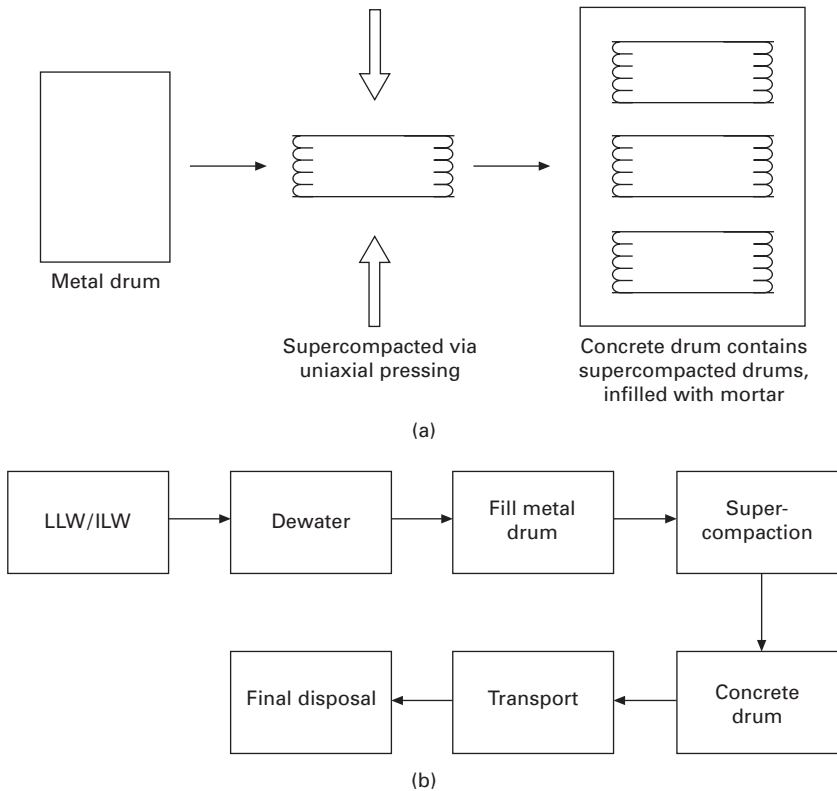
Two basic strategies can be employed. Firstly, the waste can be directly mixed with a cementitious material in a metal drum. The cementitious material is then allowed to set and the drum is sealed. However, this approach has some risks, insofar as (a) certain possible waste components can cause flash setting or can prevent setting altogether and (b) the water in the usual cementitious material yields radiolytic hydrogen and oxygen from the effect of radioactive decay of the nuclides being immobilised, and the hydrogen is a fire risk if it escapes and otherwise could deform the sealed container. On point (a), many wastes which have been in existence for many years are grossly inhomogeneous and the records of the chemical identities of the wastes are vague at best.

Hence a more popular practice is to dry the waste while it is contained in a drum, followed by uniaxial supercompaction of the drum to minimise the volume; drums are then put inside a concrete container and infilled with mortar for ultimate disposal in a shallow repository. Here there is no radiolytic hydrogen generated from aqueous material in the supercompacted drum (see below) and the radioactivity incident on the concrete container is relatively minor because of the shielding effect of the supercompacted drum and the

distance of the concrete lining from the actual radioactivity. Figure 18.2 shows a schematic of this process.

So the main question for this chapter is whether geopolymers have potential to replace standard cement mixtures for containment of LLW/ILW. A second possible application is the replacement of cement by geopolymers in repositories for such waste, noting that repositories for LLW/ILW will be essentially close to the Earth's surface.

Although there are seemingly obvious advantages of geopolymer production producing much less greenhouse gas than cement on a mass basis, dealt with elsewhere in this book, it must be remembered that when dealing with radioactive wastes, the cost of the immobilising materials is only a small component of the total costs of the whole operation because of the safety aspects of shielding and general precautions in the handling of radioactive materials. However, the greenhouse advantage over cement for use in large-scale repository construction is direct because no radioactivity would be introduced before the repository construction would be completed.



18.2 (a) Schematic of supercompaction process for LLW/ILW immobilisation; (b) flow sheet for LLW/ILW disposal.

The factors to be considered for LLW/ILW waste forms (solids for waste incorporation) are (a) knowledge of agents which give rise to flash set or set inhibition of geopolymers; (b) leach resistance relative to that of conventional cement; (c) the production of radiolytic hydrogen; (d) freeze-thaw behaviour and (e) the immobilisation of possible chemically toxic entities accompanying the radioactive ions in the waste.

We have essentially dealt with (a) above already. But there could be some merit in combining waste directly with cementitious material if flash setting is not a problem. Ca and B are the possible agents of difficulty, together with water-soluble anions. When calcium salts were added to fly ash-based geopolymers they set rapidly compared to those free of calcium salts (Lee and Deventer, 2002). It has been shown that Class C fly ash which is high in CaO (~ 22 wt%; Perera *et al.*, 2004) also sets rapidly (Nicholson *et al.*, 2005). However, the presence of Ca increases the strength in a geopolymer, hence the presence of a small amount of Ca (say 3–8 wt%) is beneficial (van Jaarsveld *et al.*, 2003; Dombrowski *et al.*, 2007). The addition of B-containing salts, such as sodium tetraborate and lithium pyroborate, increases the setting times significantly for OPC (Taylor, 1997) but does not significantly influence geopolymers in this regard (Palomo and de la Fuente, 2003). Boron is present as tetrahedral BO_4 entities in the geopolymer structure (Nicholson *et al.*, 2005). It was also found by Lee and van Deventer (2002) that anions such as Cl^- and CO_3^{2-} could possibly reduce the setting time for geopolymers, although the influence of cations accompanying these anions could well mask such effects.

Because of fire and radiation resistance criteria in nuclear regulatory tests (see Sections 18.5 and 18.6), waste form solids for immobilisation of nuclear waste preferably need to be inorganic and refractory. Water interactions with such solids can be very complex and are far from understood in detail.

18.2.1 Aqueous dissolution behaviour

While substances such as inorganic metal salts (e.g., NaCl) dissolve in water such that the cations and anions dissolve together on a stoichiometric basis until the solubility limit is reached (congruent dissolution), this is not the case for more complex compounds such as rocks, ceramics and metal alloys. Here some species dissolve preferentially, with this process being referred to as incongruent dissolution or more commonly as ‘leaching’. This process causes a nett alteration in the composition of the solid, particularly near the surface, and the whole process is diffusion controlled and non-linear in time.

More generally, the dissolution rate of a solid is a complicated function of the ratio of the solid to liquid, sample surface area, pH, temperature, composition of the aqueous medium and the leaching reaction time. Thus the dissolution process is initially characterised by a forward reaction which can be characterised by the dissolution rate at zero time and zero concentration

of dissolution products in the water. However, as dissolution proceeds, the reaction slows down because of a 'back-reaction' which tends to precipitate some of the dissolved species. Eventually an equilibrium is reached between the solid dissolution products and the solution, depending on whether the system is essentially closed insofar as it is small and bounded by a water-free zone, or is essentially unbounded and therefore open. Further complications arise when leaching is carried out in groundwaters containing substantial amounts of salts.

One of the factors involved in the choice of a solid for regulation-dictated immobilisation of radioactivity is reproducibility of the solid, and for this reason we would argue that metakaolin is by far the most reproducible aluminosilicate precursor for geopolymers and should be used in candidate geopolymers for this purpose. A somewhat negative feature, however, is that the water demand is higher for geopolymers based on metakaolin as against fly ash. While fly ash is cheaper, its composition varies from one power station to the next and even on a day-to-day basis at a given power station. Moreover fly ash consists of a complex mixture of crystalline, cryptocrystalline and amorphous entities which makes it very difficult to sort out collective aqueous dissolution mechanisms. Therefore we will mostly confine our remarks to metakaolin-based geopolymers.

The aqueous dissolution behaviour of (metakaolin-based) geopolymers is particularly complex because, as we have seen in earlier chapters of this book, we are dealing with an aluminosilicate framework which contains pore water. So two basic processes contribute to the reaction of geopolymers with water: (a) the diffusion of the pore water into the external water solution and (b) the leaching of the framework. However, it is clear from many studies that only partly reacted aluminosilicate precursors are usually also present in the geopolymer matrix and this further complicates the picture.

It is well known (see earlier chapters) that 3-D polymerisation of geopolymers maximises at around a Si/Al molar ratio of ~ 2 and that for all the oxygen in the tetrahedral framework to be fully bonded the Na/Al molar ratio should be 1, to provide full charge compensation. Relevant studies include solid-state magic angle ^{27}Al and ^{29}Si nuclear magnetic resonance (Duxson *et al.*, 2005; Blackford *et al.*, 2007) as well as compressive strength measurements (Rowles and O'Connor, 2003). Not surprisingly then, it has recently been found that aqueous dissolution is also a minimum for Si/Al values of around 2 (Aly *et al.*, 2008). As discussed in other chapters, for Si/Al molar ratios of around 1 or less, crystalline zeolite formation is favoured, especially at higher curing temperatures, whereas when the Si/Al molar ratio significantly exceeds 2 or 3, extensive 2-D networks form, which have low strength.

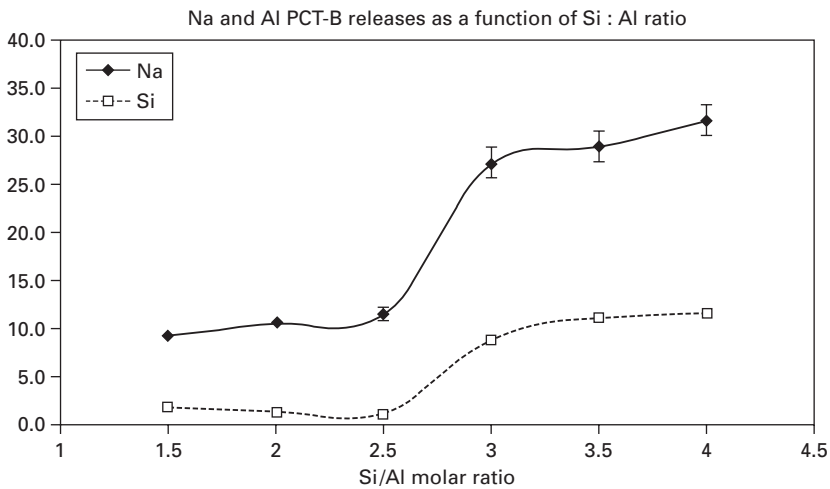
We will first consider the reaction of the tetrahedral aluminosilicate framework with water. To a first approximation, the framework can be likened to a porous aluminosilicate glass. When such a glass is immersed in water, the

first indication of reaction is an increase in the pH of the water and for solid glass this is attributed to ion exchange whereby alkali ions are transferred to the solution and protons (or H_3O^+ entities) replace the alkali ions in the glass. The continuation of this process is that the alkaline solution then attacks the aluminosilicate framework via a reaction such as:



Many studies have been made of borosilicate glasses in connection with the immobilisation of high-level nuclear waste (fission-product-rich waste derived from reprocessing of used nuclear power plant fuel-see above), and the process is basically well understood (Lutze and Ewing, 1988), although the fine detail of improvements to the net leaching rate by the addition of small amounts of other cations such as Ti, Zr, Al, Fe, Li, Zn, etc., is still empirical to some extent.

When geopolymers are leached in water, it is found that the pH of the water quickly rises and the overall release rate in terms of fractional extraction of the inventory of a particular cation is by far the highest for the alkalis (Fig. 18.3 and see, e.g., Aly *et al.*, 2008; Ly *et al.*, 2006). But it has not proved easy to separate the contributions from framework dissolution and pore water dissolution to the total alkali release. However, it has been observed that, other things being equal, the release rate of the alkalis (and Al and Si) depends strongly on the surface area to liquid ratio even in relatively dilute solutions (Vance *et al.*, 2007), something that would not be expected if pore water/solution exchange was the only contributor to the alkali release.



18.3 Percentage elemental extractions in PCT-B tests from metakaolin-based geopolymers with different Si/Al molar ratios. Al extractions all < 0.4%. ANSTO unpublished work.

Although pore water can be nearly all removed by modest heating to $\sim 300^\circ\text{C}$ (Perera *et al.*, 2005), the pore structure would remain substantially unaltered and any salts in the pore water would crystallise on the sides of the pores: when the dried solid is immersed in water, the water could penetrate into the pore structure, dissolve the salts and then the salts could diffuse back into the leach water.

Of course pore water transfer to an aqueous solution should be minimised if relatively large-scale porosity can be removed, so current efforts are directed to high-shear mixing to minimise water content and removing air bubbles.

Microstructures of geopolymers have been discussed in other chapters and the essentials are that very fine meso- and macropores (2–50 nm and 50–200 nm respectively; Roquerol *et al.*, 1999, p8) are present, even if mm-sized pores can be prevented from forming by vibration techniques. However, it is not all that likely that nm-sized pores would allow any significant porewater transfer to a leaching solution, in the absence of high external water pressures, so reduction of the larger scale porosity would seem to have the most promise for improvement of the leaching resistance.

Experiments in this laboratory are in progress to see how much water minimisation can be utilised in high-shear mixing of metakaolin-based geopolymers. To date it has been found (Walls and Kurlapski, private communication) that minimising water additions for setting can cause samples to crack upon subsequent exposure to water. We have also investigated commercial geopolymers and found in unpublished work that using milled fly ash, minimum water addition and high-shear mixing to maximise their strength, that they can fail even the HLW version of the PCT test (see Section 18.2), so it seems improbable that such water minimisation would lead to a large improvement in water leach resistance.

18.2.2 Conformance with regulatory tests

There are well-defined, short-term International Atomic Energy Authority (IAEA) plus country-specific regulatory tests for the disposal of radioactive wastes, but scientific understanding of the behaviour of the disposed waste is still necessary to assure that immobilisation will last for thousands of years or when all radioactive decay in the nominally immobilised waste has effectively ceased.

The main relevant regulatory tests are ANS 16.1 (ANS, 2003) and to a lesser extent the PCT-B test (ASTM, 2002). However, these are short-term tests and scientific understanding is still necessary to assure the immobilisation of the particular wastes for periods of thousands of years. The ANS 16.1 test involves the use of cementitious samples of known composition and $\sim 1 \times 1 \times 5$ cm in size and weighing ~ 20 g. These are immersed in ~ 200 mL of water at 20°C and leaching is allowed to proceed for 2, 7, 24, 48, 72, 96, 120 h, with longer

periods being optional. The solutions are then analysed for various cations, particularly the radioactive species. Assuming that < 20% of the inventories have been leached out of the blocks (which can be deduced from knowing the composition), the fractional inventories leached out are plotted against the square root of leaching time and effective diffusion coefficients for various elements are derived. If the diffusion coefficients are all < 10^{-6} cm²/s the solid is deemed successful in immobilising the radionuclides of interest, assuming it has a compressive strength > 3.5 MPa (IAEA, 1996).

In the PCT-B test, the sample is powdered to achieve a fraction between 100 and 200 mesh (150–75 microns). Adherent fines are then removed by washing in ethanol/methanol/acetone or preferably a non-polar solvent to remove the chances of pre-dissolution of soluble species. For each g of washed sample, 10 ml of deionised water is added and the samples are leached at 90°C for 7 days. The fractional inventories of the leached elements, notably Na and Si in the present context, are then measured and assuming these elements are present, the material is a good candidate for HLW disposal if all leached inventories correspond to < ~13% of the totals in the solid. The focus on these elements derives from the use of the PCT-B test as an indicator of the quality of HLW-bearing borosilicate glass, and it is also noteworthy that the SA/V ratio is relatively high (~ 40 cm⁻¹) in these tests. Borosilicate glasses typically give fractional release rates of the abovementioned elements in the range of 0.1–10%.

The use of the PCT-B test for candidate solids containing LLW/ILW for near-surface disposal is identical in methodology but the ‘pass mark’ for elemental leaching is 2 g/m², a factor of 3–5 lower than that for HLW (depending on the waste form density), a criterion that is adjusted to account for LLW/ILW being disposable in a near-surface repository as against a deep repository containing multiple barriers to prevent radionuclide transport to the biosphere for HLW.

While waste-free geopolymers can be fabricated and pass the HLW version of the PCT test, and on occasion the LLW version, there are strong indications that the PCT test gives early saturation effects – at times of only 1 day (Vance *et al.*, 2007) – and this is consistent with the very high early release rates determined in tests in which the SA/V ratio is low (see Section 18.2).

18.2.3 Effect of anions

The US tank wastes from Pu production during the Cold War (see Section 18.1) are classed as HLW in that country but their activities would fall into the ILW regime in many other nuclear countries. Accordingly there have been several attempts to demonstrate that geopolymers are a viable way to immobilise these wastes relative to vitrification which is the baseline technology in the US. The wastes under consideration are the liquid + sludge wastes at the

Hanford site and the Savannah River Laboratory, and the calcines at Idaho National Laboratory. The liquid wastes consist of a metal hydroxide sludge containing most of the fission products and actinides, plus a supernatant solution of mainly Na hydroxide, Na nitrate, Na nitrite and Na aluminate, together with soluble fission products such as Cs and Tc. The calcines consist of mixtures of zirconia, alumina, Ca fluoride and dolomite, plus fission products and actinides. For the liquid wastes, geopolymer formulations have been devised to immobilise simulated wastes which have been calcined after mixing with clay and sugar as a reducing agent to maximise the removal of the nitrate/nitrite plus sulphate as well as organic species (Krishnamurthy *et al.*, 2001; Siemer *et al.*, 2001b; Bao and Grutzeck, 2007); the metakaolin-based geopolymers which were mostly treated by autoclaving at $\sim 200^\circ\text{C}$ (Siemer *et al.* 2001a) could pass the HLW version of the PCT test for Na (the waste being classed as HLW in the USA), as well as display adequate compressive strength. Broadly similar results were obtained on geopolymers prepared from the Idaho National Laboratory calcines (Siemer *et al.*, 2001b).

The nitrate/nitrite and sulphate anions present in the liquid wastes normally exist in geopolymers as alkali salt solutions in the pore water and as such are very poorly immobilised when the geopolymer is exposed to water. Because these particular tank wastes have high alkali contents, it is difficult to remove the anions, even by calcination, without adding large amounts of other cations such as Al and/or reducing agents. However, fabrication of nitrate sodalites has been reported (Buhl and Lons, 1994; 1996; Buhl, 1991), although this was all done in hydrothermal preparations at temperatures well above 100°C in which the nitrate was stoichiometrically in excess of the aluminosilicate components by factors of 10 or more. Nitrate, nitrite and sulphate ions can be incorporated in cancrinite structures derived from the basic sodalite structure and can evidently be immobilised in geopolymers with Na/Al/Si ratios of around unity (Krishnamurthy *et al.*, 2001; Siemer *et al.*, 2001a; Bao and Grutzeck, 2007). Moreover, Ba hydroxide can be added to immobilise the sulphate as insoluble BaSO_4 .

18.2.4 Comparison with OPC

Cs is one of the most difficult radionuclides to immobilise because of its generally high water solubility as an alkali element and in a PCT test on a geopolymer the extraction is roughly 2 g/L (Perera *et al.*, 2006) as against 80–100 g/L for Cs in cement (Hanna *et al.*, 2001). To try to lower the Cs leach rates for cement, attempts have been made to incorporate the Cs in zeolite which is in turn embodied in cement (El-Kamash *et al.*, 2006; Perera *et al.*, 2007).

In ANS 16.1 tests on geopolymers containing simulated LLW/ILW, we found D values ($-\log_{10}$ of the derived diffusion coefficient—see Section 18.2)

(Perera *et al.*, 2007) of around 10 (i.e., considerably greater than the ‘pass mark’ of 6) for several elements, viz. Al, Na, Si, Cs, Sr, Nd and Ba.

18.2.5 Radiolytic hydrogen

In cement, the main strength-building phase is the hydrated C-S-H (Ca-Si-oxide/hydrate) phase and radiolysis will generate hydrogen (Offerman, 1989). As mentioned above, such H₂ presents a hazard. In principle, the hydrogen can be largely removed by dehydrating the cement and this would ameliorate the radiolytic H₂ problem. However heating to a few hundred °C can seriously impact the cement structure and mechanical properties because water is a component of the C-S-H phase. By contrast, geopolymers can be almost completely dehydrated by heating at 300–400°C with virtually no effect on aqueous dissolution properties (Perera *et al.*, 2006). Any organic material would also be essentially removed by such treatment, so such heating should remove the problem of radiolytic H₂ generation. Effects of such heating on their mechanical properties have not been quantified (work is in progress) but are not anticipated to be very significant from numerous laboratory observations of general friability.

18.2.6 Fire resistance

Fire resistance criteria for immobilising ILW/LLW are somewhat elastic but the IAEA recommends that attention be paid to this question (IAEA, 1996). Clearly bituminous products (see Section 18.2.9) would need to be contained in fireproof metal cans and even then, the heat of a fire would produce potential for explosion and subsequent combustion. Geopolymers have adequate fire resistance and this is well documented (Kong *et al.*, 2007, 2008).

18.2.7 Freeze-thaw behaviour

Freeze-thaw problems are basically macroscopic cracking from the expansion/contraction of hydrous phases in cementitious materials. The freeze-thaw behaviour of OPC derivatives is an important parameter but in the same way as the problem of radiolytic H₂ production can be minimised by heating geopolymers to ~300°C (Section 18.2.1), such heating also removes any potential problem of freeze-thaw behaviour in geopolymers, at least while they are not in contact with water.

18.2.8 Actual waste immobilisation in geopolymers

AllDeco Ltd, of the Slovak Republic, has developed a proprietary geopolymer matrix (called SIAL) for embedding various intermediate level wastes resulting

from Slovak power reactors (Majersy *et al.*, 2007). Some of the materials encapsulated in geopolymer matrices are bottom sludges from long-term storage of spent nuclear fuel elements, sludges from the sedimentation tank of a reactor and several other sludges. Some of the sludges are formed from an emulsified mixture of organic compounds from the cooling media and contain a large amount of calcium and magnesium hydrocarbonates. The activity of the ^{137}Cs in the sludges is $\sim 10^5 - 10^8$ Bq/L. Once these sludges were solidified in the geopolymer matrix and placed in 60 L drums, the surface dosage on the drums was $10-20$ mGy.h $^{-1}$. The D value for the ^{137}Cs in samples taken from the drum was > 8 for the ANSI 16.1 test and the compressive strength was 25 MPa. About 20 wt% (on a dry basis) of waste was encapsulated.

Organic ion exchange resins on their own and in mixtures of sludges were also encapsulated in geopolymer matrices. It was possible to encapsulate ~ 20 wt% (on a dry basis) for geopolymers compared to 10 wt% for OPC. These were placed in 200 L drums. The dosages on the drum surfaces were $130-600$ $\mu\text{Gy.h}^{-1}$ and the D value for ^{137}Cs was > 9 on cut samples from the drums. All the drums used were made from stainless steel.

The SIAL matrix (geopolymer) has been accepted by the Slovak Nuclear Authority (UJDSR) and the Czech Nuclear Authority (SUJB) for placement in their respective repositories (Majersy *et al.*, 2007). AllDeco Ltd placed these drums in the Slovak repository in 2003.

18.2.9 Alternate low-temperature products for LLW/ILW immobilisation

Alternate 'low-temperature' products to OPC and geopolymers are the Argonne Mg-K-phosphate mixtures and bitumen, as well as modified cements. As mentioned previously, OPC is a baseline product for LLW/ILW immobilisation. OPC extenders are fly ash and ground glass blast furnace slag and these have been studied extensively in this context – see, e.g., Quillin *et al.* (1994) and the reviews by Glasser (1992) and Milestone (2006). Again, however, the criticism of non-reproducibility of fly ash and ground glass blast furnace slags will apply. Shi *et al.* (2006) have also discussed the use of alkali-activated cements for immobilising radioactive waste.

For bitumen radiolytic H_2 production is generally perceived as a problem but bitumenous products are being used in Europe, with Eurobitum as a well-defined product (Chaix *et al.*, 2001; Valcke *et al.*, 2001; Sneyers and Van Iseghem, 1998). Oxalates and other radicals are radiolysis products (Valcke *et al.*, 2001); these will have complexing power and facilitate transfer of radionuclides in groundwater.

Mg-K-phosphates made by Argonne National Laboratory (ANL) workers involve combining calcined MgO with KH_2PO_4 via



as the major reaction (Singh *et al.*, 1994; Jeong *et al.*, 1996; Walker *et al.*, 2000; Langton *et al.*, 2000). This material was seen as appropriate for the immobilisation of actinides and Cs incorporated in the CST ion exchanger (Singh *et al.*, 1994). It was also argued to be good for actinides (Jeong *et al.*, 1996), while the product was also widely applicable to the toxic components of the waste via passing TCLP tests. Radioactive stability was usually assessed by the ANS 16.1 tests.

Table 18.2 summarises the key properties of candidate waste forms.

Cations which form insoluble hydroxides are clearly immobilised in non-acidic groundwaters, noting that the use of cement or geopolymers in the repository construction will promote alkalinity of any groundwater which enters the repository. Such alkalinity would not be fostered by the use of bitumen and probably not the ANL phosphate cements.

It follows from Table 18.2 that potential advantages of geopolymers for LLW/ILW immobilisation can be summarised as: (a) generally better performance in regulatory leach tests; (b) essential removal of radiolytic H₂ production (and freeze-thaw problems) can be carried out by heating at very moderate temperatures such as 300°C without any serious effects on strength or leachability; (c) demonstrated excellent fire resistance and (d) the alkalinity of geopolymers (and of course cements) would encourage the intrinsic formation of insoluble hydroxides for many fission products and actinides.

18.3 Future trends

Current work in this laboratory is investigating the dependence of leach rate in very low SA/V regimes of time, pH, water additives such as chloride and carbonate species, and temperatures between 25 and 90°C. Detailed studies of possible benefits of high-shear mixing and minimisation of water content are also in progress. Very recent work in this laboratory has showed that a change of chemistry to phosphate-based materials may also have considerable potential to improve on aluminosilicate geopolymers.

18.4 Conclusions

Geopolymers can have significant advantages over cements (other than greenhouse gas emissions during production) and other candidates for the

Table 18.2 Key properties of candidate waste forms for immobilisation of LLW/ILW

Candidate	Leachability	Water/organic content	Fire resistance
Cement	Satisfactory	Yes	Binder weakened
Geopolymers	Better than OPC	Can be eliminated	Excellent
Mg-K-phosphate	Better than OPC	Yes	??
Bitumen	Better than OPC	Yes	No

immobilisation of LLW/ILW, and it needs to be stressed that the existing volumes of these classes of nuclear waste far outweigh those of HLW. These advantages lie in lack of freeze-thaw problems and minimal production of radiolytic H_2 if a dewatering production step is inserted in the production cycle, fire resistance, and good immobilisation of radionuclides from the point of view of leaching resistance. There has been actual disposal of low-level nuclear waste in geopolymers on the industrial scale in the Slovak Republic. Even if advanced nuclear fuel cycles become widely implemented in, say, 40 or 50 years, there will always be very large amounts of LLW and ILW requiring immobilisation.

However, the aqueous dissolution behaviour of geopolymers containing a variety of LLW/ILWs in a range of groundwater types needs to be more widely investigated to assure the long-term stability of the immobilised LLW/ILW. Research is especially needed to assess geopolymers' potential as engineered barriers in repositories for nuclear and hazardous wastes. Control and minimisation of porosity at the $0.1 \mu m$ scale and above is especially needed.

18.5 Sources of further information and advice

The book entitled '*Radioactive Waste Forms for the Future*', edited by Lutze and Ewing is an excellent source of materials-related research on nuclear waste immobilisation up to the mid-1980s. The Materials Research Society have held approximately annual symposia on radioactive waste management since 1978. Glasser (1992) and Milestone (2006) have given very useful reviews of research on cements as applied to immobilisation of radioactive waste.

18.6 Acknowledgments

We wish to thank D. Brew and P. Walls for helpful discussions, and Z. Aly for carrying out most of the leaching analyses. This work was supported in part by the Cooperative Research Centre for Sustainable Resource Processing, based at Curtin University, Perth, WA.

18.7 References

- Aly, Z, Vance, E R, Perera, D S, Davis, J, Durce, D, Hanna, J V, and Griffith, C S (2008), 'Aqueous leachability of metakaolin-based geopolymers with molar ratios of Si/Al = 1.5 to 4', *J. Nucl. Mater.*, 378, 172–9.
- ANS (2003), *Measurement of Leachability of Solidified Low Level Radioactive Wastes by Short-Term Test Procedure*, ANSI/ANS-16.1-2003. American Nuclear Society, Illinois, USA.
- ASTM (2002), *Standard Test Methods for Determining Chemical Durability of Nuclear, Hazardous, and Mixed Waste Glasses and Multiphase Glass Ceramics: The Product*

- Consistency Test (PCT)*, Designation C1285-02, ASTM International, PO Box C700, West Conshohocken, PA 19428-2959, USA.
- Bao, Y, and Grutzeck, M W (2007), 'Solidification of Sodium Bearing Waste using Hydroceramic and Portland Cement Binders', in Dunn, D, Poinssot, D C, and Begg, B (eds.), *Scientific Basis for Nuclear Waste Management XII*, Materials Research Society, Warrendale, PA, USA, 233–242.
- Blackford, M G, Hanna, J V, Pike, K J, Vance E R, and Perera D S (2007), 'Transmission Electron Microscopy and Nuclear Magnetic Resonance in Geopolymers for Radioactive Waste Immobilisation', *J. Amer. Ceram. Soc.*, 90 (4), 1193–1199.
- Buhl, J-C (1991), 'The properties of salt-filled sodalites Part 2. Synthesis, decomposition reactions and phase transitions of nitrate sodalite $\text{Na}_8[\text{AlSiO}_4]_6(\text{NO}_3)_2$ ', *Thermochim. Acta*, 189, 75–82.
- Buhl, J-C, and Lons, J (1994), 'Orientational Disorder and Heterogeneous Reaction Behaviour of NO_2^- and NO_3^- Anions Inside a Sodalite Matrix', *J. Solid State Chem.*, 112, 243–250.
- Buhl, J-C, and Lons, J (1996), 'Synthesis and crystal structure of nitrate enclathrated sodalite $\text{Na}_8[\text{AlSiO}_4]_6(\text{NO}_3)_2$ ', *J. Alloys and Compounds*, 235, 41–47.
- Chaix, P, Camaro, S, Simondi, B, Vistoli, P P, and Blanc, Y (2001), 'Long-Term Behaviour of Bituminized Waste: Modelling of Auto-Irradiation and Leaching', in Hart, K P and Lumpkin, G R (eds.), *Scientific Basis for Nuclear Waste Management XXIV*, Materials Research Society, Warrendale, PA, USA, 131–139.
- Dombrowski, K, Buchwald, A, and Weil, M (2007), 'The influence of calcium content on the structure and thermal performance of fly ash based-geopolymers', *J. Mater. Sci.*, 42, 3033–3043.
- Duncan, G M (2005), 'The Nation's Largest Construction Project: Designing and Constructing Hanford's Waste Treatment Plant', *Radwaste Solutions*, Sept/Oct, 14–22.
- Duxson, P, Lukey, G C, Separovic F, and van Deventer, J S J (2005), 'Effect of Alkali Cations on Aluminum Incorporation in Geopolymeric Gels', *Ind. Eng. Chem. Res.*, 44, 832–839.
- EPA (1992), Environmental Protection Agency, *Test Methods for Evaluating Solid Waste, Physical/Chemical Methods: Method 1311: Toxicity Control Leaching Procedure*, Document SW-846.
- El-Kamash, A M, El-Nagggar, M R, and El-Dessouky, M I (2006), 'Immobilization of cesium and strontium radionuclides in zeolite-cement blends', *J. Hazardous Materials*, B136, 310–318.
- Ewing, R C (2008), 'Nuclear Fuel Cycle: Environmental Impact', *Materials Research Society Bulletin*, 33, 338–340.
- Glasser, F P (1992), 'Progress in the Immobilization of Radioactive Wastes in Cement', *Cem. Concr. Res.*, 22, 201–216.
- Hanna, J V, Aldridge, L P, and Vance, E R (2001), 'Cs Speciation in Cement', in Hart, K P and Lumpkin, G R (eds.), *Scientific Basis for Nuclear Waste Management XXIV*, Materials Research Society, Warrendale, PA, USA, 89–96.
- Herbert, A M, and Hopley, G W (2007), *Nuclear Energy Now*, John Wiley and Sons, Inc., Hoboken, NJ, USA, p. 33.
- IAEA (1996), *Requirements and methods for low and intermediate level waste package acceptability*, Report IAEA-TECDOC-864, IAEA-Vienna.
- Jeong, S, Wagh, A S, and Singh, D (1996), 'Chemically Bonded Phosphate Ceramics for Stabilizing Low-Level Radioactive Wastes, in Jain, V and Peeler, D (eds.), *Environmental*

- Issues and Waste Management Technologies in the Ceramic and Nuclear Industries II*, American Ceramic Society, Westerville, OH, USA, 179–188.
- Kong, D L Y, Sanjayan, J G, and Sagoe-Crentsil, K (2007), ‘Comparative performance of geopolymers made with metakaolin and fly ash after exposure to elevated temperatures’, *Cem. Concr. Res.*, 37, 1583–1589.
- Kong, D L Y, Sanjayan, J G, and Sagoe-Crentsil, K (2008), ‘Factors affecting the performance of metakaolin geopolymers exposed to elevated temperatures’, *J. Mater. Sci.*, 43, 824–831.
- Krishnamurthy, N, Grutzeck, M W, and Kwan, S (2001), ‘Hydroceramics for Savannah River Laboratory Sodium-Bearing Waste’, in Spearing D R, Smith, G L, and Putnam, R L (eds.), *Environmental Issues and Waste Management Technologies in the Ceramic and Nuclear Industries VI*, American Ceramic Society, Westerville, OH, USA, 337–344.
- Langton, C A, Singh, D, Wagh, A S, Tlustochowicz, and Dwyer, K (2000), ‘Phosphate Ceramic Solidification and Stabilization of Cesium-containing Crystalline Silicotitanate Resins’, in Chandler, G T and Feng, X (eds.), *Environmental Issues and Waste Management Technologies in the Ceramic and Nuclear Industries V*, American Ceramic Society, Westerville, OH, USA, 175–187.
- Lee, W K W, and van Deventer, J S J (2002), ‘The effect of ionic contamination on the early-age properties of alkali-activated fly ash-based cements’, *Cem. Concr. Res.*, 32, 577–584.
- Lutze, W, and Ewing, R C (1988), (eds.) *Radioactive Waste Forms for the Future*, North-Holland, Amsterdam.
- Ly, L, Vance, E R, Perera, D S, Aly, Z, and Olufson, K (2006), ‘Leaching of geopolymers in deionised water’, *Adv. in Mater. and Mater. Proc. J.*, 8, 236–247.
- Majersy, D, Sekely, S, and Breza, M (2007), ‘Verified possibilities of specific and historical waste solidification’, *IAEA RCM on Behaviour of cementitious materials in Long term storage and disposal of radioactive waste meeting*, 10–14 September, Moscow, Russia, CD ROM, IAEA, Vienna, Austria.
- Milestone, N B (2006), ‘Reactions in cement encapsulated nuclear wastes: Need for toolbox of different cement types’, *Adv. App. Ceram.*, 105, 13–20.
- Nicholson, C L, Murray, B J, Fletcher, R A, Brew, D R M, MacKenzie, K J D, and Schmucker, M (2005), ‘Novel geopolymer materials containing borate structural units’, in Davidovits, J (ed.), *Proceedings World Congress Geopolymer 2005*, Saint-Quentin, France, 31–33.
- Odler, I (2003), ‘The BET-specific surface area of hydrated Portland cement and related materials’, *Cem. Concr. Res.*, 33, 2049–2056.
- Offermann, P (1989), ‘Calculation of the Radiolytic Gas Production in Cemented Waste’, in Lutze, W and Ewing, R C (eds.), *Scientific Basis for Nuclear Waste Management XII*, Materials Research Society, Pittsburgh, PA, USA, 461–468.
- Palomo, A, and de la Fuente, J I L (2003), ‘Alkali-activated cementitious materials: Alternative matrices for the immobilisation of hazardous wastes-Part I. Stabilisation of boron’, *Cem. Concr. Res.*, 33, 281–288.
- Perera, D S, Nicholson, C L, Blackford, M G, Fletcher, R A, and Trautman, R L (2004), ‘Geopolymer Made Using New Zealand Fly Ash’, *J. Jap. Ceram. Soc.* 112(4), S108–S111.
- Perera, D S, Vance, E R, Cassidy, D J, Blackford, M G, Hanna, J V, and Trautman, R L (2005), ‘The Effect of Heat on Geopolymers made using Fly Ash and Metakaolinite’, in Singh, J P, Bansal, N P and Kriven, W M (eds.), *Advances in Ceramic Matrix Composites X*, American Ceramic Society, Westerville, OH, USA, 87–94.

- Perera, D S, Vance, E R, Aly, Z, Davis J, and Nicholson, C L (2006), 'Immobilization of Cs and Sr in Geopolymers with Si/Al Molar Ratios of ~ 2 ', in Herman, C C and Marra, S L (eds.), *Environmental Issues and Waste Management Technologies in the Ceramic and Nuclear Industries XI*, American Ceramic Society, Columbus, OH, USA, 91–96.
- Perera, D S, Vance, E R, Kiyama, S, Aly, Z, and Yee, P (2007), 'Geopolymers as Candidates for Low/Intermediate Level Highly Alkaline Waste', in Dunn, D, Poinssot, C D and Begg, B (eds.), *Scientific Basis for Nuclear Waste Management XXX*, Materials Research Society, Warrendale, PA, USA, 361–366.
- Quillin, K C, Duerden, S L, and Majumdar, A J (1994), 'Accelerated Ageing of Blended OPC Cements', in Barkatt, A and Van Konynenburg, R A (eds.), *Scientific Basis for Nuclear Waste Management XVII*, Materials Research Society, Pittsburgh, PA, USA, 341–348.
- Rouquerol, F, Rouquerol, J, and Sing, K (1999), *Adsorption by Powders and Porous Solids: Principles, Methodology and Applications*, Academic Press, San Diego, CA, USA, p. 8.
- Rowles, M R, and O'Connor, B H (2003), 'Chemical optimisation of the compressive strength of aluminosilicate geopolymers synthesised by sodium silicate activation of metakaolinite', *J. Mater. Chem.*, 13, 1161–1165.
- Shi, C, Krivenko, P V, and Roy, D M (2006), *Alkali-Activated Cements and Concretes*, Taylor and Francis, London and New York, pp. 313–319.
- Siemer, D D, Olanrewaju, J, Scheetz, B, Krishnamurthy, N, and Grutzeck, M W (2001a), 'Development of Hydroceramic Waste Forms', in Spearing, D R, Smith, G L and Putnam, R L, (eds.), *Environmental Issues and Waste Management Technologies in the Ceramic and Nuclear Industries VI*, American Ceramic Society, Westerville, OH, USA, 383–390.
- Siemer, D D, Olanrewaju, J, Scheetz, B, Krishnamurthy, N, and Grutzeck, M W (2001b), 'Development of Hydroceramic Waste Forms for INEEL Calcined Waste', in Spearing, D R, Smith, G L and Putnam, R L, (eds.), *Environmental Issues and Waste Management Technologies in the Ceramic and Nuclear Industries VI*, American Ceramic Society, Westerville, OH, USA, 391–398.
- Singh, D, Wagh, A S, Cunnane, J, Sutaria, M, Kurokawa, S, and Mayberry, J (1994), 'Phosphate-Bonded Ceramics as Candidate Final Waste Form Materials', in Bickford, D, Bates, S, Jain, V and Smith, G (eds.), *Environmental and Waste Management Issues in the Ceramic Industry II*, American Ceramic Society, Westerville, OH, USA, 165–174.
- Sneyers, A, and Van Iseghem, P (1998), 'The Leaching Behaviour of Bituminized Radioactive Waste in the Geologic Disposal Conditions of the Boom Clay Formation', in McKinley, I G and McCombie, C (eds.), *Scientific Basis for Nuclear Waste Management XXI*, Materials Research Society, Warrendale, PA, USA, 565–572.
- Taylor, H F W (1997), *Cement Chemistry*, 2nd edition, Thomas Telford, London, UK.
- USDOE (1982), *The Evaluation and Selection of Candidate High-level Waste Forms*, US Dept of Energy Report DOE/TIC 11611.
- Valcke, E, Sneyers, A, and Van Iseghem, P (2001), 'The Effect of Radiolytic Degradation Products of Eurobitum on the Solubility and Sorption of Pu and Am in Boom Clay, in Hart, K P and Lumpkin, G R (eds.), *Scientific Basis for Nuclear Waste Management XXIV*, Materials Research Society, Warrendale, PA, USA, pp. 141–149.
- van Jaarsveld, J G S, van Deventer, J S J, and Lukey, G C (2003), 'The characterisation of source materials in fly ash-based geopolymers', *Mater. Lett.*, 57, 1272–1280.

- Vance, E R, Perera, D S, Aly, Z, Walls, P A, Zhang, Y, Cassidy, D J, and Griffith, C S, (2007), 'Immobilisation of Cations and Anions in Geopolymers', Materials Science and Technology 2007 Conference and Exhibition, Sept 16–20, Detroit, MI, USA.
- Walls, P A, and Kurlapski, I, private communication.
- Walker, B W, Langton, C A, and Singh, D (2000), 'Phosphate bonded Solidification of Radioactive Incinerator Wastes', in Chandler, G T and Feng, X (eds.), *Environmental Issues and Waste Management Technologies in the Ceramic and Nuclear Industries V*, American Ceramic Society, Westerville, OH, USA, 169–174.

Immobilisation of toxic wastes in geopolymers

J L PROVIS, University of Melbourne, Australia

Abstract: This chapter addresses the utilisation of geopolymers in the immobilisation of a variety of different hazardous wastes. Several elements have been investigated in detail in terms of immobilisation in geopolymers, in particular Pb and Cr as wastes from the mining industry, and Cs and Sr in radioactive wastes. There are varying degrees of effectiveness observed for different elements; geopolymer chemistry appears to provide an ideal matrix for the immobilisation of low-charged cationic species, but transition metals with the ability to take on very high oxidation states tend to be problematic. Many metallic elements appear to be trapped in the geopolymer binder in the form of precipitated hydroxides; this can give very good leach resistance in near-neutral or alkaline environments but is less desirable under acidic conditions. It is important to tailor binder chemistry to match the critical species to be immobilised; some species are much more effectively treated by immobilisation in Portland cement or alkali activated slags than in geopolymers, while in other cases the opposite is true. Waste immobilisation, in geopolymers or any other class of materials, is a highly complex area requiring detailed scientific study if acceptable and predictable results are to be obtained.

Key words: geopolymer, aluminosilicate, fly ash, hazardous waste.

19.1 Introduction

Geopolymer technology has long been recognised to provide the potential for immobilisation of hazardous wastes (Comrie *et al.*, 1988) – most commonly for species falling into the vaguely defined category of ‘heavy metals,’ but also for a wide variety of other elements, ions and compounds. Immobilisation behaviour also has the potential to provide useful information about the intrinsic chemistry of the geopolymer binder, as it can depend critically on one or more of a number of factors which are often hard to measure independently.

Cement-based matrices are a well-established solution for the immobilisation of many potentially hazardous species, and their effectiveness in treating many different classes of wastes has been established over several decades (Glasser 1997, Conner and Hoeffner 1998, Malviya and Chaudhary 2006). The legislative requirements for material performance in an immobilisation scenario have in many cases been developed with respect to cement-based grouts, where a small amount of cement is added to a large volume of waste,

resulting in the formation of a contiguous but low-strength material with sufficient resistance to leaching of immobilised components. This process is also referred to as ‘solidification/stabilisation’, and alternative binders have been relatively widely sought to reduce the environmental and cost impact of using Portland cement (prepared from virgin materials) to treat wastes. The use of both ash- and slag-based alkali-activated binders in waste immobilisation was reviewed by Shi and Fernández-Jiménez (2006). The focus of this chapter will be on low-Ca systems (i.e., ash and/or metakaolin-based geopolymers); the reader is referred to that review for details of higher-Ca systems.

It is also important to note a distinction between leaching of immobilised species due to matrix degradation, and their release from a relatively intact matrix. In this chapter, the majority of the data presented represent the latter scenario, as the leaching conditions used in most tests will not be sufficiently harsh to cause severe degradation of the aluminosilicate geopolymer binder. The rate of degradation of the geopolymer binder will also depend to a significant extent on its formulation, with parameters such as water content and calcium content controlling both the porosity and chemical durability of the binder. Such issues were discussed in detail in Chapters 8 and 9, and so will not be the primary focus of this chapter.

This chapter will address the treatment of a number of different elements by immobilisation in geopolymers. The classification of potentially hazardous species into ‘heavy metals’ and ‘other’ is widespread both in immobilisation science and in toxicology; however, there is no consensus on what exactly constitutes a ‘heavy metal’ (Duffus, 2002). The classification here will therefore be presented in terms of the periodic table, with main-group elements and transition metals treated distinctly from each other, following more closely the observed trends in their behaviour when immobilised in geopolymers (van Deventer *et al.*, 2007). This chapter will not present an exhaustive listing of all research studies published for each hazardous element, particularly the more widely studied species, but rather will give an overview of the observed and/or expected performance of geopolymers in a range of immobilisation scenarios. Figure 19.1 shows the periodic table, with elements classified according to the success of published studies showing their treatment by geopolymerisation. The elements classified as ‘have been bound’ include framework-forming species, as well as elements such as N, S and Cl which are usually present as counter-ions to the species of primary interest in immobilisation studies. To be classified as ‘bound,’ an element needs to have had its availability to the environment markedly reduced by geopolymerisation; it is clear that this is far from universally observed, particularly for transition metals, and the reasons for this will be discussed throughout this chapter.

H																	He
Li	Be											B	C	N	O	F	Ne
Na	Mg											Al	Si	P	S	Cl	Ar
K	Ca	Sc	Ti	V	Cr	Mn	Fe	Co	Ni	Cu	Zn	Ga	Ge	As	Se	Br	Kr
Rb	Sr	Y	Zr	Nb	Mo	Tc	Ru	Rh	Pd	Ag	Cd	In	Sn	Sb	Te	I	Xe
Cs	Ba	*	Hf	Ta	W	Re	Os	Ir	Pt	Au	Hg	Tl	Pb	Bi	Po	At	Rn
Fr	Ra	**	Rf	Db	Sg	Bh	Hs	Mt	Ds	Rg	Uub	Uut	Uuq	Uup	Uuh	Uus	Uuo
		*	La	Ce	Pr	Nd	Pm	Sm	Eu	Gd	Tb	Dy	Ho	Er	Tm	Yb	Lu
		**	Ac	Th	Pa	U	Np	Pu	Am	Cm	Bk	Cf	Es	Fm	Md	No	Lr

-  Have been bound in geopolymers
-  Bound with limited or mixed success
-  Geopolymerisation increases availability
-  Not studied

19.1 Periodic table showing a classification of the elements that have been bound into geopolymers, based on a survey of the available literature.

19.2 Main group elements

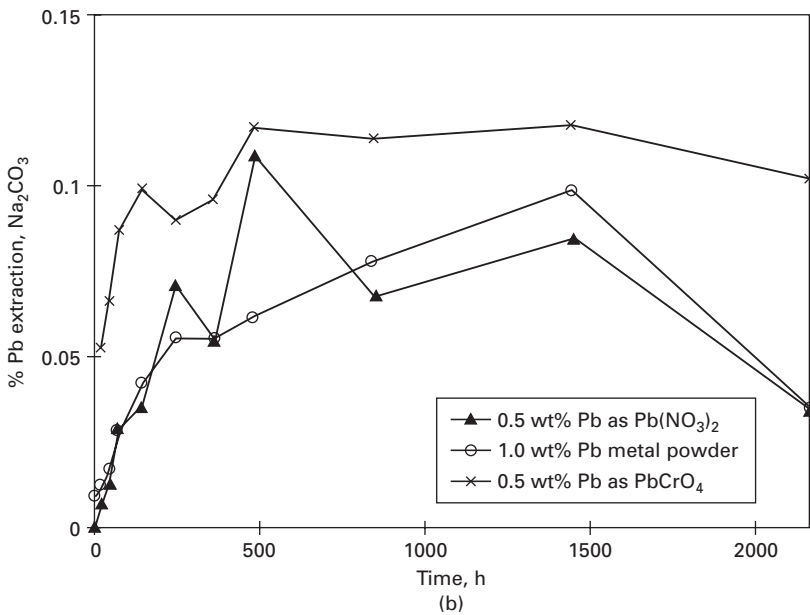
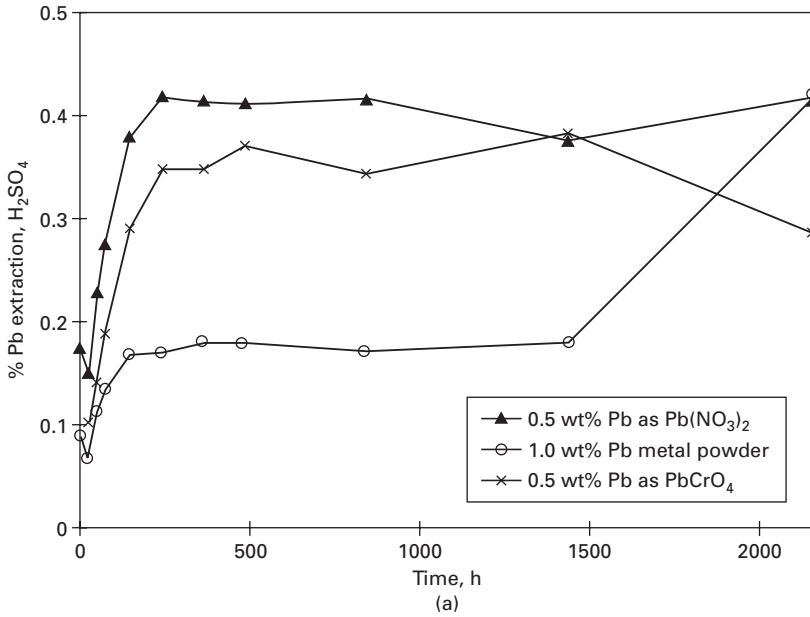
19.2.1 Lead

Lead is probably the element that has been most widely studied as a hazardous waste component for immobilisation in geopolymers. That being the case, the majority of studies have simply reported that it is effectively immobilised, rather than attempting to provide a detailed explanation for the mechanisms involved. However, there are some studies that have provided useful mechanistic information. The early work of van Jaarsveld and co-workers (van Jaarsveld *et al.*, 1997, 1998, van Jaarsveld and van Deventer 1999) showed that lead is likely to be chemically bound within the geopolymer matrix, although its specific chemical form could not be distinguished. Lead was observed to modify the pore structure formed during geopolymerisation, which, combined with its large ionic radius, led to effective immobilisation. Release of lead during batch leaching tests was found to be controlled at least partially by pore diffusion.

Palomo and Palacios (Palomo and Palacios, 2003, Palacios and Palomo, 2004) attributed the effective immobilisation of lead in hydroxide-activated fly ash geopolymers to the formation of insoluble Pb_3SiO_5 , and found that the use of a more reactive fly ash provided more effective immobilisation. The identification of Pb_3SiO_5 was tentatively supported by the results of Zhang *et al.* (2008b), although in both studies this identification was made on the basis of a single XRD peak and cannot be considered absolutely conclusive. Zhang *et al.* (2008b) also investigated the effect of the addition of Pb to a silicate-activated fly ash geopolymer in different chemical forms, as shown in Fig. 19.2.

The data shown in Fig. 19.2 indicate that the immobilisation of Pb in a geopolymer matrix is in fact attributable to chemical entrapment of Pb^{2+} in the matrix, as opposed to simple physical effects. If the lead were only physically bound, addition as sparingly soluble PbCrO_4 would be expected to give better results than where the lead is supplied as the soluble nitrate salt. The fact that there is not a significant difference between these two forms of lead in H_2SO_4 leaching, and that the nitrate salt actually outperforms the chromate in Na_2CO_3 leaching, shows that there must be chemical binding of some sort taking place.

Further indication that the binding of Pb into geopolymeric matrices is probably due to the formation of a lead silicate phase, rather than depending on sorption or physical entrapment in the geopolymeric binder, is provided by the data of Phair *et al.* (2004). These authors investigated binding of lead into fly ash geopolymers activated with different mixtures of sodium hydroxide and silicate solutions, and found that NaOH activation gave the lowest TCLP-leached lead levels, but the highest leachability of Si and Al from the geopolymeric binder. Looking at the stoichiometry of the proposed



19.2 Extraction from silicate-activated fly ash geopolymers of Pb added in different forms, under static leach conditions in (a) H₂SO₄, initially at pH 1, and (b) 5wt% Na₂CO₃ solution. Data from Zhang *et al.* (2008b).

lead silicate phase, Pb_3SiO_5 , it is apparent that high levels of dissolved silicate would not necessarily be beneficial for its formation, while silicate-activated geopolymers are well known to provide a more durable gel structure. No new crystalline phases were observed when 1 wt% Pb was added in nitrate form to a metakaolin-based geopolymer (Perera *et al.*, 2005). However, any Pb-containing phases would most likely be present in concentrations below the detection limit of laboratory XRD. Detailed atomic scale analysis will be required to conclusively determine the disposition of lead within geopolymeric binders. Techniques such as X-ray absorption spectroscopy (EXAFS and/or XANES) and ^{207}Pb NMR may be of value here, but such studies have not yet been published and necessitate relatively complex experimental procedures; the accurate use of ^{207}Pb NMR spectroscopy in particular faces several non-trivial obstacles (Dybowski and Neue, 2002).

19.2.2 Arsenic

Arsenic is a particularly important element in large-scale waste immobilisation, as it is highly toxic, soluble, and commonly part of waste streams from industries including mining and metallurgy, semiconductor manufacture, pest control, wood treatment, and paint production. Arsenic in various forms is able to be relatively successfully immobilised in Portland cement-based matrices, with the formation of sparingly soluble calcium-containing compounds (Dutre and Vandecasteele, 1998, Leist *et al.*, 2003). Its incorporation into geopolymers has been studied most widely when supplied in multicomponent mixed wastes – including mining wastes (Comrie *et al.*, 1988), paint sludges (Comrie *et al.*, 1988), wastewater treatment sludges (Hermann *et al.*, 1999), brown coal fly ash (Bankowski *et al.*, 2004a) and black coal fly ash (Álvarez-Ayuso *et al.*, 2008). In most of these studies immobilisation was reported to be relatively effective, although Álvarez-Ayuso *et al.* (2008) reported that geopolymerisation in fact mobilised more arsenic than was available from the untreated fly ash, which is of concern.

Fernández-Jiménez *et al.* (2004, 2005a) did conduct a study of arsenic immobilisation where the arsenic was supplied as NaAsO_2 , enabling more detailed analysis of specific chemical effects than is possible in multicomponent waste systems. Immobilisation was significantly better in a fly ash-based geopolymer than in comparable metakaolin-based materials, although neither system provided particularly effective immobilisation and both failed by some distance to reach the TCLP leach test requirements. Arsenic was observed in TEM to be associated with iron-rich regions derived from the fly ash, although similar behaviour was not observed when Fe_2O_3 particles were added directly to the mixture. This correlates well with the known behaviour of arsenic in contact with iron hydroxide surfaces (Sherman and Randall, 2003); this is a more likely fate for the added arsenic in geopolymers

rather than being directly bound into the geopolymer structure. The lack of immobilisation performance in metakaolin-based geopolymers is also in accord with this suggestion. Comrie *et al.* (1988) also noted that the presence of excess alkali can lead to solubilisation of arsenic (III) as arsenious acid or sodium arsenate, although they present conflicting theories regarding the desirability of this. It is therefore likely that 'real' wastes high in arsenic will either need pretreatment before geopolymerisation, and/or very careful geopolymer mix design, to ensure adequate performance in the long term.

It may also be that the use of blended ash/slag systems or other higher-Ca geopolymer systems may be beneficial, given that calcium appears to be beneficial to the chemistry of arsenic immobilisation, as well as in reduction of the porosity and permeability of geopolymers (Lloyd, 2008). However, given that treatment of high-arsenic wastes by solidification in Portland cements is in general relatively successful, this avenue may be preferred at the present time unless there is another component of the waste that severely interferes with cement setting.

19.2.3 Boron

Immobilisation of boron is an area of potential importance for alkali activation technology, given that borate salts are well known to retard the setting of Portland cement. While this can largely be overcome by controlling cement chemistry and forcing the boron to precipitate as specific phases, the availability of a matrix which does not suffer from these difficulties would certainly be considered beneficial. Boron is present at low levels in most water sources including sea water, but is found in very high concentrations in specific industrial and nuclear waste streams due to its use in semiconductor manufacture and as a neutron moderator. These streams need to be treated before release to the environment, as excessive levels of boron are well known to be hazardous in the biosphere. Boron is also a relatively common component of fly ashes, and there are legislated limits for the boron content of drinking water in some (but by no means all) jurisdictions in the developed world.

Palomo and López de la Fuente (2003) conducted a study of boron immobilisation in geopolymers, with boric acid concentrations simulating those observed in some waste streams from the nuclear industry. Boron was observed to be effectively immobilised in geopolymers; low-calcium geopolymers provided performance comparable to OPC with extra lime added (a standard means of reducing its retarding effects), while geopolymers with the same amount of lime added showed an improvement in performance by a factor of better than 20. The addition of lime is believed to cause precipitation of borate as calcium borate phases, and so it appears that the combination of

this mechanism with the entrapment provided by the geopolymeric binder is optimal in this situation.

However, the strong immobilisation performance of geopolymers without added calcium is also significant, as it indicates that a second mechanism of binding involving the aluminosilicate framework may be taking place. Nicholson *et al.* (2005) investigated this possibility further by the use of boron as an additive to geopolymers based on a Class C fly ash (~20 wt% calcium content) to control setting. Their ^{11}B MAS NMR data suggested that all boron present was in tetrahedral coordination, and this was interpreted to mean that it was playing a network-forming role in the geopolymer structure. However, the statement that all boron must be present in the geopolymer network simply because it is tetrahedral, particularly in the presence of significant quantities of calcium, must be called into question. There exist many polymorphs within the system $\text{CaB}_2\text{O}_4 \cdot x\text{H}_2\text{O}$, $x \leq 5$, several of which contain boron purely in tetrahedral coordination (Christ and Clark, 1977), and the presence of at least some proportion of the tetrahedral boron in such phases in the presence of calcium cannot be discounted. There may also be changes in leaching behaviour induced by the changes in geopolymer pore structure in the presence of calcium (Lloyd, 2008); it remains unclear how these effects all interact with each other to affect the leaching of boron.

19.2.4 Caesium and strontium

Caesium and strontium will be discussed together here, as they are most problematically found mixed (isotopes ^{137}Cs and ^{90}Sr) in low- to intermediate-level nuclear wastes, as fission products of ^{235}U . The behaviour of these elements in geopolymers has been widely studied, either separately, together or combined with other elements, e.g. molybdenum (Khalil and Merz, 1994). Caesium is known to be problematic in Portland cement systems, as these materials generally do not strongly bind alkali metal cations. Strontium is relatively well immobilised in Portland cements, as it is able to substitute for some of the calcium in calcium silicate hydrates. However, given that it readily forms a number of insoluble compounds, in particular SrCO_3 , it is not expected to be highly leachable even from matrices in which it is only physically encapsulated in such forms.

In general, caesium appears to be chemically bound into the geopolymer structure as a charge-balancing cation, filling the sites that would ordinarily be filled by sodium or potassium (Blackford *et al.*, 2007). Analogies with naturally occurring mineral structures have been used to provide arguments for the stability of aluminosilicate matrices for immobilisation of caesium and strontium (Krivenko *et al.*, 1994), although the long-term performance of these materials remains to be proven, as discussed in detail in the previous chapter. Pure caesium aluminosilicate geopolymers have also been synthesised and

studied (Berger *et al.*, 2007, Bell *et al.*, 2008), and appear to show a binder structure similar to the more 'traditional' sodium or potassium aluminosilicate systems.

Immobilisation of Cs and Sr has been achieved in geopolymers based on calcined clays (kaolinite and/or bentonite), where the hazardous elements were supplied as wood ash (Chervonnyi and Chervonnaya, 2003), simulated mixed waste powders (Khalil and Merz, 1994, Bao *et al.*, 2005) or reagent-grade chemicals (Perera *et al.*, 2006), as well as in fly ash-based geopolymers (Fernández-Jiménez *et al.*, 2005b, Perera *et al.*, 2006). A longstanding research programme in the United States has led to the development of 'hydroceramics' – predominantly metakaolin-based geopolymers cured at elevated temperatures of up to 200°C, with waste loadings of up to 25% in the form of nitrate-rich calcines (Olanrewaju, 2002, Bao *et al.*, 2005). These formulations are also often designed to approximate stable mineral structures, in particular members of the sodalite family (Siemer, 2002), and generally perform acceptably in leaching tests. A detailed analysis of the performance of geopolymers in nuclear applications was given in the previous chapter, and will not be repeated here.

19.2.5 Other main-group elements

The other main-group elements that have been treated by geopolymerisation fall neatly into two categories: radioactive waste products, and trace elements in coal ashes. In the former category, radium and uranium have both been treated by geopolymerisation with some success (Davidovits and Comrie 1988, Hermann *et al.*, 1999), although full validation of geopolymer technology for disposal of these elements has not been published as yet. Barium, selenium and antimony are found as trace elements in coals, and pass through the furnace during combustion to become concentrated in the fly ash by-products. Bankowski *et al.* (2004a, 2004b) did not show effective immobilisation of barium, with leachability reduced only due to dilution of their brown coal fly ash by mixing with metakaolin for geopolymerisation. They observed some immobilisation of selenium, but not with any particular effectiveness even at the lowest waste loadings tested.

Álvarez-Ayuso *et al.* (2008) did demonstrate significant immobilisation of barium from their black coal fly ash by geopolymerisation, but obtained no marked effect on the leachable selenium concentration. Their samples also showed mobilisation of antimony, with higher leachability from geopolymerised samples than from the untreated ash. More successful immobilisation of barium has been demonstrated by the use of a mixture of Portland cement and zeolitic tuffs (Iucolano *et al.*, 2005); it may be that the tailoring of the partially zeolitic character of geopolymers could be of value in this application.

19.3 Transition metals

19.3.1 Copper

Copper immobilisation in geopolymers has been relatively widely studied, most commonly in conjunction with Pb immobilisation to enable comparison of the behaviour of a small divalent transition metal cation with that of a large main-group metal cation (van Jaarsveld *et al.*, 1997, 1998, van Jaarsveld and van Deventer, 1999). Copper is generally somewhat less successfully immobilised in geopolymers than is lead, which is generally attributed to its smaller radius and therefore reduced tendency to become trapped in nanopore networks. The effectiveness of copper immobilisation varies dramatically between studies, with leaching extents as low as 0.5% (Zhang *et al.*, 2007) or as high as 90% (Hanzlíček and Steinerová-Vondráková, 2006) having been reported. The reason for this may lie in the details of the experimental procedures used, although neither study reports sufficient characterisation of the samples to make such identification with any certainty. Zhang *et al.* (2007) added the copper to a slag-metakaolin geopolymer as a nitrate salt and leached the samples in acetic acid according to a modified TCLP procedure, whereas Hanzlíček and Steinerová-Vondráková (2006) added the copper dissolved in 1M H₂SO₄ to a metakaolin geopolymer and leached the samples in water. It is possible that the concentrated acid present in the latter instance caused significant inhibition of the geopolymerisation reaction, although a similar lack of immobilisation performance was not observed in the case of either nickel or cobalt in that study. Mina íková and kvára (2006) were also less than entirely successful in immobilising copper in fly ash-based geopolymers, where the addition of copper as a hydrated sulfate led to a significant decrease in the strength of the matrix.

Wang *et al.* (2007) also used a fly ash-based geopolymer for sorption of Cu²⁺ from solution, and found that it displayed a much higher sorption capacity than either untreated fly ash or natural clinoptilolite zeolite. However, the sorption capacity reported was 92 mg Cu/g geopolymer, or 9.2 wt%, which seems very high to be attributable simply to Cu²⁺ ions sorbing on geopolymer particle surfaces, even taking into account the high BET surface area reported for the geopolymers. It may be that the copper in fact precipitated along with any excess alkali present as sparingly soluble Cu(OH)₂, which could lead to an increase in copper removal from solution in a batch test at an extent significantly above that which could be attributed to simple sorption processes. However, in either case, further testing and validation will certainly be required before geopolymeric sorbents find widespread use in copper removal from solution. It should also be noted that geopolymeric sorbents incorporating barium sulfate particles have been successfully used in the removal of radium from wastewater (Kunze *et al.*, 2002); this could provide an avenue for utilisation of geopolymeric sorbents.

19.3.2 Chromium

Chromium is a widespread environmental pollutant, produced by industries including electroplating, production of pigments, metal alloys, leather and textiles, as well as petroleum refining. Immobilisation of the waste streams from these and other industries is therefore of paramount importance. Hexavalent chromium is particularly toxic, and is also mobile in the environment. Cr(III) is both less toxic and less mobile, being relatively insoluble as $\text{Cr}(\text{OH})_3$ and also as mixed hydroxide phases containing some Ca (Omotoso *et al.*, 1996). Some substitution into calcium (alumino)silicate hydrate (C-A-S-H) phases is also believed to be possible (Glasser, 1997), but Cr(VI) addition tends to have deleterious effects on the strength development of Portland cement-based (OPC) systems. In OPC blends with higher Al content, CrO_4^{2-} substitution into the SO_4^{2-} sites of ettringite and hydrocalumite is also possible, although the solubilities of these phases are unsatisfactorily high for their use in immobilisation (Perkins and Palmer, 2001).

Alkali activation of slags has also been the subject of some attention in chromium immobilisation. Deja (2002) studied the immobilisation of Cr(VI) in alkali-activated slag binders, and showed that not only is this species quite effectively immobilised in these systems, but that it also leads to an improvement in mechanical strength development in both carbonate- and silicate-activated systems. This work also indicated that reducing conditions in the hydrated slag pastes (i.e., available S^{2-} ions) play a positive role in the immobilisation process by mechanisms such as partial reduction of Cr(VI) to Cr(III).

Most reports available in the literature detail difficulties in the use of geopolymer binders for immobilisation of Cr(VI). Bankowski *et al.* (2004b) did report a very slight Cr leachability from a brown coal fly ash, which was reduced to undetectable levels by encapsulation of the ash in a metakaolin-based geopolymer. However, the concentrations involved are too low to be able to report successful immobilisation. Palomo and Palacios (2003) studied fly ash activated by 8 M NaOH, doped with 2.6% Cr(VI) as CrO_3 . They found that the presence of this level of Cr(VI) significantly inhibited hardening during alkali activation, and the resulting product did not develop sufficient mechanical strength.

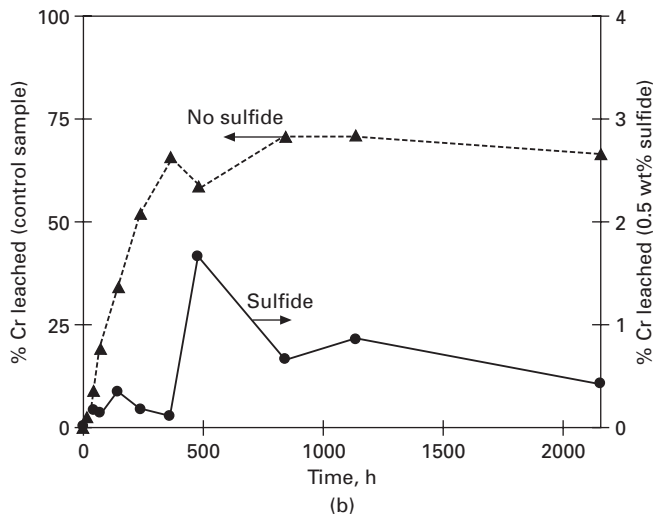
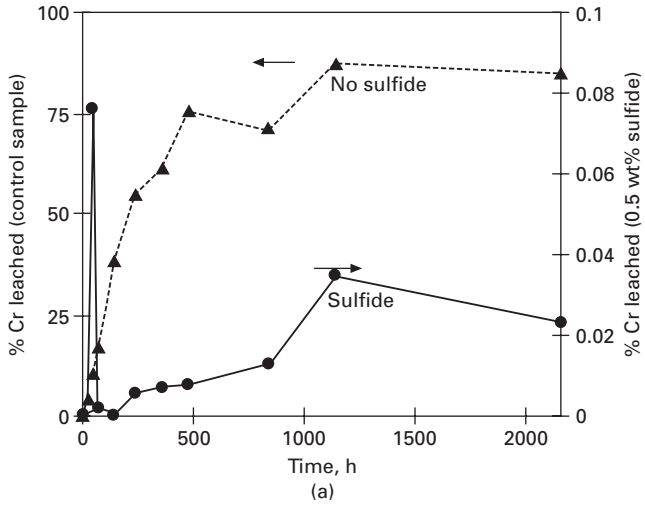
Recently, Zhang *et al.* (2008a) doped fly ash geopolymers with either 0.5% Cr(VI) as Na_2CrO_4 or 0.125% Cr(VI) as PbCrO_4 . Addition of chromium in either of these forms gave an increased compressive strength when compared with uncontaminated mortar samples. However, long-term leaching tests in different media showed that more than 75% Cr extraction was observed from Na_2CrO_4 -containing samples after 90 days in dilute H_2SO_4 , in deionised water, or in MgSO_4 or Na_2CO_3 solutions, and the Cr immobilisation performance of PbCrO_4 -containing samples was only slightly better. However, the addition of

0.5 wt% S^{2-} as Na_2S improved the immobilisation performance dramatically, as can be seen from Fig. 19.3 for leaching in deionised water. This marked decrease in chromium leach rates is also observed for leaching in salt solutions or in sulfuric acid; the acid leach is a more aggressive system and results in leaching extents on the order of 20% in the sulfide-containing system, but this is still an improvement over the 75% leaching observed in the absence of sulfide.

It is also noteworthy that supplying chromium as the highly soluble Na_2CrO_4 , and at a higher concentration, gives markedly better immobilisation in the presence of sulfide than when it is added as sparingly soluble $PbCrO_4$. This is not observed in the absence of sulfide, and provides critical information regarding the fundamental mechanisms of chromium immobilisation in geopolymers. When a soluble salt such as Na_2CrO_4 is added to a geopolymer in the absence of a reductant and the chromate is not effectively bound into the gel matrix, the Cr is readily available and leaches rapidly, so addition as $PbCrO_4$ is preferable where no sulfide is used. However, when Na_2S is added, the situation is reversed: the availability of Cr from the soluble salt means that it is more readily reduced by the S^{2-} ions and microencapsulated throughout the binder phase, possibly as insoluble $Cr(OH)_3$. If the Cr is added in sparingly soluble form, this process will not be completed prior to geopolymeric setting, and some remnant $PbCrO_4$ will then be available for leaching. This then explains the lower leach rates shown in Fig. 19.3 for the sulfide-free systems, but much higher leach rate for sulfide-containing systems, where Cr is added as $PbCrO_4$ compared to addition as Na_2CrO_4 . This has some interesting implications for the design of processes to be used in waste conditioning prior to immobilisation in geopolymeric binders; it may be that some of the steps that are commonly taken to reduce the solubility of Cr in salt form before mixing with the immobilisation matrix are in fact undesirable when the Cr is to be bound in a sulfide-containing geopolymer.

19.3.3 Zinc

The presence of zinc is well known to have deleterious effects on the setting of Portland cement, with the precipitation of calcium zincate compounds on the surfaces of cement grains severely retarding hydration (Mollah *et al.*, 1995). Zinc does also form covalent Zn-O-Si bonds (Anseau *et al.*, 2005), and so will eventually become substituted into the silicate chains of a calcium silicate hydrate gel once the system reaches the point of setting. Sodium silicate-activated slags only start to show a significant retardation at a higher level of zinc addition (Qian *et al.*, 2003), which may be attributed to the lower Ca/Si ratio of this system, as silicate complexation of zinc in the initial stages of reaction will reduce the effects of calcium zincate precipitation.



19.3 Leaching of Cr into deionised water, from samples with (a) 0.5 wt% Cr as Na₂CrO₄, and (b) 0.125 wt% Cr as PbCrO₄. Data from Zhang *et al.* (2008a).

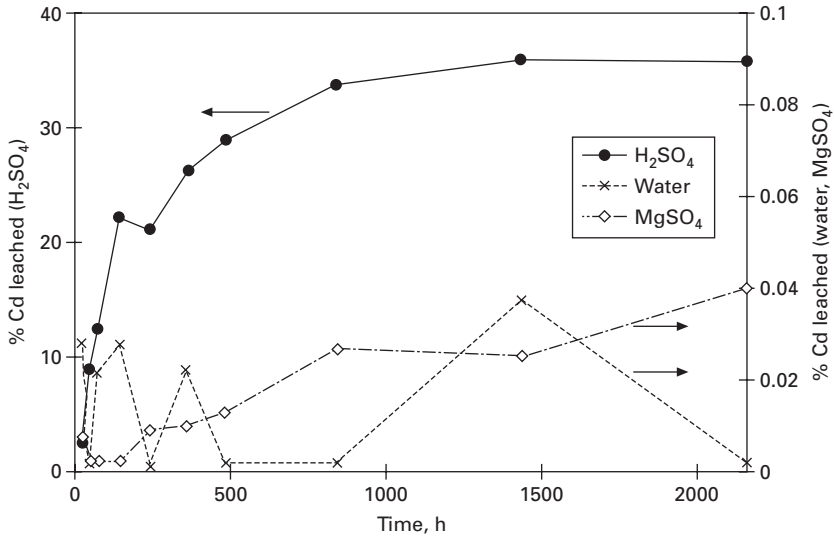
Given that calcium-zinc interactions appear detrimental in the development of an effective immobilisation matrix, it may be expected that a low-calcium geopolymer could provide desirable immobilisation properties. Few detailed studies of zinc immobilisation in geopolymers have yet been published; Minaříková and Škvára (2006) showed that the addition of ZnO to a low-Ca fly ash-based geopolymer gave around a 50% reduction in the compressive strength reached, but the relative rate of strength development was not notably

impacted, in contrast to the retardation shown in a Portland-cement based system. Immobilisation performance was good but not uniformly outstanding, and for some reason the use of potassium-based activating solutions gave a factor of 10 improvement compared to sodium-based activators. Fernández Pereira *et al.* (2009) also showed relatively good (>90%) immobilisation in geopolymerisation of a zinc-rich electric arc furnace dust.

19.3.4 Cadmium

Cadmium is another problematic transition metal, being extremely toxic and a known human carcinogen. It is commonly released to the environment as a byproduct of mining and metallurgical operations, from discarded nickel-cadmium batteries, as a contaminant in fly ash or cement kiln dust, and due to its relatively extensive use in pigments. Cadmium, being a divalent cation, is relatively successfully immobilised in Portland cement matrices, becoming substituted on calcium sites to form Ca/Cd-silicate hydrate gels (Díez *et al.*, 1997, Pomiès *et al.*, 2001). It has also been successfully treated by immobilisation in alkali silicate- or carbonate-activated slags (Deja, 2002), presumably due to similar incorporation mechanisms.

Immobilisation of cadmium in low-calcium geopolymers has not always met with a corresponding degree of success (Minaříková and Škvára, 2006, Xu *et al.*, 2006), particularly considering the very strict environmental regulations covering Cd^{2+} leachability. However, the performance of geopolymer matrices for cadmium immobilisation has also been shown to be strongly dependent on the leaching test applied (Zhang *et al.*, 2008b), as shown in Fig. 19.4. Leaching in sulfuric acid gave very poor immobilisation performance, whereas water and 5 wt% MgSO_4 solutions gave better than 99.95% immobilisation efficiency. No leaching at all was detected after 3 months' exposure to saturated Na_2CO_3 solution. These results were attributed to the solidification of cadmium as a hydroxide or related phase in the geopolymer system; it cannot form the Ca/Cd-silicate hydrate phases observed in higher-calcium systems, so the hydroxide is the most likely host phase here. The solubility of $\text{Cd}(\text{OH})_2$ will clearly be lower at elevated pH, and it appears that it is also low enough at near-neutral pH to give good immobilisation performance. However, upon exposure to a strong and/or concentrated acid, this phase is solubilised and the cadmium is released. In the context of real-world immobilisation, it is therefore recommended that treatment in a higher-calcium binder system is likely to be more beneficial than the use of geopolymers. While leaching performance is good as long as the samples remain alkaline, the chance of catastrophic immobilisation failure with a decrease in pH is not one that should be taken lightly if cadmium concentrations in the waste stream are high.



19.4 Leaching of Cd²⁺ from fly ash-based geopolymer matrices exposed to H₂SO₄ (initial pH = 1.0), deionised water and 5 wt% MgSO₄ solutions in batch leaching tests. Leaching in saturated Na₂CO₃ solution in a corresponding test showed no measurable Cd release. 0.5 wt% Cd was added as Cd(NO₃)₂; data from Zhang *et al.* (2008b).

19.3.5 Other transition metals

To briefly mention a few other studies of transition metal immobilisation: Hanzlíček and co-workers (Hanzlíček and Steinerová-Vondráková, 2006, Hanzlíček *et al.*, 2006) showed that nickel and cobalt can be relatively effectively immobilised in metakaolin-based geopolymers, and that europium (as a representative lanthanide) is sufficiently well bound to resist leaching by water but not by 1.0 M H₂SO₄. Zosin *et al.* (1998) immobilised Ru and Co along with Cs from radioactive waste streams in magnesia-iron slag based geopolymers. There have been a number of studies showing the immobilisation of different components of complex wastes, including ashes (Álvarez-Ayuso *et al.*, 2008), mining wastes (Davidovits and Comrie, 1988), and paint sludges (Comrie *et al.*, 1988). However, little detailed information regarding immobilisation mechanisms can in general be obtained from such systems, as the complex and sometimes competing effects of the different species of interest are difficult or impossible to deconvolute.

19.4 Other wastes

Geopolymers have also been used to a somewhat more limited extent in immobilisation of non-metallic wastes. Li *et al.* (2006) used fly ash-based

geopolymers as a sorbent for dyes with some success. Tavor *et al.* (2007) mixed wastewater containing phenol into the activating solution used in synthesis of geopolymers and observed a slight impact on compressive strength, although strengths exceeding 65MPa were still developed by their fly ash-based mixes. Fly ash geopolymers showed a much higher extent of immobilisation of phenol than the corresponding metakaolin-based systems, with unmeasurably low leaching at anywhere up to 1 wt% phenol in the mix. Comrie *et al.* (1988) also found good immobilisation of cyanides present in the paint sludge used in their immobilisation tests.

19.5 Conclusions

Geopolymers have been used to immobilise a wide variety of wastes. Cationic wastes are in most cases more successfully treated than those that form oxyanions or hydroxy complexes, although the addition of sulfide can aid in the immobilisation of chromium by reducing it from mobile Cr(VI) to the less soluble Cr(III). Not all wastes are as readily treated by geopolymerisation as they are by Portland cement immobilisation or alkali-activated slags, while others are treated much more effectively; it is necessary to select the most appropriate chemistry to treat each specific waste stream. Further research is required to determine the most effective geopolymer formulation for each specific waste type, as there is not expected to be a 'one size fits all' solution to the immensely complex problem of toxic waste immobilisation.

19.6 References

- Álvarez-Ayuso, E., Querol, X., Plana, F., Alastuey, A., Moreno, N., Izquierdo, M., Font, O., Moreno, T., Diez, S., Vázquez, E. and Barra, M. (2008) Environmental, physical and structural characterisation of geopolymer matrixes synthesised from coal (co-) combustion fly ashes. *Journal of Hazardous Materials*, 54, 175–183. doi:10.1016/j.jhazmat.2007.10.008.
- Anseau, M. R., Leung, J. P., Sahai, N. and Swaddle, T. W. (2005) Interaction of silicate ions with zinc(II) and aluminum(III) in alkaline aqueous solution. *Inorganic Chemistry*, 44, 8023–8032. doi:10.1021/ic050594c.
- Bankowski, P., Zou, L. and Hodges, R. (2004a) Using inorganic polymer to reduce leach rates of metals from brown coal fly ash. *Minerals Engineering*, 17, 159–166. doi:10.1016/j.mineng.2003.10.024.
- Bankowski, P., Zou, L. and Hodges, R. (2004b) Reduction of metal leaching in brown coal fly ash using geopolymers. *Journal of Hazardous Materials*, B114, 59–67. doi:10.1016/j.jhazmat.2004.06.034.
- Bao, Y., Grutzeck, M. W. and Jantzen, C. M. (2005) Preparation and properties of hydroceramic waste forms made with simulated Hanford low-activity waste. *Journal of the American Ceramic Society*, 88, 3287–3302. doi:10.1111/j.1551-2916.2005.00775.x.
- Bell, J. L., Sarin, P., Provis, J. L., Haggerty, R. P., Driemeyer, P. E., Chupas, P. J., van

- Deventer, J. S. J. and Kriven, W. M. (2008) 'Atomic structure of a cesium aluminosilicate geopolymer: A pair distribution function study,' *Chemistry of Materials*, 20(14), 4768–4776. doi:10.1021/cm703369s.
- Berger, S., Frizon, F., Fournel, V. and Cau-Dit-Comes, C. (2007) Immobilization of cesium in geopolymeric matrix: A formulation study. *12th International Congress on the Chemistry of Cement*, Montreal, Canada, Beaudoin, J. J. (Ed.).
- Blackford, M. G., Hanna, J. V., Pike, K. J., Vance, E. R. and Perera, D. S. (2007) Transmission electron microscopy and nuclear magnetic resonance studies of geopolymers for radioactive waste immobilization. *Journal of the American Ceramic Society*, 90, 1193–1199. doi:10.1111/j.1551-2916.2007.01532.x.
- Chervonnyi, A. D. and Chervonnaya, N. A. (2003) Geopolymeric agent for immobilization of radioactive ashes after biomass burning. *Radiochemistry*, 45, 182–188.
- Christ, C. L. and Clark, J. R. (1977) A crystal-chemical classification of borate structures with emphasis on hydrated borates. *Physics and Chemistry of Minerals*, 2, 59–87. doi:10.1007/BF00307525.
- Comrie, D. C., Paterson, J. H. and Ritcey, D. J. (1988) Geopolymer technologies in toxic waste management. *Proceedings of Geopolymer '88 – First European Conference on Soft Mineralogy*, Compeigne, France, Davidovits, J. and Orlinski, J. (Eds.), 107–123.
- Conner, J. R. and Hoeffner, S. L. (1998) A critical review of stabilization/solidification technology. *Critical Reviews in Environmental Science and Technology*, 28, 397–462. doi:10.1080/10643389891254250.
- Davidovits, J. and Comrie, D. C. (1988) Long term durability of hazardous toxic and nuclear waste disposals. *Proceedings of Geopolymer '88 – First European Conference on Soft Mineralogy*, Compeigne, France, Davidovits, J. and Orlinski, J. (Eds.), 125–134.
- Deja, J. (2002) Immobilization of Cr^{6+} , Cd^{2+} , Zn^{2+} and Pb^{2+} in alkali-activated slag binders. *Cement and Concrete Research*, 32, 1971–1979. doi:10.1016/S0008-8846(02)00904-3.
- Díez, J. M., Madrid, J. and Macías, A. (1997) Characterization of cement-stabilized Cd wastes. *Cement and Concrete Research*, 27, 337–343. doi:10.1016/S0008-8846(97)00017-3.
- Duffus, J. H. (2002) 'Heavy metals' - A meaningless term? *Pure and Applied Chemistry*, 74, 793–807. doi:10.1351/pac200274050793.
- Dutre, V. and Vandecasteele, C. (1998) Immobilization mechanism of arsenic in waste solidified using cement and lime. *Environmental Science and Technology*, 32, 2782–2787. doi:10.1021/es971090j.
- Dybowski, C. and Neue, G. (2002) Solid state ^{207}Pb NMR spectroscopy. *Progress in Nuclear Magnetic Resonance Spectroscopy*, 41, 153–170. doi:10.1016/S0079-6565(02)00005-5.
- Fernández-Jiménez, A., Palomo, A., Macphee, D. E. and Lachowski, E. E. (2005a) Fixing arsenic in alkali-activated cementitious matrices. *Journal of the American Ceramic Society*, 88, 1122–1126. doi:10.1111/j.1551-2916.2005.00224.x.
- Fernández-Jiménez, A., Macphee, D. E., Lachowski, E. E. and Palomo, A. (2005b) Immobilization of cesium in alkaline activated fly ash matrix. *Journal of Nuclear Materials*, 346, 185–193. doi:10.1016/j.jnucmat.2005.06.006.
- Fernández-Jiménez, A. M., Lachowski, E. E., Palomo, A. and Macphee, D. E. (2004) Microstructural characterisation of alkali-activated PFA matrices for waste immobilisation. *Cement and Concrete Composites*, 26, 1001–1006. doi:10.1016/j.cemconcomp.2004.02.034.
- Fernández Pereira, C., Luna, Y., Querol, X., Antenucci, D. and Vale, J. (2009) Waste

- stabilization/solidification of an electric arc furnace dust using fly ash-based geopolymers. *Fuel*, 88, 1185–1193. doi:10.1016/j.fuel.2008.01.021.
- Glasser, F. P. (1997) Fundamental aspects of cement solidification and stabilisation. *Journal of Hazardous Materials*, 52, 151–170. doi:10.1016/S0304-3894(96)01805-5.
- Hanzlíček, T. and Steinerová-Vondráková, M. (2006) Immobilization of toxic metals in solidified systems of siloxo-sial networks. *Journal of the American Ceramic Society*, 89, 968–970. doi:10.1111/j.1551-2916.2005.00822.x.
- Hanzlíček, T., Steinerova, M. and Straka, P. (2006) Radioactive metal isotopes stabilized in a geopolymer matrix: Determination of a leaching extract by a radiotracer method. *Journal of the American Ceramic Society*, 89, 3541–3543. doi:10.1111/j.1551-2916.2006.01024.x.
- Hermann, E., Kunze, C., Gatzweiler, R., Kießig, G. and Davidovits, J. (1999) Solidification of various radioactive residues by Géopolymère® with special emphasis on long-term stability. *Proceedings of Géopolymère '99 – Second International Conference*, Saint-Quentin, France, Davidovits, J., Davidovits, R. and James, C. (Eds.), 211–228.
- Iucolano, F., Caputo, D. and Colella, C. (2005) Permanent and safe storage of Ba²⁺ in hardened phillipsite-rich tuff/cement pastes. *Applied Clay Science*, 28, 167–173. doi:10.1016/j.clay.2004.01.011.
- Khalil, M. Y. and Merz, E. (1994) Immobilization of intermediate-level wastes in geopolymers. *Journal of Nuclear Materials*, 211, 141–148. doi:10.1016/0022-3115(94)90364-6.
- Krivenko, P. V., Skurchinskaya, J. V., Lavrinenko, L. V., Starkov, O. V. and Konovalov, E. E. (1994) Physico-chemical bases of radioactive wastes – Immobilisation in a mineral-like solidified stone. *Proceedings of the First International Conference on Alkaline Cements and Concretes*, Kiev, Ukraine, Krivenko, P. V. (Ed.), 1095–1106.
- Kunze, C., Hermann, E., Griebel, I., Kießig, G., Dullies, F. and Schreiter, M. (2002) Entwicklung und Praxiseinsatz eines hocheffizienten selektiven Sorbens für Radium. *Wasser-Abwasser*, 143, 572–577.
- Leist, M., Casey, R. J. and Caridi, D. (2003) The fixation and leaching of cement stabilized arsenic. *Waste Management*, 23, 353–359. doi:10.1016/S0956-053X(02)00116-2.
- Li, L., Wang, S. and Zhu, Z. (2006) Geopolymeric adsorbents from fly ash for dye removal from aqueous solution. *Journal of Colloid and Interface Science*, 300, 52–59. doi:10.1016/j.jcis.2006.03.062.
- Lloyd, R. R. (2008) PhD Thesis, Department of Chemical and Biomolecular Engineering, University of Melbourne, Australia.
- Malviya, R. and Chaudhary, R. (2006) Factors affecting hazardous waste solidification/stabilization: A review. *Journal of Hazardous Materials*, B137, 267–276. doi:10.1016/j.jhazmat.2006.01.065.
- Minaříková, M. and Škvára, F. (2006) Fixation of heavy metals in geopolymeric materials based on brown coal fly ash. *Ceramics-Silikaty*, 50, 200–207.
- Mollah, M. Y. A., Vempati, R. K., Lin, T. C. and Cocke, D. L. (1995) The interfacial chemistry of solidification/stabilization of metals in cement and pozzolanic material systems. *Waste Management*, 15, 137–148. doi:10.1016/0956-053X(95)00013-P.
- Nicholson, C. L., Murray, B. J., Fletcher, R. A., Brew, D. R. M., Mackenzie, K. J. D. and Schmücker, M. (2005) Novel geopolymer materials containing borate structural units. *World Congress Geopolymer 2005*, Saint-Quentin, France, Davidovits, J. (Ed.), 31–33.
- Olanrewaju, J. (2002) PhD Thesis, College of Earth and Mineral Sciences, Pennsylvania State University, USA.

- Omotoso, O. E., Ivey, D. G. and Mikula, R. (1996) Quantitative X-ray diffraction analysis of chromium(III) doped tricalcium silicate pastes. *Cement and Concrete Research*, 26, 1369–1379. doi:10.1016/0008-8846(96)00118-4.
- Palacios, M. and Palomo, A. (2004) Alkali-activated fly ash matrices for lead immobilisation: A comparison of different leaching tests. *Advances in Cement Research*, 16, 137–144. doi:10.1680/adcr.16.4.137.46661.
- Palomo, A. and Palacios, M. (2003) Alkali-activated cementitious materials: Alternative matrices for the immobilisation of hazardous wastes – Part II. Stabilisation of chromium and lead. *Cement and Concrete Research*, 33, 289–295. doi:10.1016/S0008-8846(02)00964-X.
- Palomo, A. and López De La Fuente, J. I. (2003) Alkali-activated cementitious materials: Alternative matrices for the immobilisation of hazardous wastes – Part I. Stabilisation of boron. *Cement and Concrete Research*, 33, 281–288. doi:10.1016/S0008-8846(02)00963-8.
- Perera, D. S., Aly, Z., Vance, E. R. and Mizumo, M. (2005) Immobilization of Pb in a geopolymer matrix. *Journal of the American Ceramic Society*, 88, 2586–2588. doi:10.1111/j.1551-2916.2005.00438.x.
- Perera, D. S., Vance, E. R., Aly, Z., Davis, J. and Nicholson, C. L. (2006) Immobilization of Cs and Sr in geopolymers with Si/Al ~ 2. *Ceramic Transactions*, 176, 91–96.
- Perkins, R. B. and Palmer, C. D. (2001) Solubility of chromate hydrocalumite ($3\text{CaO}\cdot\text{Al}_2\text{O}_3\cdot\text{CaCrO}_4\cdot n\text{H}_2\text{O}$) 5–75°C. *Cement and Concrete Research*, 31, 983–992. doi:10.1016/S0008-8846(01)00507-5.
- Phair, J. W., Van Deventer, J. S. J. and Smith, J. D. (2004) Effect of Al source and alkali activation on Pb and Cu immobilization in fly-ash based ‘geopolymers’. *Applied Geochemistry*, 19, 423–434. doi:10.1016/S0883-2927(03)00151-3.
- Pomiès, M.-P., Lequeux, N. and Boch, P. (2001) Speciation of cadmium in cement: Part I. Cd^{2+} uptake by C-S-H. *Cement and Concrete Research*, 31, 563–569. doi:10.1016/S0008-8846(00)00480-4.
- Qian, G., Sun, D. D. and Tay, J. H. (2003) Characterization of mercury- and zinc-doped alkali-activated slag matrix: Part II. Zinc. *Cement and Concrete Research*, 33, 1257–1262. doi:10.1016/S0008-8846(03)00046-2.
- Sherman, D. M. and Randall, S. R. (2003) Surface complexation of arsenic(V) to iron(III) (hydr)oxides: structural mechanism from ab initio molecular geometries and EXAFS spectroscopy. *Geochimica et Cosmochimica Acta*, 67, 4223–4230. doi:10.1016/S0016-7037(03)00237-0.
- Shi, C. and Fernández-Jiménez, A. (2006) Stabilization/solidification of hazardous and radioactive wastes with alkali-activated cements. *Journal of Hazardous Materials*, B137, 1656–1663. doi:10.1016/j.jhazmat.2006.05.008.
- Siemer, D. D. (2002) Hydroceramics, a ‘new’ cementitious waste form material for US defense-type reprocessing waste. *Materials Research Innovations*, 6, 96–104. doi:10.1007/s10019-002-0193-3.
- Tavor, D., Wolfson, A., Shamaev, A. and Shvartzman, A. (2007) Recycling of industrial wastewater by its immobilization in geopolymer cement. *Industrial and Engineering Chemistry Research*, 46, 6801–6805. doi:10.1021/ie0616996.
- Van Deventer, J. S. J., Provis, J. L., Duxson, P. and Lukey, G. C. (2007) Reaction mechanisms in the geopolymeric conversion of inorganic waste to useful products. *Journal of Hazardous Materials*, A139, 506–513. doi:10.1016/j.jhazmat.2006.02.044.
- Van Jaarsveld, J. G. S. and Van Deventer, J. S. J. (1999) The effect of metal contaminants on the formation and properties of waste-based geopolymers. *Cement and Concrete Research*, 29, 1189–1200. doi:10.1016/S0008-8846(99)00032-0.

- Van Jaarsveld, J. G. S., Van Deventer, J. S. J. and Lorenzen, L. (1997) The potential use of geopolymeric materials to immobilise toxic metals. 1. Theory and applications. *Minerals Engineering*, 10, 659–669. doi:10.1016/S0892-6875(97)00046-0.
- Van Jaarsveld, J. G. S., Van Deventer, J. S. J. and Lorenzen, L. (1998) Factors affecting the immobilization of metals in geopolymerized flyash. *Metallurgical and Materials Transactions B – Process Metallurgy and Materials Processing Science*, 29, 283–291. doi:10.1007/s11663-998-0032-z.
- Wang, S., Lin, L. and Zhu, Z. H. (2007) Solid-state conversion of fly ash to effective adsorbents for Cu removal from wastewater. *Journal of Hazardous Materials*, 139, 254–259. doi:10.1016/j.jhazmat.2006.06.018.
- Xu, J. Z., Zhou, Y. L., Chang, Q. and Qu, H. Q. (2006) Study on the factors of affecting the immobilization of heavy metals in fly ash-based geopolymers. *Materials Letters*, 60, 820–822. doi:10.1016/j.matlet.2005.10.019.
- Zhang, J., Provis, J. L., Feng, D. and Van Deventer, J. S. J. (2008a) The role of sulfide in the immobilization of Cr(VI) in fly ash geopolymers. *Cement and Concrete Research*, 38, 681–688. doi:10.1016/j.cemconres.2008.01.006.
- Zhang, J., Provis, J. L., Feng, D., van Deventer, J. S. J. (2008b) ‘Geopolymers for immobilization of Cr⁶⁺, Cd²⁺, and Pb²⁺’, *Journal of Hazardous Materials*, 157(2-3), 587–598. doi:10.1016/j.jhazmat.2008.01.053.
- Zhang, Y., Sun, W., Chen, Q. and Chen, L. (2007) Synthesis and heavy metal immobilization behaviors of slag based geopolymer. *Journal of Hazardous Materials*, 143, 206–213. doi:10.1016/j.jhazmat.2006.09.033.
- Zosin, A. P., Priimak, T. I. and Avsaragov, K. B. (1998) Geopolymer materials based on magnesia-iron slags for normalization and storage of radioactive wastes. *Atomic Energy*, 85, 510–514. doi:10.1007/BF02358790.

- AAFA, *see* fly ash geopolymers
- abiotic resource depletion potential, 198
- ACS-ISO, 346
- activating solutions
- geopolymers, 50–66
 - alkali hydroxide solutions, 51–6
 - alkali silicate solutions, 56–62, 64
 - other activators, 64–6
- AFt-phase, 171
- ageing, accelerated, of geopolymers, 139–64
- crystallisation during ageing of gels, 141–2
 - crystallisation during synthesis of gels, 140–1
- fly ash geopolymers, 153–63
- crystallisation of zeolites faujasite and sodium P1, 156
 - effect of ageing on strength, 153–4, 156
 - effect of zeolite crystallisation on strength, 158–63
 - elemental composition of fly ashes and GGBS, 154
 - geopolymer synthesized from FA3 and GGBS, 158
 - phase changes, 156–7
 - polished section of geopolymer synthesized from FA1, 159
 - SEM examination, 157–8
- metakaolin geopolymers, 145–53
- accelerated ageing at 95°C, 146–7
 - ageing at ambient temperature, 145–6
 - effect of alkali type, 153
 - effect of temperature, 151–2
 - mechanism of strength loss during ageing, 150–1
 - phase changes, 147–8
 - SEM examination, 149–50
 - test procedure, 144
 - tests, 142–4
 - considerations, 143–4
 - need for accelerated ageing tests, 142–3
- Al MAS NMR, 129
- albite, 186, 231
- Al:Ca ratio, 364
- alkali activated materials, 379
- see also* geopolymers
- alkali aluminosilicate, 2
- alkali hydroxide solutions, 51–6
- caesium hydroxide, 55–6
 - lithium hydroxide, 53
 - potassium hydroxide, 55
 - rubidium hydroxide, 55
 - sodium hydroxide, 53–5
 - standard enthalpies of dissolution, 52
 - viscosities as a function of molality, 51
- alkali silicate solutions, 56–62, 64
- engineering properties, 62, 64
 - density of sodium silicate solutions, 65
 - potassium silicate viscosities, 63
 - sodium silicate viscosities, 63
 - solubility and phase equilibria, 56–8
 - compositional regions, 57
 - crystallisation isotherms, 56
 - speciation, 58–62
 - ²⁹Si NMR for species identification, 59
 - silicate monomer and dimer equilibrium constants, 62
- alkali-activated cement, 414
- alkali-aggregate reaction, 384
- alkaline aluminosilicate cements
- experience of application, 257–61
 - fireproof doors for elevators, 262

- glassware furnace lining fragments, 260
- heat-resistant aerated concrete structure, 260
- testing of heat-resistant adhesive, 260
- geocement composition and pre-curing conditions
 - compressive strength, 254
 - residual strength after firing at 800°C, 254
 - shrinkage after firing at 800°C, 254
- mineral transformation depending on cation type, 230
- mix proportion, phase composition and properties, 250–7
 - compressive strength and thermal shrinkage, 252
 - isoparametric diagrams of thermal shrinkage, 259
 - optimal mixes of heat resistant Na-based geocement-based composites, 257
 - solutions for shrinkage control, 253
 - thermal shrinkage vs heating temperature, 258
- Na-K geocement – OPC clinker after firing
 - temperature of crystallisation measured by DTA, 251
 - XRD patterns after firing at 800°C, 1000°C, 1300°C, 250
- phase composition after curing, 229–50
 - alkali activated cements after firing vs cation type, 249
 - chemical composition of raw materials, 233
 - fly ash-based geocements DTA patterns, 237
 - geocements with $\text{SiO}_2/\text{Al}_2\text{O}_3$ after firing at 800°C, 236
 - hydration products composition vs geocement compositions, 234
 - phase transformation at low temperatures, 231–2
 - transformation in geological process, 229–1
- phase transformation during heating, 235–50
 - alkali activated metakaolin and fly ashes after steam curing, 244
 - aluminosilicate component type and $\text{SiO}_2/\text{Al}_2\text{O}_3$ ratio, 238, 241–3
 - cation type and direction of phase transformation, 248–50
 - effect of clay mineral and type of activator, 239–40
 - geocements after firing at 800°C, 242
 - initial alkalinity ($\text{Na}_2\text{O}/\text{Al}_2\text{O}_3$ ratio), 243, 245, 248
 - pre-curing mode, 235–6, 238
 - $\text{SiO}_2/\text{Al}_2\text{O}_3$ molar ratio and initial geocements dehydration products, 241
- phases formed in alkali activated fly ash cements
 - $\text{Na}_2\text{O}\cdot\text{Al}_2\text{O}_3\cdot 3.6\text{SiO}_2\cdot x\text{H}_2\text{O}$, 247
 - $\text{Na}_2\text{O}\cdot\text{Al}_2\text{O}_3\cdot 4.0\text{SiO}_2\cdot x\text{H}_2\text{O}$, 247
 - $0.5\text{Na}_2\text{O}\cdot\text{Al}_2\text{O}_3\cdot x\text{H}_2\text{O}\cdot 4.0\text{SiO}_2\cdot x\text{H}_2\text{O}$, 247
- relative intensity of crystallisation
 - compressive strength of ‘geocement-chamotte’ composition, 256
 - density of ‘geocement-chamotte’ composition, 256
 - residual strength of ‘geocement-chamotte’ composition, 256
 - thermal shrinkage of ‘geocement-chamotte’ composition, 256
- transformation in geological process, 230
- XRD patterns of compositions
 - $0.5\text{Na}_2\text{O}\cdot\text{Al}_2\text{O}_3\cdot 4.0\text{SiO}_2\cdot x\text{H}_2\text{O}$, 246
 - $\text{Na}_2\text{O}\cdot\text{Al}_2\text{O}_3\cdot 3.6\text{SiO}_2\cdot x\text{H}_2\text{O}$, 245
 - $\text{Na}_2\text{O}\cdot\text{Al}_2\text{O}_3\cdot 4.0\text{SiO}_2\cdot x\text{H}_2\text{O}$, 246
- alkali-silica reaction, 384
- Al–O bonds, 371
- alumina, 412
- aluminium, 42–3, 101–7
- ‘Aluminium of Greece,’ 346
- aluminium oxide, 213
- aluminosilicate, 2, 81, 122
 - dehydroxylation of 1:1 layer-lattice halloysite dehydroxylation, 298
 - kaolinite dehydroxylation, 296
 - dehydroxylation of 2:1 layer-lattice pyrophyllite dehydroxylation, 299
- geopolymers, other formation methods, 308–11
 - soft chemical synthesis, 310–11
 - solid-state synthesis, 309
- octahedral Al–O and tetrahedral Si–O sheets

- 1:1 layer lattice, 297
- 2:1 layer lattice, 297
- powder pattern of dehydroxylated halloysite, 298
- aluminosilicate calcium hydrates, 380
- aluminosilicate glass, 22
 - major oxide composition, 25
 - phase diagram, 23
 - XRD patterns before and after thermal treatment, 27
 - XRD patterns of Australian coal fly ashes, 28
- American Concrete Institute Committee 217, 225, 363
- analcime, 96, 142, 186, 231, 232, 252
- anorthite, 345
- anorthoclase, 231
- ANS 16.1 test, 410, 412–13
- antimony, 429
- argon, 324
- Argonne National Laboratory, 414
- arsenic, 426–7
- arsenious acid, 427
- AS1530 4, 328
- ASTM C150, 385
- ASTM C595, 385
- ASTM C684, 143
- ASTM C1157, 385
- ASTM C1260-94, 180, 181
- ASTM E119, 328
- Attenuated Total Reflectance-Fourier Transform Infrared Spectroscopy, 120
- Australian Standard AS3600, 217, 219, 222
- Australian Standard AS3972, 387–9
- Aznalcollar mine, 267
- back-reaction, 408
- barium, 429
- barium hydroxide, 412
- bentonite, 429
- Bingham visco-plastic fluid model, 127
- bitumen, 414
- bitumenisation, 405
- black coal fly ash, 426
- blast furnace slag, *see* ground granulated blast furnace slag
- boron, 427–8
- borosilicate glass, 409, 411
- Bragg diffraction condition, 334
- brown coal fly ash, 426
- Brunauer-Emmett Teller, 404
- BS 1881, 143
- cadmium, 434
- caesium, 428–9
- caesium aluminosilicate, 78–9, 428
- caesium hydroxide, 55–6
- calcined kaolinite clay, *see* metakaolin
- calcium, 84, 125
- calcium aluminate cement, 139, 144, 333
- calcium (alumino) silicate hydrate, 431
- calcium ferronickel slags, 369, 371
- calcium fluoride, 412
- calcium hydroxide, 333, 338
- calcium oxide, 212, 345
- calcium silicate hydrates, 143, 335, 338, 361, 364, 370, 413, 428
 - gel, 167, 352
- calcium silicates, 81, 228
 - hydrated, 90
- calcium zincate, 432
- calorimetry, 125–6
- capillary water absorption coefficients, 280
- carbon cap-and-trade system, 394
- cementation, 405
- cementitious gels, 89–92
 - C-S-H gel structural model, 90
 - proposed structural model for N-A-S-H gel, 91
- cenospheres, 20
- Certified Emission Reductions, 397
- chabazite, 142, 231, 232, 309
- chabazite-Na, 96, 109
- chamotte, 186, 261
- chemical durability, of geopolymers, 167–90
 - acid attack, 172–6
 - changes in mineralogy of mortars, 176
 - compressive strength of Portland cement and alkali activated fly ash, 173
 - mechanical strength of AAFA and OPC mortars, 175
 - mechanism of corrosion, 172
 - alkali silica reaction, 180–1, 183
 - formation of expansive products by ASR, 181
 - zeolite transformation, 181
 - frost attack, 189–90
 - general aspects, 167–8
 - high temperature and fire resistance, 183–9

- resistance to corrosion of steel reinforcement, 176–9, 180
- sulphate attack and sea water attack resistance, 168–71
- chert, 384
- chromite, 345
- chromium, 431–2
- class C ash, 40–1
- class F ash, 18, 39–40
- clays
 - calcined, 429
 - conventional and alternative methods of pre-treatment, 294–312
 - reproduction of thermal dehydroxylation effects
 - chemical pre-treatment, 306–8
 - mechanochemical processing, 304–6
 - planetary ball mill and vibratory mill, 304
 - reproduction of thermal dehydroxylation effects, 302, 304–6
- Clean Development Mechanism project, 395, 397
- Climate Change Levy, 395
- clinoptilolite, 142
- CML method, 198
- coal, 16
- coal fly ash
 - chemistry, and inorganic polymer cements, 15–33
 - aluminosilicate glass chemistry, 22
 - glass behaviour in IPC formation, 29–32
 - glass chemistry, 24–6
 - major minerals in Australian bituminous coals, 19
 - origin and history, 16–19
 - particle morphology, 19–22
- coal fly ash glass
 - chemistry, 24–6
 - ASG oxide composition, 25
 - XRD patterns of ASG before and after thermal treatment, 27
 - XRD patterns of Australian coal fly ashes, 28
 - in IPC formation, 29–32
 - two dimensional structure of crystalline and vitreous silica, 30
- coalification, 16
- cobalt, 435
- coefficient of variation, 285
- computed tomography, 336
- congruent dissolution, 407
- construction industry
 - addressing standards and regulations framework, 385–90
 - drivers for standards development, 386–7
 - insurance and risk assessment, 389–90
 - long-term global standards development, 388
 - material flow for cement, 386
 - prescription vs performance standards, 387–8
 - short-term regulatory barriers, 388–9
- cement market analysis, 390–1
- cement production in 2005, 391
- direct CO₂ emissions from cement production, 392
- drivers for cement demand, 390–1
- global cement demand by region and country, 392
- size of cement market, 390
- total estimated CO₂ emission of geopolymer binder, 394
- commercialisation of geopolymers, 379–400
- effect of climate change and carbon trading on opportunities, 393–8
 - carbon trading market, 397–8
 - different emission reduction instruments, 394–6
 - life cycle analysis, 393–4
 - tax, trade and permit allocation, 396–7
- opportunities for AAM, 398–9
 - carbon trading opportunities, 399
 - focus on climate change, 398
 - ‘green’ as competitive advantage in market, 398
 - overcoming regulatory obstacles, 399
- reasons for not commercialising AAM technology, 381–3
 - barriers overcome, 384
 - brief history of R&D and commercial efforts, 381–3
 - remaining barriers, 384–5
- copper, 430
- corundum, 261, 334
- creep coefficient, 222
- cristobalite, 26, 241, 242, 335, 345
- crystallisation, 24, 140

- C-S-H gel, *see* calcium silicate
 cumulative energy demand, 198
- Davidovits geopolymer synthesis, 308
 dealumination, 174, 175
 deconvolution, 77–8
 dehydroxylation, 318
 devitrification, 24
 differential scanning calorimetry, 324
 quasi-isothermal modulated, 125
 differential temperature analysis, 324
 Diffrac_{plus} Software, 347
 diffraction techniques, 127–9
 dilatometry, 316, 324
 DIN 38414 – S4, 289
 DIN EN 206-1//DIN 1045-2, 204, 205, 206
 diopside, 361, 370
 dissolution-precipitation phenomenon, 168
 dolomite, 412
 dry-curing, 216
 DTA, *see* differential temperature analysis
 dyes, 436
- Ecoinvent database, 197
 E-Crete, 388
 EDXRD, *see* energy dispersive X-ray
 diffractometry
 efflorescence, 55
 electric arc slag, 345
 energy dispersive X-ray diffractometry, 128,
 129, 132
 Engelhardt equation, 99
 Environmental scanning electron microscopy,
 130
 ettringite, 171, 223, 431
 Eurobitum, 414
 Eurocode (EN1991-1-2:2002), 328
 Eurocode (EN1991-1-2 [40]), 329, 330
 European Union Emission Trading Scheme,
 395, 397
 europium, 435
 EXAFS, 426
- faujasites, 141, 148, 156, 157, 168, 231
 fayalite, 345, 360, 361, 362
 Fe:Cr ratio, 364
 feldspars, 141, 183, 230
 feldspathoids, 185, 230
 ferrihydrite, 325, 335
 fly ash, 2, 4–5, 39–42, 345, 352
 class C ash, 40–1
 class F ash, 39–40
 pseudo-ternary composition, 40
 and glass chemistry, 41–2
 geopolymerisation, 41
 nanostructure/microstructure, 89–114
 cementitious gels, 89–92
 geopolymer microstructure, 111–14
 N-A-S-H gel, 96–9, 101–11
 polymerisation, 92–6
- fly ash geopolymers
 alkali-activated, mechanical strength, 175
 alkali-silica reaction-induced expansion,
 181
 changes in mineralogy of mortars, 176
 compressive strength evolution
 activated with NaOH and with sodium
 silicate solution, 169
 alkali activated, exposed to acid
 solutions, 173
 mortars activated with a sodium
 silicate solution, 170
 mortars activated with an 8M NaOH
 solution, 170
 diffractograms of samples tested at
 ambient and at high temperatures,
 186
 effect of accelerated ageing
 high calcium, 155
 low calcium, 155
 effect of changes in activator composition
 on ageing, 160
- FA3 paste
 activated with varying alkali content,
 161
 zeolite P content, 162
 flexural and compressive strengths, 187
 fracture surface before and after high
 temperature exposure, 337
 leaching of Cd²⁺ from matrices, 435
 low-calcium concrete, engineering
 properties, 211–25
 mechanical strength evolution, 332
 mercury intrusion porosimetry data, 338
 microanalysis of solution N-activated
 mortar subjected to accelerated
 test, 182
 SEM back-scattered electron image of
 FA1 paste, 162
 silicate-activated, extraction of Pb, 425
 strength development profiles of
 geopolymer mortars, 154

- TGA/DTA results, 325
- thermal expansion showing regional breakdown, 317
- thermal shrinkage, 322
- variation in i_{corr} vs time, 179
- variation in residual bending and compressive strength in cold samples, 185
- forsterite, 345
- Fourier Transform Infrared spectroscopy, 365–8
- freeze-thaw-resistant concrete, 204, 205
- FRITSCH pulveriser, 345
- FTIR, *see* Fourier Transform Infrared spectroscopy
- FTIR Spectrometer Model 1000, 347

- gallio germanates, 312
- gallium-germanium analogue, 309
- garnets, 228
- gehlenite, 335
- gel nuclei, 124
- general blended cement, 388
- geopolymer concrete, 212
 - compressive strength, 221
 - effect on compressive strength
 - curing time, 215
 - water-to-geopolymer solids ratio, 214
 - engineering properties, 211–25
 - heat-cured
 - acid resistance, 224
 - and ambient-cured, drying shrinkage, 223
 - change in compressive strength, 221
 - total strain and drying shrinkage strain, 222
 - indirect tensile splitting strength, 219
 - long-term properties, 219–24
 - compressive strength, 219–21
 - creep and drying shrinkage, 221–2
 - sulphate resistance, 222–4
 - sulphuric acid resistance, 224
 - mean compressive strength and unit-weight, 220
 - mixture design, production, and curing, 213–16
 - curing, 215–16
 - mixture design, 213–14
 - production, 215
 - mixture proportions, 214
 - mixture proportions tested in hydrocarbon fire, 329
 - modulus of elasticity in compression, 218
 - short-term properties, 216–19
 - behaviour in compression, 216–18
 - indirect tensile strength, 218–19
 - unit-weight, 219
 - stress-strain relation in compression, 217
- Geopolymer conferences, 2
- geopolymer kinetic phenomena, 123
- geopolymeric binders
 - calcination operations influence in mine waste reactivity, 268–71
 - compressive strength
 - according to curing time, 277
 - of alkali activated mine waste mud mortars, 271
 - relationship with modulus of elasticity, 282
 - vs $\text{H}_2\text{O}/\text{Na}_2\text{O}$ molar ratio, 276
 - vs NaOH concentration, 273–4
 - durability and environmental performance, 286–9
 - abrasion resistance, 286–7
 - abrasion resistance with Los Angeles test, 287
 - acid resistance, 287–8
 - contaminant concentration in wastewater, 289
 - environmental assessment, 288–9
 - water quality according to Portuguese Decree 236/98, 290
 - weight loss after acid attack, 288
 - future research trends, 289, 291
 - physical and mechanical properties, 276–86
 - adhesion characterisation, 283–6
 - bond strength coefficient of variation, 285
 - capillary water absorption coefficients, 280
 - modulus elasticity vs molar ratio, 282
 - setting time, 278
 - slant shear test results, 284
 - slant specimen with monolithic failure, 283
 - specimens with adhesive failure, 285
 - static modulus of elasticity, 281
 - unrestrained shrinkage, 279–80
 - water absorption, 280
 - workability, 276–8

- strength gain and mix design parameters, 271–5
 - calcium hydroxide and sodium hydroxide concentration, 271–3, 275
 - H₂O/Na₂O molar ratio, 275
 - mortar composition (C105-C116), 272
 - mortar composition (C126-C128), 278
- unrestrained shrinkage, 279
- utilisation of mining wastes in production, 267–91
- geopolymerisation, 3, 38, 43, 60, 216, 223
 - kinetics, 118–33
- geopolymers, 1–7
 - accelerated ageing, 139–64
 - crystallisation during ageing of gels, 141–2
 - crystallisation during synthesis of gels, 140–1
 - geopolymers synthesised from fly ash, 153–63
 - geopolymers synthesised from metakaolin, 145–53
 - tests, 142–4
 - activating solutions, 50–66
 - alkali hydroxide solutions, 51–6
 - alkali silicate solutions, 56–62, 64
 - other activators, 64–6
 - applications
 - fire protection, 6
 - host matrix in waste encapsulation, 6
 - low-cost ceramic, 6
 - reduced CO₂ construction material, 6
 - cement thermal expansion, 323
 - chemical durability, 167–90
 - acid attack, 172–6
 - alkali silica reaction, 180–1, 183
 - frost attack, 189–90
 - general aspects, 167–8
 - high temperature and fire resistance, 183–9
 - resistance to corrosion of steel reinforcement, 176–9, 180
 - sulphate attack and sea water attack resistance, 168–71
 - commercialisation for construction, 379–400
 - addressing standards and regulations framework, 385–90
 - alkaline activation, 380–1
 - cement market analysis, 390–1
 - effect of climate change and carbon trading on opportunities, 393–8
 - opportunities for alkali activated materials, 398–9
 - reasons for not commercialising AAM technology, 381–5
 - compressive strength
 - addition of silica sand or CaO, 352
 - fly ash/red mud addition, 353
 - glass content, 354
 - immersed in various solutions, 358
 - paste composition, 355
 - pozzolan or kaolinite addition, 351
 - pre-curing period, 356
 - subjected to high temperature heating, 359
 - vs addition of kaolinite or metakaolinite, 351
 - vs temperature and heating time, 355
 - vs temperature when kaolinite or metakaolinite is added, 350
 - conclusions, 6–7
 - durability studies, 356–59
 - engineering properties of geopolymer concrete, 211–25
 - geopolymer concrete, 212
 - long-term properties, 219–24
 - mixture design, production, and curing, 213–16
 - short-term properties, 216–19
 - factors affecting compressive strength, 347–56
 - additives, 349–53
 - alkali hydroxide/alkali silicate concentration, 347–8
 - paste composition, 353–4
 - thermal treatment, 354–6
 - fly ash
 - nanostructure/microstructure, 89–114
 - history of technology, 1–3
 - immersed in various solutions
 - conductivity vs time evolution, 358
 - Eh (mV) vs time evolution, 357
 - pH vs time evolution, 357
 - immobilisation of toxic wastes, 421–36
 - main group elements, 424–29
 - other wastes, 435–6
 - transition metals, 430–5
 - life-cycle analysis, 194–208
 - assessment, 195–8

- comparison of geopolymers to other product systems, 202–8
- geopolymers and utilisation of secondary resources, 208–9
- influence of composition on environmental impacts, 198–200
- production influence on environmental impacts, 200–2
- lithium geopolymer precursor MAS NMR spectra, 310
- low-calcium slags for strength and durability improvement, 343–71
 - backscattered image of slag-glass geopolymer, 364
 - binder element spectrum, 367
 - composition of slag-kaolinite geopolymers, 354
 - elemental mapping of slag-glass geopolymers, 365
 - experimental synthesis conditions, 360
 - FTIR spectra of slag and geopolymers T1, T2, T3 and T4, 367
 - glass grains element spectrum, 366
 - mineralogical studies, 360–69
 - prospects for industrial application, 369
 - slag grains element spectrum, 366
 - TGA curves for geopolymers T1, T2, T3 and T4, 368
- materials and methodology, 345–7
 - chemical analysis of raw material and additives, 345
 - XRD pattern of slag, 346
- metakaolin
 - nanostructure/microstructure, 72–85
- mineralogical studies, 360–69
 - FTIR, 365–68
 - SEM, 362–5
 - TGA, 368–9
 - XRD, 360–2
- Na-, Na + K, and K-activated, thermal shrinkage, 320
- non-thermally activated clays in production, 294–312
 - 1:1 layer-lattice aluminosilicate minerals dehydroxylation, 296, 298
 - 2:1 layer-lattice aluminosilicate minerals dehydroxylation, 299
 - methods of reproducing the effects of thermal dehydroxylation, 302, 304–8
 - other formation methods of aluminosilicate geopolymers, 308–11
 - reactions of thermally dehydroxylated clays with alkali, 300–2
- nuclear waste immobilisation, 401–16
 - cementitious LLW/ILW waste forms, 405–15
 - future trends, 415
 - nuclear waste around the world, 401–4
- precursor design, 37–45
 - aluminium availability, 42–3
 - designing one-part geopolymer cements, 44–5
 - fly ash, 39–42
 - future cement industry, 45
 - metallurgical slags, 38
- prepared from undehydroxylated 2:1 layer-lattice aluminosilicate
 - 11.7T ^{27}Al MAS NMR, 307
 - 11.7T ^{29}Si MAS NMR, 307
 - XRD powder pattern, 307
- producing fire- and heat-resistant, 227–63
 - alkaline cements phase composition after curing, 229–50
 - experience of application, 257–61
 - mix proportion, phase composition and properties, 250–7
- science, 4–5
- slag-based geopolymers compressive strength evolution
 - vs % w/w addition of Na_2SiO_3 , 349
 - vs alkali hydroxide concentration, 348
 - vs KOH concentration, 349
- synthesis kinetics
 - calorimetry, 125–6
 - chemical steps involved in binder formation, 119
 - diffraction techniques, 127–9
 - FTIR spectra of geopolymer development, 121
 - microscopy, 130
 - modelling, 130–2, 133
 - nuclear magnetic resonance, 129–30
 - rheology, 126–7
 - in situ* infrared spectroscopy, 119–25
 - synthesis kinetics, 118–33

- synthesised from starting materials
 - subjected to various pretreatments
 - 11.7T²⁷Al MAS NMR spectra, 303
 - XRD powder patterns, 301
- terminology, 3–4
- thermal properties, 315–39
 - fire resistance, 327–30
 - high temperature applications, 338–9
 - mechanical strength evolution, 330–3
 - microstructural changes, 335–38
 - phase changes at elevated temperatures, 333–5
 - thermal expansion, 316–23
 - thermoanalysis, 324–5
 - thermophysical properties, 326
- XRD patterns
 - geopolymers P80, P200 and P800, 362
 - geopolymers T1, T2, T3 and T4, 360
 - glass-kaolinite and glass geopolymers, 363

see also specific geopolymers
- GGBS, *see* ground granulated blast furnace slag
- glass, 345, 346
- glass chemistry, 41–2
- glass-kaolinite, 362
- global warming potential, 196
- Golden Bay Cement, 383
- granite aggregates, 323
- ground granulated blast furnace slag, 38, 154, 158
 - strength development profiles of geopolymer mortars, 154
- gunnite, 339
- GWP, *see* global warming potential
- gypsum, 171, 223
- halloysite, 305, 309
 - chemical pre-treatment, 306–8
 - acid treatment, 306–8
 - alkali treatment, 308
 - dehydroxylation, 298
 - effect of various pre-treatments, 305
 - powder pattern of dehydroxylated halloysite, 298
- Hanna EC215 conductivity meter, 347
- hazardous wastes, immobilisation by
 - geopolymers, 421–36
 - extraction from silicate-activated fly ash geopolymers of Pb, 425
 - leaching of Cd²⁺ from fly ash-based geopolymer matrices, 435
 - leaching of Cr into deionised water, 433
- main group elements, 424–29
 - arsenic, 426–7
 - boron, 427–28
 - caesium and strontium, 428–9
 - lead, 424, 426
 - other main-group elements, 429
- other wastes, 435–6
- periodic table of elements bound to
 - geopolymers, 423
- transition metals, 430–5
 - cadmium, 434
 - chromium, 431–2
 - copper, 430
 - other transition metals, 435
 - zinc, 432–4
- HDPE, *see* high-density polyethylene
- heat curing
 - effects on environmental impact indicators, 202
 - effects on environmental impact of geopolymer production, 202
- hematite, 235, 236, 325, 335, 361, 370
- herschelite, 142, 148, 231, 232
- high level waste, 401
- high-density polyethylene, 206–8
- high-energy grinding, 304–6
- HLW, *see* high level waste
- hot plate test method, 326
- hydrocalumite, 431
- hydrocarbon fire, 328–9
- hydroceramics, 80, 429
- hydroxylation, 93
- hydroxysodalite, 148, 160, 186, 231, 360, 361
- Idaho National Laboratory, 412
- illite, 362
- ILW, *see* intermediate level waste
- in situ* infrared spectroscopy, 119–25
- incongruent dissolution, 407
- 'induction period,' 121
- inorganic polymer cements
 - and fly ash chemistry, 15–33
- Instron servomechanical machine, 186
- intermediate level waste, 402
- International Atomic Energy Authority, 404, 410
- International Energy Agency, 390, 391
- inter-particle speciation, 20–1
- intra-particle speciation, 21
- IPCs, *see* inorganic polymer cements

- ISO 834, 189, 329
ISO standards 14040 ff, 195
isothermal conduction calorimetry, 125
- JEOL JSM-5400 scanning electron microscope, 347
Journal of Materials Science, 381
- kaliophilite, 319, 334
kalsilite, 183
kaolinite, 73, 296, 345, 349, 360, 362, 429
kaolinite dehydroxylate, *see* metakaolinite
KBr pellet technique, 347
K:Ca ratio, 364
kinetic model, 61
K-PSS, 172
- labradorite, 249
LARCO S.A Larymna ferronickel plant, 345
leaching, 407
lead, 424, 426
leucite, 183, 249, 319, 334
life-cycle analysis, of geopolymers, 194–209, 393
 assessment, 195–8
 database, 197
 impact assessment method, 198
 methodology, 195–7
 utilised inventories with data source and quality, 198
comparison of geopolymers to other product systems, 202–8
 geopolymer coating vs HDPE liner systems in sewage sludge pipes, 206–8
 geopolymer vs cement concrete, 203–6
comparison of mass balances and GWP results, 200
composition of geopolymer and cement concrete, 205
effects of heat curing
 environmental impact indicators, 202
 environmental impact of geopolymer production, 202
framework according to ISO Standard 14040 series, 196
geopolymers and utilisation of secondary resources, 208–9
impact categories, 197
influence on environmental impacts
 geopolymer composition, 198–200
 geopolymer production, 200–2
results
 geopolymers and cement concrete, 205
 geopolymers coating and HDPE lining, 207
steps, 195–7
 goal and scope, 196
 impact assessment, 196–7
 interpretation, 197
 inventory analysis, 196
system boundaries
 for comparison of different geopolymer composition, 199
 for comparison of geopolymer coating and HDPE lining, 207
 for comparison of geopolymer concrete and cement concrete production, 205
 for identification of relevant production processes, 201
- lime, 335
Linde A, 96
lithium hydroxide, 53
LLW, *see* low level waste
Lone Star, 382
Los Angeles abrasion apparatus, 286
low level waste, 402
low-calcium slags, for geopolymer strength and durability improvement, 343–71
Lowenstein rule, 107
low-temperature inorganic polymer glass, 126
- maghemite, 360, 361
Magic Angle Spinning Nuclear Magnetic Resonance, 428
magnesium silicates, 228
magnetite, 345, 360, 361
Master Builders, 383
Materials Data JADE 6.0 software, 268
mercury intrusion porosimetry, 336
metakaolin, 2, 4–5
 compressive strength during ageing at 23°C, 145
 compressive strength during ageing at 95°C, 146
 correlation between compressive strength and Na-P1 content, 148

- density and thermal conductivity, 326
- effect of ageing temperature and time on zeolite crystallisation, 152
- fractional elemental extractions in PCT-B tests, 409
- geopolymer structure, 72–85
 - calcium, 84
 - compressive strengths, 82
 - geopolymer formation, 75–6
 - geopolymerisation, 75–6
 - layered structure of kaolinite, 74
 - Metastar x-ray analysis, 74
 - microstructure, 81–2
 - nanostructure, 76–81
 - SEM images of microstructure of synthesized geopolymers, 83
- mechanical strength evolution, 332
- mercury intrusion porosimetry data, 338
- microstructure, 149
- restructuring of geopolymer gel, 149
- TGA-DTA curves, 324
- X-ray diffraction patterns, 147
- metakaolinite, 294, 296, 345, 349, 361
- metallurgical slags, 38
- Metastar 402, 74
- Mg-K-phosphate mixtures, 414
- microscopy, 130
- microstructure
 - fly ash, 111–14
 - alkali activation, 113
 - SEM images of original morphology, 111
 - zeolite SEM images, 112
 - metakaolin, 81–2
- mine wastes
 - calcination effects on XRD diffraction, 270
 - calcination operation influence on reactivity, 268–71
 - chemical composition and specific surface, 269
 - compressive strength according to thermal treatment, 270
 - and concrete substrate interfacial transition zone, 286
 - for geopolymeric binder production, 267–91
 - XRD patterns of mine wastes treated at different temperatures, 269
- minimum cement content, 385
- mining wastes, *see* mine wastes
- modulus of elasticity, 217–18
- montmorillonite, 299
- mordenite, 231
- MTS 1600 load frame, 346
- mullite, 20, 243, 271, 302, 334
- muscovite, 268, 299
- Na:Al:Si ratios, 412
- nanostructures
 - metakaolin, 76–81
 - nuclear magnetic resonance, 76–8
 - structural models, 79–81
 - X-ray pair distribution function analysis, 78–9
- N-A-S-H gel, *see* sodium aluminosilicate gel
- National Allocation Plans, 395
- natrolite, 362
- natural clinoptilolite zeolite, 430
- nepheline, 186, 228, 229, 231, 319, 334, 335
- nickel, 435
- nitrogen, 324
 - adsorption/desorption, 336
- NMR spectroscopy, 426
- Nordtest NT Fire 046, 328
- nuclear magnetic resonance, 76–8, 129–30, 316
 - ²⁹Si NMR spectra of geopolymers, 77
- nuclear waste
 - around the world, 401–4
 - cementitious LLW/ILW waste forms, 405–15
 - actual waste immobilisation in geopolymers, 413–14
 - alternate low-temperature products, 414–15
 - aqueous dissolution behaviour, 407–10
 - comparison with OPC, 412–13
 - conformance with regulatory tests, 410–11
 - effect of anions, 411–12
 - factors to be considered, 407
 - fire resistance, 413
 - flow sheet for disposal, 406
 - freeze-thaw behaviour, 413
 - key properties of candidate waste forms for immobilisation, 415
 - radiolytic hydrogen, 413
 - strategies for immobilisation, 405
 - supercompaction process for immobilisation, 406

- drums containing LLW stored at ANSTO, 403
- half-lives and decay modes of fission products and actinides, 402
- immobilisation by geopolymers, 401–16
 - advantages, 415
 - future trends, 401–16
- olivine group, 361
- 'Ongoing gel rearrangement and crystallisation,' 129
- opal, 384
- OPC, *see* Portland cements
- orthoclase, 231, 362
- Ostwald's rule, 99, 141, 148, 241
- OTIS company, 261
- Oxford energy dispersive X-ray spectrometer, 347
- paint sludges, 426
- PCT-B, 410, 411
- Perkin Elmer Thermogravimetric Analyser TGA 6, 347
- perlite, 261
- phase equilibria, and solubility, 56–8
- phenols, 436
- philipsite, 109, 142, 153, 309
- pirssonite, 362
- plagioclases, 231
- planetary ball mill, 304–5
- plombierite, 157
- Poisson's ratio, 218
- pollucite, 78–9, 334
- polycondensation, 93
- polymerisation, 92–6
 - coagulation–condensation, 93–4
 - condensation–crystallisation, 94–6
 - conceptual model for geopolymerisation, 95
 - destruction–coagulation, 93
- Portland cement-based system, 38
- Portland cements, 127, 140, 195, 204, 205, 405, 426, 427
 - alkali-silica reaction-induced expansion, 181
 - carbon dioxide emission, 211
 - compared with geopolymer concrete, 211–25
 - compressive strength evolution
 - exposed to 5% sodium and magnesium sulphate solutions, 169
 - exposed to acid solutions, 173
 - concrete mechanical properties
 - degradation, 333
 - flexural and compressive strengths, 187
 - mechanical strength, 175
 - mixture proportions tested in hydrocarbon fire, 329
 - thermal expansion, 323
 - variation in i_{corr} vs time, 179
 - variation in residual bending and compressive strength in cold samples, 185
- Portuguese Decree 236/98, 289
- Portuguese kaolin, 302
- Portuguese Standard LNEC E398-1993, 279
- potassium aluminosilicate system, 429
- potassium chabazite, 153
- potassium hydroxide, 55
- potassium sialate, 183
- pozzolan, 345, 350
- precipitation, 94–5
- pre-curing, 235
- price instrument, 394
- 'pseudo-plastic' behaviour, 188
- Pyrament, 382–3
- pyrophyllite, 299, 302, 306
- quantity instrument, 394
- quartz, 241, 243, 268, 321, 323, 335, 345, 360, 361, 362
- quartzite, 384
- radium, 429
- red mud, 345, 346, 352
- reinforced concrete structures, 176
- Réunion Internationale des Laboratoires et Experts des Matériaux, 388
- rheology, 126–7
- Rietveld refinement, 333
- Roman *opus caementicium*, 141
- rubidium hydroxide, 55
- scanning electron microscopy, 336, 362–5
- selenium, 429
- SEM, *see* scanning electron microscopy
- shotcrete, 339
- Si MAS NMR, 129
- SIAL, 413
- Si:Al ratio, 147, 174, 315, 318, 321, 324, 334, 363, 408
- sialate bond, 4

- Siemens D500 diffractometer, 347
 silica, 345
 silica sand, 345, 351
 silicon, 97–9
 silicon carbide, 261
 silicon oxide, 213
 Siloxo Pty. Ltd., 383
 Si-O-Al bonds, 174, 359
 Si-O-T bonds, 120
 Slovak power reactors, 414
 sodium, 107–11
 sodium aluminate, 412
 sodium aluminium oxide, 361
 sodium aluminium silicate carbonate, 308
 sodium aluminosilicate, 180, 184
 sodium aluminosilicate gel, 96–9, 101–11,
 162, 229, 231
 role of aluminium, 101–7
²⁷Al MAS-NMR spectra of ash pastes,
 104
 central component of ²⁷Al MAS-NMR
 spectra of fly ash pastes, 105–6
 mechanical strength, 103
 role of silicon in gel structure, 97–9, 101
 nanostructural model, 102
²⁹Si MAS-NMR spectra of type F fly
 ash, 98
²⁹Si NMR spectra of alkaline
 solutions, 100
 role of sodium, 107–11
 central component of 180-day ²³Na
 MAS NMR spectra for ash pastes,
 110
 central component of ²³Na MAS
 NMR spectra for ash pastes, 108
 soluble sodium variation, 109
 sodium aluminosilicate system, 429
 sodium arsenate, 427
 sodium carbonate, 232
 sodium chabazite, 148, 151, 157
 sodium hydroxide, 53–5, 122, 278, 412
 phase diagram, 54
 solids, 213
 solution, 212
 sodium nitrate, 412
 sodium nitrite, 412
 sodium P1, 151
 sodium silicate solution, 212, 213
 soil-cement, 380
 sol-gel process, 92
 ‘Solidification and hardening,’ 128
 solidification/stabilisation, 422
 solid-state magic angle, 408
 solubility, and phase equilibria, 56–8
 steam-curing, 216
 strained quartz crystals, 384
 strontium, 428–30
 super plasticiser, 204, 212, 213, 215, 278
 supplementary cementitious materials, 387
 synthesis kinetics, of geopolymers, 118–33
 apparatus used for EDXRD experiments,
 128
 calorimetry, 125–6
 changes in intensity at 960cm⁻¹, 124
 diffraction techniques, 127–9
 experimental EDXRD vs model
 predictions, 132
 FTIR spectra, 121
 kinetic analysis sample activated
 with different concentrations of
 NaOH, 123
 with 6M NaOH, 122
 microscopy, 130
 modelling, 130–1, 133
 NaOH concentration ratio and
 geopolymer gel growth rate,
 118–33
 nuclear magnetic resonance, 129–30
 potassium silicate/metakaolin geopolymer
 system EDXRD data, 129
 quasi-isothermal DSC data, 126
 reaction process described by reaction
 kinetic model, 131
 rheology, 126–7
in situ infrared spectroscopy, 119–25
 TCLP test, *see* Toxicity Characteristic
 Leaching Procedure
 TGA, *see* thermogravimetric analysis
 thermal expansion, of geopolymers, 316–23
 common coarse aggregates, 323
 comparison with ordinary Portland
 cement, 322
 fly ash geopolymers, 321–2
 influencing factors, 319–21
 alkali activator, 320
 compositional ratio, 321
 source material type, 321
 water content, 319–20
 metakaolin geopolymers, 321
 thermal properties, of geopolymers, 315–39
 fire resistance, 327–30

- concrete slabs tested for hydrocarbon fire exposure, 330
- fire test results, 329–30
- Portland cement and geopolymer concrete mixture tested in hydrocarbon fire, 329
- specimens after fire test, 331
- standard fire curves, 327–29
- temperature vs time relationship of standard fire, 328
- time vs temperature curve of typical room fire, 327
- high temperature applications, 338–9
- mechanical strength evolution, 330–3
 - comparison to ordinary Portland cement, 332–3
- microstructural changes, 335–38
 - pore structure evolution, 336–38
- phase changes at elevated temperatures, 333–5
 - geopolymer paste formation and destruction, 334–5
 - phases formed from secondary material, 335
- shrinkage/expansion characteristics of geopolymers, 317
- TGA/DTA, 324–5
- thermal conductivity, 326
- thermal expansion, 316–23
 - comparison with ordinary Portland cement, 322
 - fly ash geopolymers, 321–2
 - geopolymer concrete, 323
 - influencing factors, 319–1
 - metakaolin geopolymers, 321
- thermoanalysis, 324–5
- thermophysical properties, 326
- thermodynamics
- thermogravimetric analysis, 316, 324, 368–9
- thermonatrite, 362
- titanium, 21
- tobermorite, 157
- tonnes CO₂ equivalent, 393
- Toxicity Characteristic Leaching Procedure test, 404, 426
- transmission electron microscope, 336
- tridymite, 335, 345, 362
- trona, 232, 361, 362
- tungsten mine waste mud, 278, 229
- uranium, 429
- V.D. Glukhovskiy Institute, 261
- vermiculite, 261
- vibratory mill, 304–6
- Vicat needle, 278, 289
- Vicat penetration test, 280
- wastewater treatment sludges, 426
- water-to-cement ratio, 214, 316, 386
- WINFIT software, 104–5
- XANES, 426
- X-ray absorption spectroscopy, 426
- X-ray diffraction, 333, 360–2
- X-ray pair distribution function analysis, 78–9
 - pollucite vs caesium aluminosilicate pair distribution function, 79
- XRD, *see* X-ray diffraction
- Young's modulus, 318, 320, 330
- Zeobond, 389
- zeolite, 80
 - see also* specific zeolites
- zeolite Na-P1, 148
- zeolite P, 109
- zeolite precursor, 141, 229, 231, 238
- zeolite synthesis, 123
- zeolites, *see* specific mineral species
- zinc, 432–4
- zirconia, 412
- Zn-O-Si bonds, 432